MICROBIAL LIFE UNDER STRESS: BIOCHEMICAL, GENOMIC, TRANSCRIPTOMIC, PROTEOMIC, BIOINFORMATICS, EVOLUTIONARY ASPECTS AND BIOTECHNOLOGICAL APPLICATIONS OF POLY-EXTREMOPHILIC BACTERIA, VOLUME II

EDITED BY: Davide Zannoni, Claudia P. Saavedra, Gloria Paz Levicán and Martina Cappelletti

PUBLISHED IN: Frontiers in Microbiology

frontiers Research Topics

ISSN 1664-8714
ISBN 978-2-88976-446-4
DOI 10.3389/978-2-88976-446-4

About Frontiers

Frontiers is more than just an open-access publisher of scholarly articles: it is a pioneering approach to the world of academia, radically improving the way scholarly research is managed. The grand vision of Frontiers is a world where all people have an equal opportunity to seek, share and generate knowledge. Frontiers provides immediate and permanent online open access to all its publications, but this alone is not enough to realize our grand goals.

Frontiers Journal Series

The Frontiers Journal Series is a multi-tier and interdisciplinary set of open-access, online journals, promising a paradigm shift from the current review, selection and dissemination processes in academic publishing. All Frontiers journals are driven by researchers for researchers; therefore, they constitute a service to the scholarly community. At the same time, the Frontiers Journal Series operates on a revolutionary invention, the tiered publishing system, initially addressing specific communities of scholars, and gradually climbing up to broader public understanding, thus serving the interests of the lay society, too.

Dedication to Quality

Each Frontiers article is a landmark of the highest quality, thanks to genuinely collaborative interactions between authors and review editors, who include some of the world's best academicians. Research must be certified by peers before entering a stream of knowledge that may eventually reach the public - and shape society; therefore, Frontiers only applies the most rigorous and unbiased reviews.
Frontiers revolutionizes research publishing by freely delivering the most outstanding research, evaluated with no bias from both the academic and social point of view. By applying the most advanced information technologies, Frontiers is catapulting scholarly publishing into a new generation.

What are Frontiers Research Topics?

Frontiers Research Topics are very popular trademarks of the Frontiers Journals Series: they are collections of at least ten articles, all centered on a particular subject. With their unique mix of varied contributions from Original Research to Review Articles, Frontiers Research Topics unify the most influential researchers, the latest key findings and historical advances in a hot research area! Find out more on how to host your own Frontiers Research Topic or contribute to one as an author by contacting the Frontiers Editorial Office: frontiersin.org/about/contact

MICROBIAL LIFE UNDER STRESS: BIOCHEMICAL, GENOMIC, TRANSCRIPTOMIC, PROTEOMIC, BIOINFORMATICS, EVOLUTIONARY ASPECTS AND BIOTECHNOLOGICAL APPLICATIONS OF POLY-EXTREMOPHILIC BACTERIA, VOLUME II

Topic Editors:
Davide Zannoni, University of Bologna, Italy
Claudia P. Saavedra, Andres Bello University, Chile
Gloria Paz Levicán, University of Santiago, Chile
Martina Cappelletti, University of Bologna, Italy

Citation: Zannoni, D., Saavedra, C. P., Levicán, G. P., Cappelletti, M., eds. (2022). Microbial Life Under Stress: Biochemical, Genomic, Transcriptomic, Proteomic, Bioinformatics, Evolutionary Aspects and Biotechnological Applications of Poly-Extremophilic Bacteria, Volume II. Lausanne: Frontiers Media SA.
doi: 10.3389/978-2-88976-446-4

Table of Contents

frontiers | Frontiers in Microbiology

EDITORIAL
published: 26 May 2022
doi: 10.3389/fmicb.2022.910962

Editorial: Microbial Life Under Stress: Biochemical, Genomic, Transcriptomic, Proteomic, Bioinformatics, Evolutionary Aspects, and Biotechnological Applications of Poly-Extremophilic Bacteria, Volume II

Davide Zannoni[1]*, *Claudia Saavedra*[2], *Gloria Levicán*[3] and *Martina Cappelletti*[1]

[1] Department of Pharmacy and Biotechnology, University of Bologna, Bologna, Italy, [2] Facultad de Ciencias de la Vida, Universitad Andres Bello, Santiago, Chile, [3] Departamento de Biología, Facultad de Química y Biología, Universidad de Santiago de Chile (USACH), Santaigo, Chile

Keywords: environmental stress, molecular mechanisms, extremophiles, adaptive evolution, resistance

OPEN ACCESS

Edited and reviewed by:
Andreas Teske,
University of North Carolina at Chapel Hill, United States

***Correspondence:**
Davide Zannoni
davide.zannoni@unibo.it

Specialty section:
This article was submitted to Extreme Microbiology, a section of the journal Frontiers in Microbiology

Received: *01 April 2022*
Accepted: *13 April 2022*
Published: *26 May 2022*

Citation:
Zannoni D, Saavedra C, Levicán G and Cappelletti M (2022) Editorial: Microbial Life Under Stress: Biochemical, Genomic, Transcriptomic, Proteomic, Bioinformatics, Evolutionary Aspects, and Biotechnological Applications of Poly-Extremophilic Bacteria, Volume II. Front. Microbiol. 13:910962. doi: 10.3389/fmicb.2022.910962

Editorial on the Research Topic

Microbial Life Under Stress: Biochemical, Genomic, Transcriptomic, Proteomic, Bioinformatics, Evolutionary Aspects, and Biotechnological Applications of Poly-Extremophilic Bacteria, Volume II

Habitats defined as "extremes" exist across the entire planet. They can be widely different in their physico-chemical features as they include a diverse array of harsh parameters thought to preclude the existence of living organisms, such as temperature, pH, salinity, radiation, pressure, low water activity, low nutrients, and even the presence of toxic agents such as metals and/or metalloids. Organisms capable of surviving or thriving in those habitats are named "extremophiles" and the vast majority of them are prokaryotes, which is not surprising as they show a remarkable reservoir of genomes allowing them to grow in a great variety of hostile niches. Interestingly, several harsh conditions may occur simultaneously and the microorganisms able to withstand them are called "poly-extremophiles". Although many bacterial species from all kinds of extreme environments have been isolated and described in the last decades, very little is known about the molecular strategies and physiology that allow them to grow in such critical conditions.

The aim of this Research Topic on Microbial Life Under Stress (Volume II) is to address this issue by applying multidisciplinary approaches for integrating data from biochemical, genomic, transcriptomic, proteomic, bioinformatics, and evolutionary studies of bacteria from extreme and poly-extreme environments. This Research Topic consists of 14 original articles by numerous authors actively engaged in the study of microbiology, biochemistry, and omic-research of extremophiles. The present Editorial can be divided into four sections which include groups of articles on different genera and species of acidophiles, studies on microorganisms from arid/desiccated environments but also from habitats at low and high temperatures, and finally, a set of papers on extremophiles capable of coping with extreme levels of radiation, pressure, and toxic metals.

Sulfate-reducing bacteria (SRB) are polyextremophiles as they grow at low-pH, high-metal concentration, and high-salinity conditions. These microorganisms are known to catalyze the precipitation of metals in the form of their sulfides and to neutralize the acidity of low pH-drainage environments through proton consumption. In their research article, Sanchez-Andrea et al. reports and describes the isolation of a novel genus of moderately acidophilic SRB, *Acididesulfobacillus acetoxydans* gen. nov. sp. nov. strain INE, able to grow at pH 3.8. Bioreactor studies show that strain INE is capable of completely oxidizing organic acids to CO_2, a rare property among acidophilic SRB, while comparative proteogenomics and membrane lipid analysis indicate the presence of saturated ether-bound lipids as a protection mechanism against acid stress.

In another paper by Gonzalez-Rosales at al., integrative genomics was applied to investigate the evolution of extreme acidophiles belonging to the Acidithiobacillia class. Phylogenetic reconstruction revealed the genes and mechanisms, defined as first and second lines of defense, which are involved in the exclusion and/or extrusion of protons along with the biosynthesis of hopanoids for membrane stabilization, that are crucial in explaining the acidophilic lifestyle of these microorganisms.

Acidihalobacter is a genus of acidophilic, Gram-negative bacteria, known for its ability to oxidize pyrite minerals in the presence of high amounts of chloride ions, a rare property among iron-sulfur oxidizing acidophiles. A phylogenetic analysis of four genomes of this genus *(A. prosperus* DSM 5130Y, *A. yilgarnensis* DSM 105917T, *A. aeolians* DSM 14174T, and *A. ferrooxidans* DSM 14175T) performed by Boase et al. shows that they all root to the Chromatiales class consisting of mostly halophilic microorganisms. The study provides evidence that a series of acid tolerance mechanisms found in Acidihalobacter genomes were acquired by horizontal gene transfer (HGT) from other acidophilic lineages, allowing the genus members to cope with acid stress. These mechanisms include multiple potassium transporters, chloride/proton antiporters, glutamate- and arginine-decarboxylase systems, and both squalene and hopanoid synthesis.

Large-scale outdoor cultivation of autotrophic microalgae is strongly favored by extreme environmental conditions, e.g., very low pH, in order to prevent contamination and predation. In search for new extremophilic microalgae suitable for large-scale production, Abiusi et al. examined six microalgal strains of the genera *Stichococcus*, *Chlamydomonas*, *Viridiella,* and *Galdieria*, which are able to grow at pH < 3. Several strains were cultivated at variable light intensities and acidic pHs and their autotrophic biomasses were compared with one of the most productive microalgae, *Chlorella sorokiniana* SAG 211-8K grown at pH 6.8. Notably, five of the tested strains displayed autotrophic biomass productivities slightly (10%) or moderately (39%) lower than *C. sorokiniana* indicating the potential use of these microalgae for biomass production under acidic conditions.

Microbiological soil crusts are communities of microorganisms on the soil surface of arid and semi-arid ecosystems. They perform important ecological roles including carbon fixation, nitrogen fixation, and soil stabilization. The paper by Jiang et al. describes the properties of *Modestobacter deserti* sp. nov., a novel phosphate-solubilizing actinobacterium isolated from soil crust samples of the Tengger Desert, China. Whole-genome analysis revealed the presence of a set of genes coding for alkaline phosphatases, phosphate transport, trehalose-phosphate synthase, and trehalose 6-phosphatase along with other genes helping this microorganism to cope with harsh conditions prevalent in deserts. In this respect, the Salar of Atacama in the Chilean Central Andes harbors unique microbial ecosystems due to the high altitude, low oxygen pressure, high solar radiation, and high salinity. The paper by Vignale et al. expands our knowledge of these extreme habitats, through the characterization of 20 previously unexplored Andean microbial ecosystems (both prokaryotic and eukaryotic taxa) in eight different lakes and wetlands. Conversely, Fuentes et al. examined the variation in microbial communities down to a depth of 3.4 m in the hyperarid Yungay region of the Atacama Desert. They found that the moisture content changed from 2 to 11% with depth, with different distributions of bacterial phyla in three zones, namely: A. *Deinococcota*, *Halobacterota,* and *Latescibacterota*; B. *Crenarchaeota* and *Fusobacteriota*; and C. *Fervibacteria* and *Campilobacterota* (at 0–60 cm, 60–220 cm, and 220–340 cm, respectively). It was concluded that the moisture content, total carbon, pH, and electric conductivity were the best predictors of microbial richness and diversity while total sulfur and phosphorus contents were predictive of community compositions.

In recent years, shallow water hydrothermal vents have been explored for investigating the effects of ocean acidification on microbial communities as vent emissions can release high amounts of CO_2, causing local pH reduction. However, this phenomenon is often blurred by the emission of other gas species and metals, making this environment highly dynamic. Sciutteri et al. examined the composition and functional profiles of microbial biofilms in Levante Bay (Vulcano Island, Italy, Mediterranean Sea), a well-studied shallow-water hydrothermal vent. Analysis of 16S rRNA transcripts revealed that the composition of the microbial populations varies at very small spatial scales, reflecting the strong influence of H_2S gas emission as a selection factor for sulfide-dependent and chemolithoautothrophic bacteria. Another example of an extreme marine environment is represented by deep ocean waters and Arctic/Antarctic areas where the temperature is below 0°C. These habitats are colonized by psychrophiles, which are microorganisms thriving at temperatures around the freezing point of water. *Colwelia psychrerythraea* 34H is a Gram-negative psychrophile, isolated from Arctic marine sediments and is considered a model organism for studying adaptive strategies at low temperatures. The paper by Casillo et al. reports that *C. psychrerythraea* generates a series of unusual membrane and extracellular matrix glycopolymers in response to temperature fluctuations. The effects of climate change on environmental microorganisms and in particular on the increase in temperatures in the polar regions were addressed by Garcia-Descalzo et al. who performed a comparative proteomic analysis of psychrophilic (*Shewanella frigidimarina* and *Psychrobacter frigidicola*) vs. mesophilic (*Shewanella oneidensis*) bacterial species. The results show a greater versatility of acclimatization

for the genus *Shewanella* with respect to *Psychrobacter*. Furthermore, chaperons play a pivotal role in withstanding temperature changes as they form complexes with other proteins, thus establishing a cooperation with transmembrane proteins, elongation factors, and proteins acting against oxidative damage. The effects of temperature as an abiotic stress factor at the transcriptional level were examined by Guo et al. in *Rhodosporidium kratochvilovae* YM25235, a cold-adapted oleaginous yeast strain that can grow at 15°C. They discover that temperatures around 10–15°C induce substantial changes in the expression of different genes in many fungal genera as part of the process known as the cold-shock response. Comparing the RNA transcriptomic data at 15 and 30°C, ∼1,300 differentially expressed genes (DEGs), primarily related to metabolic and cellular processes, cell organelles, and catalytic activities, were identified, providing crucial information on the use of this organism for the production of polyunsaturated fatty acids.

Microbes colonizing the deep seas and oceans represent a large fraction of the biosphere. Therefore, shedding light on their metabolic processes is helpful for understanding global energy cycling. The paper by Zhang et al. that *Iocasia fonsfrigidae* NS-1 gen. nov., sp. nov., a novel Gram-negative anaerobe isolated from deep-sea cold seeps in the South China Sea, metabolizes multiple carbohydrates including xylan, alginate, starch, and lignin. Their anaerobic metabolism generates fermentation products such as hydrogen, lactate, butyrate, and ethanol. The evidence presented predicts that *Iocasia* sp. could be a metabolic partner of other cold-seep microorganisms thriving at the expense of these small macromolecules.

The bacterium *Deinococcus radiodurans* shows remarkable resistance to a range of damage caused by ionizing radiation, desiccation, UV radiation, and oxidizing agents. Although it is known that these multiple resistance phenotypes stem from efficient DNA repair processes, the mechanisms underlying these extraordinary repair capabilities remain poorly understood. Recently, a protein homolog containing a metalloenzyme domain (DRJAMM) with Zn^{2+}-dependent deubiquitase activity was reported in *D. radiodurans*. In their paper, Cai et al. show that DRJAMM has efficient *in vitro* catalytic activity in the presence of Mn^{2+}, Ca^{2+}, Mg^{2+}, and Ni^{2+} in addition to Zn^{2+} along with a strong adaptability to a wide range of temperatures. Furthermore, DRJAMM was shown to counteract oxidant processes and it was also required for anaerobic DMSO-respiration.

Bioleaching of copper sulfides is a crucial aspect of iron- and sulfur-oxidizing acidophilic microorganisms in the heap/dump mining industry. The paper by Bobadilla and Poblete-Castro examines in detail the dynamics of biofilm formation using *Leptospirillum* spp. and *Acidithiobacillus thiooxidans* (in a ratio of 3:1) during bioleaching of primary copper sulfide minerals (bornite, Cu_5FeS_4 and chalcopyrite, $CuFeS_2$) at 30°C. The results show that *A. thiooxidans* cells are able to develop as a biofilm on the surface of bornite while *Leptospirillum* spp. are detected in planktonic form, underlying the role of biofilm formation in the bioleaching process of copper sulfides.

Finally, I would like to mention, on behalf of the co-editors Claudia Saavedra, Gloria Levicán, and Martina Cappelletti, that this Research Topic on Microbial Life Under Stress, is dedicated to the memory of my friend and colleague Claudio Vasquez who died prematurely in July 2020. The remembrance I have of Claudio is that of a generous, authentic, outgoing, and lively man. He was a lover of life and good foods, and, last but not least, a scientist who raised a group of excellent young researchers in his laboratory in Santiago, Chile. My biggest regret is not having had many more opportunities to meet him but for sure Claudio will remain in my thoughts for years to come.

AUTHOR CONTRIBUTIONS

DZ wrote the first draft of the manuscript. DZ, CS, GL, and MC contributed to the final version of the manuscript. All authors contributed to the article and approved the submitted version.

FUNDING

This work was supported by Fondecyt grant N° 1211386 from the government of Chile (to GL), by Fondecyt 1210633 (to CS) and by RFO-2021 UniBo (to MC).

Conflict of Interest: The authors declare that the research was conducted in the absence of any commercial or financial relationships that could be construed as a potential conflict of interest.

Publisher's Note: All claims expressed in this article are solely those of the authors and do not necessarily represent those of their affiliated organizations, or those of the publisher, the editors and the reviewers. Any product that may be evaluated in this article, or claim that may be made by its manufacturer, is not guaranteed or endorsed by the publisher.

frontiers in Microbiology

ORIGINAL RESEARCH
published: 16 September 2021
doi: 10.3389/fmicb.2021.727105

Genome-Wide Transcriptional Changes of *Rhodosporidium kratochvilovae* at Low Temperature

Rui Guo, Meixia He, Xiaoqing Zhang, Xiuling Ji, Yunlin Wei, Qi-Lin Zhang and Qi Zhang**

Faculty of Life Science and Technology, Kunming University of Science and Technology, Kunming, China

Rhodosporidium kratochvilovae strain YM25235 is a cold-adapted oleaginous yeast strain that can grow at 15°C. It is capable of producing polyunsaturated fatty acids. Here, we used the Nanopore Platform to first assemble the *R. kratochvilovae* strain YM25235 genome into a 23.71 Mb size containing 46 scaffolds and 8,472 predicted genes. To explore the molecular mechanism behind the low temperature response of *R. kratochvilovae* strain YM25235, we analyzed the RNA transcriptomic data from low temperature (15°C) and normal temperature (30°C) groups using the next-generation deep sequencing technology (RNA-seq). We identified 1,300 differentially expressed genes (DEGs) by comparing the cultures grown at low temperature (15°C) and normal temperature (30°C) transcriptome libraries, including 553 significantly upregulated and 747 significantly downregulated DEGs. Gene ontology and pathway enrichment analysis revealed that DEGs were primarily related to metabolic processes, cellular processes, cellular organelles, and catalytic activity, whereas the overrepresented pathways included the MAPK signaling pathway, metabolic pathways, and amino sugar and nucleotide sugar metabolism. We validated the RNA-seq results by detecting the expression of 15 DEGs using qPCR. This study provides valuable information on the low temperature response of *R. kratochvilovae* strain YM25235 for further research and broadens our understanding for the response of *R. kratochvilovae* strain YM25235 to low temperature.

Keywords: *Rhodosporidium kratochvilovae*, low temperature, genome sequencing, differential expressed genes, RNA-Seq, qPCR

OPEN ACCESS

Edited by:
Gloria Paz Levicán, University of Santiago, Chile

Reviewed by:
Fang-Fang Wang, Institute of Microbiology, Chinese Academy of Sciences (CAS), China
Sujit Jagtap, University of Illinois at Urbana-Champaign, United States

****Correspondence:***
Qi-Lin Zhang
zhangql@kust.edu.cn
Qi Zhang
qzhang37@kust.edu.cn

Specialty section:
This article was submitted to Extreme Microbiology, a section of the journal Frontiers in Microbiology

Received: *18 June 2021*
Accepted: *26 August 2021*
Published: *16 September 2021*

Citation:
Guo R, He M, Zhang X, Ji X, Wei Y, Zhang Q-L and Zhang Q (2021) Genome-Wide Transcriptional Changes of Rhodosporidium kratochvilovae at Low Temperature. Front. Microbiol. 12:727105. doi: 10.3389/fmicb.2021.727105

INTRODUCTION

One of the crucial ecological factors associated with abiotic stress is low temperatures, which can disrupt microbial homeostasis and affect the biological functions of cells (García-Ríos et al., 2017; Wang et al., 2020). In addition, low temperatures can severely inhibit fungal growth and may also kill it (Wang et al., 2014; Long et al., 2015). Although 10–18°C is considered as a low temperature range for fungus, these are permissive temperature (García-Ríos et al., 2017). Currently, the understanding of the molecular mechanisms of response in fungus to low temperature stress has been explored. For example, several fungal genera adapt to low temperature by changing the expression of different genes as part of the process known as the cold-shock response that has been investigated in *Saccharomyces cerevisiae* (Aguilera et al., 2007). During adaptation, several cold response-related genes, including those involved in energy preservation, detoxification,

osmolyte production, protein folding support, and maintenance of membrane fluidity, are activated (Murata et al., 2006). Growth capacity diminishes as the temperature decreases below the optimum temperatures. Studies in *Neurospora crassa* have demonstrated a high accumulation of mRNAs of carotenoid genes to reduce oxidative stress under low temperature (Castrillo et al., 2018). These results suggest that differentially expressed genes (DEGs) play a key role under low temperature stress in fungi. Therefore, the identification of genes associated with low temperature response and intensive exploration for molecular mechanisms in response to low temperature at the level of gene expression in fungi are necessary.

Rhodosporidium species have been reported to be capable of synthesizing some value-added compounds with a wide industrial usage, such as lipid (Uprety et al., 2017), carotenoids (Buzzini et al., 2007), enzymes (MacDonald et al., 2016), polyunsaturated fatty acids (PUFAs) (Ageitos et al., 2011; Cui et al., 2016; Wang et al., 2017; He et al., 2019) and sugar alcohols including D-arabitol and galactitol (Jagtap and Rao, 2018; Jagtap et al., 2019). As a species of the genus *Rhodosporidium*, *Rhodosporidium kratochvilovae* strain YM25235 (isolated from Chenghai Lake, Yunnan, China) is a cold-adapted oleaginous fungal yeast strain that can grow at 15°C (He et al., 2019), and it is capable of producing PUFAs (Cui et al., 2016; Wang et al., 2017; He et al., 2019). PUFAs are involved in the maintenance of optimal physical and biological properties of cell membranes, which is an essential adaptation strategy in microorganisms against cold stress (Clarke, 2001; Sampath and Ntambi, 2004). Certain fungi produce high levels of PUFAs in response to low temperature (Calvo et al., 2001; Wang et al., 2017). We had previously reported that the strain YM25235 at 15°C produced high amounts of linoleic acid (LA, C18:2Δ9,12) and α-linolenic acid (ALA, C18:3Δ9,12,15), and the inhibition of PUFA biosynthesis negatively influenced the cold adaptation of YM25235 (Cui et al., 2016; Wang et al., 2017). In addition, cold-adapted fungal yeasts have attracted the wide attention of several scientists worldwide because of their significant potential for application in diverse industries (Margesin and Miteva, 2011; Carrasco et al., 2017). These fungal species have evolved physiological strategies to survive in cold climates, including modulation of enzyme kinetics and membrane fluidity (Firdaus-Raih et al., 2018).

For *R. kratochvilovae*, Miccoli et al. (2018) have completed whole genome sequencing of the strain LS11, and several other *Rhodosporidium* strains have also been sequenced (Hu and Ji, 2016; Zhang et al., 2016; Tran et al., 2019). In addition, multi-omics analyses of the oleaginous fungal yeast *Rhodosporidium toruloides* were conducted to shield lights on Pi-limitation-induced lipid accumulation (Wang et al., 2018). By comparing microbial growth and gene expression patterns, several studies demonstrated that expression levels of genes that encode carotenoid biosynthesis were altered in response to light change (Pham et al., 2020). Dinh et al. (2019) reconstructed a genome-scale model of *R. toruloides* IFO0880's metabolic network. However, changes in the gene expression profile of these fungal yeasts, especially *R. kratochvilovae*, under temperature stress have not been investigated.

We performed this study to gain a comprehensive understanding of the molecular adaptation mechanisms to low temperatures in *R. kratochvilovae* strain YM25235 from the perspective of gene expression. The whole genome of *R. kratochvilovae* strain YM25235 was sequenced. Subsequently, based on RNA-seq data and the above-sequenced genome of strain YM25235, DEGs were identified between *R. kratochvilovae* at low temperature (15°C) and normal temperature (30°C) groups. Furthermore, we performed annotation of *R. kratochvilovae* strain YM25235 genes and functional enrichment analysis [Gene Ontology (GO) and Kyoto Encyclopedia of Genes and Genomes (KEGG) pathway] of DEGs. The DEGs were summarized, and several key pathways involved in low temperature stress tolerance were obtained from the list of KEGG terms enriched by the DEGs. This study will provide insights into the molecular adaptation mechanisms of *R. kratochvilovae* strain YM25235 under low temperature stress.

MATERIALS AND METHODS

Culture Conditions and Cell Sample Preparation

For whole genome sequencing, *R. kratochvilovae* strain YM25235 was grown in yeast extract peptone dextrose (YPD: 1% yeast extract, 2% peptone, and 2% glucose) broth at 30°C to logarithmic growth phase (OD_{600} = 1.60). For RNA-seq, *R. kratochvilovae* strain YM25235 was pre-incubated in YPD broth at 30°C for 24 h and then was exposed to 15 and 30°C for another 8 h, with the final OD_{600} values of ∼2.1 and ∼2.3, respectively, with three technical replicates collected for each sample. The culture broth was centrifuged at 5,000 × *g* for 10 min at 4°C. For cell disruption, the culture pellets were ground in liquid nitrogen.

DNA Extraction, Genome Sequencing, and Assembly

Total DNA of *R. kratochvilovae* strain YM25235 was extracted using Wizard Genomic DNA Purification Kit (Promega, Madison, WI, United States). The next experimental procedures were performed according to the standard protocols provided by Oxford Nanopore Technologies (ONT). To optimize the sequencing experiments and improve the throughput, a library was constructed using the SQK-LSK109 Ligation Sequencing Kit. Then, the library was sequenced on the Nanopore PromethION platform. After sequencing, the downstream sequencing data were analyzed by basecalling programs using the Albacore software from the MinKNOW package to convert the raw sequencing data from FAST5 format to FASTQ format (Wick et al., 2019). Further filtering for the adaptor, low quality, and short reads (<2,000 bp in length) resulted in total dataset clean reads. Canu v1.5 software was used to correct the filtered subreads (Koren et al., 2017). Next, we assembled the subreads after error correction using the wtdbg software to obtain the final genome with high accuracy (Ruan and Li, 2019). The BUSCO v2.0 software was used to assess the completeness of the

R. kratochvilovae strain YM25235 genome assembly (Simão et al., 2015).

Functional Annotation of the Genome

Because of the relatively low conservation of repeat sequences among different species, predictions of repeat sequences for a particular species require the construction of specific repeat sequence databases. Therefore, we used four software, including LTR_FINDER v1.05, MITE-Hunter, RepeatScout v1.05, and PILER-DF v2.4, to construct a repeat sequence database for the genome of *R. kratochvilovae* strain YM25235 based on the methods of structural and *de novo* predictions (Edgar and Myers, 2005; Price et al., 2005; Xu and Wang, 2007; Han and Wessler, 2010). Classification of the repeat sequences was performed using the PASTE Classifier software (Wicker et al., 2007). The type of the classified repeat sequences was subsequently annotated using the Repbase database (Jurka et al., 2005). Repeat sequences in the genome of *R. kratochvilovae* strain YM25235 were searched in the RepeatMasker v4.0.6 database (Chen, 2004).

The gene structure was predicted using *de novo* predictions and homologous protein search. Transcript evidence from sequencing transcriptome was used to validate the coding regions of genes. Finally, the prediction results from the three methods were intersected as the final sets of protein-coding genes. In particular, *de novo* prediction was performed using GenScan, Augustus v2.4, GlimmerHMM v3.0.4, GeneID v1.4, SNAP (version 2006–07–28) (Burge and Karlin, 1997; Stanke and Waack, 2003; Korf, 2004; Majoros et al., 2004; Alioto et al., 2018). Homologous protein-based predictions were implemented using GeMoMa v1.3.1 (Keilwagen et al., 2016); and transcript-based predictions were conducted using the PASA v2.0.2 software (Campbell et al., 2006). The intersection of the results from three methods was obtained by using EVM v1.1.1 (Haas et al., 2008).

To obtain functional annotation information of *R. kratochvilovae* strain YM25235 genes, the predicted gene sequences were annotated by searching them in the following gene collections using the BLAST tool: Cluster of orthologous groups for eukaryotic complete genomes (KOG) (Tatusov et al., 2000), KEGG (Kanehisa et al., 2004), Swiss-Prot (Boeckmann et al., 2003), and non-redundant protein sequence database (Nr) (Deng et al., 2006). Based on the searched results from the Nr database, the GO annotation information of genes was extracted using the in-house Perl script (Ashburner et al., 2000; Conesa et al., 2005). In addition, domains of the protein sequence of each gene were searched in the Pfam database using the Hmmer software (Eddy, 1998; Finn et al., 2016).

Extraction of RNA, Library Construction, and Sequencing

Total RNA of *R. kratochvilovae* strain YM25235 was purified using RNeasy Mini Kit (Qiagen, Valencia, CA, United States). After extraction of total RNA from the samples, the quality of total RNA [i.e., RNA integrity number (RIN) values, 28S/18S and concentration] was determined using the Agilent 2100 Bioanalyzer (Agilent RNA 6000 Nano Kit). The purity of the samples was assessed using a UV spectrophotometer NanoDrop^{TM}, ND-1000 (Thermo Scientific, United States). Next, the cDNA library was constructed. In brief, *R. kratochvilovae* strain YM25235 mRNA was enriched using magnetic beads with oligo (dT). The resulting mRNA was fragmented by adding an appropriate amount of the shearing reagent under high temperature conditions so that the interrupted mRNA was used as a template for the first-strand cDNA synthesis. Subsequently, the second strand cDNA was synthesized, purified using commercial kits, and sticky ends were repaired. The base "a" was added to the 3′ end of the cDNA and adaptors were ligated, followed by fragment size selection and PCR amplification. The quality of the constructed libraries was checked using the Agilent 2100 Bioanalyzer (Agilent Technologies, United States) and ABI StepOnePlus Real-Time PCR System.

Raw reads generated by RNA sequencing (RNA-seq) were filtered to obtain clean data by removing low-quality reads, adapter contamination, and reads with excessive unknown bases (Cock et al., 2010). Clean reads were mapped to the

TABLE 1 | List of randomly selected 15 differentially expressed genes (DEGs).

Gene name	Log_2FoldChange (Treatment/Control)	Gene symbol	Pathway	P_{adj}
Aryl-alcohol dehydrogenase	−2.9209	AAD	MAPK signaling pathway-yeast	2.61E-53
LigA	2.5233	LigA	Amino sugar and nucleotide sugar metabolism	1.72E-10
Alcohol dehydrogenase	−3.6458	Adh	Amino sugar and nucleotide sugar metabolism	1.83E-117
Acetolactate synthase	1.6086	ALS	Butanoate metabolism	1.31E-22
GTP cyclohydrolase II	−5.0704	GCH2	NA	3.12E-115
4-Coumarate-CoA ligase	−2.0127	4CCL	NA	1.05E-07
Cell cycle checkpoint protein rad17	−1.4118	rad17	Cell cycle-yeast	4.50E-16
Sulfate permease	1.8478	SLP	NA	0.00126
Isocitrate lyase	−2.8528	ICL	Metabolic pathways	3.76E-28
Proteophosphoglycan ppg4	1.9823	ppg4	NA	1.25E-40
ATP phosphoribosyltransferase	2.0123	hisG	Metabolic pathways	2.62E-52
GCN5-related *N*-acetyltransferase	1.3899	GNAT	NA	9.88E-13
MFS multidrug transporter	−1.9306	MFSmdf	Amino sugar and nucleotide sugar metabolism	8.21E-33
Cytosine-purine permease	−2.4662	FCY	MAPK signaling pathway-yeast	6.64E-27
RTA-like protein	−1.9852	RTK	Amino sugar and nucleotide sugar metabolism	2.59E-44

reference genome of *R. kratochvilovae* strain YM25235 to avoid contaminants caused by non-*R. kratochvilovae* strain YM25235 reads using Hierarchical Indexing for Spliced Alignment of Transcripts (HISAT) (Kim et al., 2015).

Quantification of Gene Expression and Identification of Differentially Expressed Genes

Clean reads were mapped to the reference gene sequences using Bowtie 2 (Langmead and Salzberg, 2012). Next, the expression of genes was assessed based on Fragments Per Kilobase per Million (FPKM) values calculated by RSEM (RNA-Seq by Expectation Maximization) methods (Li and Dewey, 2011). DEGs were identified using the DESeq2 software, an R program suitable for the identification of DEGs from high-throughput sequencing data between the control and treatment groups (Love et al., 2014). The DEGs with fold change (FC) ≥ 2 ($|\log_2 \text{ratio}| \geq 1$) and *p*-values (Wald test in Deseq2) corrected by a false discovery rate (corrected *p*-values) < 0.05 were identified as DEGs.

Functional Enrichment Analysis of Differentially Expressed Genes

To further elucidate the biased biological function of DEGs and signaling pathways, the functional analyses of DEGs were performed using the Blast2GO pipeline (Conesa et al., 2005). The annotated functional terms of DEGs were clustered through the Functional Annotation Clustering tool in the KOBAS software (Xie et al., 2011). The KEGG pathways from each clustered set with an FDR-value < 0.01 were considered to be significantly enriched. Furthermore, the redundant GO terms were systematically discarded using GO trimming (Jantzen et al., 2011).

Validation of RNA-Seq Data and Gene Expression Analysis by qPCR

To validate the results of RNA-seq, 15 DEGs were randomly selected for downstream quantitative real-time PCR (qPCR) analysis, with three biological replicates (**Table 1**). Parallelly, we obtained the corresponding control sample in the same manner. Purification and evaluation of total RNA were performed using the above-mentioned methods ("Extraction of RNA, Library Construction, and Sequencing"). This was performed thrice independently to generate three biological replicates.

Specific primers used in the qPCR analysis were designed automatically using the Beacon Designer 7 (**Supplementary Table 1**). For the preparation of cDNA libraries, the first-strand cDNA was synthesized from total RNA using the PrimeScript RT reagent kit with gDNA eraser (TaKaRa, Tokyo, Japan). Next, we used RNase-free water to dilute the preliminary cDNA solution (final concentration, 100 ng/μL). Next, qPCR was performed on the Light Cycler 480 Real-Time PCR System (Roche, Basel, Switzerland) using the Bestar SYBR Green qPCR Master mix (DBI Bioscience, Shanghai, China). The qPCR reaction of each gene in each sample was independently repeated thrice, and experiments were performed in three biological replicates. The qPCR amplification steps were a holding stage at 95°C for 5 min, followed by the cycling stage with 40 cycles of 94°C for 10 s and 60°C for 40 s. The subsequent melt curve stage consisted of 95°C for 15 s, 60°C for 1 min, and 95°C for 15 s. Small subunit rRNA (SSU rRNA) was used as an internal control. The relative expression of target genes was calculated by comparison with SSU rRNA using the $2^{-\Delta\Delta Ct}$ method. The final results are shown as means ± standard deviations (SD) (Livak and Schmittgen, 2001).

RESULTS

Summary and Assembly Information of Genome Sequencing Data

A total of 4,795,537,118 bp raw data of *R. kratochvilovae* strain YM25235 were obtained from the Nanopore sequencer. Furthermore, 4,578,684,148 bp clean data were obtained. Sequencing depth was 193.04× and the total length of the assembled complete genome was 23.71 Mb, which is higher than that of *R. kratochvilovae* strain LS11 (22.11 Mb), *R. toruloides*

TABLE 2 | Genome assembly results statistics.

Item	
Scaffold features	
Total number	46
Total length (bp)	23,718,404
N50 (bp)	1,067,950
N90 (bp)	255,572
Max length (bp)	2,421,707
Mean Qual	8.92
Sequence GC content (%)	67.30
Genome features	
Genome assembly (Mb)	18,229,638
Number of protein-coding genes	8,472
Average gene length (bp)	2,151.75
Average coding sequence length (bp)	229.57
Exon length (nt)	14,092,373
Average exon length (nt)	240.24
Exon number	58,660
Average exon number	6.92
intron length (nt)	4,137,265
Average intron length (nt)	82.44
intron number	50,188
Average intron number	5.92

TABLE 3 | BUSCO evaluation statistics.

Item	
Complete BUSCOs(C)	246 (84.83%)
Complete and single-copy BUSCOs(S)	226 (77.93%)
Complete and duplicated BUSCOs(D)	20 (6.90%)
Fragmented BUSCOs(F)	21 (7.24%)
Missing BUSCOs(M)	23 (7.93%)
Total Lineage BUSCOs	290

strain NP11 (20.22 Mb), and *R. paludigena* (20.66 Mb). The N50 length of the assembly was 1,067,950 bp, which is higher than that of *R. kratochvilovae* strain LS11 (704,466 bp), *R. toruloides* strain NP11 (163,970 bp), and *R. paludigena* (371,695 bp). The average GC content of *R. kratochvilovae* strain YM25235 genome (67.30%) is higher than that of *R. kratochvilovae* strain LS11 (66.60%), *R. toruloides* strain NP11 (62.00%), and *R. paludigena* (64.3%). A total of 8,472 genes were identified in the genome of *R. kratochvilovae* strain YM25235, with an average length of 2,151 bp. The number of coding sequence (CDS) was 57,762, and the average length of CDS was 229.57 bp; the average number of CDS per gene was 6.82 bp. The number of introns was 50,188 bp and the average length of the intron was 82.44 bp. Each gene average contained 5.92 introns (**Table 2**). The results of BUSCO showed that 84.83% of the genes were completed (**Table 3**), indicating the high quality and completeness of the current genome (Jiang et al., 2019).

Gene Prediction and Annotation

Among the 7,907 predicted genes, 7,859 (99.39%) genes could be annotated by BLASTN (*E*-value $< 1e^{-5}$) using NCBI Nr databases based on sequence homology. It should be noted that among these genes assigned to Nr database, the top three species of matched genes number are *R. toruloides* (6,180, 78.69%), followed by *R. glutinis* (1,087, 13.84%) and *Microbotryum violaceum* (226, 2.88%). In addition, 4,602 (58.20%), 4,963 (62.77%), and 7,862 (99.43%) genes could be annotated according to the KOG (**Figure 1**), SwissProt, and TrEMBL databases, respectively. Furthermore, 2,288 genes could be classified into three GO categories: cellular component, biological process, and molecular function (**Figure 2A**). To gain further insights into the gene function of *R. kratochvilovae* strain YM25235, we analyzed 3,143 genes and plotted the KEGG annotation classification statistics (**Figure 2B**). Summary for number of genes annotated in each database is shown in **Supplementary Table 2**. In addition, a repeat sequence of 557,107 bp was obtained, accounting for 2.35% of all sequences (**Table 4**).

Summary of Transcriptome Sequencing Data

After filtering the raw data, a total of 32.34 and 31.12 million clean reads were obtained for the treatment and control groups, respectively. The percentage of reads mapping to the *R. kratochvilovae* strain YM25235 genome was 81.1% in the treatment group and 75.9% in the control group. Uniform alignment rates across samples indicate the comparability of data between the samples (**Table 5**). The number of predicted novel genes was 40, and a total of 8,048 expressed genes were detected, including 8,008 known genes and 40 predicted novel genes. A total of 5,227 novel transcripts were detected, of which 4,840 belonged to the novel alternatively spliced isoforms of known protein-coding genes, 40 transcripts of novel

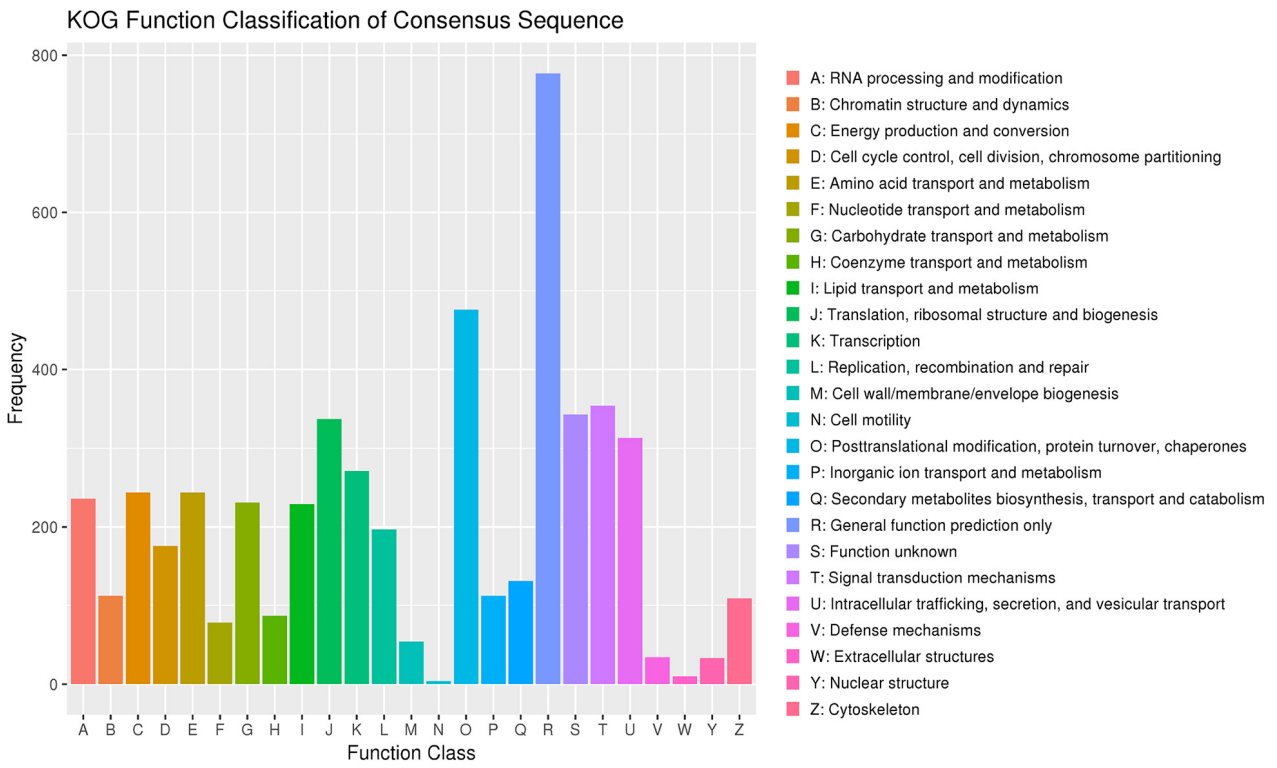

FIGURE 1 | The Eukaryotic Orthologous Groups (KOG) classification of proteins in *Rhodosporidium kratochvilovae* strain YM25235. The distribution of predicted proteins from *R. kratochvilovae* strain YM25235 genome according to the functional class by KOG database.

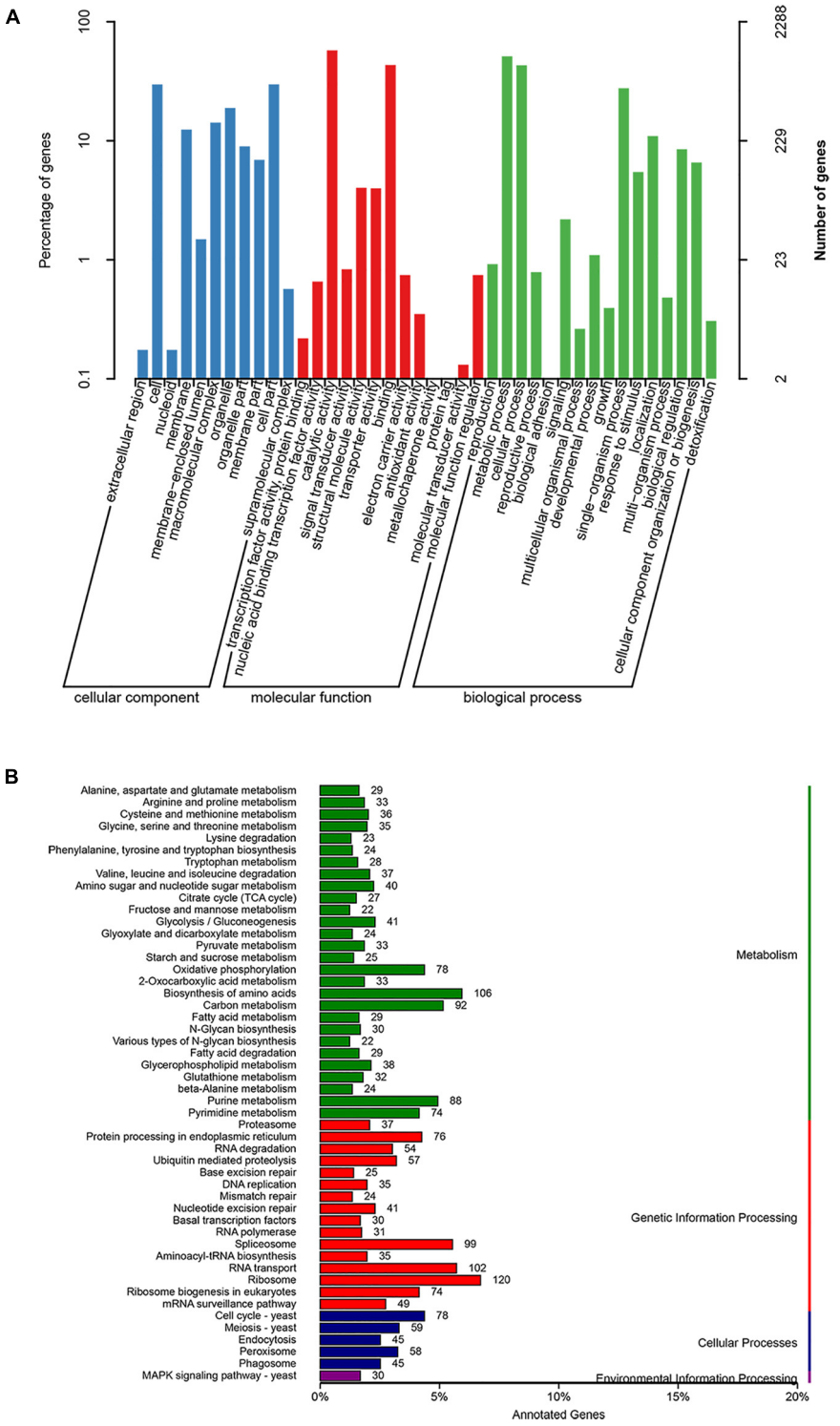

FIGURE 2 | Gene ontology (GO) and Kyoto Encyclopedia of Genes and Genomes (KEGG) classifications of proteins in *R. kratochvilovae* strain YM25235. Distribution of predicted proteins from *R. kratochvilovae* strain YM25235 genome by **(A)** GO and **(B)** KEGG databases.

protein-coding genes, and the remaining 347 to long non-coding RNAs. For the functional annotation, the reference gene set was aligned with sequences from major databases, including Swiss-Prot, Nr, GO, and KEGG. We performed principal component analysis (PCA) among all the samples (**Supplementary Figure 1**).

TABLE 4 | Statistics of repeat sequence classification results.

Type	Number	Length (bp)	Percentage (%)
ClassI	430	453,925	1.91
ClassI/DIRS	2	12,801	0.05
ClassI/LINE	131	66,539	0.28
ClassI/LTR/Copia	144	138,439	0.58
ClassI/LTR/Gypsy	136	229,148	0.97
ClassI/PLE| LARD	9	3,072	0.01
ClassI/TRIM	8	8,355	0.04
ClassII	47	8,908	0.04
ClassII/MITE	39	8,502	0.04
ClassII/TIR	7	395	0.00
ClassII/Unknown	1	11	0.00
PotentialHostGene	6	2,805	0.01
Unknown	315	92,433	0.39
Total	483	557,107	2.35

TABLE 5 | Statistics of reads mapped to the genome of six samples.

Sample	Total CleanReads	Total MappingRatio (%)	Uniquely MappingRatio (%)
15-1	29,677,882	81.15	65.05
15-2	32,297,704	80.80	64.29
15-3	35,027,652	81.49	64.47
30-1	27,093,510	68.71	55.08
30-2	33,998,322	79.80	63.60
30-3	32,269,496	79.19	63.11

Identification of Differential Gene Expression

Overall, 1,300 genes were significantly determined to be DEGs, which comprised 553 upregulated and 747 downregulated DEGs (**Figure 3**). They occupied 16.19% of all genes that were identified in this study. The top 10 DEGs with the most dramatic expression changes were listed in **Table 6**. The top three most upregulated DEGs were histone-binding protein RBBP4, molecular chaperone GrpE, protein of pyridoxal phosphate phosphatase-related family (*PLPP*). The three most downregulated DEGs were NADH oxidase (*Nox*), glycosyltransferase family 31 protein (*GT31*), and esterase/lipase (*LIP*). In addition, a minority of DEGs were annotated to hypothetical proteins, indicating their unknown functions. The qPCR analysis for all 15 DEGs represents a close correlation (Pearson's correlation coefficients = 0.815, $p < 0.01$) in fold changes for DEGs between RNA-seq and qPCR (**Figure 4**), suggesting the accuracy of RNA-seq and DEG analyses.

GO and KEGG Enrichment Analyses of DEGs

All DEGs were divided into three GO categories: biological process (19 terms), molecular function (18 terms), and cellular component (6 terms) (**Figure 5**). Among the BP terms, the three GO terms containing the highest number of DEGs were metabolic process, cellular process, and cellular component organization or biogenesis. Moreover, some BP terms involving response to low temperature were detected, such as biological process, negative regulation of biological process and growth. In the MF category, catalytic activity, binding, and transporter activity were the top three terms, and for the CC category, cell, cell part, and membrane were the top three terms. In addition, the membrane part ranked fourth.

In the pathway enrichment analysis, 107 KEGG pathways were enriched by DEGs (**Supplementary Table 3**). Furthermore, the top 20 KEGG pathways were enriched by DEGs and are presented in **Figure 6**. MAPK signaling pathway-yeast (ko04011) and metabolic pathways (ko01100) contained the most DEGs. The remaining KEGG terms were primarily associated with amino acid metabolism [e.g., alanine, aspartate, and glutamate metabolism (ko00250), valine, leucine, and isoleucine degradation (ko00310), and lysine degradation (ko00310)], carbohydrate metabolism [e.g., amino sugar and nucleotide sugar metabolism (ko00520) and propanoate metabolism (ko00640)], lipid metabolism [i.e., steroid biosynthesis (ko00100)], cell growth and death (i.e., cell cycle-yeast [ko04111] and meiosis yeast (ko04113), and translation [i.e., RNA transport (ko03013) and mRNA surveillance pathway (ko03015)]. In addition, all 1,300 DEGs included in different pathways were listed in **Supplementary File 2** List of DEGs.

DISCUSSION

Compared with several *Rhodosporidium* strains that have been sequenced, *R. kratochvilovae* strain YM25235 was isolated from Chenghai Lake in Yunnan, China. This plateau lake locates at the border of Tibet Plateau and Yunnan plateau, where the water temperature ranges from 2 to 31°C, with an average temperature of about 15°C (Wan et al., 2005). The high-quality genomic and transcriptomic data of *R. kratochvilovae* strain YM25235 were obtained and the molecular mechanism regarding low temperature response of *R. kratochvilovae* strain YM25235 was explored in this study. The comparative transcriptomic analysis of *R. kratochvilovae* strain YM25235 treated by low temperature and control temperature identified several DEGs primarily involved in BP functions (e.g., metabolism, regulation processes, and stress response). It was established that low temperature induced changes in the biological process of *R. kratochvilovae* strain YM25235. In addition, the terms associated with metabolism were overrepresented (77, 71.96% of all terms) among the enriched KEGG pathways and adjustment of metabolism function due to gene expression changes primarily contributed to the low temperature response of *R. kratochvilovae* strain YM25235.

In particular, steroids can serve as important components of cell membranes, which can alter the fluidity of cell membranes (Fernández-Cabezón et al., 2018). Moreover, triterpenoid serves as a precursor for steroid biosynthesis (Davis and Croteau, 2000). In this study, several KEGG pathways involved in sesquiterpenoid and triterpenoid biosynthesis were significantly enriched. This evidence suggested that steroids could act as a crucial factor for changes in the protective ability

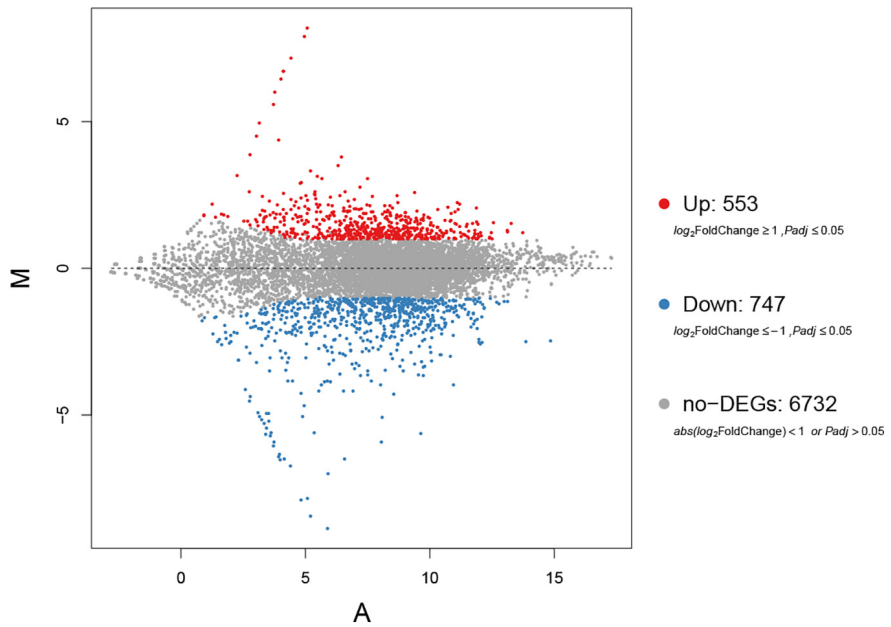

FIGURE 3 | A volcano plot of differentially expressed genes (DEGs). The red spots indicate significant upregulation, whereas blue spots indicate significant downregulation. The black spots signify no significantly changed genes.

TABLE 6 | List of top 10 most upregulated and downregulated DEGs.

GeneID	log_2FoldChange (Treatment/Control)	P_{adj}	Gene description	Gene symbol
The 10 most upregulated genes				
EVM0004254	8.1856	6.22E-51	Histone-binding protein RBBP4	*RBBP4*
EVM0001626	7.9172	6.52E-46	Molecular chaperone GrpE	*GrpE*
EVM0005149	7.1616	1.97E-35	Protein of pyridoxal phosphate phosphatase-related family	*PLPP*
EVM0003618	6.7268	5.77E-30	Transcription factor	*TF*
EVM0000292	6.7266	4.83E-30	GDP-fucose protein O-fucosyltransferase family protein	*POFUT1*
EVM0002391	6.4524	1.45E-26	Nucleus export protein Brr6	*Brr6*
EVM0004860	6.0137	6.14E-22	Hypothetical protein	/
EVM0004609	5.5868	1.35E-17	Arylamine *N*-acetyltransferase 1	*NAT1*
EVM0001661	4.9611	1.99E-13	GATA-binding transcription factor	*GATA*
EVM0003124	4.5093	1.71E-10	Methyltransferase type 11	*MCAG_03950*
The 10 most down-regulated genes				
EVM0008135	−8.8632	2.02E-77	NADH oxidase	*Nox*
EVM0004703	−8.4488	1.77E-55	Glycosyltransferase family 31 protein	*GT31*
EVM0004035	−7.8793	3.70E-46	Esterase/lipase	*LIP*
EVM0004698	−7.8304	4.84E-50	Hypothetical protein	/
EVM0001923	−7.0013	6.58E-27	Transcription regulator HTH	*HTH*
EVM0002712	−6.7289	2.10E-28	Phenol 2-monooxygenase	*pheA*
EVM0007841	−6.5184	1.87E-27	Putative Nucleoside-diphosphate-sugar epimerase	*ytbQ*
EVM0004887	−6.4840	3.33E-101	Pyridoxine biosynthesis protein	*PDX1*
EVM0004965	−6.4789	3.67E-26	Zinc finger, RING-type protein	*Znf_RING*
EVM0006689	−6.4149	2.88E-26	Hypothetical protein	/

of *R. kratochvilovae* strain YM25235 against low temperature by altering the fluidity of cell membranes. Therefore, genes involved in steroid products are useful targets in genetic manipulation to improve the cold resistance of *R. kratochvilovae* strain YM25235. Another analysis revealed that the DEGs of the biosynthesis of steroid pathway were overwhelmingly upregulated (**Supplementary Figure 2**), further supporting that *R. kratochvilovae* strain YM25235 adapts to the low

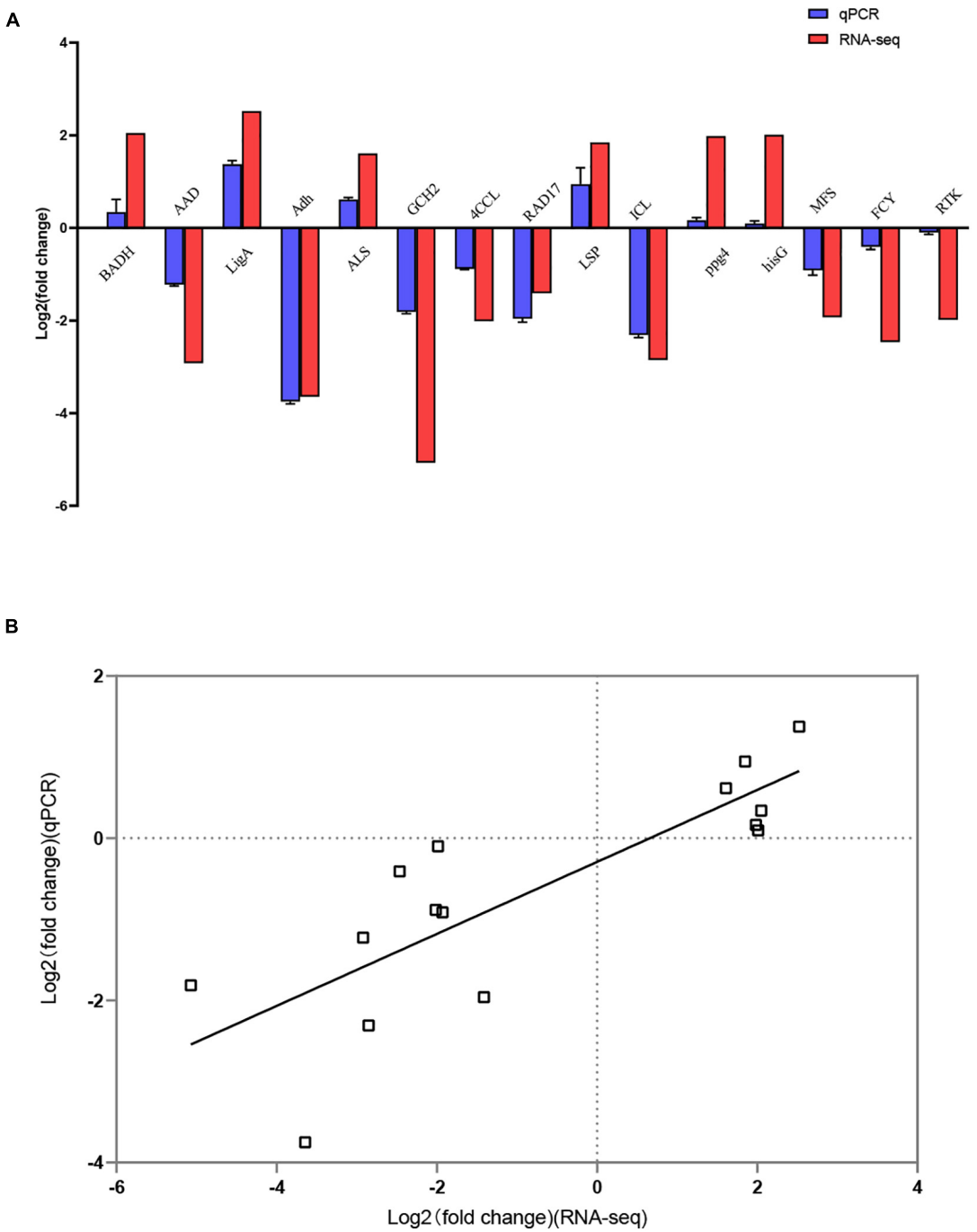

FIGURE 4 | Confirmation of RNA-seq results by quantitative real-time PCR (qPCR). **(A)** Comparison of the fold change in expression of 15 selected DEGs as detected using RNA-seq and qPCR. **(B)** Correlation of the fold change in the expression of 15 DEGs analyzed by RNA-seq and qPCR.

temperature environment by adjusting the biosynthesis of steroids. Ubiquinone and other terpenoid quinone are involved in MVA (Dallner and Sindelar, 2000). The MVA pathway, in turn, is upstream of not only steroid biosynthesis but also carotenoid biosynthesis (Katsuki and Bloch, 1967; Groeneveld, 1999). However, carotenoids could modulate membrane fluidity because carotenoids can stabilize the membrane to respond to low temperature (Chattopadhyay et al., 1997; Jagannadham et al., 2000). Low temperature stress also leads to increased intracellular reactive oxygen species (ROS) (Gasch, 2003), more carotenoids biosynthesis can mitigate cellular damage caused by ROS (Breierová et al., 2018). In this study, ubiquinone and other terpenoid quinone biosynthesis were significantly enriched. Certain amino acids, including alanine, aspartate, glutamate, and

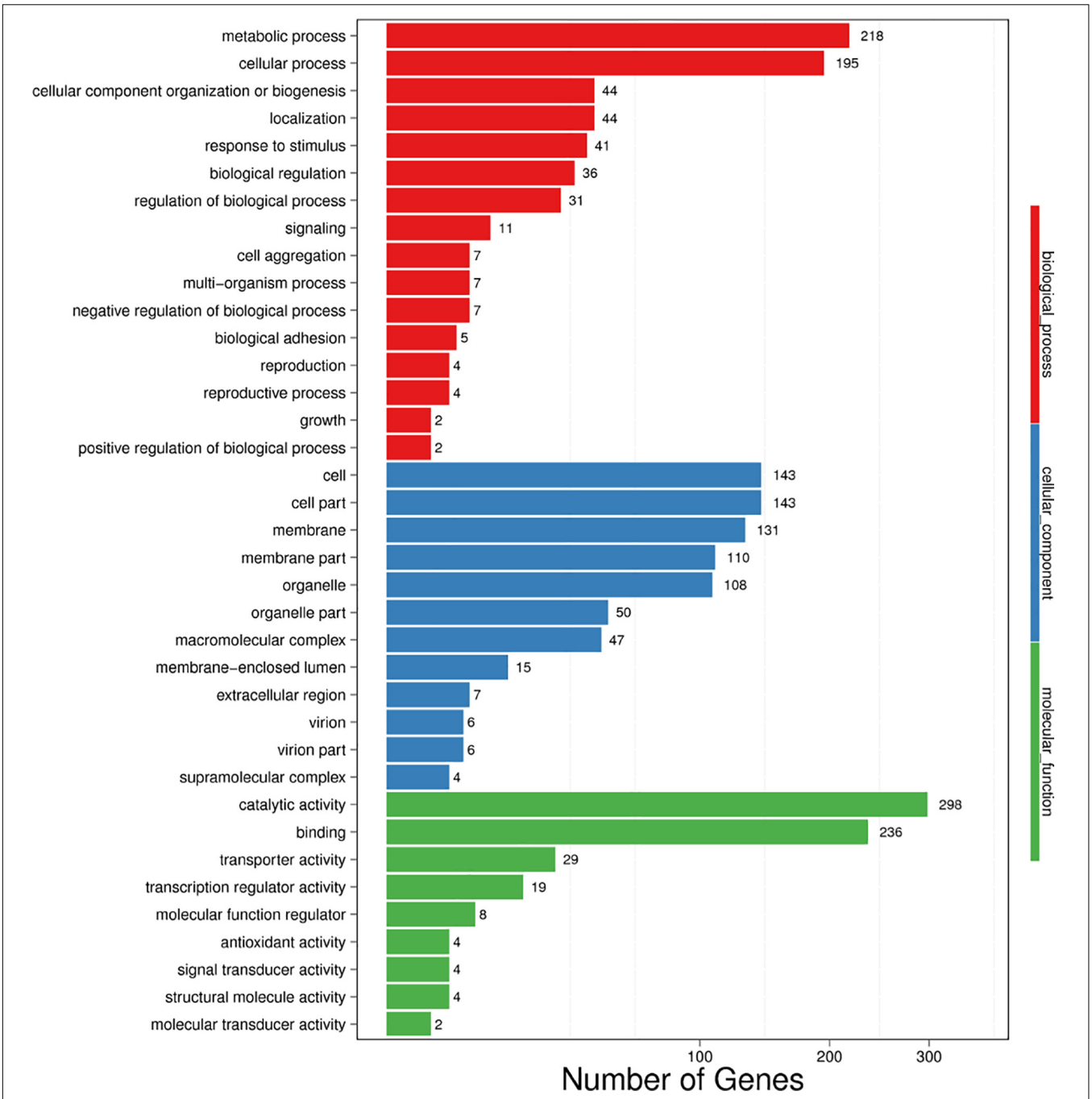

FIGURE 5 | Vertical histogram presentation of DEG-enriched GO terms. BP (red): biological process, CC (blue): cellular component, and MF (green): molecular function.

phenylalanine metabolic pathways were enriched, suggesting an altered utilization of amino acids by *R. kratochvilovae* strain YM25235 at low temperature, similar to the findings reported by Beltran et al. (2007). In addition, glutathione metabolism was significantly enriched, glutathione (GSH) protects the cells by neutralizing (i.e., reducing) ROS (Wu et al., 2004), Thus, GSH might protect *R. kratochvilovae* strain YM25235 from increased ROS at low temperature. In addition, the DNA replication, mismatch repair, and nucleotide excision repair pathways were enriched in the current study. Previous studies have reported genes whose expression is affected by low temperature associated with DNA replication (Driessen et al., 2014). Thus, it can be inferred that the changes occurring in the levels of DNA replication might be involved in the important biological processes in *R. kratochvilovae* strain YM25235 acting at low temperature. Moreover, most of the downregulated DEGs were

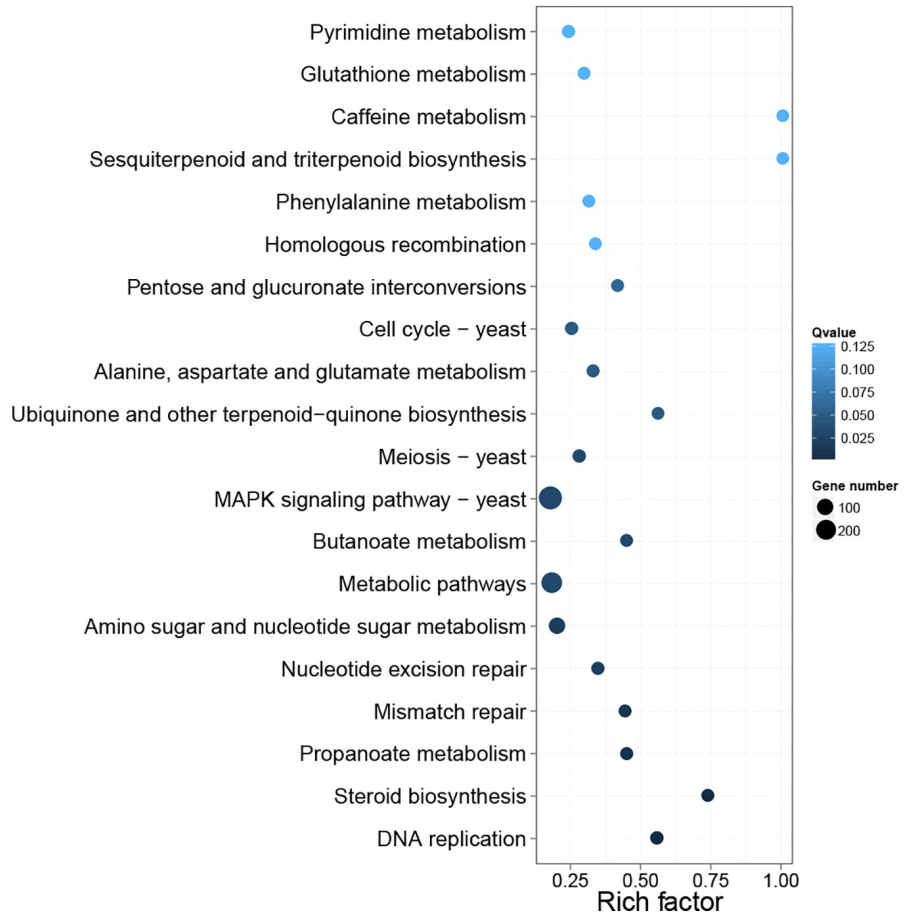

FIGURE 6 | Top 20 differential gene pathway enrichment results. The X-axis represents the enrichment factor value, and the Y-axis represents the pathway name. Color represents the *Q* value, with smaller values representing more significant enrichment results. The size of the dots represents the number of DEGs. Rich factor refers to the enrichment factor value, and a larger value indicates a more pronounced enrichment result.

related to propanoate metabolism, valine, leucine, and isoleucine degradation, pentose, and glucuronate interconversion. We speculate that low temperature limits the progression of these biological responses (**Supplementary Figure 2**).

MAPKs are serine/threonine kinases that, when phosphorylated, enter the nucleus and phosphorylate several transcription factors, enzymes, and other proteins that modulate the cellular activity (Cowan and Storey, 2003). The MAPK gene family is well known for its function in transmitting stress signals from the environment to the cell nucleus (Cowan and Storey, 2003). Significant enrichment of the MAPK pathway in this study indicated the implication of MAPKs in transmitting stress signals from the environment to the cell nucleus in *R. kratochvilovae* strain YM25235 at low temperature. Traditionally, the HOG pathway, a conserved MAPK cascade, has been considered a specific signaling pathway, responding to changes in external solute concentrations (Hohmann, 2002; Westfall et al., 2004). However, the HOG pathway was demonstrated to function as a transducer of cold stimuli (Panadero et al., 2006). *Hog1*, as a key gene of the HOG pathway was implicated in response to low temperature stress in our lab study (unpublished). However, *Hog1* was not identified as a DEG in this study. We speculate that this process is achieved at the protein level or by certain other mechanisms and is not manifested by differences in the transcript levels.

The top 10 identified DEGs might play a key role for *R. kratochvilovae* strain YM25235 when grown at low temperature. The *RBBP4* gene has been reported to regulate signaling through the MAPK pathway (Li et al., 2019). The activity of GrpE, a nucleotide exchange factor for the heat shock protein DnaK, is downregulated in response to increasing temperature (Bracher and Verghese, 2015). In this study, the expression of *GrpE* significantly increased at low temperature, indicating that *GrpE* is a key molecule participating in the response of *R. kratochvilovae* strain YM25235 to low temperature. The nucleus export protein Brr6 is involved in mRNA and protein export from the nucleus and contribute to mitosis (Lo Presti et al., 2007). The translational activity of mRNA-based protein biosynthesis greatly decreased at low temperatures (Jones and Inouye, 1996). Vitamin B6 as oxygen reactive species scavengers and factors was able to increase resistance to biotic and abiotic stress (Ehrenshaft et al., 1999; Bilski et al., 2000).

This vitamin comprises six interconvertible pyridine compounds (vitamers) such as pyridoxal 5'-phosphate (PLP) and five others (ShuoHao et al., 2019). Gene that codes a protein of pyridoxal phosphate phosphatase-related family (PLPP) were significantly upregulated in this study, indicating that *PLPP* plays a key role in responding to low temperature. In this study, the transcript levels of certain genes involved in regulating the transcription were significantly changed at low temperature. *HTH* and *GATA* were detected with significant changes at the transcript level. Most of these proteins were transcription activators and are known to negatively regulate their expression (Baumeister et al., 1992). Thus, the results revealed potential key roles of these genes for *R. kratochvilovae* strain YM25235 to grow at low temperature. Notably, the functions of several top DEGs remain largely unexplored, and they cannot be linked well to the response of *R. kratochvilovae* strain YM25235 to low temperature. However, this study is the first to reveal their acute response of *R. kratochvilovae* strain YM25235 to low temperature.

Membrane rigidity increases when cells are incubated at low temperatures *in vitro* (Hayashi and Maeda, 2006). Microorganisms overcome the membrane stiffness at low temperatures by adapting to the environment to keep the membrane fluidity constant to a degree (Morgan-Kiss et al., 2006). To accomplish this, cold stress triggers a coordinated response that induces fatty acid desaturases and dehydrogenases, which in turn increase the ratio of polyunsaturated to saturated fatty acids and/or actually decrease the length of fatty acid chains in the membrane (Dickens and Thompson, 1981; Avery et al., 1995; Carty et al., 1999). The PUFAs association with low temperature response in *R. kratochvilovae* strain YM25235 has been confirmed in our previous study (Cui et al., 2016). However, no pathway and no DEGs related to PUFA biosynthesis were significantly enriched in this study. This is because the response to low temperature stress is a complex process. We speculate that this process may be achieved at the protein level or by certain other mechanisms and is not manifested by differences in the transcript levels.

CONCLUSION

In this study, the genome-wide transcriptional changes of *R. kratochvilovae* strain YM25235 at low temperature was obtained by whole genome sequencing of *R. kratochvilovae* strain YM25235 and transcriptome sequencing from low temperature (15°C) and normal temperature (30°C) groups. Likewise, this study also showed that there exist genes whose functions are still not known and certain mechanisms of response to low temperature cannot be elucidated. Further experimental verifications are needed. Notably, despite the DEGs obtained in this study are related to low temperature response, further verification for DEGs directly involved in the response is required in the future.

DATA AVAILABILITY STATEMENT

The datasets presented in this study can be found in online repositories. The names of the repository/repositories and accession number(s) can be found below: https://www.ncbi.nlm.nih.gov/, PRJNA739038 (genome sequencing and assembly) and PRJNA739250 (Transcriptome).

AUTHOR CONTRIBUTIONS

RG, QZ, and Q-LZ contributed to the conception and design of the study. RG and XZ did the laboratory work and acquired all raw data. RG and MH did the bioinformatic analyses. YW and XJ provided the research materials. RG wrote the first draft of the manuscript. QZ and Q-LZ wrote sections of the manuscript. All authors contributed to manuscript revision, read, and approved the submitted version.

FUNDING

This work was supported by the National Natural Science Foundation of China (31960466 and 31660454).

SUPPLEMENTARY MATERIAL

The Supplementary Material for this article can be found online at: https://www.frontiersin.org/articles/10.3389/fmicb.2021.727105/full#supplementary-material

REFERENCES

Ageitos, J. M., Vallejo, J. A., Veiga-Crespo, P., and Villa, T. G. (2011). Oily yeasts as oleaginous cell factories. *Appl. Microbiol. Biotechnol.* 90, 1219–1227. doi: 10.1007/s00253-011-3200-z

Aguilera, J., Randez-Gil, F., and Prieto, J. A. (2007). Cold response in *Saccharomyces cerevisiae*: new functions for old mechanisms. *FEMS Microbiol. Rev.* 31, 327–341. doi: 10.1111/j.1574-6976.2007.00066.x

Alioto, T., Blanco, E., Parra, G., and Guigó, R. (2018). Using geneid to Identify Genes. *Curr. Protoc. Bioinform.* 64:e56. doi: 10.1002/cpbi.56

Ashburner, M., Ball, C. A., Blake, J. A., Botstein, D., Butler, H., Cherry, J. M., et al. (2000). Gene ontology: tool for the unification of biology. *Nat. Genet.* 25, 25–29. doi: 10.1038/75556

Avery, S. V., Lloyd, D., and Harwood, J. L. (1995). Temperature-dependent changes in plasma-membrane lipid order and the phagocytotic activity of the amoeba *Acanthamoeba castellanii* are closely correlated. *Biochem. J.* 312, 811–816. doi: 10.1042/bj3120811

Baumeister, R., Müller, G., Hecht, B., and Hillen, W. (1992). Functional roles of amino acid residues involved in forming the alpha-helix-turn-alpha-helix operator DNA binding motif of Tet repressor from Tn10. *Proteins* 14, 168–177. doi: 10.1002/prot.340140204

Beltran, G., Rozès, N., Mas, A., and Guillamón, J. M. (2007). Effect of low-temperature fermentation on yeast nitrogen metabolism. *World J. Microbiol. Biotechnol.* 23, 809–815. doi: 10.1007/s11274-006-9302-6

Bilski, P., Li, M., Ehrenshaft, M., Daub, M., and Chignell, C. (2000). Vitamin B6 (pyridoxine) and its derivatives are efficient singlet oxygen quenchers and potential fungal antioxidants. *Photochem. Photobiol.* 71, 129–134. doi: 10.1562/0031-865520000710129SIPVBP2.0.CO2

Boeckmann, B., Bairoch, A., Apweiler, R., Blatter, M.-C., Estreicher, A., Gasteiger, E., et al. (2003). The SWISS-PROT protein knowledgebase and its supplement

TrEMBL in 2003. *Nucleic Acids Res.* 31, 365–370. doi: 10.1093/nar/gkg095

Bracher, A., and Verghese, J. (2015). The nucleotide exchange factors of Hsp70 molecular chaperones. *Front. Mol. Biosci.* 2:10. doi: 10.3389/fmolb.2015.00010

Breierová, E., Čertík, M., Márová, I., and Vadkertiová, R. (2018). The effect of Zn(II) ions and reactive oxygen on the uptake of zinc and production of carotenoids by selected red yeasts. *Chem. Biodiv.* 15:e1800069. doi: 10.1002/cbdv.201800069

Burge, C., and Karlin, S. (1997). Prediction of complete gene structures in human genomic DNA. *J. Mol. Biol.* 268, 78–94. doi: 10.1006/jmbi.1997.0951

Buzzini, P., Innocenti, M., Turchetti, B., Libkind, D., van Broock, M., and Mulinacci, N. (2007). Carotenoid profiles of yeasts belonging to the genera *Rhodotorula, Rhodosporidium, Sporobolomyces*, and *Sporidiobolus*. *Can. J. Microbiol.* 53, 1024–1031. doi: 10.1139/W07-068

Calvo, A. M., Gardner, H. W., and Keller, N. P. (2001). Genetic connection between fatty acid metabolism and sporulation in *Aspergillus nidulans*. *J. Biol. Chem.* 276, 25766–25774. doi: 10.1074/jbc.M100732200

Campbell, M. A., Haas, B. J., Hamilton, J. P., Mount, S. M., and Buell, C. R. (2006). Comprehensive analysis of alternative splicing in rice and comparative analyses with Arabidopsis. *BMC Genom.* 7:327. doi: 10.1186/1471-2164-7-327

Carrasco, M., Alcaíno, J., Cifuentes, V., and Baeza, M. (2017). Purification and characterization of a novel cold adapted fungal glucoamylase. *Microbial. Cell Factories* 16:75. doi: 10.1186/s12934-017-0693-x

Carty, S. M., Sreekumar, K. R., and Raetz, C. R. H. (1999). Effect of cold shock on lipid a biosynthesis in *Escherichia coli*. *J. Biol. Chem.* 274, 9677–9685. doi: 10.1074/jbc.274.14.9677

Castrillo, M., Luque, E. M., Pardo-Medina, J., Limón, M. C., Corrochano, L. M., and Avalos, J. (2018). Transcriptional basis of enhanced photoinduction of carotenoid biosynthesis at low temperature in the fungus *Neurospora crassa*. *Res. Microbiol.* 169, 78–89. doi: 10.1016/j.resmic.2017.11.003

Chattopadhyay, M., Jagannadham, M., Vairamani, M., and Shivaji, S. (1997). Carotenoid pigments of an Antarctic psychrotrophic bacterium *Micrococcus roseus*: temperature dependent biosynthesis, structure, and interaction with synthetic membranes. *Biochem. Biophys. Res. Commun.* 239, 85–90. doi: 10.1006/bbrc.1997.7433

Chen, N. (2004). Using repeat masker to identify repetitive elements in genomic sequences. *Curr. Protoc. Bioinform.* Chapter 4:Unit4.10. doi: 10.1002/0471250953.bi0410s05

Clarke, S. D. (2001). Polyunsaturated fatty acid regulation of gene transcription: a molecular mechanism to improve the metabolic syndrome. *J. Nut.* 131, 1129–1132. doi: 10.1093/jn/131.4.1129

Cock, P. J., Fields, C. J., Goto, N., Heuer, M. L., and Rice, P. M. (2010). The sanger FASTQ file format for sequences with quality scores, and the Solexa/Illumina FASTQ variants. *Nucleic Acids Res.* 38, 1767–1771. doi: 10.1093/nar/gkp1137

Conesa, A., Gotz, S., Garcia-Gomez, J. M., Terol, J., Talon, M., and Robles, M. (2005). Blast2GO: a universal tool for annotation, visualization and analysis in functional genomics research. *Bioinformatics* 21, 3674–3676. doi: 10.1093/bioinformatics/bti610

Cowan, K. J., and Storey, K. B. (2003). Mitogen-activated protein kinases: new signaling pathways functioning in cellular responses to environmental stress. *J. Exp. Biol.* 206, 1107–1115. doi: 10.1242/jeb.00220

Cui, J., He, S., Ji, X., Lin, L., Wei, Y., and Zhang, Q. (2016). Identification and characterization of a novel bifunctional Δ12/Δ15-fatty acid desaturase gene from Rhodosporidium kratochvilovae. *Biotechnol. Lett.* 38, 1155–1164. doi: 10.1007/s10529-016-2090-7

Dallner, G., and Sindelar, P. J. (2000). Regulation of ubiquinone metabolism. *Free Radical Biol. Med.* 29, 285–294. doi: 10.1016/s0891-5849(00)00307-5

Davis, E. M., and Croteau, R. (2000). "Cyclization Enzymes in the Biosynthesis of Monoterpenes, Sesquiterpenes, and Diterpenes," in *Biosynthesis: Aromatic Polyketides, Isoprenoids, Alkaloids*, eds F. J. Leeper and J. C. Vederas (Berlin: Springer Berlin Heidelberg), 53–95. doi: 10.1007/3-540-48146-X_2

Deng, Y. Y., Li, J. Q., Wu, S. F., Zhu, Y., Chen, Y. W., and He, F. C. (2006). Integrated nr database in protein annotation system and its localization. *Computer Eng.* 32, 71–72.

Dickens, B. F., and Thompson, G. A. (1981). Rapid membrane response during low-temperature acclimation Correlation of early changes in the physical properties and lipid composition of *Tetrahymena microsomal* membranes. *Biochim. et Biophys. Acta (BBA) Biomembranes* 644, 211–218. doi: 10.1016/0005-2736(81)90377-1

Dinh, H. V., Suthers, P. F., Chan, S. H. J., Shen, Y., Xiao, T., Deewan, A., et al. (2019). A comprehensive genome-scale model for *Rhodosporidium toruloides* IFO0880 accounting for functional genomics and phenotypic data. *Metabolic Eng. Commun.* 9:e00101. doi: 10.1016/j.mec.2019.e00101

Driessen, R. P. C., Sitters, G., Laurens, N., Moolenaar, G. F., Wuite, G. J. L., Goosen, N., et al. (2014). Effect of temperature on the intrinsic flexibility of DNA and its interaction with architectural proteins. *Biochemistry* 53, 6430–6438. doi: 10.1021/bi500344j

Eddy, S. R. (1998). Profile hidden markov models. *Bioinformatics* 14, 755–763. doi: 10.1093/bioinformatics/14.9.755

Edgar, R. C., and Myers, E. W. (2005). PILER: identification and classification of genomic repeats. *Bioinformatics* 21(Suppl. 1), i152–i158. doi: 10.1093/bioinformatics/bti1003

Ehrenshaft, M., Bilski, P., Li, M. Y., Chignell, C. F., and Daub, M. E. (1999). A highly conserved sequence is a novel gene involved in de novo vitamin B6 biosynthesis. *Proc. Natl. Acad. Sci. U.S.A.* 96, 9374–9378. doi: 10.1073/pnas.96.16.9374

Fernández-Cabezón, L., Galán, B., and García, J. L. (2018). New insights on steroid biotechnology. *Front. Microbiol.* 9:958. doi: 10.3389/fmicb.2018.00958

Finn, R. D., Coggill, P., Eberhardt, R. Y., Eddy, S. R., Mistry, J., Mitchell, A. L., et al. (2016). The Pfam protein families database: towards a more sustainable future. *Nucleic Acids Res.* 44, D279–D285. doi: 10.1093/nar/gkv1344

Firdaus-Raih, M., Hashim, N. H. F., Bharudin, I., Abu Bakar, M. F., Huang, K. K., Alias, H., et al. (2018). The *Glaciozyma antarctica* genome reveals an array of systems that provide sustained responses towards temperature variations in a persistently cold habitat. *PLoS One* 13:e0189947. doi: 10.1371/journal.pone.0189947

García-Ríos, E., Morard, M., Parts, L., Liti, G., and Guillamón, J. M. (2017). The genetic architecture of low-temperature adaptation in the wine yeast *Saccharomyces cerevisiae*. *BMC Genom.* 18:159. doi: 10.1186/s12864-017-3572-2

Gasch, A. P. (2003). "The environmental stress response: a common yeast response to diverse environmental stresses," in *Yeast Stress Responses*, eds S. Hohmann and W. H. Mager (Berlin: Springer Berlin Heidelberg), 11–70. doi: 10.1007/3-540-45611-2_2

Groeneveld, H. W. (1999). Tracing steroid synthesis in plants. *Crit. Rev. Biochem. Mol. Biol.* 34, 59–69. doi: 10.1080/10409239991209192

Haas, B. J., Salzberg, S. L., Zhu, W., Pertea, M., Allen, J. E., Orvis, J., et al. (2008). Automated eukaryotic gene structure annotation using evidencemodeler and the program to assemble spliced alignments. *Genome Biol.* 9:R7. doi: 10.1186/gb-2008-9-1-r7

Han, Y., and Wessler, S. R. (2010). MITE-hunter: a program for discovering miniature inverted-repeat transposable elements from genomic sequences. *Nucleic Acids Res.* 38:e199. doi: 10.1093/nar/gkq862

Hayashi, M., and Maeda, T. (2006). Activation of the HOG pathway upon cold stress in *Saccharomyces cerevisiae*. *J. Biochem.* 139, 797–803. doi: 10.1093/jb/mvj089

He, J., Cui, Z., Ji, X., Luo, Y., Wei, Y., and Zhang, Q. (2019). Novel histidine kinase gene HisK2301from *Rhodosporidium kratochvilovae* contributes to cold adaption by promoting biosynthesis of polyunsaturated fatty acids and glycerol. *J. Agric. Food Chem.* 67, 653–660. doi: 10.1021/acs.jafc.8b04859

Hohmann, S. (2002). Osmotic stress signaling and osmoadaptation in yeasts. *Microbiol. Mol. Biol. Rev. MMBR* 66, 300–372. doi: 10.1128/MMBR.66.2.300-372.2002

Hu, J., and Ji, L. (2016). Draft genome sequences of *Rhodosporidium toruloides* strains ATCC 10788 and ATCC 10657 with compatible mating types. *Genome Announ.* 4:e00098-16. doi: 10.1128/genomeA.00098-16

Jagannadham, M. V., Chattopadhyay, M. K., Subbalakshmi, C., Vairamani, M., Narayanan, K., Mohan Rao, C., et al. (2000). Carotenoids of an Antarctic psychrotolerant bacterium, Sphingobacterium antarcticus, and a mesophilic bacterium, *Sphingobacterium multivorum*. *Arch. Microbiol.* 173, 418–424. doi: 10.1007/s002030000163

Jagtap, S. S., Bedekar, A. A., Liu, J.-J., Jin, Y.-S., and Rao, C. V. (2019). Production of galactitol from galactose by the oleaginous yeast *Rhodosporidium toruloides* IFO0880. *Biotechnol. Biofuels* 12:250. doi: 10.1186/s13068-019-1586-5

Jagtap, S. S., and Rao, C. V. (2018). Production of d-arabitol from d-xylose by the oleaginous yeast *Rhodosporidium toruloides* IFO0880. *Appl. Microbiol. Biotechnol.* 102, 143–151. doi: 10.1007/s00253-017-8581-1

Jantzen, S. G., Sutherland, B. J., Minkley, D. R., and Koop, B. F. (2011). GO trimming: systematically reducing redundancy in large gene ontology datasets. *BMC Res. Notes* 4:267. doi: 10.1186/1756-0500-4-267

Jiang, W., Lv, Y., Cheng, L., Yang, K., Bian, C., Wang, X., et al. (2019). Whole-genome sequencing of the giant devil catfish, *Bagarius yarrelli*. *Genome Biol. Evol.* 11, 2071–2077. doi: 10.1093/gbe/evz143

Jones, P. G., and Inouye, M. (1996). RbfA, a 30S ribosomal binding factor, is a cold-shock protein whose absence triggers the cold-shock response. *Mol. Microbiol.* 21, 1207–1218. doi: 10.1111/j.1365-2958.1996.tb02582.x

Jurka, J., Kapitonov, V. V., Pavlicek, A., Klonowski, P., Kohany, O., and Walichiewicz, J. (2005). Repbase update, a database of eukaryotic repetitive elements. *Cytogenet Genome Res.* 110, 462–467. doi: 10.1159/000084979

Kanehisa, M., Goto, S., Kawashima, S., Okuno, Y., and Hattori, M. (2004). The KEGG resource for deciphering the genome. *Nucleic Acids Res.* 32, D277–D280. doi: 10.1093/nar/gkh063

Katsuki, H., and Bloch, K. (1967). Studies on the biosynthesis of ergosterol in yeast: formation of methylated intermediates. *J. Biol. Chem.* 242, 222–227. doi: 10.1016/S0021-9258(19)81452-7

Keilwagen, J., Wenk, M., Erickson, J. L., Schattat, M. H., Grau, J., and Hartung, F. (2016). Using intron position conservation for homology-based gene prediction. *Nucleic Acids Res.* 44:e89. doi: 10.1093/nar/gkw092

Kim, D., Langmead, B., and Salzberg, S. L. (2015). HISAT: a fast spliced aligner with low memory requirements. *Nat. Methods* 12, 357–360. doi: 10.1038/nmeth.3317

Koren, S., Walenz, B. P., Berlin, K., Miller, J. R., Bergman, N. H., and Phillippy, A. M. (2017). Canu: scalable and accurate long-read assembly via adaptive k-mer weighting and repeat separation. *Genome Res.* 27, 722–736. doi: 10.1101/gr.215087.116

Korf, I. (2004). Gene finding in novel genomes. *BMC Bioinform.* 5:59. doi: 10.1186/1471-2105-5-59

Langmead, B., and Salzberg, S. L. (2012). Fast gapped-read alignment with bowtie 2. *Nat. Methods* 9, 357–359. doi: 10.1038/nmeth.1923

Li, B., and Dewey, C. N. (2011). RSEM: accurate transcript quantification from RNA-Seq data with or without a reference genome. *BMC Bioinform.* 12:323. doi: 10.1186/1471-2105-12-323

Li, Y. D., Lv, Z., Xie, H. Y., and Zheng, S. S. (2019). Retinoblastoma binding protein 4 up-regulation is correlated with hepatic metastasis and poor prognosis in colon cancer patients. *Hepatobil. Pancreat. Dis. Int.* 18, 446–451. doi: 10.1016/j.hbpd.2019.08.006

Livak, K. J., and Schmittgen, T. D. (2001). Analysis of relative gene expression data using real-time quantitative PCR and the $2-\Delta\Delta CT$ method. *Methods* 25, 402–408. doi: 10.1006/meth.2001.1262

Lo Presti, L., Cockell, M., Cerutti, L., Simanis, V., and Hauser, P. M. (2007). Functional characterization of Pneumocystis carinii brl1 by transspecies complementation analysis. *Eukaryot Cell* 6, 2448–2452. doi: 10.1128/EC.00321-07

Long, Y., Yan, J., Song, G., Li, X., Li, X., Li, Q., et al. (2015). Transcriptional events co-regulated by hypoxia and cold stresses in *Zebrafish larvae*. *BMC Genomics* 16:385. doi: 10.1186/s12864-015-1560-y

Love, M. I., Huber, W., and Anders, S. (2014). Moderated estimation of fold change and dispersion for RNA-seq data with DESeq2. *Genome Biol.* 15:550. doi: 10.1186/s13059-014-0550-8

MacDonald, M. C., Arivalagan, P., Barre, D. E., MacInnis, J. A., and D'Cunha, G. B. (2016). *Rhodotorula glutinis* Phenylalanine/tyrosine ammonia lyase enzyme catalyzed synthesis of the methyl ester of para-hydroxycinnamic acid and its potential antibacterial activity. *Front. Microbiol.* 7:281. doi: 10.3389/fmicb.2016.00281

Majoros, W. H., Pertea, M., and Salzberg, S. L. (2004). Tigr scan and glimmer HMM: two open source ab initio eukaryotic gene-finders. *Bioinformatics* 20, 2878–2879. doi: 10.1093/bioinformatics/bth315

Margesin, R., and Miteva, V. (2011). Diversity and ecology of psychrophilic microorganisms. *Res. Microbiol.* 162, 346–361. doi: 10.1016/j.resmic.2010.12.004

Miccoli, C., Palmieri, D., De Curtis, F., Lima, G., Ianiri, G., and Castoria, R. (2018). Complete genome sequence of the biocontrol agent yeast *Rhodotorula kratochvilovae* strain LS11. *Genome Announ.* 6:e00120-18. doi: 10.1128/genomeA.00120-18

Morgan-Kiss, R. M., Priscu, J. C., Pocock, T., Gudynaite-Savitch, L., and Huner, N. P. A. (2006). Adaptation and acclimation of photosynthetic microorganisms to permanently cold environments. *Microbiol. Mol. Biol. Rev. MMBR* 70, 222–252. doi: 10.1128/MMBR.70.1.222-252.2006

Murata, Y., Homma, T., Kitagawa, E., Momose, Y., Sato, M. S., Odani, M., et al. (2006). Genome-wide expression analysis of yeast response during exposure to 4 C. *Extremophiles* 10, 117–128. doi: 10.1007/s00792-005-0480-1

Panadero, J., Pallotti, C., Rodríguez-Vargas, S., Randez-Gil, F., and Prieto, J. A. (2006). A downshift in temperature activates the high osmolarity glycerol (HOG) pathway, which determines freeze tolerance in *Saccharomyces cerevisiae**. *J. Biol. Chem.* 281, 4638–4645. doi: 10.1074/jbc.M512736200

Pham, K. D., Shida, Y., Miyata, A., Takamizawa, T., Suzuki, Y., Ara, S., et al. (2020). Effect of light on carotenoid and lipid production in the oleaginous yeast Rhodosporidium toruloides. *Biosci. Biotechnol. Biochem.* 84, 1501–1512. doi: 10.1080/09168451.2020.1740581

Price, A. L., Jones, N. C., and Pevzner, P. A. (2005). De novo identification of repeat families in large genomes. *Bioinformatics* 21(Suppl. 1), i351–i358. doi: 10.1093/bioinformatics/bti1018

Ruan, J., and Li, H. (2019). Fast and accurate long-read assembly with wtdbg2. *Nat. Methods* 17, 155–158. doi: 10.1101/530972

Sampath, H., and Ntambi, J. M. (2004). Polyunsaturated fatty acid regulation of gene expression. *Nutrit. Rev.* 62, 333–339. doi: 10.1111/j.1753-4887.2004.tb00058.x

ShuoHao, H., Jing, L., Jie, Z., JianYun, Z., and LongQuan, H. (2019). Identification and characterization of a pyridoxal 5'-phosphate phosphatase in tobacco plants. *Plant Sci.* 278, 88–95. doi: 10.1016/j.plantsci.2018.10.014

Simão, F., Waterhouse, R. M., Panagiotis, I., Kriventseva, E. V., and Zdobnov, E. M. (2015). BUSCO: assessing genome assembly and annotation completeness with single-copy orthologs. *Bioinformatics* 31, 3210–3212. doi: 10.1093/bioinformatics/btv351

Stanke, M., and Waack, S. (2003). Gene prediction with a hidden Markov model and a new intron submodel. *Bioinformatics* 19(Suppl. 2), ii215–ii225. doi: 10.1093/bioinformatics/btg1080

Tatusov, R. L., Galperin, M. Y., Natale, D. A., and Koonin, E. V. (2000). The COG database: a tool for genome-scale analysis of protein functions and evolution. *Nucleic Acids Res.* 28, 33–36. doi: 10.1093/nar/28.1.33

Tran, T. N., Ngo, D.-H., Nguyen, N. T., and Ngo, D.-N. (2019). Draft genome sequence data of Rhodosporidium toruloides VN1, a strain capable of producing natural astaxanthin. *Data Brief* 26:104443. doi: 10.1016/j.dib.2019.104443

Uprety, B. K., Dalli, S. S., and Rakshit, S. K. (2017). Bioconversion of crude glycerol to microbial lipid using a robust oleaginous yeast *Rhodosporidium toruloides* ATCC 10788 capable of growing in the presence of impurities. *Energy Conv. Manag.* 135, 117–128. doi: 10.1016/j.enconman.2016.12.071

Wan, G. J., Chen, J. A., Wu, F. C., Xu, S. Q., Bai, Z. G., Wan, E. Y., et al. (2005). Coupling between 210Pbex and organic matter in sediments of a nutrient-enriched lake: an example from Lake Chenghai, China. *Chem. Geol.* 224, 223–236. doi: 10.1016/j.chemgeo.2005.07.025

Wang, C., Chen, Y., Zhou, H., Li, X., and Tan, Z. (2020). Adaptation mechanisms of *Rhodococcus* sp. CNS16 under different temperature gradients: Physiological and transcriptome. *Chemosphere* 238:124571. doi: 10.1016/j.chemosphere.2019.124571

Wang, J., Chen, W., Nian, H., Ji, X., Lin, L., Wei, Y., et al. (2017). Inhibition of polyunsaturated fatty acids synthesis decreases growth rate and membrane fluidity of *Rhodosporidium kratochvilovae* at low temperature. *Lipids* 52, 729–735. doi: 10.1007/s11745-017-4273-y

Wang, Q., Tan, X., Jiao, S., You, F., and Zhang, P. J. (2014). Analyzing cold tolerance mechanism in transgenic zebrafish (Danio rerio). *PLoS One* 9:e102492. doi: 10.1371/journal.pone.0102492

Wang, Y., Zhang, S., Zhu, Z., Shen, H., Lin, X., Jin, X., et al. (2018). Systems analysis of phosphate-limitation-induced lipid accumulation by the oleaginous yeast *Rhodosporidium toruloides*. *Biotechnol. Biofuels* 11:148. doi: 10.1186/s13068-018-1134-8

Westfall, P. J., Ballon, D. R., and Thorner, J. (2004). When the stress of your environment makes you go hog wild. *Science* 306:1511. doi: 10.1126/science.1104879

Wick, R. R., Judd, L. M., and Holt, K. E. (2019). Performance of neural network basecalling tools for Oxford Nanopore sequencing. *Genome Biol.* 20:129. doi: 10.1186/s13059-019-1727-y

Wicker, T., Sabot, F., Hua-Van, A., Bennetzen, J. L., Capy, P., Chalhoub, B., et al. (2007). A unified classification system for eukaryotic transposable elements. *Nat. Rev. Genet.* 8, 973–982. doi: 10.1038/nrg2165

Wu, G., Fang, Y.-Z., Yang, S., Lupton, J. R., and Turner, N. D. (2004). Glutathione metabolism and its implications for health. *J. Nut.* 134, 489–492. doi: 10.1093/jn/134.3.489

Xie, C., Mao, X., Huang, J., Ding, Y., Wu, J., Dong, S., et al. (2011). KOBAS 2.0: a web server for annotation and identification of enriched pathways and diseases. *Nucleic Acids Res.* 39(Suppl. 2), W316–W322. doi: 10.1093/nar/gkr483

Xu, Z., and Wang, H. (2007). LTR_FINDER: an efficient tool for the prediction of full-length LTR retrotransposons. *Nucleic Acids Res.* 35, W265–W268. doi: 10.1093/nar/gkm286

Zhang, S., Skerker, J. M., Rutter, C. D., Maurer, M. J., Arkin, A. P., and Rao, C. V. (2016). Engineering *Rhodosporidium toruloides* for increased lipid production. *Biotechnol. Bioeng.* 113, 1056–1066. doi: 10.1002/bit.25864

Conflict of Interest: The authors declare that the research was conducted in the absence of any commercial or financial relationships that could be construed as a potential conflict of interest.

Publisher's Note: All claims expressed in this article are solely those of the authors and do not necessarily represent those of their affiliated organizations, or those of the publisher, the editors and the reviewers. Any product that may be evaluated in this article, or claim that may be made by its manufacturer, is not guaranteed or endorsed by the publisher.

frontiers in Microbiology

ORIGINAL RESEARCH
published: 22 October 2021
doi: 10.3389/fmicb.2021.761997

Biofilm Formation Is Crucial for Efficient Copper Bioleaching From Bornite Under Mesophilic Conditions: Unveiling the Lifestyle and Catalytic Role of Sulfur-Oxidizing Bacteria

*Roberto A. Bobadilla-Fazzini and Ignacio Poblete-Castro**

Biosystems Engineering Laboratory, Department of Chemical Engineering, Universidad de Santiago de Chile (USACH), Santiago, Chile

OPEN ACCESS

Edited by:
Davide Zannoni, University of Bologna, Italy

Reviewed by:
Raymond J. Turner, University of Calgary, Canada
Olli Heikki Tuovinen, The Ohio State University, United States

***Correspondence:**
Ignacio Poblete-Castro
ignacio.poblete.c@usach.cl

Specialty section:
This article was submitted to Extreme Microbiology, a section of the journal Frontiers in Microbiology

Received: *20 August 2021*
Accepted: *27 September 2021*
Published: *22 October 2021*

Citation:
Bobadilla-Fazzini RA and Poblete-Castro I (2021) Biofilm Formation Is Crucial for Efficient Copper Bioleaching From Bornite Under Mesophilic Conditions: Unveiling the Lifestyle and Catalytic Role of Sulfur-Oxidizing Bacteria. Front. Microbiol. 12:761997. doi: 10.3389/fmicb.2021.761997

Biofilm formation within the process of bioleaching of copper sulfides is a relevant aspect of iron- and sulfur-oxidizing acidophilic microorganisms as it represents their lifestyle in the actual heap/dump mining industry. Here, we used biofilm flow cell chambers to establish laminar regimes and compare them with turbulent conditions to evaluate biofilm formation and mineralogic dynamics through QEMSCAN and SEM-EDS during bioleaching of primary copper sulfide minerals at 30°C. We found that laminar regimes triggered the buildup of biofilm using *Leptospirillum* spp. and *Acidithiobacillus thiooxidans* (inoculation ratio 3:1) at a cell concentration of 10^6 cells/g mineral on bornite (Cu_5FeS_4) but not for chalcopyrite ($CuFeS_2$). Conversely, biofilm did not occur on any of the tested minerals under turbulent conditions. Inoculating the bacterial community with ferric iron (Fe^{3+}) under shaking conditions resulted in rapid copper recovery from bornite, leaching 40% of the Cu content after 10 days of cultivation. The addition of ferrous iron (Fe^{2+}) instead promoted Cu recovery of 30% at day 48, clearly delaying the leaching process. More efficiently, the biofilm-forming laminar regime almost doubled the leached copper amount (54%) after 32 days. In-depth inspection of the microbiologic dynamics showed that bacteria developing biofilm on the surface of bornite corresponded mainly to *At. Thiooxidans*, while *Leptospirillum* spp. were detected in planktonic form, highlighting the role of biofilm buildup as a means for the bioleaching of primary sulfides. We finally propose a mechanism for bornite bioleaching during biofilm formation where sulfur regeneration to sulfuric acid by the sulfur-oxidizing microorganisms is crucial to prevent iron precipitation for efficient copper recovery.

Keywords: ***Leptospirillum* spp.**, ***Acidithiobacillus thiooxidans*, biofilm, chalcopyrite, bornite**

INTRODUCTION

One of the most important challenges that face the copper industry is the development of sustainable technologies to leach complex ores composed of mixed copper mineral species in low grades, with a prevalence of primary copper sulfides. The major component of these materials is usually chalcopyrite ($CuFeS_2$), followed by bornite (Cu_5FeS_4) (Panda et al., 2015). To this end, bioleaching has emerged as an efficient technology to leach secondary sulfides under mesophilic conditions (ambient temperature) (Bustos et al., 1993) and primary sulfides mostly under thermophilic conditions above 60°C (Duarte et al., 1993) or at moderate thermophilic (45–50°C) in stirred tank bioreactors (Cancho et al., 2007; Hedrich et al., 2018). Recently, acidophilic bacterial consortia recovered 43% of copper from chalcopyrite using shake flasks at room temperature (25–30°C) (Ma et al., 2018). In another study utilizing a bioleaching column coupled with a fuel cell, the system yielded 244 mg L^{-1} of copper from 150 g of chalcopyrite at 30°C in 320 days (Huang et al., 2019).

In the case of bornite, studies have shown bioleaching activity under mesophilic conditions compared with abiotic controls (Jun et al., 2008; Bevilaqua et al., 2010). Besides, researchers have proposed a galvanic effect with chalcopyrite accelerating the oxidative dissolution of bornite in the presence of microorganisms (Wang et al., 2016). Inoculation of the moderate thermophilic *Leptospirillum ferriphilum and Acidithiobacillus caldus* in shaking flasks at 45°C enabled the conversion of bornite into several intermediates including covellite (CuS) and isocubanite ($CuFe_2S_3$) through the bioleaching process, with a final copper extraction of 70% (Hong et al., 2019).

Finally, several works have established the high bioleaching efficiency of thermophiles over chalcopyrite (Petersen and Dixon, 2002), but none of them uncovered the role of biofilm formation in this process. Recently, a study reported biofilm development over chalcopyrite under moderate thermophilic conditions, where *L. ferriphilum* was inoculated at a high concentration (above 10^8 cells/g mineral) in the presence of under-stoichiometric iron concentrations (Bellenberg et al., 2018). A few studies have specifically addressed mesophilic biofilm formation on chalcopyrite, with researchers postulating that high precipitation of jarosite and elemental sulfur restrict biofilm development (Lei et al., 2009), while others identified microcolonies of *At. ferrooxidans* and *L. ferriphilum* forming a monolayered biofilm under short contacting periods (Africa et al., 2010).

Here, we demonstrated that mesophilic inoculation of bacteria with iron- and sulfur-oxidizing capacity in a flow cell chamber enables the detailed study of biofilm development on bornite resembling heap/dump bioleaching conditions when assuming a homogeneous packed bed behavior, where liquid percolation is driven by gravity through the ore particle surface. The biofilm-promoting laminar regime improved the copper leaching rate compared with stirred conditions in the presence of ferrous iron (Fe^{2+}) and highlighted the importance of biofilm formation and its microbial composition to explain the mode of action and lifestyle of acidophiles carrying iron and sulfur oxidization during bornite bioleaching for copper extraction.

MATERIALS AND METHODS

Consortium and Culture Conditions

The acidophilic consortium used in this study was obtained by enrichment from ore samples from mining regions in Chile. This consortium was maintained in batch aerated bubble column reactors at 30°C in modified 9K mineral salt medium [990 mg/L of $(NH_4)_2SO_4$, 145 mg/L of $NaH_2PO_4{\cdot}H_2O$, 52 mg/L of KH_2PO_4, 100 mg/L of $MgSO_4{\cdot}7H_2O$, and 21 mg/L of $CaCl_2$] (Bobadilla-Fazzini et al., 2011), adjusted to pH 1.6 and containing soluble iron (5 g/L Fe^{2+}), elemental sulfur (5 g S^0/L), and chalcopyrite concentrate (0.2/L) as energy sources. The microbial composition analyses were performed by specific q-PCR determination as previously described (Bobadilla-Fazzini et al., 2011) indicated 76% abundance of *Leptospirillum* spp. and 24% of *Acidithiobacillus* spp.

Mineral Samples

High-purity chalcopyrite (optical mineralogical characterization as 90.07% chalcopyrite, 0.10 covellite, 7.11% pyrite, and 2.72% unspecified gangue) and bornite (optical mineralogical characterization as 74.91% bornite, 15,89% Cc, 0.16% chalcopyrite, 0.79% digenite, 0.09% covellite, 0.35% rutile, 1.69% hematite, and 6.13% unspecified gangue) were obtained by manual picking from ore samples from the Geological Department of the Universidad de Chile. Samples were ground and sieved with 325 Tyler mesh, which means that all particles were below 0.044 mm.

Screening Bioleaching Assays

Every mineral sample was attached to a plastic tape to cover a surface of approximately 1.5 × 1.5 cm registering the exact mass of mineral. The plastic tape with the bound mineral was attached to the bottom of a six-well plate with the mineral facing upward. Turbulent flow of culture medium (8 ml per well) was carried out using modified 9K medium either including ferric (0.7 g Fe^{3+}/L) or ferrous iron (0.7 g Fe^{2+}/L) as sulfate salts and incubating the plate at 30°C and 150 rpm under non-sterile conditions and including mesophilic inoculation. The acidophilic consortium was added to the solution to reach an initial density of 10^6 cells/g mineral. For both conditions (with and without inoculation) three to five replicates were set up for every analyzed time. The solution obtained was directly sampled at the end of the assay without solid washing. Evaporation was prevented with a hermetic plastic cover on top of each six-well plate.

Flow Cell Bioleaching Assays

A set of custom-made flow cells with a lower inlet and an overflow chamber was done in acrylic, recirculating a volume of 100–200 ml of culture minimal medium (Bobadilla-Fazzini, 2017). Every mineral sample was attached to a plastic tape in order to cover a surface of approximately 1.5 × 1.5 cm registering the exact mass of the mineral. The plastic tape with the bound

mineral was attached to a glass slide that was placed on the top of the flow cell with the mineral facing downward. Flow was set at a free-stream fluid velocity of 0.02 cm/s and pipe diameter of 0.3 cm, where a laminar flow was assured (Reynolds number below 10) of culture-modified 9K medium with ferrous iron (0.7 g Fe^{2+}/L) with a peristaltic recirculation pump and avoiding turbulent flow placing a bubble trap between the pump and the flow cell inlet. Mesophilic inoculation was done adding the acidophilic consortium to the solution to reach an initial density of 10^6 cells/g of mineral just at the beginning of the incubation. All conditions were set up for every analyzed time in triplicate. All flow cells were incubated at 30°C under non-sterile conditions assuming solution saturation for oxygen and carbon dioxide. The recirculating solution was periodically sampled, and evaporation was compensated with pure water before each sampling time.

Biofilm and Microbial Analysis

Measurements were done directly on mineral samples and solutions stopping three flow cell replicates for every condition and analyzed time. Cell concentration in the recirculating solution was done by direct chamber counting under phase-contrast microscope (Thoma Chamber, depth 0.010 mm). Further strain proportion was determined by specific q-PCR determination as previously described (Bobadilla-Fazzini et al., 2011). Briefly, purified genomic DNA was extracted and analyzed with total bacteria 16S rRNA gene region primers (forward 5′-GTGCCAGCMGCCGCGGTAA-3′, reverse 5′-CCGTCAATTCCTTTGAGTTT-3′), total Archaea 16S rRNA gene region primers (forward 5′-ACGGGGCG CAGCAGGCGCGA-3′, reverse 5′-YCCGGCGTTGAMTCCAA TT-3′), 16S rRNA gene for *Acidithiobacillus thiooxidans* (forward 5′-TAATATCGCCTGCTGTTGAC-3′, reverse 5′-TTTCACGACAGACCTAATG-3) and 16S rRNA gene for *Leptospirillum* spp. (forward 5′-TGAGGGGACTGCCAGCGAC-3′, reverse 5′-CTAGACGGGTACCTTGTTAC-3′). Alternatively, for biofilm analysis, previously designed fluorescent *in situ* hybridization (FISH) method and probes were used for *Leptospirillum* spp. (FISH-FAM: 5′-CGCTTCCCTC TCCCAGCCT-3′) (Bond and Banfield, 2001) and *Acidithiobacillus* spp. (5′-ACCAAACATCTAGTATTCATCG-3′) (Peccia et al., 2000).

Chemical Analysis

Total iron and copper were determined by Atomic Absorption Spectrometry (Perkin Elmer Analyst 400), and Fe(II) by the o-phenantroline method (Kolthoff and Sandell, 1963).

Mineralogical Analysis

For every sample, one section was dried overnight for mineralogical analysis, and the other section taken for SEM-EDS analysis (FEI Quanta 250) after sputter coating with gold. Mineralogical analysis was performed directly over the dry mineral samples at different times by bulk mineralogical analysis (BMA) with QEMSCAN Express equipment (FEI). The analytic methodology chosen was a combination of bulk mineral analysis with linear intercept method and a high-density field scan analysis (2.5 μm × 2.5-μm pixel size) with a minimum of 200,000 pixel analysis/sample in order to obtain a general mineral overview and a detailed mineral association mapping.

RESULTS AND DISCUSSION

Mesophilic bioleaching has been used at an industrial scale for secondary copper sulfide ores, but not for the primary ones like chalcopyrite, given the low copper recovery and slow kinetics (Córdoba et al., 2008). For low-grade primary copper sulfide ores, a few industrial bioleaching applications are in the advanced stages to make the copper extraction economically feasible, to some extent, because of our inability to capture the lifestyle and growth development of the leaching microorganisms during copper recovery from actual primary ores. Thus, we investigated the capabilities of *Leptospirillum* spp. and *At. thiooxidans* to form biofilm on primary copper sulfides utilizing a standardized and reproducible flow cell approach that resembles heap/dump bioleaching conditions. It is important to highlight that most studies today employed primary copper sulfide high-purity minerals with concentrates added at low pulp densities and high cell loads in shaking flasks (Corkhill et al., 2008; Wang et al., 2016; Bellenberg et al., 2018). These growth conditions are optimal for homogeneous mixing and planktonic microbial growth, but certainly not for biofilm development (Tolker-Nielsen and Sternberg, 2011). First, we set the screening assay under turbulent flow regimes to mimic shaking flask liquid homogeneous conditions (**Figure 1A**). On the other hand, the method for studying bacterial biofilm development uses cell flow chambers under laminar regimes (Tolker-Nielsen and Sternberg, 2011; Crusz et al., 2012). **Figure 1B** depicts the components that comprise the cell chambers to study metal-leaching acidophiles. We found that the bubble trap is essential for attaining a homogeneous flow and proper propagation of acidophilic microorganisms (Crusz et al., 2012). We next placed on top of the cell chamber, in various sets of experiments, high-purity natural primary copper sulfide minerals to evaluate biofilm formation and copper extraction and finally compare it with turbulent conditions. Importantly, the minerals were not cleansed by acid solutions (HCl) nor autoclaved since these procedures alter the surface of the material, provoking initial leaching of copper and eliminating native microorganisms inhabiting these primary copper sulfide materials (Cerda et al., 2018).

Chalcopyrite Bioleaching

Mineralogical analyses were done on the head mineral to confirm chalcopyrite purity (**Figure 2A**, time 0) and at the end of the bioleaching assay to record possible transformations (**Figure 2A**, 30 and 60 days). Chalcopyrite inspection before bioleaching by QEMSCAN-BMA indicated a purity of 70% (previously estimated over 90% by optical microscopy), with a significant 16% of unclassified minerals (**Figure 2A**), with a clean surface as observed by SEM (**Figure 2C**). Under shaking conditions, precipitates completely covered the chalcopyrite surface after 30 days of bioleaching, partially classified as potassium and/or sodium jarosite based on the EDS elemental identification (**Figure 2D**). This was not the case for chalcopyrite bioleached

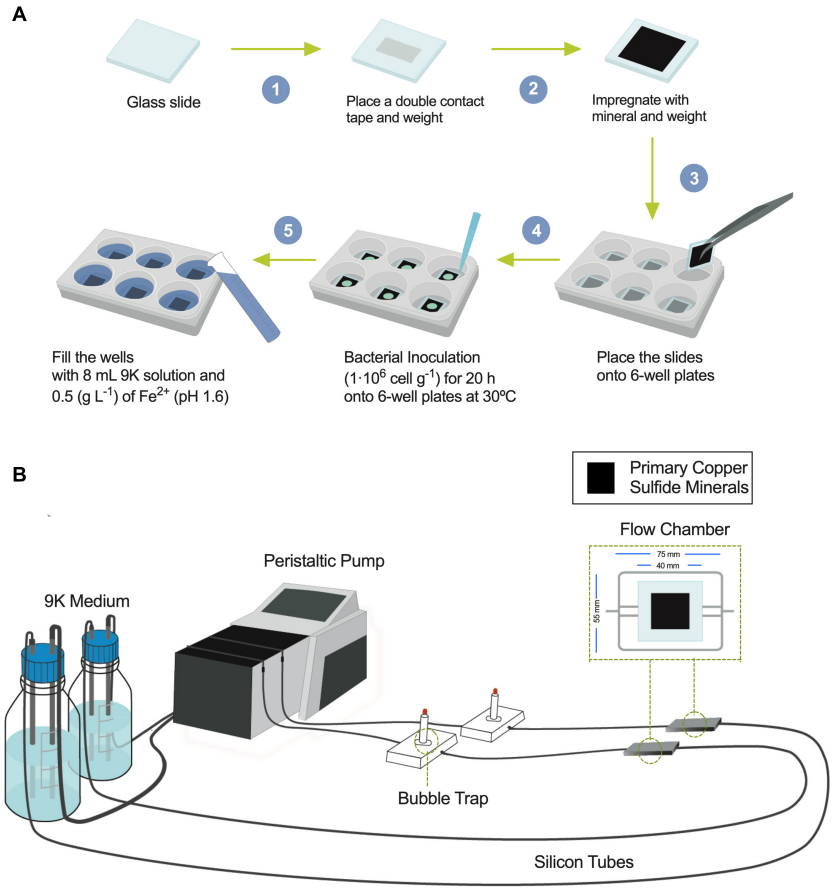

FIGURE 1 | Diagrams showing the flow chamber for biofilm formation and the screening assay under shaking conditions. **(A)** Screening procedure scheme to bioleach copper from primary copper sulfides in mesophilic conditions (30°C) under shaking using six-well plates with inoculation of bacterial acidophiles. **(B)** Flow cell model and assembly diagram of bioleaching copper from primary copper sulfides under laminar regimes and buildup biofilm composed of acidophilic bacterial consortium growing at 30°C.

under laminar regimes as the micrographs show low precipitates, and EDS analysis remained constant (**Figure 2E**).

Using the laminar flow chamber, the final mineralogical analysis showed significant variations with an increment in chalcopyrite proportion to 78% and reduced unclassified material to 11%, probably indicating the removal of initially present impurities from the mineral surface. On the contrary, in the turbulent flow regime, the mineralogical analysis was almost unable to identify chalcopyrite at the end of the assay (only 2% identification at day 30), while the unclassified raised to 94% attributed mainly to not identified mixed phases (**Figure 2A**, 30 and 60 days), indicating major mineral surface coverage by formed precipitates including potassium and/or sodium jarosite as indicated by EDS (**Figure 2D**). The screening bioleaching assay and the laminar flow condition showed a low copper recovery of 6% in 30 days incubated at 30°C and maintaining this copper level until day 60 (**Figures 2A,B**). Biofilm formation did not occur under turbulent or laminar flow regimes (**Figures 2D,E**). These results are in agreement with those previously published by Lei et al. (2009). Some studies describe biofilm buildup on the altered surface of the chalcopyrite in a short period where chalcopyrite was either previously electro-oxidized resulting in S^0, CuS, and S^{2-} that promote bacterial attachment (García-Meza et al., 2013), or crushed down to a size of less than 80 μm and finally polished (Yang et al., 2015). Other works using batch stirred bioreactors set at 42°C and inoculated with *L. ferriphilum*, *Sulfobacillus* spp., and *A. caldus* showed 94% extraction of the available copper in the concentrate, where chalcopyrite remained intact during the leaching process (6% of the remaining Cu) (Spolaore et al., 2011; Hedrich et al., 2016). This confirms that even at moderate thermophilic conditions and employing a different acidophilic consortium from this study, it is challenging to leach the copper content from this primary sulfide mineral.

Bornite Bioleaching

Considering that chalcopyrite is commonly associated with bornite in nature and that a galvanic couple between these two minerals has been described (Wang et al., 2016), the next step was to analyze the mesophilic bioleaching process correlated with highly pure bornite. We first inoculated the same proportion of the acidophilic bacterial consortium used

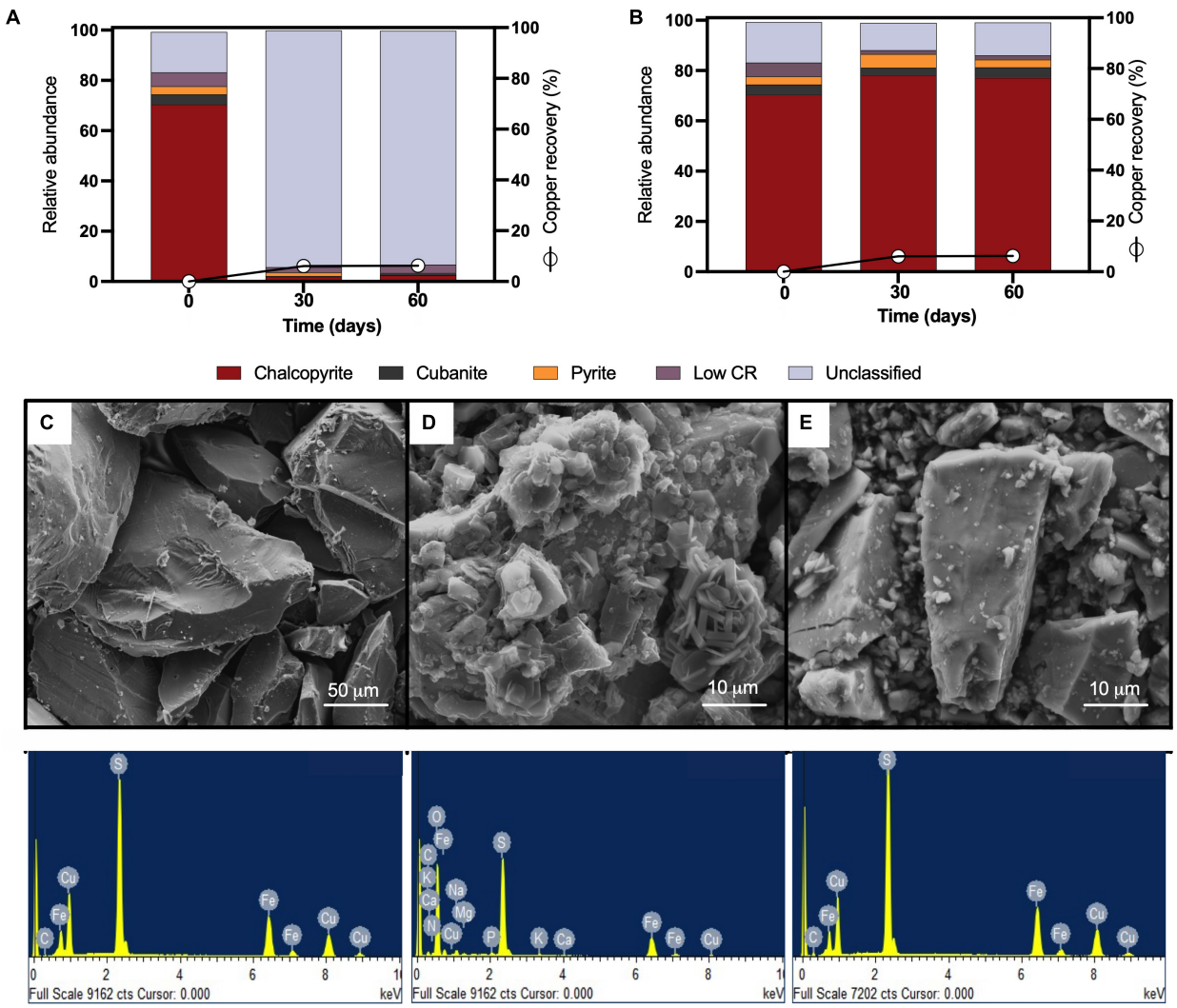

FIGURE 2 | QEMSCAN-BMA analysis of high-purity natural chalcopyrite before bioleaching (t0) and after flow cell bioleaching assay (30 days) for **(A)** turbulent and **(B)** laminar conditions. **(C)** SEM image and EDS spectrum of high purity chalcopyrite before bioleaching. SEM images and EDS spectra of high-purity chalcopyrite after 30 days of **(D)** turbulent (screening method) and **(E)** laminar flow mesophilic bioleaching (flow cell method). Low CR: no mineral detection.

for chalcopyrite along with the addition of ferric iron (0.7 g Fe^{3+}/L), which enabled the rapid recovery of copper from bornite (40%) after 10 days of cultivation under stirring conditions (**Figure 3A**). Previous studies showed accelerated bornite leaching in the presence of external ferric iron addition (Hidalgo et al., 2019), and on the contrary, the screening bioleaching assays carried out with the addition of ferrous iron (0.7 g Fe^{2+}/L) exhibited a copper extraction close to 30% after 48 days at 30°C (**Figure 3B**). In parallel, the laminar regime leached 54% of the Cu content at day 32, with no further Cu recovery until day 48 (**Figure 3C**), illustrating the importance of the process set up and bacterial attachment to accelerate copper bioleaching from bornite at 30°C.

QEMSCAN-BMA recorded 32% bornite purity before bioleaching (estimated at 75% by optical microscopy) with an unclassified mineral fraction close to a third (time 0 in **Figures 3A–C**). The mineralogical dynamics of mesophilic bioleaching indicated in both regimens (turbulent and laminar flow) the intermediate formation of idaite (Cu_3FeS_4) in the first stage of bioleaching. Chalcopyrite detection was attributed to ferric ion precipitation masking further bornite/idaite detection (**Figures 3A–C**), though former studies consider it as part of the bornite (bio)leaching mechanism (Pal-ing, 2018). Turbulent and laminar flow regimes were initially inoculated including external ferrous iron (Fe^{2+}) addition; in the turbulent regime, only a slight iron-oxidizing activity was observed until day 20 (**Figure 4A**) with a concomitant microbial growth, stopped by a significant pH increase (pH 4.25, data not shown) and consequent iron precipitation (**Figure 4A**). Interestingly, biofilm formation was observed only under laminar flow conditions, with a significant alteration in the bornite surface and an exopolysaccharide (EPS)

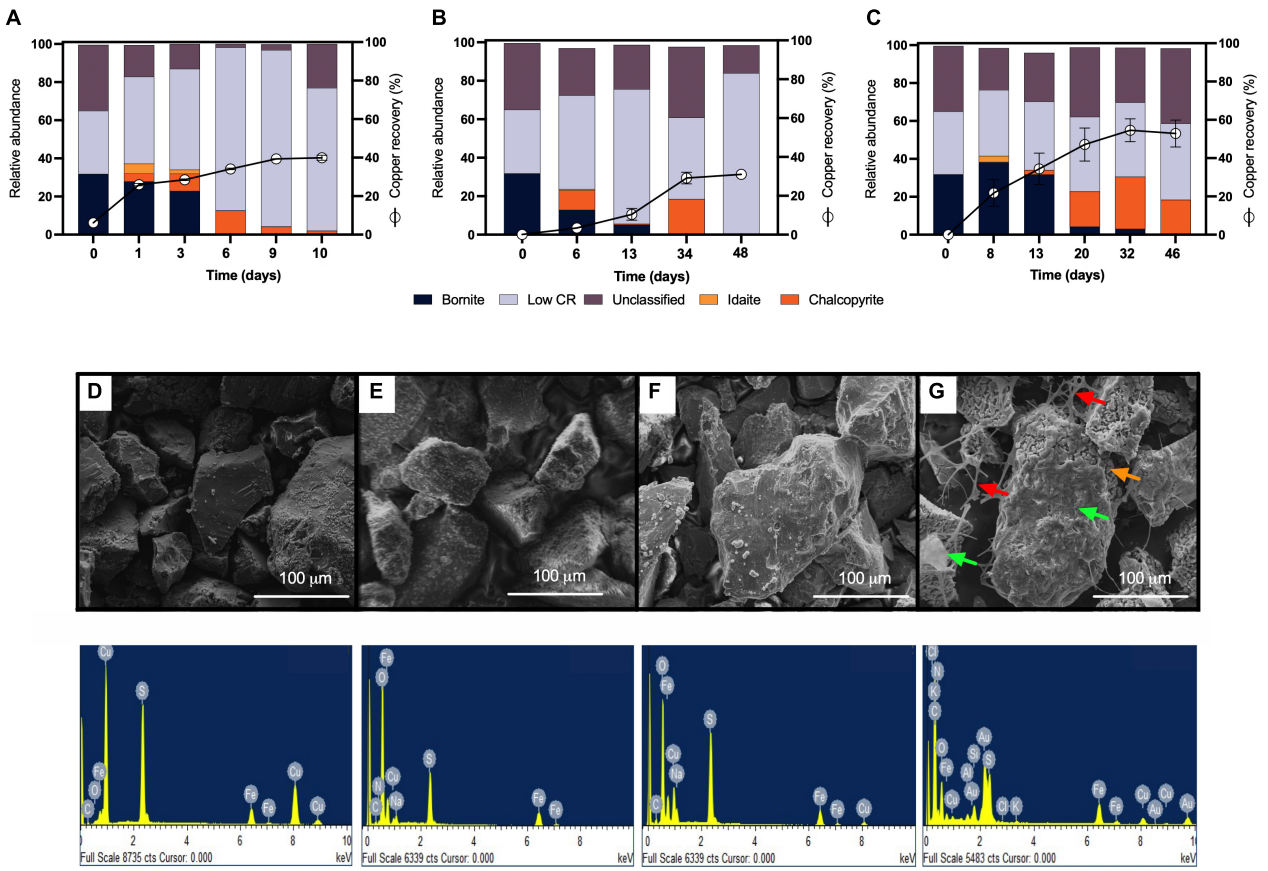

FIGURE 3 | Mineralogical dynamics, SEM images, and EDS spectra of high-purity natural bornite bioleaching under mesophilic (30°C) inoculation. **(A)** Turbulent flow bioleaching with addition of ferric iron (screening method), **(B)** turbulent flow bioleaching with addition of ferrous iron (screening method), **(C)** laminar flow bioleaching (flow cell method). SEM images and EDS spectra for **(D)** bornite before bioleaching, **(E)** bornite after 10 days (40% Cu recovery) under turbulent flow mesophilic bioleaching (screening method), **(F)** bornite after 48 days (30% Cu recovery) under turbulent flow mesophilic bioleaching with addition of ferrous iron (screening method), **(G)** bornite after 46 days (54% Cu recovery) under laminar flow mesophilic bioleaching (flow cell method). Red, orange, and green arrows indicate exopolysaccharide (EPS) network, altered mineral, biofilm formation, respectively. Low CR: no mineral detection.

network (**Figure 3G**, indicated with red arrows), compared with turbulent flow conditions where no biofilm formation was encountered with the initial addition of ferric nor ferrous iron (**Figure 3F**). Biofilm development mediated initially by EPS production during bioleaching depends on several factors including mineral type (Gehrke et al., 1998), process temperature (Zeng et al., 2010; Barahona et al., 2014), and the presence of organic compounds such as D-galactose (Saavedra et al., 2020) and sodium glucoronate (Bellenberg et al., 2015). For instance, pyrite is an excellent sulfide mineral for biofilm formation under acidic conditions as a strong electrochemical interaction occurs between the synthesized EPS-Fe^{3+} and the negatively charged mineral surface (Gehrke et al., 1998; Bellenberg et al., 2015). It differs highly compared with chalcopyrite, where EPS synthesis occurs only when inoculated at a high cell density (Lei et al., 2009; Yang et al., 2015; Bellenberg et al., 2018), with some studies using more than 10^9 cells/g mineral as initial biomass (Lei et al., 2009). Unfortunately, this biomass loading is impractical at the industrial mining scale for cooper bioleaching of primary sulfur-bearing ores. It is clear that further investigation aiming at promoting biofilm development on chalcopyrite at mesophilic conditions is necessary under different flow regimes, varying the type and abundance of acidophilic consortia, resembling industrial operations, and taking care of the mineral characteristics, initial cell density, and avoiding major mineral pretreatments to make the process economically feasible.

Microbial Analysis During Bornite Bioleaching

Considering the extensive copper recovery from bornite under the laminar flow regime, which was not seen here for the turbulent condition in the presence of ferrous iron (Fe^{2+}), we next performed a dynamic microbial analysis during biofilm formation. Initial inoculation of the acidophilic consortium in a proportion 3:1 (*Leptospirillum* spp.:*At. thiooxidans*) was followed under the laminar flow condition, revealing the predominance of the iron oxidizers in solution until the end of the assay and the appearance of unidentified (possibly mineral native bacteria)

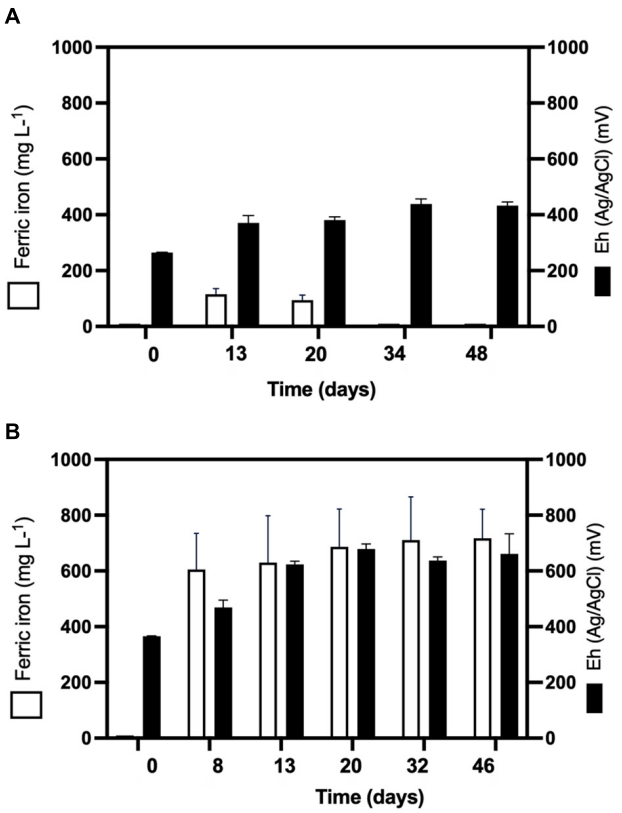

FIGURE 4 | Ferric ion (Fe^{3+}) formation and oxidation–reduction potential (Eh) during **(A)** turbulent flow bioleaching with addition of ferrous iron (700 mg/L) (screening method) and **(B)** laminar flow mesophilic bioleaching with addition of ferrous iron (700 mg/L) (flow cell method).

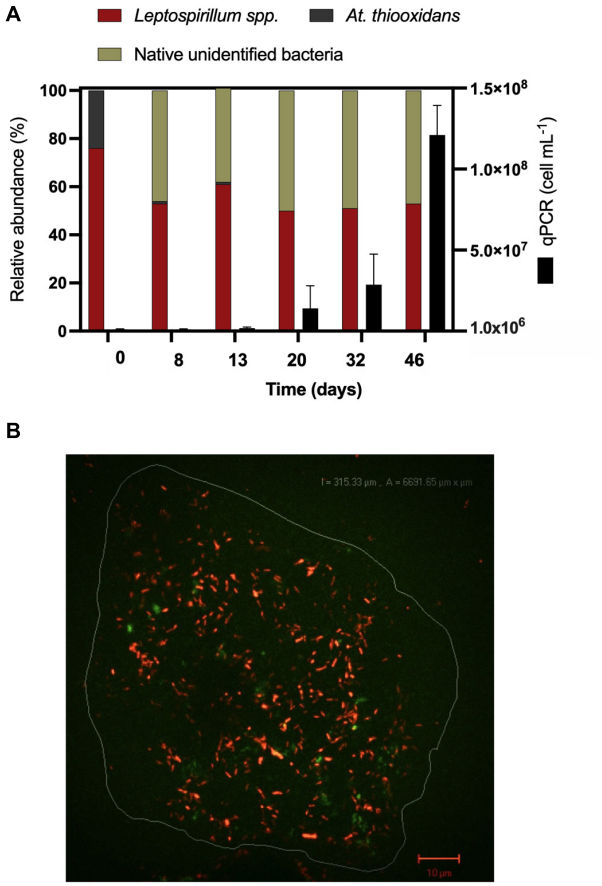

FIGURE 5 | Microbiological determinations during high-purity natural bornite bioleaching under mesophilic (30°C) inoculation with external ferrous iron (Fe^{2+}) addition in laminar flow bioleaching (flow cell method). **(A)** Microbial dynamics in the recirculating solution *via* qPCR and cell counts. **(B)** Representative biofilm composition by FISH (30 days) where the image corresponds to overlap of FISH-Cy3 (red, *Acidithiobacillus* spp.) and FISH-FAM (green, *Leptospirillum* spp.).

in planktonic form (**Figure 5A**). After day 20, the iron present in the solution was detected in the ferric form (**Figure 4B**), correlating with the increment in the total iron-oxidizing bacteria in the recirculating solution (**Figure 4B**). However, FISH analysis indicated the prevalence of *Acidithiobacillus* spp. in the biofilm (**Figure 5B**), opening the discussion concerning the interaction and relevance of both planktonic and sessile microbial populations. On the one hand, the planktonic iron oxidizers recycle the ferric ion that actively (bio)leach the mineral surface, a phenomenon initially favored under turbulent conditions (Hong et al., 2019) based on the screening copper recovery kinetics observed (**Figure 3**). However, the lack of biofilm formation with the presence of microbes with sulfur-oxidizing activity did not generate the required acid production to balance its consumption during the microbial iron-oxidation process (**Figure 4A**), avoiding further copper extraction from bornite (**Figure 3B**). Clearly, this is not representative of the industrial heap/dump copper mining operations, where the kinetics of microbial iron and sulfur oxidation occur at a different pace. In this sense, the laminar flow biofilm analysis shows that the attached microbial population is mainly composed of sulfur-oxidizing bacterial species (**Figure 5B**), most likely due to mineral surface elemental sulfur accumulation (Lei et al., 2009; Bobadilla-Fazzini, 2017). This phenomenon can be considered useful in terms of initial mineral surface exposure to the ferric leaching agent, though detrimental due to extensive biofilm growth and mineral surface hindering at a later process stage, perhaps requiring specific conditions to tailor microbial composition for efficient copper extraction.

EDS analyses confirmed the expected bornite atomic composition before bioleaching (**Figure 3D**), and the altered bornite surface with the impoverishment of copper during bioleaching (**Figure 3F**), validating the identification of idaite by QEMSCAN. Moreover, EDS analysis showed that during the turbulent flow screening method, the precipitates formed over the surface of bornite appears to be sodium jarosite [$NaFe_3(OH)_6(SO_4)_2$] due to notable increments in oxygen and sodium (**Figure 3E**), as recently reported for ferric sulfate pretreatment followed by moderate thermophilic bioleaching (Liu et al., 2020). On the other hand, the surface EDS analysis

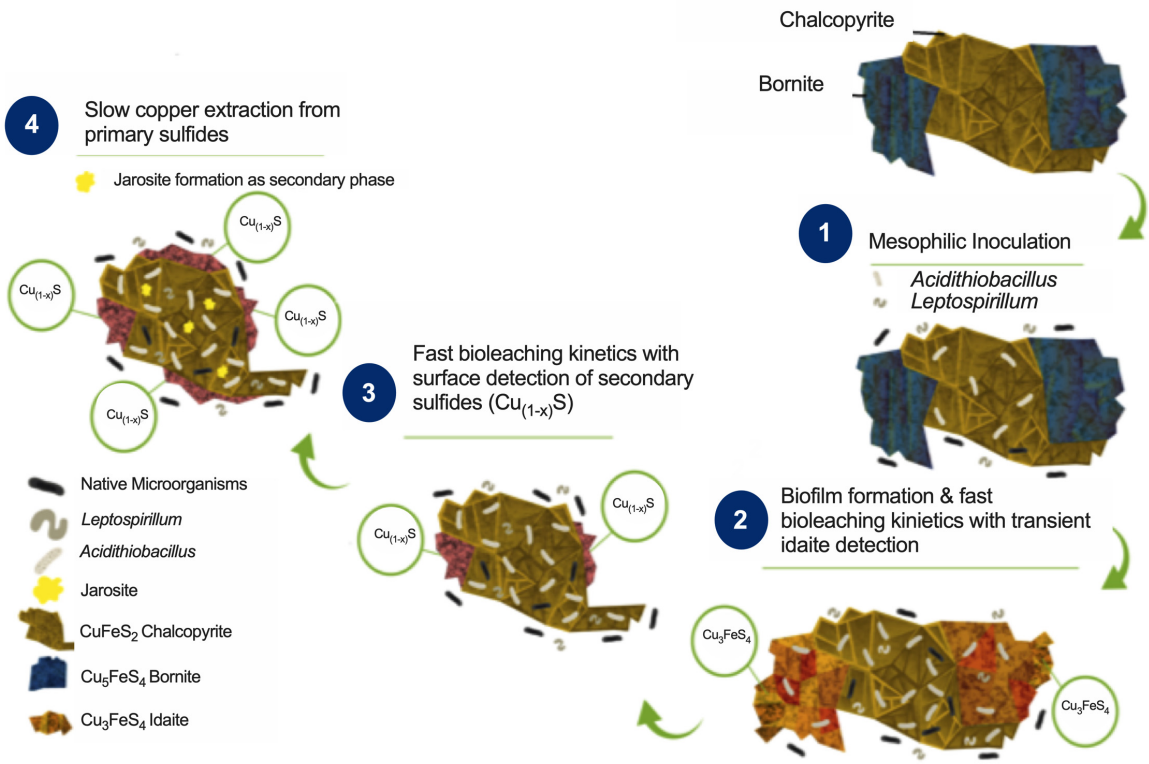

FIGURE 6 | Proposed bioleaching mechanism for primary copper sulfides bornite and chalcopyrite under mesophilic inoculation of bacteria with iron- and sulfur-oxidizing activity forming biofilm.

of laminar flow cell bornite showed no sodium at all but high carbon proportions indicating the organic nature of the biofilm formed (**Figure 3G**).

Mechanism for Bornite Bioleaching During Biofilm Formation

Combining the biofilm development, ferric profile, and the mineralogical QEMSCAN and EDS analyses, it is possible to propose a mechanism for bornite bioleaching under laminar flow conditions (**Figure 6**). Previous studies have shown two stages for bornite ferric leaching (Pesic and Olson, 1984), with an initial leaching rate significantly dependent on ferric ion concentration and with no elemental sulfur formation leading to idaite:

$$Cu_5FeS_4 + 4Fe^{3+} \longrightarrow Cu_3FeS_4 + 2Cu^{2+} + 4Fe^{2+} \quad (1)$$

Indeed, the ferrous iron oxidation is mediated by *Leptospirillum* spp. yielding the ferric form:

$$2Fe^{2+} + 1/2O_2 + 2H^{+} \longrightarrow 2Fe^{3+} + H_2O \quad (2)$$

This first stage is observed in our analysis from the beginning of the process until days 34 and 13 for turbulent and laminar flow with ferrous iron addition, respectively, with a corresponding copper extraction close to 30% (**Figure 3**). In the second stage, a slow leaching rate of idaite arises independent of ferric ion concentration (**Figure 3C**) where the sulfur produced is proportional to copper dissolved and tending to envelop the residue mineral particles, therefore, being the limiting step:

$$Cu_3FeS_4 + 8Fe^{3+} \longrightarrow S^0 + 3Cu^{2+} + 9Fe^{2+} \quad (3)$$

Here, the iron- and sulfur-oxidizing microorganisms exert a catalyzing role, with the pH maintenance as a critical aspect in order to prevent ferric ion precipitation (**Figure 4B**), a role exerted by the sulfur-oxidizing biofilm controlling the leaching kinetics (**Figure 5B**):

$$S^0 + 3O_2 + 2H_2O \longrightarrow 2SO4^{2-} + 4H^{+} \quad (4)$$

These results confirm that mesophilic biofilm occurs extensively over bornite under laminar flow regimes, modifying its surface in a very different way than ferric leaching does

under turbulent flow conditions (Hong et al., 2019; Liu et al., 2020). In addition, as the buildup of biofilm comprises several stages, initiating with the bacterial adherence to the surface, then the cells aggregate entering a phase of irreversible attachment, maturation, and finally dispersion (Garnett and Matthews, 2012). This process could explain the significantly higher copper recovery levels compared with shaking conditions (**Figures 3B,C**).

More precipitates are observed under turbulent conditions masking the proper quantification of the resulting iron sulfide compounds (**Figure 3**). Overall, the flow cell chamber is a more appropriated approach to studying biofilm formation and mineralogic dynamics that resemble the heap bioleaching of this abundant primary copper sulfide.

CONCLUSION

The main copper minerals worldwide correspond to primary sulfides chalcopyrite and bornite, so it is crucial to understand the microbial variations affecting their efficient copper extraction. In this sense, this work shows that the standard approaches of bioleaching tests under stirring conditions prevent biofilm formation on bornite and chalcopyrite at 30°C. In addition, we determine that biofilm development is not feasible on chalcopyrite even under laminar flow mesophilic conditions, posing a great challenge for copper hydrometallurgy. Successfully, the biofilm-forming laminar regime improves almost twice the leached copper content of bornite compared with stirring conditions in the presence of ferrous iron (Fe^{2+}), reducing the time from 48 to 32 days of cultivation. For the first time, we demonstrated that the main microorganisms comprising the biofilm development on bornite are sulfur-oxidizing bacteria, while the ferrous-oxidizing bacteria are in planktonic form. This lifestyle of acidophiles explains the accelerated pace of copper recovery during biofilm formation, where the action of sulfur-oxidizing bacteria maintains the low pH *via* sulfuric acid formation, thus, preventing iron precipitation. The next step toward sustainable copper hydrometallurgy is to develop a process that promotes biofilm formation on the surface of chalcopyrite under mesophilic or moderate thermophilic conditions to extract copper from this bulk material efficiently, pointing to the creation of novel acidophilic microbial consortia.

DATA AVAILABILITY STATEMENT

The raw data supporting the conclusions of this article will be made available by the authors, without undue reservation.

AUTHOR CONTRIBUTIONS

RB-F performed experiments, analyzed the data, and wrote the manuscript. IP-C analyzed the data and wrote the manuscript. Both authors contributed to the article and approved the submitted version.

FUNDING

This work was supported in part by ANID-PIA-Anillo INACH ACT192057 and by DICYT-USACH.

REFERENCES

Africa, C.-J., Harrison, S. T. L., Becker, M., and van Hille, R. P. (2010). In situ investigation and visualisation of microbial attachment and colonisation in a heap bioleach environment: the novel biofilm reactor. *Miner. Eng.* 23, 486–491. doi: 10.1016/j.mineng.2009.12.011

Barahona, S., Dorador, C., Zhang, R., Aguilar, P., Sand, W., Vera, M., et al. (2014). Isolation and characterization of a novel Acidithiobacillus ferrivorans strain from the Chilean Altiplano: attachment and biofilm formation on pyrite at low temperature. *Res. Microbiol.* 165, 782–793. doi: 10.1016/j.resmic.2014.07.015

Bellenberg, S., Barthen, R., Boretska, M., Zhang, R., Sand, W., and Vera, M. (2015). Manipulation of pyrite colonization and leaching by iron-oxidizing *Acidithiobacillus* species. *Appl. Microbiol. Biotechnol.* 99, 1435–1449. doi: 10.1007/s00253-014-6180-y

Bellenberg, S., Buetti-Dinh, A., Galli, V., Ilie, O., Herold, M., Christel, S., et al. (2018). Automated microscopic analysis of metal sulfide colonization by acidophilic microorganisms. *Appl. Environ. Microbiol.* 84:e01835-18. doi: 10.1128/AEM.01835-18

Bevilaqua, D., Garcia, O. Jr., and Tuovinen, O. H. (2010). Oxidative dissolution of bornite by *Acidithiobacillus ferrooxidans*. *Process Biochem.* 45, 101–106. doi: 10.1016/j.procbio.2009.08.013

Bobadilla-Fazzini, R. A. (2017). Mineralogical dynamics of primary copper sulfides mediated by acidophilic biofilm formation. *Solid State Phenomena* 262, 325–329. doi: 10.4028/www.scientific.net/SSP.262.325

Bobadilla-Fazzini, R. A., Levican, G., and Parada, P. (2011). Acidithiobacillus thiooxidans secretome containing a newly described lipoprotein Licanantase enhances chalcopyrite bioleaching rate. *Appl. Microbiol. Biotechnol.* 89, 771–780. doi: 10.1007/s00253-010-3063-8

Bond, P. L., and Banfield, J. F. (2001). Design and performance of rRNA targeted oligonucleotide probes for in situ detection and phylogenetic identification of microorganisms inhabiting acid mine drainage environments. *Microb. Ecol.* 41, 149–161. doi: 10.1007/s002480000063

Bustos, S., Castro, S., and Montealegre, R. (1993). The Sociedad Minera Pudahuel bacterial thin-layer leaching process at Lo Aguirre. *FEMS Microbiol. Rev.* 11, 231–235. doi: 10.1111/j.1574-6976.1993.tb00289.x

Cancho, L., Blázquez, M. L., Ballester, A., González, F., and Muñoz, J. A. (2007). Bioleaching of a chalcopyrite concentrate with moderate thermophilic microorganisms in a continuous reactor system. *Hydrometallurgy* 87, 100–111. doi: 10.1016/j.hydromet.2007.02.007

Cerda, C. P., Taboada, M. E., Jamett, N. E., Ghorbani, Y., and Hernández, P. C. (2018). Effect of pretreatment on leaching primary copper sulfide in acid-chloride media. *Minerals* 8:1. doi: 10.3390/min8010001

Córdoba, E. M., Muñoz, J. A., Blázquez, M. L., González, F., and Ballester, A. (2008). Leaching of chalcopyrite with ferric ion. Part IV: the role of redox potential in the presence of mesophilic and thermophilic bacteria. *Hydrometallurgy* 93, 106–115. doi: 10.1016/j.hydromet.2007.11.005

Corkhill, C. L., Wincott, P. L., Lloyd, J. R., and Vaughan, D. J. (2008). The oxidative dissolution of arsenopyrite (FeAsS) and enargite (Cu3AsS4) by *Leptospirillum ferrooxidans*. *Geochim. Cosmochim. Acta* 72, 5616–5633. doi: 10.1016/j.gca.2008.09.008

Crusz, S. A., Popat, R., Rybtke, M. T., Cámara, M., Givskov, M., Tolker-Nielsen, T., et al. (2012). Bursting the bubble on bacterial biofilms: a flow cell methodology. *Biofouling* 28, 835–842. doi: 10.1080/08927014.2012.716044

Duarte, J. C., Estrada, P. C., Pereira, P. C., and Beaumont, H. P. (1993). Thermophilic vs. mesophilic bioleaching process performance. *FEMS Microbiol. Rev*. 11, 97–102. doi: 10.1111/j.1574-6976.1993.tb00272.x

García-Meza, J. V., Fernández, J. J., Lara, R. H., and González, I. (2013). Changes in biofilm structure during the colonization of chalcopyrite by *Acidithiobacillus thiooxidans*. *Appl. Microbiol. Biotechnol.* 97, 6065–6075. doi: 10.1007/s00253-012-4420-6

Garnett, J. A., and Matthews, S. (2012). Interactions in bacterial biofilm development: a structural perspective. *Curr. Protein Pept. Sci.* 13, 739–755. doi: 10.2174/138920312804871166

Gehrke, T., Telegdi, J., Thierry, D., and Sand, W. (1998). Importance of extracellular polymeric substances from *Thiobacillus ferrooxidans* for bioleaching. *Appl. Environ. Microbiol.* 64, 2743–2747. doi: 10.1128/AEM.64.7.2743-2747.1998

Hedrich, S., Guézennec, A.-G., Charron, M., Schippers, A., and Joulian, C. (2016). Quantitative monitoring of microbial species during bioleaching of a copper concentrate. *Front. Microbiol.* 7:2044. doi: 10.3389/fmicb.2016.02044

Hedrich, S., Joulian, C., Graupner, T., Schippers, A., and Guézennec, A.-G. (2018). Enhanced chalcopyrite dissolution in stirred tank reactors by temperature increase during bioleaching. *Hydrometallurgy* 179, 125–131. doi: 10.1016/j.hydromet.2018.05.018

Hidalgo, T., Kuhar, L., Beinlich, A., and Putnis, A. (2019). Kinetics and mineralogical analysis of copper dissolution from a bornite/chalcopyrite composite sample in ferric-chloride and methanesulfonic-acid solutions. *Hydrometallurgy* 188, 140–156. doi: 10.1016/j.hydromet.2019.06.009

Hong, M., Wang, X., Wu, L., Fang, C., Huang, X., Liao, R., et al. (2019). Intermediates transformation of bornite bioleaching by *Leptospirillum ferriphilum* and *Acidithiobacillus caldus*. *Minerals* 9:159. doi: 10.3390/min9030159

Huang, T., Wei, X., and Zhang, S. (2019). Bioleaching of copper sulfide minerals assisted by microbial fuel cells. *Bioresour. Technol.* 288:121561. doi: 10.1016/j.biortech.2019.121561

Jun, W., Qin, W.-Q., Zhang, Y.-S., Yang, C.-R., Zhang, J.-W., Nai, S.-S., et al. (2008). Bacterial leaching of chalcopyrite and bornite with native bioleaching microorganism. *Trans. Nonferrous Met. Soc. China* 18, 1468–1472. doi: 10.1016/S1003-6326(09)60027-3

Kolthoff, J. M., and Sandell, E. B. (1963). *Textbook of Quantitative Inorganic Chemistry*. New York, NY: Macmillan. !

Lei, J., Huaiyang, Z., Xiaotong, P., and Zhonghao, D. (2009). The use of microscopy techniques to analyze microbial biofilm of the bio-oxidized chalcopyrite surface. *Miner. Eng.* 22, 37–42. doi: 10.1016/j.mineng.2008.03.012

Liu, S., Hong, M., Wang, X., Yang, B., Lin, H., Lin, M., et al. (2020). Pretreatment with acidic ferric sulfate leaching promotes the bioleaching of bornite. *Hydrometallurgy* 196:105349. doi: 10.1016/j.hydromet.2020.105349

Ma, L., Wang, X., Liu, X., Wang, S., and Wang, H. (2018). Intensified bioleaching of chalcopyrite by communities with enriched ferrous or sulfur oxidizers. *Bioresour. Technol.* 268, 415–423. doi: 10.1016/j.biortech.2018.08.019

Pal-ing, K. J. (2018). *The Mechanism of Bornite Leaching: Insights From Mineralogical and Textural Characterisation*. Ph.D thesis. Perth: Murdoch University.

Panda, S., Akcil, A., Pradhan, N., and Deveci, H. (2015). Current scenario of chalcopyrite bioleaching: a review on the recent advances to its heap-leach technology. *Bioresour. Technol.* 196, 694–706. doi: 10.1016/j.biortech.2015.08.064

Peccia, J., Marchand, E. A., Silverstein, J., and Hernandez, M. (2000). Development and application of small-subunit rRNA probes for assessment of selected *Thiobacillus* species and members of the genus *Acidiphilium*. *Appl. Environ. Microbiol.* 66, 3065–3072. doi: 10.1128/AEM.66.7.3065-3072.2000

Pesic, B., and Olson, F. A. (1984). Dissolution of bornite in sulfuric acid using oxygen as oxidant. *Hydrometallurgy* 12, 195–215. doi: 10.1016/0304-386X(84)90034-3

Petersen, J., and Dixon, D. G. (2002). Thermophilic heap leaching of a chalcopyrite concentrate. *Miner. Eng.* 15, 777–785. doi: 10.1016/S0892-6875(02)00092-4

Saavedra, A., Aguirre, P., and Gentina, J. C. (2020). Biooxidation of iron by *Acidithiobacillus ferrooxidans* in the presence of D-galactose: understanding its influence on the production of EPS and cell tolerance to high concentrations of iron. *Front. Microbiol.* 11:759. doi: 10.3389/fmicb.2020.00759

Spolaore, P., Joulian, C., Gouin, J., Morin, D., and d'Hugues, P. (2011). Relationship between bioleaching performance, bacterial community structure and mineralogy in the bioleaching of a copper concentrate in stirred-tank reactors. *Appl. Microbiol. Biotechnol.* 89, 441–448. doi: 10.1007/s00253-010-2888-5

Tolker-Nielsen, T., and Sternberg, C. (2011). Growing and analyzing biofilms in flow chambers. *Curr. Protoc. Microbiol.* 21:1B–2. , doi: 10.1002/9780471729259.mc01b02s21

Wang, J., Tao, L., Zhao, H., Hu, M., Zheng, X., Peng, H., et al. (2016). Cooperative effect of chalcopyrite and bornite interactions during bioleaching by mixed moderately thermophilic culture. *Miner. Eng.* 95, 116–123. doi: 10.1016/j.mineng.2016.06.006

Yang, Y., Tan, S. N., Glenn, A. M., Harmer, S., Bhargava, S., and Chen, M. (2015). A direct observation of bacterial coverage and biofilm formation by *Acidithiobacillus ferrooxidans* on chalcopyrite and pyrite surfaces. *Biofouling* 31, 575–586. doi: 10.1080/08927014.2015.1073720

Zeng, W., Qiu, G., Zhou, H., Liu, X., Chen, M., Chao, W., et al. (2010). Characterization of extracellular polymeric substances extracted during the bioleaching of chalcopyrite concentrate. *Hydrometallurgy* 100, 177–180. doi: 10.1016/j.hydromet.2009.11.002

Conflict of Interest: The authors declare that the research was conducted in the absence of any commercial or financial relationships that could be construed as a potential conflict of interest.

Publisher's Note: All claims expressed in this article are solely those of the authors and do not necessarily represent those of their affiliated organizations, or those of the publisher, the editors and the reviewers. Any product that may be evaluated in this article, or claim that may be made by its manufacturer, is not guaranteed or endorsed by the publisher.

frontiers in Microbiology

ORIGINAL RESEARCH
published: 28 October 2021
doi: 10.3389/fmicb.2021.762076

Geobiology of Andean Microbial Ecosystems Discovered in Salar de Atacama, Chile

Federico A. Vignale[1,2], Daniel Kurth[1], Agustina I. Lencina[1], Daniel G. Poiré[3], Elizabeth Chihuailaf[4], Natalia C. Muñoz-Herrera[4], Fernando Novoa[4], Manuel Contreras[4], Adrián G. Turjanski[2] and María E. Farías[1]**

[1] Laboratorio de Investigaciones Microbiológicas de Lagunas Andinas (LIMLA), Planta Piloto de Procesos Industriales Microbiológicos (PROIMI), CCT, CONICET, San Miguel de Tucumán, Argentina, [2] Laboratorio de Bioinformática Estructural, Instituto de Química Biológica de la Facultad de Ciencias Exactas y Naturales (IQUIBICEN)-CONICET, Universidad de Buenos Aires, Buenos Aires, Argentina, [3] Centro de Investigaciones Geológicas (CIG), Universidad Nacional de La Plata (UNLP)-CONICET, La Plata, Argentina, [4] Centro de Ecología Aplicada (CEA), Santiago, Chile

OPEN ACCESS

Edited by:
Claudia P. Saavedra, Andres Bello University, Chile

Reviewed by:
Aharon Oren, The Hebrew University of Jerusalem, Israel
Francisco Remonsellez, Catholic University of the North, Chile

***Correspondence:**
Federico A. Vignale
vignalefede@gmail.com
María E. Farías
mefarias2009@gmail.com

Specialty section:
This article was submitted to Extreme Microbiology, a section of the journal Frontiers in Microbiology

Received: *20 August 2021*
Accepted: *28 September 2021*
Published: *28 October 2021*

Citation:
Vignale FA, Kurth D, Lencina AI, Poiré DG, Chihuailaf E, Muñoz-Herrera NC, Novoa F, Contreras M, Turjanski AG and Farías ME (2021) Geobiology of Andean Microbial Ecosystems Discovered in Salar de Atacama, Chile. Front. Microbiol. 12:762076. doi: 10.3389/fmicb.2021.762076

The Salar de Atacama in the Chilean Central Andes harbors unique microbial ecosystems due to extreme environmental conditions, such as high altitude, low oxygen pressure, high solar radiation, and high salinity. Combining X-ray diffraction analyses, scanning electron microscopy and molecular diversity studies, we have characterized twenty previously unexplored Andean microbial ecosystems in eight different lakes and wetlands from the middle-east and south-east regions of this salt flat. The mats and microbialites studied are mainly formed by calcium carbonate (aragonite and calcite) and halite, whereas the endoevaporites are composed predominantly of gypsum and halite. The carbonate-rich mats and microbialites are dominated by *Bacteroidetes* and *Proteobacteria* phyla. Within the phylum *Proteobacteria*, the most abundant classes are *Alphaproteobacteria*, *Gammaproteobacteria* and *Deltaproteobacteria*. While in the phylum *Bacteroidetes*, the most abundant classes are *Bacteroidia* and *Rhodothermia*. *Cyanobacteria*, *Chloroflexi*, *Planctomycetes*, and *Verrucomicrobia* phyla are also well-represented in the majority of these systems. Gypsum endoevaporites, on the contrary, are dominated by *Proteobacteria*, *Bacteroidetes*, and *Euryarchaeota* phyla. The *Cyanobacteria* phylum is also abundant in these systems, but it is less represented in comparison to mats and microbialites. Regarding the eukaryotic taxa, diatoms are key structural components in most of the microbial ecosystems studied. The genera of diatoms identified were *Achnanthes*, *Fallacia*, *Halamphora*, *Mastogloia*, *Navicula*, *Nitzschia*, and *Surirella*. Normally, in the mats and microbialites, diatoms form nano-globular carbonate aggregates with filamentous cyanobacteria and other prokaryotic cells, suggesting their participation in the mineral precipitation process. This work expands our knowledge of the microbial ecosystems inhabiting the extreme environments from the Central Andes region, which is important to ensure their protection and conservation.

Keywords: Andean lakes, microbial mats, microbialites, endoevaporites, extremophiles

INTRODUCTION

The Salar de Atacama (**Figure 1**), located in the Chilean Central Andes, is one of the Earth's largest evaporite basins (ca. 3,000 km^2) (Alonso and Risacher, 1996). It comprises numerous hypersaline lakes, locally called "lagunas," at the edge of which evaporitic crusts form. A combination of extreme environmental conditions, such as high altitude, low barometric pressure, high solar and UV radiation, low rates of precipitation, high rates of evaporation, high salinity, strong winds, wide daily range in temperatures and the occurrence of hydrothermal activity makes this area one of the best primitive Earth analogs. Consequently, the study of the Andean microbial ecosystems (AMEs) that thrive in this environment may help us improve our understanding of the earliest complex ecosystems on Earth, as well as provide information for the search for life on other planets (Cabrol et al., 2009; Vignale et al., 2021).

In recent years, a variety of AMEs have been reported and studied in the Salar de Atacama. These include microbial mats at Laguna Cejar (∼2,300 m a.s.l.) (Rasuk et al., 2016), Laguna Tebenquiche (∼2,340 m a.s.l.) (Thiel et al., 2010; Farías et al., 2014; Fernandez et al., 2016; Kurth et al., 2021), Laguna Chaxa (∼2,300 m a.s.l.) (Thiel et al., 2010), and Laguna Brava (∼ 2,300 m a.s.l.) (Farías et al., 2014; Farias et al., 2017; Kurth et al., 2021); microbialites at Laguna Brava (Farías et al., 2014; Farias et al., 2017) and Laguna Interna (∼2,300 m a.s.l.) (Osman et al., 2021); and gypsum endoevaporites at Laguna de la Piedra (∼2,300 m a.s.l.) (Stivaletta et al., 2011) and Laguna Tebenquiche (Farías et al., 2014; Fernandez et al., 2016). Microbial mats are vertically laminated biofilms that occasionally lithify, forming organosedimentary structures called microbialites (Stolz, 2000). The mineralization of mats can be microbially induced or microbially influenced. In the former, microbial metabolic activities (e.g., photosynthesis, sulfate reduction, nitrate-driven sulfide oxidation) induce conditions for mineral precipitation, while in the latter, external environmental processes (e.g., degassing, evaporation) create the conditions for mineral precipitation. An organic matrix comprised of extracellular polymeric substances (EPS) is, however, involved in both microbially mediated mineralizations providing a template for mineral nucleation (Dupraz and Visscher, 2005; Dupraz et al., 2009). In the high-altitude Andean lakes (HAALs) of the Central Andes, both mineralization processes take place (Gomez et al., 2014, 2018; Vignale et al., 2021). Evaporites, on the other hand, are salt deposits precipitated from a saturated brine via solar evaporation (Warren, 2016). Occasionally, they present endolithic microbial communities named endoevaporites. The minerals that form the evaporites, mainly halite (NaCl) and gypsum ($CaSO_4{\cdot}2H_2O$), provide protection against desiccation and UV-B radiation but allow photosynthetically active radiation (400–700 nm) to pass through, which is important for the development of photoautotrophs (Stivaletta et al., 2011; Rasuk et al., 2014; Fernandez et al., 2016; Vignale et al., 2021).

The aim of this study is to expand our knowledge of the AMEs in the extreme environments of Salar de Atacama. To fulfill this objective, first we identified previously unknown microbial ecosystems (biofilms, microbial mats, microbialites, and endoevaporites) in eight different lakes and wetlands from Salar de Atacama, and then we analyzed the composition of their mineral phase and microbiota. Finally, we performed comparative analyses of the data to determine if there was a correlation between these features.

MATERIALS AND METHODS

Sample Collection

In the first place, a delimitation of the study area (**Figure 1**) was performed through the analysis of satellite and aerial images obtained from Google Earth and a DJI® Mavic Pro drone, respectively. Afterward, three field campaigns (24–28 November 2017, 24–26 November 2018, and 17 May 2018) were carried out to explore the respective area and search for AMEs.

In total, twenty previously undescribed AMEs were identified in eight different lakes and wetlands from the middle-east and south-east regions of Salar de Atacama. These are a floating biofilm from Tilopozo (T); microbial mats from Aguas de Quelana (Q1 and Q2), Laguna Salada (S1), Laguna La Punta (P1 and P2) and Laguna Brava (B1); microbialites from Laguna Chaxa (CH1, CH2, and CH3), Laguna Interna (I), Laguna La Punta (P3) and Laguna Brava (B2, B3, and B4); endoevaporites from Laguna Barros Negros (BN1, BN2, and BN3); a microbial community within an Andean flamingo (*Phoenicoparrus andinus*) mound nest from Laguna Salada (S2) and a sediment-associated microbial community from Aguas de Quelana (Q3).

Bulk samples were taken from the respective AMEs to perform mineralogy and scanning electron microscopy (SEM) analyses. These samples were stored in the dark at 4°C, and processed within 1–2 weeks. Additionally, samples were taken from different layers of the AMEs to perform 16S rRNA diversity analyses (**Table 1**). These samples were stored in RNAlater® solution (Thermo Fisher Scientific, United States) at 4°C in the dark, and processed within a week.

Bulk Mineralogy Analyses

The mineral composition of the samples was determined by X-ray diffraction (XRD) analyses, which were carried out on finely ground sample material (<20 μm) employing a PANalytical X'Pert Pro Multipurpose Powder Diffractometer, with a Cu X-ray source ($k\alpha$ = 1.5403 Å), operated at 40 kV and 40 mA at Centro de Investigaciones Geológicas (CIG), La Plata, Argentina. The dried and ground samples were scanned from 2 to 40 2θ, with a scanning speed of 0.04°/s and a time per step of 0.50 s. For each XRD pattern, semi-quantification of the minerals was obtained from the intensity of the main peaks (Schultz, 1964; Moore and Reynolds, 1989). The mineral composition of the samples was used to perform a chloride, sulfate and carbonate ternary diagram with the R package ggtern (Hamilton and Ferry, 2018).

Scanning Electron Microscopy (SEM) Analyses

Samples were fixed overnight at 4°C in modified Karnovsky fixative, composed of formaldehyde (8% v/v), glutaraldehyde

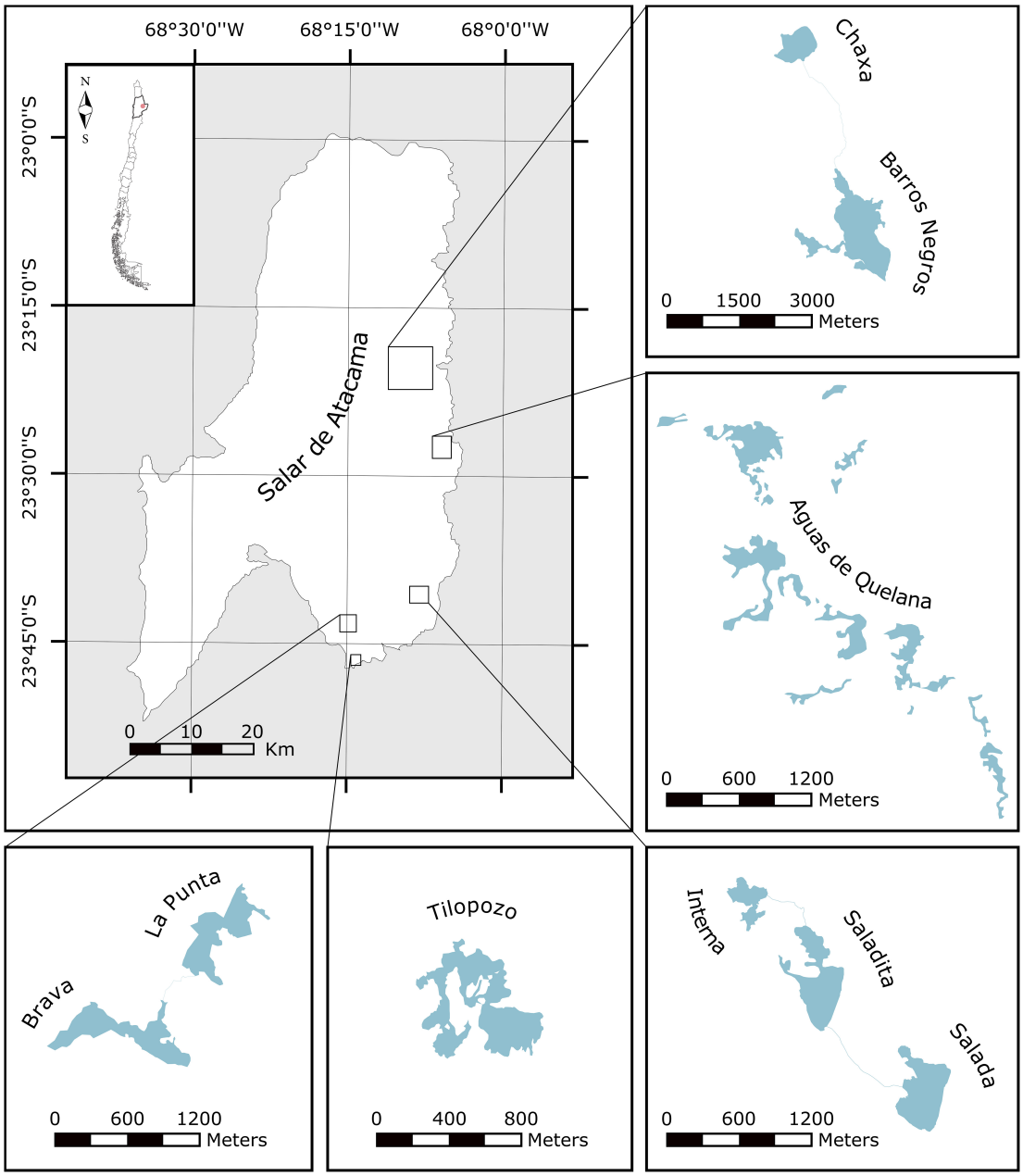

FIGURE 1 | Location of the study area which consists of a system of several lakes and wetlands. The eight lakes and wetlands of this study are outlined in the five respective inserts.

(16% v/v) and phosphate-buffered saline (PBS; 0.2 M, pH 7.4). Afterward, the samples were washed three times with PBS and calcium chloride ($CaCl_2$) for 10 min, and fixed with osmium tetroxide (2% v/v) overnight. Finally, after washing twice with ethanol (30% v/v) for 10 min, the samples were dried at critical point and sputtered with gold. Specimens were observed under vacuum using a Zeiss Supra 55VP (Carl Zeiss NTS GmbH, Germany) scanning electron microscope at Centro Integral de Microscopía Electrónica (CIME), Tucumán, Argentina. Biofilm from Tilopozo could not be imaged using SEM due to difficulties encountered during sample preparation. Identification of diatom taxa, based on morphological features of their frustules, was carried out employing SEM images and identification keys (Cristóbal et al., 2020). The morphological features analyzed were: size, shape and symmetry of valves; presence, location and structure of the axial area; presence, location and structure of raphe; presence of septa; presence and structure of costae; location, structure and density of striae; and presence of stauros, among others.

TABLE 1 | Overview of samples used to perform 16S rRNA diversity analyses, locations and coordinates.

Sample label	Lake/ Wetland	Sample description	GPS location [UTM]	Elevation [m]
CH1	Chaxa	Biofilm over microbialite	584877 E, 7419856 N	2,305
CH2A	Chaxa	Microbial mat over microbialite, first layer	584754 E, 7419856 N	2,305
CH2B	Chaxa	Microbial mat over microbialite, second layer	584754 E, 7419856 N	2,305
CH2C	Chaxa	Microbial mat over microbialite, third layer	584754 E, 7419856 N	2,305
CH3	Chaxa	Biofilm over microbialite	584877 E, 7419709 N	2,305
BN1A	Barros Negros	Endoevaporite, first layer	584580 E, 7416203 N	2,305
BN1B	Barros Negros	Endoevaporite, second layer	584580 E, 7416203 N	2,305
BN1C	Barros Negros	Endoevaporite, third layer	584580 E, 7416203 N	2,305
BN2A	Barros Negros	Endoevaporite, first layer	586132 E, 7416056 N	2,305
BN2B	Barros Negros	Endoevaporite, second layer	586132 E, 7416056 N	2,305
BN3A	Barros Negros	Endoevaporite, first layer	586132 E, 7416056 N	2,305
BN3B	Barros Negros	Endoevaporite, second layer	586132 E, 7416056 N	2,305
BN3C	Barros Negros	Endoevaporite, third layer	586132 E, 7416056 N	2,305
Q1A	Aguas de Quelana	Microbial mat, first layer	592225 E, 7408159 N	2,305
Q1B	Aguas de Quelana	Microbial mat, second layer	592225 E, 7408159 N	2,305
Q1C	Aguas de Quelana	Microbial mat, third layer	592225 E, 7408159 N	2,305
Q2A	Aguas de Quelana	Microbial mat, first layer	592048 E, 7405582 N	2,305
Q2B	Aguas de Quelana	Microbial mat, second layer	592048 E, 7405582 N	2,305
Q2C	Aguas de Quelana	Microbial mat, third layer	592048 E, 7405582 N	2,305
Q3	Aguas de Quelana	Sediment	592248 E, 7409988 N	2,305
IA	Interna	Microbial mat over microbialite, first layer	586221 E, 7382261 N	2,305
IB	Interna	Microbial mat over microbialite, second layer	586221 E, 7382261 N	2,305
IC	Interna	Microbial mat over microbialite, third layer	586221 E, 7382261 N	2,305
S1A	Salada	Microbial mat, first layer	587747 E, 7380714 N	2,305
S1B	Salada	Microbial mat, second layer	587747 E, 7380714 N	2,305
S2A	Salada	Endolithic microbial community inhabiting an Andean flamingo mound nest, first layer	587635 E, 7380585 N	2,305
S2B	Salada	Endolithic microbial community inhabiting an Andean flamingo mound nest, second layer	587635 E, 7380585 N	2,305
T	Tilopozo	Floating biofilm	577847 E, 7370337 N	2,312
P1A	La Punta	Microbial mat associated with vegetation, first layer	578154 E, 7376594 N	2,305
P1B	La Punta	Microbial mat associated with vegetation, second layer	578154 E, 7376594 N	2,305
P1C	La Punta	Microbial mat associated with vegetation, third layer	578154 E, 7376594 N	2,305
P2A	La Punta	Microbial mat associated with vegetation, first layer	577965 E, 7376601 N	2,305
P2B	La Punta	Microbial mat associated with vegetation, second layer	577965 E, 7376601 N	2,305
P2C	La Punta	Microbial mat associated with vegetation, third layer	577965 E, 7376601 N	2,305
P3	La Punta	Biofilm over microbialite	577784 E, 7376362 N	2,305
B1A	Brava	Microbial mat, first layer	576689 E, 7376362 N	2,305
B1B	Brava	Microbial mat, second layer	576689 E, 7376362 N	2,305
B1C	Brava	Microbial mat, third layer	576689 E, 7376362 N	2,305
B2	Brava	Biofilm over microbialite	576689 E, 7375484 N	2,305
B3A	Brava	Microbial mat over microbialite, first layer	575982 E, 7375291 N	2,305
B3B	Brava	Microbial mat over microbialite, second layer	575982 E, 7375291 N	2,305
B4A	Brava	Microbial mat over microbialite, first layer	576459 E, 7375524 N	2,305
B4B	Brava	Microbial mat over microbialite, second layer	576459 E, 7375524 N	2,305
B4C	Brava	Microbial mat over microbialite, third layer	576459 E, 7375524 N	2,305

DNA Extraction and Amplicon Sequencing

Total genomic DNA was isolated from the samples, detailed in **Table 1**, using the FastDNA® SPIN Kit for Soil (MP Biomedicals, United States) according to the protocol provided by the manufacturer. DNA yield (ng μl^{-1})

was quantified spectrophotometrically with a NanoDrop 2000c Spectrophotometer (Thermo Fisher Scientific, United States). NanoDrop was also used to estimate the purity of the extracted DNA. Sample BN3A could not be further processed as not enough DNA was extracted from it. The hypervariable regions V3 and V4 of the bacterial and archaeal 16S rRNA gene were amplified using the primers Bakt_341F (CCTACGGGNGGCWGCAG) and Bakt_805R (GACTACHVGGGTATCTAATCC). The amplicons obtained were sequenced by Macrogen Inc., (Seoul, South Korea) using an Illumina MiSeq sequencer platform. Raw sequences were submitted to the ENA Project database under the accession number PRJEB44218.

Bioinformatics

Raw Sequence data were analyzed with the software package QIIME 2 v.2018.2, following the tutorials provided by the developers (Caporaso et al., 2010; Bolyen et al., 2018). Taxonomic annotation was performed in QIIME 2 using the SILVA database (No. 132, April 2018) (Quast et al., 2013) trained with 16S rRNA genes grouped in OTUs with 97% similarity. OTUs classified as coming from chloroplast or mitochondria were removed before further analyses. The R package phyloseq (McMurdie and Holmes, 2013) was used to calculate alpha diversity metrics (Chao1, ACE, Shannon and Simpson) after rarefying the data, and perform a principal coordinate analysis (PCoA) based on Bray-Curtis dissimilarity. The R package vegan (Oksanen et al., 2013) was used to perform a redundancy analysis (RDA) and correlate mineralogy with the microbial composition of the samples. Permutational ANOVA (PERMANOVA) tests were also carried out with the R package vegan to evaluate the PCoA and RDA analyses.

RESULTS

Microbial Ecosystems Discovered in Salar de Atacama

The exploration carried out in the middle-east and south-east regions of Salar de Atacama allowed us to identify and study twenty previously unreported AMEs in eight different lakes and wetlands: Laguna Chaxa, Laguna Barros Negros, Aguas de Quelana, Laguna Interna, Laguna Salada, Laguna La Punta, Laguna Brava, and Tilopozo.

Laguna Chaxa is a small lake (∼0.35 km^2 area) from the middle-east region of Salar de Atacama (**Figure 1**). A previous study reported the presence of red–purple-colored microbial mats developing in this lake (Thiel et al., 2010). In addition to these microbial mats, we have discovered modern microbialites developing in this environment (**Figure 2**). Some of these microbialites are covered by black or pink biofilms (CH1 and CH3, respectively), while others are covered by microbial mats that usually display a sequence of (from top to bottom) pink/orange, green and purple colored layers (CH2).

Two kilometers south from Laguna Chaxa is Laguna Barros Negros (∼1.38 km^2 area) (**Figure 1**). In this lake, contrary to Laguna Chaxa, we have identified numerous microbial communities developing inside evaporite deposits (endoevaporites) forming colored strata (**Figure 2**). Normally, a yellow/orange layer (ca. 0.5–2 cm thick) is visible on the top, followed by a green layer of similar thickness (BN2). In some cases, a third purple layer is visible at the bottom as well (BN1 and BN3).

Aguas de Quelana is a wetland complex (∼1.5 km^2 area) also located in the middle-east region of Salar de Atacama (**Figure 1**). Neither microbialites nor endoevaporites could be identified in the explored area of this environment. Nevertheless, microbial mats (Q1 and Q2) and pink/orange sediment-associated microbial communities (Q3) were observed along the shorelines (**Figure 2**). Like the endoevaporites from Laguna Barros Negros, the microbial mats form colored strata. Normally, the first layer (rich in EPS) varies in color and thickness (ca. 0.1–0.3 cm) from one mat to another, while the second and third layers are green and purple, respectively, and usually have a similar thickness (ca. 0.2 cm). Occasionally, a dark layer can be found at the bottom as well. When mats are exposed to the air, a white evaporitic crust covers their surface. Cerebroid, snake and globular morphologies have been observed in these microbial mats, which usually accumulate gas at the subsurface.

Laguna Interna (∼0.08 km^2 area) and Laguna Salada (∼0.18 km^2 area) are two connected lakes located in the south-east region of Salar de Atacama (**Figure 1**). In Laguna Interna, we have discovered modern microbialites (I) that exhibit a laminated mesostructure (stromatolites), covered by microbial mats that usually display a sequence of (from top to bottom) pink/orange, green and purple colored layers (**Figure 2**). These microbialites are similar to those recently reported in this environment (Osman et al., 2021). In Laguna Salada, on the contrary, we have identified microbial mats (S1) that form colored strata (**Figure 2**). Typically, a pink/orange layer (ca. 0.1–0.2 cm thick) is visible on the top, followed by a green layer of similar thickness. Some of these microbial mats are close to Andean flamingo mound nests which are, in most of the cases, no longer used by the wading birds. The dissection of these mound nests revealed endolithic microbial communities (S2) forming colored strata, similar to the ones present in the evaporite deposits from Laguna Barros Negros (**Figure 2**). As far as we know, this is the first work to report a microbial ecosystem of this kind in the Central Andes.

Laguna La Punta (∼0.16 km^2 area) and Laguna Brava (∼0.20 km^2 area) are two connected lakes from the south of Salar de Atacama that have already been explored (**Figure 1**). Nevertheless, in both lakes, we have identified previously unknown microbial mats and microbialites. In Laguna La Punta, we have discovered microbial mats associated with vegetation (P1 and P2) that usually display a sequence of (from top to bottom) pink/orange, green and purple colored layers, with cerebroid, snake and globular morphologies, as well as microbialites covered by black biofilms (P3) (**Figure 2**). Whereas in Laguna Brava, we have discovered red-green-colored microbial mats (B1), oncoids (microbialites that display a concentrically laminated mesostructure) (Logan et al., 1964) covered by black biofilms (B2) and microbialites covered by microbial mats (B3 and B4) that usually display a sequence of (from top to bottom) pink/orange, green and purple colored layers (**Figure 2**).

FIGURE 2 | General views of the AMEs discovered in Salar de Atacama. CH1, CH2 and CH3, Microbialites from Laguna Chaxa; BN1, BN2 and BN3, Endoevaporites from Laguna Barros Negros; Q1 and Q2, Microbial mats from Aguas de Quelana; Q3, Sediment-associated microbial community from Aguas de Quelana; I, Microbialite from Laguna Interna; S1, Microbial mat from Laguna Salada; S2, Microbial community within an Andean flamingo mound nest from Laguna Salada; P1 and P2, Microbial mats from Laguna La Punta; P3, Microbialite from Laguna La Punta; B1, Microbial mat from Laguna Brava; B2, B3 and B4, Microbialites from Laguna Brava; T, Floating biofilm from Tilopozo.

The last system prospected was Tilopozo (~0.34 km^2 area), a wetland complex located in the south region of Salar de Atacama (**Figure 1**). Compared to the other systems studied, we have not identified in this environment carbonate or evaporite deposits associated with microbial communities. Instead, we have discovered green floating biofilms (T) covering a great proportion of the wetland surface (**Figure 2**).

Mineralogical Analyses

X-ray diffraction analyses were carried out on the samples collected (**Supplementary Figures 1–3**) to determine and compare the mineralogical composition of the AMEs studied (**Figure 3** and **Supplementary Table 1**). The endoevaporites from Laguna Barros Negros (BN1, BN2 and BN3), as well as the microbial community within the Andean flamingo mound nest from Laguna Salada (S2) are mainly formed by gypsum (ca. 40–65%) and halite (ca. 10–65%), which probably explain their morphological similarities. As the endoevaporite BN3 was located in a drier area compared to the rest of the endoevaporites from Laguna Barros Negros, it also contains a considerable amount (ca. 25%) of anhydrite ($CaSO_4$).

The microbial mats from Aguas de Quelana (Q2) and Laguna Salada (S1) are comprised predominantly of halite (ca. 25–65%), aragonite ($CaCO_3$) (ca. 25–40%) and calcite ($CaCO_3$) (ca. 25–40%). Whereas the microbial mats from Laguna La Punta (P1 and P2) and Laguna Brava (B1), as well as the pink/orange sediment

from Aguas de Quelana (Q3), are composed mainly of halite (ca. 10–80%) and aragonite (ca. 10–80%), but do not contain great amounts of calcite (ca. 1–3%). This is also observed in the microbial mat Q1 from Aguas de Quelana, which is deficient in calcite (ca. 1%) but contains a considerable amount of aragonite (ca. 40%), halite (ca. 40%) and gypsum (ca. 25%).

The microbialites from Laguna Chaxa (CH1, CH2 and CH3), Laguna Brava (B3 and B4) and Laguna La Punta (P3), the stromatolite from Laguna Interna (I), and the oncoid from Laguna Brava (B2) are mostly formed by aragonite (ca. 10–80%) and halite (ca. 10–80%). In addition to these minerals, the stromatolite from Laguna Interna (I) contains a great proportion of calcite (ca. 25%), and the microbialite from Laguna La Punta (P3) contains considerable amounts of gypsum (ca. 10%) and opal-A ($SiO_2 \cdot nH_2O$) (ca. 10%).

The floating biofilm from Tilopozo (T) has a mineralogical composition quite different from the rest of the microbial ecosystems studied. Although its principal component is calcite (ca. 65%), it also contains clay (ca. 25%), dolomite ($CaMg(CO_3)_2$) (ca. 25%), quartz (SiO_2) (ca. 10%), siderite ($FeCO_3$) (ca. 10%) and dawsonite ($NaAlCO_3(OH)_2$) (ca. 10%) in great proportion.

Scanning Electron Microscopy Analyses

Scanning electron microscopy analyses were performed on the samples to study the association of the prokaryotic and eukaryotic microorganisms with the minerals present in the AMEs studied (**Figure 4** and **Supplementary Figures 4–6**). The SEM images obtained from the microbialite samples (**Figure 4A** and **Supplementary Figure 4**) revealed the presence of diatoms (*Bacillariophyceae*), filamentous cyanobacteria and other prokaryotic cells (cocci and bacilli) forming nano-globular carbonate aggregates, which suggests their participation in the mineral precipitation process (Gomez et al., 2018). Based on morphological characteristics, we could identify at least four families of diatoms: *Achnanthaceae* (*Achnanthes* spp.), *Bacillariaceae* (*Nitzschia* spp.), *Catenulaceae* (*Halamphora* spp.), and *Naviculaceae* (*Navicula* spp.). A multicellular eukaryotic organism was also identified in one of the microbialite samples (CH1). This was a free-living roundworm (*Nematoda*) that, based on the shape of its mouth (hollow tube) (**Supplementary Figure 4**), feeds on the prokaryotes that cover the microbialites (McSorley, 1997).

The SEM images of the endoevaporites and the endolithic microbial community inhabiting the Andean flamingo mound nest (**Figure 4B** and **Supplementary Figure 5**) also revealed the presence of diatoms, filamentous cyanobacteria and other prokaryotic cells (bacilli). In this case, the identified families of diatoms were *Achnanthaceae* (*Achnanthes* spp.) and *Naviculaceae* (*Navicula* spp.). But compared to the microbialite systems, the number of diatoms and filamentous cyanobacteria in these systems seemed to be lower.

In the microbial mats and pink/orange sediment (**Figure 4C** and **Supplementary Figure 6**), the SEM images showed a great number of diatoms, filamentous cyanobacteria, and other prokaryotic cells (cocci and spirochetes). Like in the microbialites, these microorganisms form aggregates with precipitation of nano-globular carbonates, suggesting their participation in the mineral precipitation process (Gomez et al., 2018). The families of diatoms identified in the microbial mats were *Achnanthaceae* (*Achnanthes* spp.), *Bacillariaceae* (*Nitzschia* spp.), *Catenulaceae* (*Halamphora* spp.), *Mastogloiaceae* (*Mastogloia* spp.), *Naviculaceae* (*Navicula* spp.), and *Surirellaceae* (*Surirella* spp.), while the families of diatoms identified in the pink/orange sediment were *Achnanthaceae* (*Achnanthes* spp.), *Bacillariaceae* (*Nitzschia* spp.), *Catenulaceae* (*Halamphora* spp.), *Mastogloiaceae* (*Mastogloia* spp.), *Naviculaceae* (*Navicula* spp.), *Sellaphoraceae* (*Fallacia* spp.), and *Surirellaceae* (*Surirella* spp.). Free-living roundworms were also observed in the microbial mats (P1 and P2), supporting their role as bacterivorous in these systems.

Taxonomy-Based Analyses

Molecular diversity analyses based on the small subunit ribosomal (SSU) rRNA of *Bacteria* and *Archaea* were carried out on the samples (**Table 1**) to determine the prokaryotic composition of the AMEs studied. The results revealed that the taxonomic composition of prokaryotes not only differs between types of AMEs, but also between their layers (**Figure 5**).

The dominant phyla in the majority of the microbial mats are *Bacteroidetes* (ca. 8.78–66.95%) and *Proteobacteria* (ca. 8.59–52.96%), followed by *Cyanobacteria* (ca. 0.41–29.15%), *Firmicutes* (ca. 0.02–27.19%), *Chloroflexi* (ca. 0–23.10%), and *Spirochetes* (ca. 0.02–18.44%). *Planctomycetes* (ca. 0.48–19.27%) and *Verrucomicrobia* (ca. 0.41–5.33%) phyla are also well-represented (**Figure 5A**). Within the phylum *Proteobacteria*, the most abundant classes are *Alphaproteobacteria* (ca. 5.23–31.23%), *Gammaproteobacteria* (ca. 1.09–27.24%), and *Deltaproteobacteria* (ca. 0.35–17.29%) (**Supplementary Figures 7**, **8**). While in the phylum *Bacteroidetes*, the most abundant classes are *Bacteroidia* (ca. 0.54–62.70%) and *Rhodothermia* (ca. 0.38–29.85%) (**Supplementary Figures 7**, **9**).

In most carbonate microbialites, *Proteobacteria* (ca. 24.28–50.00%) and *Bacteroidetes* (ca. 11.14–47.73%) are the dominant phyla, followed by *Cyanobacteria* (ca. 1.87–18.08%) and *Chloroflexi* (ca. 0.01–12.89%). *Planctomycetes* (ca. 0.51–21.55%) and *Verrucomicrobia* (ca. 0.30–12.59%) phyla are also abundant, especially in Laguna Brava samples. Contrary to microbial mats, the phylum *Firmicutes* is underrepresented in the majority of the microbialites, except in the ones from Laguna La Punta (P3), Laguna Interna (I) and Laguna Brava (B3) (ca. 44.37%, 1.84–19.83%, and 2.68–12.45%, respectively) (**Figure 5A**). Within the phylum *Proteobacteria*, the most abundant classes are *Alphaproteobacteria* (ca. 10.97–32.96%), *Gammaproteobacteria* (ca. 3.74–24.20%) and *Deltaproteobacteria* (ca. 0.62–18.12%) (**Supplementary Figures 7**, **8**). Whereas in the phylum *Bacteroidetes*, the most abundant classes are *Bacteroidia* (ca. 1.82–29.32%) and *Rhodothermia* (ca. 0.59–26.29%) (**Supplementary Figures 7**, **9**). Like in microbial mats and microbialites, the dominant phyla in the pink/orange sediment are *Proteobacteria* (ca. 38.47%) and *Bacteroidetes* (ca. 31.01%), followed by *Chloroflexi* (ca. 6.79%), *Spirochetes* (ca. 4.15%), and *Cyanobacteria* (ca. 3.74%) (**Figure 5A**).

The taxonomic composition of gypsum endoevaporites differs greatly from that of microbial mats and microbialites.

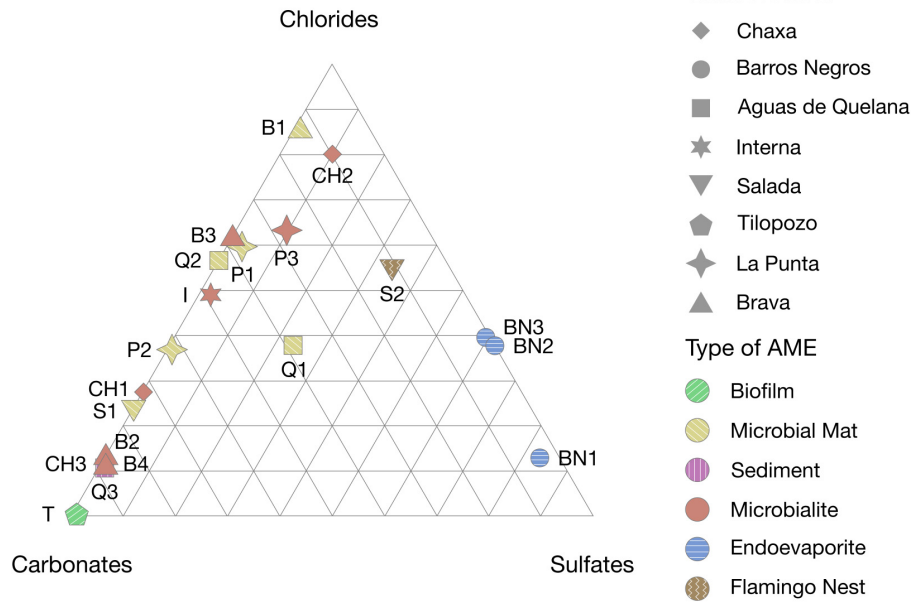

FIGURE 3 | Ternary diagram representing the mineral composition of the AMEs. The shapes and colors indicate the location and type of AME, respectively.

Proteobacteria (ca. 14.03–48.24%), *Bacteroidetes* (ca. 21.29–44.39%), and *Euryarchaeota* (ca. 0.40–43.04%) phyla dominate the majority of these microbial ecosystems. The *Cyanobacteria* phylum is also abundant (ca. 0.24–14.36%), but in comparison to microbial mats and microbialites, it is less represented (**Figure 5A**). Within the phylum *Proteobacteria*, the most abundant classes are *Alphaproteobacteria* (ca. 8.39–23.79%) and *Gammaproteobacteria* (ca. 4.58–23.04%). *Deltaproteobacteria* class is present, but underrepresented (ca. 1.06–2.63%) (**Supplementary Figures 7**, **8**). The most abundant classes in the *Bacteroidetes* phylum are *Rhodothermia* (ca. 20.40–41.99%) and *Bacteroidia* (ca. 0.88–4.98%). Interestingly, in all the endoevaporites, *Rhodothermia* class is more abundant than *Bacteroidia* class. However, in most of the microbial mats and microbialites, *Bacteroidia* class is more abundant than *Rhodothermia* class (**Supplementary Figures 7**, **9**). Within the *Euryarchaeota* phylum, the dominant class is *Halobacteria* (ca. 0.40–43.05%) (**Supplementary Figure 7**). Another interesting observation is the low proportion of *Firmicutes* (ca. 0.06–3.05%), *Spirochetes* (ca. 0.02–1.39%), *Verrucomicrobia* (ca. 0.02–1.23%), *Chloroflexi* (ca. 0.00–0.39%), and *Deinococcus-Thermus* (0.01–0.29%) phyla, which are normally well-represented in the microbial mats and microbialites. The taxonomic composition of the Andean flamingo mound nest resulted to be similar to that of gypsum endoevaporites, with *Proteobacteria* (ca. 18.45–48–63%), *Euryarchaeota* (ca. 14.56–47.94%) and *Bacteroidetes* (ca. 17.27–24.60%) as the dominant phyla (**Figure 5A**).

Regarding the taxonomic depth distributions (**Figure 5B**), in the microbial mats, *Deinococcus-Thermus* (1° layer: 0–14.93%, 2° layer: 0–4.66%, 3° layer: 0–0.51%), *Firmicutes* (1° layer: 0.09–27.19%, 2° layer: 0.02–16.16%, 3° layer: 0.03–0.90%) and *Bacteroidetes* (1° layer: 23.04–66.95%, 2° layer: 11.79–25.72%, 3° layer: 8.78–18.78%) taxa normally reduce their abundance with depth. While *Calditrichaeota* (1° layer: 0–0.22%, 2° layer: 0–0.12%, 3° layer: 0–3.76%), *Chloroflexi* (1° layer: 0–3.98%, 2° layer: 0–20.11%, 3° layer: 0.05–23.10%), *Spirochetes* (1° layer: 0.02–1.98%, 2° layer: 0.08–18.44%, 3° layer: 0.02–15.43%), *Deltaproteobacteria* (1° layer: 0.35–2.73%, 2° layer: 1.48–5.82%, 3° layer: 5.68–17.29%), and *Planctomycetes* (1° layer: 0.48–3.09%, 2° layer: 1.63–10.83%, 3° layer: 2.17–19.27%) taxa increase it. The *Cyanobacteria* phylum, contrary to other taxa, is more abundant in the middle layers than in the upper or lower ones (1° layer: 1.73–22.32%, 2° layer: 4.55–29.15%, 3° layer: 0.41–10.90%). With regard to *Gammaproteobacteria* (1° layer: 1.09–26.45%, 2° layer: 2.18–27.03%, 3° layer: 1.75–27.24%) and *Alphaproteobacteria* (1° layer: 5.79–22.04%, 2° layer: 5.24–31.22%, 3° layer: 5.79–19.38%) taxa, no common patterns are observed. Although the microbialites CH2, I, B3, and B4 are covered by microbial mats, their taxa do not present depth-related distribution patterns. In the endoevaporites and the Andean flamingo mound nest, the only depth-related distribution pattern observed is the abundance increase of *Patescibacteria* phylum with depth (1° layer: 0–1.15%, 2° layer: 0.29–3.90%, 3° layer: 0.51–2.58%).

Diversity Analyses

Alpha diversity metrics (Chao1 and Shannon indexes) were estimated, after even subsampling (rarefaction), to determine the community structure of each sample (**Figure 6A** and **Supplementary Table 2**). The comparison of these metrics, evaluated with Wilcoxon rank-sum test (Mann-Whitney) (Wilcoxon, 1945), revealed that both richness and diversity do not differ significantly ($P > 0.05$) between types of AMEs, nor between layers.

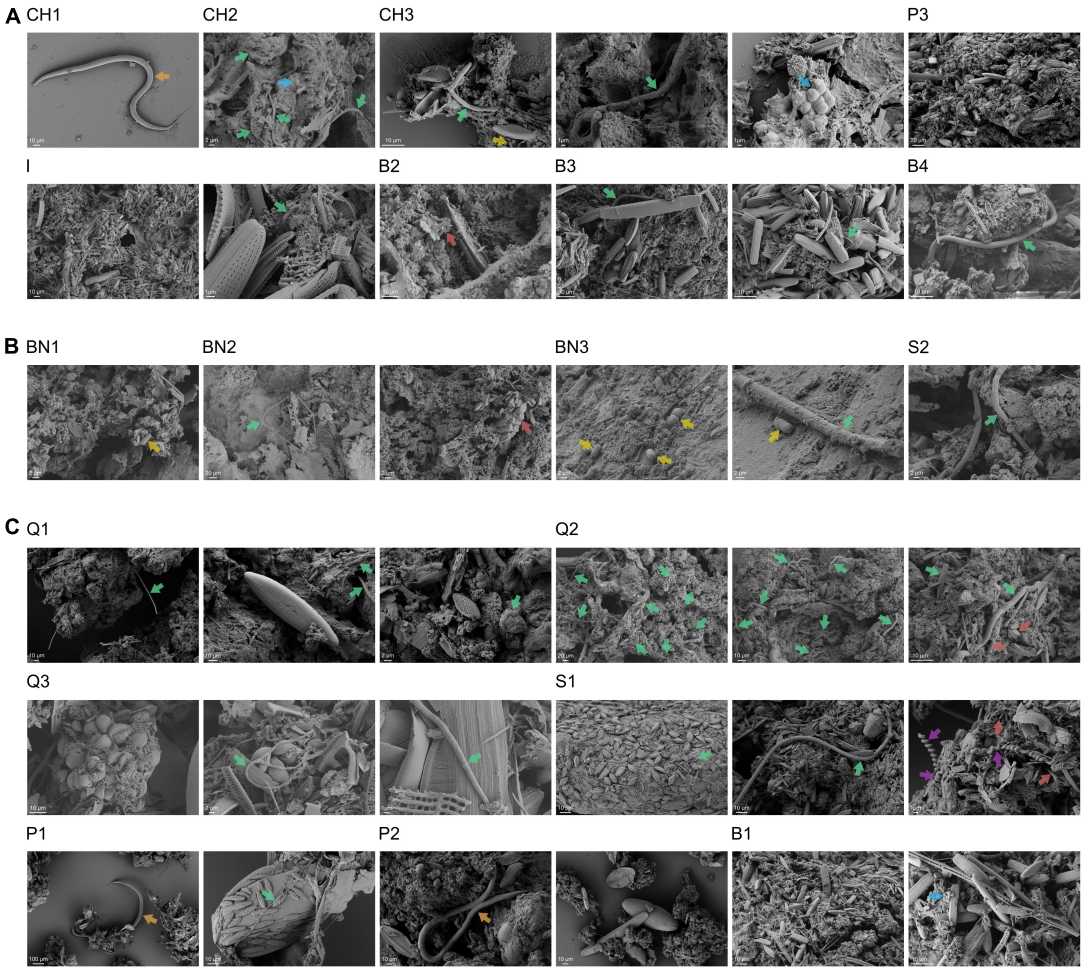

FIGURE 4 | Diatoms, filamentous cyanobacteria and other prokaryotic cells form nano-globular carbonate aggregates in most of the AMEs. **(A)** SEM images of the microbialites. CH1, CH2 and CH3, Microbialites from Laguna Chaxa; P3, Microbialite from Laguna La Punta; I, Microbialite from Laguna Interna; B2, B3 and B4, Microbialites from Laguna Brava. **(B)** SEM images of the endolithic microbial communities. BN1, BN2 and BN3, Endoevaporites from Laguna Barros Negros; S2, Microbial community within an Andean flamingo mound nest from Laguna Salada. **(C)** SEM images of the microbial mats and the pink/orange sediment. Q1 and Q2, Microbial mats from Aguas de Quelana; Q3, Sediment-associated microbial community from Aguas de Quelana; S1, Microbial mat from Laguna Salada; P1 and P2, Microbial mats from Laguna La Punta; B1, Microbial mat from Laguna Brava. Different recognized structures are marked with an arrow. Green arrow, Filamentous cyanobacterium; Blue arrow, Coccus; Yellow arrow, Bacillus; Purple arrow, Spirochete; Orange arrow, Nematode; Red arrow, Mineral grain.

Beta diversity was assessed through a principal coordinate analysis (PCoA) based on Bray-Curtis dissimilarity between endoevaporite, microbial mat, and microbialite samples (**Figure 6B**). Floating biofilm, sediment and Andean flamingo mound nest samples were not included as random factors as they do not present replicates. The PCoA plot showed a clear separation of the samples based on the type of AME (PERMANOVA, $R^2 = 0.152$, $P < 0.001$) and the site (PERMANOVA, $R^2 = 0.335$, $P < 0.001$) (**Supplementary Table 3**), with the largest variation observed between gypsum endoevaporites, and carbonate mats and microbialites (Axis 1, **Figure 6B**). Therefore, a redundancy analysis (RDA) was carried out to evaluate further the relationship between the mineralogy and the community composition of the samples (**Figure 6C**). The RDA plot confirmed what was observed in the PCoA analysis. Gypsum (PERMANOVA, $P < 0.001$) and anhydrite (PERMANOVA, $P < 0.01$) compositions are significantly correlated with the community composition of the endoevaporites, while calcite (PERMANOVA, $P < 0.001$) and aragonite (PERMANOVA, $P < 0.001$) compositions are significantly correlated with the community composition of the mats and microbialites (**Supplementary Table 4**).

DISCUSSION

The exploration of high-altitude lakes and wetlands in the middle-east and south-east regions of Salar de Atacama revealed a great number of previously undescribed AMEs, including floating biofilms, sediment-associated microbial communities, microbial mats, microbialites, endoevaporites and endolithic microbial communities inhabiting Andean flamingo mound

FIGURE 5 | Taxonomic composition of prokaryotes in the AMEs. **(A)** Relative abundance of the twenty major phyla in the different samples. B, Biofilm; MM, Microbial mat; S, Sediment; MI, Microbialite; EV, Endoevaporite; FN, Andean flamingo mound nest. **(B)** Graphical summary of taxa depth distributions observed in the microbial mats.

nests. Nevertheless, not all types of AMEs were found in every prospected environment. Floating biofilms were described in Tilopozo; sediment-associated microbial communities were reported in Laguna Salada; microbial mats were found in Aguas de Quelana, Laguna Salada, Laguna La Punta and Laguna Brava; microbialites were observed in Laguna Chaxa, Laguna Interna, Laguna La Punta and Laguna Brava; endoevaporites were detected in Laguna Barros Negros; and endolithic microbial communities inhabiting Andean flamingo mound nests were discovered in Laguna Salada. The presence of different types of AMEs in the lakes and wetlands studied could be partially explained by their distinct environmental and geochemical conditions (Stivaletta et al., 2011; Gomez et al., 2014; Suosaari et al., 2016; Bougeault et al., 2020; Vignale et al., 2021). Among these AMEs, the endolithic microbial community inhabiting the Andean flamingo mound nest could be considered one of the most interesting findings. Thus far, endoevaporites were the only microbial endolithic communities reported in the Central Andes environments (Vignale et al., 2021). Therefore, this discovery opens the possibility of finding new types of microbial endolithic communities in the salt flats of the region. Endolithic microorganisms are often the main form of life in

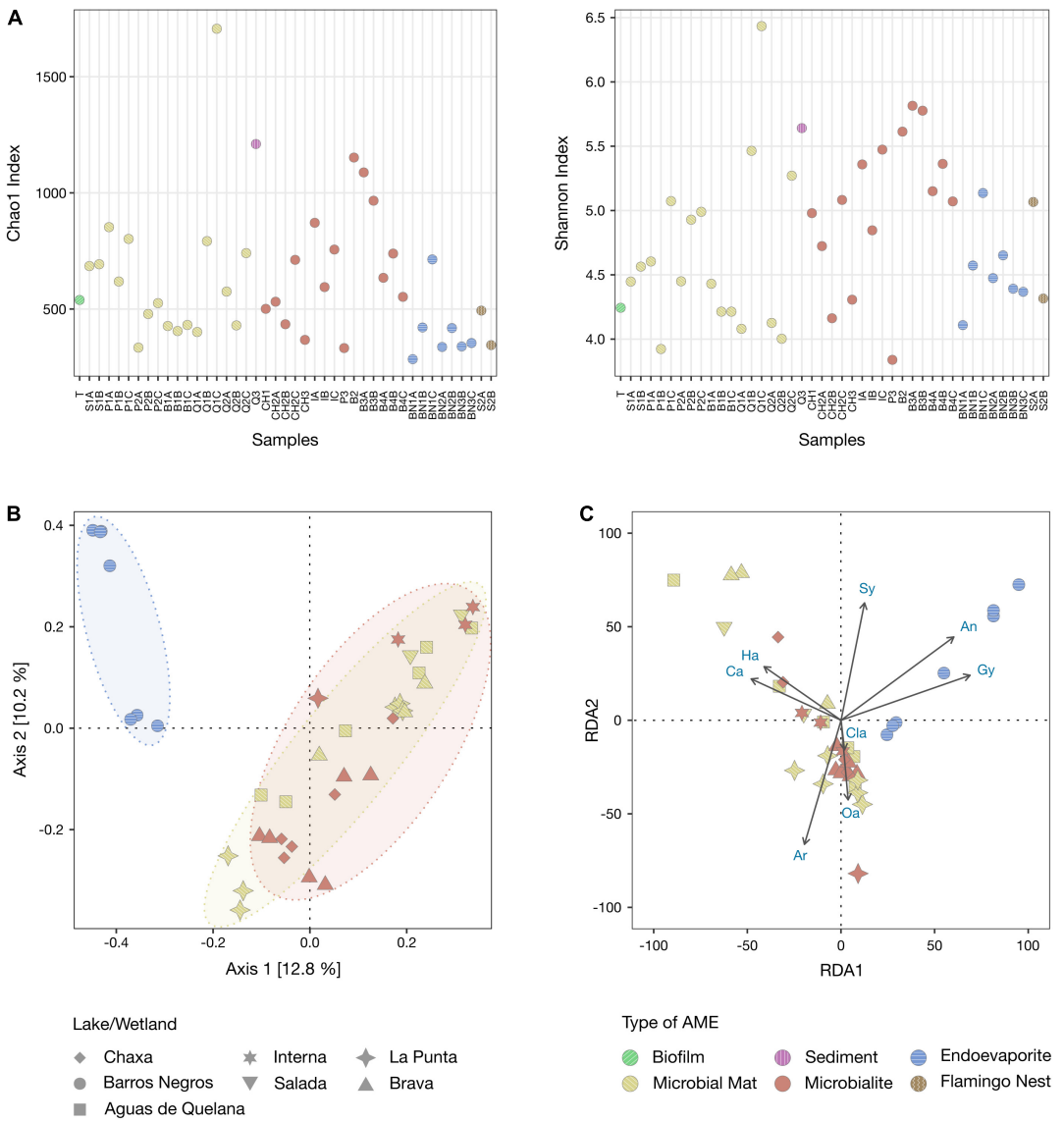

FIGURE 6 | Diversity analyses of the AMEs. **(A)** Comparison of alpha diversity metrics between samples. Left, richness estimates (Chao1 index) for the different samples. Right, diversity estimates (Shannon index) for the different samples. **(B)** Principal coordinate analysis (PCoA) based on Bray-Curtis dissimilarity between endoevaporite, microbial mat, and microbialite samples. **(C)** Redundancy analysis (RDA) of the relationship between minerals and endoevaporite, microbial mat, and microbialite samples. Arrows indicate the direction and magnitude of minerals associated with the samples. Ha, Halite; Ca, Calcite; Ar, Aragonite; Oa, Opal-A; Cla, Clay; Gy, Gypsum; An, Anhydrite; Sy, Sylvite.

the most extreme terrestrial climates, and thus could provide important clues about ancient life on the Earth or elsewhere in the Solar System (Walker et al., 2005).

The XRD analyses revealed diverse mineralogical compositions in the AMEs studied. Microbial mats and microbialites found in Laguna Chaxa, Aguas de Quelana, Laguna Interna, Laguna Salada, Laguna La Punta and Laguna Brava are mainly formed by halite and calcium carbonate, like the majority of the mats and microbialites previously described in Salar de Atacama (Thiel et al., 2010; Farías et al., 2014; Farias et al., 2017; Farías, 2020). However, in all the microbialites, calcium carbonate is mostly present as aragonite. While, in some microbial mats, calcium carbonate is present both as aragonite and calcite. There are several factors that could favor the precipitation of calcium carbonate as calcite or as aragonite. The presence of sulfate (SO_4^{2-}) or magnesium (Mg^{2+}) in solution (Berner, 1975; Walter, 1986), as well as a high rate of carbonate precipitation (Given and Wilkinson, 1985), could favor precipitation of aragonite. Whereas, the presence of phosphate (PO_4^{3-}) or iron (Fe^{2+}) in solution (Meyer, 1984; Walter, 1986) could favor precipitation of calcite. As we do not have measurements of these parameters, we cannot be certain which factor favors the precipitation of calcium carbonate as calcite or as aragonite in the microbial mats and microbialites

from this study. Therefore, water geochemical analyses should be carried out in the future to assess this interrogation. Contrary to microbial mats and microbialites, the endoevaporites from Laguna Barros Negros are mainly formed by gypsum and halite, like the previously studied endoevaporites from Laguna Tebenquiche (Farías et al., 2014; Fernandez et al., 2016). This mineral composition is also observed in the Andean flamingo mound nest from Laguna Salada, which could be explained by the fact that Andean flamingos build their mound nests with mud from the salt flat (Brown and King, 2005).

The SEM images of the microbial mats and microbialites studied revealed filamentous cyanobacteria and other prokaryotic cells (cocci, bacilli, and spirochetes) associated with diatom frustules forming nano-globular carbonate aggregates. Diatoms and cyanobacteria fix carbon dioxide and release oxygen through photosynthesis, which increases alkalinity and promotes carbonate precipitation (Dupraz and Visscher, 2005; Dupraz et al., 2009). The large amounts of EPS produced by them also influence carbonate precipitation, as the EPS matrix provides a template for carbonate nucleation (Dupraz and Visscher, 2005; Dupraz et al., 2009). Therefore, the formation of these nano-globular carbonate aggregates might suggest their participation in the mineral precipitation process (Gomez et al., 2018). Although diatoms and cyanobacteria seem to be key structural components in all the AMEs studied, a lower number of them were observed in the endoevaporites than in the microbial mats and microbialites. Microorganisms that colonize gypsum evaporites extract water from the gypsum crystals to withstand desiccation (Huang et al., 2020). However, under severe xeric conditions, this mechanism might not be enough for the development of diatoms and cyanobacteria, which could explain their lower abundance in the evaporite deposits. This hypothesis is supported by the lower abundance of cyanobacteria in the endoevaporite BN3 (ca. 0.24–0.28%), which is rich in anhydrite, than in the endoevaporites BN1 and BN2 (ca. 5.72–14.36% and 0.35–11.57%, respectively). The growth of diatoms in the gypsum evaporites could also be affected by a low silicon concentration in these systems (Martin-Jezequel et al., 2000). Most genera of diatoms identified in this work (*Navicula*, *Halamphora*, *Nitzschia*, *Achnanthes*, *Surirella*, and *Mastogloia*) have also been reported in other AMEs from the Central Andes (Farías et al., 2013, 2014; Rasuk et al., 2014; Albarracín et al., 2015; Gomez et al., 2018), which suggests a wide distribution of these taxa in the Central Andes environments.

Regarding the prokaryotic composition, differences have been observed between gypsum endoevaporites and carbonate mats and microbialites. Gypsum endoevaporites are dominated by *Proteobacteria*, *Bacteroidetes*, and *Euryarchaeota* phyla. The high halotolerance of *Bacteroidetes* and *Euryarchaeota* species could explain their great abundance in this type of AME (Farías et al., 2014). On the contrary, *Firmicutes*, *Spirochetes*, *Verrucomicrobia*, *Chloroflexi*, and *Deinococcus-Thermus* phyla are underrepresented. Probably, the moisture conditions of the evaporite deposits are not suitable for the correct growth of these microorganisms. Interestingly, a similar taxonomic composition has been observed in other gypsum endoevaporites from Salar de Atacama (Farías et al., 2014; Fernandez et al., 2016), which suggests a correlation between the microbiota and the mineralogy. Carbonate mats and microbialites are dominated by *Bacteroidetes* and *Proteobacteria* phyla, followed by *Cyanobacteria*, *Chloroflexi*, *Planctomycetes*, and *Verrucomicrobia* phyla. Oxygenic and anoxygenic phototrophs from *Cyanobacteria*, *Chloroflexi*, and *Proteobacteria* phyla, as well as sulfate reducers from *Deltaproteobacteria* class, increase alkalinity and promote carbonate precipitation, which could explain their great abundance in these types of AMEs (Dupraz et al., 2009). Other carbonate-rich mats and microbialites from Salar de Atacama (Farías et al., 2014; Fernandez et al., 2016) present a similar taxonomic composition, which further suggests a correlation between the microbiota and the mineralogy. Due to the previous observations, we performed a RDA analysis evaluated with a PERMANOVA test, and confirmed that gypsum, anhydrite, calcite and aragonite compositions are significantly correlated with the community composition of the samples. In the future, this could help us better understand the role of prokaryotes in the formation of the AMEs (Dupraz and Visscher, 2005; Dupraz et al., 2009).

The taxonomy-based analyses also revealed that certain microbial groups are arranged in a vertically organized structure in the microbial mats. This structure is normally determined by steep and fluctuating gradients of light, oxygen, hydrogen sulfide and pH, among other physicochemical gradients (Dupraz and Visscher, 2005; Dupraz et al., 2009). *Bacteroidetes*, *Firmicutes*, and *Deinococcus-Thermus* phyla are more abundant in the upper layers, probably due to the high resistance of their species to desiccation and/or ionizing radiation (Makarova et al., 2001; Rainey et al., 2005; Galperin, 2013; Yu et al., 2015). Species of the *Cyanobacteria* phylum are generally found in great proportion in the intermediate layers, a few millimeters beneath the surface, where they are protected from the harsh conditions of the environment to perform oxygenic photosynthesis (Stal, 1995). Whereas species of the *Chloroflexi*, *Deltaproteobacteria*, *Planctomycetes*, *Spirochetes*, and *Calditrichaeota* taxa are more abundant in the lower layers, which are normally anoxic. This could be partially explained by the metabolic activities carried out by them. *Chloroflexi* species consume fermentation products and perform anoxygenic photosynthesis (Lee et al., 2014), *Deltaproteobacteria* and *Planctomycetes* species grow anaerobically reducing sulfate and oxidizing ammonium, respectively (Madigan et al., 2017), while *Spirochetes* and *Calditrichaeota* species degrade organic compounds under anoxic conditions (Marshall et al., 2017; Dong et al., 2018).

CONCLUSION

The exploration carried out in the middle-east and south-east regions of Salar de Atacama allowed us to identify twenty previously unknown AMEs. The analyses performed on these AMEs revealed that (1) their mineralogical composition consists mainly of sulfates and/or calcium carbonates, the latter mostly present as aragonite; (2) their prokaryotic composition is correlated with their mineralogy; and (3) most harbor

numerous diatom frustules forming nano-globular carbonate aggregates with cyanobacteria and other prokaryotic cells, which suggests the participation of these microorganisms in the mineral precipitation process.

Nevertheless, to have a better comprehension of the AMEs in the Salar de Atacama, further analyses need to be performed to confirm the participation (directly or indirectly) of diatoms and other eukaryotes in the mineral precipitation process; determine the seasonal variations of the environmental factors and their effect on the prokaryotic composition; and elucidate the metabolic potential of their microorganisms in terms of resistance to environmental conditions.

This work has expanded our comprehension of the AMEs inhabiting the high-altitude lakes and wetlands from the Central Andes region and we hope it will provide a stimulus to further study and preserve these unique ecosystems.

DATA AVAILABILITY STATEMENT

The datasets presented in this study can be found in online repositories. The names of the repository/repositories and accession number(s) can be found below: ENA, PRJEB44218.

AUTHOR CONTRIBUTIONS

FV conducted the experiments for the project, analyzed data, and drafted the manuscript. DK and AT assisted with bioinformatic analysis. AL assisted with the interpretation of SEM images. DP assisted with mineralogy analysis. EC, NM-H, FN, and MC performed sampling. MF obtained funding for the original project idea, performed sampling and supervised the findings of this work. All authors assisted in the reviewing and editing of the manuscript.

FUNDING

This work was supported by the Company Albemarle Ltda Chile and the Scientific and Technological Research Fund from Argentina (FONCyT, PICT V 2015/3825). FV and AL are CONICET doctoral fellows.

SUPPLEMENTARY MATERIAL

The Supplementary Material for this article can be found online at: https://www.frontiersin.org/articles/10.3389/fmicb.2021.762076/full#supplementary-material

REFERENCES

Albarracín, V. H., Kurth, D., Ordoñez, O. F., Belfiore, C., Luccini, E., Salum, G. M., et al. (2015). High-up: a remote reservoir of microbial extremophiles in central Andean wetlands. *Front. Microbiol.* 6:1404. doi: 10.3389/fmicb.2015.01404

Alonso, H., and Risacher, F. (1996). Geoquímica del Salar de Atacama, parte 1: origen de los componentes y balance salino. *Rev. Geol. Chile* 23, 113–122.

Berner, R. A. (1975). The role of magnesium in the crystal growth of calcite and aragonite from sea water. *Geochim. Cosmochim. Acta* 39, 489–504. doi: 10.1016/0016-7037(75)90102-7

Bolyen, E., Rideout, J. R., Dillon, M. R., Bokulich, N. A., Abnet, C., Al-Ghalith, G. A., et al. (2018). QIIME 2: reproducible, interactive, scalable, and extensible microbiome data science. *PeerJ* [Preprint]. doi: 10.7287/peerj.preprints.27295v2

Bougeault, C., Durlet, C., Vennin, E., Muller, E., Ader, M., Ghaleb, B., et al. (2020). Variability of carbonate isotope signatures in a hydrothermally influenced system: insights from the Pastos Grandes Caldera (Bolivia). *Minerals* 10:989. doi: 10.3390/min10110989

Brown, C., and King, C. (2005). *Flamingo Husbandry Guidelines; A Joint Effort of the AZA and EAZA in Cooperation with WWT*. Dallas: Dallas Zoo.

Cabrol, N. A., McKay, C. P., Grin, E. A., Kiss, K. T., Ács, É, Tóth, B., et al. (2009). "Signatures of habitats and life in Earth's high-altitude lakes: clues to Noachian aqueous environments on Mars," in *The Geology of Mars: Evidence From Earth-based Analogs Cambridge Planetary Science*, ed. M. G. Chapman (Cambridge: Cambridge University Press), 460.

Caporaso, J. G., Kuczynski, J., Stombaugh, J., Bittinger, K., Bushman, F. D., Costello, E. K., et al. (2010). QIIME allows analysis of high-throughput community sequencing data. *Nat. Methods* 7, 335–336. doi: 10.1038/nmeth.f.303

Cristóbal, G., Blanco, S., and Bueno, G. (eds) (2020). *Modern Trends in Diatom Identification*. Cham: Springer.

Dong, X., Greening, C., Brüls, T., Conrad, R., Guo, K., Blaskowski, S., et al. (2018). Fermentative Spirochaetes mediate necromass recycling in anoxic hydrocarbon-contaminated habitats. *ISME J.* 12, 2039–2050. doi: 10.1038/s41396-018-0148-3

Dupraz, C., Reid, R. P., Braissant, O., Decho, A. W., Norman, R. S., and Visscher, P. T. (2009). Processes of carbonate precipitation in modern microbial mats. *Earth-Sci. Rev.* 96, 141–162. doi: 10.1016/j.earscirev.2008.10.005

Dupraz, C., and Visscher, P. T. (2005). Microbial lithification in marine stromatolites and hypersaline mats. *Trends Microbiol.* 13, 429–438. doi: 10.1016/j.tim.2005.07.008

Farías, M. E., Contreras, M., Rasuk, M. C., Kurth, D., Flores, M. R., Poiré, D. G., et al. (2014). Characterization of bacterial diversity associated with microbial mats, gypsum evaporites and carbonate microbialites in thalassic wetlands: tebenquiche and La Brava, Salar de Atacama, Chile. *Extremophiles* 18, 311–329. doi: 10.1007/s00792-013-0617-6

Farías, M. E. (ed.) (2020). *Microbial Ecosystems in Central Andes Extreme Environments: Biofilms, Microbial Mats, Microbialites and Endoevaporites*. Cham: Springer.

Farías, M. E., Rascovan, N., Toneatti, D. M., Albarracín, V. H., Flores, M. R., Poiré, D. G., et al. (2013). The discovery of stromatolites developing at 3570 m above sea level in a high-altitude volcanic Lake Socompa, Argentinean Andes. *PLoS One* 8:e53497. doi: 10.1371/journal.pone.0053497

Farias, M. E., Rasuk, M. C., Gallagher, K. L., Contreras, M., Kurth, D., Fernandez, A. B., et al. (2017). Prokaryotic diversity and biogeochemical characteristics of benthic microbial ecosystems at La Brava, a hypersaline lake at Salar de Atacama, Chile. *PLoS One* 12:e0186867. doi: 10.1371/journal.pone.0186867

Fernandez, A. B., Rasuk, M. C., Visscher, P. T., Contreras, M., Novoa, F., Poire, D. G., et al. (2016). Microbial diversity in sediment ecosystems (evaporites domes, microbial mats, and crusts) of hypersaline Laguna Tebenquiche, Salar de Atacama, Chile. *Front. Microbiol.* 7:1284. doi: 10.3389/fmicb.2016.01284

Galperin, M. Y. (2013). Genome diversity of spore-forming Firmicutes. *Microbiol. Spectr.* 1:2012. doi: 10.1128/microbiolspectrum.TBS-0015-2012

Given, R. K., and Wilkinson, B. H. (1985). Kinetic control of morphology, composition, and mineralogy of abiotic sedimentary carbonates. *J. Sediment. Res.* 55, 109–119.

Gomez, F. J., Kah, L. C., Bartley, J. K., and Astini, R. A. (2014). Microbialites in a high-altitude Andean lake: multiple controls on carbonate precipitation and lamina accretion. *Palaios* 29, 233–249. doi: 10.2110/palo.2013.049

Gomez, F. J., Mlewski, C., Boidi, F. J., Farías, M. E., and Gérard, E. (2018). Calcium carbonate precipitation in diatom-rich microbial mats: the Laguna Negra hypersaline lake, Catamarca, Argentina. *J. Sediment. Res.* 88, 727–742. doi: 10.2110/jsr.2018.37

Hamilton, N. E., and Ferry, M. (2018). ggtern: ternary Diagrams Using ggplot2. *J. Stat. Softw.* 87, 1–17. doi: 10.18637/jss.v087.c03

Huang, W., Ertekin, E., Wang, T., Cruz, L., Dailey, M., DiRuggiero, J., et al. (2020). Mechanism of water extraction from gypsum rock by desert colonizing microorganisms. *Proc. Natl. Acad. Sci. U. S. A.* 117, 10681–10687. doi: 10.1073/pnas.2001613117

Kurth, D., Elias, D., Rasuk, M. C., Contreras, M., and Farías, M. E. (2021). Carbon fixation and rhodopsin systems in microbial mats from hypersaline lakes Brava and Tebenquiche, Salar de Atacama, Chile. *PLoS One* 16:e0246656. doi: 10.1371/journal.pone.0246656

Lee, J. Z., Burow, L. C., Woebken, D., Everroad, R. C., Kubo, M. D., Spormann, A. M., et al. (2014). Fermentation couples Chloroflexi and sulfate-reducing bacteria to Cyanobacteria in hypersaline microbial mats. *Front. Microbiol.* 5:61. doi: 10.3389/fmicb.2014.00061

Logan, B. W., Rezak, R., and Ginsburg, R. N. (1964). Classification and environmental significance of algal stromatolites. *J. Geol.* 72, 68–83. doi: 10.1086/626965

Madigan, M. T., Bender, K. S., Buckley, D. H., Matthew Sattley, W., and Stahl, D. A. (2017). *Brock Biology of Microorganisms, Global Edition*. New York: Pearson Higher Ed.

Makarova, K. S., Aravind, L., Wolf, Y. I., Tatusov, R. L., Minton, K. W., Koonin, E. V., et al. (2001). Genome of the extremely radiation-resistant bacterium Deinococcus radiodurans viewed from the perspective of comparative genomics. *Microbiol. Mol. Biol. Rev.* 65, 44–79. doi: 10.1128/MMBR.65.1.44-79.2001

Marshall, I. P. G., Starnawski, P., Cupit, C., Fernández Cáceres, E., Ettema, T. J. G., Schramm, A., et al. (2017). The novel bacterial phylum Calditrichaeota is diverse, widespread and abundant in marine sediments and has the capacity to degrade detrital proteins. *Environ. Microbiol. Rep.* 9, 397–403. doi: 10.1111/1758-2229.12544

Martin-Jezequel, V., Hildebrand, M., and Brzezinski, M. A. (2000). Silicon metabolism in diatoms: implications for growth. *J. Phycol.* 36, 821–840. doi: 10.1046/j.1529-8817.2000.00019.x

McMurdie, P. J., and Holmes, S. (2013). phyloseq: an R package for reproducible interactive analysis and graphics of microbiome census data. *PLoS One* 8:e61217. doi: 10.1371/journal.pone.0061217

McSorley, R. (1997). *Soil Inhabiting Nematodes, Phylum Nematoda*. Florida: Institute of Food and Agriculture Sciences.

Meyer, H. J. (1984). The influence of impurities on the growth rate of calcite. *J. Cryst. Growth* 66, 639–646. doi: 10.1016/0022-0248(84)90164-7

Moore, D. M., and Reynolds, R. C. Jr. (1989). *X-ray Diffraction and the Identification and Analysis of Clay Minerals*. Oxford: Oxford University Press.

Oksanen, J., Blanchet, F. G., Kindt, R., Legendre, P., Minchin, P. R., O'hara, R. B., et al. (2013). *Community Ecology Package. R package version 2*.

Osman, J. R., Viedma, P., Mendoza, J., Fernandes, G., DuBow, M. S., and Cotoras, D. (2021). Prokaryotic diversity and biogeochemical characteristics of field living and laboratory cultured stromatolites from the hypersaline Laguna Interna, Salar de Atacama (Chile). *Extremophiles* 25, 327–342. doi: 10.1007/s00792-021-01232-1

Quast, C., Pruesse, E., Yilmaz, P., Gerken, J., Schweer, T., Yarza, P., et al. (2013). The SILVA ribosomal RNA gene database project: improved data processing and web-based tools. *Nucleic Acids Res.* 41, D590–D596. doi: 10.1093/nar/gks1219

Rainey, F. A., Ray, K., Ferreira, M., Gatz, B. Z., Nobre, M. F., Bagaley, D., et al. (2005). Extensive diversity of ionizing-radiation-resistant bacteria recovered from Sonoran Desert soil and description of nine new species of the genus Deinococcus obtained from a single soil sample. *Appl. Environ. Microbiol.* 71, 5225–5235. doi: 10.1128/AEM.71.9.5225-5235.2005

Rasuk, M. C., Fernández, A. B., Kurth, D., Contreras, M., Novoa, F., Poiré, D., et al. (2016). Bacterial diversity in microbial mats and sediments from the Atacama Desert. *Microb. Ecol.* 71, 44–56. doi: 10.1007/s00248-015-0649-9

Rasuk, M. C., Kurth, D., Flores, M. R., Contreras, M., Novoa, F., Poire, D., et al. (2014). Microbial characterization of microbial ecosystems associated to evaporites domes of gypsum in Salar de Llamara in Atacama desert. *Microb. Ecol.* 68, 483–494. doi: 10.1007/s00248-014-0431-4

Schultz, L. G. (1964). *Quantitative Interpretation of Mineralogical Composition from X-ray and Chemical Data for the Pierre Shale*. Virginia: USGS.

Stal, L. J. (1995). Physiological ecology of cyanobacteria in microbial mats and other communities. *New Phytol.* 131, 1–32. doi: 10.1111/j.1469-8137.1995.tb03051.x

Stivaletta, N., Barbieri, R., Cevenini, F., and López-García, P. (2011). Physicochemical conditions and microbial diversity associated with the evaporite deposits in the Laguna de la Piedra (Salar de Atacama, Chile). *Geomicrobiol. J.* 28, 83–95. doi: 10.1080/01490451003653102

Stolz, J. F. (2000). "Structure of microbial mats and biofilms," in *Microbial Sediments*, eds R. E. Riding and S. M. Awramik (Berlin: Springer), 1–8.

Suosaari, E. P., Pamela Reid, R., Abreu Araujo, T. A., Playford, P. E., Holley, D. K., Mcnamara, K. J., et al. (2016). Environmental pressures influencing living stromatolites in Hamelin Pool, Shark Bay, Western Australia. *Palaios* 31, 483–496. doi: 10.2110/palo.2016.023

Thiel, V., Tank, M., Neulinger, S. C., Gehrmann, L., Dorador, C., and Imhoff, J. F. (2010). Unique communities of anoxygenic phototrophic bacteria in saline lakes of Salar de Atacama (Chile): evidence for a new phylogenetic lineage of phototrophic Gammaproteobacteria from pufLM gene analyses. *FEMS Microbiol. Ecol.* 74, 510–522. doi: 10.1111/j.1574-6941.2010.00966.x

Vignale, F. A., Lencina, A. I., Stepanenko, T. M., Soria, M. N., Saona, L. A., Kurth, D., et al. (2021). Lithifying and non-lithifying microbial ecosystems in the wetlands and salt flats of the central Andes. *Microb. Ecol.* doi: 10.1007/s00248-021-01725-8 [Epub Online ahead of print].

Walker, J. J., Spear, J. R., and Pace, N. R. (2005). Geobiology of a microbial endolithic community in the Yellowstone geothermal environment. *Nature* 434, 1011–1014. doi: 10.1038/nature03447

Walter, L. M. (1986). Relative Efficiency of Carbonate Dissolution and Precipitation During Diagenesis: A Progress Report on the Role of Solution Chemistry. Available Online at: http://archives.datapages.com/data/sepm_sp/SP38/Relative_Efficiency_of_Carbonate_Dissolution.pdf (accessed November 05, 2020)

Warren, J. K. (2016). *Evaporites: A Geological Compendium*. Berlin: Springer.

Wilcoxon, F. (1945). Individual comparisons by ranking methods. *Biometr. Bull.* 1, 80–83. doi: 10.2307/3001968

Yu, L. Z., Luo, X.-S., Liu, M., and Huang, Q. (2015). Diversity of ionizing radiation-resistant bacteria obtained from the Taklimakan Desert. *J. Basic Microbiol.* 55, 135–140. doi: 10.1002/jobm.201300390

Conflict of Interest: The authors declare that the research was conducted in the absence of any commercial or financial relationships that could be construed as a potential conflict of interest.

Publisher's Note: All claims expressed in this article are solely those of the authors and do not necessarily represent those of their affiliated organizations, or those of the publisher, the editors and the reviewers. Any product that may be evaluated in this article, or claim that may be made by its manufacturer, is not guaranteed or endorsed by the publisher.

frontiers in Microbiology

ORIGINAL RESEARCH
published: 05 November 2021
doi: 10.3389/fmicb.2021.742798

Properties of *Modestobacter deserti* sp. nov., a Kind of Novel Phosphate-Solubilizing Actinobacteria Inhabited in the Desert Biological Soil Crusts

*Zhu-Ming Jiang[1], Bing-Huo Zhang[2], Hong-Min Sun[1], Tao Zhang[1], Li-Yan Yu[1] and Yu-Qin Zhang[1]**

[1]*Institute of Medicinal Biotechnology, Chinese Academy of Medical Sciences & Peking Union Medical College, Beijing, China,* [2]*College of Life Science, Jiujiang University, Jiujiang, China*

OPEN ACCESS

Edited by:
Martina Cappelletti, University of Bologna, Italy

Reviewed by:
Haiyuan Cai, University of Maryland, Baltimore County, United States
Yuli Wei, Shanghai Ocean University, China
Intikhab Alam, King Abdullah University of Science and Technology, Saudi Arabia
Fatemeh Salimi, Damghan University, Iran

***Correspondence:**
Yu-Qin Zhang
zhyuqin@126.com

Specialty section:
This article was submitted to Extreme Microbiology, a section of the journal Frontiers in Microbiology

Received: *02 August 2021*
Accepted: *05 October 2021*
Published: *05 November 2021*

Citation:
Jiang Z-M, Zhang B-H, Sun H-M, Zhang T, Yu L-Y and Zhang Y-Q (2021) Properties of Modestobacter deserti sp. nov., a Kind of Novel Phosphate-Solubilizing Actinobacteria Inhabited in the Desert Biological Soil Crusts. Front. Microbiol. 12:742798. doi: 10.3389/fmicb.2021.742798

Three Gram-stain-positive, aerobic, motile actinobacterial strains designated as CPCC 205119^T, CPCC 205215, and CPCC 205251 were isolated from different biological soil crust samples collected from Tengger Desert, China. The 16S rRNA gene sequence comparison of these three strains showed they had almost identical 16S rRNA genes, which were closely related to members of the family *Geodermatophilaceae*, with the highest similarities of 96.3–97.3% to the species of *Modestobacter*. In the phylogenetic tree based on 16S rRNA gene sequences, these isolates clustered into a subclade next to the branch containing the species of *Modestobacter lapidis* and *Modestobacter multiseptatus*, within the lineage of the genus *Modestobacter*. The comparative genomic characteristics (values of ANI, dDDH, AAI, and POCP) and the phenotypic properties (morphological, physiological, and chemotaxonomic characteristics) of these isolates readily supported to affiliate them to the genus *Modestobacter* as a single separate species. For which, we proposed that the isolates CPCC 205119^T, CPCC 205215, and CPCC 205251 represent a novel species of the genus *Modestobacter* as *Modestobacter deserti* sp. nov. CPCC 205119^T (=I12A-02624 = NBRC 113528^T = KCTC 49201^T) is the type strain. The genome of strain CPCC 205119^T consisted of one chromosome (4,843,235 bp) containing 4,424 coding genes, 48 tRNA genes, five rRNA genes, three other ncRNA genes, and 101 pseudogenes, with G + C content of 74.7%. The whole-genome sequences analysis indicated that this species contained alkaline phosphatase genes (*phoA*/*phoD*), phosphate transport-related genes (*phoU*, *phnC*, *phnD*, *phnE*, *phoB*, *phoH*, *phoP*, *phoR*, *pitH*, *ppk*, *pstA*, *pstB*, *pstC*, and *pstS*), trehalose-phosphate synthase gene (*otsA*), trehalose 6-phosphate phosphatase gene (*otsB*) and other encoding genes for the properties that help the microorganisms to adapt to harsh environmental conditions prevalent in deserts. Strains of this species could solubilize tricalcium phosphate [$Ca_3(PO_4)_2$] and phytin, assimilate pyrophosphate, thiophosphate, dithiophosphate, phosphoenol pyruvate, 2-deoxy-d-glucose-6-phosphate, and cysteamine-S-phosphate.

Keywords: *Modestobacter deserti*, average nucleotide identity, pan-genome, phenotype, genotype, biological soil crusts

INTRODUCTION

Water scarcity, violent temperature fluctuation, strong ultraviolet radiation, and low-substrate supply are the key abiotic stress factors for life in desert environments. Microbiological soil crusts, the primary stage of biological soil crusts, contribute greatly in stabilization of the sandy surface, soil formation, and carbon and nitrogen assimilation, which provide foundation for other organisms to survive. The "National Desert Ecological Reserve" (NDER) located in Shapotou desert region, on the south east edge of the Tengger Desert, south to the Yellow River, in the northwest of China is the first Chinese NDER. This NDER acts as a model for studying the development of biological soil crusts. Previous study (Sun et al., 2015) found that the members of the family *Geodermatophilaceae* (Normand, 2006) were ubiquitous in different types of crusts in Shapotou NDER. Among the validly described species of the family *Geodermatophilaceae*, most validly described type strains, especially the *Modestobacter* (a major genus in the family *Geodermatophilaceae*) members were isolated from harsh environments, including desert soils (Busarakam et al., 2016; Golińska et al., 2020), sandstone (Trujillo et al., 2015), stone surfaces (Normand et al., 2012; Montero-Calasanz et al., 2019), as well as the newly recognized species *Modestobacter excelsi*[1] from a high altitude Atacama Desert soil (Golinska et al., 2020). The genome study of *Modestobacter* revealed that the multiple copies of genes, such as *coxSML* (carbon monoxide dehydrogenase related genes), *katA* (catalase coding gene), and *uvrACD* (UvrABC system protein coding genes; Chouaia et al., 2012; Gtari et al., 2012; Sghaier et al., 2016) may serve as the genetic basis to help the strains to adapt to extreme ecological niches. Therefore, *Modestobacter* strains from the desert biological soil crusts may be ideal model microorganisms to investigate the microbiological soil crusts development in depth. At the time of writing, the genus *Modestobacter* comprised of 11 validly named species.[1] Generally, the members of the genus *Modestobacter* are characterized as Gram-staining-positive, aerobic, pink-pigmented, and short rod-shaped actinobacteria, with major polar lipid composition of diphosphatidylglycerol (DPG), phosphatidylglycerol (PG), phosphatidylethanolamine (PE), phosphatidylmethylethanolamine (PME), phosphatidylinositol (PI), and phosphatidylinositol mannosides (PIM). The major respiratory quinone is MK-9(H_4), and MK-8(H_4), MK-9(H_6), MK-9(H_2), and MK-10(H_4) may be present. Major fatty acids are iso-$C_{16:0}$ and iso-$C_{15:0}$. The DNA G+C content ranges from 68 to 74.1%.

The primary goal of the present research was to collect and identify the *Modestobacter* cultures from Shapotou NDER, and study the properties of *Modestobacter* members inhabiting in the biological soil crusts in desert niches. The detailed phenotypic and genotypic properties resulted from these strains could be helpful to systematically demonstrate their ecological adaptation mechanism and their ecological function. As a result, strains CPCC 205119^T, CPCC 205215, and CPCC 205251 were isolated from biological soil crusts collected from Tengger Desert, showing phosphate-solubilizing activity. Based on the phenotypic and genotypic data, a novel species *Modestobacter deserti* sp. nov. is proposed, with the isolate CPCC 205119^T as the type strain.

[1]https://lpsn.dsmz.de/genus/modestobacter

Abbreviations: ANI, Average nucleotide identity; dDDH, Digital DNA–DNA hybridization; AAI, Amino acid identity; POCP, Percentage of conserved proteins; BSCs, Biological soil crusts.

MATERIALS AND METHODS

Acquisition of Samples

The moss-dominated soil crusts samples designated IMB12100 and IMB12108 were collected from Cuiliu ditch (37°25′38″N, 104°35′9″E, 1,691 mH) and Yiwan spring (37°35′50″N, 104°34′59″E, 1,329 mH), respectively, and the cyanobacteria-dominated soil crusts sample CCL12125 was from the North-road experimental area (37°25′38″N, 104°35′8″E, 1,340 mH), in the middle of Shapotou NDER (36°39′–37°41′N, 104°25′–105°40′E, 1,300–1,700 mH). Different samples were sealed in sterilized envelopes following collection and taken to the laboratory within 1 week of collection. All samples were immediately processed for the isolation of microorganisms after arriving at the laboratory, and the remaining samples were maintained at −80°C.

Isolation and Identification of *Modestobacter* Strains

Dilution plating method was employed for the isolation of microorganisms from the sand samples. Approximately 0.2–0.3 ml of the 10^{-3} dilution was dropped into isolation agar Petri dishes and spread evenly on the surface. The isolation medium of PYG (g L^{-1}; peptone 3, yeast extract 5, glycerol 10, glycine betaine 1.25, sodium pyruvate 1.25, and pH 7.5) and agar (1.5% w/v) was prepared and autoclaved separately, to avoid high H_2O_2 concentration in media prepared by autoclaving agar and phosphate buffer together (Tanaka et al., 2014), and then mixed the agar with the nutrient content when cooling to 55°C. Subsequently, supplemented with 0.1% (*v*/*v*) of compound trace salts solution ($FeSO_4{\cdot}7H_2O$ 0.2 g, $MnCl_2{\cdot}2H_2O$ 0.1 g, $ZnSO_4{\cdot}7H_2O$ 0.1 g, sterilized water 100 ml), 1% (*v*/*v*) of compound vitamin mixture (vitamin B1 1 mg, vitamin B2 1 mg, vitamin B3 1 mg, vitamin B6 1 mg, phenylalanine 1 mg, biotin 1 mg, alanine 0.3 mg, suspended in 100 ml sterilized water) and cycloheximide to the final concentration of 50 mg L^{-1}. Vitamin mixture and cycloheximide were all filter-sterilized.

The Petri dishes spread with soil suspension were incubated at 28°C for 3 weeks and distinct colonies were streaked into newly prepared PYG agar dishes to purify the cultures. The purified isolates were maintained on PYG slants at 4°C and also as glycerol suspensions (20%, *v*/*v*) at −80°C.

The *Modestobacter*-like strains were primarily identified according to the 16S rRNA gene sequence comparison following next steps.

Extraction of genomic DNA and PCR amplification of the strain's 16S rRNA gene were carried out as described by Li et al. (2007). The obtained sequence was compared with available 16S rRNA gene sequences from GenBank using the BLAST program and the EzTaxon-e server[2] to determine an approximate taxonomic affiliation (Yoon et al., 2017a). Multiple sequence alignment and analysis of the data were performed by using the molecular evolutionary genetics analysis (MEGA) software package version X (Kumar et al., 2018). The phylogenetic trees were reconstructed by the software package MEGA version X using the neighbour-joining (Kimura, 1979) and confirmed by maximum-likelihood (Felsenstein, 1981) and maximum-parsimony (Kluge and Farris, 1969) tree-making methods. Bootstrap analysis with 1,000 replicates was performed to obtain the confidence level of the branches (Felsenstein, 1985).

Growth Conditions and Morphological Tests

Growth characteristics of the strains were tested using ISP 2 (Shirlng and Gottlieb, 1966), GYM ($g\,L^{-1}$; glucose 4, yeast extract 4, malt extract 10, calcium carbonate 2, pH 7.5), Tryptic soy agar (TSA, Difco), Reasoner's 2A agar (R2A, Difco), nutrition agar (NA), and PYG agar. The temperature range for growth was tested at 4, 10, 15, 20, 28, 30, 32, 35, 37, and 40°C using ISP 2 broth for cultivation 2 weeks. The pH range (5.0–12.0, at intervals of 1 pH unit) for growth was observed in ISP 2 broth using the buffer system described by Xu et al. (2005). Tolerance to NaCl was examined using GYM broth as the basal medium with different NaCl concentrations [0–10% (*w*/*v*; at 1% intervals)].

Colonies characteristics and pigments production were observed and recorded after 3-day incubation on GYM agar[3] at 28°C. The Gram reaction was tested by the standard Gram-staining method as described by Magee et al. and observed using light microscopy (BH-2, Olympus). Motility of cells was examined on GYM semi-solid medium agar (0.3%, *w*/*v*) and then checked using light microscopy. The cellular morphology of the test strains was studied using transmission electron microscopy (JEOL JEM-1010) after 6-day incubation on GYM semi-solid slant agar. Before cells were mounted on formvar-coated copper grids (Electron Microscopy Science), they were negatively stained using 2% (*w*/*v*) uranyl acetate for 15 s.

Physiological Tests

The reference strains of *M. lapidis* DSM 100206^T and *M. multiseptatus* DSM 44406^T obtained from DSMZ were carried out some assays in parallel.

The assimilation of carbon compounds, nitrogen sources, phosphorus, and sulfur sources were tested at 28°C using Biolog GEN III, PM3B, and PM4A Microplates, respectively, in an Omnilog device (BIOLOG Inc., Hayward, CA, United States). Other metabolic characters were determined by API 50CH and API ZYM test kits (bioMerieux) according to the manufacturer's instructions. Results were evaluated after incubation at 28°C for 72–168 h. The oxidase activity was detected using API oxidase reagent (bioMeriéux) according to the manufacturer's instructions. The catalase activity was determined by observation of bubble production in 3% (*v*/*v*) H_2O_2. The abilities of strains to produce H_2S and indole, hydrolysis of cellulose, gelatin, and starch were examined according to previously described procedures (Zhou et al., 1998; Yuan et al., 2008).

The ability of these three strains and the reference strains *M. lapidis* DSM 100206^T and *M. multiseptatus* DSM 44406^T to solubilize insoluble phosphate were determined on plates using phosphate-solubilizing media and confirmed using broth culture method (Zhang et al., 2016), with little modification addressed as follows.

Inocula for phosphate solubilization test were prepared from culture grown in GYM broth (28°C, 3 days). Cultures were centrifuged (4,860 *g*, 20 min, 4°C), and the collected biomass re-suspended in small aliquots of sterilized distilled water. Cell suspension, adjusted to approximately 1×10^6 CFU/ml, was inoculated into the phosphate-solubilizing medium ($g\,L^{-1}$) [glucose, 10; $(NH_4)_2SO_4$, 0.5; $MgSO_4{\cdot}7H_2O$, 0.3; NaCl, 0.3; KCl, 0.3; $FeSO_4{\cdot}4H_2O$, 0.036; $MnSO_4{\cdot}4H_2O$, 0.03; insoluble phosphorus sources, 2 (including tricalcium phosphate or phytin); distilled water, 1,000 ml; pH 7.0]. For the control, the bacterial cell inoculum was replaced with sterile water. Culture broth was centrifuged (4,860 *g*, 20 min, 4°C) on the 2nd day of incubation, and the amount of available phosphorus in the supernatant determined colorimetrically using standard protocol as described previously (Ministry of Agriculture of the People's Republic of China, 2010).

Reaction mixture containing 5 ml supernatant, 5 ml Mo-Sb reagent solution were adjusted to a final volume of 50 ml with distilled water, briefly mixed and kept incubated at 20°C for 30 min. Absorbance of the reaction mixture was monitored at 700 nm against a standard of potassium phosphate. The Mo-Sb reagent solution contained (per liter) sulfuric acid, 2.87 mol; ammonium molybdate, 8.1 mmol; antimonyl potassium tartrate, 1.5 mmol; ascorbic acid, 85.2 mmol (added into the solution just before use).

Concentration of the available phosphorus in the culture media was calculated based on the following equation:

$$X = \frac{(P \times V1 \times K)}{V2}$$

where X represents available phosphorus in the culture media; P, available phosphorus calculated for a reaction mixture; $V1$, total volume of reaction mixture; $V2$ volume of culture supernatant added in the reaction mixture; K, the dilution ratio used for measuring the absorbance.

Chemotaxonomic Tests

Biomass for chemotaxonomic studies of the strains was obtained by cultivation in flasks on a rotary shaker (180 rpm) using GYM broth at 28°C for 4 days except that cellular fatty acid extraction and analysis were conducted using the cultures harvested from Tryptic soy broth (TSB). The diagnostic isomers of diaminopimelic acid in the whole cell hydrolysates (4N

[2]http://eztaxon-e.ezbiocloud.net

[3]https://www.dsmz.de/collection/catalogue/details/culture/DSM-100206

HCl, 100°C, 15 h) of these strains were subjected to thin-layer chromatography on cellulose plates using the solvent system of Schleifer and Kandler (1972). The sugar analysis of whole cell hydrolysates followed procedures described by Staneck and Roberts (1974). Polar lipids were extracted and examined by two-dimensional TLC and identified using previously described procedures (Minnikin et al., 1984). Menaquinones were isolated using the method of Collins et al. (1977) and were analysed by HPLC (Groth et al., 1997). Analysis of the whole cell fatty acid pattern followed the described methods using the MIDI system (Microbial ID, Inc., Newark, Del; Kroppenstedt, 1985; Meier et al., 1993). MIDI Sherlock Version 6.0 and ACTIN1 database were employed for this analysis.

Whole-Genomic Study

Genome Sequencing and Assembly

The whole-genome sequencing was implemented using an Illumina HiSeq 4000 system (Illumina, SanDiego, CA, United States) at the Beijing Genomics Institute (Shenzhen, China). Genomic DNA was sheared randomly to construct three read libraries with length of 300 bp by a Bioruptor ultrasonicator (Diagenode, Denville, NJ, United States) and physico-chemical methods. The paired-end fragment libraries were sequenced according to the Illumina HiSeq 4000 system's protocol. Raw reads of low quality from paired-end sequencing (those with consecutive bases covered by fewer than five reads) were discarded. The sequenced reads were assembled using SOAPdenovo v1.05 software.

Genome Component Prediction

Gene prediction was performed on the genome assembly by glimmer3[4] with Hidden Markov models. The tRNAscan-SE (Lowe and Eddy, 1997), RNAmmer, and the Rfam databases were employed for sorting of tRNA, rRNA, and sRNAs, respectively. The tandem repeats annotation was obtained using the Tandem Repeat Finder,[5] and the minisatellite DNA and microsatellite DNA selected based on the number and length of repeat units. The Genomic Island Suite of Tools (GIST) used for genomicis lands analysis[6] with IslandPath-DIOMB, SIGI-HMM, IslandPicker method. Prophage regions were predicted using the PHAge Search Tool (PHAST) web server[7] and CRISPR identification using CRISPRFinder.

Gene Annotation

Rapid Annotation using Subsystem Technology (RAST; Aziz et al., 2008) was applied for annotation of the assembled whole genomic sequences of the family *Geodermatophilaceae*. The protein sequence of each genome annotated by RAST was used for downstream analysis such as stress-responding genes retrieval, pan-genome analysis, and calculation of AAI and POCP values. For pathway analysis, the predicted proteins sequences were uploaded to KEGG Automatic Annotation Server with "for prokaryotes" and "bidirectional best hit" options. The website of UniProt[8] was implemented for the validation of stress response genes. Predictions of gene clusters for natural products were performed using antiSMASH (Blin et al., 2019).

Whole Genome Based Taxonomy

Genomic robust indexes, i.e., ANI (average nucleotide identity), dDDH (digital DNA-DNA hybridisation), AAI (average amino identity), and POCP (percentage of conserved proteins) were calculated for the definition and classification of the novel species of the genus *Modestobacter*. ANI Calculator (Yoon et al., 2017b),[9] Genome-to-Genome Distance Calculator (Meier-Kolthoff et al., 2013),[10] Average Amino acid Identity (Rodriguez-R and Konstantinidis, 2016),[11] and POCP described by Qin et al. (2014) were used to calculate the ANI, dDDH, AAI, and POCP, respectively.

Bacterial Pan-genome Analysis (BPGA) pipeline was applied for analysis of the genomic diversity of the *Modestobacter* members. The protein sequences of strains CPCC 205119^T, CPCC 205215, and CPCC 205251 were annotated by RAST 2.0. The protein sequences of other *Modestobacter* strains were accessed from NCBI. Pan-genome analysis was performed by BPGA 1.3 using default settings (Chaudhari et al., 2016), and the pan- and core-genome analysis of the *Modestobacter* spp. was also performed by using the Roary pipeline (Page et al., 2015). A total of 22 protein sequence files annotated from the 22 corresponding strains' whole genome sequences were used to generate orthologous gene/protein clusters (homologous families) by USEARCH clustering tool and construct the phylogenetic tree using the concatenated core genes by BPGA. Except the strain *M. lacusdianchii* JXJ CY 19^T, without available genome sequence in the database, all other 22 strains were also included in the 16S rRNA gene phylogenetic tree. Each homologous family was given a conserved value (CV) based on the frequency it occurs in the three genomes. Different CV reflects the distribution frequency of the homologous gene in these three strains. The larger CV indicates that the gene is more widely distributed in the strains of the species *M. deserti* sp. nov. and the more conserved the gene family is in the species *M. deserti*. In the pan-genome of the three strains, if the CVs of some homologous families were 3, these homologous families were considered as the part of core genome; those homologous families with the CV of 2 or 1 were regarded as accessory genes or unique genes, respectively. The core, accessory, unique and exclusively absent genes were retrieved using USEARCH clustering tool. BPGA performed the evolutionary analysis based on concatenated core gene alignments and binary (presence/absence) pan-matrix. Gene matrix was calculated using similarity or dissimilarity in contribution of genes to orthologous gene clusters. For core genome based phylogenetic tree, BPGA first extracted the protein sequences (excluding

[4]http://www.cbcb.umd.edu/software/glimmer/
[5]http://tandem.bu.edu/trf/trf.html
[6]http://www5.esu.edu/cpsc/bioinfo/software/GIST/
[7]http://phast.wishartlab.com/
[8]https://www.uniprot.org/
[9]https://www.ezbiocloud.net/tools/ani
[10]https://ggdc.dsmz.de/
[11]http://enve-omics.ce.gatech.edu/aai/

paralogs) from 20 random orthologous gene clusters to generate core genome phylogeny tree. BPGA automated multiple sequences alignments using MUSCLE. All alignments were concatenated and a neighbor-joining phylogenetic tree was constructed.

RESULTS AND ANALYSIS

Isolation and Identification of *Modestobacter* Strains

Strains designated as CPCC 205119^T and CPCC 205215 were isolated from moss-dominated soil crust samples IMB12100 and IMB12108, respectively, and strain CPCC 205251 was acquired from cyanobacteria-dominated soil crust sample CCL12125, collected from Shapotou NDER in Tengger Desert, China.

The complete 16S rRNA gene sequences of strains CPCC 205119^T (1,529 bp), CPCC 205215 (1,529 bp), and CPCC 205251 (1,529 bp) were obtained. Pairwise alignment indicated that these three newly isolated strains contained almost identical 16S rRNA genes. BLAST search results showed that they exhibited the highest similarities with the validly described species of the genus *Modestobacter*, i.e., *M. lapidis* DSM 100206^T (97.3%), *M. multiseptatus* DSM 44406^T (97.3%), and other type strains of the genus *Modestobacter* (<97.0%). These similarity values were all lower than 98.65%, which was proposed by Kim et al. as the threshold for differentiating two genic species according to the 16S rRNA gene similarity (Kim et al., 2014). In the Neighbour-Joining phylogenetic tree based on the 16S rRNA gene sequences, strains CPCC 205119^T, CPCC 205215, and CPCC 205251 formed a stable subclade next to the subclade containing *M. lapidis* DSM 100206^T and *M. multiseptatus* DSM 44406^T in the genus of *Modestobacter* lineage, within the family *Geodermatophilaceae* (**Figure 1**), which showed almost the same case in maximum-parsimony, maximum-likelihood trees. These results indicated these three strains could be affiliated to the genus of *Modestobacter* as a distinct species.

Genome-Based Classification

Assembly sequences for the draft genomes of CPCC 205119^T, CPCC 205215, and CPCC 205251 were deposited in GenBank with the accession number JAAGWK000000000, WGGQ00000000, and JAABOZ000000000. The detailed genome repertoires were given in the supplementary materials (**Supplementary Table S1**). In the phylogenetic tree based on the concatenated core genes, strains CPCC 205119^T, CPCC 205215, and CPCC 205251 clustered in a unique branch in the lineage of the genus *Modestobacter*, with the closest evolutionary distance with the branch formed by *M. lapidis* DSM 100206^T and *M. multiseptatus* DSM 44402 (**Supplementary Figure S1**). The dDDH values between strain CPCC 205119^T and their closest phylogenic neighbors ranged in 20.4–22.7%, which was far below than the cut-off value (70%) used to classify bacterial strains of the same species (Auch et al., 2010); the ANI values between strain CPCC 205119^T and their closest phylogenic neighbors ranged in 79.5–79.7%, which were also much lower than the threshold for bacterial species delineation (95–96%; Kim et al., 2014); the AAI values between strain CPCC 205119^T and their closest phylogenic neighbors ranged in 71.1–71.8%, which were also much lower than the threshold for bacterial species delineation (~ 90%; Rodriguez-R and Konstantinidis, 2014); the POCP values between strain CPCC 205119^T and their closest phylogenic neighbors ranged in 53.4–58.5%, which were all higher than threshold for bacterial genus delineation (50%), while lower than the threshold for bacterial species delineation (70%; Qin et al., 2014; **Table 1**). While the pairwise values of dDDH, ANI and AAI and POCP among these three strains readily confirmed to classify these three strains as one species (**Supplementary Table S2**). Therefore, the above results strongly supported the proposal that the three strains represent a single novel species (*M. deserti* sp. nov.) of the genus *Modestobacter*. The calculated G+C contents of these strains were in the range of 74.6–74.7%.

Genes Associated With Stress Response

The whole genome of strains CPCC 205119^T, CPCC 205215, and CPCC 205251 contained 4,480, 4,443, and 4,523 genes, respectively (**Supplementary Table S1**). The strains *M. lapidis* DSM 100206^T isolated from building rock surface and *M. multisptatus* DSM 44402 isolated from Antarctica's dry and cold Valley composed of 4,366 and 6,094 genes, respectively, which were included as reference. The putative stress-responding related genes were retrieved in the whole genome DNA annotation results (**Figure 2**). The heat shock response related genes (*clpB*, *dnaK*, *dnaJ*, *grpE*, and *hrcA* gene; Li et al., 2011), the cold shock response related genes (*cspA*, *cspC*; Essoussi et al., 2010), osmotic stress related genes (*aglF, aglG, otsA, otsB, treS, treY, treZ, opuAA, opuAB, opuAC*, and *opuD*; Kempf and Bremer, 1995; Pan et al., 2008; Reina-Bueno et al., 2012), oxidative stress-related genes (*bcp*, *btuE*, *efeB*, *katA*, *katE*, *katG*, *sodN* and *soxR*; Martindale and Holbrook, 2002), carbon source starvation stress-related genes (*csrA*; Romeo et al., 1993; Romeo, 1998), UV-radiation-resistant genes (*uvrA*, *uvrB*, *uvrC*, and *uvrD*; Long et al., 2020), DNA repair related genes (*recA*, *recF*, *recG*, *recN*, *recO*, *recQ*, and *recR*; Hickson, 2003; Manthei et al., 2015), heat-resistant esterase coding genes [esterase (EC 3.1.1.X) coding genes; Essoussi et al., 2010; Jaouani et al., 2012], alkaline phosphatase genes (*phoA*/*phoD*), pyrophosphatase coding gene (*ppa*), and phytase coding gene (*phyC*; Pasamontes et al., 1997), phosphate starvation-inducible protein coding gene (*phoH*), phosphate transport-related genes (*phoU*, *phnC*, *phnD*, *phnE*, *phoB*, *phoH*, *phoP*, *phoR*, *pitH*, *ppk*, *pstA*, *pstB*, *pstC*, and *pstS*; Song et al., 2020), carbon monoxide assimilation-related genes (*coxLSM* gene cluster, *coxD* and *coxE*; Lorite et al., 2000), rhodopsin-encoding genes (*bop*; Shand and Betlach, 1994), arsenate resistance genes (*arsC*; Chouaia et al., 2012), copper resistance related genes (*cop*), various metal resistance genes (*czcD*), DNA inducible enzyme gene (*dnaG*), thioredoxin reductase gene (*trx*), and mitomycin free radical oxidase gene (*mcrA*; Normand et al., 2012) were predicted from all or partial of these strains. A total of 99 copies, 100 copies, 101 copies, 99 copies, and 111 copies of stress response related genes accounted for 2.21, 2.25, 2.23, 2.26, and 1.82%, respectively,

in their whole genomes. These data showed stress-responding related genes seemed richer in the microorganisms inhabited in deserts (these three newly isolates) and the rock surface (*M. lapidis* DSM 100206^T) than that in Antarctica's Valley (*M. multisptatus* DSM 44402).

Pan-genome Analysis of the Species *Modestobacter deserti*

A total of 13,532 protein-coding genes (**Table 2**) were sorted from the genomes of these three strains of the species *M. deserti*, which were divided into 4,592 homologous families by cluster analysis. Histograms were constructed according to different CVs (**Figure 3A**). Among them, there were a total of 4,282 core genes commonly shared by these three strains (CV = 3), accounting for about 93.2% of the total number of homologous gene families. The accessory genes (188 genes; CV = 2) accounted for about 4.1% of the homologous gene families in the newly proposed species. The proportion of the unique genes (122 genes; CV = 1) was about 2.7% (**Supplementary Figure S2**).

The relationship between the pan-genome size and the number of genomes of the species, and the relationship between the number of core genes and the number of genomes were deduced (**Figure 3B**) by using all the protein sequences extracted from these three strains of the species *M. deserti*. The functional relationship between pan-genome size (f_{pan}) and the number of genomes (n) was obtained by fitting, as follows:

$$f_{pan}(n) = 4450.13 \times n^{0.0306539}$$

Meanwhile, the functional relationship between the number of core genes (f_{core}) and the number of genomes (n) was obtained by fitting, as follows:

$$f_{core}(n) = 4534 \times e^{-0.0202158n}$$

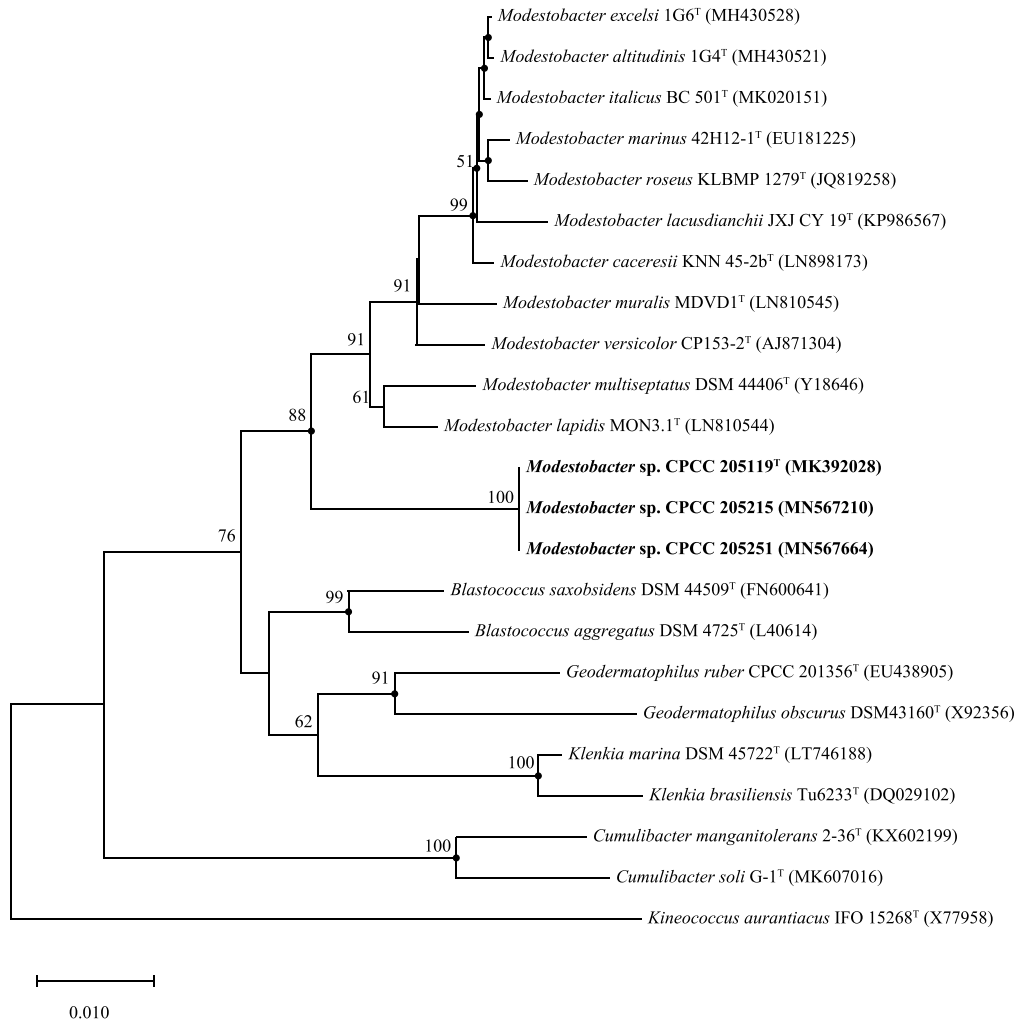

FIGURE 1 | Neighbour-joining tree based on 16S rRNA gene sequences showing the relationship of the strains CPCC 205119^T, CPCC 205215, and CPCC 205251 with representatives of the family *Geodermatophilaceae*. Filled circles indicate that the corresponding nodes were also recovered in the trees generated with the maximum-likelihood and maximum-parsimony methods. Bootstrap values (>50%) are shown as percentages of 1,000 replicates. Bar, 1 nt substitutions per 100 nt.

TABLE 1 | The values of ANI, dDDH, AAI, and POCP of the whole genome DNA assembly sequences between the strain CPCC 205119^T and the closest phylogenic neighbours.

	CPCC 205119^T			
	ANI (%)	**dDDH (%)**	**AAI (%)**	**POCP (%)**
Modestobacter lapidis DSM 100206^T	79.7	22.7	71.8	58.5
Modestobacter multiseptatus DSM 44402	79.5	20.4	71.1	53.4

ANI, values of average nucleotide identity; dDDH, digital DNA–DNA hybridization; AAI, average amino acid identity; POCP, percentage of conserved proteins.

TABLE 2 | The pan-genome profile of the species *Modestobacter deserti* sp. nov.

Genome number	Organism name	No. of core genes	No. of accessory genes	No. of unique genes	No. of exclusively absent genes
1	*M. deserti* CPCC 205119^T	4,282	158	42	30
2	*M. deserti* CPCC 205215	4,282	55	45	133
3	*M. deserti* CPCC 205251	4,282	163	35	25

It could be observed from the pan-genome fitting curve in the **Figure 3B** that, with the increasing number of sequenced genomes, the pan-genome size tended to a plateau. Accordingly, it could be inferred that the pan-genome of the novel species *M. deserti* was almost closed.

Out of 4,592 genes (clusters), BPGA could map 2,508 (54.6%) to KEGG (Kyoto Encyclopedia of Genes and Genomes) pathways, i.e., core genes (2,457, 98.0%), accessory genes (47, 1.9%) and unique genes (4, 0.1%). Having filtered some KEGG pathway related to eukaryotes, we obtained an overview on the metabolic pathway corresponding to the gene(s) in the pan-genome of the species *M. deserti*. A large number of core genes (2,305, 15.6%) were involved in carbohydrate metabolism, amino acid metabolism (14.3%), some other elementary metabolism (biosynthesis of amino acids, 4.9%; carbon metabolism, 4.6%; fatty acid metabolism, 1.8%; 2-oxocarboxylic acid metabolism, 1.1% and degradation of aromatic compounds, 0.5%; 12.8%), energy metabolism (6.8%), metabolism of cofactors and vitamins (5.6%), lipid metabolism (5.3%), nucleotide metabolism (5.3%), and membrane transport (5.1%). Accessory and unique genes appeared to be enriched in membrane transport, carbohydrate metabolism, as well as metabolism of cofactors and vitamins. Among the accessory genes (41), the major portion of genes seemed related to membrane transport (19.5%), metabolism of cofactors and vitamins (14.6%), carbohydrate metabolism (12.2%), amino acid metabolism (9.8%), some other elementary metabolism (biosynthesis of amino acids, 4.9%; carbon metabolism, 2.4% and fatty acid metabolism, 2.4%; 9.8%), signal transduction (9.8%), signal transduction (9.8%). Unique genes (4) seemed to be mainly enriched in carbohydrate metabolism (75%), and carbon metabolism (25%; **Figure 4**).

Phenotypic Properties

Morphological and Physiological Characteristics

Orange to red colored colonies with a maximum diameter of 1.1 mm were opaque, convex and irregular circle on ISP 2, GYM, TSA, R_2A, NA, and PYG agar after incubation for 72 h at 28°C. No diffusible pigments were observed on any tested media. Cells of strains CPCC 205119^T, CPCC 205215, and CPCC 205251 were aerobic, Gram-staining-positive, non-spore-forming, cocci (diameter of 0.5–0.8 μm) and/or short rods (0.5–0.6 μm in width and 0.8–1.1 μm in length), motile with polar flagella. Bud-like structure was observed for some cells (**Figure 5**). These three strains grew well on ISP 2 agar and GYM agar, moderate growth occurred on and R_2A agar, TSA, NA and PYG media. Growth of these strains was observed at 10–37°C, pH 6.0–11.0, in ISP 2 medium with the presence of 0–3% (*w*/*v*) NaCl. The optimum growth occurred at 28–32°C, pH 6.0–8.0, with the absence of NaCl. The catalase, oxidase and phosphate solubilizing activity of these strains were positive. None of these strains can hydrolyze gelatin, CM-cellulose (carboxymethyl cellulose), urea and starch. Nitrate was not reduced and H_2S was not produced.

Detailed physiological and biochemical characteristics of these strains from Biolog GEN III, PM3B, and PM4A Microplates, and API 50CH and API ZYM test kits are given in the description of the species and in the supplementary materials as **Supplementary Table S3**.

In the liquid culture assay, strains CPCC 205119^T, CPCC 205215, and CPCC 205251 could solubilize tricalcium phosphate [$Ca_3(PO_4)_2$] and phytin with a detection of additional available phosphorus of (4.72 ± 0.34) mg/L and (36.78 ± 1.75) mg/L, respectively.

Chemotaxonomic Characteristics

These three isolates were found to contain alanine, glutamic acid, glycine, and *meso*-diaminopimelic (*meso*-DAP) in the cell wall. Whole-cell hydrolysates yielded arabinose, glucose and ribose. The cellular polar lipids contained DPG, PE, PG, PI and PIM, PME as well as small amounts of unidentified phospholipid (UPL) and aminophospholipid (APL; **Supplementary Figure S3**). In the menaquinones extraction, tetrahydrogenated menaquinones with nine isoprene units as the predominant isoprenologue, i.e., MK-9(H_4) (78.8–82.3% of total menaquinone composition) with minor amounts of MK-8(H_4) (17.7–21.2%); The cellular fatty acids were $C_{18:1}\omega9c$ (18.9–29.7%), iso-$C_{16:0}$ (11.2–20.9%), $C_{16:0}$ (6.7–11.0%), $C_{17:1}\omega8c$ (4.2–11.8%), $C_{16:1}\omega7c$ (6.6–9.0%), iso-$C_{15:0}$ (6.1–8.0%), $C_{18:0}$ (4.3–5.8%; **Supplementary Table S4**).

Taxonomic Study Conclusion

The 16S rRNA gene sequence comparison results and the phylogenic analysis suggest that strains CPCC 205119^T, CPCC 205215, and CPCC 205251 represent a single novel species of the genus

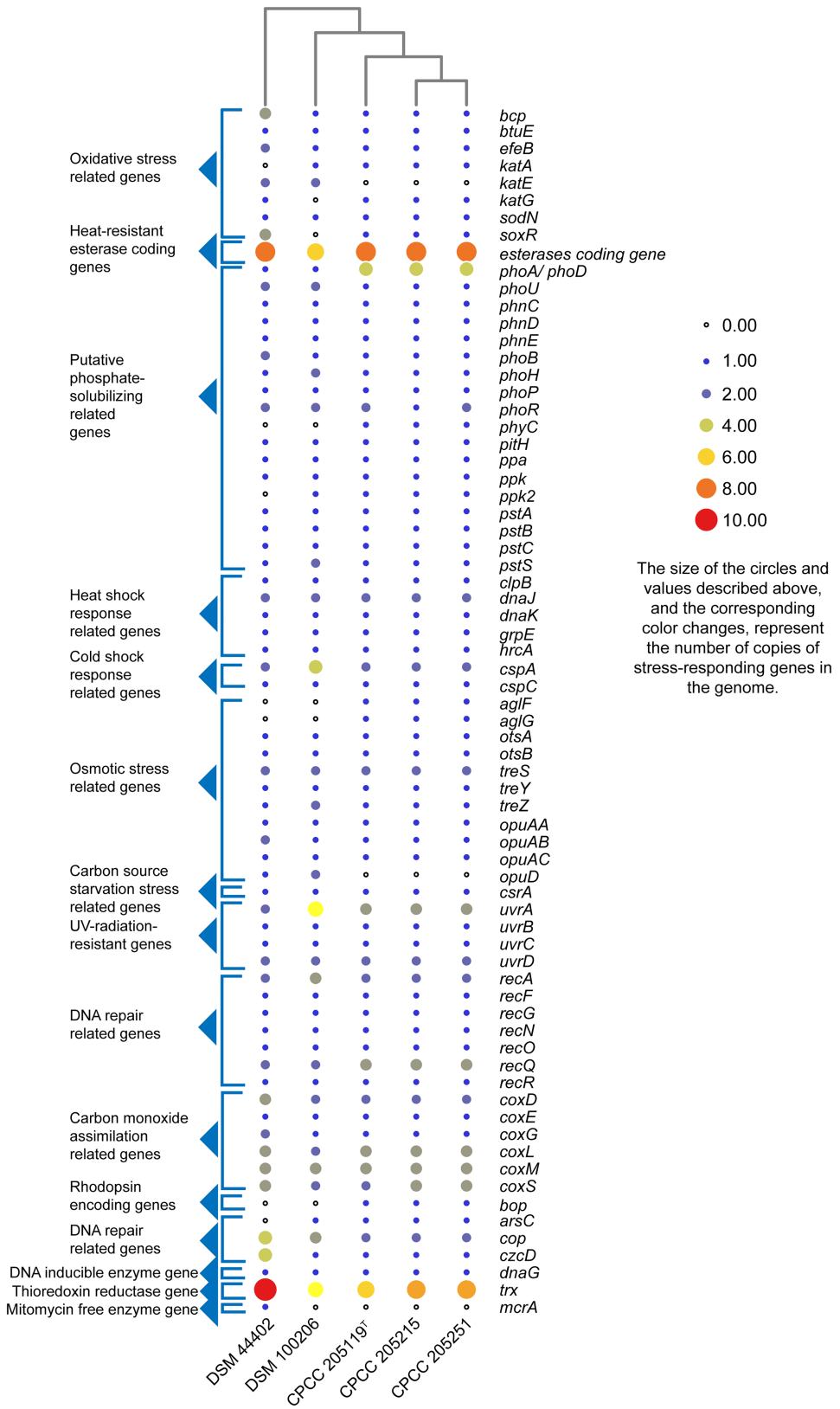

FIGURE 2 | Heatmap of putative stress-responding genes predicted in the genomes of strains CPCC 205119^{T}, CPCC 205215, CPCC 205251, and their closest phylogenic neighbors according to the copy number of the genes from the Rapid Annotation using Subsystem Technology (RAST) annotation.

Modestobacter. This proposal was well approved by the whole genome research repertoires including ANI, dDDH, AAI, POCP, and the pan-genome phylogenic analysis. The phenotypic properties of strains CPCC 205119^{T}, CPCC 205215, and CPCC 205251, such as the assimilation of carbon sources and chemotaxonomic characteristics (**Table 3**) well supported the classification these three stains as one so far unknown species in the genus *Modestobacter*. Therefore, based on the above phenotypic and genotypic data, we suggested to establish a new species in the genus *Modestobacter*, for which the name *M. deserti* sp. nov. was proposed, with strain CPCC 205119^{T} as the type strain.

Description of *Modestobacter deserti* sp. nov.

Modestobacter deserti sp. nov. (de.ser'ti. L. gen. n. *deserti* of a desert, where the organisms were acquired).

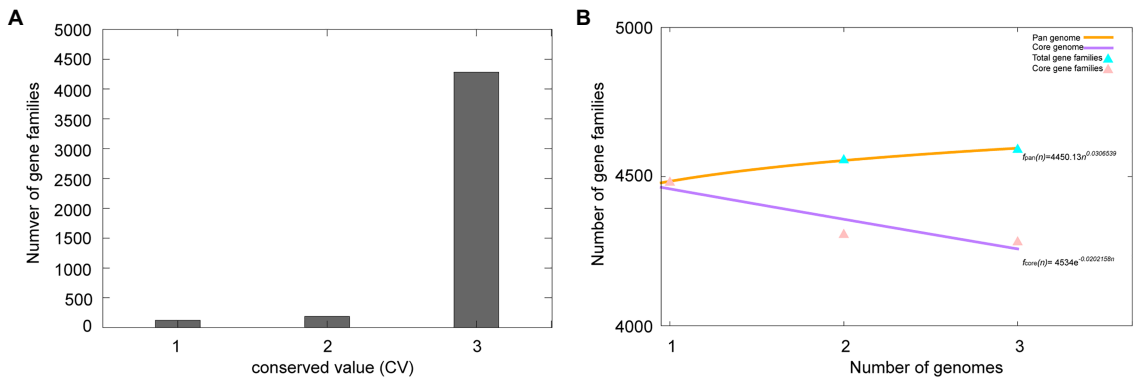

FIGURE 3 | Overview of the pan-genome generated by Bacterial Pan-genome Analysis (BPGA) using three strains of the species *Modestobacter deserti*. **(A)** The gene family frequency spectrum. **(B)** The pan genome profile trends of the species *Modestobacter deserti* obtained using clustering tools USEARCH.

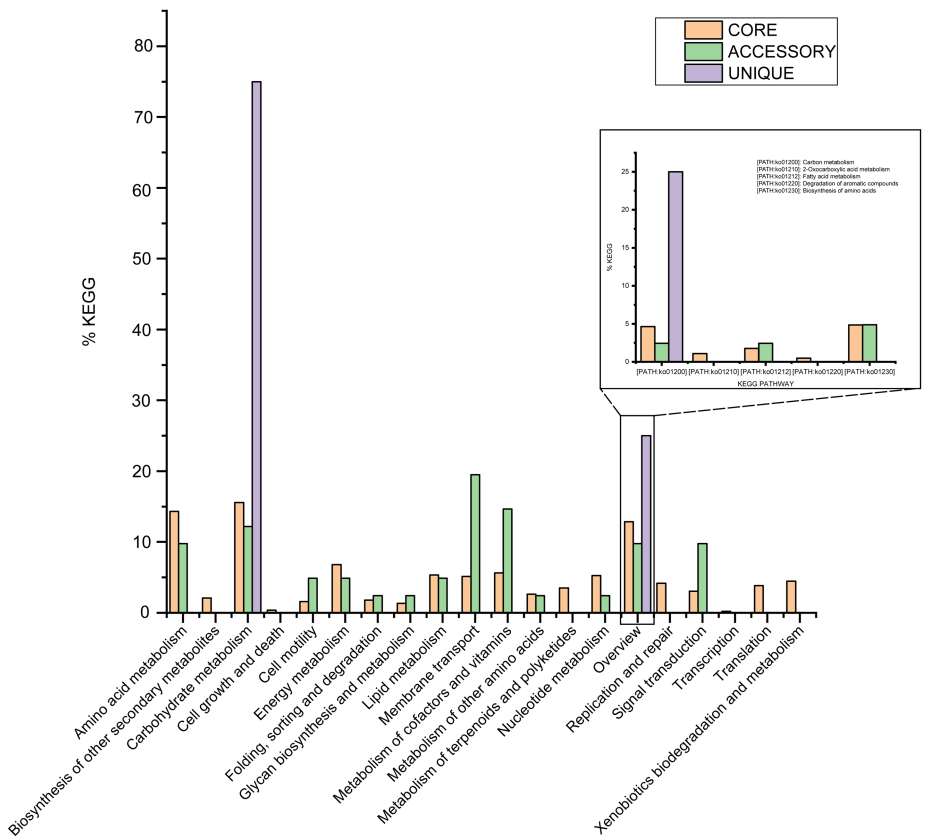

FIGURE 4 | The assigned metabolic pathways associated with the core, accessory, and unique genes among the species *Modestobacter deserti* from the KEGG database.

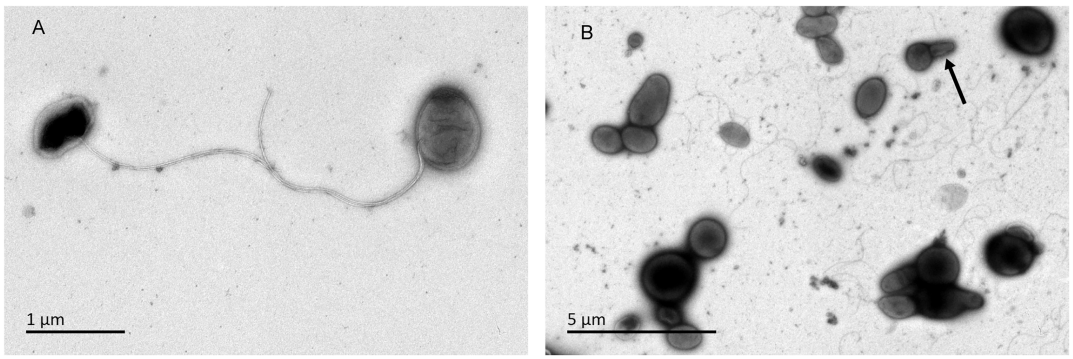

FIGURE 5 | Transmission electron micrograph of strain CPCC 205119^T grown on GYM semi-solid medium (0.3% agar) for 7 days at 28°C. Bar, 2 μm. **(A)** Showing the flagella; **(B)** arrow, indicating the bud-like structure.

TABLE 3 | Differentiating phenotypic characteristics of strain CPCC 205119^T, CPCC 205215, CPCC 205251, and their phylogenetically related species of the genus *Modestobacter*.

Characteristic	1	2	3	4	5
Colony colour	Orange or pink	Orange or pink	Orange or pink	Orange, black or yellow white	Pale pink
Flagella	+	+	+	+	–
Temperature for growth (°C)					
Range	10–37	10–37	10–37	20–37	0–28
Optimum	28–30	28–30	28–30	28	19–21
pH for growth					
Range	6.0–11.0	6.0–11.0	6.0–11.0	6.0–9.0	4.0–9.5
Optimum	7.0–8.0	7.0–8.0	7.0–8.0	7.5	8.0–8.5
Tolenrance of NaCl (%)	0–3	0–3	0–3	0–8	0–6
Reduction of nitrate	–	–	–	+	+
Urease	+	+	+	+	–
Production of H_2S	–	–	–	–	+
Enzyme activities (API ZYM)					
Acid phosphatase, esterase (C4), esterase lipase (C8), leucine arylamidase, valine arylamidase, naphthol-AS-B1-phosphohydrolase, β-glucosidase	+	+	+	+	–
Alkaline phosphatase, lipase (C14), trypsin, α-galactosidase, β-galactosidase	+	+	+	–	–
Utilization of (Biolog GEN III)					
Dextrin	+	+	+	+	–
d-fructose-6-PO_4, inosine	+	–	–	+	+
d-fucose, l-rhamnose	–	–	–	–	+
d-galactose, d-mannose, d-salicin, α-d-lactose	+	+	+	–	+
d-glucose-6-PO_4	+	–	–	+	–
d-melibiose, gentiobiose	–	–	–	+	–
d-rnaffinose	–	–	–	+	+
Glucuronamide	–	+	–	+	–
N-acetyl-d-glucosamine, *N*-acetyl-β-d-mannosamine	–	–	–	–	+
d-arabitol, d-mannitol	–	–	–	–	+
d-sorbitol	–	–	–	+	–
Glycerol	+	+	+	–	+
myo-inositol	+	–	+	–	+

(Continued)

TABLE 3 | Continued

Characteristic	1	2	3	4	5
d-serine	–	–	–	+	–
l-alanine, l-arginine, l-histidine	–	–	–	–	+
l-glutamic acid	+	+	+	–	+
Gelatin	+	+	+	+	–
Acetoacetic acid	–	+	+	+	+
Bromo-succinic acid, d-malic acid, propionic acid	+	+	+	+	–
Citric acid, d-galacturonic acid, l-pyroglutamic acid, *p*-hydroxy-phenylacetic acid	–	–	–	+	–
d-saccharic acid, l-lactic acid, *β*-Hydroxy-D,l-butyric acid	–	–	–	–	+
d-aspartic acid, mucic acid, quinic acid, *α*-keto-glutaric acid	–	–	–	+	+
d-gluconic acid	+	–	–	–	+
Formic acid	–	+	–	–	–
Methyl pyruvate, *α*-hydroxy-butyric acid	–	+	+	–	–
Pectin	–	+	+	+	–
Tween 40	+	+	+	–	–
DNA G+C content (%)	74.6	74.7	74.7	72	69.9
Phospholipids profile	APL1, APL2, DPG, PE, PG, PI, PIM, PME, UPL	APL1, APL2, DPG, PE, PG, PI, PIM, PME, UPL	APL1, APL2, DPG, PE, PG, PI, PIM, PME, UPL	DPG, PE, PG, PI, PIM	DPG, PE, PG, PI
Major Menaquinone(s)	MK-9(H_4)	MK-9(H_4)	MK-9(H_4)	MK-9(H_4)	MK-9(H_4), MK-8(H_4) and MK-9(H_6)
Fatty acids components (>5%)	$C_{18:1}$ *ω9c*, iso-$C_{16:0}$, $C_{16:0}$, iso- $C_{15:0}$, $C_{16:1}$ *ω7c*, $C_{18:0}$	$C_{18:1}$ *ω9c*, iso-$C_{16:0}$, $C_{17:1}$ *ω8c*, iso- $C_{15:0}$, $C_{16:1}$ *ω7c*, $C_{16:0}$	$C_{18:1}$ *ω9c*, $C_{17:1}$ *ω8c*, iso-$C_{16:0}$, $C_{16:1}$ *ω7c*, $C_{16:0}$, iso- $C_{15:0}$, $C_{18:0}$	iso-$C_{16:0}$, iso-$C_{15:0}$, $C_{16:1}$ *ω9c*, $C_{16:0}$, $C_{17:1}$ *ω9c*	iso-$C_{16:0}$, $C_{18:1}$, anteiso-$C_{17:0}$, cycle-$C_{19:0}$
Isolation source	Cyanobacteria-dominated soil crusts of the Tengger Desert, China	Moss-dominated soil crusts of the Tengger Desert, China	Cyanobacteria-dominated soil crusts of the Tengger Desert, China	Surface of deteriorated sandstone of a historic building, Spain	Soils from Linnaeus Terrace, Antarctica

1, CPCC 205119^T (data from this study); 2, CPCC 205215 (data from this study); 3, CPCC 205251 (data from this study); 4, M. lapidis DSM 100206^T (Trujillo et al., 2015); 5, M. multiseptatus DSM 44406^T (Golińska et al., 2020). All strains are Gram-reaction-positive, positive for motility, catalase and oxidase; contain meso-diaminopimelic in the cell wall and arabinose, glucose and ribose in the whole-cell hydrolysis. In API ZYM kits, all strains are positive for α-chymotrypsin, α-glucosidase and cystine arylamidase, negative for α-fucosidase, α-galactosidase, α-Mannosidase, N-acetyl-β-glucosaminidase and β-glucuronidase. In Biolog GEN III (MicroPlate), all strains are positive for acetic acid, α-d-glucose, α-keto-butyric acid, d-cellobiose, d-fructose, d-maltose, d-trehalose, d-turanose, l-aspartic acid, l-malic acid, and sucrose assimilation; negative for the utilization of 3-methyl glucose, acetoacetic acid, d-glucuronic acid, d-lactic acid methyl ester, d-serine, formic acid, glycyl-l-proline, l-fucose, l-galactonic acid lactone, l-serine, methyl pyruvate, N-acetyl-neuraminic acid, N-acetyl-d-galactosamine, stachyose, β-methyl-d-glucoside and γ-amino-butryric acid. DPG, diphosphatidylglycerol; PE, phosphatidylethanolamine; PME, phosphatidylmethylethanolamine; PG, phosphatidylglycerol; PI, phosphatidylinositol; PIM, phosphatidylinositol mannoside; APL, aminophospholipid; UPL, unidentified phospholipid. +, Positive; –, negative.

Cells are aerobic, Gram-staining-positive, cocci- to rod-shaped, motile, and non-sporing actinobacterium. The colonies are irregular, opaque, orange-red on most tested media. Grows at 10–37°C and pH 6.0–11.0, with optima at 28–30°C and pH 7.0–8.0, respectively. Grows in NaCl at concentrations up to not more than 3%. The activity of oxidase and catalase is positive. The production of H_2S, indole and melanin, hydrolysis of gelatin, starch, and cellulose are negative. Cells are positive for acid phosphatase, alkaline phosphatase, cystine arylamidase, esterase lipase (C8), esterase (C4), leucine arylamidase, lipase (C14), naphthol-AS-B1-phosphohydrolase, trypsin, valine arylamidase, *α*-glucosidase, *β*-glucosidase, *β*-galactosidase, and weekly positive for *α*-chymotrypsin, *α*-galactosidase in API ZYM strip. Acetic acid, bromo-succinic acid, D-cellobiose, Dextrin, D-fructose, D-galactose, D-malic acid, D-maltose, D-mannose, D-salicin, D-trehalose, D-turanose, gelatin, glycerol, L-aspartic acid, L-glutamic acid, L-malic acid, propionic acid, sucrose, Tween 40, *α*-D-glucose, *α*-D-lactose, and *α*-keto-butyric acid can be utilized as sole carbon sources in Biolog GEN III Micro-Plates. Acid is produced from esculin ferric citrate and potassium 5-ketogluconate. Cell wall contains alanine, glutamic acid, glycine and *meso*-diaminopimelic as diagnostic amino acids. The whole-cell hydrolysis contains arabinose, galactose, ribose and traces of glucose. The cellular polar lipid system includes DPG, PE, PG, PI, and PIM, as well as small amount of APL. The predominant respiratory quinone is MK-9(H_4), with minor of MK-8(H_4). The major fatty acids are $C_{18:1}\omega9c$, iso-$C_{16:0}$, $C_{16:0}$, iso-$C_{15:0}$, and $C_{16:1}\omega7c$. The G+C content of the genomic DNA is 74.7%. The type strain is CPCC 205119^T (=I12A-02624^T = NBRC 113528^T = KCTC 49201^T), isolated from the moss-dominated soil crust from the Shapotou NDER located in Tengger Desert situated at the Ningxia Hui

Autonomous Region, the north of China. The assembly sequences for the draft genome of CPCC 205119^T has been deposited in GenBank with the accession number JAAGWK000000000.

DISCUSSION

Based on the genomic information, we summarized genetic characteristics of the novel species *M. deserti* sp. nov. accommodating three isolates from the desert microbiological soil crusts. The detailed phenotypic properties illustrated the abilities of these strains to adapt to environmental stress.

In core genome of the species *M. deserti*, 37 gene clusters (1.6%) were mapped to bacterial chemotaxis (ko02030, pathway number in KEGG Orthology) and flagellar assembly (ko02040) pathway which was related to cell motility (KO09142, KEGG Orthology number). These gene clusters, including chemotaxis family related genes *cheA*, *cheB*, *cheR*, *cheW*, *cheY*, *mcp*, *motA*, *motB*, *rbsB*, *tar*, and *tap*, flagellar basal-body rod protein coding genes *flgB* and *flgC*, flagellar basal-body rod modification protein coding gene *flgD*, flagellar hook protein coding genes *flgE* and *flgL*, flagellar biosynthesis protein coding genes *flhA*, *flhB*, *fliP*, *fliQ*, and *fliR*, RNA polymerase sigma factor for flagellar operon coding gene *fliA*, flagellin coding gene *fliC*, flagellar hook-basal body complex protein coding gene *fliE*, flagellar M-ring protein coding gene *fliF*, flagellar motor switch protein coding genes *fliG and fliY*, flagellum-specific ATP synthase gene *fliI*, flagellar motor switch protein coding gene *fliM*. These genes might encode some factors and proteins to help the cells to adapt to harsh environment by sensing chemical gradients in their habitats and then move toward more favorable conditions. The interaction between above factors and proteins caused a change in behavior, such as in direction or speed of rotation of flagella (Miller et al., 2009).

Phosphorus (P) acquisition and assimilation are of fundamental importance in cell physiology because P is a kind of required nutrient in many of the metabolic and energy-producing pathways in bacteria. The phosphorus sources include organic phosphorus and inorganic phosphorus. Bacteria transport inorganic phosphate by high affinity phosphate transport system PstSCAB coded by the *pstSCAB* operon (Hudek et al., 2016; Martín and Liras, 2021), PhnCDE transport system (coded by the *phnCDE* gene clusters; Hove-Jensen et al., 2010) and Pit transport systems (coded by *pitH* gene; Hoffer et al., 2001). Both transport systems are regulated by the two-component system PhoR-PhoP or PhoR-PhoB, and also interact with the phosphate modulator PhoU. To respond to phosphate limitation, some bacteria species may trigger the expression of genes encoding extracellular enzymes, including alkaline phosphatases PhoA (coded by *phoA* gene), PhoC (coded by *phoC* gene), and the phospholipase PhoD (coded by *phoD* gene; Apel et al., 2007; Moura et al., 2001). In the KAAS annotation results of the three strains, phosphate ABC transporters corresponding genes *pstS, pstA*, *pstB*, and *pstC*, phosphonate ABC transporters related genes *phnD*, *phnE* and *phnC*, two component system related genes phoR and phoD were all sorted.

The phenotypic assays showed that all the three strains could assimilate pyrophosphate, thiophosphate, dithiophosphate, phosphoenol pyruvate, 2-deoxy-D-glucose 6-phosphate, and cysteamine-S-phosphate, especially, they could solubilize tricalcium phosphate [$Ca_3(PO_4)_2$] and phytin.

Assignment of metabolic pathways *via* the KEGG database, 2-deoxy-D-glucose-6-phosphate (C06369), dithiophosphate, phosphoenol pyruvate (C00074), and pyrophosphate (C00013) could be predicted from these three strains' metabolic pathway. In the RAST annotation results (**Figure 2**), the phytase coding gene (*phyC*) was retrieved from all the three genomes. It could be proposed that phytase could catalyze the hydrolysis of inorganic orthophosphate from phytin (Kerovuo et al., 1998).

At the genomic level, alkaline phosphatase genes (*phoA, phD*) and phosphate transport-related genes (*phoU*, *phnC*, *phnD*, *phnE*, *phoB*, *phoP*, *phoR*, *pitH*, *pstA*, *pstB*, and *pstC*, and *pstS*), as well as inorganic pyrophosphatase coding gene (*ppa*), phytase coding gene (*phyC*), phosphate starvation-inducible protein coding gene (*phoH*), and a polyphosphate kinase coding gene (*ppk*) were retrieved from all these three genomes (**Figure 2**). Alkaline phosphatase A was a kind of nonspecific phosphate monoesterase. Alkaline phosphatase D with broad substrate specificity has phosphatase activity toward nucleotide and sugar phosphates (without phosphodiesterase activity; Gomez and Ingram, 1995).

All the genomes of these three strains contained one copy of *aglF* gene (*α*-glucoside transport system permease protein AglF coding gene), one copy of *aglG* gene (*α*-glucoside transport system permease protein AglG coding gene), one copy of *otsA* gene (trehalose-phosphate synthase gene), one copy of *otsB* gene (trehalose 6-phosphate phosphatase gene), two copies of *treS* genes (maltose alpha-D-glucosyltransferase gene), one copy of *treY* gene (maltooligosyl trehalose synthase gene), and one copy of *treZ* gene (malto-oligosyltrehalose trehalohydrolase gene). The proteins coded by these genes reported to be involved in the pathway of trehalose uptake and biosynthesis, which is part of starch and sucrose metabolism (ko00500), and these proteins were supposed to respond to the osmotic stress (Boos et al., 1990; Pan et al., 2008; Reina-Bueno et al., 2012; Chen et al., 2017; MacIntyre et al., 2020). Accumulated trehalose seems to have a major role in protecting the cells from osmotic pressure imbalance. As a major compatible solute, trehalose is involved in the osmotic stress response, cellular adaptation and survival to heat and desiccation stress (Reina-Bueno et al., 2012). The physiological tests results showed that strains CPCC 205119^T, CPCC 205215, and CPCC 205251 could assimilate D-trehalose, which might contributed to maintaining the osmotic balance inside and outside the cell.

In the core genome of the species *M. deserti*, 96 gene clusters (4.2%) were mapped to replication and repair (KO09124) contained DNA replication (ko03030), base excision repair (ko03410), nucleotide excision repair (ko03420), mismatch repair (ko03430), homologous recombination (ko03440), and non-homologous end-joining (ko03450) pathway, such as *uvrA* (UvrABC system protein A coding gene), *uvrB* (UvrABC system protein B coding gene), *uvrC* (UvrABC system protein C coding gene), *uvrD* (DNA helicase II coding gene), *recA* (protein RecA

coding gene), *recB* (RecBCD enzyme subunit RecB coding gene), *recC* (RecBCD enzyme subunit RecC coding gene), *recD* (RecBCD enzyme subunit RecD coding gene), *recF* (DNA replication and repair protein RecF coding gene), *recG* (ATP-dependent DNA helicase RecG coding gene), *recO* (DNA repair protein RecO coding gene), *recQ* (ATP-dependent DNA helicase RecQ coding gene), and *recR* (recombination protein RecR coding gene). Thirty-seven gene clusters (1.5%) were mapped to carbon fixation pathways in prokaryotes (ko00720), such as *coxS* (carbon monoxide dehydrogenase small chain coding gene), *coxM* (carbon monoxide dehydrogenase medium chain coding gene), and *coxL* (carbon monoxide dehydrogenase large chain coding gene). In the core genome, *katG* gene (catalase-peroxidase coding gene) was retrieved, and the protein coded by this gene could protect strains against toxic reactive oxygen species (ROS) including hydrogen peroxide as well as organic peroxides. The gene *csrA* was also retrieved from the core genome, this key regulator could bind to mRNA to regulate the gene expression, thereby, shift from rapid growth to stress survival, or might help the strain to survive in low carbon habitats by activating peptide uptake (Schultz and Matin, 1991; Lucchetti-Miganeh et al., 2008; Rasmussen et al., 2013).

These three strains of the species *M. deserti* showed a wide substrate-assimilation spectrum, including monosaccharide, oligosaccharide, polysaccharide (dextrin), glycerol, hexosephosphates, amino acids, carboxylic acids, fatty acids, and phosphate esters (**Supplementary Table S3**), which led to the assumption that these strains have evolved to enable access to various carbon sources or to be involved in catabolic pathways. Abundant and various of substrates that could be assimilated contain ester bonds. Own to the abundance of esterases (EC 3.1.1.X) in the strains, they could hydrolyze these ester bonds. So, these esterases might promote these strains survival abilities in dry environments (Bornscheuer, 2002).

Actinobacteria have been well recognized as the prolific producers of natural compounds (Hu et al., 2019; Yang et al., 2021). Typically, *Streptomyces* spp. and *Micromonospora* spp. are rich in secondary metabolite synthesis gene clusters (dozens; Carro et al., 2018; Kim et al., 2019). However, the results from antiSMASH database showed that in these three strains of the species *M. deserti*, only seven secondary metabolite gene clusters with moderate similarities to previously described secondary metabolite biosynthetic gene clusters were retrieved (**Supplementary Table S5**). These gene clusters exhibited 16–100% similarities to previously reported secondary metabolite biosynthetic gene clusters, such as 5-isoprenylindole-3-carboxylate *β*-D-glycosyl easter, alkyl-O-dihydrogeranyl-methoxyhydroquinones, arsono-polyketide, desferrioxamine, hiroshidine, isorenieratene and tallysomysin A gene clusters. While abundant stress-responding genes were found in the core genome of the newly established species, which were proposed to contribute greatly to their survival abilities in harsh desert environments. Therefore, the species *M. deserti* might serve as research model organisms for poineer microorganisms adaption and evolution in extreme environments.

DATA AVAILABILITY STATEMENT

The datasets presented in this study can be found in online repositories. The names of the repository/repositories and accession number(s) can be found in the article/**Supplementary Material**. The DDBJ/EMBL/GenBank accession numbers for the 16S rRNA gene sequences of strains CPCC 205119^T, CPCC 205215 and CPCC 205251 are MK392028, MN567210 and MN567664, respectively. This whole genome shotgun projects of strains CPCC 205119^T, CPCC 205215 and CPCC 205251 have been deposited at DDBJ/ENA/GenBank under the accession numbers JAAGWK000000000, WGGQ00000000 and JAABOZ000000000, respectively.

AUTHOR CONTRIBUTIONS

Z-MJ, B-HZ, and H-MS carried out the experiments and prepared the manuscript. TZ and L-YY collected the samples. Y-QZ designed the research and analyzed the data. All authors contributed to the article and approved the submitted version.

FUNDING

This research was supported by National Natural Science Foundation of China (32170021 and 31670010), Beijing Natural Science Foundation (5212018), the National Infrastructure of Microbial Resources (NIMR-2021-3), and CAMS Innovation Fund for Medical Sciences (CIFMS; 2016-I2M-2-002).

SUPPLEMENTARY MATERIAL

The Supplementary Material for this article can be found online at: https://www.frontiersin.org/articles/10.3389/fmicb.2021.742798/full#supplementary-material

REFERENCES

Apel, A. K., Sola-Landa, A., Rodríguez-García, A., and Martín, J. F. (2007). Phosphate control of *phoA*, *phoC* and *phoD* gene expression in *Streptomyces coelicolor* reveals significant differences in binding of PhoP to their promoter regions. *Microbiology* 153, 3527–3537. doi: 10.1099/mic.0.2007/007070-0

Auch, A. F., von Jan, M., Klenk, H. P., and Göker, M. (2010). Digital DNA-DNA hybridization for microbial species delineation by means of genome-to-genome sequence comparison. *Stand. Genomic Sci.* 2, 117–134. doi: 10.4056/sigs.531120

Aziz, R. K., Bartels, D., Best, A. A., DeJongh, M., Disz, T., Edwards, R. A., et al. (2008). The RAST server: rapid annotations using subsystems technology. *BMC Genomics* 9:75. doi: 10.1186/1471-2164-9-75

Blin, K., Shaw, S., Steinke, K., Villebro, R., Ziemert, N., Lee, S. Y., et al. (2019). antiSMASH 5.0: updates to the secondary metabolite genome mining pipeline. *Nucleic Acids Res.* 47, W81–W87. doi: 10.1093/nar/gkz310

Boos, W., Ehmann, U., Forkl, H., Klein, W., Rimmele, M., and Postma, P. (1990). Trehalose transport and metabolism in *Escherichia coli*. *J. Bacteriol.* 172, 3450–3461. doi: 10.1128/jb.172.6.3450-3461.1990

Bornscheuer, U. T. (2002). Microbial carboxyl esterases: classification, properties and application in biocatalysis. *FEMS Microbiol. Rev.* 26, 73–81. doi: 10.1111/j.1574-6976.2002.tb00599.x

Busarakam, K., Bull, A. T., Trujillo, M. E., Riesco, R., Sangal, V., van Wezel, G. P., et al. (2016). *Modestobacter caceresii* sp. nov., novel actinobacteria with an insight into their adaptive mechanisms for survival in extreme hyper-arid Atacama Desert soils. *Syst. Appl. Microbiol.* 39, 243–251. doi: 10.1016/j.syapm.2016.03.007

Carro, L., Nouioui, I., Sangal, V., Meier-Kolthoff, J. P., and Trujillo, M. E., Montero-Calasanz, M. D. C., et al. (2018). Genome-based classification of micromonosporae with a focus on their biotechnological and ecological potential. *Sci. Rep.* 8:525. doi: 10.1038/s41598-017-17392-0

Chaudhari, N. M., Gupta, V. K., and Dutta, C. (2016). BPGA- an ultra-fast pan-genome analysis pipeline. *Sci. Rep.* 6:24373. doi: 10.1038/srep24373

Chen, X., An, L., Fan, X., Ju, F., Zhang, B., Sun, H., et al. (2017). A trehalose biosynthetic enzyme doubles as an osmotic stress sensor to regulate bacterial morphogenesis. *PLoS Genet.* 13:e1007062. doi: 10.1371/journal.pgen.1007062

Chouaia, B., Crotti, E., Brusetti, L., Daffonchio, D., Essoussi, I., Nouioui, I., et al. (2012). Genome sequence of *Blastococcus saxobsidens* DD2, a stone-inhabiting bacterium. *J. Bacteriol.* 194, 2752–2753. doi: 10.1128/JB.00320-12

Collins, M. D., Pirouz, T., Goodfellow, M., and Minnikin, D. E. (1977). Distribution of menaquinones in actinomycetes and corynebacteria. *J. Gen. Microbiol.* 100, 221–230. doi: 10.1099/00221287-100-2-221

Essoussi, I., Ghodhbane-Gtari, F., Amairi, H., Sghaier, H., Jaouani, A., Brusetti, L., et al. (2010). Esterase as an enzymatic signature of *Geodermatophilaceae* adaptability to Sahara desert stones and monuments. *J. Appl. Microbiol.* 108, 1723–1732. doi: 10.1111/j.1365-2672.2009.04580.x

Felsenstein, J. (1981). Evolutionary trees from DNA sequences: a maximum likelihood approach. *J. Mol. Evol.* 17, 368–376. doi: 10.1007/BF01734359

Felsenstein, J. (1985). Confidence limits on phylogenies: an approach using the bootstrap. *Evolution* 39, 783–791. doi: 10.1111/j.1558-5646.1985.tb00420.x

Golinska, P., Montero-Calasanz, M. D. C., Świecimska, M., Yaramis, A., Igual, J. M., Bull, A. T., et al. (2020). *Modestobacter excelsi* sp. nov., a novel actinobacterium isolated from a high altitude Atacama Desert soil. *Syst. Appl. Microbiol.* 43:126051. doi: 10.1016/j.syapm.2019.126051

Golińska, P., Świecimska, M., Montero-Calasanz, M. D. C., Yaramis, A., Igual, J. M., Bull, A. T., et al. (2020). *Modestobacter altitudinis* sp. nov., a novel actinobacterium isolated from Atacama Desert soil. *Int. J. Syst. Evol. Microbiol.* 70, 3513–3527. doi: 10.1099/ijsem.0.004212

Gomez, P. F., and Ingram, L. O. (1995). Cloning, sequencing and characterization of the alkaline phosphatase gene (*phoD*) from *Zymomonas mobilis*. *FEMS Microbiol. Lett.* 125, 237–245. doi: 10.1111/j.1574-6968.1995.tb07364.x

Groth, I., Schumann, P., Rainey, F. A., Martin, K., Schuetze, B., and Augsten, K. (1997). *Demetria terragena* gen. nov., sp. nov., a new genus of actinomycetes isolated from compost soil. *Int. J. Syst. Bacteriol.* 47, 1129–1133. doi: 10.1099/00207713-47-4-1129

Gtari, M., Essoussi, I., Maaoui, R., Sghaier, H., Boujmil, R., Gury, J., et al. (2012). Contrasted resistance of stone-dwelling *Geodermatophilaceae* species to stresses known to give rise to reactive oxygen species. *FEMS Microbiol. Ecol.* 80, 566–577. doi: 10.1111/j.1574-6941.2012.01320.x

Hickson, I. D. (2003). RecQ helicases: caretakers of the genome. *Nat. Rev. Cancer* 3, 169–178. doi: 10.1038/nrc1012

Hoffer, S. M., Uden, N., and Tommassen, J. (2001). Expression of the *pho* regulon interferes with induction of the *uhpT* gene in *Escherichia coli* K-12. *Arch. Microbiol.* 176, 370–376. doi: 10.1007/s002030100339

Hove-Jensen, B., Rosenkrantz, T. J., Zechel, D. L., and Willemoës, M. (2010). Accumulation of intermediates of the carbon-phosphorus lyase pathway for phosphonate degradation in *phn* mutants of *Escherichia coli*. *J. Bacteriol.* 192, 370–374. doi: 10.1128/JB.01131-09

Hu, X. W., Hu, X. X., Hu, X. M., Li, S. F., Li, L. L., Yu, L. Y., et al. (2019). Cytotoxic and antibacterial cervinomycins B1-4 from a *Streptomyces* species. *J. Nat. Prod.* 82, 2337–2342. doi: 10.1021/acs.jnatprod.9b00198

Hudek, L., Premachandra, D., Webster, W. A., and Bräu, L. (2016). Role of phosphate transport system component PstB1 in phosphate internalization by *Nostoc punctiforme*. *Appl. Environ. Microbiol.* 82, 6344–6356. doi: 10.1128/AEM.01336-16

Jaouani, A., Neifar, M., Hamza, A., Chaabouni, S., Martinez, M. J., and Gtari, M. (2012). Purification and characterization of a highly thermostable esterase from the actinobacterium *Geodermatophilus obscurus* strain G20. *J. Basic Microbiol.* 52, 653–660. doi: 10.1002/jobm.201100428

Kempf, B., and Bremer, E. (1995). OpuA, an osmotically regulated binding protein-dependent transport system for the osmoprotectant glycine betaine in *Bacillus subtilis*. *J. Biol. Chem.* 270, 16701–16713. doi: 10.1074/jbc.270.28.16701

Kerovuo, J., Lauraeus, M., Nurminen, P., Kalkkinen, N., and Apajalahti, J. (1998). Isolation, characterization, molecular gene cloning, and sequencing of a novel phytase from *Bacillus subtilis*. *Appl. Environ. Microbiol.* 64, 2079–2085. doi: 10.1128/AEM.64.6.2079-2085.1998

Kim, B., Han, S. R., Lamichhane, J., Park, H., and Oh, T. J. (2019). Draft genome analysis of antimicrobial *Streptomyces* isolated from himalayan lichen. *J. Microbiol. Biotechnol.* 29, 1144–1154. doi: 10.4014/jmb.1906.06037

Kim, M., Oh, H. S., Park, S. C., and Chun, J. (2014). Towards a taxonomic coherence between average nucleotide identity and 16S rRNA gene sequence similarity for species demarcation of prokaryotes. *Int. J. Syst. Evol. Microbiol.* 64, 346–351. doi: 10.1099/ijs.0.059774-0

Kimura, M. (1979). The neutral theory of molecular evolution. *Sci. Am.* 241, 98–100, 102, 108 passim. doi:10.1038/scientificamerican1179-98

Kluge, A. G., and Farris, J. S. (1969). Quantitative phyletics and the evolution of anurans. *Syst. Zool.* 18, 1–32. doi: 10.2307/2412407

Kroppenstedt, R. M. (1985). Fatty acid and menaquinone analysis of actinomycetes and related organisms. *Soc. Appl. Bacteriol. Tech. Ser.* 173–199.

Kumar, S., Stecher, G., Li, M., Knyaz, C., and Tamura, K. (2018). MEGA X: molecular evolutionary genetics analysis across computing platforms. *Mol. Biol. Evol.* 35, 1547–1549. doi: 10.1093/molbev/msy096

Li, J. S., Bi, Y. T., Dong, C., Yang, J. F., and Liang, W. D. (2011). Transcriptome analysis of adaptive heat shock response of *Streptococcus thermophilus*. *PLoS One* 6:e25777. doi: 10.1371/journal.pone.0025777

Li, W. J., Xu, P., Schumann, P., Zhang, Y. Q., Pukall, R., Xu, L. H., et al. (2007). *Georgenia ruanii* sp. nov., a novel actinobacterium isolated from forest soil in Yunnan (China), and emended description of the genus *Georgenia*. *Int. J. Syst. Evol. Microbiol.* 57, 1424–1428. doi: 10.1099/ijs.0.64749-0

Long, L. J., Lee, P. H., Small, E. M., Hillyer, C., Guo, Y., and Osley, M. A. (2020). Regulation of UV damage repair in quiescent yeast cells. *DNA Repair* 90:102861. doi: 10.1016/j.dnarep.2020.102861

Lorite, M. J., Tachil, J., Sanjuan, J., Meyer, O., and Bedmar, E. J. (2000). Carbon monoxide dehydrogenase activity in *Bradyrhizobium japonicum*. *Appl. Environ. Microbiol.* 66, 1871–1876. doi: 10.1128/AEM.66.5.1871-1876.2000

Lowe, T. M., and Eddy, S. R. (1997). tRNAscan-SE: a program for improved detection of transfer RNA genes in genomic sequence. *Nucleic Acids Res.* 25, 955–964. doi: 10.1093/nar/25.5.955

Lucchetti-Miganeh, C., Burrowes, E., Baysse, C., and Ermel, G. (2008). The post-transcriptional regulator CSRA plays a central role in the adaptation of bacterial pathogens to different stages of infection in animal hosts. *Microbiology* 154, 16–29. doi: 10.1099/mic.0.2007/012286-0

MacIntyre, A. M., Barth, J. X., Pellitteri-Hahn, M. C., Scarlett, C. O., Genin, S., and Allen, C. (2020). Trehalose synthesis contributes to osmotic stress tolerance and virulence of the bacterial wilt pathogen *Ralstonia solanacearum*. *Mol. Plant-Microbe Interact.* 33, 462–473. doi: 10.1094/MPMI-08-19-0218-R

Manthei, K. A., Hill, M. C., Burke, J. E., Butcher, S. E., and Keck, J. L. (2015). Structural mechanisms of DNA binding and unwinding in bacterial RecQ helicases. *Proc. Natl. Acad. Sci. U. S. A.* 112, 4292–4297. doi: 10.1073/pnas.1416746112

Martín, J. F., and Liras, P. (2021). Molecular mechanisms of phosphate sensing, transport and signalling in *Streptomyces* and related *Actinobacteria*. *Int. J. Mol. Sci.* 22:1129. doi: 10.3390/ijms22031129

Martindale, J. L., and Holbrook, N. J. (2002). Cellular response to oxidative stress: signaling for suicide and survival. *J. Cell. Physiol.* 192, 1–15. doi: 10.1002/jcp.10119

Meier, A., Kirschner, P., Schröder, K. H., Wolters, J., Kroppenstedt, R. M., and Böttger, E. C. (1993). *Mycobacterium intermedium* sp. nov. *Int. J. Syst. Bacteriol.* 43, 204–209. doi: 10.1099/00207713-43-2-204

Meier-Kolthoff, J. P., Auch, A. F., Klenk, H. P., and Göker, M. (2013). Genome sequence-based species delimitation with confidence intervals and improved distance functions. *BMC Bioinformatics* 14:60. doi: 10.1186/1471-2105-14-60

Miller, L. D., Russell, M. H., and Alexandre, G. (2009). Diversity in bacterial chemotactic responses and niche adaptation. *Adv. Appl. Microbiol.* 66, 53–75. doi: 10.1016/s0065-2164(08)00803-4

Ministry of Agriculture of the People's Republic of China (2010). General technical requirements for production strain quality of microbial fertilizer (NY/T 1847–2010). 4–5.

Minnikin, D. E., O'Donnell, A. G., Goodfellow, M., Alderson, G., Athalye, M., Schaal, A., et al. (1984). An integrated procedure for the extraction of bacterial isoprenoid quinones and polar lipids. *J. Microbiol. Methods* 2, 233–241. doi: 10.1016/0167-7012(84)90018-6

Montero-Calasanz, M. D. C., Yaramis, A., Nouioui, I., Igual, J. M., Spröer, C., Castro, J. F., et al. (2019). *Modestobacter italicus* sp. nov., isolated from Carrara marble quarry and emended descriptions of the genus *Modestobacter* and the species *Modestobacter marinus*, *Modestobacter multiseptatus*, *Modestobacter roseus* and *Modestobacter versicolor*. *Int. J. Syst. Evol. Microbiol.* 69, 1537–1545. doi: 10.1099/ijsem.0.003282

Moura, R. S., Martı, J. F., Martı, N. A., and Liras, P. (2001). Substrate analysis and molecular cloning of the extracellular alkaline phosphatase of *Streptomyces griseus*. *Microbiology* 147, 1525–1533. doi: 10.1099/00221287-147-6-1525

Normand, P. (2006). *Geodermatophilaceae* fam. nov., a formal description. *Int. J. Syst. Evol. Microbiol.* 56, 2277–2278. doi: 10.1099/ijs.0.64298-0

Normand, P., Gury, J., Pujic, P., Chouaia, B., Crotti, E., Brusetti, L., et al. (2012). Genome sequence of radiation-resistant *Modestobacter marinus* strain BC501, a representative actinobacterium that thrives on calcareous stone surfaces. *J. Bacteriol.* 194, 4773–4774. doi: 10.1128/JB.01029-12

Page, A. J., Cummins, C. A., Hunt, M., Wong, V. K., Reuter, S., Holden, M., et al. (2015). Roary: rapid large-scale prokaryote pan genome analysis. *Bioinformatics* 31, 3691–3693. doi: 10.1093/bioinformatics/btv421

Pan, Y. T., Carroll, J. D., Asano, N., Pastuszak, I., Edavana, V. K., and Elbein, A. D. (2008). Trehalose synthase converts glycogen to trehalose. *FEBS J.* 275, 3408–3420. doi: 10.1111/j.1742-4658.2008.06491.x

Pasamontes, L., Haiker, M., Wyss, M., Tessier, M., and Loon-van, A. P. (1997). Gene cloning, purification, and characterization of a heat-stable phytase from the fungus *Aspergillus fumigatus*. *Appl. Environ. Microbiol.* 63, 1696–1700. doi: 10.1128/aem.63.5.1696-1700.1997

Qin, Q. L., Xie, B. B., Zhang, X. Y., Chen, X. L., Zhou, B. C., Zhou, J., et al. (2014). A proposed genus boundary for the prokaryotes based on genomic insights. *J. Bacteriol.* 196, 2210–2215. doi: 10.1128/JB.01688-14

Rasmussen, J. J., Vegge, C. S., Frokiaer, H., Howlett, R. M., Krogfelt, K. A., Kelly, D. J., et al. (2013). *Campylobacter jejuni* carbon starvation protein a (CSTA) is involved in peptide utilization, motility and agglutination, and has a role in stimulation of dendritic cells. *J. Med. Microbiol.* 62, 1135–1143. doi: 10.1099/jmm.0.059345-0

Reina-Bueno, M., Argandona, M., Nieto, J. J., Hidalgo-Garcia, A., Iglesias-Guerra, F., Delgado, M. J., et al. (2012). Role of trehalose in heat and desiccation tolerance in the soil bacterium *Rhizobium etli*. *BMC Microbiol.* 12:207. doi: 10.1186/1471-2180-12-207

Rodriguez-R, L. M., and Konstantinidis, K. (2014). Bypassing cultivation to identify bacterial species. *Microbe Magazine* 9, 111–118. doi: 10.1128/microbe.9.111.1

Rodriguez-R, L. M., and Konstantinidis, K. T. (2016). The enveomics collection: a toolbox for specialized analyses of microbial genomes and metagenomes. *PeerJ Preprints* 4:e1900v1. doi: 10.7287/peerj.preprints.1900v1

Romeo, T. (1998). Global regulation by the small RNA-binding protein CsrA and the non-coding RNA molecule CsrB. *Mol. Microbiol.* 29, 1321–1330. doi: 10.1046/j.1365-2958.1998.01021.x

Romeo, T., Gong, M., Liu, M. Y., and Brun-Zinkernagel, A. M. (1993). Identification and molecular characterization of csrA, a pleiotropic gene from *Escherichia coli* that affects glycogen biosynthesis, gluconeogenesis, cell size, and surface properties. *J. Bacteriol.* 175, 4744–4755. doi: 10.1128/jb.175.15.4744-4755.1993

Schleifer, K. H., and Kandler, O. (1972). Peptidoglycan types of bacterial cell walls and their taxonomic implications. *Bacteriol. Rev.* 36, 407–477. doi: 10.1128/br.36.4.407-477.1972

Schultz, J. E., and Matin, A. (1991). Molecular and functional characterization of a carbon starvation gene of *Escherichia coli*. *J. Mol. Biol.* 218, 129–140. doi: 10.1016/0022-2836(91)90879-B

Sghaier, H., Hezbri, K., Ghodhbane-Gtari, F., Pujic, P., Sen, A., Daffonchio, D., et al. (2016). Stone-dwelling actinobacteria *Blastococcus saxobsidens*, *Modestobacter marinus* and *Geodermatophilus obscurus* proteogenomes. *ISME J.* 10, 21–29. doi: 10.1038/ismej.2015.108

Shand, R. F., and Betlach, M. C. (1994). bop gene cluster expression in bacteriorhodopsin-overproducing mutants of *Halobacterium halobium*. *J. Bacteriol.* 176, 1655–1660. doi: 10.1128/jb.176.6.1655-1660.1994

Shirlng, E. B., and Gottlieb, D. (1966). Methods for characterization of *Streptomyces* species. *Int. J. Syst. Bacteriol.* 16, 313–340. doi: 10.1099/00207713-16-3-313

Song, Y., Jiang, C. Y., Liang, Z. L., Wang, B. J., Jiang, Y., Yin, Y., et al. (2020). *Casimicrobium huifangae* gen. nov., sp. nov., a Ubiquitous "Most-Wanted" core bacterial taxon from municipal wastewater treatment plants. *Appl. Environ. Microbiol.* 86:e02209-19. doi: 10.1128/AEM.02209-19

Staneck, J. L., and Roberts, G. D. (1974). Simplified approach to identification of aerobic actinomycetes by thin-layer chromatography. *Appl. Microbiol.* 28, 226–231. doi: 10.1128/am.28.2.226-231.1974

Sun, H. M., Zhang, T., Yu, L. Y., Sen, K., and Zhang, Y. Q. (2015). Ubiquity, diversity and physiological characteristics of *Geodermatophilaceae* in Shapotou National Desert Ecological Reserve. *Front. Microbiol.* 6:1059. doi: 10.3389/fmicb.2015.01059

Tanaka, T., Kawasaki, K., Daimon, S., Kitagawa, W., Yamamoto, K., Tamaki, H., et al. (2014). A hidden pitfall in the preparation of agar media undermines microorganism cultivability. *Appl. Environ. Microbiol.* 80, 7659–7666. doi: 10.1128/AEM.02741-14

Trujillo, M. E., Goodfellow, M., Busarakam, K., and Riesco, R. (2015). *Modestobacter lapidis* sp. nov. and *Modestobacter muralis* sp. nov., isolated from a deteriorated sandstone historic building in Salamanca, Spain. *Antonie Van Leeuwenhoek* 108, 311–320. doi: 10.1007/s10482-015-0482-7

Xu, P., Li, W. J., Tang, S. K., Zhang, Y. Q., Chen, G. Z., Chen, H. H., et al. (2005). *Naxibacter alkalitolerans* gen. nov., sp. nov., a novel member of the family '*Oxalobacteraceae*' isolated from China. *Int. J. Syst. Evol. Microbiol.* 55, 1149–1153. doi: 10.1099/ijs.0.63407-0

Yang, X., Zhu, Z. H., Ji, X., Liu, Z. M., Zhang, H., and Wei, B. (2021). Complete genome sequence of *Micromonospora craniellae* LHW63014T, a potential metal ion-chelating agent producer. *Mar. Genomics* 57:100830. doi: 10.1016/j.margen.2020.100830

Yoon, S. H., Ha, S. M., Kwon, S., Lim, J., Kim, Y., Seo, H., et al. (2017a). Introducing EzBioCloud: a taxonomically united database of 16S rRNA gene sequences and whole-genome assemblies. *Int. J. Syst. Evol. Microbiol.* 67, 1613–1617. doi: 10.1099/ijsem.0.001755

Yoon, S.-H., Ha, S.-M., Lim, J., Kwon, S., and Chun, J. (2017b). A large-scale evaluation of algorithms to calculate average nucleotide identity. *Antonie Van Leeuwenhoek* 110, 1281–1286. doi: 10.1007/s10482-017-0844-4

Yuan, L. J., Zhang, Y. Q., Guan, Y., Wei, Y. Z., Li, Q. P., Yu, L. Y., et al. (2008). *Saccharopolyspora antimicrobica* sp. nov., an actinomycete from soil. *Int. J. Syst. Evol. Microbiol.* 58, 1180–1185. doi: 10.1099/ijs.0.65532-0

Zhang, B. H., Salam, N., Cheng, J., Li, H. Q., Yang, J. Y., Zha, D. M., et al. (2016). *Modestobacter lacusdianchii* sp. nov., a phosphate-solubilizing actinobacterium with ability to promote microcystis growth. *PLoS One* 11:e0161069. doi: 10.1371/journal.pone.0161069

Zhou, Z. H., Liu, Z. H., Qian, Y. D., Kim, S. B., and Goodfellow, M. (1998). *Saccharopolyspora spinosporotrichia* sp. nov., a novel actinomycete from soil. *Int. J. Syst. Bacteriol.* 48(Pt 1), 53–58. doi: 10.1099/00207713-48-1-53

Conflict of Interest: The authors declare that the research was conducted in the absence of any commercial or financial relationships that could be construed as a potential conflict of interest.

Publisher's Note: All claims expressed in this article are solely those of the authors and do not necessarily represent those of their affiliated organizations, or those of the publisher, the editors and the reviewers. Any product that may be evaluated in this article, or claim that may be made by its manufacturer, is not guaranteed or endorsed by the publisher.

frontiers in Microbiology

ORIGINAL RESEARCH
published: 24 November 2021
doi: 10.3389/fmicb.2021.725159

Iocasia fonsfrigidae NS-1 gen. nov., sp. nov., a Novel Deep-Sea Bacterium Possessing Diverse Carbohydrate Metabolic Pathways

*Jing Zhang[1,2,3,4,5], Yuechao Zhang[6], Rui Liu[1,2,4], Ruining Cai[1,2,3,4], Fanghua Liu[6] and Chaomin Sun[1,2,4]**

[1] CAS Key Laboratory of Experimental Marine Biology and Center of Deep-Sea Research, Institute of Oceanology, Chinese Academy of Sciences, Qingdao, China, [2] Laboratory for Marine Biology and Biotechnology, Qingdao National Laboratory for Marine Science and Technology, Qingdao, China, [3] College of Earth Science, University of Chinese Academy of Sciences, Beijing, China, [4] Center for Ocean Mega-Science, Chinese Academy of Sciences, Qingdao, China, [5] School of Life Sciences, Hebei University, Baoding, China, [6] Key Laboratory of Coastal Biology and Biological Resources Utilization, Yantai Institute of Coastal Zone Research, Chinese Academy of Sciences, Yantai, China

Resolving metabolisms of deep-sea microorganisms is crucial for understanding ocean energy cycling. Here, a strictly anaerobic, Gram-negative strain NS-1 was isolated from the deep-sea cold seep in the South China Sea. Phylogenetic analysis based on 16S rRNA gene sequence indicated that strain NS-1 was most closely related to the type strain *Halocella cellulosilytica* DSM 7362^T (with 92.52% similarity). A combination of phylogenetic, genomic, and physiological traits with strain NS-1, was proposed to be representative of a novel genus in the family Halanaerobiaceae, for which *Iocasia fonsfrigidae* NS-1 was named. It is noteworthy that *I. fonsfrigidae* NS-1 could metabolize multiple carbohydrates including xylan, alginate, starch, and lignin, and thereby produce diverse fermentation products such as hydrogen, lactate, butyrate, and ethanol. The expressions of the key genes responsible for carbohydrate degradation as well as the production of the above small molecular substrates when strain NS-1 cultured under different conditions, were further analyzed by transcriptomic methods. We thus predicted that part of the ecological role of *Iocasia* sp. is likely in the fermentation of products from the degradation of diverse carbohydrates to produce hydrogen as well as other small molecules, which are in turn utilized by other members of cold seep microbes.

Keywords: fermentation, hydrogen, carbohydrates, cold seep, microcompartment

OPEN ACCESS

Edited by:
Martina Cappelletti, University of Bologna, Italy

Reviewed by:
David C. B. Taras, Boehringer Ingelheim, Germany
Kaoru Nakasone, Kindai University, Japan
Fatemeh Salimi, Damghan University, Iran

***Correspondence:**
Chaomin Sun
sunchaomin@qdio.ac.cn

Specialty section:
This article was submitted to Extreme Microbiology, a section of the journal Frontiers in Microbiology

Received: *15 June 2021*
Accepted: *27 September 2021*
Published: *24 November 2021*

Citation:
Zhang J, Zhang Y, Liu R, Cai R, Liu F and Sun C (2021) Iocasia fonsfrigidae NS-1 gen. nov., sp. nov., a Novel Deep-Sea Bacterium Possessing Diverse Carbohydrate Metabolic Pathways. Front. Microbiol. 12:725159. doi: 10.3389/fmicb.2021.725159

INTRODUCTION

Microbes inhabiting the deep sea represent a large portion of the biosphere, and resolving their ecology is crucial for understanding global ocean processes (Baker et al., 2021). In recent years, with more and more new species available in laboratory conditions, deep-sea sediments have been a prominent source of new lineages in the tree of life (Imachi et al., 2011, 2014; Hug et al., 2016; Nakahara et al., 2019; Lewis et al., 2020). Detailed investigations and comparisons of the metabolic potentials of these new lineages uncover key previously undescribed steps in element and nutrient cycling driven by previously uncultured microbes (Shah et al., 2017; Henson et al., 2018; Zhang et al., 2020). A recently isolated free-living representative of *Candidatus* Izemoplasma from the

deep sea, which could degrade and utilize extracellular DNA (Zheng et al., 2021), was a good representative. Despite the global importance of these microorganisms, the majority of deep-sea microbial diversity remains uncultured and poorly characterized (Baker et al., 2021).

In the deep-sea ecosystem, heterotrophic microorganisms play an important role in the marine carbon cycle by breaking down polysaccharides and other organic biomass (Azam, 1998). The anaerobic degradation of organic matter involves complex microbial food chains, starting with the hydrolysis of macromolecular structures by extracellular enzymes and the formation of organic molecules small enough to be taken up by microorganisms (Arnosti, 2003; Liu et al., 2018). Microbial cells take advantage of these small organic molecules (such as sugars, amino acids, fatty acid, organic acids, and so on) through multistep fermentation processes with the production of a range of volatile fatty acids (VFAs), such as formate, acetate, propionate, and butyrate, together with H_2 and CO_2. Usually, these VFAs are electron donors that support the growth of diverse bacteria (Gittel et al., 2008; Zhang et al., 2019b; Choi et al., 2021).

Hydrothermal vents and cold seep zones are two special habitats in the deep sea. These habitats are always dark, and have extreme temperatures, and are rich in heavy metals and toxic substrates (Zhang et al., 2020; Zhou et al., 2020; Ma et al., 2021). The cold seep ecosystem is characterized by methane-rich migration, authigenic carbonate minerals, and chemosynthetic communities (Feng et al., 2018). Due to the distinct biogeochemistry dominated by fluid flow and hydrocarbon transport at the cold seep ecosystems, methanotrophs, hydrocarbon degraders, sulfate-reducing and sulfide-oxidizing bacteria are usually the key functional groups (Pachiadaki and Kormas, 2013). Taxonomically, the predominant bacterial communities in the cold seep are Proteobacteria, Firmicutes, Actinobacteria, Bacteroidetes, Planctomycetes, Nitrospirae, and Chloroflexi (Du et al., 2011; Jiao et al., 2015; Cui et al., 2019; Li et al., 2019). Notably, frequently reported fermentation microbiota are classified within the phyla of Bacteroidetes, Firmicutes, and Planctomycetes (Sun et al., 2016; Schwalm and Groisman, 2017; Zhang et al., 2017; Dedysh and Ivanova, 2019). The phylum Firmicutes is one of the predominant phyla in the cold seep, they include bacteria possessing diverse characteristics and have been abundantly detected in hydrate-bearing and crude oil deposit sites (Orcutt et al., 2010; Yamane et al., 2011). Clostridia are anaerobic Firmicutes producing a large array of metabolites by utilizing simple and complex carbohydrates and are often involved in the decomposition and recycling of organic matter (Penning and Conrad, 2006). The Clostridial bacteria are sometimes symbiotic with other organisms due to their production of alcohol (Ren et al., 2016), butanol (Lee et al., 2008), CO_2, H_2, and CO, through the fermentation of complex carbohydrates (Tracy et al., 2012), and several of the above products are important materials for the production of methane (Schink and Stams, 2013). Clostridia were found to be closely related to Methanogenesis and might be easy to understand (Sasaki et al., 2011). Undoubtedly, Clostridia are essential heterotrophic bacteria contributing to the whole bacterial community (Tracy et al., 2012). However, the studies of metabolic potentials conducted by deep-sea Clostridia lag well behind because of sampling and cultivation difficulties.

In the current study, a detailed description of the phenotypic traits, genomic data, and carbohydrate metabolisms was analyzed through biochemical and transcriptomic methods of the novel strain NS-1, which allows for the reconstruction of the metabolic potential and lifestyle of a novel Clostridial bacterium from the deep-sea. Based on the description of strain NS-1, we propose a novel species in a novel genus with strain NS-1 as its type strain, *Iocasia fonsfrigidae* gen. nov., sp. nov. Overall, this study widens understanding of diverse anaerobic categories and potential ecological roles in the deep-sea cold seep.

MATERIALS AND METHODS

Isolation and Cultivation of Strain NS-1

Strain NS-1 was isolated from sedimentary samples (7–19 cm below the seabed) collected by ROV (remotely operated vehicle) *KEXUE* from the cold seep in the South China Sea (119°17′04.956″E, 22°06′58.384″N), at a depth of approximately 1,143 m in September of 2017. The temperature of the sampling site was 3.75°C, and the pH was 7.68 (Zhang et al., 2020), the total organic matter composition was about 0.6–0.9% (wt, %) (Li et al., 2016). The enrichment medium (EM) was modified from Zhang (2007) and contained 6.5 g PIPES, 25 g NaCl, 2.7 g $MgSO_4{\cdot}7H_2O$, 4.3 g $MgCl_2{\cdot}6H_2O$, 2.84 g Na_2SO_4, 0.25 g NH_4Cl, 0.5 g KCl, 0.14 g $CaCl_2{\cdot}2H_2O$, 0.14 g $K_2HPO_4{\cdot}3H_2O$, 0.002 g $Fe(NH_4)_2(SO_4)_2{\cdot}6H_2O$, 0.1 g yeast extract, 20 mM sodium lactate, 0.5 g cysteine-HCl and 0.001 g resazurin in 1,000 mL sea water filtered with 0.22μm filter membrane. The pH was adjusted to 6.5 with 2 M NaOH and the medium was boiled for several rounds to remove dissolved oxygen. Then 1 mL trace mineral element solution [containing 29 g $Na_2EDTA{\cdot}2H_2O$, 3.26 g $MnSO_4{\cdot}H_2O$, 1.8 g $CoCl_2{\cdot}6H_2O$, 1 g $ZnSO_4{\cdot}7H_2O$, 0.11 g $NiSO_4{\cdot}6H_2O$, 0.1 g $CuSO_4{\cdot}5H_2O$, 0.1 g H_3BO_3, 0.1 g $KAl(SO_4)_2{\cdot}12H_2O$, 0.1 g $Na_2MoO_4{\cdot}2H_2O$, 0.1 g $Na_2WO_4{\cdot}2H_2O$, 0.05 g Na_2SeO_3 in 1,000 mL Milli-Q water] and 10 mL vitamin solution (containing 2 mg biotin, 2 mg folic, 10 mg pyridoxine phosphate, 5 mg thiamine, 5 mg riboflavin, 5 mg niacin, 5 mg calcium pantothenate, 0.1 mg cobalamin, 5 mg para-aminobenzoic, and 5 mg thioctic acid in 1,000 mL Milli-Q water) were added to the autoclaved EM after being filtered with 0.22 μm filter membrane. Approximately 0.5 g sediment sample was added to 100 mL of EM and enriched for one month at 37°C. Unless otherwise specified, isolation and cultivation of microbes were performed by strict anaerobic procedures in an anaerobic chamber filled with 5% H_2, 5%CO_2, and 90% N_2. To obtain pure cultures, enrichment was serially diluted tenfold in roll-tubes containing EM supplemented with 15 g/L agar (Hungate, 1969).

Purified strain NS-1 was cultured at 37°C in the PTYG medium containing 5 g peptone, 5 g tryptone, 10 g yeast extract, 4 g glucose, 5 g NaCl, 0.5 g cysteine-HCl, and 0.001 g resazurin in 1,000 mL artificial sea water (ASW). The ASW contained: 24.47 g NaCl, 3.917 g Na_2SO_4, 0.664 g KCl, 0.024 g SrCl, 4.981 g $MgCl_2{\cdot}6H_2O$, 1.102 g $CaCl_2$, 0.192 g $NaHCO_3$, 0.026 g H_3BO_4

and 0.0039 g NaF per 1 l of Milli-Q water. The pH was adjusted to between 7.2 and 7.5 using 1 M NaOH.

Analysis of Physiological Characteristics of Strain NS-1

Strain NS-1 was tested for the Gam reaction by using the Gram-staining method. Morphological characteristics of the cells were observed by transmission electron microscope (TEM) (HT7700, Hitachi, Japan) at 100.0 kV and zoom in 2,000. Determination of the temperature range for bacterial growth was tested using the PTYG medium over the range of 4–60°C (4, 16, 20, 28, 37, 45, and 60°C) for one week. To determine the need for NaCl for growth, NaCl-free artificial sea water was used to prepare the PTYG medium with different concentrations of NaCl. Briefly, 10 mL NaCl-free PTYG was respectively supplemented with 0, 12.5, 25, 50, 75, 100, 125, 150, 200, and 250 g/L NaCl, which was added into 15 mL Hungate tubes, and the culture was conducted at 37°C for one week. The pH range of growth was tested in triplicate from pH 3.36 to pH 9.36 (3.36, 4.04, 4.75, 5.32, 5.90, 6.48, 6.97, 7.6, 8.08, 8.45, 8.61, and 9.36), and 0.1 M citrate/sodium citrate buffer and 0.1M Tris-HCl/Tris-base buffer were used to prepare the PTYG medium, and the cultivation was performed for one week at 37°C. Susceptibility to antibiotics of strain NS-1 was tested in the PTYG medium supplemented with different antibiotics. The following antibiotics (Solarbio, Beijing) at an appropriate final concentration were tested: ampicillin (100 μg/mL), chloramphenicol (20 μg/mL), erythromycin (20 μg/mL), gentamicin (20 μg/mL), kanamycin (100 μg/mL), rifampicin (50 μg/mL), streptomycin (30 μg/mL), and vancomycin (30 μg/mL).

The anaerobic fermentation of carbon substrates by strain NS-1 was performed in triplicate by using the PTY medium (containing 5 g peptone, 5 g tryptone, 10 g yeast extract, 5 g NaCl, 0.5 g cysteine-HCl, and 0.001 g resazurin in 1,000 mL ASW) supplemented with different substrates at a final concentration of 0.5% (w/v). The use of different substrates was determined by comparison of the final biomass of strain NS-1. The following substrates were tested: L-arabinose, D-fructose, glucose, xylan, maltose, D-mannose, rhamnose, alginate, starch, sucrose, xylose, sodium ligninsulfonate (lignin), and galactose. PTY medium supplemented with different substrates were set as blank prior to incubation, and cultures without substrate in PTY medium were set as the control group.

Bacterial growth was monitored by measuring the amount of whole cell proteins (Begemann et al., 2012). Briefly, 0.5 mL culture was used to measure the whole cell proteins, cells were collected by centrifugation (8,000 rpm, 10 min, 4°C) washed twice with 10 mM PBS (pH = 7.4), and resuspend in 0.2 mL NaOH (0.1 M). Samples were boiled for 10 min and frozen in the refrigerator, repeated twice to break the cell completely. The major fermentation products of different substrates were determined after 48 h culture by High Performance Liquid Chromatography (HPLC) and gas chromatography (GC) as described previously (Zhang et al., 2019a). All samples were set up in triplicate and the final results were corrected by deducting the corresponding blank.

All statistically significant differences between groups were determined using Student's *t*-test, and the Levene test was used to test whether the variance between the two groups was homogeneous. Statistical analysis was performed by SPSS Statistics 20 and $p < 0.05$ was considered as a significant difference. Congo red at a final concentration of 1 mg/mL was added to the PTY solid medium, supplemented with 1% carboxymethyl cellulose (CMC) to determine the CMC degradation ability of strain NS-1. For fatty acid composition assay, cell grown in PTYG medium were harvested after 48 h of incubation. The extracted fatty acids were analyzed by using an Agilent 6890 gas chromatograph (Agilent Technologies) and identified by using the Microbial Identification System operating manual (MIDI, 2008). Polar lipids of strain NS-1 were extracted using a chloroform/methanol system and analyzed by two-dimensional TLC (Thin Layer Chromatography) on silica gel 60 F254 aluminum-backed thin-layer plates (Merck). The plate dotted with the sample was subjected to two-dimensional development, with the first solvent system of chloroform: methanol: water (65: 25: 4, by Vol.) and the second solvent of chloroform: glacial acetic acid: methanol: water (80:18:12:5, by Vol.). Phosphomolybdate, ninhydrin, molybdenum blue, and 1-methylnaphthol were chosen as the chromogenic agents.

Phylogenetic Analysis

Genomic DNA of strain NS-1 was extracted from the isolates, and PCR was performed to amplify the 16S rRNA gene sequence using primers 27F (5′-3′ AGAGTTTGATCMTGGCTCAG) and 1492R (5′-3′ TCAGGYTACCTTGTTACGACTT) as described previously (Wu et al., 2016). A phylogenetic tree based on the 16S rRNA gene for strain NS-1 and close phylogenetic relatives were created using MEGA X (Kumar et al., 2018). The tree was constructed by the maximum-likelihood method and the bootstrap support value 1,000.

Genome Sequencing and Analysis

The genome of strain NS-1 was completely sequenced by Novogene Bioinformatic Technology Co. Ltd, Beijing, China using PacBio RSII. Pairwise genome comparison was performed with Average Nucleotide Identity (ANI) (Pritchard et al., 2016). Comparative genome analysis between strain NS-1 and *Halocella* sp. SP3-1 was carried out by using the MUMmer package (Delcher et al., 2003; Li and Ji, 2014). A detailed blast was run in Galaxy (Cock et al., 2015) to further compare the similarity of each coding sequence (CDS) in the two genomes.

Transcriptional Profiling of Strain NS-1 Cultured With Different Carbohydrates

For transcriptomic profiling, strain NS-1 was grown in 10 mL PTY medium supplemented with CMC, rhamnose, lignin, and glucose at a final concentration of 0.5% (w/v), respectively. Cells cultured in the PTY medium were set as the control group. All samples were set up in triplicate. Cells were harvested after 24 h of incubation by centrifugation at 12,000 *g* for 10 min at 4°C. Three biologically repeated samples were mixed. Then the pellets were washed with 10 mM phosphate buffer solution

(PBS pH 7.4), and total RNAs were extracted with Trizol reagent. Transcriptomic profiling was performed by Novogene Bioinformatics Technology Co. Ltd (Beijing, China) as described previously (Zhu et al., 2017). Raw data were filtered by removing reads containing adapter, reads containing poly-N, and low-quality reads. HTSeq v0.6.1 was used to count the read numbers mapped to each gene. The FPKM (Fragments Per Kilobase of transcript sequence per million of base pairs sequenced) of each gene was calculated based on the length of the gene and the read count mapped to this gene. Differential expression analysis of the two groups was performed using the DESeq R (1.18.0). The resulting *P*-values were adjusted using Benjamini and Hochberg's approach for controlling the false discovery rate. Genes with an adjusted *P*-value < 0.05 found by DESeq were assigned as differentially expressed. To investigate the functional genes expressed under the treatment of different substrates, the relative expression of differentially expressed genes (DEGs) was further analyzed via heat-map (Deng et al., 2014) based on the $\log_2$(ΔFPKM-values). The ΔFPKM-values indicated the FPKM deviations between the substrate supplemented and the control group. The DEGs with different ΔFPKM-values, related to degradation of polysaccharide, production of ethanol, acetate, and hydrogen were chosen based on their reported function in the CAZY family, KEGG database, and previous studies (Xu et al., 2013 Land et al., 2020).

RESULTS

Isolation, Identification, and Characterization of the Novel Strain NS-1

We isolated the novel bacterial strains inhabiting the deep-sea cold seeps to gain insights into the diverse microbe-driven anaerobic metabolisms in the deep biosphere. As a result, a strictly anaerobic bacterial strain, designated NS-1, was isolated by several rounds of purification using the roll-tube method (Hungate, 1969). Analysis of the 16S rRNA sequence (1,444 bp) of strain NS-1 (accession No. MK418264.1) showed that it was a member of the family Halanaerobiaceae and possessed 92.52% sequence similarity (the highest score) with *Halocella cellulosilytica* DSM 7362^T, a cellulose degradation bacterium isolated from the hypersaline (Simankova et al., 1993).

Cells of strain NS-1 are long rods (0.2–0.3 μm in width, 6–10 μm in length), Gram-negative, and motile by flagella (**Figure 1**). The temperature and pH ranges for growth are 20–45°C and pH 6.5–8, and optimal growth occurs at 37°C and pH 7.0. The strain requires sodium chloride for growth at a concentration range of 12.5–150 g/L (optimal at 25–75 g/L). By measuring the amount of whole cellular protein of strain NS-1 growing under different conditions, it was clear that the growth of this bacterium was significantly increased with the supplement of respectively L-arabinose, fructose, galactose, glucose, xylan, maltose, D-mannose, rhamnose, starch, and sucrose in PTY medium (**Figure 2**). Due to the decolorization of the medium supplementing with lignin (**Supplementary Figure 1**), we deduced that the utilization of lignin occurred, though the growth of strain NS-1 was not significantly increased

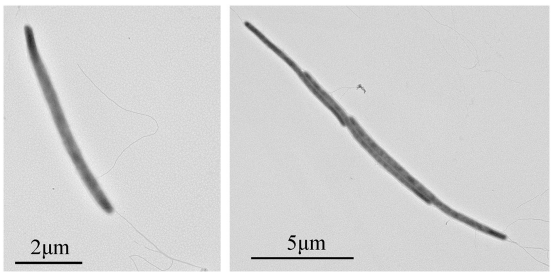

FIGURE 1 | Transmission electron microscope observation of *I. fonsfrigidae* NS-1.

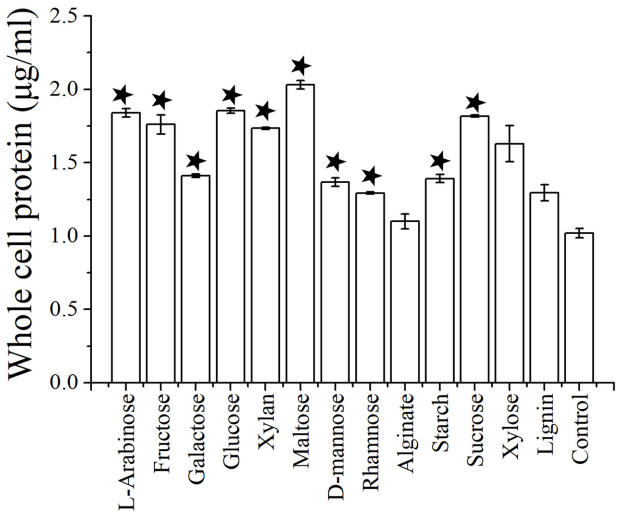

FIGURE 2 | The growth assay of *I. fonsfrigidae* NS-1 under different carbohydrates by measuring the whole cellular protein. The error bars indicate the standard deviation (S.D.) from three different biological replicates. All statistically significant differences between groups were determined using Student's *t*-test. The asterisk above each column indicates the growth of strain NS-1 is significantly ($p < 0.05$) promoted by the corresponding substrate.

by the supplementation of lignin. Considering that strain NS-1 was closely related to the cellulose degrading bacterium, *H. cellulosilytica*, its cellulose degradation ability was tested. As expected, the CMC was observed to be consumed by strain NS-1 after three days of cultivation (**Supplementary Figure 2A**). Meanwhile, transparent zones appeared when strain NS-1 was cultured in the medium containing CMC supplementing with Congo red (**Supplementary Figures 2B,C**), indicating strain NS-1 could degrade CMC. The products of glucose fermentation are acetate, ethanol, lactate, butyrate, hydrogen, and carbon dioxide. The predominant membrane fatty acids comprise 15:0 anteiso (23.71%), 14:0 (17.93%), 15:0 iso (12.02%), and 16:0 (9.99%). The composition of polar lipids was diphosphatidylglycerol (DPG), phosphatidylglycerol (PG), unidentified phosphoglycolipids (PGL), and two unidentified glycolipids (GL) (**Supplementary Figure 3**). Strain NS-1 is sensitive to ampicillin (100 μg/mL), erythromycin (20 μg/mL),

and rifampicin (50 μg/mL), while resistant to vancomycin (30 μg/mL), kanamycin (100 μg/mL), gentamicin (20 μg/mL), chloramphenicol (20 μg/mL), and streptomycin (30 μg/mL) (**Table 1**).

To further understand the characteristics of strain NS-1, its complete genome was sequenced. The size of the complete genome sequence of strain NS-1 is 3,926,493 bp with a G + C content of 35.72%. The genome harbors 3,700 coding sequences (CDSs), and 3,641 of them encode proteins. The genome of strain NS-1 contains a complete set of gene encoding enzymes related to glycolysis and pentose phosphate pathways, which are closely associated with carbohydrate metabolisms (**Supplementary Figure 4**). Correspondingly, quite a number of genes belonging to the CAZY family were identified in the genome (**Supplementary Table 1**). Among them the cellulase (*GM661_14245*) cellodextrinase (*GM661_08065*) and cellobiose phosphorylase (*GM661_04220*, *GM661_08070*, *GM661_08075*, *GM661_15060,* and *GM661_15065*) were responsible for the metabolism of cellulose, and the alpha-amylase (*GM661_00120*, *GM661_01725*, *GM661_02625,* and *GM661_03140*) was

TABLE 1 | Characteristics of strain NS-1 and other type strains of the genera in the family Halanaerobiaceae.

Strains	**NS-1**	***Halocella cellulosilytica* [1]**	***Halothermothrix orenii* [2]**	***Halarsenatibacter silvermanii* [3]**	***Halanaerobium praevalens* [4]**
Type strain	KCTC 15988 MCCC 1K04439	DSM 7362	DSM 9562	DSM 21684	DSM 2228
Cell size	0.2–0.3 × 6–10 μm	0.4–0.6 × 3.8–12 μm	0.4–0.6 × 10–20 μm	0.5 × 3 μm	0.9–1.1 × 2–2.6 μm
Morphology	Long rods	Rods	Rods	Curved rods	Rods
Motility	+*, flagella	+, peritrichous flagella	+, peritrichous flagella	+, paired subpolar flagella	–
Endospores	–*	–	–	–	–
Spheroplasts	–	+	NA	–	–
Gas vesicles	–	NA#	NA	–	NA
NaCl range	1.25–15%	5–20%	4–20%	20–35%	2–30%
NaCl optimum	2.5–7.5%	15%	10%	35%	13%
pH range	6.5–8	5.5–8.5	5.5–8.2	8.7–9.8	6.0–9.0
pH optimum	7	7	6.5–7.0	9.4	7.0–7.4
Temperature range	20–45°C	20–50°C	45–68°C	28–55°C	5–50°C
Temperature optimum	37°C	39°C	60°C	44°C	37°C
Carbohydrate utilized	+	+	+	–	+
Antibiotic sensitivity	Ampicillin (100 μg/mL), erythromycin (20 μg/mL) and rifampicin (50 μg/mL)	NA	NA	NA	NA
Antibiotic resistance	Vancomycin (30 μg/mL), kanamycin (100 μg/mL), gentamicin (20 μg/mL), chloramphenicol (20 μg/mL) and streptomycin (30 μg/mL)	NA	NA	NA	NA
Products of fermentation	Acetate, ethanol, lactate, butyrate, propionate H_2, CO_2	Acetate, ethanol, lactate, H_2, CO_2	Acetate, ethanol, H_2, CO_2	Not fermentative	Acetate, butyrate, propionate, H_2, CO_2
Major fatty acids	14:0 15:0 iso 15:0 anteiso	14:0 16:0 15:0 anteiso	14:0 15:0 iso 16:0	15:0 iso 18:0 17:0 iso 16:0	14:0 16:0 16:1
G + C content of DNA (mol%)	35.72	29	39.6	45.2	27
Sample source and site	Sediment, cold seep, South China Sea	Sediment, lake Sivash, Crimea	Sediment, hypersaline lake, Tunisia	Sediment, Searles Lake, CA, United States	Sediment, Great Salt Lake, UT, United States

** " + " indicates the strain has that capability; "–" indicates the strain lacks that capability.*

#NA indicates not available.

Related references cited in this table, (1) (Simankova et al., 1993), (2) (Cayol et al., 1994), (3) (Blum et al., 2009), and (4) (Zeikus et al., 1983).

responsible for the degradation of starch. In comparison, genes related to the tricarboxylic acid (TCA) cycle are incomplete, indicating the key roles of carbohydrate metabolism toward energy production in strain NS-1.

Phylogenetic analysis was conducted based on the 16S rRNA sequence of strain NS-1 and other species in the family Halanaerobiaceae (**Figure 3**). The low similarity between strain NS-1 and the genus *Halocella* indicated that this isolate represented a novel species of a potential novel genus as described before (Tindall et al., 2010; Yarza et al., 2014). Moreover, a phylogenomic analysis was performed based on the genomic information of strain NS-1 and other species in the family Halanaerobiaceae (**Supplementary Figure 5**). Therefore, we proposed strain NS-1 to be classified as the type strain of a novel species in a novel genus, for which the name *Iocasia fonsfrigidae* gen. nov., sp. nov. was proposed.

Characterization of Anaerobic Metabolism of *Iocasia fonsfrigidae* NS-1

As *I. fonsfrigidae* NS-1 was a strictly anaerobic bacterium utilizing various substrates as carbon sources (**Table 1**), we further particularly investigated its metabolic details toward different carbohydrates. To further explore the process of carbohydrate degradation by strain NS-1, fermentation products (including acetate, ethanol, butyrate, hydrogen, and carbon dioxide) from different substrates were determined. The production of hydrogen was significantly increased by the supplementation of fructose, L-galactose, glucose, xylan, D-maltose, alginate, starch, sucrose, or xylose (**Figure 4A**). The generation of carbon dioxide was significantly increased by almost all the tested carbohydrates (**Figure 4B**). The amount of produced acetate was significantly increased by supplementation of galactose or alginate, while markedly decreased by the supplement of L-arabinose, fructose, glucose, or rhamnose (**Figure 4C**). The production of butyrate was significantly increased by L-arabinose, fructose, galactose, glucose, xylan, D-mannose, rhamnose, sucrose, xylose, or lignin (**Figure 4D**). The yield of ethanol was significantly increased by the supplement of glucose or maltose, while it evidently decreased by supplementing rhamnose, alginate, or lignin (**Figure 4E**). Overall, *I. fonsfrigidae* NS-1 was shown to utilize diverse carbohydrates and thereby produce many small molecular substrates such as acetate, ethanol, butyrate, hydrogen, and carbon dioxide.

Transcriptomic Profiling of Carbohydrates Degradation by Strain NS-1

According to the results of the substrate degradation assays performed above (**Figures 3**, **4**), we were clear that strain NS-1 could use a variety of mono- and polysaccharides. To

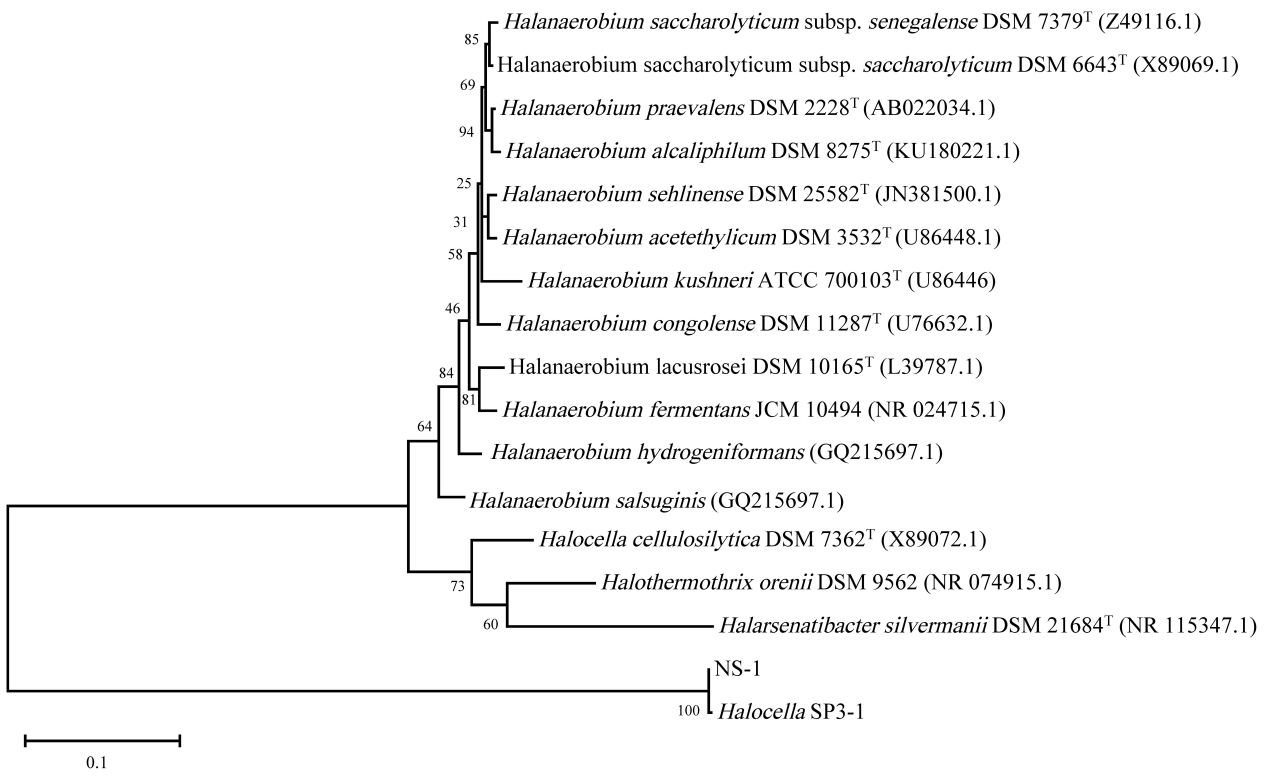

FIGURE 3 | The consensus phylogenetic tree of strain NS-1 with other related relatives in the family Halanaerobiaceae obtained from the GenBank (accession numbers of different 16S rRNA sequences are indicated after the species name). The tree was constructed by the maximum-likelihood method and the bootstrap support values 1,000.

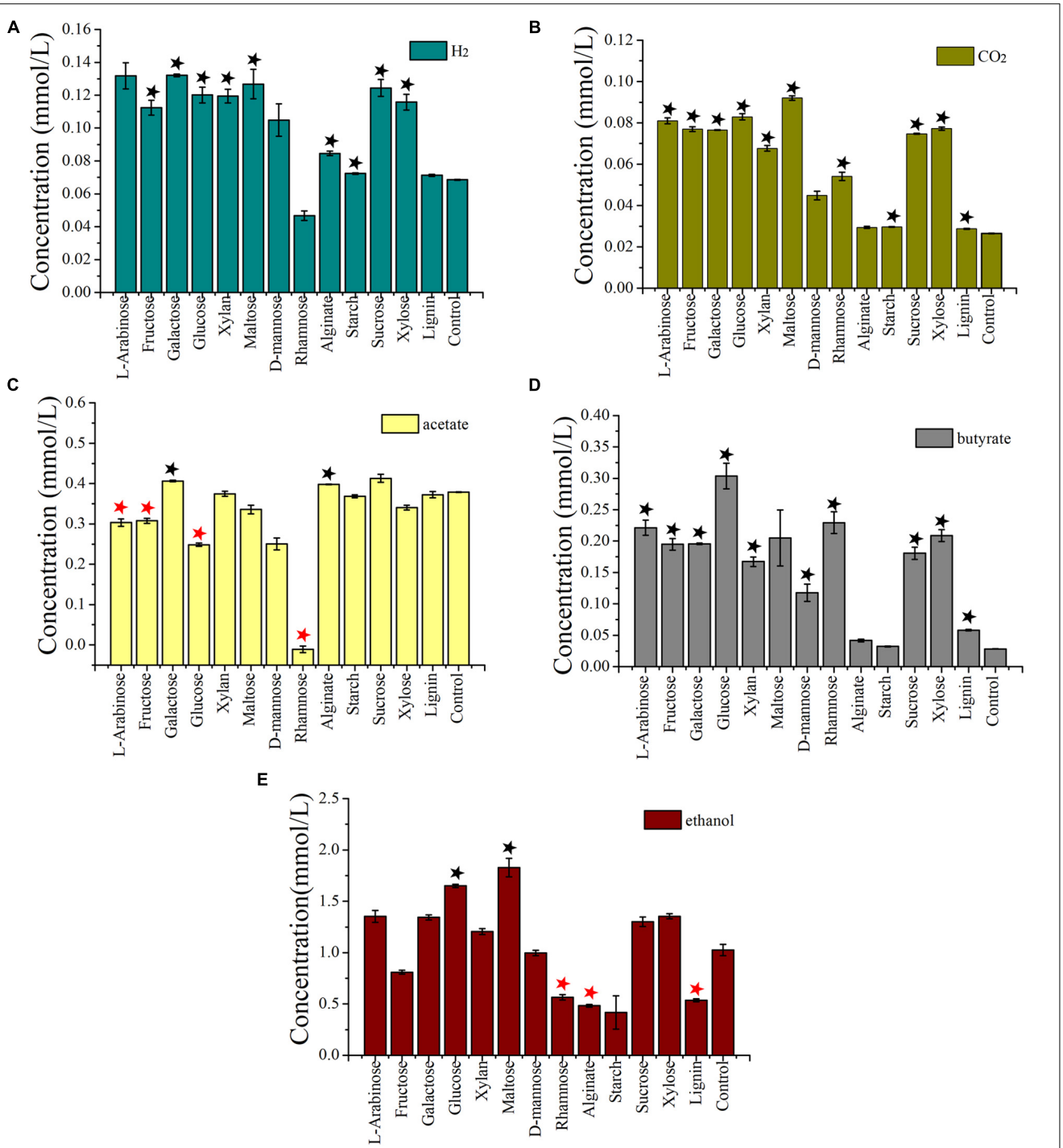

FIGURE 4 | Detection and quantification of the production of H_2 **(A)**, CO_2, **(B)**, acetate **(C)**, butyrate **(D)**, and ethanol **(E)** by *I. fonsfrigidae* NS-1 incubated in the medium supplemented with different carbohydrates. The error bars indicate the standard deviation (S.D.) from three different biological replicates. All statistically significant differences between groups were determined using Student's *t*-test. Asterisk indicates the production is significantly ($p < 0.05$) promoted (the black one) or inhibited (the red one).

get further insights into the possible degradation process, a transcriptomic analysis of strain NS-1 incubated in the presence of different carbohydrates was performed. CMC, lignin, glucose, and rhamnose were chosen as representative substrates, according to their effects on the metabolism of strain NS-1. Among them, CMC and lignin are two kinds of difficult-to-degrade polysaccharides and utilization of rhamnose could dramatically decrease the production of hydrogen and acetate.

Moreover, glucose is a commonly used monosaccharide for energy production and growth promotion of many bacteria. Based on the transcriptomic results, the global distribution of differentially expressed genes (DEGs) was indicated in the volcano plot (**Supplementary Figure 6**). The expressions of 130, 571, 476, and 592 genes were most up-regulated, while 130, 586, 441, and 694 genes were down-regulated in CMC, rhamnose, lignin, and glucose supplemented groups compared to the control group, respectively, indicating expressions of more genes were dramatically changed in the glucose supplemented group than those in other groups.

To investigate the functional genes expressed under the treatment of different substrates, the relative expression of DEGs was further analyzed via heat-map (Deng et al., 2014) based on the $\log_2$(ΔFPKM-values) (**Supplementary Table 3**). The ΔFPKM-values indicated the FPKM deviations between the substrate supplemented and the control group. By comparing the DEGs under different substrate supplement conditions, the most up-regulated or down-regulated genes that may be related to the degradation of carbohydrates, production of hydrogen, acetate, and ethanol were analyzed (**Figure 5**). Genes encoding CAZY family proteins related to carbohydrate degradation exhibited different expression levels according to different supplementing substrates. Of note, genes encoding cellodextrinase (*GM661_08065*) and glycosyltransferase (*GM661_08070* and *GM661_08075*) showed a relatively higher expression level in the CMC treatment group than other groups, which strongly indicated their potential function toward CMC degradation. These three genes belonged to the glycosyl hydrolase superfamily with putative

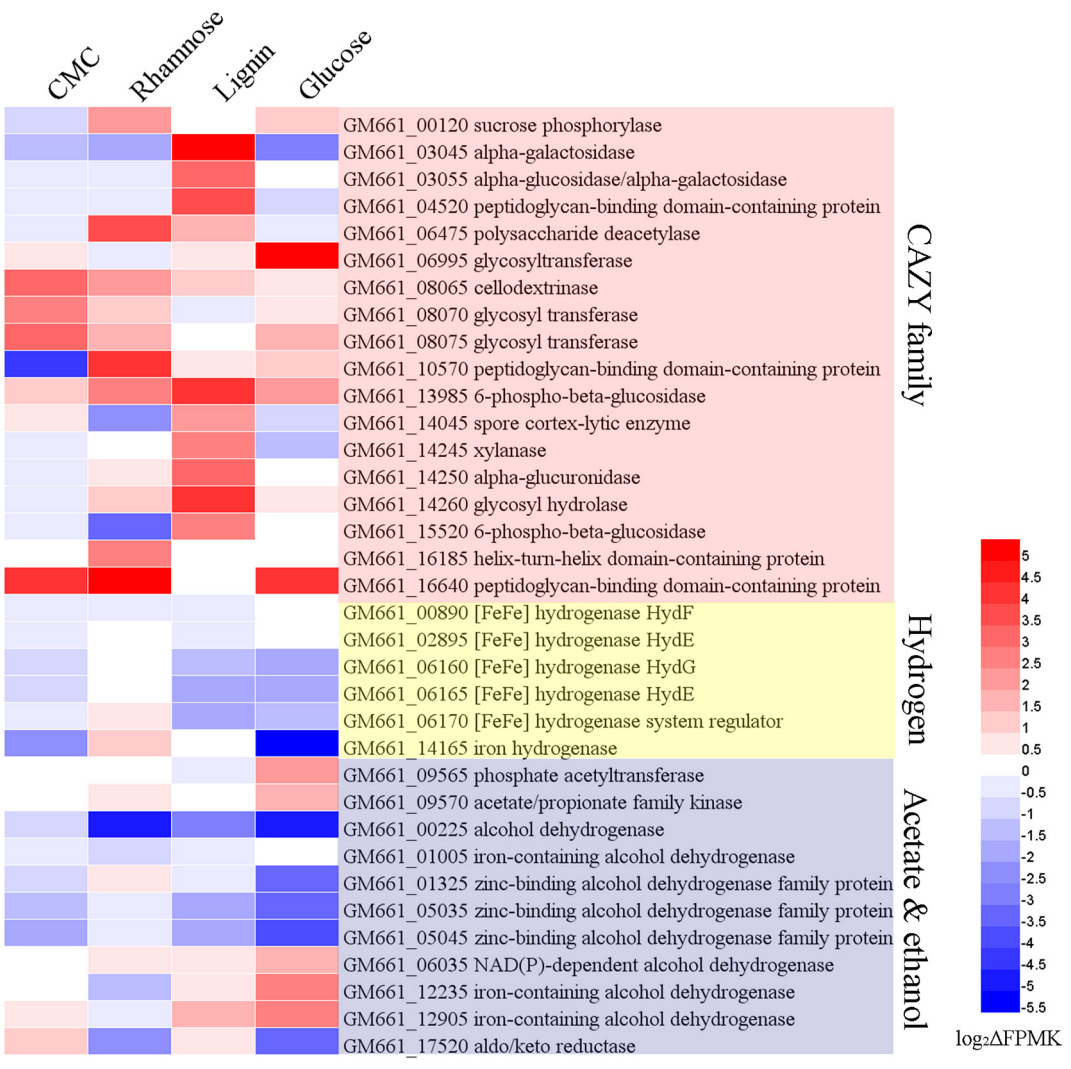

FIGURE 5 | Transcriptomic analysis of *I. fonsfrigidae* NS-1 cultured in medium supplemented with different carbohydrates. Heat map showing differentially expressed genes encoding proteins associated with CAZY family, hydrogen, alcohol, and acetate production, which were respectively labeled with different colors. The color coding was related to the $\log_2$ ΔFPMK values, the red colors represented a higher expression level and the blue ones represented a lower expression level. The heat map is generated by the Heml 1.0.3.3 software.

carbohydrate binding domain (CBM), consistent with their potential cellulolytic function. The most up-regulated genes related to CMC degradation strongly indicated that CMC was an available substrate for strain NS-1.

As for the degradation of lignin, expressions of genes encoding alpha-galactosidase (*GM661_03045* and *GM661_03055*), peptidoglycan-binding domain-containing protein (*GM661_04520*), 6-phospho-beta-glucosidase (*GM661_13985*), spore cortex-lytic enzyme (*GM661_14045*), xylanase (*GM661_14245*), alpha-glucuronidase (*GM661_14250*), glycosyl hydrolase (*GM661_14260*), 6-phospho-beta-glucosidase (*GM661_15520*), and helix-turn-helix domain-containing protein (*GM661_16185*) were most up-regulated in the lignin supplement group than the other three groups. On the other hand, expressions of genes encoding sucrose phosphorylase (*GM661_00120*), polysaccharide deacetylase (*GM661_06475*), peptidoglycan-binding domain-containing protein (*GM661_10570*), helix-turn-helix domain-containing protein (*GM661_16185*), and peptidoglycan-binding domain-containing protein (*GM661_16640*) were markedly increased and these genes were considered to be key genes for the metabolism of rhamnose. Similarly, glycosyltransferase (*GM661_06995*) was the most up-regulated gene in the glucose treatment group and we thus propose that it is important in the glucose metabolism of strain NS-1.

Producing a large amount of hydrogen was an important metabolic feature of strain NS-1 in the presence of diverse carbohydrates (**Figure 4A**). Correspondingly, expressions of many genes related to hydrogen production were regulated under different treatments. Among them, expressions of genes encoding [FeFe] hydrogenase (*GM661_06160* and *GM661_06165*), [FeFe] hydrogenase system regulator (*GM661_06170*), and iron hydrogenase (*GM661_14165*) were most up- or down-regulated in the presence of different substrates, indicating the evident effects of different substrates on the production of hydrogen. Combining the production of hydrogen (**Figure 4A**) and the DEGs under the treatment of rhamnose and glucose (**Figure 5**), we found a negative relationship between the production of hydrogen and [FeFe]-hydrogenase related genes. The [FeFe]-hydrogenase was reported with particularly high turnover activities for both the release and oxidation of hydrogen (Land et al., 2020), and based on our results, we tended to believe that the main function of [FeFe]-hydrogenase in strain NS-1 was hydrogen oxidation.

Acetate was an important intermediate in a variety of metabolic processes, and its production was determined by indeterminate factors (Tracy et al., 2012). Up-regulated acetate/propionate family kinase (*GM661_09570*) and phosphate acetyltransferase (*GM661_09565*) in the glucose supplemented group, and up-regulated acetate/propionate family kinase (*GM661_09570*) in the rhamnose supplemented group might explain the decreased production of acetate in **Figure 4C**. As for the production of ethanol, we found two up-regulated iron-containing alcohol dehydrogenase (*GM661_12235* and *GM661_12905*) in the glucose supplemented group, which may be responsible for the increased production of ethanol.

It is noteworthy that an intact cluster containing genes encoding the different components responsible for ethanolamine and propanediol metabolism, as well as proteins constituting the bacterial microcompartment (BMC) were identified in the genome of strain NS-1 (**Figure 6A**). Moreover, the expression levels of most of these genes were up-regulated in the medium supplemented with CMC, lignin, or glucose (**Figure 6B**), strongly indicating ethanolamine and propanediol metabolisms were performed in BMC and affected by metabolized products from different carbohydrates.

Comparative Genomic Analysis Between Strain NS-1 and *Halocella* sp. SP3-1

Recently, a genome sequence of *Halocella* sp. SP3-1 has been published (Heng et al., 2019) (accession number GCF_003953895.1), however, no further study was performed except the genome sequencing and polysaccharide hydrolase analysis. The 16S rRNA gene of strain NS-1 shared a high similarity of 99.58% with *Halocella* sp. SP3-1. The ANI between strain NS-1 and the *Halocella* sp. SP3-1 was 97.64%, which was higher than the accepted threshold (ANI value of 95–96%) for the same species (Richter and Rosselló-Móra, 2009). The ANI values between strain NS-1 and other types of strains in the family Halanaerobiaceae were lower than the accepted threshold (**Supplementary Table 4**). The high similarity of the 16S rRNA gene and the ANI value strongly indicated that *Halocella* sp. SP3-1 and strain NS-1 belonged to the same species. Logically, full polyphasic taxonomic description and detailed physiological characteristics were necessary before claiming a novel microorganism (Imachi et al., 2014; Oren, 2014), thus *Halocella* sp. SP3-1 needs to be recognized without valid standing in nomenclature. In the current study, we proposed that *Halocella* sp. SP3-1 belongs to the new species *Iocasia fonsfrigidae*. Considering that these two strains were isolated from different environments, a genomic comparison between these two strains was performed to identify the potential differences between these two strains. Although the genomic alignment analysis between strain NS-1 and *Halocella* sp. SP3-1 showed a very high similarity (**Supplementary Figure 7**), many proteins specifically existed in the genome of strain NS-1 but are absent in *Halocella* sp. SP3-1 were identified by Galaxy (Cock et al., 2015), such as proteins related to ABC transporters, PTS sugar transporters, type II secretion systems, type I-B and type III-B CRISPR associated proteins, proteins involved in carbohydrate metabolisms, and clusters of proteins related to ethanolamine and propanediol metabolism and BMC (**Supplementary Tables 1, 2**).

Description of *Iocasia* gen. nov.

Iocasia (I.o.c.a.s'ia L.fem. n. *Iocasia* arbitrary name formed from the acronym of the Institute of Oceanology, Chinese Academy of Sciences). *Iocasia* gen. nov. belong to the family Halanaerobiaceae. Cells are long rods, with 0.2–0.3 × 6–10 μm. Cells were strictly anaerobic and moderately halophilic. Cells are Gram-negative and motile by flagella. The G + C content was between 35.1 and 35.72%. The type species is *I. fonsfrigidae* which

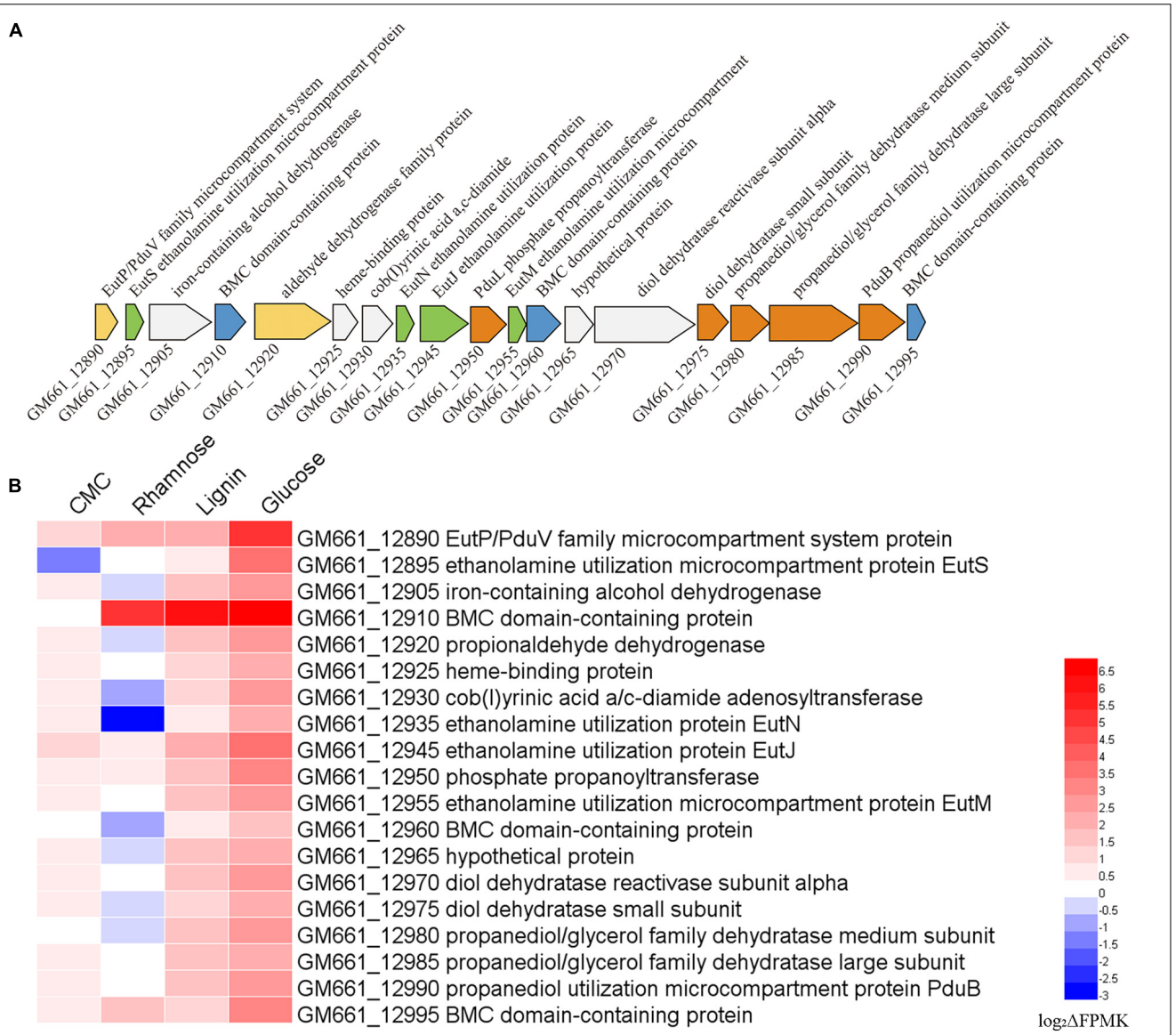

FIGURE 6 | Transcriptomic analysis showing ethanolamine and propanediol metabolisms of *I. fonsfrigidae* NS-1 were affected by the presence of different carbohydrates and might be performed in microcompartment (BMC). **(A)** Gene cluster containing genes encoding different components responsible for ethanolamine and propanediol metabolism, as well as proteins constituting the bacterial BMC identified in the genome of *I. fonsfrigidae* NS-1. **(B)** Heat map showing the different expression levels of the genes belonging to the cluster shown in panel A when *I. fonsfrigidae* NS-1 incubated in the medium supplemented with different carbohydrates. The color coding was related to the $\log_2 \Delta$FPMK values, the red colors represented a higher expression level and the blue ones represented a lower expression level. The heat map is generated by the Heml 1.0.3.3 software.

was isolated from cold seep sediment from the South China Sea (**Supplementary Table 5**).

Description of *Iocasia fonsfrigidae* sp. nov.

Iocasia fonsfrigidae (fo.ns.fri.gi.da'e. L. m. n. fons seep; L. fem. frigida cold: N. L. gen. n. fonsfrigidae of the cold seep). Cells are long rods (0.2–0.3 μm in width, 6–10 μm in length), Gram-negative and motile by flagella. The temperature and pH ranges for growth are 16–45°C and pH 6.5–8, and optimal growth occurs at 37°C and pH 7.0. The strain requires sodium chloride for growth at a concentration range of 12.5–150 g/L (optimal at 25–75 g/L). Substrates used as carbon sources are arabinose, D-fructose, galactose, glucose, xylose, maltose, D-mannose, rhamnose, alginate, sucrose, xylan, starch, lignin, and carboxymethylcellulose (CMC). The products of glucose fermentation are acetate, ethanol, lactate, butyrate, hydrogen, and carbon dioxide. The predominant membrane fatty acids comprise 15:0 anteiso (23.71%), 14:0 (17.93%), 15:0 iso (12.02%), and 16:0 (9.99%). The composition of polar lipids was diphosphatidylglycerol (DPG), phosphatidylglycerol

(PG), unidentified phosphoglycolipids (PGL), and two unidentified glycolipids (GL). Strain NS-1 is sensitive to ampicillin, erythromycin, and rifampicin, while resistant to vancomycin, kanamycin, gentamicin, chloramphenicol, and streptomycin. The type strain NS-1^T (KCTC 15988^T = MCCC 1K04439^T) was isolated from deep-sea sediment of cold seep, China, and deposited in Marine Culture Collection of China and Korea Collection for Type Cultures.

DISCUSSION

The estimated total microbial abundance was about 2.9×10^{29} cells in the global subseafloor sediment, and the living biomass was 10–45% lower than this estimate (Kallmeyer et al., 2012). These microbial communities process both organic and inorganic carbon and contribute to the cycling of nutrients such as sulfur, nitrogen, and iron (Parkes et al., 2014). To explore the potential novel metabolisms and ecological roles of microorganisms in the subseafloor, pure isolates are necessary. However, due to the sampling and cultivation limitations, most of the microorganisms in the subseafloor are uncultured (Martiny, 2019), especially those in deep-sea special environments such as hydrothermal vents and cold seep areas. In the present study, a novel genus and species *Iocasia fonsfrigidae* NS-1 belonging to the family Halanaerobiaceae was isolated from the deep-sea cold seep, and its physiological, phylogenetics, genomic, and metabolic traits were investigated in detail.

The family Halanaerobiaceae belong to the class Clostridia in the phylum Firmicutes was created in 1995 (Rainey et al., 1995). It contained 4 genera including *Halanaerobium* (Zeikus et al., 1983), *Halocella* (Simankova et al., 1993), *Halothermothrix* (Cayol et al., 1994), and *Halarsenatibacter* (Oremland et al., 2005; Blum et al., 2009). Most isolated species in Halanaerobiaceae belong to the genus *Halanaerobium* (Oren, 2014). All previous Halanaerobiaceae species were isolated from saline, sediments of salt or hypersaline lakes, offshore fields, petroleum reservoirs, and fermented puffer fish ovaries (Oren, 2014). *I. fonsfrigidae* NS-1 represents the first member of Halanaerobiaceae isolated from the sediment of a deep-sea cold seep. The natural habitats for these known Halanaerobiaceae populations reflect their capacity to tolerate a broad range of salt concentrations. Compared with other members of Halanaerobiaceae, *I. fonsfrigidae* NS-1 showed a relatively lower tolerance to the presented salt content in the medium, which could be a long-term adaptation to the original ecological habitat. The isolation of *I. fonsfrigidae* NS-1 from the cold seep strongly indicates that there exists a wide range of living habitats of Halanaerobiaceae, and their potential metabolic differences need further study in the future.

The ability to metabolize diverse carbohydrates by *I. fonsfrigidae* NS-1 is consistent with other members in the family Halanaerobiaceae (Blum et al., 2009). Strain NS-1 was shown to degrade cellulose (**Supplementary Figure 2**), and most marine cellulolytic bacteria belong to the genera *Bacillus* and *Clostridium* (Castro da Silva and de Souza Lima, 2017). The discovery of cellulolytic function in the genus *Iocasia* provides evidence for the microorganisms that possess the capability to decompose high-molecular-weight organic matter in the anaerobic sediment of the deep sea. Moreover, the whole cell protein was increased in the lignin supplemented group, which indicated that the novel isolated strain has a strong ability to decompose refractory polysaccharide. Strain NS-1 could produce a large number of different fermentation products including hydrogen, alcohol, acetate, and butyrate, and the amount of these small molecular substrates varied accordingly to the substrate categories (**Figure 4**). Notably, alginate could significantly increase the production of hydrogen and acetate (**Figures 4A,C**) without a significant increase in growth (**Figure 2**). Therefore, acting as an active degrader of organic matter in anaerobic sediments, which are inhabited by large amounts of autotrophic-heterotrophic microorganisms, *I. fonsfrigidae* NS-1 is proposed to promote the elements and nutrient cycling in the dark biosphere by providing a variety of small molecular organic nutrients.

Comparative genomic results indicated that strain NS-1 and *Halocella* sp. SP3-1 probably belong to the same species (**Supplementary Figure 6**). The most obvious difference between these two strains is the presence of a variety of genes associated with BMC constitution and ethanolamine and propanediol metabolism in the genome of strain NS-1 but the absence in the genome of *Halocella* sp. SP3-1 (**Figure 6A**). BMCs are organelles that encapsulate functionally linked enzymes within a proteinaceous shell. They play crucial roles in carbon dioxide fixation in autotrophs (Rae et al., 2013) and the catabolism of organic substrates in heterotrophs (Kofoid et al., 1999; Erbilgin et al., 2014). They were reported to be involved in the degradation of a number of plant and algal cell wall derived sugars, and L-fucose and L-rhamnose could promote the formation of BMCs in *Planctomyces limnophilus* (Erbilgin et al., 2014). It was also reported that BMCs were responsible for the degradation of plant saccharides (Erbilgin et al., 2014). Correspondingly, the expression levels of most genes in the BMC related gene cluster were dramatically up-regulated when supplementing CMC, lignin, or glucose in the medium (**Figure 6B**), strongly suggesting that ethanolamine and propanediol metabolisms were affected by the metabolized products of different carbohydrates such as ethanol and propanol (**Figure 6B**). The existence of BMC in strain NS-1 may contribute to metabolic versatility, and provide a competitive advantage in specific environmental niches.

Taken together, based on the isolate *I. fonsfrigidae* NS-1, we explored its physiology, genomic traits, phylogenetics, and metabolisms in detail, through bioinformatics, biochemical and transcriptomic methods, and proposed a model describing its central metabolic pathways (**Supplementary Figure 4**). The metabolisms of diverse carbohydrates (such as cellulose, lignin) are crucial for the complete metabolic network of this novel strain and closely link to other important metabolic processes like ethanolamine and propanediol, which are conducted in the BMC. Besides the contribution of diverse and enormous small molecular organic matter to the surrounding environment, it is also proposed that it might be involved in elements cycling such as sulfur and metal ions, which need to be investigated further in the future.

DATA AVAILABILITY STATEMENT

The NCBI GenBank accession numbers for the 16S rRNA gene sequence and whole genome sequence (WGS) of strain NS-1 are MK418264.1 and CP046640, respectively. The access number for the original transcriptome data is PRJNA666065 in the NCBI GenBank.

AUTHOR CONTRIBUTIONS

JZ and CS conceived and designed the study. JZ performed the most of the experiments. YZ and FL measured the anaerobic products of NS-1. RL collected the samples. JZ, RC, and CS analyzed the data. JZ wrote the manuscript. CS revised the manuscript. All authors read and approved the final manuscript.

FUNDING

This work was funded by the Strategic Priority Research Program of the Chinese Academy of Sciences (Grant No. XDA22050301), China Ocean Mineral Resources R&D Association Grant (Grant No. DY135-B2-14), National Key R&D Program of China (Grant No. 2018YFC0310800), the Taishan Young Scholar Program of Shandong Province (Grant No. tsqn20161051), and Qingdao Innovation Leadership Program (Grant No. 18-1-2-7-zhc) for CS.

SUPPLEMENTARY MATERIAL

The Supplementary Material for this article can be found online at: https://www.frontiersin.org/articles/10.3389/fmicb.2021.725159/full#supplementary-material

REFERENCES

Arnosti, C. (2003). "13 - microbial extracellular enzymes and their role in dissolved organic matter cycling," in *Aquatic Ecosystems*, eds S. E. G. Findlay and R. L. Sinsabaugh (Burlington, VT: Academic Press).

Azam, F. (1998). Microbial control of oceanic carbon flux: the plot thickens. *Science* 280, 694–696. doi: 10.1126/SCIENCE.280.5364.694

Baker, B. J., Appler, K. E., and Gong, X. (2021). New microbial biodiversity in marine sediments. *Annu. Rev. Mar. Sci.* 13, 161–175. doi: 10.1146/ANNUREV-MARINE-032020-014552

Begemann, M., Mormile, M. R., Sitton, O., Wall, J. D., and Elias, D. A. (2012). A streamlined strategy for biohydrogen production with *Halanaerobium hydrogeniformans*, an alkaliphilic bacterium. *Front. Microbiol.* 3:93. doi: 10.3389/FMICB.2012.00093

Blum, J. S., Han, S., Lanoil, B., Saltikov, C., Witte, B., Tabita, F. R., et al. (2009). Ecophysiology of "*Halarsenatibacter silvermanii*" strain SLAS-1T, gen. nov., sp. nov., a facultative chemoautotrophic arsenate respirer from salt-saturated Searles Lake. *California. Appl Environ. Microbiol.* 75, 1950–1960. doi: 10.1128/AEM.02614-08

Castro da Silva, M. A., and de Souza Lima, A. O. (2017). "Diversity and prospection of South Atlantic Ocean microorganisms," in *Diversity and Benefits of Microorganisms from the Tropics*, eds J. L. de Azevedo and M. Carolina Quecine (Switzerland: Springer).

Cayol, J.-L., Ollivier, B., Patel, B., Prensier, G., Guezennec, J., and Garcia, J.-L. (1994). Isolation and characterization of *Halothermothrix orenii* gen. nov., sp. nov., a halophilic, thermophilic, fermentative, strictly anaerobic bacterium. *Int J Syst Evol. Microbiol.* 44, 534–540. doi: 10.1099/00207713-44-3-534

Choi, O., Cha, S.-J., Kim, H., Kim, H., and Sang, B.-I. (2021). Dynamic changes of microbiome with the utilization of volatile fatty acids as electron donors for denitrification. *Water* 13:1556. doi: 10.3390/W13111556

Cock, P. J. A., Chilton, J. M., Grüning, B., Johnson, J. E., and Soranzo, N. (2015). NCBI BLAST+ integrated into Galaxy. *GigaScience* 4:39. doi: 10.1186/s13742-015-0080-7

Cui, H., Su, X., Chen, F., Holland, M., Yang, S., Liang, J., et al. (2019). Microbial diversity of two cold seep systems in gas hydrate-bearing sediments in the South China Sea. *Mar. Environ. Res.* 144, 230–239. doi: 10.1016/J.MARENVRES.2019.01.009

Dedysh, S. N., and Ivanova, A. A. (2019). Planctomycetes in boreal and subarctic wetlands: diversity patterns and potential ecological functions. *FEMS Microbiol. Ecol.* 95:227. doi: 10.1093/femsec/fiy227

Delcher, A. L., Salzberg, S. L., and Phillippy, A. M. (2003). Using MUMmer to identify similar regions in large sequence sets. *Curr. Protocols Bioinform.* Chapter 10, Unit10.3. doi: 10.1002/0471250953.bi1003s00

Deng, W., Wang, Y., Liu, Z., Cheng, H., and Xue, Y. (2014). HemI: a toolkit for Illustrating heatmaps. *PLoS One* 9:e111988. doi: 10.1371/JOURNAL.PONE.0111988

Du, J., Xiao, K., Huang, Y., Li, H., Tan, H., Cao, L., et al. (2011). Seasonal and spatial diversity of microbial communities in marine sediments of the South China Sea. *Anton. Van Leeuw.* 100, 317–331. doi: 10.1007/S10482-011-9587-9

Erbilgin, O., McDonald, K. L., and Kerfeld, C. A. (2014). Characterization of a Planctomycetal organelle: a novel bacterial microcompartment for the aerobic degradation of plant saccharides. *Appl. Environ. Microbiol.* 80, 2193–2205. doi: 10.1128/AEM.03887-13

Feng, D., Qiu, J.-W., Hu, Y., Peckmann, J., Guan, H., Tong, H., et al. (2018). Cold seep systems in the South China Sea: an overview. *J. Asian Earth Sci.* 168, 3–16. doi: 10.1016/J.JSEAES.2018.09.021

Gittel, A., Mußmann, M., Sass, H., Cypionka, H., and Könneke, M. (2008). Identity and abundance of active sulfate-reducing bacteria in deep tidal flat sediments determined by directed cultivation and CARD-FISH analysis. *Environ. Microbiol.* 10, 2645–2658. doi: 10.1111/J.1462-2920.2008.01686.X

Heng, S., Sutheeworapong, S., Prommeenate, P., Cheevadhanarak, S., Kosugi, A., Pason, P., et al. (2019). Complete genome sequence of *Halocella sp*. strain SP3-1, an extremely halophilic, glycoside hydrolase-and bacteriocin-producing bacterium isolated from a salt evaporation pond. *Microbiol. Resour Announc.* 8:e01696-18. doi: 10.1128/MRA.01696-18

Henson, M. W., Lanclos, V. C., Faircloth, B. C., and Thrash, J. C. (2018). Cultivation and genomics of the first freshwater SAR11 (LD12) isolate. *ISME J.* 12, 1846–1860. doi: 10.1038/S41396-018-0092-2

Hug, L. A., Baker, B. J., Anantharaman, K., Brown, C. T., Probst, A. J., Castelle, C. J., et al. (2016). A new view of the tree of life. *Nat. Microbiol.* 1:16048. doi: 10.1038/NMICROBIOL.2016.48

Hungate, R. (1969). "A roll tube method for cultivation of strict anaerobes," in *Methods in Microbiology*, ed. J. N. A. D. Ribbons (New York, NY: Academic Press).

Imachi, H., Aoi, K., Tasumi, E., Saito, Y., Yamanaka, Y., Saito, Y., et al. (2011). Cultivation of methanogenic community from subseafloor sediments using a continuous-flow bioreactor. *ISME J.* 5, 1913–1925. doi: 10.1038/ISMEJ.2011.64

Imachi, H., Sakai, S., Lipp, J. S., Miyazaki, M., Saito, Y., Yamanaka, Y., et al. (2014). *Pelolinea submarina* gen. nov., sp. nov., an anaerobic, filamentous bacterium of the phylum Chloroflexi isolated from subseafloor sediment. *Int. J. Syst. Evol. Microbiol.* 64, 812–818. doi: 10.1099/IJS.0.057547-0

Jiao, L., Su, X., Wang, Y., Jiang, H., Zhang, Y., and Chen, F. (2015). Microbial diversity in the hydrate-containing and -free surface sediments in the Shenhu area. South China Sea. *Geosci. Front.* 6, 627–633. doi: 10.1016/J.GSF.2014.04.007

Kallmeyer, J., Pockalny, R., Adhikari, R. R., Smith, D. C., and D'Hondt, S. (2012). Global distribution of microbial abundance and biomass in subseafloor sediment. *Proc. Natl. Acad. Sci. U S A.* 109, 16213–16216. doi: 10.1073/pnas.1203849109

Kofoid, E., Rappleye, C., Stojiljkovic, I., and Roth, J. (1999). The 17-gene ethanolamine (eut) operon of *Salmonella typhimurium* encodes five

homologues of carboxysome shell proteins. *J. Bacteriol.* 181, 5317–5329. doi: 10.1128/JB.181.17.5317-5329.1999

Kumar, S., Stecher, G., Li, M., Knyaz, C., and Tamura, K. (2018). MEGA X: molecular evolutionary genetics analysis across computing platforms. *Mol. Biol. Evol.* 35, 1547–1549. doi: 10.1093/molbev/msy096

Land, H., Senger, M., Berggren, G., and Stripp, S. T. (2020). Current state of [FeFe]-Hydrogenase research: biodiversity and spectroscopic investigations. *ACS CATAL* 10, 7069–7086. doi: 10.1021/acscatal.0c01614

Lee, S. Y., Park, J. H., Jang, S. H., Nielsen, L. K., Kim, J., and Jung, K. S. (2008). Fermentative butanol production by clostridia. *Biotechnol. Bioeng.* 101, 209–228. doi: 10.1002/BIT.22003

Lewis, W. H., Tahon, G., Geesink, P., Sousa, D. Z., and Ettema, T. J. G. (2020). Innovations to culturing the uncultured microbial majority. *Nat. Rev. Microbiol.* 19, 225–240. doi: 10.1038/S41579-020-00458-8

Li, J., Li, L., Bai, S., Ta, K., Xu, H., Chen, S., et al. (2019). New insight into the biogeochemical cycling of methane, S and Fe above the sulfate-methane transition zone in methane hydrate-bearing sediments: a case study in the Dongsha area, South China Sea. *Deep-Sea Res. Part I-Oceanogr. Res. Pap.* 145, 97–108. doi: 10.1016/J.DSR.2019.01.011

Li, N., Feng, D., Chen, L., Wang, H., and Chen, D. (2016). Using sediment geochemistry to infer temporal variation of methane flux at a cold seep in the South China Sea. *Mar. Petroleum Geol.* 77, 835–845. doi: 10.1016/j.marpetgeo.2016.07.026

Li, Y., and Ji, Z. (2014). A local alignment of DNA based on parallelized MUMmer algorithm. *Int. Conference Nat. Comput.* 2014, 401–406.

Liu, Q., Fang, J., Li, J., Zhang, L., Xie, B.-B., Chen, X.-L., et al. (2018). Depth-Resolved variations of cultivable bacteria and their extracellular enzymes in the water column of the new britain trench. *Front. Microbiol.* 9:135. doi: 10.3389/fmicb.2018.00135

Ma, N., Sha, Z., and Sun, C. (2021). Formation of cadmium sulfide nanoparticles mediates cadmium resistance and light utilization of the deep-sea bacterium *Idiomarina sp*. OT37-5b. *Environ. Microbiol.* 23, 934–948. doi: 10.1111/1462-2920.15205

Martiny, A. C. (2019). High proportions of bacteria are culturable across major biomes. *ISME J.* 13, 2125–2128. doi: 10.1038/s41396-019-0410-3

MIDI (2008). *Sherlock Microbial Identification System Operating Manual*. Newark: DE: MIDI Inc.

Nakahara, N., Nobu, M. K., Takaki, Y., Miyazaki, M., Tasumi, E., Sakai, S., et al. (2019). *Aggregatilinea lenta* gen. nov., sp. nov., a slow-growing, facultatively anaerobic bacterium isolated from subseafloor sediment, and proposal of the new order *Aggregatilineales ord*. nov. within the class Anaerolineae of the phylum Chloroflexi. *Int. J. Syst. Evol. Microbiol.* 69, 1185–1194. doi: 10.1099/IJSEM.0.003291

Orcutt, B. N., Joye, S. B., Kleindienst, S., Knittel, K., Ramette, A., Reitz, A., et al. (2010). Impact of natural oil and higher hydrocarbons on microbial diversity, distribution, and activity in Gulf of Mexico cold-seep sediments. *Deep-sea Res. Part II-Topical Stud. Oceanography* 57, 2008–2021. doi: 10.1016/J.DSR2.2010.05.014

Oremland, R. S., Kulp, T. R., Blum, J. S., Hoeft, S. E., Baesman, S., Miller, L. G., et al. (2005). A microbial arsenic cycle in a salt-saturated, extreme environment. *Science* 308, 1305–1308. doi: 10.1126/science.1110832

Oren, A. (2014). "The order Halanaerobiales, and the families Halanaerobiaceae and Halobacteroidaceae," in *The Prokaryotes: Firmicutes and Tenericutes*, eds E. Rosenberg, E. F. DeLong, S. Lory, E. Stackebrandt, and F. Thompson (Berlin: Springer).

Pachiadaki, M. G., and Kormas, K. A. (2013). Interconnectivity vs. isolation of prokaryotic communities in European deep-sea mud volcanoes. *Biogeosciences* 10, 2821–2831. doi: 10.5194/BG-10-2821-2013

Parkes, R. J., Cragg, B., Roussel, E., Webster, G., Weightman, A., and Sass, H. (2014). A review of prokaryotic populations and processes in sub-seafloor sediments, including biosphere:geosphere interactions. *Mar. Geol.* 352, 409–425. doi: 10.1016/J.MARGEO.2014.02.009

Penning, H., and Conrad, R. (2006). Carbon isotope effects associated with mixed-acid fermentation of saccharides by *Clostridium papyrosolvens*. *Geochim Cosmochim Acta* 70, 2283–2297. doi: 10.1016/j.gca.2006.01.017

Pritchard, L., Glover, R. H., Humphris, S., Elphinstone, J. G., and Toth, I. K. (2016). Genomics and taxonomy in diagnostics for food security: soft-rotting enterobacterial plant pathogens. *Anal. Methods* 8, 12–24. doi: 10.1039/C5AY02550H

Rae, B. D., Long, B. M., Badger, M. R., and Price, G. D. (2013). Functions, compositions, and evolution of the two types of carboxysomes: polyhedral microcompartments that facilitate CO2 fixation in *Cyanobacteria* and some *Proteobacteria*. *Appl. Environ. Microbiol.* 77, 357–379. doi: 10.1128/MMBR.00061-12

Rainey, F. A., Zhilina, T. N., Boulygina, E. S., Stackebrandt, E., Tourova, T. P., and Zavarzin, G. A. (1995). The taxonomic status of the fermentative halophilic anaerobic bacteria: description of *Haloanaerobiales ord*. nov., *Halobacteroidaceae fam*. nov., *Orenia gen*. nov., and further taxonomic rearrangements at the genus and species level. *Anaerobe* 1:185. doi: 10.1006/ANAE.1995.1018

Ren, C., Wen, Z., Xu, Y., Jiang, W., and Gu, Y. (2016). Clostridia: a flexible microbial platform for the production of alcohols. *Curr. Opin. Chem. Biol.* 35, 65–72. doi: 10.1016/J.CBPA.2016.08.024

Richter, M., and Rosselló-Móra, R. (2009). Shifting the genomic gold standard for the prokaryotic species definition. *Proc. Natl. Acad. Sci. U S A.* 106, 19126–19131. doi: 10.1073/PNAS.0906412106

Sasaki, D., Hori, T., Haruta, S., Ueno, Y., Ishii, M., and Igarashi, Y. (2011). Methanogenic pathway and community structure in a thermophilic anaerobic digestion process of organic solid waste. *J. Biosci. Bioeng.* 111, 41–46. doi: 10.1016/J.JBIOSC.2010.08.011

Schink, B. S., and Stams, A. J. M. (2013). "Syntrophism among prokaryotes," in *The Prokaryotes*, (eds) E. Rosenberg, E. F. DeLong, S. Lory, E. Stackebrandt, F. Thompson (Berlin: Springer).

Schwalm, N. D., and Groisman, E. A. (2017). Navigating the gut buffet: control of polysaccharide utilization in *Bacteroides spp*. *Trends Microbiol.* 25, 1005–1015. doi: 10.1016/J.TIM.2017.06.009

Shah, V., Chang, B. X., and Morris, R. M. (2017). Cultivation of a chemoautotroph from the SUP05 clade of marine bacteria that produces nitrite and consumes ammonium. *ISME J.* 11, 263–271. doi: 10.1038/ISMEJ.2016.87

Simankova, M., Chernych, N., Osipov, G., and Zavarzin, G. (1993). *Halocella cellulolytica* gen. nov., sp. nov., a new obligately anaerobic, halophilic, cellulolytic bacterium. *Syst. Appl. Microbiol.* 16, 385–389. doi: 10.1016/S0723-2020(11)80270-5

Sun, C., Fu, G.-Y., Zhang, C.-Y., Hu, J., Xu, L., Wang, R.-J., et al. (2016). Isolation and complete genome sequence of *Algibacter alginolytica* sp. nov., a novel seaweed-degrading *Bacteroidetes bacterium* with diverse putative polysaccharide utilization loci. *Appl. Environ. Microbiol.* 82, 2975–2987. doi: 10.1128/AEM.00204-16

Tindall, B. J., Rosselló-Móra, R., Busse, H.-J., Ludwig, W., and Kämpfer, P. (2010). Notes on the characterization of prokaryote strains for taxonomic purposes. *Int. J. Syst. Evol. Microbiol.* 60, 249–266. doi: 10.1099/IJS.0.016949-0

Tracy, B. P., Jones, S. W., Fast, A. G., Indurthi, D. C., and Papoutsakis, E. T. (2012). Clostridia: the importance of their exceptional substrate and metabolite diversity for biofuel and biorefinery applications. *Curr. Opin. Biotech.* 23, 364–381. doi: 10.1016/J.COPBIO.2011.10.008

Wu, S., Liu, G., Jin, W., Xiu, P., and Sun, C. (2016). Antibiofilm and anti-infection of a marine bacterial exopolysaccharide against *Pseudomonas aeruginosa*. *Front. Microbiol.* 7:102. doi: 10.3389/fmicb.2016.00102

Xu, S.-Y., He, P.-Q., Dewi, S.-Z., Zhang, X.-L., Ekowati, C., Liu, T.-J., et al. (2013). Hydrogen-Producing microflora and Fe–Fe hydrogenase diversities in seaweed bed associated with marine hot springs of Kalianda. Indonesia. *Curr. Microbiol.* 66, 499–506. doi: 10.1007/S00284-013-0302-0

Yamane, K., Hattori, Y., Ohtagaki, H., and Fujiwara, K. (2011). Microbial diversity with dominance of 16S rRNA gene sequences with high GC contents at 74 and 98 °C subsurface crude oil deposits in Japan. *FEMS Microbiol. Ecol.* 76, 220–235. doi: 10.1111/J.1574-6941.2011.01044.X

Yarza, P., Yilmaz, P., Pruesse, E., Glöckner, F. O., Ludwig, W., Schleifer, K.-H., et al. (2014). Uniting the classification of cultured and uncultured bacteria and archaea using 16S rRNA gene sequences. *Nat. Rev. Microbiol.* 12, 635–645. doi: 10.1038/NRMICRO3330

Zeikus, J., Hegge, P., Thompson, T., Phelps, T., and Langworthy, T. (1983). Isolation and description of *Haloanaerobium praevalens* gen. nov., and sp. nov., an obligately anaerobic halophile common to Great Salt Lake sediments. *Curr. Microbiol.* 9, 225–233. doi: 10.1007/BF01567586

Zhang, J., Liu, R., Xi, S., Cai, R., Zhang, X., and Sun, C. (2020). A novel bacterial thiosulfate oxidation pathway provides a new clue about the formation of zero-valent sulfur in deep sea. *ISME J.* 14, 2261–2274. doi: 10.1038/s41396-020-0684-5

Zhang, X. (2007). *Marine Microbiology*. Qingdao: Qingdao China Ocean University Press.

Zhang, X., Zeng, X., Li, X., Alain, K., Jebbar, M., and Shao, Z. (2017). *Anaeromicrobium sediminis* gen. nov., sp. nov., a fermentative bacterium isolated from deep-sea sediment. *Int. J. Syst. Evol. Microbiol.* 67, 1462–1467. doi: 10.1099/IJSEM.0.001739

Zhang, Z., Li, J., Hao, X., Gu, Z., and Xia, S. (2019b). Electron donation characteristics and interplays of major volatile fatty acids from anaerobically fermented organic matters in bioelectrochemical systems. *Environ. Technol.* 40, 2337–2344. doi: 10.1080/09593330.2018.1441334

Zhang, Y., Xiao, L., Wang, S., and Liu, F. (2019a). Stimulation of ferrihydrite nanorods on fermentative hydrogen production by *Clostridium pasteurianum*. *Bioresour. Technol.* 283, 308–315. doi: 10.1016/J.BIORTECH.2019.03.088

Zheng, R., Liu, R., Shan, Y., Cai, R., Liu, G., and Sun, C. (2021). Characterization of the first cultured free-living representative of *Candidatus Izemoplasma* uncovers its unique biology. *ISME J.* 15, 2676–2691. doi: 10.1038/S41396-021-00961-7

Zhou, L., Cao, L., Wang, X., Wang, M., Wang, H., Zhong, Z., et al. (2020). Metal adaptation strategies of deep-sea *Bathymodiolus mussels* from a cold seep and three hydrothermal vents in the West Pacific. *Sci. Total Environ.* 707:136046. doi: 10.1016/J.SCITOTENV.2019.136046

Zhu, Y., Ma, N., Jin, W., Wu, S., and Sun, C. (2017). Genomic and transcriptomic insights into Calcium Carbonate biomineralization by marine *Actinobacterium Brevibacterium linens* BS258. *Front. Microbiol.* 8:602. doi: 10.3389/FMICB.2017.00602

Conflict of Interest: The authors declare that the research was conducted in the absence of any commercial or financial relationships that could be construed as a potential conflict of interest.

Publisher's Note: All claims expressed in this article are solely those of the authors and do not necessarily represent those of their affiliated organizations, or those of the publisher, the editors and the reviewers. Any product that may be evaluated in this article, or claim that may be made by its manufacturer, is not guaranteed or endorsed by the publisher.

frontiers in Microbiology

ORIGINAL RESEARCH
published: 27 January 2022
doi: 10.3389/fmicb.2022.820907

Acid Tolerant and Acidophilic Microalgae: An Underexplored World of Biotechnological Opportunities

Fabian Abiusi[1], Egbert Trompetter[1], Antonino Pollio[2], Rene H. Wijffels[1,3] and Marcel Janssen[1]*

[1]Bioprocess Engineering, AlgaePARC, Wageningen University and Research, Wageningen, Netherlands, [2]Department of Biology, University of Naples Federico II, Naples, Italy, [3]Faculty of Biosciences and Aquaculture, Nord University, Bodø, Norway

Despite their large number and diversity, microalgae from only four genera are currently cultivated at large-scale. Three of those share common characteristics: they are cultivated mainly autotrophically and are extremophiles or tolerate "extreme conditions." Extreme growth conditions aid in preventing contamination and predation of microalgae, therefore facilitating outdoor cultivation. In search for new extremophilic algae suitable for large-scale production, we investigated six microalgal strains able to grow at pH below 3 and belonging to four genera; *Stichococcus bacillaris* ACUF158, *Chlamydomonas acidophila* SAG 2045, and *Chlamydomonas pitschmannii* ACUF238, *Viridiella fridericiana* ACUF035 and *Galdieria sulphuraria* ACUF064 and ACUF074. All strains were cultivated autotrophically at light intensity of 100 and 300 μmol m^{-2} s^{-1} and pH between 1.9 and 2.9. The autotrophic biomass productivities were compared with one of the most productive microalgae, *Chlorella sorokiniana* SAG 211-8K, grown at pH 6.8. The acid tolerant strains have their autotrophic biomass productivities reported for the first time. Mixotrophic and heterotrophic properties were investigated when possible. Five of the tested strains displayed autotrophic biomass productivities 10–39% lower than *Chlorella sorokiniana* but comparable with other commercially relevant neutrophilic microalgae, indicating the potential of these microalgae for autotrophic biomass production under acidic growth conditions. Two acid tolerant species, *S. bacillaris* and *C. acidophila* were able to grow mixotrophically with glucose. *Chlamydomonas acidophila* and the two Galdieria strains were also cultivated heterotrophically with glucose at various temperatures. *Chlamydomonas acidophila* failed to grow at 37°C, while *G. sulphuraria* ACUF64 showed a temperature optimum of 37°C and *G. sulphuraria* ACUF74 of 42°C. For each strain, the biomass yield on glucose decreased when cultivated above their optimal temperature. The possible biotechnological applications of our findings will be addressed.

Keywords: extremophilic microalgae, biomass productivity, mixotrophy, biomass yield on substrate, temperature optima, *Galdieria*, *Chlamydomonas acidophila*, *Stichococcus bacillaris*

OPEN ACCESS

Edited by:
Davide Zannoni, University of Bologna, Italy

Reviewed by:
Shuhao Huo, Jiangsu University, China
Saikat Chakraborty, Indian Institute of Technology Kharagpur, India

****Correspondence:***
Fabian Abiusi
fabian.abiusi@gmail.com

Specialty section:
This article was submitted to Extreme Microbiology, a section of the journal Frontiers in Microbiology

Received: *23 November 2021*
Accepted: *06 January 2022*
Published: *27 January 2022*

Citation:
Abiusi F, Trompetter E, Pollio A, Wijffels RH and Janssen M (2022) Acid Tolerant and Acidophilic Microalgae: An Underexplored World of Biotechnological Opportunities. Front. Microbiol. 13:820907. doi: 10.3389/fmicb.2022.820907

INTRODUCTION

Microalgae are a diverse, polyphyletic group of organisms, boasting estimated species number between 2,00,000 and several million (Norton et al., 1996). In addition to cultivating microalgae for food and feed they also hold promise for a plethora of new products and applications. Microalgae are commonly grown exploiting their photoautotrophic capacity (henceforth referred to as autotrophic), in which cells harvest light energy, use carbon dioxide (CO_2) as a carbon source, and release oxygen (O_2) as a byproduct. Alternatives to autotrophic cultures are chemo-organotrophic (henceforth referred to as heterotrophic) cultures in which organic carbon, such as sugars and organic acids, are used as carbon sources in the absence of light. Despite the enormous diversity, only four genera of microalgae are cultivated at large-scale: *Arthrospira* (Spirulina), *Chlorella*, *Dunaliella*, and *Haematococcus* (Pulz and Gross, 2004). Excluding *Chlorella*, which is mainly produced heterotrophically in fermenters utilizing glucose or acetic acid (Iwamoto, 2004), the other three genera mentioned are cultivated mainly autotrophically and are extremophiles or tolerate "extreme conditions."

Extreme conditions are, for example, unusually high or low temperature, high or low pH, or high osmotic pressure. If a strain has at least one of its growth optima falling into such a range, it is considered an extremophile, and if it has more than one optimum in such categories, the term is "poly-extremophile." *Spirulina* is cultivated in alkaline media (pH 8.5–10.5), *Dunaliella* at high NaCl concentrations (35–300 g/L; Oren, 2014) and also *Haematococcus* can tolerate high salinity, which is used to promote accumulation of the red pigment astaxanthin within the cells (Oslan et al., 2021). Extreme growth conditions aid in preventing contamination and predation of microalgae, therefore facilitating their outdoor cultivation.

Bacterial contamination is a notable challenge when microalgae are cultivated in a medium containing organic carbon, as microalgae have a growth rate one order of magnitude lower than their competitors. In order to avoid bacterial contaminations, heterotrophic cultivation of microalgae is performed in bioreactors, where all inputs (liquid media or gasses) are sterilized and the process is optimized to operate axenically. With some microalgal species, autotrophic and heterotrophic cultivation can be combined in so-called "mixotrophic" cultivation. In this trophic mode, light and organic carbon are simultaneously provided and both heterotrophic and autotrophic metabolisms operate concurrently within a single microalgal monoculture. Mixotrophic cultivation can significantly increase biomass productivity and concentration, while utilizing light energy with the same photosynthetic efficiency of an autotrophic culture (Abiusi et al., 2020a,b).

When sunlight is used as a light source, mixotrophic cultivation of microalgae is performed in photobioreactors, characterized by high surface/volume ratio to maximize the light supply rate (Posten, 2009). Although it might be technically feasible to operate closed sunlit photobioreactors without bacterial contamination, maintaining axenic conditions in an outdoor photobioreactor, especially when a medium contains a source of organic carbon is challenging. In a pursuit of a strategy to prevent bacterial contamination under mixotrophic conditions, Henkanatte-Gedera et al. (2017) demonstrated that lowering pH of unsterilized urban primary effluent to a value of 2 resulted in a complete removal of pathogens and reduced the initial bacterial population by 98%, allowing an acidophilic microalgae to be the primary organism growing in such a nutrient-rich medium. Contamination by unwanted microorganisms is not only a challenge in the presence of an organic substrate. There is a wide diversity of protist taxa (e.g., amoeba, flagellates, and ciliates) able to graze on microalgae, threatening the commercial success of the developing microalgal industry (Day et al., 2017). Several studies demonstrate that pH affects microbial community diversity more than any other parameter tested (Merino et al., 2019). Moreover, it is well documented that few ciliate and rotifer can survive pH below 3 (Seckbach, 2007).

During the last two decades, increasing attention has been paid toward acidophilic and acid tolerant microalgae and their possible biotechnological applications such as the production of acid stable pigments (Rahman et al., 2017; Ferraro et al., 2020a), rare earth metal biorecovery (Minoda et al., 2015), extremozymes (Rahman et al., 2020) and extremolytes (Martinez-Garcia and van der Maarel, 2016). Despite their potential, most of the research on acidophilic microalgae has been focused on one species only: *Galdieria sulphuraria* (Sydney et al., 2019).

The aim of this study was to find microalgal strains able to grow at low pH sufficiently to exhibit potential for large-scale production with or without utilizing organic carbon. In order to achieve this goal, we investigated the autotrophic biomass productivities of six acid tolerant microalgal strains at pH below 3 and compared their productivity with the neutrophilic *Chlorella sorokiniana*. Three strains were chosen since there were previous reports on their ability to use glucose, namely: *Stichococcus bacillaris* ACUF158, *Chlamydomonas acidophila* SAG 2045, and *Chlamydomonas pitschmannii* ACUF238 (Martinez et al., 1987; Pollio et al., 2005; Spijkerman, 2007). *Viridiella fridericiana* ACUF035 was suggested from the Algal Collection of University Federico II of Naples (ACUF) due to good autotrophic performance. Two strains of *G. sulphuraria*, the most studied acidophilic microalgae species, were compared with the acid tolerant strains. *Galdieria sulphuraria* ACUF064 and ACUF074 were selected based on the results of a screening of 42 *Galdieria* strains (Graziani et al., 2013) as they displayed the best autotrophic and heterotrophic growth rates. The acid tolerant microalgae strains performing well autotrophically were then also cultivated mixotrophically and, when possible, heterotrophically.

MATERIALS AND METHODS

Organism, Media, and Cultivation Conditions

Seven microalgal strains were used in this study. *Stichococcus bacillaris* ACUF158, *C. pitschmannii* ACUF238, *V. fridericiana* ACUF035, *G. sulphuraria* ACUF064, and *G. sulphuraria* ACUF074

were obtained from the Algal Collection of University Federico II of Naples (ACUF). *Chlamydomonas acidophila* SAG 2045 and *C. sorokiniana* SAG 211-8K were obtained from the algae culture collection of Göttingen University (SAG). For each strain maintenance flasks were prepared. Maintenance cultures were cultivated autotrophically by placing 250 ml flasks in an incubator with orbital shaker set at 100 rpm. Incubator headspace was enriched with 2% v/v CO_2 and the flasks were illuminated 24/24 from the top by fluorescent lamps at a photon flux density (PFD) of 100 µmol $m^{-2} s^{-1}$.

Chlorella sorokiniana SAG 211-8K was cultivated at pH 6.8 ± 0.1 at 37°C in M8a medium (Abiusi et al., 2020a) with ammonium chlorine as a nitrogen source. All the other strains were cultivated initially at pH 2.1 ± 0.2 adjusting the pH with 2 M H_2SO_4. The medium was prepared according to Abiusi et al. (2021) composed of the following salts (in mol L^{-1}): $2.2\,10^{-3}$ KH_2PO_4, $20.0\,10^{-3}$ $(NH_4)_2SO_4$, $1.6\,10^{-3}$ $MgSO_4\,7\,H_2O$, $0.1\,10^{-3}$ $CaCl_2$, $0.16\,10^{-3}$ EDTA ferric sodium salt, $0.05\,10^{-3}$ $Na_2EDTA\,2H_2O$, $0.9\,10^{-3}$ NaCl, $0.2\,10^{-3}$ H_3BO_3, $20.2\,10^{-6}$ $MnCl_2\,4H_2O$, $20.6\,10^{-6}$ $ZnCl_2$, $8.0\,10^{-6}$ $CuSO_4\,5H_2O$, $4.1\,10^{-6}$ $Na_2MoO_4\,2H_2O$, and $4.2\,10^{-6}CoCl_2\,6H_2O$. If no growth was observed, pH was increased to 2.9 ± 0.2. The two *Galdieria* strains were maintained at 37°C, while the other acid tolerant strains were placed in two different incubators, set at 25 and 37°C.

Autotrophic Flasks Experiment

In this study, we assessed the autotrophic performance of four acid tolerant microalgal strains, with a pH optimum above 3 but able to grow at pH 3 or lower, namely: *S. bacillaris* ACUF158, *C. acidophila* SAG 2045, *C. pitschmannii* ACUF238, *V. fridericiana* ACUF035, and two acidophilic strains *G. sulphuraria* ACUF064 and *G. sulphuraria* ACUF074, with a pH optimum below 3.

The autotrophic growth of these six microalgal strains was studied in 250 ml flasks filled with 100 ml of culture in a home-made incubator described by Abiusi et al. (2020a) and depicted in **Figure 1**. In this incubator illumination was provided 24/24 from below using warm-white LED at a PFD of 100 ± 15 and 300 ± 25 µmol $m^{-2} s^{-1}$. The position of each flask in the incubator was changed daily to minimize differences in light intensity within the incubator. Flasks were stirred at 100 rpm with a magnetic rod and the headspace of the incubator was enriched with 4.5% v/v CO_2.

The four acid tolerant strains were cultivated at a temperature and pH in which growth was observed during the pre-cultivation summarized in **Table 1**. The two acidophilic *G. sulphuraria* strains were cultivated at pH 1.8 ± 0.2. In each experiment, pH was measured at the beginning and at the end of the experiment. The neutrophilic strain *C. sorokiniana* SAG 211-8K and the two *G. sulphuraria* strains were cultivated at 37°C.

Each experiment was conducted in duplicate. Maintenance flasks were used as inoculum. Cultures were pre-cultivated using the maintenance flasks as inoculum and cultures were adapted to the respective light and temperature settings for at least 1 week. Provided that linear growth was observed during this adaptation time, the pre-culture was used as an inoculum for the actual autotrophic experiment starting at an optical density 1.2 ± 0.3 at 100 µmol $m^{-2} s^{-1}$ and 4.5 ± 1.2 at 300 µmol $m^{-2} s^{-1}$ measured at 750 nm (OD_{750}).

During the batch, one or two samples per day were taken from each flask to measure OD_{750} and the photosystem II maximum quantum yield of photochemistry (*QY* or Fv/Fm). The microalgal concentration was assessed by converting OD_{750} into biomass concentration (C_x $g_x\,L^{-1}$), using OD_{750}/C_x linear correlation pre-determined for each strain and light intensity. The validity of this correlation was confirmed at the end of each experiment by an additional measurement of dry weight and optical density. The volumetric biomass production rate r_x ($g_x\,L^{-1}\,day^{-1}$) was calculated from a linear regression of the increase of biomass concentration (C_x) over time during the batch.

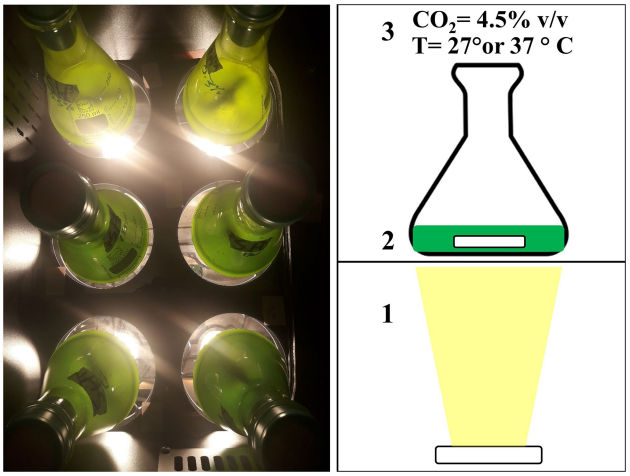

FIGURE 1 | Picture (left) and schematic view of the incubator used during the autotrophic experiment. Light was provided from below using a LED (1), flasks were stirred at 100 rpm with a magnetic rod (2), and the head space of the incubator was enriched with 4.5% v/v carbon dioxide (CO_2; 3). Temperature of the incubator was maintained constant, either at 27°C or at 37°C, depending on the experiment (3).

TABLE 1 | Temperature and pH used during the autotrophic experiment.

Strain	pH optimum	pH	T (C°)
Chlorella sorokiniana SAG 211-8K	Neutrophilic	6.8 ± 0.1	37
Galdieria sulphuraria ACUF064	Acidophilic	1.9 ± 0.2	37
Galdieria sulphuraria ACUF074	Acidophilic	2.0 ± 0.2	37
Viridiella fridericiana ACUF035	Acid tolerant	2.1 ± 0.2	27
Chlamydomonas acidophila SAG 2045	Acid tolerant	2.2 ± 0.1	27
Stichococcus bacillaris ACUF158	Acid tolerant	2.9 ± 0.3	27
Chlamydomonas pitschmannii ACUF238	Acid tolerant	2.8 ± 0.2	27

The pH was measured at the beginning and at the end of the experiment and is reported with the SD of the two measurements.

Mixotrophic Microplate Experiment

The ability of *S. bacillaris* ACUF158, *C. acidophila* SAG 2045, and *V. fridericiana* ACUF035 to grow mixotrophically utilizing glycerol, acetic acid, and glucose under 24/24 lighting was tested

in 24-well microplates at pH 2.9 ± 0.2 (Costar 3524, Corning, United States). Glucose, acetic acid, and glycerol were supplemented to the autotrophic medium based on their carbon content. In order to provide 1 g L^{-1} of organic carbon, 2.75 g L^{-1}, 2.50 g L^{-1}, and 2.56 g L^{-1} of glucose monohydrate, acetic acid, and glycerol were used. The mixotrophic performance was evaluated using an autotrophic culture grown under the same conditions in a medium without an organic carbon source as a reference.

Maintenance cultures were diluted to an OD_{750} of 0.3–0.6 with the specific media required and each well was filled with 1 ml of this culture. Each medium was tested in triplicate. The 24-well plates were placed in an incubator at 25°C, headspace was enriched with 2% v/v CO_2 and shaken at 100 rpm (orbital shaker). Light was provided from the top by fluorescent lamps (Sylvania *CF*-LE 55 W) giving a light intensity of 75 μmol m^{-2} s^{-1}. Microalgal growth was followed by measuring OD_{680} and OD_{750} using a plate reader (Infinite Nanoquant M200, Tecan, Switzerland). The ratio OD_{680}/OD_{750} was used as an indicator for the amount of chlorophyll per unit biomass and therefore of possible bacterial contaminations.

Heterotrophic Flasks Experiment

Chlamydomonas acidophila SAG 2045, *G. sulphuraria* ACUF064, and *G. sulphuraria* ACUF074, where cultivated heterotrophically under the same conditions used for the autotrophic experiment but supplementing the medium with 2.75 g L^{-1} glucose monohydrate without illumination. The experiment was conducted using the same procedure described by Abiusi et al. (2021). Several temperatures were tested. At each temperature cultures were adapted to heterotrophic growth for at least 2 weeks. Specific growth rate (μ) was calculated by plotting the natural logarithm of OD_{750} over time of cultures growing exponentially.

During the experiments, multiple samples were taken per day until glucose was depleted. The concentration of microalgae was assessed by measuring optical density at 750 nm (OD_{750}). A 1 ml aliquot of sample was centrifuged to obtain a clear supernatant for the glucose concentration measurement. The microalgae concentration was assessed by converting OD_{750} into C_x using a OD_{750}/C_x linear correlation pre-determined for each strain and temperature. The validity of this correlation was confirmed at the end of each experiment by an additional measurement of dry weight and optical density.

The heterotrophic biomass yield on substrate ($Y_{x/s}$, $g_x g_s^{-1}$) was calculated using the following equation:

$$Y_{x/s} = \frac{C_{xe} - C_{x0}}{S_0 - S_e}$$

where C_{x0}/C_{xe} and S_0/S_e are the biomass and the glucose concentrations (g L^{-1}) respectively at the start and the end of the exponential phase.

Analytical Methods

The PFD (μmol m^{-2} s^{-1}) was measured with a LI-COR 190-SA 2π PAR quantum sensor and dry weight concentration (C_x, $g_x L^{-1}$), optical density at 750 nm (OD_{750}), and the photosystem II maximum quantum yield of photochemistry (*QY* or Fv/Fm) were determined according to Abiusi et al. (2020a). The presence of possible microbial contaminants was assessed both by optical and fluorescent microscopy after staining the sample with SYBER green I (Sigma-Aldrich, United States) according to Abiusi et al. (2020a).

Samples were taken aseptically from flasks one or two times per day. In the heterotrophic experiment, aliquots of 1 ml were centrifuged at 20,000 rpm (10 min). The supernatant was immediately analyzed for glucose content. Glucose concentration was determined using a bioanalyzer (YSI 2700, YSI Life Sciences, United States) that couples an enzymatic reaction of glucose with electrochemical detection.

Statistical Analysis

Autotrophic and heterotrophic experiments were conducted in biological duplicate ($n = 2$), while mixotrophic experiment in biological triplicate ($n = 3$). Figures reported the SD of these replicates. Significant difference between strains cultivated in flasks under autotrophic and heterotrophic condition or between autotrophic and mixotrophic culture in microplate were analyzed by one-way ANOVA. The significance level was $p < 0.05$.

RESULTS

Autotrophic Growth

Four acid tolerant and two acidophilic microalgae strains were tested for their autotrophic performance at two light intensities (100 and 300 μmol m^{-2} s^{-1}) and compared to the neutrophilic *C. sorokiniana* SAG 211-8K. Maintenance cultures were prepared before initiating the experiment. These were kept at a pH 2.0 ± 0.2 at 37°C. For the acid tolerant strains additional maintenance cultures were kept at 25°C. At pH 2.0 ± 0.2 no growth was obtained in *C. pitschmannii* ACUF238 and *S. bacillaris* ACUF158 cultures regardless of the temperature applied. For this reason, the pH was increased to 2.9 ± 0.2. After the increase of pH those two strains succeeded in growing at 25°C but not at 37°C. *Viridiella fridericiana* ACUF035 and *C. acidophila* SAG 2045 successfully grew at pH 2.1 ± 0.2 but no growth was observed at 37°C. The presence in the medium of two buffers, by $H_3PO_4 \rightleftharpoons H_2PO_4^- + H^+$ ($pKa_1 = 2.14$) and $H_2SO_4 + H_2O \rightleftharpoons H^+ + HSO^-_4$ ($pK_{a1} = 1.92$), maintained the pH stable across the experiments. **Table 1** summarizes the final temperatures and pH used during the autotrophic experiment at two light intensities.

All of the tested strains succeeded in growing at 100 μmol m^{-2} s^{-1} (**Figure 2**; **Supplementary Figures 1–7**). No significant difference ($p < 0.05$) was found between the biomass productivities of *S. bacillaris* and *C. sorokiniana* (0.6 g L^{-1} day^{-1}), while the other five strains had a biomass productivity 25–72% lower than *C. sorokiniana*. When the strains were cultivated at 300 μmol m^{-2} s^{-1}, *C. pitschmannii* did not grow and *C. sorokiniana* expressed the highest productivity (1.1 g L^{-1} day^{-1}). The other five strains showed a productivity which was 10–39% lower than *C. sorokiniana*. Given the poor autotrophic

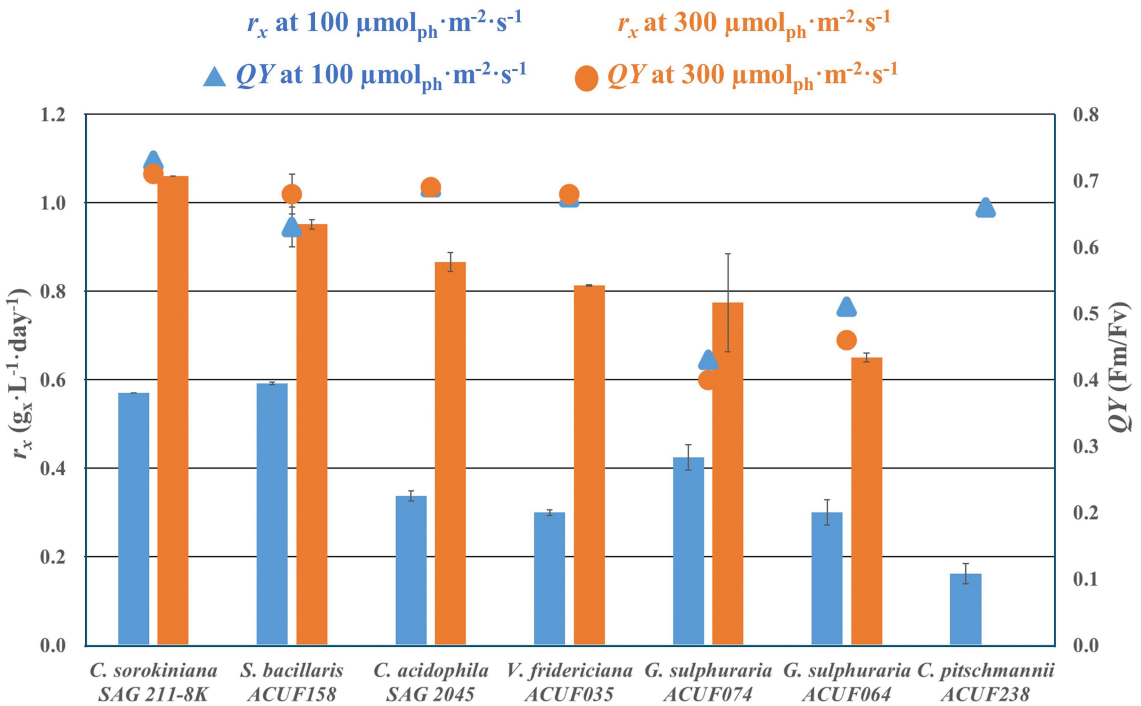

FIGURE 2 | Volumetric biomass production rate r_x ($g_x L^{-1} day^{-1}$) and photosystem II maximum quantum yield of photochemistry (QY, F_v/F_m) of autotrophic culture grown at 100 and 300 µmol $m^{-2} s^{-1}$. The data are presented as average of the biological duplicate ($n = 2$) and reported with the SD of the measurements.

performance of *C. pitschmannii*, this strain was discontinued from further investigations.

The photosystem II maximum quantum yields of photochemistry were between 0.66 and 0.73 in *C. sorokiniana* and the acid tolerant strains with no significantly differences ($p < 0.05$) between 100 and 300 µmol $m^{-2} s^{-1}$. At 100 µmol $m^{-2} s^{-1}$, *G. sulphuraria* ACUF064 and *G. sulphuraria* ACUF074 had QY 30% lower than other strains. The QY of both strains significantly decreased ($p > 0.05$) further at 300 µmol $m^{-2} s^{-1}$, resulting in a QY of 0.46 ± 0.1 for *G. sulphuraria* ACUF064 and of 0.40 ± 0.1 for *G. sulphuraria* ACUF074.

Mixotrophic Growth

The ability of *S. bacillaris* ACUF158, *C. acidophila* SAG 2045, and *V. fridericiana* ACUF35 to utilize glucose, acetic acid, and glycerol in presence of light was tested on 24-well microplates (**Figure 3**). The final OD_{750} reached for *S. bacillaris* ACUF158 and *C. acidophila* SAG 2045 grown in presence of glucose was significantly higher than the autotrophic cultures grown under similar conditions. In both strains OD_{680}/OD_{750} remained constant suggesting that the cultures were axenic and that glucose boosted algal growth. Microscopic observation from samples taken at the end of the experiment confirmed axenicity (**Supplementary Figures 8–10**). *Viridiella fridericiana* ACUF35 was growing similarly in the presence of glucose as the corresponding autotrophic culture indicating that the culture was not able to utilize this substrate. Glycerol did not have any effect on the three tested strains, while acetic acid was lethal for all of them.

Heterotrophic Growth

Heterotrophic experiments were conducted with *C. acidophila* SAG 2045, *G. sulphuraria* ACUF064, and *G. sulphuraria* ACUF074 to determine specific growth rate (μ) and biomass yield on substrate ($Y_{x/s}$) using glucose. Cultures were adapted for 2 weeks before starting the experiment under heterotrophic conditions. During this adaptation period, the cultures were diluted regularly with fresh medium to maintain exponential growth. During the adaptation time, all the cultures lost their pigmentation and became pale. *Chlamydomonas acidophila* cultivated at 25°C had a specific growth rate of 0.52 day^{-1} and a biomass yield on substrate of 0.4 $g_x g_s^{-1}$, while no growth was observed at 37°C (**Figure 4**).

The two *G. sulphuraria* strains grown at 37°C had similar specific growth rates and biomass yields on substrate, 0.75 day^{-1} and 0.5 $g_x g_s^{-1}$ (**Figure 4**). When temperature was increased to 42°C the specific growth rate of *G. sulphuraria* ACUF064 decreased to 0.33 day^{-1}, while the specific grow rate of *G. sulphuraria* ACUF074 increased to 1.04 day^{-1} to decline again to 0.41 day^{-1} at 47°C. For each strain, the biomass yield on glucose decreased as soon as it was cultivated above its optimal temperature.

DISCUSSION

In the present study six microalgal strains, belonging to four different microalgal genera, were cultivated autotrophically at a pH below 3, under similar conditions. The autotrophic

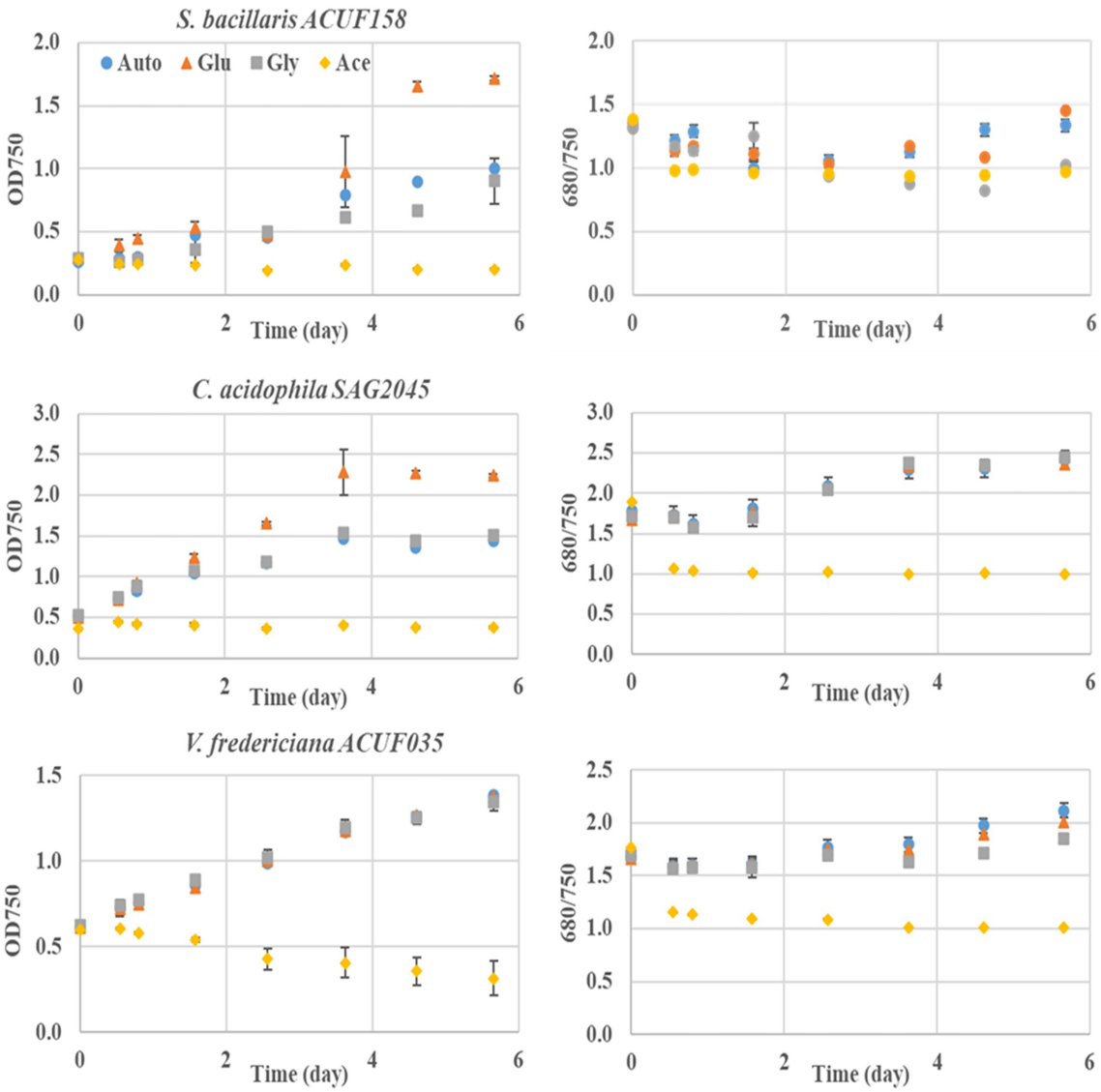

FIGURE 3 | Mixotrophic performance in the presence of 1 g/L of individual carbon source such as glucose (triangle), glycerol (square), and acetic acid (diamond) of three acid tolerant microalgal cultivated at pH 2.9 ± 0.2 strains under 24/24 lighting. An autotrophic culture (dot) is used as reference.

performances of those six microalgal strains were compared with neutrophilic *C. sorokiniana* SAG 211-8K, which is one of the fastest growing microalgae (Cuaresma et al., 2009). Five of the tested strains showed an autotrophic biomass productivity which was 10–39% lower than *C. sorokiniana* but comparable with other commercially relevant neutrophilic microalgae such as *Isocrysis lutea* (Gao et al., 2020), *Rhodomonas* sp. (Oostlander et al., 2020), and *Nannochloropsis* sp. (Benvenuti et al., 2016) indicating the potential of these microalgae for autotrophic biomass production under acidic growing conditions.

Literature concerning autotrophic productivity of acid tolerant microalgae grown below pH 3 is limited. Most studies on acid tolerant microalgae isolated from acid waters are not focusing on biomass production but were conducted from taxonomic (Albertano et al., 1991, 2000), evolutionary (Costas et al., 2007), or ecological viewpoints (Aguilera et al., 2007). In the present work, autotrophic biomass productivities of the studied acid tolerant strains are reported for the first time. One of the few previous works on biomass productivity of an acid tolerant microalgae was conducted by Cuaresma et al. (2011) in a 1 L photobioreactor. The authors cultivated a newly isolated acid tolerant *C. acidophila* strain at pH 2.5 obtaining a biomass areal productivity of 20 $g\,m^{-2}\,day^{-1}$. The acid tolerant strains used in our study displayed a biomass areal productivity of 15–18 $g\,m^{-2}\,day^{-1}$ when cultivated at 300 $\mu mol\,m^{-2}\,s^{-1}$. Those areal productivities were derived from the volumetric productivity considering the bottom of the flask as illuminated surface (**Figure 1**). The resulting areal productivities obtained in flasks with the two *G. sulphuraria* strains are comparable to the productivities observed in our

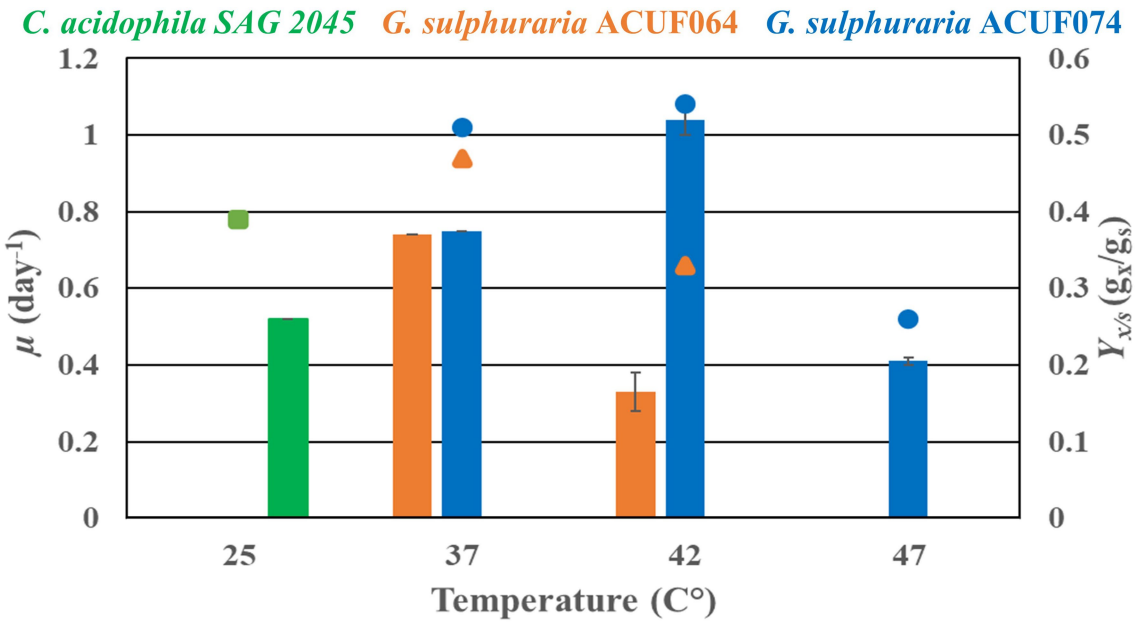

FIGURE 4 | Heterotrophic specific growth rate (μ) and biomass yield substrate ($Y_{x/s}$) of *Chlamydomonas acidophila* SAG 2045 (green), *Galdieria sulphuraria* ACUF064 (orange), and *Galdieria sulphuraria* ACUF074 (blue) grown on glucose at different temperatures.

two recent studies in a 2 L photobioreactor (Abiusi et al., 2021, 2022). The data obtained from our flask incubator (**Figure 1**) therefore represents cultivation in a bench-scale photobioreactor. This is due to the specific setup of our experiment where algae, grown in flasks at a controlled temperature and elevated CO_2, are illuminated from below which leads to a high surface/volume ratio (50.3 m^{-1}) and a high light supply rate. The high light regime can also explain why linear growth was maintained until a high biomass concentration of 9 g L^{-1} was reached (**Supplementary Figures 1–6**).

Other studies on acid tolerant strains often report only the autotrophic specific growth rate (μ) measured in the exponential growth phase (Gerloff-Elias et al., 2005; Olivieri et al., 2011). Although, the specific growth rate is not sufficient to predict biomass productivity, it may be used to compare different conditions and to give a first indication of the autotrophic growth potential of the strain. Olivieri et al. (2011) studied the autotrophic growth rate of *S. bacillaris* ACUF158 at pH 3.3, 6, and 8.3. In their study, *S. bacillaris* ACUF158 displayed a pH optimum of 6 with a μ of 0.79 day^{-1}, while at pH 3.3 it was reduced to 0.33 day^{-1}. In our experiments, *S. bacillaris* was cultivated at pH similar to the lowest pH tested by Olivieri et al. (2011) and we observed a similar growth rate.

In the only previous study on *C. acidophila* SAG 2045 (Gerloff-Elias et al., 2005), the authors reported two autotrophic pH optimums at pH 3 and 5 with maximum specific growth rate of 0.8 day^{-1}. Gerloff-Elias et al. (2005) compared *C. acidophila* SAG 2045 at pH 3 and 5 to the neutrophilic *Chlamydomonas reinhardtii* SAG 11-32b grown at neutral pH reporting similar growth rate. The higher dark respiration rates found in *C. acidophila* were compensated by higher photosynthetic rates.

The poorest autotrophic performance in our experiment was observed from *C. pitschmannii* ACUF238. The only previous study on *C. pitschmannii* ACUF238 regards the eco-physiological characterization and isolation of the strain (Pollio et al., 2005). Growth optimum at pH 2.5 and temperature 37°C were found, while in our study the strain failed to grow under such conditions. Large intraspecific variations in key ecophysiological traits are common within natural populations. The *C. pitschmannii* strains were isolated by serial dilution from the site of Pisciarelli in mid-2003 and were immediately used for the experiments reported in Pollio et al. (2005). During long-term maintenance in the following 18 years, the strains have been treated against bacteria and fungi contamination and re-isolated. The combination of high nutrient concentrations provided by the culture media and the stability of light and temperature conditions (60 µmol m^{-2} s^{-1} and 24 ± 1°C, respectively) could have led to a laboratory selection of neutrophilic isolates with a temperature optimum closer to 25°C possibly explaining the disparities between the studies.

Another important observation in our work is that two acid tolerant species, *C. acidophila* SAG 2045 and *S. bacillaris* ACUF158, were able to grow mixotrophically with glucose displaying a higher growth rate than the corresponding autotrophic culture. In a previous study by Cuaresma et al. (2011), *C. acidophila* was cultivated mixotrophically without CO_2 addition using acetic acid, glycerol, glucose, glycine, or starch as the sole carbon source. *Chlamydomonas acidophila* was able to utilize the tested organic substrates, except for acetic acid, but the growth rate and final biomass produced were significantly lower than, or in the case of glucose, similar, to the autotrophic control. A different strain used in our study may explain the variance between our results

and Cuaresma et al. (2011). Our recent studies demonstrated that mixotrophy is a promising strategy to even double the biomass productivity (Abiusi et al., 2020b, 2021). Mixotrophic production of microalgae is already used at industrial scale to decrease microalgal production costs (Iwamoto, 2004; Ganuza and Tonkovich, 2016). We believe that mixotrophic cultivation of acid tolerant and acidophilic microalgae, by reducing the risk of contamination, will further facilitate this cultivation strategy.

We further studied glucose assimilation cultivating *C. acidophila* SAG 2045 under strictly heterotrophic conditions (no light) at 25°C. The heterotrophic specific growth rate (μ), we observed in this study ($0.52\,day^{-1}$) was comparable with the autotrophic μ of $0.72\,day^{-1}$ observed by Gerloff-Elias et al. (2006) at 25°C. In the same study, the temperature optimum of *C. acidophila* SAG 2045 was reported to be 20°C with a drop of 25% in μ at 25°C. Suboptimal temperature might also explain the low biomass yield on substrate ($Y_{x/s}$) ($0.39\ g_x g_s^{-1}$) found in our study. In fact, a $Y_{x/s}$ of $0.7\ g_x g_s^{-1}$ has been previously reported in other *Chlymidomonas* species (Chen and Johns, 1996). Biomass yield on glucose is known to decrease as soon as the temperature optimum is exceeded, as also confirmed by the two *Galdieria* strains (**Figure 4**).

Glucose also increased the growth rate of *S. bacillaris* ACUF158 under mixotrophic conditions. Martinez et al. (1987) isolated a *S. bacillaris* from a sugar factory and reported that the mixotrophic growth rate was about 70% higher than autotrophic growth rate. Moreover, the same authors indicated that, when cultivated at neutral pH *S. bacillaris* could use sucrose, fructose, citrate, and acetate as carbon sources. At pH 3 in our mixotrophic experiments, acetic acid was lethal to all tested species. This was expected since acetic acid has a pKa of 4.76, so in our medium at pH 3 it was mainly present in the protonated form. Acetic acid can therefore enter the cell through passive diffusion. Once inside the cell, where the pH is close to neutrality, the undissociated acetic acid causes intracellular acidification. To counteract this acidification, protons have to be pumped out of the cells dissipating the proton motive force across the plasma membrane (Guldfeldt and Arneborg, 1998).

The most studied acidophilic microalgae species is *G. sulphuraria* with a growing research interest observed in the last decade (Sydney et al., 2019). *Galdieria sulphuraria* has been proposed as a novel source of protein (Abiusi et al., 2022), dietary fibers (Graziani et al., 2013), antioxidants (Carfagna et al., 2016) and of the blue pigment C-phycocyanin (Wan et al., 2016). For a long time, *G. sulphuraria* has been considered extremely photosensitive with light inhibition occurring at intensities above $200\,\mu mol\,m^{-2}\,s^{-1}$ (Brock, 1978; Sloth et al., 2006) recently it was demonstrated (Abiusi et al., 2021); however, that *G. sulphuraria* ACUF064 can be cultivated at high light intensity by optimizing the specific light supply rate. This was done by optimizing the biomass concentration in the reactor (Abiusi et al., 2021). In the present work. we cultivated two *G. sulphuraria* strains at 100 and $300\,\mu mol\,m^{-2}\,s^{-1}$ and started the experiment at biomass concentrations of $0.9\,g\,L^{-1}$ and $1.5\,g\,L^{-1}$, respectively (**Supplementary Figures 5, 6**). At these biomass concentrations, the specific light supply rate was below 9.5 $\mu mol_{ph}\,g_x^{-1}\,s^{-1}$, the upper limit previously reported for photoinhibition (Abiusi et al., 2021). Absence of photoinhibition was confirmed by the photosystem II maximum quantum yield (*QY*, Fv/Fm) which was in a higher range reported for *G. sulphuraria* (Abiusi et al., 2021; Uwizeye et al., 2021). Moreover, linear growth was observed from the first day (**Supplementary Figures 5, 6**) further confirming the adaptation of those strains for both the light intensities applied. These results obtained with two strains, confirm that *G. sulphuraria* can successfully be cultivated autotrophically at a high light intensity with a good biomass productivity.

Graziani et al. (2013) performed the largest screening ever performed on *G. sulphuraria*, comparing autotrophic and heterotrophic specific growth rates of 42 strains belonging to ACUF. In the autotrophic screening, the *G. sulphuraria* strains were cultivated at pH 1.5, 36°C without CO_2 addition and the medium contained only $40\,mg\,L^{-1}$ of nitrogen, 14 times lower than the nitrogen concentration used in our work. Heterotrophic cultivation was conducted using 3% glycerol as the source of organic carbon. *Galdieria sulphuraria* ACUF064 was the best performing strain under both autotrophic and heterotrophic conditions. *Galdieria sulphuraria* ACUF064 had a similar autotrophic μ as *G. sulphuraria* ACUF074 but under heterotrophic conditions, the μ of *G. sulphuraria* ACUF064 was the double of *G. sulphuraria* ACUF074, $1.0\,day^{-1}$ and $0.5\,day^{-1,}$ respectively. The difference in heterotrophic μ between our study and Graziani et al. (2013), may be explained by different growing conditions (e.g., medium composition, organic substrate).

The lack of standardized procedures in the screening of acid tolerant and acidophilic microalgae was the main cause of the discrepancies between our findings and the previous studies. Moreover, previous studies mainly measured the specific growth rate (μ), which is not sufficient to predict bulk growth at biomass concentrations used in large scale production. Commercial production of microalgae is better characterized by linear growth, such as volumetric ($g\,L^{-1}\,day^{-1}$) or areal ($g\,m^{-2}\,day^{-1}$) productivity. Van Wagenen et al. (2014) proposed a microplate-based method for high-throughput screening of microalgae, based on the measurement of two input parameters: specific growth rate as a function of light intensity and light absorbance coefficient. Using these two inputs it was possible to predict the volumetric biomass productivity. This type of a high-throughput screening procedures can offer a solution to obtain industrially relevant information on algal strains. Despite hundreds of microalgal strains able to grow at pH below 3 having been isolated (D'Elia et al., 2018) and kept at culture collections, information on the biomass productivities of these strains are limited to a few. Standardized high-throughput screenings are required to exploit the potential of unexplored groups of microalgae.

Future Outlook

In this study, we demonstrated that microalgae cultivated at pH below 3 can have biomass productivities comparable to neutrophilic strains. In this section, we will discuss possible

advantages and biotechnological applications of acid tolerant and acidophilic microalgae.

Biomass productivity of an illuminated algal culture can be doubled by utilizing a mixotrophic cultivation strategy (Abiusi et al., 2020a, 2022). In the current study, two acid tolerant strains, *C. acidophila* SAG 2045 and *S. bacillaris* ACUF158, demonstrated an increased growth rate when cultivated in the presence of glucose, while *G. sulphuraria* is known to be able to grow mixotrophically on glucose and glycerol (Sloth et al., 2006). Mixotrophic cultivation of those acid tolerant and acidophilic strains is expected to further increase biomass productivity making them more productive than most of the neutrophilic microalgal strains cultivated autotrophically. When neutrophilic microalgae are cultivated in presence of organic substrate, contamination by heterotrophic bacteria and fungi is a considerable challenge (Unnithan et al., 2014). Contaminating microbes have a growth rate faster than microalgae and can therefore outcompete algae for organic carbon utilization. Cultivating microalgae at low pH can be a worthwhile strategy to prevent contaminants. Previous works indicated that *G. sulphuraria* can be cultivated axenically in a lab scale mixotrophic reactor for over a month (Abiusi et al., 2021, 2022). Another work reports that at pH 2 *G. sulphuraria* was the main organism growing in unsterilized primary municipal waste water (Henkanatte-Gedera et al., 2017). Moreover, the low pH reduced the initial bacterial population by 98% and removed all the pathogens originally present in the waste water. Therefore, cultivation of microalgae at low pH might offer a means to bioremediate urban waste water (di Cicco et al., 2021) or valorize agro-industrial side streams (Scherhag and Ackermann, 2020), while minimizing the risk of contaminations by unwanted microorganisms.

Acid tolerant and acidophilic microalgae are often found in mining effluents characterized by low pH and high concentration of heavy metals (Dean et al., 2019). One exciting application is the use of those microalgae in rare earth metal biorecovery (Minoda et al., 2015). Numerous metals, including rare earth elements, can be readily dissolved in aqueous acid and selectively bioaccumulated in acidophilic microalgae from which they are then recovered.

Extremophilic organisms have also received increasing attention for the production of metabolites and enzymes that are commercially relevant for chemical, pharmaceutical, and food industries. Extremophiles have already been used for the production of extremozymes able to catalyze chemical reactions at an unusually high or low pH, temperature, or pressure. Such enzymes broaden the operational range of bioprocesses. Recently, the presence glucoamylases active at pH 2–2.5 and 80°C have been demonstrated in *G. sulphuraria* (Rahman et al., 2020). In the whole genome analysis of *G. sulphuraria*, a range of genes with high similarity with other extremozymes have been identified (Shrestha and Weber, 2007), which gives an indication that extremophilic microalgae can be used as a source extremozymes.

Extremophiles can also be used to produce extremolytes (Malavasi et al., 2020), small organic molecules, which allow extremophiles to withstand their extreme environments. They might have bioactive properties usable for medical purposes and in food industry (Becker and Wittmann, 2020). Floridoside is a glycoside accumulated by almost all red algae, including *G. sulphuraria,* under a high osmotic pressure (Martinez-Garcia and van der Maarel, 2016). This compound has been proposed for preventing biofouling in aquaculture (Callow and Callow, 2002), as a potential therapeutic agent to modulate immune response (Kim et al., 2013) and to promote bone formation (Ryu et al., 2015). The development of industrial applications for floridoside is hindered by low availability. *Galdieria sulphuraria* is demonstrated to accumulate high concentration of this compound and is a promising organism for industrial production of floridoside (Martinez-Garcia and van der Maarel, 2016).

Finally, acidophilic microalgae have been envisaged as novel source of pigments such as lutein (Cuaresma et al., 2011) and C-phycocyanin (Abiusi et al., 2022). C-phycocyanin extracted from several members of the cyanidiales family, known acid and thermophilic organisms, have reportedly exceptional thermo- and acid stability (Rahman et al., 2017; Ferraro et al., 2020a). The higher stability compared to the C-phycocyanin of other microalgae (e.g., *Spirulina*) is due to a residue mutation on the outside of the conserved regions (Ferraro et al., 2020b). Those traits open the opportunity to use said pigments in commonly pasteurized sparkling beverages, characterized by a low pH.

Acid tolerant and acidophilic microalgae have applications in several industrial processes such as the ones listed in this section. However, most of the current knowledge on possible new products and applications comes almost solely from studies conducted on *G. sulphuraria*. The combination of high throughput screening and omics techniques can be employed to select new productive strains as source of high value compounds.

CONCLUSION

In the present study, six microalgal strains were cultivated at a pH below 3. Utilizing acid growth conditions is a strategy to prevent unwanted microbial contaminations in autotrophic and specifically mixotrophic microalgae cultivation. Five of the tested strains showed an autotrophic biomass productivity comparable with other commercially relevant neutrophilic microalgae, indicating the potential of these microalgae for autotrophic biomass production. Two strains were also able to grow mixotrophically on glucose displaying higher growth rates than the corresponding autotrophic cultures. The ability to grow heterotrophically on glucose was tested on three strains. All of the strains grown heterotrophically lost their pigmentation in the darkness and displayed a specific growth rate between 0.5 and 1 day^{-1}, comparable to other commercially relevant microalgal species. Due to the reduced risk of microbial contaminations and biomass productivity comparable to neutrophilic microalgae, acid tolerant, and acidophilic microalgae are promising candidates for mass cultivation.

DATA AVAILABILITY STATEMENT

The raw data supporting the conclusions of this article will be made available by the authors, without undue reservation.

AUTHOR CONTRIBUTIONS

FA designed and conducted experiments, analyzed and interpretated the data, and drafted the manuscript. ET conducted a part of the experiments and analyzed the corresponding data. AP provided the strains and assisted with interpretation of the data. RW obtained funding and assisted with interpretation of the data. MJ contributed to the design of the experiments, interpreted data, and drafted the manuscript. All authors contributed to the article and approved the submitted version.

FUNDING

This work was supported by AlgaePARC, Wageningen University.

SUPPLEMENTARY MATERIAL

The Supplementary Material for this article can be found online at: https://www.frontiersin.org/articles/10.3389/fmicb.2022.820907/full#supplementary-material

REFERENCES

Abiusi, F., Fernández, P. M., Canziani, S., Janssen, M., Wijffels, R. H., and Barbosa, M. (2022). Mixotrophic cultivation of *Galdieria sulphuraria* for C-phycocyanin and protein production. *Algal Res.* 61:102603. doi: 10.1016/j.algal.2021.102603

Abiusi, F., Trompetter, E., Hoenink, H., Wijffels, R. H., and Janssen, M. (2021). Autotrophic and mixotrophic biomass production of the acidophilic *Galdieria sulphuraria* ACUF 64. *Algal Res.* 60:102513. doi: 10.1016/j.algal.2021.102513

Abiusi, F., Wijffels, R. H., and Janssen, M. (2020a). Doubling of microalgae productivity by oxygen balanced mixotrophy. *ACS Sust. Chem. Eng.* 8, 6065–6074. doi: 10.1021/acssuschemeng.0c00990

Abiusi, F., Wijffels, R. H., and Janssen, M. (2020b). Oxygen balanced mixotrophy under day-night cycles. *ACS Sust. Chem. Eng.* 8, 11682–11691. doi: 10.1021/acssuschemeng.0c03216

Aguilera, A., Zettler, E., Gómez, F., Amaral-Zettler, L., Rodríguez, N., and Amils, R. (2007). Distribution and seasonal variability in the benthic eukaryotic community of Río Tinto (SW, Spain), an acidic, high metal extreme environment. *Syst. Appl. Microbiol.* 30, 531–546. doi: 10.1016/j.syapm.2007.05.003

Albertano, P., Ciniglia, C., Pinto, G., and Pollio, A. (2000). The taxonomic position of Cyanidium, Cyanidioschyzon and *Galdieria*: an update. *Hydrobiologia* 433, 137–143. doi: 10.1023/A:1004031123806

Albertano, P., Pinto, G., Pollio, A., and Taddei, R. (1991). Physiological, biochemical, and ultrastructural characters of some strains of *Viridiella fridericiana* (Chlorophyta, Chlorococcales). *Arch. Protistenkd.* 139, 117–123. doi: 10.1016/S0003-9365(11)80013-8

Becker, J., and Wittmann, C. (2020). Microbial production of extremolytes—high-value active ingredients for nutrition, health care, and well-being. *Curr. Opin. Biotechnol.* 65, 118–128. doi: 10.1016/j.copbio.2020.02.010

Benvenuti, G., Lamers, P. P., Breuer, G., Bosma, R., Cerar, A., Wijffels, R. H., et al. (2016). Microalgal TAG production strategies: why batch beats repeated-batch. *Biotechnol. Biofuels* 9:64. doi: 10.1186/s13068-016-0475-4

Brock, T. D. (1978). *Thermophilic Microorganisms and Life at High Temperatures*. New York, NY: Springer, 255–302.

Callow, M. E., and Callow, J. E. (2002). Marine biofouling: a sticky problem. *Biologist* 49, 10–14.

Carfagna, S., Bottone, C., Cataletto, P. R., Petriccione, M., Pinto, G., Salbitani, G., et al. (2016). Impact of sulfur starvation in autotrophic and heterotrophic cultures of the extremophilic microalga *Galdieria phlegrea* (Cyanidiophyceae). *Plant Cell Physiol.* 57, 1890–1898. doi: 10.1093/pcp/pcw112

Chen, F., and Johns, M. R. (1996). Heterotrophic growth of *Chlamydomonas reinhardtii* on acetate in chemostat culture. *Process Biochem.* 31, 601–604. doi: 10.1016/S0032-9592(96)00006-4

Costas, E., Flores-Moya, A., Perdigones, N., Maneiro, E., Blanco, J. L., García, M. E., et al. (2007). How eukaryotic algae can adapt to the Spain's Rio Tinto: a neo-Darwinian proposal for rapid adaptation to an extremely hostile ecosystem. *New Phytol.* 175, 334–339. doi: 10.1111/j.1469-8137.2007.02095.x

Cuaresma, M., Casal, C., Forján, E., and Vílchez, C. (2011). Productivity and selective accumulation of carotenoids of the novel extremophile microalga *Chlamydomonas acidophila* grown with different carbon sources in batch systems. *J. Ind. Microbiol. Biotechnol.* 38, 167–177. doi: 10.1007/s10295-010-0841-3

Cuaresma, M., Janssen, M., Vílchez, C., and Wijffels, R. H. (2009). Productivity of *Chlorella sorokiniana* in a short light-path (SLP) panel photobioreactor under high irradiance. *Biotechnol. Bioeng.* 104, 352–359. doi: 10.1002/bit.22394

D'Elia, L., del Mondo, A., Santoro, M., de Natale, A., Pinto, G., and Pollio, A. (2018). Microorganisms from harsh and extreme environments: a collection of living strains at ACUF (Naples, Italy). *Ecol. Quest.* 29, 63–74. doi: 10.12775/EQ.2018.023

Day, J. G., Gong, Y., and Hu, Q. (2017). Microzooplanktonic grazers—a potentially devastating threat to the commercial success of microalgal mass culture. *Algal Res.* 27, 356–365. doi: 10.1016/j.algal.2017.08.024

Dean, A. P., Hartley, A., McIntosh, O. A., Smith, A., Feord, H. K., Holmberg, N. H., et al. (2019). Metabolic adaptation of a *Chlamydomonas acidophila* strain isolated from acid mine drainage ponds with low eukaryotic diversity. *Sci. Total Environ.* 647, 75–87. doi: 10.1016/j.scitotenv.2018.07.445

di Cicco, M. R., Iovinella, M., Palmieri, M., Lubritto, C., and Ciniglia, C. (2021). Extremophilic microalgae *Galdieria* gen. for urban wastewater treatment: current state, the case of "POWER" system, and future prospects. *Plants* 10:2343. doi: 10.3390/plants10112343

Ferraro, G., Imbimbo, P., Marseglia, A., Illiano, A., Fontanarosa, C., Amoresano, A., et al. (2020a). A thermophilic C-phycocyanin with unprecedented biophysical and biochemical properties. *Int. J. Biol. Macromol.* 150, 38–51. doi: 10.1016/j.ijbiomac.2020.02.045

Ferraro, G., Imbimbo, P., Marseglia, A., Lucignano, R., Monti, D. M., and Merlino, A. (2020b). X-ray structure of C-phycocyanin from *Galdieria phlegrea*: determinants of thermostability and comparison with a C-phycocyanin in the entire phycobilisome. *Biochim. Biophys. Acta Bioenerg.* 1861:148236. doi: 10.1016/j.bbabio.2020.148236

Ganuza, E., and Tonkovich, A. L. (2016). "Heliae development, LLC: an industrial approach to mixotrophy in microalgae," in *Industrial Biorenewables*. ed. Pablo Domínguez de María 323–339.

Gao, F., Teles, I., Wijffels, R. H., and Barbosa, M. J. (2020). Process optimization of fucoxanthin production with *Tisochrysis lutea*. *Bioresour. Technol.* 315:123894. doi: 10.1016/j.biortech.2020.123894

Gerloff-Elias, A., Barua, D., Mölich, A., and Spijkerman, E. (2006). Temperature- and pH-dependent accumulation of heat-shock proteins in the acidophilic green alga *Chlamydomonas acidophila*. *FEMS Microbiol. Ecol.* 56, 345–354. doi: 10.1111/j.1574-6941.2006.00078.x

Gerloff-Elias, A., Spijkerman, E., and Pröschold, T. (2005). Effect of external pH on the growth, photosynthesis and photosynthetic electron transport of *Chlamydomonas acidophila* Negoro, isolated from an extremely acidic lake (pH2.6). *Plant Cell Environ.* 28, 1218–1229. doi: 10.1111/j.1365-3040.2005.01357.x

Graziani, G., Schiavo, S., Nicolai, M. A., Buono, S., Fogliano, V., Pinto, G., et al. (2013). Microalgae as human food: chemical and nutritional characteristics

of the thermo-acidophilic microalga *Galdieria sulphuraria*. *Food Funct.* 4, 144–152. doi: 10.1039/C2FO30198A

Guldfeldt, L. U., and Arneborg, N. (1998). Measurement of the effects of acetic acid and extracellular pH on intracellular pH of nonfermenting, individual saccharomyces cerevisiae cells by fluorescence microscopy. *Appl. Environ. Microbiol.* 64, 530–534. doi: 10.1128/AEM.64.2.530-534.1998

Henkanatte-Gedera, S. M., Selvaratnam, T., Karbakhshravari, M., Myint, M., Nirmalakhandan, N., van Voorhies, W., et al. (2017). Removal of dissolved organic carbon and nutrients from urban wastewaters by *Galdieria sulphuraria*: laboratory to field scale demonstration. *Algal Res.* 24, 450–456. doi: 10.1016/j.algal.2016.08.001

Iwamoto, H. (2004). "11 industrial production of microalgal cell-mass and secondary products–major industrial species," in *Handbook of Microalgal Culture: Biotechnology and Applied Phycology*. ed. Amos Richmond 255–263.

Kim, M. J., Li, Y. X., Dewapriya, P., Ryu, B., and Kim, S. K. (2013). Floridoside suppresses pro-inflammatory responses by blocking MAPK signaling in activated microglia. *BMB Rep.* 46, 398–403. doi: 10.5483/BMBRep.2013.46.8.237

Malavasi, V., Soru, S., and Cao, G. (2020). Extremophile microalgae: the potential for biotechnological application. *J. Phycol.* 56, 559–573. doi: 10.1111/jpy.12965

Martinez, F., Avendaño, M. D. C., Marco, E., and Orus, M. I. (1987). Algal population and auxotrophic adaptation in a sugar refinery wastewater environment. *J. Gen. Appl. Microbiol.* 33, 331–341. doi: 10.2323/jgam.33.331

Martinez-Garcia, M., and van der Maarel, M. J. E. C. (2016). Floridoside production by the red microalga *Galdieria sulphuraria* under different conditions of growth and osmotic stress. *AMB Express* 6:71. doi: 10.1186/s13568-016-0244-6

Merino, N., Aronson, H. S., Bojanova, D. P., Feyhl-Buska, J., Wong, M. L., Zhang, S., et al. (2019). Living at the extremes: extremophiles and the limits of life in a planetary context. *Front. Microbiol.* 10:780. doi: 10.3389/fmicb.2019.00780

Minoda, A., Sawada, H., Suzuki, S., Miyashita, S., Inagaki, K., Yamamoto, T., et al. (2015). Recovery of rare earth elements from the sulfothermophilic red alga *Galdieria sulphuraria* using aqueous acid. *Appl. Microbiol. Biotechnol.* 99, 1513–1519. doi: 10.1007/s00253-014-6070-3

Norton, T. A., Melkonian, M., and Andersen, R. A. (1996). Algal biodiversity. *Phycologia* 35, 308–326. doi: 10.2216/i0031-8884-35-4-308.1

Olivieri, G., Marzocchella, A., Andreozzi, R., Pinto, G., and Pollio, A. (2011). Biodiesel production from *Stichococcus* strains at laboratory scale. *J. Chem. Technol. Biotechnol.* 86, 776–783. doi: 10.1002/jctb.2586

Oostlander, P. C., van Houcke, J., Wijffels, R. H., and Barbosa, M. J. (2020). Optimization of *Rhodomonas* sp. under continuous cultivation for industrial applications in aquaculture. *Algal Res.* 47:101889. doi: 10.1016/j.algal.2020.101889

Oren, A. (2014). The ecology of *Dunaliella* in high-salt environments. *J. Biol. Res.* 21:23. doi: 10.1186/s40709-014-0023-y

Oslan, S. N. H., Shoparwe, N. F., Yusoff, A. H., Rahim, A. A., Chang, C. S., Tan, J. S., et al. (2021). A review on *Haematococcus pluvialis* bioprocess optimization of green and red stage culture conditions for the production of natural astaxanthin. *Biomolecules* 11:256. doi: 10.3390/biom11020256

Pollio, A., Cennamo, P., Ciniglia, C., de Stefano, M., Pinto, G., Huss, A. R., et al. (2005). *Chlamydomonas pitschmannii* Ettl, a little known species from thermoacidic environments. *Protist* 156, 287–302. doi: 10.1016/j.protis.2005.04.004

Posten, C. (2009). Design principles of photo-bioreactors for cultivation of microalgae. *Eng. Life Sci.* 9, 165–177. doi: 10.1002/elsc.200900003

Pulz, O., and Gross, W. (2004). Valuable products from biotechnology of microalgae. *Appl. Microbiol. Biotechnol.* 65, 635–648. doi: 10.1007/s00253-004-1647-x

Rahman, D. Y., Sarian, F. D., and van der Maarel, M. J. E. C. (2020). Biomass and phycocyanin content of heterotrophic *Galdieria sulphuraria* 074G under maltodextrin and granular starches–feeding conditions. *J. Appl. Phycol.* 32, 51–57. doi: 10.1007/s10811-019-01957-9

Rahman, D. Y., Sarian, F. D., van Wijk, A., Martinez-Garcia, M., and van der Maarel, M. J. E. C. (2017). Thermostable phycocyanin from the red microalga Cyanidioschyzon merolae, a new natural blue food colorant. *J. Appl. Phycol.* 29, 1233–1239. doi: 10.1007/s10811-016-1007-0

Ryu, B. M., Li, Y. X., Kang, K. H., Kim, S. K., and Kim, D. G. (2015). Floridoside from *Laurencia undulata* promotes osteogenic differentiation in murine bone marrow mesenchymal cells. *J. Funct. Foods* 19, 505–511. doi: 10.1016/j.jff.2015.09.022

Scherhag, P., and Ackermann, J.-U. (2020). Removal of sugars in wastewater from food production through heterotrophic growth of *Galdieria sulphuraria*. *Eng. Life Sci.* 21, 233–241. doi: 10.1002/elsc.202000075

Seckbach, J. (2007). *Algae and Cyanobacteria in Extreme Environments*. Dordrecht: Springer.

Shrestha, R., and Weber, A. (2007). Acidothermophilic red microalga *Galdieria sulphuraria*: from genome to an extracellular glucoamylase active at extreme low pH and high temperature. *J. Phycol.* 43, 23–24.

Sloth, J. K., Wiebe, M. G., and Eriksen, N. T. (2006). Accumulation of phycocyanin in heterotrophic and mixotrophic cultures of the acidophilic red alga *Galdieria sulphuraria*. *Enzym. Microb. Technol.* 38, 168–175. doi: 10.1016/j.enzmictec.2005.05.010

Spijkerman, E. (2007). Phosphorus acquisition by *Chlamydomonas acidophila* under autotrophic and osmo-mixotrophic growth conditions. *J. Exp. Bot.* 58, 4195–4202. doi: 10.1093/jxb/erm276

Sydney, E. B., Schafranski, K., Barretti, B. R., Sydney, A. C. N., Zimmerman, J. F. D., Cerri, M. L., et al. (2019). Biomolecules from extremophile microalgae: from genetics to bioprocessing of a new candidate for large-scale production. *Process Biochem.* 87, 37–44. doi: 10.1016/j.procbio.2019.09.012

Unnithan, V., Unc, A., and Smith, G. B. (2014). Mini-review: a priori considerations for bacteria–algae interactions in algal biofuel systems receiving municipal wastewaters. *Algal Res.* 4, 35–40. doi: 10.1016/j.algal.2013.11.009

Uwizeye, C., Decelle, J., Jouneau, P. H., Flori, S., Gallet, B., Keck, J. B., et al. (2021). Morphological bases of phytoplankton energy management and physiological responses unveiled by 3D subcellular imaging. *Nat. Commun.* 12:1049. doi: 10.1038/s41467-021-21314-0

Van Wagenen, J., Holdt, S. L., de Francisci, D., Valverde-Pérez, B., Plósz, B. G., and Angelidaki, I. (2014). Microplate-based method for high-throughput screening of microalgae growth potential. *Bioresour. Technol.* 169, 566–572. doi: 10.1016/j.biortech.2014.06.096

Wan, M., Wang, Z., Zhang, Z., Wang, J., Li, S., Yu, A., et al. (2016). A novel paradigm for the high-efficient production of phycocyanin from *Galdieria sulphuraria*. *Bioresour. Technol.* 218, 272–278. doi: 10.1016/j.biortech.2016.06.045

Conflict of Interest: The authors declare that the research was conducted in the absence of any commercial or financial relationships that could be construed as a potential conflict of interest.

Publisher's Note: All claims expressed in this article are solely those of the authors and do not necessarily represent those of their affiliated organizations, or those of the publisher, the editors and the reviewers. Any product that may be evaluated in this article, or claim that may be made by its manufacturer, is not guaranteed or endorsed by the publisher.

frontiers in Microbiology

ORIGINAL RESEARCH
published: 28 January 2022
doi: 10.3389/fmicb.2021.756867

DRJAMM Is Involved in the Oxidative Resistance in *Deinococcus radiodurans*

Jianling Cai†, Chaoming Pan†, Ye Zhao, Hong Xu, Bing Tian, Liangyan Wang and Yuejin Hua**

Ministry of Education Key Laboratory of Biosystems Homeostasis and Protection, Institute of Biophysics, College of Life Sciences, Zhejiang University, Hangzhou, China

Proteins containing JAB1/MPN/MOV34 metalloenzyme (JAMM/MPN$^+$) domains that have Zn^{2+}-dependent deubiquitinase (DUB) activity are ubiquitous across among all domains of life. Recently, a homolog in *Deinococcus radiodurans*, DRJAMM, was reported to possess the ability to cleave DRMoaD-MoaE. However, the detailed biochemical characteristics of DRJAMM *in vitro* and its biological mechanism *in vivo* remain unclear. Here, we show that DRJAMM has an efficient *in vitro* catalytic activity in the presence of Mn^{2+}, Ca^{2+}, Mg^{2+}, and Ni^{2+} in addition to the well-reported Zn^{2+}, and strong adaptability at a wide range of temperatures. Disruption of *drJAMM* led to elevated sensitivity in response to H_2O_2 *in vivo* compared to the wild-type R1. In particular, the expression level of MoaE, a product of DRJAMM cleavage, was also increased under H_2O_2 stress, indicating that DRJAMM is needed in the antioxidant process. Moreover, DRJAMM was also demonstrated to be necessary for dimethyl sulfoxide respiratory system in *D. radiodurans*. These data suggest that DRJAMM plays key roles in the process of oxidative resistance in *D. radiodurans* with multiple-choice of metal ions and temperatures.

Keywords: *Deinococcus*, JAMM/MPN$^+$, deubiquitinase, antioxidation, DMSO

OPEN ACCESS

Edited by:
Davide Zannoni, University of Bologna, Italy

Reviewed by:
Min-Kyu Kim, Korea Atomic Energy Research Institute (KAERI), South Korea
Deepti Harinder, Indian Institute of Technology Bombay (IIT Bombay), India

****Correspondence:***
Liangyan Wang
liangyanwang@zju.edu.cn
Yuejin Hua
yjhua@zju.edu.cn

† These authors have contributed equally to this work and share first authorship

Specialty section:
This article was submitted to Extreme Microbiology, a section of the journal Frontiers in Microbiology

Received: *11 August 2021*
Accepted: *23 December 2021*
Published: *28 January 2022*

Citation:
Cai J, Pan C, Zhao Y, Xu H, Tian B, Wang L and Hua Y (2022) DRJAMM Is Involved in the Oxidative Resistance in Deinococcus radiodurans. Front. Microbiol. 12:756867. doi: 10.3389/fmicb.2021.756867

INTRODUCTION

Proteins containing JAMM/MPN$^+$ domain (JAMMs) have been found in prokaryotes, eukaryotes, and archaea. They play important roles in all kinds of cellular processes such as DNA repair (Zeqiraj et al., 2015), pre-mRNA-processing (Galej et al., 2014), and sulfur mobilization to form molybdenum cofactors (Cao et al., 2015). Generally, JAMMs cleave the ubiquitin-like small archaeal modifier proteins (SAMP1/2) or MoaD-MoaE in the presence of Zn^{2+}, for instance, HvJAMM1 (Hepowit et al., 2012), PfHAMM1 (Cao et al., 2017), and CSN5 (Altmann et al., 2017). It is worth noting that the MPN domain super-family has two main subclasses: MPN$^+$ and MPN$^-$. The MPN$^+$ domain-containing proteins are zinc-dependent isopeptidases with the conserved sequence (E-x[2]-H-S/T-H-x[7]-S-x[2]-D) (Cope et al., 2002; McCullough et al., 2004; Moretti et al., 2010). The functional activity of zinc-dependent isopetidases involves zinc bound to the proteins via two histidines and one aspartic acid residues, such as AMSH (Davies et al., 2011) and CSN5 (Echalier et al., 2013), which are JAMM/MPN$^+$ proteins and have the similar organization and composition. The proteins of the MPN$^-$ family lack catalytic activity due to the absence of pivotal residues in the typical JAMM motif and are usually found in pairs in multi-protein complexes with JAMM$^+$

proteins. For example, the eIF3 and COP9 complex has eIF3f and CSN5 representatives of the JAMM/MPN$^+$ family and MPN$^-$ family members, namely eIF3h and CSN6 (Zhou et al., 2008; Sharon et al., 2009).

After decades of research, it has been found that the action of deubiquitinating enzymes or DUBs controls most ubiquitination events dynamically (Amerik and Hochstrasser, 2004). In addition, the deubiquitination process is achieved by hydrolyzing the last residue of the isopeptide bond after Gly76 or the peptide bond of the polyubiquitin chains connected to Met1 (Wilkinson, 1997; Love et al., 2007). According to the structural analysis of the active domain, DUBs can be divided into five subfamilies: the Ub C-terminal hydrolases (UCHLs), the Ub-specific proteases (UBPs), ovarian tumor proteases (OTUs), the Josephin domain proteases (JDs), and JAB1/MPN/MOV34 (JAMMs) (Nijman et al., 2005). For example, in *Haloferax volcanii*, HvJAMM1 can cleave proteins attached to SAMP1 by linear and isopeptide bonds, and the C-terminal diglycine motif of SAMP1 is not required for HvJAMM1 mediated-cleavage of linear protein fusions (Hepowit et al., 2012). In *Pyrococcus furiosus,* the PFJAMM1 can identify SAMP2 with accuracy, regardless of the target protein connected to the C-terminal Gly of the SAMP2 (Cao et al., 2017). In eukaryotes, AMSH is demonstrated to have DUB activity (Kyuuma et al., 2006).

Deinococcus radiodurans is well-known for its powerful capacity to endure extreme stresses such as ionizing radiation (IR), desiccation, and oxidation (Makarova et al., 2001; Daly, 2012). Studies demonstrated that oxidative stress is incurred by reactive oxygen species (ROS) (Goswami et al., 2006). The antioxidant defense mechanism of *D. radiodurans* is active against all three main ROS, including hydroxyl radicals (OH·), superoxide radicals ($O_2{\cdot}^-$), and hydrogen peroxide (H_2O_2). To remove the dangerous ROS and adapt to the oxygen-rich environment of Earth, *D. radiodurans* has evolved a variety of mechanisms to cope with stressful situations. For example, MnSOD (DR1279), a superoxide dismutase (SOD) of *D. radiodurans,* scavenges the superoxide more efficiently than its homologs in humans and *Escherichia coli* due to a more rapid protonation and release of H_2O_2 (Abreu et al., 2008). As reported, *D. radiodurans* contains a high concentration of manganese and keeps high intracellular total manganese to total iron ratio of 0.24 compared to that of radiation-sensitive bacteria (< 0.01 in *E. coli*) (Daly et al., 2004). And *D. radiodurans* contains three eukaryotic-type catalases, which are constitutively expressed in normal conditions (Lipton et al., 2002; Jeong et al., 2016). These findings give us insights into understanding the oxidative damage response mechanisms in *D. radiodurans*, while numerous genes related to oxidative resistance in *D. radiodurans* have not been clearly studied in detail (Yang et al., 2014).

Recently, *dr_0402* has been found to encode the JAMM/MPN protein, and the product of its expression, DRJAMM, could cleave the MoaD-MoaE fusion protein (DR2607) and generate a C-terminal Gly residue (Yang et al., 2018). MoaD-MoaE is known as the MPT synthase that catalyzes the formation of MPT from cyclic pyranopterin monophosphate (cPMP) converted from 5′-GTP, while the two sulfur molecules on cPMP are carried as thiosulfates on the C-terminal glycine of MoaD (Leimkuhler et al., 2001; Zupok et al., 2019). During the formation of MPT, the substrate pocket of MoaE can bound the cPMP, MPT, and the C-terminal of MoaD. It has been shown that the utilitarian action of MoaD-MoaE as an MPT synthase must be cut-activated by JAMMs (Cao et al., 2015; Narrandes et al., 2015). In addition, MoaD and MoaE are essential for molybdenum cofactor (Moco)-dependent dimethyl sulfoxide (DMSO) reductase activity in archaea (Miranda et al., 2011). However, only one pair of DRMoaD-MoaE fusion protein is encoded in *D. radiodurans*, and the detailed catalytic activity of DRJAMM *in vitro* and its biological significance *in vivo* are still unknown.

In the present study, we found that DRJAMM could efficiently cleave DRMoaD-MoaE not only in the presence of Zn^{2+} but also in the presence of other metal ions *in vitro* under either low or high temperatures. Meanwhile, mutation of *drJAMM* led to a decreased survival rate and elevated transcriptional levels of DMSO reductase in response to H_2O_2 *in vivo* compared to the wild-type R1, indicating that DRJAMM plays an important role in the antioxidant process of the organism.

RESULTS

DRJAMM Cleaving Activity Is Dependent on a Variety of Metal Irons

In previous study, MoaD-MoaE has been shown to play an irreplaceable role in the transformation of cyclic pyranopterin monophosphate (cPMP) into molybdopterin (MPT) in *E. coli* (Neumann et al., 2009). To confirm the importance of DRJAMM to MPT synthase, cPMP was oxidized into its stable fluorescence derivatives, compound Z (Wuebbens and Rajagopalan, 1995; Dahl et al., 2013). When the amount of cPMP was set to 100% in *drJAMM* mutant strain, it was not detected in wild-type R1 strain and *drJAMM* complementary strain (**Supplementary Figure 1**), indicating that DRJAMM is essential for the activation of DRMoaD-MoaE.

It has been previously revealed that DRJAMM requires Zn^{2+} to cleave the MoaD-MoaE fusion protein (Yang et al., 2018). However, we found that other metal ions could also catalyze this cleavage activity *in vitro*, such as Mn^{2+}, Mg^{2+}, Ca^{2+}, and Ni^{2+} (**Figure 1A**). The remaining DRMoaD-MoaE fragments were quantified using ImageJ software (National Institutes of Health, United States) to demonstrate the catalytic efficiency of DRJAMM in the presence of different metal ions, as shown in **Figure 1B**. Unexpectedly, DRJAMM displayed the highest catalytic efficiency in the presence of Ca^{2+}, about threefold higher than that of Zn^{2+} (**Figure 1B**). In addition, high temperatures did not inhibit the activity of JAMMs. Since the catalytic function of PfJAMM1 was the best at 100°C in *Pyrococcus furiosus* (Cao et al., 2017), we set a series of temperature gradients and found that the DRJAMM exhibits catalytic activities at different temperatures. Surprisingly, DRMoaD-MoaE is stably degraded by DRJAMM even under high temperatures (**Figure 1C**). These results suggested that the enzyme activity of DRJAMM has strong adaptability to a wide range of temperatures, even above 100°C.

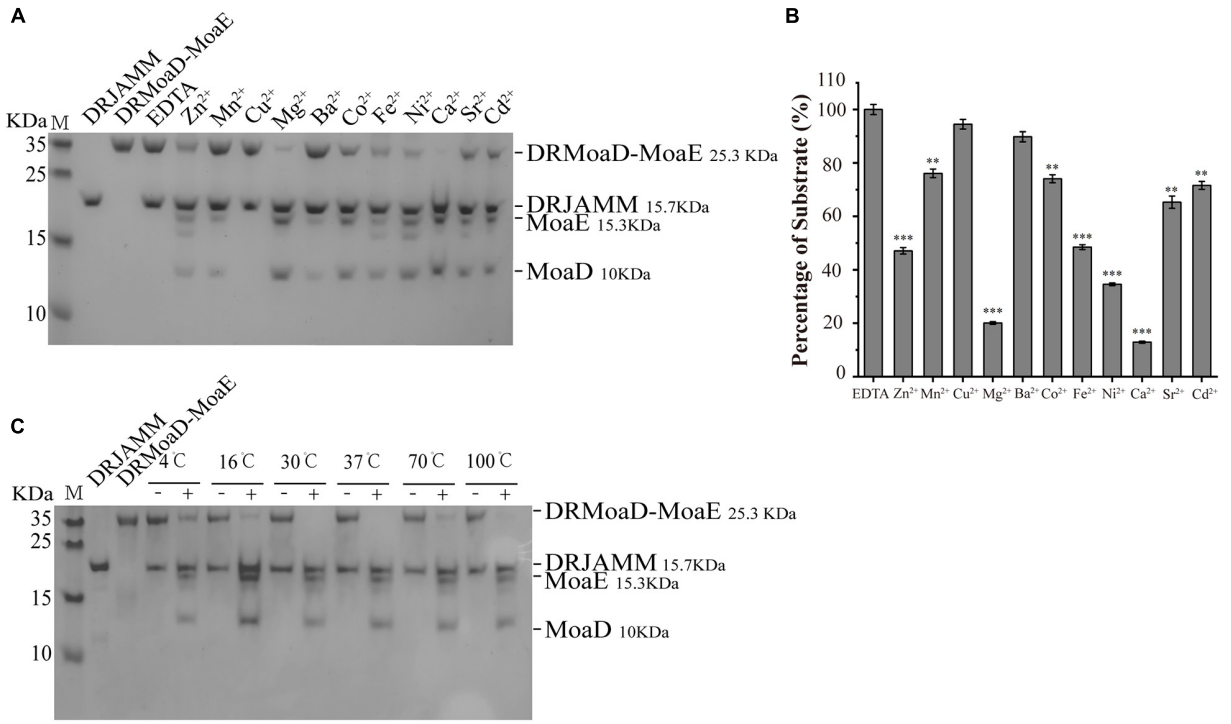

FIGURE 1 | The metal ion preference and temperature adaptability of DRJAMM activity. **(A)** Analysis of ion effects on DRJAMM function. The reaction of 10 μM DRMoaD-MoaE and 40 μM DRJAMM was incubated at 37°C for 30 min with 0.4 mM metal ions. Products were separated with Tricine-SDS-PAGE. **(B)** Values are the means of three independent assays (mean ± SD), $^{**}p < 0.01$, $^{***}p < 0.001$. **(C)** Analysis of temperature effects on DRJAMM function. Reactions were conducted similar to panel A but with the temperature gradient increased from 4 to 100°C. "−" represents EDTA control, " + " represents Ca^{2+} treatment.

drJAMM Is Involved in the Antioxidative Process

To investigate the function of DRJAMM in *D. radiodurans*, a *drJAMM* (Δ*dr_0402*) knockout mutant was constructed and the cell survival rate and cell growth curves were measured (**Figures 2A–C**). It was shown that the mutant Δ*drJAMM* was not sensitive to UV radiation but declined significantly under H_2O_2 (0–80 mM) than the R1 (wild-type). The sensitivity is nearly disappeared after complementation with *drJAMM* (Δ*dr_0402_Cwt*) in the mutant. However, the Δ*drJAMM* growth curve displayed no change during a stationary phase of approximately 30 h (**Figure 2C**), indicating that the *drJAMM* mutation does not influence the growth rate of *D. radiodurans* but affects its response to oxidative stress.

Further analysis of oxidative stress survival with a spot-test method also demonstrated that the mutant is highly sensitive to H_2O_2, and could not endure 80 mM H_2O_2, but could be recovered after gene complementation (**Figure 2D**). Hence, the ROS level was measured to verify the role of *drJAMM* in the antioxidant process of *D. radiodurans*. As shown in **Figure 2E**, the ROS accumulation level in mutant was about 1.3-fold than that of R1 following 40 mM H_2O_2 treatment, while 1.5-fold higher after 80 mM H_2O_2 treatment. Furthermore, the ROS level in the mutant rises with the increase in H_2O_2 concentration, which was found to be restored to wild-type levels in the complementary strain. This suggests that the absence of *drJAMM* will cause the accumulation of ROS. Therefore, *drJAMM* is critical for the antioxidation process in *D. radiodurans*.

Levels of DRJAMM and DRMoaD-MoaE Increase Under Oxidative Stress

To test the cleavage efficiency of DRJAMM (DR0402) to DRMoaD-MoaE (DR2607) during antioxidant processes, a His-tag was fused to the C-terminal of DRJAMM and DRMoaD-MoaE *in situ*. The transcriptional and expressional levels of *drJAMM* and *drMoaD-MoaE* were analyzed using qRT-PCR and western blot assays following H_2O_2 treatment in the wild-type R1 strain. The mRNA levels of *drJAMM* and *drMoaD-MoaE* are increased under H_2O_2 treatment (**Figure 3A**), suggesting that they both may be involved in the oxidative resistance of *D. radiodurans*. Similarly, western blot assays showed that the expression of DRJAMM and DRMoaD-MoaE are both remarkably elevated about 1.5-fold and 3-fold, respectively, following H_2O_2 treatment, while the expression level of DRMoaE is also increased significantly about 1.5-fold (**Figures 3B–E**), indicating that the cleavage activity of DRJAMM might be necessary for oxidative resistance.

DRJAMM Is Required for Dimethyl Sulfoxide Respiration System

DMSO reductase activity is dependent on molybdenum cofactor (Moco) synthesis that requires JAMM/MPN

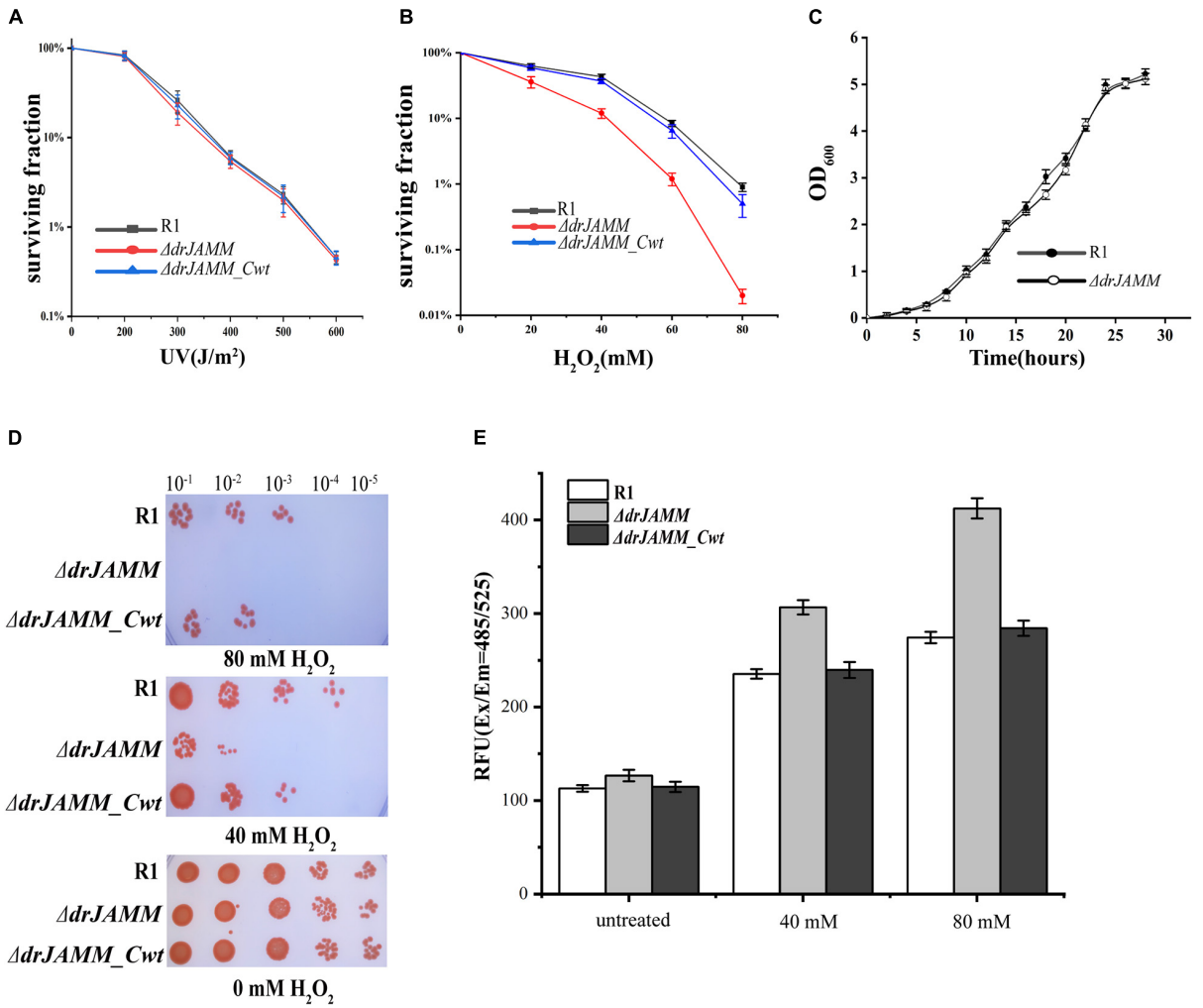

FIGURE 2 | Phenotypes of the *D. radiodurans* wild-type strain (R1), the mutant Δ*drJAMM* (Δ*dr_0402*), and Δ*drJAMM* compensatory stain (Δ*dr_0402_Cwt*). **(A,B)** Survival curves of the strains under H_2O_2 (0–80 mM) and UV (0–600 J/m^2) treatment, respectively. **(C)** Growth curves of *D. radiodurans* wild-type strain and Δ*drJAMM* mutant strain. The data represent the means of the three replicates. **(D)** Following incubation with 0, 40, or 80 mM H_2O_2 for 30 min, the strains were spotted onto TGY plates. The numbers above the figure represent the dilution ratio of cultures. **(E)** The level of ROS accumulation in cells after 0, 40, and 80 mM H_2O_2 treatment, respectively. "Untreated" represents a concentration of 0 mM H_2O_2. RFU means relative fluorescence units.

metalloprotease (Miranda et al., 2011). Sequence alignment suggested that *dr_0397* encode a molybdopterin oxidoreductase that has been shown to play a role in dimethyl sulfoxide respiration in *Rhodobacter capsulatus* (Solomon et al., 2000), and is homologous to *E. coli* DMSO reductase (**Supplementary Figure 2**).

To confirm whether the absence of *drJAMM* will affect the DMSO respiration system in *D. radiodurans*, the transcriptional levels of DMSO reductase were measured using qRT-PCR. Compared with wild-type R1, the mRNA levels of the DMSO reductase are more strongly elevated in Δ*drJAMM* following exposure to H_2O_2, though the levels are also induced in R1 (**Figure 4A**), suggesting deletion of *drJAMM* causes a large demand for DMSO reductase in the antioxidant process. In the absence of DMSO, the growth of all strains was inhibited, while the addition of DMSO restarted growth. However, the growth of Δ*drJAMM* is still in stagnation after adding DMSO (**Figure 4B**), indicating that *drJAMM* is necessary for the DMSO respiration system. In *Haloferax volcanii*, the JAMM/MPN$^+$ metalloprotease HvJAMM1 can activate MPT synthase, and anaerobic growth using DMSO as a terminal electron acceptor can be used as a method to monitor the activation of MPT synthase by HvJAMM1 (Hepowit et al., 2012).

To further investigate the function of DRJAMM in the DMSO respiration system, the wild-type R1, *drJAMM* mutant strain, and *drJAMM* complementary strain were grown to OD_{600} = 1.0 under aerobic conditions, and then incubated with DMSO under anaerobic conditions. The DMSO reductase activity was not detected in the cell lysate of *drJAMM* mutant strain, but could be readily detected in wild-type R1 and *drJAMM* complementary strain (**Figure 4C**), suggesting that DRJAMM is important for the maturation of DMSO reductase protein.

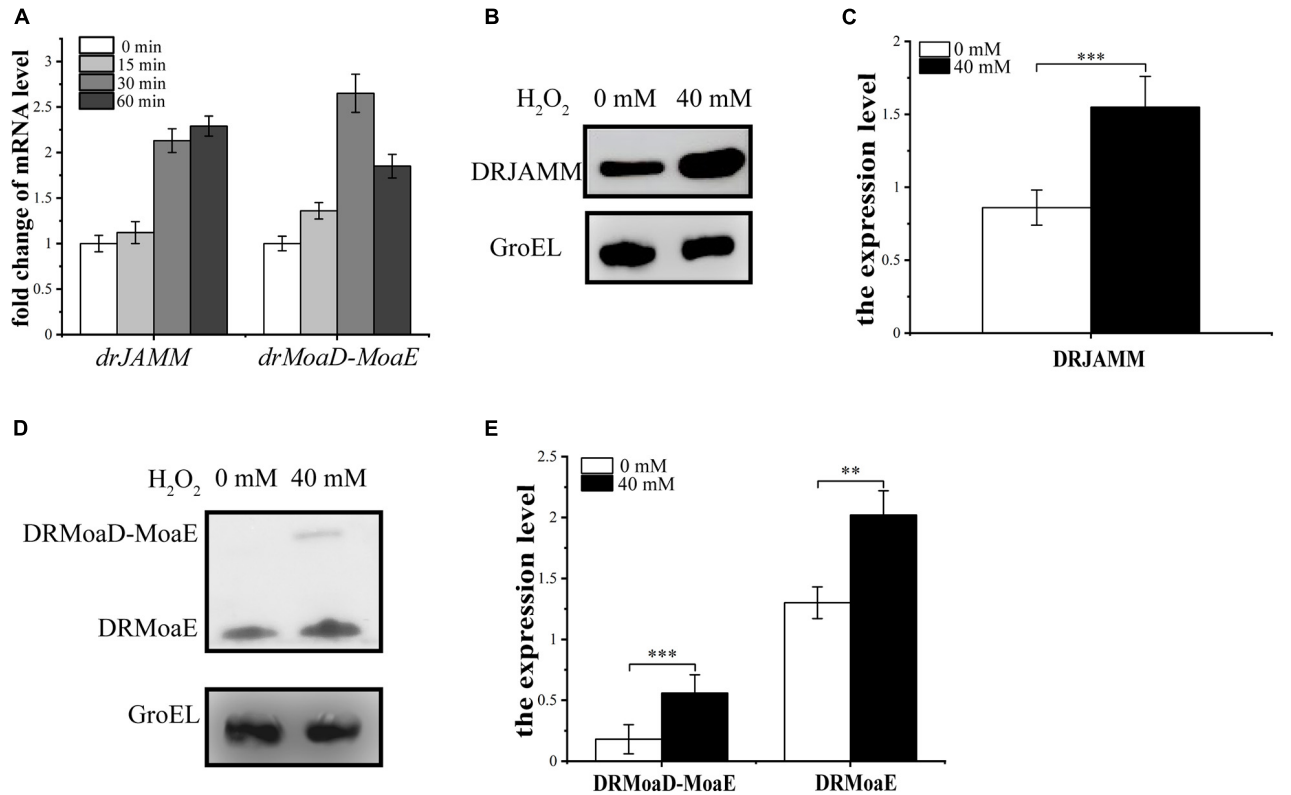

FIGURE 3 | Analysis of transcriptional and expressional levels of *drJAMM* and *drMoaD-MoaE* under oxidative stress. **(A)** The mRNA levels of *drJAMM* and *drMoaD-MoaE* after exposure to 40 mM H_2O_2 for 15, 30, and 60 min. **(B,C)** The expression level of DRJAMM in the presence or absence of H_2O_2. GroEL was used as a control, and an anti-GroEL antibody was used for detection. The relative band strength was scanned and quantified from three independent experiment using ImageJ software. The expression level of each protein was normalized based on the expression level of GroEL, $^{**}p < 0.01$, $^{***}p < 0.001$. **(D,E)** The expression level of DRMoaD-MoaE and DRMoaE in the presence or absence of H_2O_2. GroEL was used as a control, and an anti-GroEL antibody was used for detection. The expression level of each protein was normalized based on the expression level of GroEL. Values were means of three independent assays (mean ± SD), $^{**}p < 0.01$, $^{***}p < 0.001$.

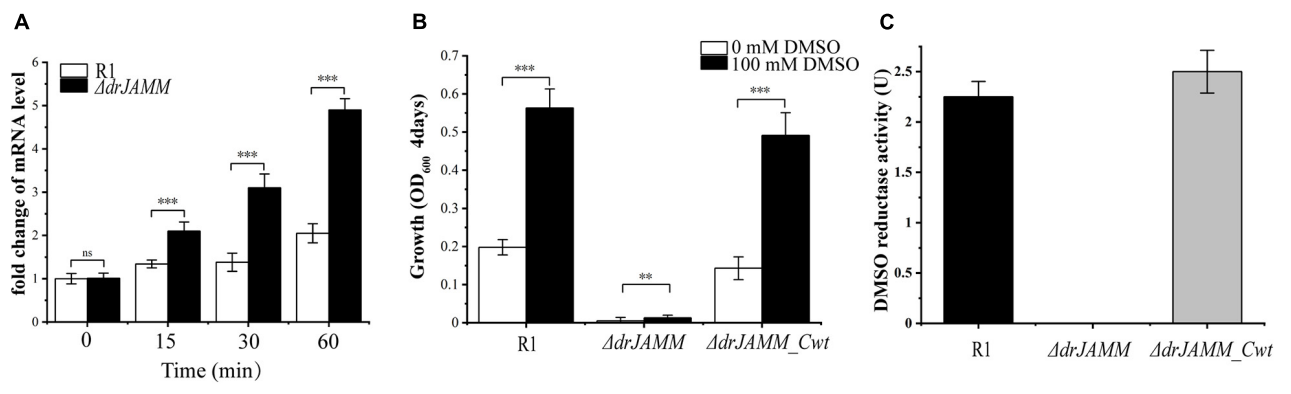

FIGURE 4 | Determination of levels of DMSO reductase under oxidative stress, growth of strains under anaerobic conditions, and the activity of DMSO reductase. **(A)** The mRNA levels of the DMSO reductase at different times following exposure to 40 mM H_2O_2 in R1 and Δ*drJAMM*. Values were means of three independent assays (mean ± SD), *ns*, not significant, $^{***}p < 0.001$. **(B)** Anaerobic growth of R1, Δ*drJAMM* and Δ*drJAMM_Cwt* in medium containing 0 or 100 mM DMSO for 4 days. Values were means of three independent assays (mean ± SD), $^{**}p < 0.01$, $^{***}p < 0.001$. **(C)** The DMSO reductase activity was monitored with nitrogen at A600 nm. The U was defined as 1 μmol substrate consumed per minute at room temperature. Values were means of three independent assays (mean ± SD).

DISCUSSION

A broad spectrum of species encoding JAMM/MPN domain proteins are dependent on Zn^{2+}. For instance, the activity of HvJAMM1 can be activated by the addition of excess $ZnCl_2$ (Hepowit et al., 2012), and the loss of structural zinc leads to a significant reduction in the thermal stability of AMSH (Bueno et al., 2015). However, in the present study, the JAMM/MPN + protein DRJAMM could be activated by different metal ions such as Mn^{2+}, Mg^{2+}, Ca^{2+}, and Ni^{2+} besides Zn^{2+}. Interestingly, more and more multi-metal-dependent nucleic acid enzymes (NAE) have been found to choose sulfophilic metal based on the characteristics of the reaction, or to perform the response through polymetallic collaboration (Zhou and Liu, 2018). Hence, as to how different metal particles control the action of DRJAMM amid the antioxidant handle, and whether there are numerous administrative components like multi-metal-dependent NAE needs further structural explanation.

Usually, proteins will be denatured and lose their function at high temperatures (Bischof and He, 2005). However, DRJAMM displayed stable protease activity even at 100°C. From the perspective of genome evolution, it is proposed that *D. radiodurans* has obtained many genes from *Thermus thermophilus* (Makarova et al., 2001), which may explain the resistance of high temperatures by DRJAMM.

A previous study revealed that HvJAMM1 regulates sumoylation and HvJAMM1-type proteins are thought to release SAMP (Hepowit et al., 2012). Meanwhile, DRJAMM contains a conserved motif similar to HvJAMM1 (Yang et al., 2018), and has the same reaction product MoaE (Hepowit et al., 2012). MoaE usually forms the MPT synthase with MoaD that shares a common globular β-grasp fold with Ub (Narrandes et al., 2015; Yang et al., 2018). For example, TtuB is a bacterial ubiquitin-like protein that has a similar globular β-grasp fold to the Ub of archaea (Shigi, 2012). In addition, DRMoaE is also associated with the function of ubiquitin-like (Ubl) proteins (Humbard et al., 2010). We speculated that Ubl protein modification system may exist in *D. radiodurans* and DRJAMM might play an important role.

Previous studies showed that BRCC36 is a JAMM (JAB1/MPN/Mov34 metalloenzyme) domain DUB enzyme and is involved in the DNA damage response (Patterson-Fortin et al., 2010). Although the survival rate of Δ*drJAMM* is identical to R1 under UV stress (**Supplementary Figure 3**), the growth of this mutant is dramatically inhibited relative to the wild-type R1 under H_2O_2 stress. Simultaneously, the mRNA level of DRJAMM is significantly increased under oxidative stress, implying the importance of this protein in improving oxidation resistance.

According to previous studies, MoaD-MoaE in molybdenum cofactor (Moco) biosynthesis was able to catalyze some redox reactions *in vivo* (Zupok et al., 2019). In the present study, we found the expression levels of DRMoaE and DRJAMM are increased simultaneously under oxidative stress, indicating that DRJAMM is necessary for DRMoaE activation. A recent study revealed that HvJAMM1 plays an important role in releasing MoaE in Moco biosynthesis through deubiquitination (Cao et al., 2015). Therefore, DRJAMM might participate in the antioxidant process by cleaving the DRMoaD-MoaE fusion protein to release MoaE in *D. radiodurans*.

As an essential enzyme in the Moco biosynthesis pathway of bacteria, MoaE is located upstream of MobB, while MobB is responsible for forming molybdenum guanine dinucleotide commonly found in the DMSO reductase family (McLuskey et al., 2003; Miranda et al., 2011). The SAMP1-MoaE is ineffective in DMSO respiration, and this process requires metalloprotease HvJAMM1 (Cao et al., 2015). Under anaerobic conditions, wild-type R1 and complementary strains can remain in abnormal growth, while growth of the *drJAMM* knockout strain is almost completely stopped. After supplement with DMSO, the mutant still showed weak growth, while both wild-type R1 and the complementary strain recovered. Furthermore, the DMSO reductase activity is nearly completely lost in the *drJAMM* mutant strain. These results verified that *drJAMM* is necessary for the DMSO respiratory system in *D. radiodurans*.

In addition, a variety of microorganisms grow through the respiration of DMSO as an electron acceptor, and several DMSO respiratory systems with different compositions have been identified (Miralles-Robledillo et al., 2019). In a previous study, the thioredoxin (Trx) system, which is composed of NADPH, thioredoxin reductase (TrxR), and thioredoxin, provides the electrons to thiol-dependent peroxidases (peroxiredoxins) to remove ROS, and contributes to the resistance toward oxidative stress in *D. radiodurans* (Holmgren, 2000). Here, the levels of DMSO reductase in *D. radiodurans* are gradually increased under oxidative stress, especially in *drJAMM* knockout strains, implying that DMSO respiratory systems might be involved in the oxidation resistance similar to the Trx system, and *drJAMM* could play an important role in this process.

Taken together, DRJAMM is essential for resistance to oxidative stress and the DMSO respiration system in *D. radiodurans* (**Figure 5**). When oxidative damage is encountered, DRMoaD-MoaE is cleaved by DRJAMM to produce DRMoaE, which ultimately affects the DMSO reductase involved in the antioxidant process as demonstrated in *E. coli* (Leimkuhler, 2020). Overall, our findings provide new insights into the role of the JAMM/MPN domain proteins DRJAMM, which can accommodate a multiple-choice of metal ions and temperatures in *D. radiodurans* under oxidative stress.

MATERIALS AND METHODS

Strains and Growth Conditions

All strains, plasmids and primers used in this study are listed in **Supplementary Tables 1, 2**. *E. coli* strains were grown in Luria-Bertani (LB) liquid medium (1% tryptone, 0.5% yeast extract, and 1% sodium chloride) or on agar (1.5% Bacto-agar) plates supplemented at 37°C with appropriate antibiotics. All *D. radiodurans* strains were grown at 30°C in tryptone glucose yeast extract (TGY) liquid media or on agar plates (0.5% tryptone, 0.1% glucose, and 0.3% yeast extract) supplemented with appropriate antibiotics.

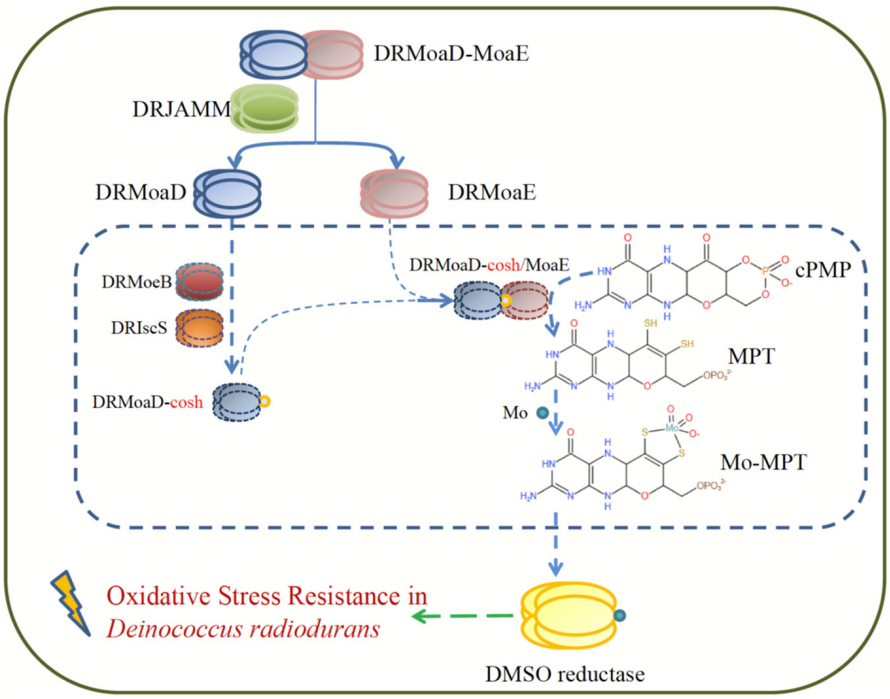

FIGURE 5 | A model of resistance to oxidative stress involving DRJAMM in *D. radiodurans*. Upon oxidative stress, DRMoaD-MoaE is cleaved by DRJAMM to produce DRMoaE and activates the DMSO reductase that participates in the antioxidant process of *D. radiodurans* through the Moco biosynthesis pathway.

Expression and Purification of Proteins

The *dr_0402* and *dr_2607* genes were amplified and cloned into a modified pET28a expression vector at *Nde*I and *Bam*HI site (**Supplementary Table 2**), respectively (Li et al., 2019). Then, the constructed plasmids were transformed into *E. coli* BL21 (DE3), and induced in LB medium containing 50 μg/mL kanamycin and 0.4 mM isopropyl-β-D-thiogalactopyranoside (IPTG) at 30°C for 5 h. Cells were collected and resuspended in lysis buffer (20 mM Tris–HCl, pH 8.0; 500 mM NaCl; 5% (w/v) glycerol; 3 mM β-mercaptoethanol and 9 mM imidazole), followed by sonication. After centrifugation at 20,000 g for 30 min at 4°C, the supernatant was purified using a Ni-NTA column (1 mL, GE Healthcare Biosciences, United States) equilibrated with buffer A (20 mM Tris–HCl, pH 8.0; 500 mM NaCl; 5% (w/v) glycerol and 3 mM β-mercaptoethanol), and washed by buffer B (20 mM Tris–HCl, pH 8.0; 500 mM NaCl; 5% (w/v) glycerol; 3 mM β-mercaptoethanol; 500 mM imidazole). Finally, the proteins were concentrated and purified using a Superdex75 column (GE Healthcare Biosciences, United States), DRJAMM was eluted with buffer C (20 mM Tris–HCl, pH 8.0; 200 mM KCl; and 1 mM EDTA), DRMoaD-MoaE was eluted with buffer D (20 mM Tris-HCl, pH 8.0; and 200 mM KCl).

DRJAMM Activity Assays

The DRJAMM (DR0402) activity assays were performed as described previously with minor modifications (Yang et al., 2018). The 40 μM of DRJAMM and 10 μM of DRMoaD-MoaE were added into the reaction buffer (100 mM KCl; 20 mM Tris-HCl, pH 8.0; and 1 mM dithiothreitol), and then 0.4 mM of different metal ions were added into samples. The reactions with 0.4 mM Ca^{2+} were incubated at 4, 16, 30, 37, 70, and 100°C for 30 min, respectively, and quenched by the addition of SDS loading buffer followed by immediate boiling. The products were identified by Tricine-SDS-PAGE (12%).

Construction of Mutant Strains

The mutant strains were constructed by a tripartite ligation method, as described previously (He et al., 2020). Briefly, the DNA fragment upstream of *dr_0402* was amplified by PCR using the primers Δ*dr_0402*-p1 and Δ*dr_0402*-p2, which was digested with *Bam*HI (**Supplementary Table 2**). The DNA fragment downstream of *dr_0402* was amplified by PCR using the primers Δ*dr_0402*-p3 and Δ*dr_0402*-p4, which were digested with *Hin*dIII (downstream) (**Supplementary Table 2**). The digested fragment was connected to a streptomycin resistance gene. After the triplet ligation product was transformed into the *D. radiodurans* wild-type R1 strain, the mutant colonies were then selected on TGY plates containing 10 μg/ml streptomycin, and confirmed by genomic PCR using primers Δ*dr_0402*-p5 and Δ*dr_0402*-p6, and DNA sequencing. For complementary strain construction, the wild type *dr_0402* was amplified by PCR using Δ*dr_0402_Cwt*-F and Δ*dr_0402_Cwt*-R, and cloned into the plasmid pRADK containing the *D. radiodurans* groEL promoter; and then transformed into the Δ*dr_0402* mutant strain to obtain the complementary strain Δ*dr_0402_Cwt*.

Western Blot Analysis

Western blotting was used to confirm protein expression levels were performed as described previously (Dai et al., 2018). The

6 × His-tag was fused to the C-terminus of DRJAMM and DRMoaD-MoaE using tripartite ligation and a double-crossover recombination method. Mouse anti-6 × His tag (Proteintech, United States) was used to detect DRJAMM, DRMoaD-MoaE, and MoaE in the strains. The pre-stained marker was used as reference (Thermo Fisher, United States). The expression level of GroEL was detected using a rabbit anti-GroEL polyclonal antibody (Sigma, United States) in *D. radiodurans*, which was used as the internal control.

Real-Time Quantitative PCR

Real-time quantitative PCR (qRT-PCR) was used to measure *dr_0402* and *dr_2607* gene expression under oxidative stress, as described previously (Dai et al., 2020). First, *D. radiodurans* cells were grown to OD_{600} = 1.0 and treated with 40 mM H_2O_2 for 30 min. Then, the cells were collected by centrifugation at 5,000 g for 3 min at 4°C. Total RNA was extracted from 5 mL cell cultures using TRIZOL reagent (Invitrogen, Carlsbad, CA, United States). The qRT-PCR experiments were performed using SYBR Premix Ex Taq (TaKaRa Biotechnology, Japan). The primers used in this experiment are listed in **Supplementary Table 2**. The data were collected and the difference in relative transcription abundance level was calculated. Glyceraldehyde 3-phosphate dehydrogenase (GADPH) encoded by the gene *dr_1343* was used as the internal control.

Survival Curves, Growth Curves, and Phenotypic Analyses

To measure the survival curves and observe phenotypes under H_2O_2 treatment, the wild-type *D. radiodurans* R1 and Δ*dr_0402* were grown to OD_{600} = 1.0, and then treated with different concentrations of H_2O_2 for 30 min. After the reaction, the residual H_2O_2 was cleared away by adding excess catalase, and then the sample was plated on TGY plates. All the experiments were repeated three times. To measure the growth curve, the wild-type *D. radiodurans* R1 and Δ*dr_0402* were cultured to OD_{600} = 1.0 at 30°C and then 500 μl was transferred into 100 ml of fresh TGY medium without antibiotics. OD_{600} values were measured every 1 or 2 h.

Antioxidation Activity Measurements

2′,7′-dichlorofluorescein diacetate (DCFH-DA) was used as a molecular probe hydrolysis to generate DCFH, ROS can oxidize DCFH to generate DCF with fluorescence, which can be measured using a fluorescence spectrometer (SpectraMax M5, United States) with an excitation wavelength of 485 nm and emission wavelength of 525 nm. *D. radiodurans* R1 and the mutant strains were grown to OD_{600} = 1.0 and washed three times with PBS buffer. Pellets were incubated with DCFH-DA at 37°C for 30 min. After incubation, cells were washed three times with PBS buffer and resuspended in 2 mL PBS buffer, and then 1 ml sample was treated with 0, 40, and 80 mM H_2O_2 for 30 min, respectively. The accumulation of ROS was measured the manufacturer's protocol (Beyotime Biotechnology, China).

Dimethyl Sulfoxide Analyses

DMSO analyses were performed as described previously (Cao et al., 2015). In brief, the strains were grown aerobically to OD_{600} = 1.0. For anaerobic growth, the strains were transferred to TGY medium containing 100 mM DMSO as a terminal electron acceptor at 30°C for 4 days.

Dimethyl Sulfoxide Reductase Activity Assay

DMSO reductase activity assay was performed as described previously (Miranda et al., 2011). A total of 250 mL of TGY cultures of each strain were grown to OD_{600} = 1.0, harvested by centrifugation, washed in 15 mL buffer A (50 mM Tris-HCl, pH 7.5; 1 mM EDTA, pH 8.0; 2 M NaCl), resuspended in 20 mL buffer A, and lysed by ultrahigh pressure homogenizer (Shanghailitu, China), successively. Cell lysates were clarified by centrifugation (15,000 rpm, 30 min), and protein concentrations were measured using the Bradford assay kit (Beyotime Biotechnology, China). The DMSO reductase activity was monitored at A_{600nm} (15 s intervals for 3.5 min). Assays (4 mL) included cell lysate (1–1.5 mg protein), 0.3 mM methyl viologen in buffer A, and the top filled with nitrogen. The mixture was titrated to 1–1.2 A_{600nm} units with fresh 20 mM odium dithionite ($Na_2S_2O_4$) in 20 mM sodium bicarbonate ($NaHCO_3$) prior to the addition of 10 mM DMSO. One unit (U) of enzyme activity was defined as 1-μm substrate consumed per minute at room temperature, with an extinction coefficient A_{600nm} of 13.6 ($mM^{-1}{\cdot}cm^{-1}$) for methyl viologen.

DATA AVAILABILITY STATEMENT

The original contributions presented in the study are included in the article/**Supplementary Material**, further inquiries can be directed to the corresponding author/s.

AUTHOR CONTRIBUTIONS

YH conceived the project. JC, CP, LW, and YH designed the experiments and drafted the manuscript. JC constructed the vectors and mutants and purified the proteins. CP was responsible for qRT-PCR, enzyme activity, and phenotype analysis. JC, BT, HX, and YZ participated in the data analysis. All authors reviewed the manuscript and approved the version to be published.

FUNDING

This work was supported by the National Key Research and Development Program of China (2017YFA0503900), the grants from National Natural Science Foundation of China (31870051, 31670065), and the Project for Experimental Technology of Zhejiang University (SJS202012).

SUPPLEMENTARY MATERIAL

The Supplementary Material for this article can be found online at: https://www.frontiersin.org/articles/10.3389/fmicb.2021.756867/full#supplementary-material

REFERENCES

Abreu, I. A., Hearn, A., An, H., Nick, H. S., Silverman, D. N., and Cabelli, D. E. (2008). The kinetic mechanism of manganese-containing superoxide dismutase from *Deinococcus radiodurans*: a specialized enzyme for the elimination of high superoxide concentrations. *Biochemistry* 47, 2350–2356. doi: 10.1021/bi7016206

Altmann, E., Erbel, P., Renatus, M., Schaefer, M., Schlierf, A., Druet, A., et al. (2017). Azaindoles as zinc-binding small-molecule inhibitors of the JAMM protease CSN5. *Angew. Chem. Int. Ed. Engl.* 56, 1294–1297. doi: 10.1002/anie.201608672

Amerik, A. Y., and Hochstrasser, M. (2004). Mechanism and function of deubiquitinating enzymes. *Biochim. Biophys. Acta* 1695, 189–207. doi: 10.1016/j.bbamcr.2004.10.003

Bischof, J. C., and He, X. M. (2005). Thermal stability of proteins. *Cell Injury Mech. Resp. Rep.* 1066, 12–33. doi: 10.1196/annals.1363.003

Bueno, A. N., Shrestha, R. K., Ronau, J. A., Babar, A., Sheedlo, M. J., Fuchs, J. E., et al. (2015). Dynamics of an Active-Site Flap contributes to catalysis in a JAMM Family Metallo Deubiquitinase. *Biochemistry* 54, 6038–6051. doi: 10.1021/acs.biochem.5b00631

Cao, S., Engilberge, S., Girard, E., Gabel, F., Franzetti, B., and Maupin-Furlow, J. A. (2017). Structural insight into Ubiquitin-Like protein recognition and oligomeric states of JAMM/MPN(+) proteases. *Structure* 25, 823–833 e826. doi: 10.1016/j.str.2017.04.002

Cao, S., Hepowit, N., and Maupin-Furlow, J. A. (2015). Ubiquitin-like protein SAMP1 and JAMM/MPN+ metalloprotease HvJAMM1 constitute a system for reversible regulation of metabolic enzyme activity in Archaea. *PLoS One* 10:e0128399. doi: 10.1371/journal.pone.0128399

Cope, G. A., Suh, G. S., Aravind, L., Schwarz, S. E., Zipursky, S. L., Koonin, E. V., et al. (2002). Role of predicted metalloprotease motif of Jab1/Csn5 in cleavage of Nedd8 from Cul1. *Science* 298, 608–611. doi: 10.1126/science.1075901

Dahl, J. U., Radon, C., Buhning, M., Nimtz, M., Leichert, L. I., Denis, Y., et al. (2013). The sulfur carrier protein TusA has a pleiotropic role in *Escherichia coli* that also affects molybdenum cofactor biosynthesis. *J. Biol. Chem.* 288, 5426–5442. doi: 10.1074/jbc.M112.431569

Dai, J., Gao, K., Yao, T., Lu, H., Zhou, C., Guo, M., et al. (2020). Late embryogenesis abundant group3 protein (DrLEA3) is involved in antioxidation in the extremophilic bacterium *Deinococcus radiodurans*. *Microbiol. Res.* 240:126559. doi: 10.1016/j.micres.2020.126559

Dai, S., Jin, Y., Li, T., Weng, Y., Xu, X., Zhang, G., et al. (2018). DR1440 is a potential iron efflux protein involved in maintenance of iron homeostasis and resistance of *Deinococcus radiodurans* to oxidative stress. *PLoS One* 13:e0202287. doi: 10.1371/journal.pone.0202287

Daly, M. J. (2012). Death by protein damage in irradiated cells. *DNA Repair* 11, 12–21. doi: 10.1016/j.dnarep.2011.10.024

Daly, M. J., Gaidamakova, E. K., Matrosova, V. Y., Vasilenko, A., Zhai, M., Venkateswaran, A., et al. (2004). Accumulation of Mn(II) in, *Deinococcus radiodurans* facilitates gamma-radiation resistance. *Science* 306, 1025–1028. doi: 10.1126/science.1103185

Davies, C. W., Paul, L. N., Kim, M. I., and Das, C. (2011). Structural and thermodynamic comparison of the catalytic domain of AMSH and AMSH-LP: nearly identical fold but different stability. *J. Mol. Biol.* 413, 416–429. doi: 10.1016/j.jmb.2011.08.029

Echalier, A., Pan, Y. B., Birol, M., Tavernier, N., Pintard, L., Hoh, F., et al. (2013). Insights into the regulation of the human COP9 signalosome catalytic subunit, CSN5/Jab1. *Proc. Natl. Acad. Sci. U.S.A.* 110, 1273–1278. doi: 10.1073/pnas.1209345110

Galej, W. P., Nguyen, T. H. D., Newman, A. J., and Nagai, K. (2014). Structural studies of the spliceosome: zooming into the heart of the machine. *Curr. Opin. Struct. Biol.* 25, 57–66. doi: 10.1016/j.sbi.2013.12.002

Goswami, M., Mangoli, S. H., and Jawali, N. (2006). Involvement of reactive oxygen species in the action of ciprofloxacin against *Escherichia coli*. *Antimicrob. Agents Chemother.* 50, 949–954. doi: 10.1128/AAC.50.3.949-954.2006

He, Y., Wang, Y., Qin, C., Xu, Y., Cheng, K., Xu, H., et al. (2020). Structural and functional characterization of a unique AP endonuclease from *Deinococcus radiodurans*. *Front. Microbiol.* 11:1178. doi: 10.3389/fmicb.2020.01178

Hepowit, N. L., Uthandi, S., Miranda, H. V., Toniutti, M., Prunetti, L., Olivarez, O., et al. (2012). Archaeal JAB1/MPN/MOV34 metalloenzyme (HvJAMM1) cleaves ubiquitin-like small archaeal modifier proteins (SAMPs) from protein-conjugates. *Mol. Microbiol.* 86, 971–987. doi: 10.1111/mmi.12038

Holmgren, A. (2000). Antioxidant function of thioredoxin and glutaredoxin systems. *Antioxid. Redox Signal.* 2, 811–820. doi: 10.1089/ars.2000.2.4-811

Humbard, M. A., Miranda, H. V., Lim, J. M., Krause, D. J., Pritz, J. R., Zhou, G., et al. (2010). Ubiquitin-like small archaeal modifier proteins (SAMPs) in *Haloferax volcanii*. *Nature* 463, 54–60. doi: 10.1038/nature08659

Jeong, S. W., Jung, J. H., Kim, M. K., Seo, H. S., Lim, H. M., and Lim, S. (2016). The three catalases in *Deinococcus radiodurans*: only two show catalase activity. *Biochem. Biophys. Res. Commun.* 469, 443–448. doi: 10.1016/j.bbrc.2015.12.017

Kyuuma, M., Kikuchi, K., Kojima, K., Sugawara, Y., Sato, M., Mano, N., et al. (2006). AMSH, an ESCRT-III associated enzyme, deubiquitinates cargo on MVB/late endosomes. *Cell Struct. Funct.* 31, 159–172. doi: 10.1247/csf.06023

Leimkuhler, S. (2020). The biosynthesis of the molybdenum cofactors in *Escherichia coli*. *Environ. Microbiol.* 22, 2007–2026. doi: 10.1111/1462-2920.15003

Leimkuhler, S., Wuebbens, M. M., and Rajagopalan, K. V. (2001). Characterization of *Escherichia coli* MoeB and its involvement in the activation of molybdopterin synthase for the biosynthesis of the molybdenum cofactor. *J. Biol. Chem.* 276, 34695–34701. doi: 10.1074/jbc.M102787200

Li, S., Cai, J., Lu, H., Mao, S., Dai, S., Hu, J., et al. (2019). N (4)-cytosine DNA methylation is involved in the maintenance of genomic stability in *Deinococcus radiodurans*. *Front. Microbiol.* 10:1905. doi: 10.3389/fmicb.2019.01905

Lipton, M. S., Pasa-Tolic, L., Anderson, G. A., Anderson, D. J., Auberry, D. L., Battista, K. R., et al. (2002). Global analysis of the *Deinococcus radiodurans* proteome by using accurate mass tags. *Proc. Natl. Acad. Sci. U.S.A.* 99, 11049–11054. doi: 10.1073/pnas.172170199

Love, K. R., Catic, A., Schlieker, C., and Ploegh, H. L. (2007). Mechanisms, biology and inhibitors of deubiquitinating enzymes. *Nat. Chem. Biol.* 3, 697–705. doi: 10.1038/nchembio.2007.43

Makarova, K. S., Aravind, L., Wolf, Y. I., Tatusov, R. L., Minton, K. W., Koonin, E. V., et al. (2001). Genome of the extremely radiation-resistant bacterium *Deinococcus radiodurans* viewed from the perspective of comparative genomics. *Microbiol. Mol. Biol. Rev.* 65, 44–79. doi: 10.1128/MMBR.65.1.44-79.2001

McCullough, J., Clague, M. J., and Urbe, S. (2004). AMSH is an endosome-associated ubiquitin isopeptidase. *J. Cell Biol.* 166, 487–492. doi: 10.1083/jcb.200401141

McLuskey, K., Harrison, J. A., Schuttelkopf, A. W., Boxer, D. H., and Hunter, W. N. (2003). Insight into the role of *Escherichia coli* MobB in molybdenum cofactor biosynthesis based on the high resolution crystal structure. *J. Biol. Chem.* 278, 23706–23713. doi: 10.1074/jbc.M301485200

Miralles-Robledillo, J. M., Torregrosa-Crespo, J., Martinez-Espinosa, R. M., and Pire, C. (2019). DMSO Reductase family: phylogenetics and applications of extremophiles. *Int. J. Mol. Sci.* 20:3349. doi: 10.3390/ijms20133349

Miranda, H. V., Nembhard, N., Su, D., Hepowit, N., Krause, D. J., Pritz, J. R., et al. (2011). E1-and ubiquitin-like proteins provide a direct link between protein conjugation and sulfur transfer in Archaea. *Proc. Natl. Acad. Sci. U.S.A.* 108, 4417–4422. doi: 10.1073/pnas.1018151108

Moretti, J., Chastagner, P., Gastaldello, S., Heuss, S. F., Dirac, A. M., Bernards, R., et al. (2010). The translation initiation factor 3f (eIF3f) exhibits a deubiquitinase activity regulating notch activation. *PLoS Biol.* 8:e1000545. doi: 10.1371/journal.pbio.1000545

Narrandes, N. C., Machowski, E. E., Mizrahi, V., and Kana, B. D. (2015). Cleavage of the moaX-encoded fused molybdopterin synthase from *Mycobacterium tuberculosis* is necessary for activity. *BMC Microbiol.* 15:22. doi: 10.1186/s12866-015-0355-2

Neumann, M., Mittelstadt, G., Seduk, F., Iobbi-Nivol, C., and Leimkuhler, S. (2009). MocA is a specific cytidylyltransferase involved in molybdopterin cytosine dinucleotide biosynthesis in *Escherichia coli*. *J. Biol. Chem.* 284, 21891–21898. doi: 10.1074/jbc.M109.008565

Nijman, S. M. B., Luna-Vargas, M. P. A., Velds, A., Brummelkamp, T. R., Dirac, A. M. G., Sixma, T. K., et al. (2005). A genomic and functional inventory of deubiquitinating enzymes. *Cell* 123, 773–786. doi: 10.1016/j.cell.2005.11.007

Patterson-Fortin, J., Shao, G., Bretscher, H., Messick, T. E., and Greenberg, R. A. (2010). Differential regulation of JAMM domain deubiquitinating enzyme activity within the RAP80 complex. *J. Biol. Chem.* 285, 30971–30981. doi: 10.1074/jbc.M110.135319

Sharon, M., Mao, H., Boeri Erba, E., Stephens, E., Zheng, N., and Robinson, C. V. (2009). Symmetrical modularity of the COP9 signalosome complex suggests its multifunctionality. *Structure* 17, 31–40. doi: 10.1016/j.str.2008.10.012

Shigi, N. (2012). Posttranslational modification of cellular proteins by a ubiquitin-like protein in bacteria. *J. Biol. Chem.* 287, 17568–17577. doi: 10.1074/jbc.M112.359844

Solomon, P. S., Shaw, A. L., Young, M. D., Leimkuhler, S., Hanson, G. R., Klipp, W., et al. (2000). Molybdate-dependent expression of dimethylsulfoxide reductase in *Rhodobacter capsulatus*. *FEMS Microbiol. Lett.* 190, 203–208. doi: 10.1111/j.1574-6968.2000.tb09287.x

Wilkinson, K. D. (1997). Regulation of ubiquitin-dependent processes by deubiquitinating enzymes. *FASEB J.* 11, 1245–1256.

Wuebbens, M. M., and Rajagopalan, K. V. (1995). Investigation of the early steps of molybdopterin biosynthesis in *Escherichia*-Coli through the use of *in-vivo* labeling studies. *J. Biol. Chem.* 270, 1082–1087. doi: 10.1074/jbc.270.3.1082

Yang, P., Chen, Z., Shan, Z., Ding, X., Liu, L., and Guo, J. (2014). Effects of FMN riboswitch on antioxidant activity in *Deinococcus radiodurans* under H(2)O(2) stress. *Microbiol. Res.* 169, 411–416. doi: 10.1016/j.micres.2013.09.005

Yang, Y. M., Won, Y. B., Ji, C. J., Kim, J. H., Ryu, S. H., Ok, Y. H., et al. (2018). Cleavage of molybdopterin synthase MoaD-MoaE linear fusion by JAMM/MPN(+) domain containing metalloprotease DR0402 from *Deinococcus radiodurans*. *Biochem. Biophys. Res. Commun.* 502, 48–54. doi: 10.1016/j.bbrc.2018.05.117

Zeqiraj, E., Tian, L., Piggott, C. A., Pillon, M. C., Duffy, N. M., Ceccarelli, D. F., et al. (2015). Higher-order assembly of BRCC36-KIAA0157 is required for DUB activity and biological function. *Mol. Cell* 59, 970–983. doi: 10.1016/j.molcel.2015.07.028

Zhou, M., Sandercock, A. M., Fraser, C. S., Ridlova, G., Stephens, E., Schenauer, M. R., et al. (2008). Mass spectrometry reveals modularity and a complete subunit interaction map of the eukaryotic translation factor eIF3. *Proc. Natl. Acad. Sci. U.S.A.* 105, 18139–18144. doi: 10.1073/pnas.0801313105

Zhou, W. H., and Liu, J. W. (2018). Multi-metal-dependent nucleic acid enzymes. *Metallomics* 10, 30–48. doi: 10.1039/c7mt00268h

Zupok, A., Iobbi-Nivol, C., Mejean, V., and Leimkuhler, S. (2019). The regulation of Moco biosynthesis and molybdoenzyme gene expression by molybdenum and iron in bacteria. *Metallomics* 11, 1602–1624. doi: 10.1039/c9mt00186g.a

Conflict of Interest: The authors declare that the research was conducted in the absence of any commercial or financial relationships that could be construed as a potential conflict of interest.

Publisher's Note: All claims expressed in this article are solely those of the authors and do not necessarily represent those of their affiliated organizations, or those of the publisher, the editors and the reviewers. Any product that may be evaluated in this article, or claim that may be made by its manufacturer, is not guaranteed or endorsed by the publisher.

frontiers in Microbiology

ORIGINAL RESEARCH
published: 07 February 2022
doi: 10.3389/fmicb.2021.794743

Influence of Physical-Chemical Soil Parameters on Microbiota Composition and Diversity in a Deep Hyperarid Core of the Atacama Desert

Bárbara Fuentes[1], Alessandra Choque[1,2], Francisco Gómez[1], Jaime Alarcón[3], Eduardo Castro-Nallar[3], Franko Arenas[2], Daniel Contreras[2], Ramona Mörchen[4], Wulf Amelung[4], Claudia Knief[5], Ghazal Moradi[6], Erwin Klumpp[6], Claudia P. Saavedra[7], Jörg Prietzel[8], Wantana Klysubun[9], Francisco Remonsellez[1,10] and Roland Bol[6,11]**

[1] Departamento de Ingeniería Química, Universidad Católica del Norte, Antofagasta, Chile, [2] Programa de Doctorado en Ciencias Mención Geología, Universidad Católica del Norte, Antofagasta, Chile, [3] Center for Bioinformatics and Integrative Biology, Universidad Andres Bello, Santiago, Chile, [4] Institute of Crop Science and Resource Conservation, Soil Science and Soil Ecology, University of Bonn, Bonn, Germany, [5] Institute of Crop Science and Resource Conservation, Molecular Biology of the Rhizosphere, University of Bonn, Bonn, Germany, [6] Institute of Bio and Geosciences, Agrosphere (IBG-3), Forschungszentrum Jülich GmbH, Jülich, Germany, [7] Laboratorio de Microbiología Molecular, Departamento de Ciencias Biológicas, Facultad de Ciencias de la Vida, Universidad Andrés Bello, Santiago, Chile, [8] Wissenschaftszentum Weihenstephan, Technical University München, Freising, Germany, [9] Synchrotron Light Research Institute, Nakhon Ratchasima, Thailand, [10] Centro de Investigación Tecnológica del Agua en el Desierto-CEITSAZA, Universidad Católica del Norte, Antofagasta, Chile, [11] School of Natural Sciences, Environment Centre Wales, Bangor University, Bangor, United Kingdom

OPEN ACCESS

Edited by:
Mark Alexander Lever, ETH Zürich, Switzerland

Reviewed by:
Alfonso F. Davila, National Aeronautics and Space Administration (NASA), United States
Charles K. Lee, University of Waikato, New Zealand

***Correspondence:**
Francisco Remonsellez
fremonse@ucn.cl
Roland Bol
r.bol@fz-juelich.de

Specialty section:
This article was submitted to Extreme Microbiology, a section of the journal Frontiers in Microbiology

Received: *14 October 2021*
Accepted: *24 December 2021*
Published: *07 February 2022*

Citation:
Fuentes B, Choque A, Gómez F, Alarcón J, Castro-Nallar E, Arenas F, Contreras D, Mörchen R, Amelung W, Knief C, Moradi G, Klumpp E, Saavedra CP, Prietzel J, Klysubun W, Remonsellez F and Bol R (2022) Influence of Physical-Chemical Soil Parameters on Microbiota Composition and Diversity in a Deep Hyperarid Core of the Atacama Desert. Front. Microbiol. 12:794743. doi: 10.3389/fmicb.2021.794743

The extreme environmental conditions and lack of water on the soil surface in hyperarid deserts hamper microbial life, allowing only highly specialized microbial communities to the establish colonies and survive. Until now, the microbial communities that inhabit or have inhabited soils of hyperarid environments at greater depths have been poorly studied. We analyzed for the first time the variation in microbial communities down to a depth of 3.4 m in one of the driest places of the world, the hyperarid Yungay region in the Atacama Desert, and we related it to changes in soil physico-chemical characteristics. We found that the moisture content changed from 2 to 11% with depth and enabled the differentiation of three depth intervals: (i) surface zone A (0–60 cm), (ii) intermediate zone B (60–220 cm), and (iii) deep zone C (220–340 cm). Each zone showed further specific physicochemical and mineralogical features. Likewise, some bacterial phyla were unique in each zone, i.e., members of the taxa *Deinococcota*, *Halobacterota*, and *Latescibacterota* in zone A; *Crenarchaeota*, *Fusobacteriota*, and *Deltaproteobacterium* Sva0485 in zone B; and *Fervidibacteria* and *Campilobacterota* in zone C, which indicates taxon-specific preferences in deep soil habitats. Differences in the microbiota between the zones were rather abrupt, which is concomitant with abrupt changes in the physical-chemical parameters. Overall, moisture content, total carbon (TC), pH, and electric conductivity (EC) were most predictive of microbial richness and diversity, while total sulfur (TS) and total phosphorous (TP) contents were additionally

predictive of community composition. We also found statistically significant associations between taxa and soil properties, most of which involved moisture and TC contents. Our findings show that under-explored habitats for microbial survival and existence may prevail at greater soil depths near water or within water-bearing layers, a valuable substantiation also for the ongoing search for biosignatures on other planets, such as Mars.

Keywords: deep soil, physicochemical properties, microbiota, hyperarid soil, Atacama Desert

INTRODUCTION

The hyperarid region of the Atacama Desert is in the south of this desert as part of the Aguas Blancas (AB) basin. This region is surrounded by mountain ranges that limit its extension to the Coastal Cordillera to the west and the Cordillera de Domeyko to the east (Bonilla, 1972). The mean annual precipitation is less than 1 mm yr^{-1} (Houston and Hartley, 2003; Houston, 2006), with precipitation (Pp) to potential evapotranspiration (PET) ratios of Pp/PET < 0.05 (UNEP, 1997). While the crest line of the coastal range blocks any incoming marine fog by approximately 100 km, this promotes a "fog shadow" in the area where some "Mars-like soils" mostly dominate (Navarro-González et al., 2003; Gómez-Silva et al., 2008). At present, this hyperarid core of the desert is also devoid of plant growth. However, several studies have shown that the Atacama Desert had humid periods in the past that varied from the current arid or hyperarid conditions (Sáez et al., 2016; Pfeiffer et al., 2018; Ritter et al., 2018).

Despite the hyperarid conditions of the soils, the existence of past and recent signals of life has been shown. A study by Wang et al. (2021) identified fingerprints of past biological activity in the Atacama Desert using phosphate oxygen (^{18}O) isotopes. Others works have reported the existence of unexpectedly large microbial populations in the hyperarid soils, especially in very particular and extreme habitats, such as the underside of quartz rocks (Warren-Rhodes et al., 2006), inside of halite evaporates (Wierzchos et al., 2006), fumaroles at the Andes Mountains, and in caves of the Coastal range (Azua-Bustos et al., 2012; Bull and Asenjo, 2013). Liquid water availability and solar radiation are the main life-controlling factors in the Atacama Desert (Bull and Asenjo, 2013). Despite the significantly challenging environmental conditions, microorganisms and organic matter have also been detected in the surface and subsurface layers of the hyperarid soils of the Atacama Desert (Mörchen et al., 2019; Warren-Rhodes et al., 2019; Knief et al., 2020). In particular, the surface soils of the Yungay area have been widely studied regarding their microbial diversity. It has been shown that microbial life can even be detected under low water availability (Connon et al., 2007; Azua-Bustos et al., 2012, 2015, 2018, 2020; Fletcher et al., 2012; Crits-Christoph et al., 2013; Neilson et al., 2017; Warren-Rhodes et al., 2019; Schulze-Makuch et al., 2021). Furthermore, DNA-based sequence analyses revealed that bacterial communities in this hyperarid core display varied but relatively low levels of diversity and that water availability and salt contents are key factors shaping the hyperarid Atacama soil microbiome (Crits-Christoph et al., 2013; Warren-Rhodes et al., 2019; Knief et al., 2020). While Neilson et al. (2017) found that community richness and diversity were positively correlated with soil humidity, other studies highlighted that sudden 'large' inputs of water into regions that had remained hyperarid for millions of years can be harmful to surface soil microbial species, especially those specifically adapted to extremely low water availability (Azua-Bustos et al., 2018). Although biosignatures and microbial life have been poorly studied in the depth of this hyperarid environment, the first evidence for metabolically active microbial communities and patterns specifically adapted to this harsh climate exists (Schulze-Makuch et al., 2018). In this matter, Warren-Rhodes et al. (2019) analyzed the spatial distribution of microbial communities between 0 and 80 cm; surprisingly, they found significant subsurface microbial communities that existed related to residual sediment moisture. This study also highlighted the influence of soluble salts and mineralogy on water availability and likely microbial life in the deeper parts of the soil. More recently, Azua-Bustos et al. (2020) found a diverse microbial community and biosignatures in humid smectite-rich subsurface layers in the hyperarid core of the Atacama Desert (at 30-40 cm depth), and Schulze-Makuch et al. (2021) showed that hypolithically colonized rocks are microbial hotspots in this desert environment.

Considering the varying minerals detected in various soil layers of the hyperarid core, such as halite, calcite, smectite, montmorillonite, dolomite, and others (Ewing et al., 2006; Fuentes et al., 2014; Azua-Bustos et al., 2020), it can be expected that the overall physicochemical properties and the microbial communities would also differ along these various layers within a soil profile. Nevertheless, microbial life in the subsurface soil of hyperarid Yungay and its relationship to physicochemical variations in soil properties have been poorly studied thus far. Therefore, we aimed to dig deeper into hyperarid soil, unraveling the deeper soil microbiota and relating it to variations in soil properties.

MATERIALS AND METHODS

Study Site in the Hyperarid Core of the Atacama Desert

The study site is in the Yungay area of the Aguas Blancas (AB) basin (between 24°01′ and 24°16′ S; elevation range of 1,000–1,300 m.a.s.l.). It is situated southeast of Antofagasta within the hyperarid core of the Atacama Desert. The positional

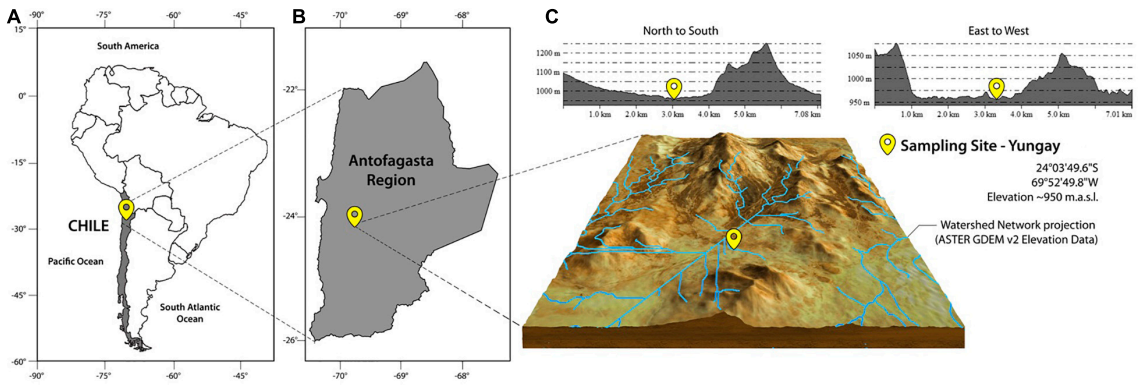

FIGURE 1 | Location of the study site in Yungay, in the hyperarid core, Atacama Desert. **(A)** Chile, **(B)** Antofagasta Region, **(C)** Yungay in the hyperarid core.

coordinates are 24°03′49.6″S, 69°52′49.8″W (**Figure 1**). Note that the surrounding area has also been studied by Pfeiffer et al. (2018) and Azua-Bustos et al. (2020). Some of our findings are in accordance with Pfeiffer et al. (2018), e.g., anhydrite polygons at the surface and needle fiber calcite in the soil profile. A soil scarp generated previously by a trench excavator was used in this study. Within the escarpment, we dug into the surface to freshly expose the upper part (2.2 m) of profile. Subsequently, we then continue digging below the surface till a depth of 1.2 m. Thus obtaining an overall profile of 3.4 m (**Figure 2**).

Physical-Chemical and Mineralogical Characterization of the Soil Profile

Soil samples were taken in March 2017. The soil profile was sampled at 10 cm depth intervals until a final depth of 340 cm. Before the sampling procedure, the surface area was cleaned and cut back into its exposure. We took soil samples immediately after excavating a specific depth layer to avoid effects of the exposure of the soil to ambient air and temperature. Soil samples were manually taken and stored in plastic bags. Additionally, soil samples for microbiological analyses were collected in sterile tubes by using plastic gloves and shovels properly cleaned with ethanol to avoid contamination. All samples were taken to the laboratory in Antofagasta and Germany to conducted physicochemical, mineralogical, and microbiological analyses. The moisture content (MC) of the soil samples was measured immediately in the laboratory in Antofagasta by drying soil at 105°C in an oven and calculating the loss of weight after drying. Electric conductivity (EC) and pH were measured in a soil-distilled water suspension with a solution ratio of 1:2.5. The total contents of C, N, S, and TOC were determined by elemental analysis employing approx. 20 mg of sample material (Vario Micro Cube, Elementar, Hanau, Germany; ISO 10694, 1995). For the determination of TOC contents, inorganic carbon was removed with 20% HCl for 2 h. Total P, reactive P that corresponds to inorganic P, and unreactive P (URP) (which includes organic P and polyphosphates in soils) were determined by the extraction method proposed by Saunders and Williams (1955). The P concentration was measured by the method of Murphy and Riley (1962). P in the soil samples was also analyzed to determine the contribution of different P forms to total P by K-edge XANES spectroscopy at beamline 8 of the Synchrotron Light Research Institute (SLRI) in Nakhon Ratchasima, Thailand (Klysubun et al., 2019). XANES spectra acquisitions and the evaluation of the standard compounds were performed according to Werner and Prietzel (2015). The reference compounds were published by Prietzel et al. (2016). Sequential P fractionation was conducted according to Hedley et al. (1982) with modifications. Briefly, 0.3 g of soil samples was shaken in 30 ml of extractant solution. The order of extractants used was deionized water, 0.5 M $NaHCO_3$ (pH 8.5), 0.1 M NaOH, and 1 M HCl. P not extracted by these solutions was classified as residual P. The amount of inorganic P (Pi) in each extract was determined by Murphy and Riley (1962). Selected soil samples of the soil profile were subjected to X-ray diffraction (XRD) to analyze its mineral compounds. XRD analysis was conducted with a Siemens Model D5000 diffractometer (Cu Kα 1).

Statistical Analysis of Soil Physicochemical Data

Based on the MC distribution along the soil profile, it was possible to distinguish and propose three distinct zones in the soil profile: surface zone A (0–60 cm), intermediate zone B (60–220 cm), and deep zone C (220–340 cm). For each zone, a linear regression was calculated for moisture content depending on depth. All data obtained were tested for normality of distribution by using a Shapiro–Wilk test ($n < 50$ for each defined zone). As the distribution was not normal, a non-parametric Friedman test for related samples was used to determine significant variations ($p < 0.05$) in the distribution of MC, TC, TOC, TN, TS and TP between the proposal zonification. All statistical analyses were performed with IBM SPSS Statistical software version 21.

DNA Extraction, Sequencing and Taxonomic Analysis

Twenty grams of soil was suspended in 40 ml nuclease-free water in sterile Falcon tubes as described previously (Finstad et al., 2017) and then filtered through a 0.22 μm

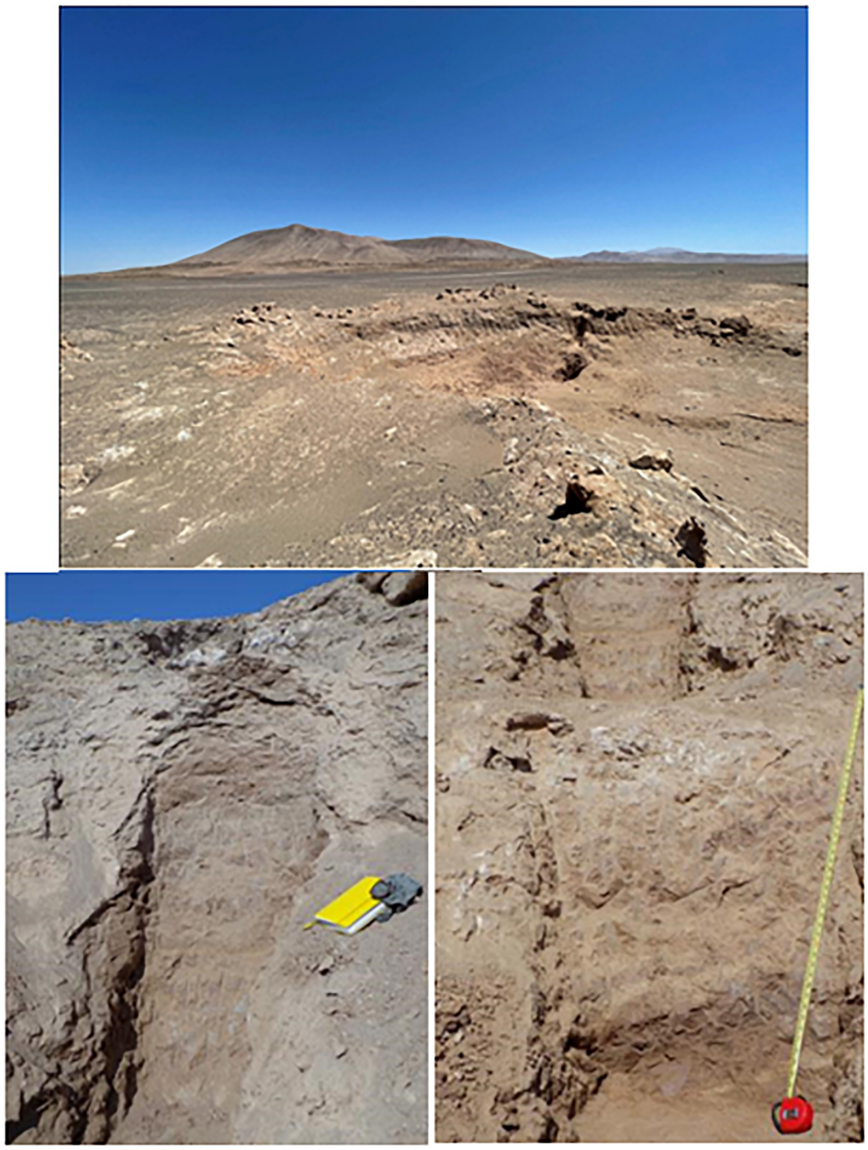

FIGURE 2 | Images of soil sampling site in Yungay hyperarid core, Atacama Desert.

sterilized filter (Millipore). DNA was extracted from the material on filter paper using the QIAGEN DNeasy PowerSoil Kit according to the manufacturer's instructions. The quantity of DNA extracted was measured using a Qubit fluorimeter with high sensitivity reagent kit. The 16S rRNA gene was amplified using primers 515F and 806R, targeting the V4 region of the 16S rRNA gene with approx. 235 bp amplicon length (Caporaso et al., 2012). Sequencing was performed on an Illumina MiSeq platform in a 150 bp paired-end cycle run. Sequencing was performed at the Environmental Sample Preparation and Sequencing Facility, Argonne National Laboratory. Samples were demultiplexed using the split_libraries_fastq.py module from QIIME 1.9 [16S: –barcode_type 12; ITS1: –rev_comp_barcode] (Caporaso et al., 2010), and amplicon sequence variants (ASVs) were inferred with DADA2 v1.10.1 (Callahan et al., 2016) using [truncLen = c(140,135), maxN = 0, maxEE = c(2,2), truncQ = 2, rm.phix = TRUE]. Error rate learning, dereplication, and merging were performed using default settings. After building an ASV table and removing chimeras, taxonomic assignment was obtained by analyzing reads against the Silva v138 database (Quast et al., 2013) using DADA2 Ribosomal Database Project's (RDP) naive Bayesian classifier (Wang et al., 2007). ASVs identified as Eukarya, Chloroplast, Mitochondria and *Escherichia/Shigella*, *Staphylococcus*, *Corynebacterium*, *Lactobacillus* and *Streptococcus* were removed (Eisenhofer et al., 2019). Moreover, the R package decontam was used to identify and remove contaminants using the "frequency" and "prevalence" methods (Davis et al., 2018). Finally, samples

with fewer than 1000 reads were discarded to avoid relying on taxonomic classification with low support. Water blanks and mock communities (Zymo microbiomics standard) were included to assess contamination and accuracy. ASV sequences were aligned with DECIPHER v3.8 (Wright, 2016).

Statistical Analysis of Amplicon Data

All statistical analyses were conducted in R v3.5.2 and RStudio v1.1.463 (RStudio Team, 2016) using ampvis2 v2.4.5 (Andersen et al., 2018), microbiomeSeq v0.1,[1] phyloseq v1.26.1 (McMurdie and Holmes, 2013), stats v3.5.2 (R Core Team, 2018), effects v4.1-4 (Fox, 2003) and bipartite v2.14 (Dormann et al., 2008). Plots were generated using ggplot2 v3.1.1 (Wickham, 2016) and basic R functions. The alpha diversity indices Chao1, Shannon and Fisher were calculated using phyloseq and subjected to normality tests (Shapiro–Wilk). Generalized linear models (GLMs) were built to test the effects of soil variables on alpha diversity indices. This was done using the "glm" function for the stats package, with the argument family = "Gaussian" and a p value threshold of <0.05 for significant predictors. All models were plotted using the R package effects, and residuals were analyzed for normality and homoscedasticity. Ampvis2 was used to perform a redundancy analysis (RDA) on Hellinger-transformed ASV abundances constrained by the soil zone. The argument envfit_numeric was added to display numerical soil variables as vectors. The MicrobiomeSeq package was used to evaluate the relationship between the taxa agglomerated to their best taxonomy and numerical soil variables based on Pearson's correlation, adjusting for multiple testing using the Benjamini-Hochberg correction (0.05 p value threshold) and for taxa + groups. Finally, for a two-dimensional matrix between taxa and sample origin (Zone), a bipartite network analysis was performed to visualize the distribution of phyla among soil zones based on their relative abundances using the plot web function from the bipartite R package (Dormann et al., 2008) with the default method cca, which leads to as few crossings of interactions as possible.

RESULTS

Characterization of the Soil Profile

According to the World Reference Base for Soil Resources, the soil profile can be classified as a Gypsisol. The profile and the complete description are given in **Supplementary Figure 1**. At the surface of the profile, fine sediments with desiccation cracks were recognized to develop over a massive chloride and sulfate salt layer with a thickness of 0.5 m. The sediments were finer below 2 m depth, and the soil particles had higher moisture contents than in the upper layers. The soil MC increased along with the soil profile (**Figure 3**). Considering that liquid water availability is one of the main life-controlling factors in the Atacama Desert (Bull and Asenjo, 2013), we propose three major zones in the profile based on linear regression analysis of the MC indicating changes with depth (**Figure 3**). These three proposed zones were surface zone A (0–60 cm, n: 6) with a slope of 0.066% moisture cm^{-1} R2: 0.71; intermediate zone B (60–220 cm, n: 16) with a slope of 0.073% moisture cm^{-1} R2: 0.80; and deep zone C (220–340 cm, n: 12) with a slope of 0.143% moisture cm^{-1} R2: 0.77. Moreover, soil MC increased significantly ($p < 0.05$, Friedman test) in the three proposal zones. In surface zone A, the MC increased from 0.66 to 5%. Additionally, we identified an evaporation layer between 0 and 20 cm within zone A, reflected by the lowest moisture content values registered in the soil profile (0.66%). In intermediate zone B, the moisture content increased to 15% at the 220 cm soil depth. In deep zone C, the moisture content reached a maximum of 21% at 330 cm soil depth. A local minimum of 3% moisture content between 220 and 240 cm depth was noted.

Within the three zones, we found different minerals (**Supplementary Table 1**). In surface zone A, the predominant minerals were halite, bassanite, anhydrite, albite, and calcite albite. Intermediate zone B was dominated by anorthite, calcite, albite, montmorillonite, and orthoclase. Deep zone C was composed of a wet clay-rich soil layer with high amounts of muscovite (approximately 20%) and lower abundances of chlorite (approximately 4%) (**Supplementary Table 1**). The values of pH along the soil profile were alkaline. However, it was also possible to detect significant differences in the three-zone intervals ($p < 0.05$, Friedman test). The average pH values were 8.3 in surface zone A, 9.0 in intermediate zone B, and 8.9 in deep zone C (**Figure 3**). High EC values were detected in zone A, and then a constant decrease was observed along with the soil profile. Significant differences in EC were found in the three-zone intervals ($p < 0.05$, Friedman test). The average EC value in surface zone A was 107 mS cm^{-1}, 22.1 mS cm^{-1} in intermediate zone B and 14.3 mS cm^{-1} in deep zone C (**Figure 3**).

Distribution of C, N, P, and S in the Soil Profile

The contents of TC in surface zone A varied between 190 and 1125 μg C g^{-1}, while in intermediate zone B, the values ranged from 135 to 280 μg C g^{-1}. In deep zone C, the values ranged from 140 to 540 μg C g^{-1}, reaching the maximum value in this zone at an interval of 310–330 cm (**Figure 4**). There were significant differences between the means of TC in the three proposal zones ($p < 0.05$, Friedman test). Concerning the TOC, the values were low along the soil profile (**Figure 4**). In zone A, TOC ranged between 160 and 310 μg TOC g^{-1} with a high value at 10 cm depth. In zone B, the TOC values were relatively constant, at approximately 140–170 μg TOC g^{-1}. Instead, we detected elevated TOC concentrations in deep zone C at 240 and 300 cm depths (190 μg TOC g^{-1}). However, there were no significant differences between the means of TOC in the three proposal zones ($p > 0.05$, Friedman test). On the other hand, the TN concentrations generally decreased with increasing soil depth (**Figure 4**). Thus, TN concentrations were highest in surface zone A (with a maximum value of 1, 594 μg N g^{-1} at 50 cm depth), while in zones B and C, TN decreased from 628 to 39 μg N g^{-1} and 628 to 134 μg N g^{-1}, respectively. There were no significant differences between TN means in the three-zone

[1]https://github.com/umerijaz/microbiomeSeq

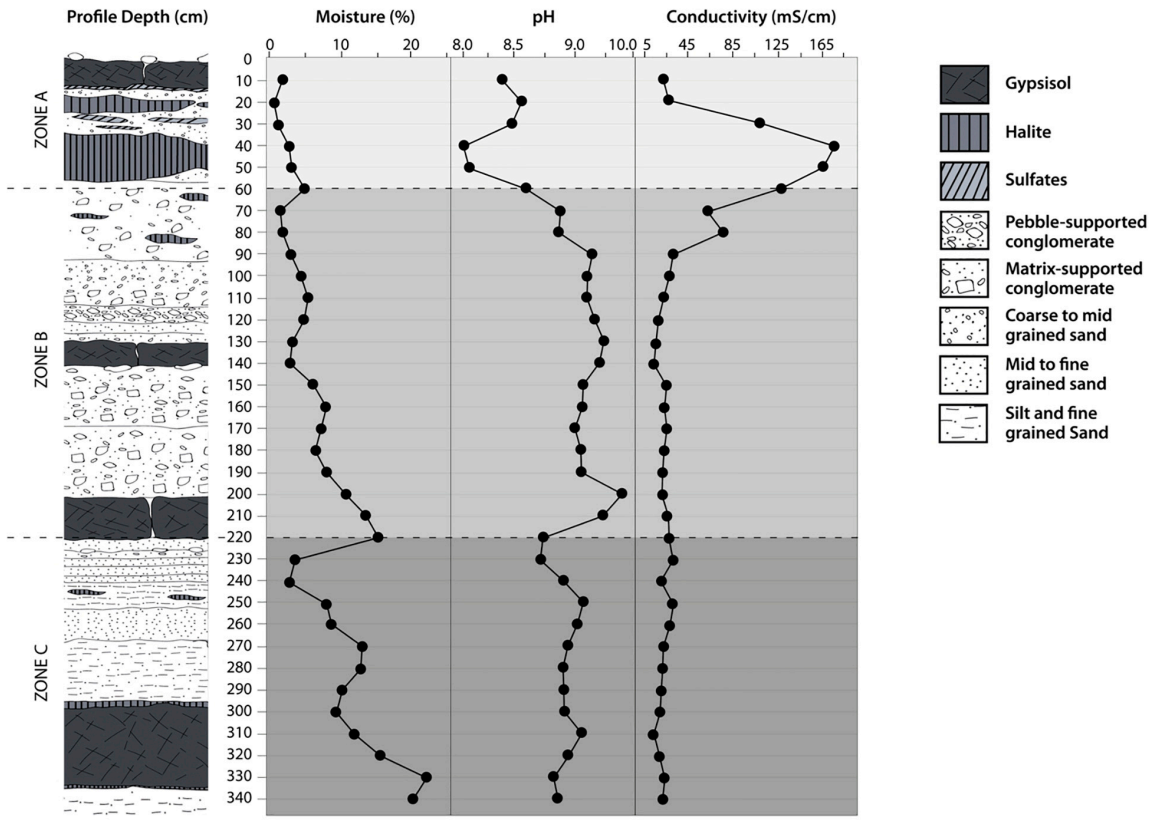

FIGURE 3 | Distribution of the soil profile parameters at the Yungay site in the Atacama Desert. Moisture content (%), pH value and electric conductivity (EC).

intervals ($p > 0.05$, Friedman test). Similarly, high TS contents were measured in the first 50 cm of soil depth (surface zone A), ranging from 23.9 to 35.3 mg S g^{-1} soil (**Figure 4**). These values rapidly declined in zones B and C. In intermediate zone B, TS decreased from 4595 to 234 μg Sg^{-1}. In deep zone C, TS tended to decrease except for a spike between 230 and 250 cm depth (deep zone C). There were significant differences between TS means in the three-zone intervals ($p < 0.05$, Friedman test).

In contrast to TC, TN, and TS, TP increased in the soil profile. TP showed minimal values in surface zone A (122–216 μg Pg^{-1} at 30–50 cm depth) (**Figure 4**). Overall, TP concentrations increased into intermediate zone B (from 509 to 840 μg Pg^{-1}). In deep zone C, PT decreased at 230-240 cm depth to increase to 783 μg Pg^{-1} at 340 cm depth. There were significant differences between TP means in the three-zone intervals ($p < 0.05$, Friedman test).

Reactive P (or inorganic P) dominated the soil profile (**Figure 4**), representing over 88% of TP in all samples. The difference between TP and reactive P is explained by the presence of unreactive P (URP) compounds, including condensed phosphates and organic P. Considering the generally low TOC contents, low amounts of organic P could be expected. However, it was possible to detect three small peaks of the URP: 42.7, 87.7 and 87.7 μg URP kg^{-1} at 140, 210, and 320 cm soil depths along with the soil profile. The latter two signals coincided with increasing TOC concentrations in depth. The easily extractable P (the sum of Pi-H_2O and Pi-$NaHCO_3$) only accounted for 1.0–5.6% of the total P (**Supplementary Table 2**). The highest P was present in the Pi-HCl fraction (> 94%), highlighting that a high P was bound to calcium. Additionally, XANES P speciation confirmed that most P (90-100% of total P) was present as apatite-P (**Supplementary Table 3**). Some P (< 10% of total P) was Ca-bound organic P; higher concentrations of Pi-H_2O were observed in intermediate zone B and deep zone C (8.1–20.6 μg Pg^{-1}) than in surface zone A (1.9–2.2 μg Pg^{-1}). A similar trend was observed for the Pi-NaOH fraction, with high values found in zones B and C (0.8–3.7 μg Pg^{-1}) compared with surface zone A (0.3–1.1 μg Pg^{-1}).

Microbial Community Analysis

The Yungay depth profile showed low DNA concentrations in the range of 1.15–11.8 ng g^{-1} soil. Amplicon sequencing revealed that the phyla *Proteobacteria*, *Actinobacteria*, *Bacteroidota* and *Firmicutes* had the highest prevalence in the soil profile (**Figure 5** and **Supplementary Figure 2**). While *Proteobacteria* and *Bacteroidota* were abundant in all three zones, microbial composition at the family level (**Figure 5**) and a bipartite network analysis (**Supplementary Figure 3**) showed that several families and phyla were predominantly detected within one of the three zones, suggesting that communities are structured throughout the soil profile. Soil surface microbial communities

were dominated by *Actinobacteria*, *Proteobacteria* and *Firmicutes* (10–20 cm). In general, *Firmicutes* exhibited a slightly greater detection frequency in surface zone A than in zone C, while it was not detected in zone B. Within *Firmicutes*, the occurrence of the families *Lachnospiraceae* and *Bacillaceae* was limited to zone A, while *Oscillospiraceae* and *Salisediminibacter* incerta sedis occurred only in zone C (wetter conditions). Similarly, the actinobacterial families had different niches, with *Sporichthyaceae* being only detected in layers of zones B and C, while *Illumatobacteraceae* were only present in different layers within zone A. *Verrucomicrobiota* and *Planctomycetota* were exclusively present in deep zone C (**Figure 5** and **Supplementary Figure 3**). Moreover, the deepest part of the profile was dominated by *Proteobacteria*, especially by the families *Comamonadaceae* (330–340 cm) and *Marinobacteraceae* (320–330 cm). The family *Sphingomonadaceae* of *Proteobacteria* showed a high abundance in several layers of zone B but a lower abundance in zone C (**Figure 5**). Some further lower-abundant phyla that were unique for a specific zone were *Deinococcota*, *Halobacterota*, and *Latescibacterota* in surface zone A; *Crenarchaeota*, *Fusobacteriota*, and Sva0485 (deltaproteobacteria) in intermediate zone B; and *Campilobacterota* and *Fervidibacteria* in deep zone C (**Supplementary Figure 3**). Remarkably, *Cyanobacteria* of the class *Oxyphotobacteria* were detected with low prevalence in various samples across the soil profile (**Supplementary Figure 2**).

We also tested to what extent the properties of the soil explained the microbial community structure. We found that microbial communities were to some extent structured by depth, as samples from either zone A, B, or C were more similar within each zone than between zones (**Figure 6**; polygons). Higher levels of TC, TS, and EC were preferentially associated with microbial communities from zone A, while higher moisture contents, depth, and total and inorganic P were associated with microbial communities from zone C (**Figure 6**). Finally, we explored associations between the relative abundance of microbial community members and soil variables as a soil zone function (**Figure 7**). We found statistically significant positive correlations between taxa and soil properties, most of which involved moisture and TC contents (**Figure 7**). Some taxa were weakly negatively associated with pH value or positively associated with EC as well as TN and TS and PT contents. We also correlated alpha diversity measures to soil properties and observed that the moisture content, TC, pH, and EC correlated positively with microbial richness and diversity (**Supplementary Figure 4** and **Supplementary Table 4**; positive slope; Chao1), while TS and TP contents correlated negatively with diversity (**Supplementary Figure 4**; negative slope).

DISCUSSION

Properties of the Soil Profile and Zonification Proposal

Climatic factors (mainly low precipitation and high temperature) limit biological productivity and activity, chemical reactions, and weathering (Plaza et al., 2018). Consequently, in hyperarid soils, a relatively poor carbon content, low microbial activity, and low soil weathering would be expected (Ewing et al., 2006; Mörchen et al., 2019; Knief et al., 2020). However, in this study, we show that it is possible to find an abundance of MC in deep hyperarid soils, affecting soil and microbial parameters. Then, we proposed three zones (surface zone A, intermediate zone B and deep zone C) considering the significant difference in the MC ($p < 0.05$ Friedman test). These zones also showed significant variations in pH, EC, TC, TS and TP ($p < 0.05$ Friedman test). Instead, at least two zones were similar in terms of TOC and TN ($P > 0.05$ Friedman test). The increase in MC in the depth soil was observed in the soil profile (**Figure 3**). Recently, wet layers below the surface of the hyperarid core of the Atacama have been reported (Azua-Bustos et al., 2020). Although the origin of water is outside the scope of this study, plausible water deep sources could be related to the unusual rain events that took place during March 2015, as have been indicated by Azua-Bustos et al. (2020). Precipitation events could lead to a reload of deep groundwater system present in the Aguas Blancas basin (Dirección General de Aguas, 2017). It has a low recharge rate, limited to very sporadic rare wet events (Herrera and Custodio, 2014). Whether, larger rainfall events have a longer lasting impact on the moisture content in the deepest part of soils or sediments in the region is still unresolved.

The entire soil profile showed alkaline pH values and high EC, which is frequent in other soils of the Atacama Desert (Connon et al., 2007; Fuentes et al., 2014; Knief et al., 2020). However, slightly lower pH values were observed in surface zone A, while the highest EC was detected in this zone. As expected in these environments, the soil is rich in salt minerals, which result in elevated EC in the entire profile (>5 mS cm^{-1}); however, in surface zone A, the soil is exceptionally saline, reaching values over 100 mS cm^{-1}. The highest EC value of 185 mS cm^{-1} was recorded at 40 cm depth and was related to salt minerals such as halite, albite, calcite, anorthite, and darapskite (**Supplementary Table 1**). Decreasing precipitation and increasing evapotranspiration reduce the loss of salts by leaching, leading to the accumulation of calcium carbonate and gypsum and relatively high pH typical of dryland soils (Plaza et al., 2018). The minerals found in the soil profile (**Supplementary Table 1**) resemble those that have previously been detected in surface and subsurface soils of the Yungay area (Ewing et al., 2006; Fuentes et al., 2014; Azua-Bustos et al., 2020). Complementarily, a soil profile study in the Yungay region by Ewing et al. (2006) revealed a similar stratification of soil with quartz, gypsum, anhydrite, chlorite (0–12 cm), anorthite (39–71 cm) and halite (102–122 cm). However, deeper soil horizons have not been analyzed in a hyperarid desert to date. On the other hand, Crits-Christoph et al. (2013) also found a significant and direct inverse relationship between pH and EC values in surface soils of the hyperarid core in the Atacama Desert. The increased solubility of Ca^{2+} ions would give a possible reason for the negative relationship between pH and EC in saline conditions under ambient atmospheric CO_2 concentrations that lead to a release of hydrogen ions. Other soil parameters, such as $CaCO_3$, gypsum and clay contents, did not appear to have a prominent

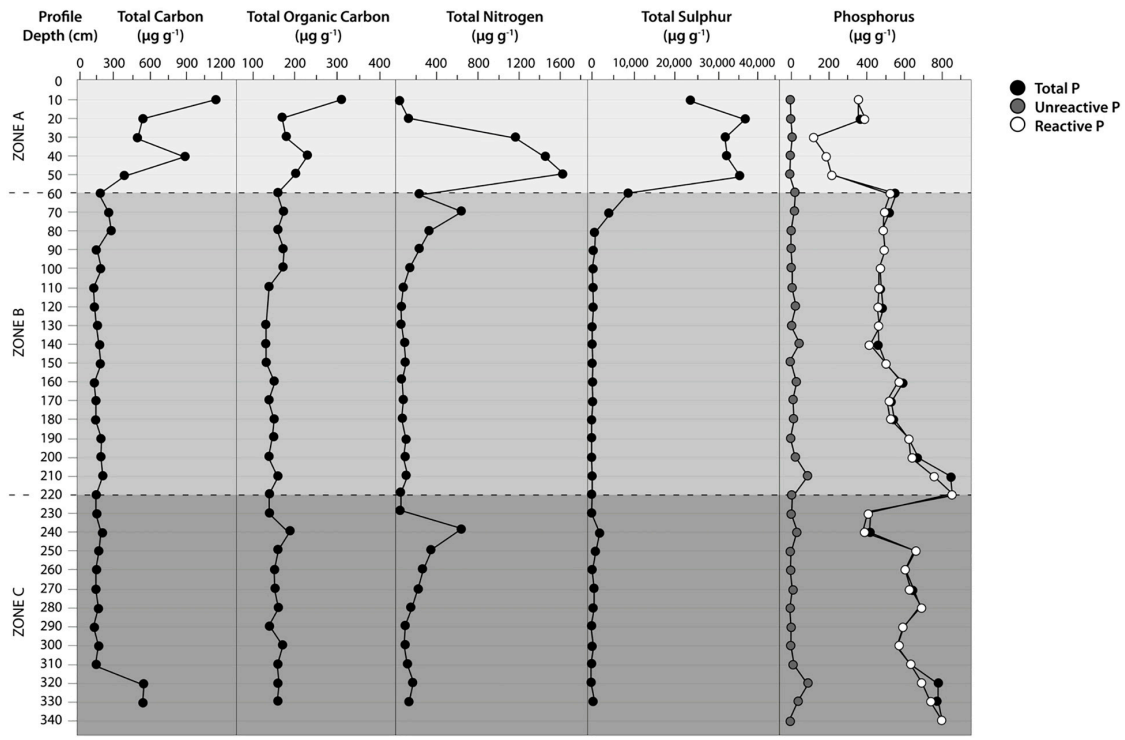

FIGURE 4 | Distribution of the soil profile parameters at the Yungay site in the hyperarid core of the Atacama Desert. Total Carbon (TC), Total Organic Carbon (TOC), Total Nitrogen (TN), Total Sulfur (TS), Total Phosphorus (TP), Reactive Phosphorus (RP), Unreactive Phosphorus (UNP).

effect on soil pH as the concentration of soluble Ca^{2+} ions increased (Al-Busaidi and Cookson, 2003).

Interestingly, Azua-Bustos et al. (2020) confirmed the existence of a widespread and sustained phenomenon of subsurface water at Yungay due to the interstratified wet clay-bearing layer. XRD showed that montmorillonite was detected in separate soil intervals in zone B (**Supplementary Table 1**). Meanwhile, muscovite and chlorite were predominant in deep zone C. These clays retain moisture at greater soil depths and reinforce the findings of Azua-Bustos et al. (2020), who investigated an interstratified wet clay-bearing layer in the upper 30 cm of a soil profile. It contained 42.8 wt% clay, mainly illite–smectite, a group of expandible clays 2:1, such as montmorillonite. Azua-Bustos et al. (2020) stated that these wet clay-rich layers play a significant role in life while preserving biosignatures in the hyperarid core of the Atacama Desert. Furthermore, in these moist smectite-rich layers were even able to detect metabolically active microorganisms protected from extremely harsh conditions at the surface.

In our study, TC was higher than TOC, which was low in the soil profile. Dryland soils store vast amounts of inorganic C. In particular, the soil inorganic C content at any depth up to 2 m is positively related to aridity (Plaza et al., 2018). Valdivia-Silva et al. (2012) indicated that the top 1 m soil layer of hyperarid lands contains ∼11.6 Tg of organic carbon and 344.6 Tg of carbonate carbon. Previous studies in the same place have indicated that the total stored carbon was 30.8-fold that of organic carbon alone (Valdivia-Silva et al., 2012). In zones B and C, it was possible to detect some peaks of TOC. In this sense, Mörchen et al. (2019) demonstrated that C accrual shifted from preferential C enrichment in topsoil to subsoil, thereby providing the potential for deep(er) biosphere food webs and revealing the future need to dig into the soil to discover traces of life in comparable environments. On the other hand, clay minerals in soil have an active role in the OC stock or C sequestration in soils (Zhong et al., 2018; Churchman et al., 2020). Organomineral interactions depend on cation bridges involving Ca ions in neutral to alkaline soils. Various organomineral interactions lead to aggregations of clay particles and organic materials, stabilizing both the soil structure and the carbon compounds within the aggregates (Oades, 1988).

The highest TN concentrations in surface zone A originated from N minerals such as darapskite (37.6%) and nitratine (2.8%) (**Figure 4** and **Supplementary Table 1**). It has been shown that the nitrate deposits present in the Atacama Desert are of atmospheric origin and formed through photochemical reactions (Ericksen, 1981; Melchiorre et al., 2018). Additionally, high contents of TS were measured in the first 50 cm depth (surface zone A); these values rapidly declined to below 500 $\mu g\ Sg^{-1}$ in zone B and then stayed below that value throughout the profile, except for a slight spike in TS contents between 230–250 cm depth (zone C). Anhydrous sulfate phases were typical in the surface layers, and the uppermost units had the least water-soluble phases. In the 0–10 cm surface layer, sulfur minerals such as

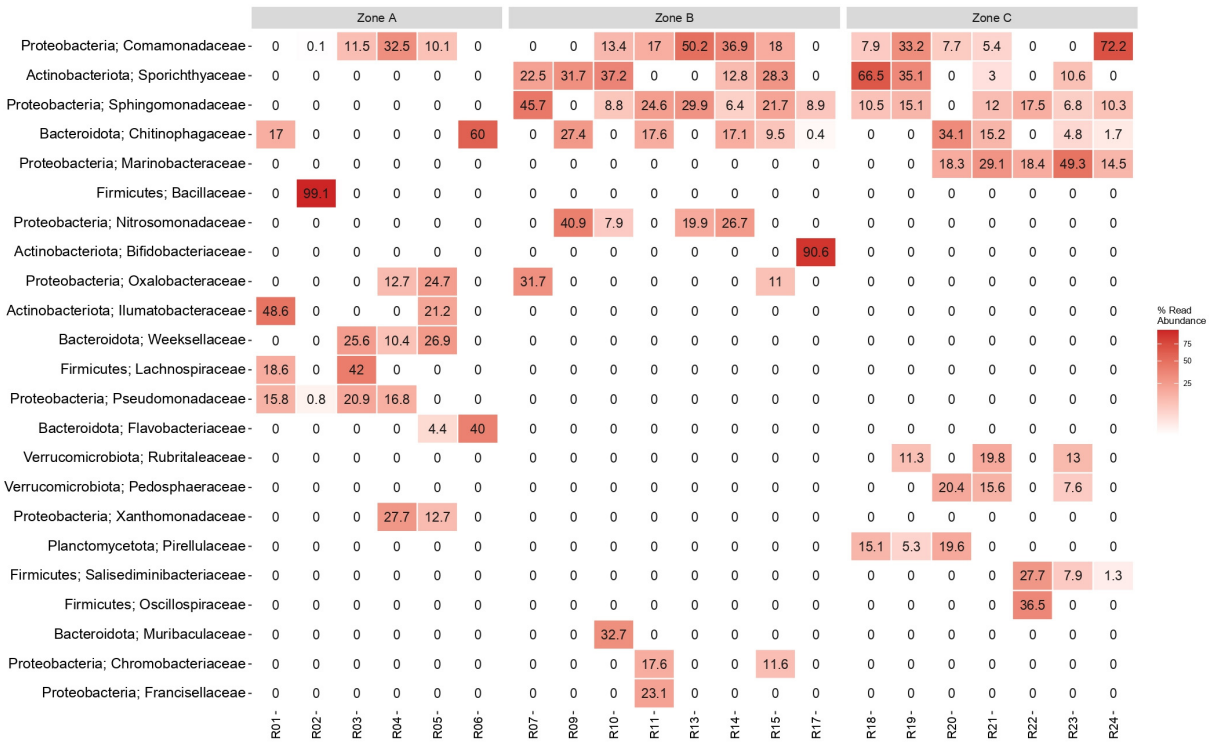

FIGURE 5 | Most abundant bacterial families in samples of the soil profile in the hyperarid core of the Atacama Desert. The heatmap shows the top 10 most abundant families per zone (total 23 families). Taxa are sorted according to overall abundance (%). R01: (0–10 cm); R02: (10–20 cm); R03: (20–30 cm); R04: (30–40 cm); R05: (40–50 cm); R06: (50–60 cm); R07: (60–70 cm); R09: (80–90 cm); R10: (90–100 cm); R11: (100–110 cm); R13: (120–130 cm); R14: (130–140 cm); R15: (140–150 cm); R17: (210–220 cm); R18: (240–250 cm); R19: (250–260 cm); R20: (260–270 cm); R21: (270–280 cm); R22: (290–300 cm); R23: (320–330 cm); R24: (330–340 cm).

Bassanita (11.6%), anhydrite (4.4%) and gypsum (1.3%) were predominant. Similar results for TOC and S contents were reported for the 0-80 cm soil depth by Warren-Rhodes et al. (2019).

Studies of P dynamics in hyperarid soils have received much less attention, even though P is an essential nutrient for life. Inorganic P (mainly in the Pi-HCl fraction) was dominant around the soil profile, which is in agreement with Wang et al. (2021). However, bioavailable P and colloidal P have been found in the surface sediments of the Atacama Desert, partly even correlating with soil microbial biomass (Warren-Rhodes et al., 2019; Knief et al., 2020; Moradi et al., 2020). Ca-P bonding forms identified by XANES were dominant, as reported earlier by Moradi et al. (2020) using colloid analyses. Higher concentrations of Pi-H_2O (representing inorganic labile P) were observed in intermediate zone B and deep zone C (8.1–20.6 $\mu g\ Pg^{-1}$) (**Supplementary Table 2**), reflecting that an increase in soil MC increases simultaneously with the availability of P. In this regard, mineralogy, associated subsoil moisture and resulting improvements in available P concentrations founded conditions that enabled the existence of a microbial biosphere within the hyperarid core of the Atacama Desert. Dryland soils also exhibit larger labile inorganic and apatite P contents but are more deficient in organic, occluded, and secondary mineral P (Plaza et al., 2018).

Increased aridity and temperature may also decouple the spatial variability of soil nutrient stocks and cycling in global drylands (Plaza et al., 2018). In the hyperarid core, the surface is devoid of vegetation; it is expected that the cycles of the nutrients carbon (C), nitrogen (N) and phosphorus (P) in the soil are mainly controlled by geochemical factors. This is in contrast with the soil-plant systems in less arid parts of the world. These cycles are coupled with biological (photosynthesis, respiration, and decomposition) and geochemical (physical and chemical weathering) processes. Aridity tends to decrease soil organic C and total N contents to different extents while increasing total and labile inorganic P, which could be related to increased P release by rock physical weathering and minimal P uptake by plants (Plaza et al., 2018).

Microbial Community Composition

The microbial composition in the soil core was dominated by *Proteobacteria, Actinobacteria, Bacteroidetes* and *Firmicutes* in all studied depth zones (**Figure 5** and **Supplementary Figures 2**, **3**). However, community composition varied with soil depth, which is consistent with other studies focusing on bacterial community variations in the surface and subsurface of this harsh environment (Crits-Christoph et al., 2013; Warren-Rhodes et al., 2019). The distribution of phyla in zone A of our study is partially in agreement with previous

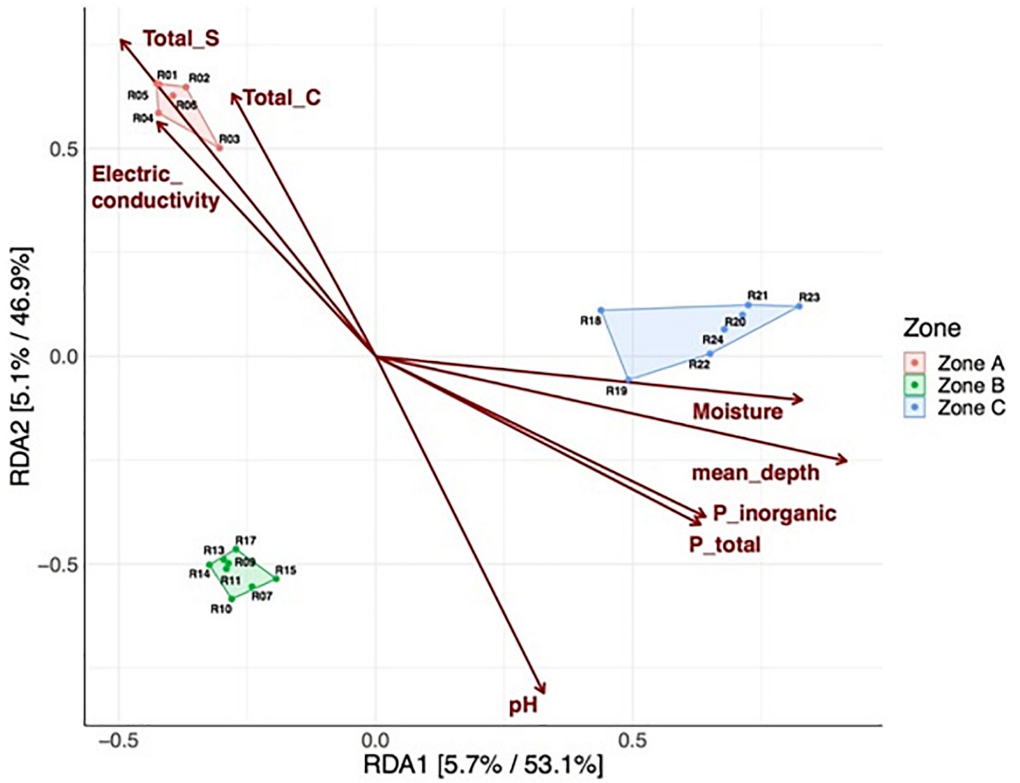

FIGURE 6 | Redundancy analysis (RDA) of Hellinger transformed amplicon sequence variant (ASV) relative abundances. Each point corresponds to a soil sample from a specific depth layer, and its relative distance indicates the level of similarity to all other samples. Polygons and colors label each of the three soil zones. The arrows indicate the explanatory power of the soil parameters concerning the observed variation in community composition. Insignificant soil parameters are not shown. For both axes, the percentages indicate the variance explained in the unconstrained and constrained analysis. Total sulfur (TS), total carbon (TC), total phosphorus (P_Total), unreactive phosphorus or inorganic phosphorus (P_inorganic).

surface sediment-based studies (Crits-Christoph et al., 2013; Schulze-Makuch et al., 2018; Warren-Rhodes et al., 2019; Knief et al., 2020). Other studies by Neilson et al. (2012) demonstrated that *Actinobacteria* and *Chloroflexi* dominate soil microbial communities in the hyperarid margin of the Atacama Desert, with extremely low levels of *Acidobacteria, Alpha-* and *Betaproteobacteria*. Neilson et al. (2017) also found that bacterial communities in soils of the Atacama Desert are mostly dominated by *Actinobacteria*, *Chloroflexi, Proteobacteria* and *Gemmatimonadetes*. Recently, Knief et al. (2020) showed the dominance of different groups of *Actinobacteria*, *Proteobacteria* and *Chloroflexi* in soils of the Atacama Desert. Connon et al. (2007) detected *Actinobacteria, Proteobacteria* and *Firmicutes* in Yungay surface soils (0–2 cm and 2–20 cm). Thus, this microbial description is in accordance with the results of our study. Recently, bacterial, and archaeal communities from hypolithic microhabitats were analyzed in the Atacama Desert to specifically identify the potentially viable microbiota (intracellular DNA versus extracellular DNA), showing habitat-specific communities dominated by bacteria. Proteobacteria were almost exclusively identified in the extracellular DNA pool in Yungay Salar halite nodules and gypsum crusts (representing an indicator for a previously existing community in this location), and *Cyanobacteria* showed the most abundant intracellular DNA in these hypolithic environments (Schulze-Makuch et al., 2021). In our case, the presence of active microbiota in deep soil remains to be addressed in future studies because we must determine if the extraction method used affected the intra- and extracellular DNA amount. The microbiological findings mentioned above show that although endolithic and hypolithic communities have been extensively studied in hyperarid surface soils of the Atacama Desert near the Yungay area (e.g., Warren-Rhodes et al., 2006; Schulze-Makuch et al., 2021), our results indicate that *Cyanobacteria* of the class *Oxyphotobacteri*a were detected with low prevalence in some of the samples of the soil profile (**Supplementary Figure 2**). Despite ecological range of *Cyanobacteria* appeared to be restricted to environments with at least occasional expose to sunlight, their presence also extends down to the deep terrestrial biosphere (Puente-Sánchez et al., 2018). A few studies have reported the presence of *Cyanobacteria* in deep subsurface environments (e.g., Kormas et al., 2003; Rastogi et al., 2010; Hubalek et al., 2016; Puente-Sánchez et al., 2018). The discussion of its origin is limited, in which it has been proposed that bloom of aquatic *Cyanobacteria* had been trapped thousands of years ago into a groundwater aquifer with no further connection with the surface (Hubalek et al., 2016), and

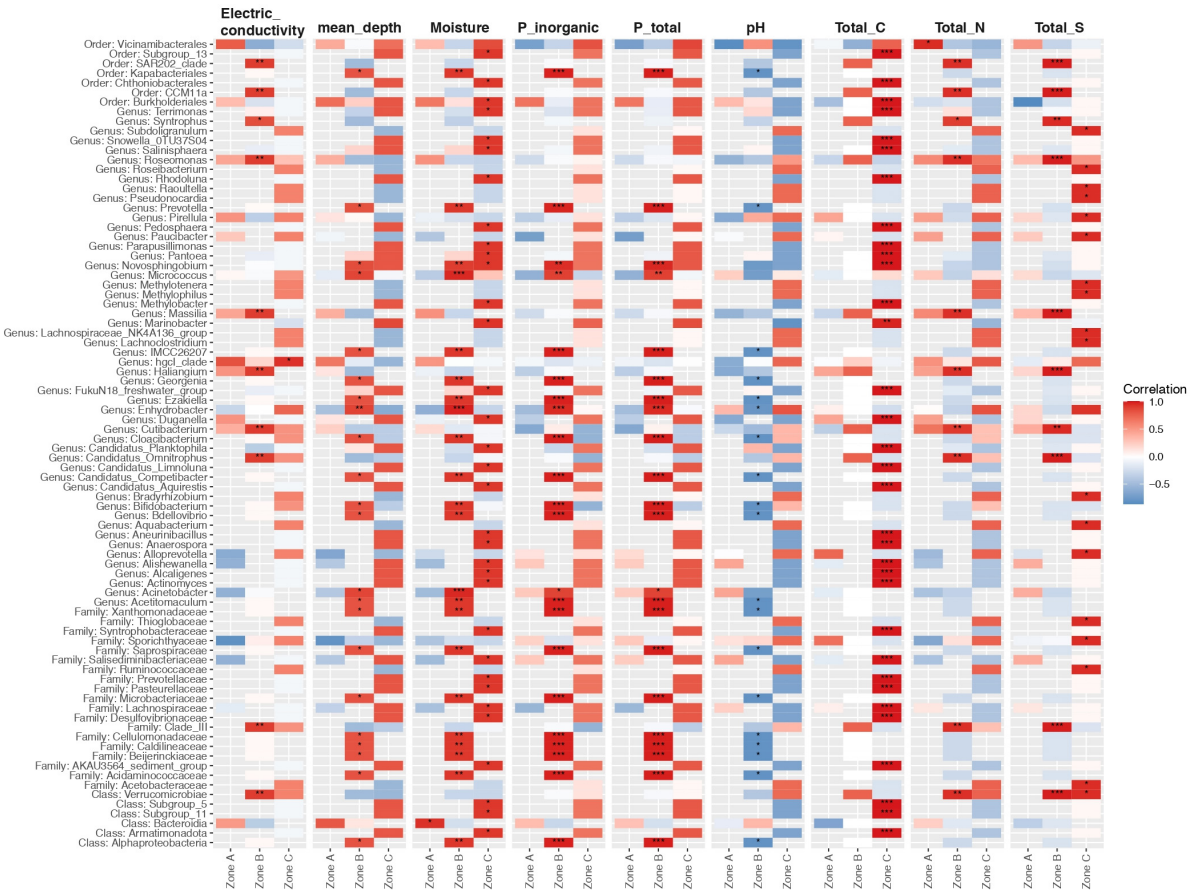

FIGURE 7 | Relationship between the 50 most correlated taxa and soil variables grouped by soil zone. Asterisks show the level of significance (*p value < 0.05, **p value < 0.01, ***p value < 0.001; Pearson correlation). Comparisons were adjusted for multiple testing using the Benjamini-Hochberg correction. Red, blue, and white indicate positive, negative, and no correlation, respectively. Taxa represent the best-hit taxonomic classification.

that the presence of *Cyanobacteria* in the continental subsurface were related to surface rock-dwelling lineages known for their high tolerance to environmental and nutritional stress (Puente-Sánchez et al., 2018). In our case, it is difficult to indicate the presence of living *Cyanobacteria* in the soil samples but this type of microorganisms in the depth soil could be related to microbial transport due surface run off rainfall events indicated by Azua-Bustos et al. (2020), and we also suggest the discovery of ancient extracellular DNA.

Moreover, our results suggest that higher moisture content, TC, pH, and EC contents favored microbial communities with more taxa that were more evenly represented (**Supplementary Figure 4** and **Supplementary Table 4**). Soil moisture is essential for bacterial diversity in desert ecosystems (Bottos et al., 2020). Additionally, moisture could be ancillary to other factors in shaping bacterial diversity. Moreover, the clay-rich layers can act as a possible "water reservoir" and help shape microbial life conditions and associated "hotspot" biosignals at greater soil depths.

The salinity of the soil, reflected by the electrical conductivity, was high along the entire soil profile (**Figure 3**). It seems to shape bacterial communities due to intense selective pressure, as few bacteria are capable of growing over large gradients of salt concentrations. We measured exceptionally high EC values (over 25 to 187 mS cm^{-1}) in surface zone A, while in intermediary zone B and depth zone C, the EC values fluctuated between 5 and 24 mS cm^{-1}. However, we did not observe a particular accumulation of halophilic taxa in zone A; rather, they were present in all zones. Nevertheless, EC had a significant effect on the bacterial community structure (**Figure 6** and **Supplementary Figure 4**). Interestingly, some of the families present in the soil profile are known to include halophilic taxa or have been shown to be present in other saline environments, such as *Proteobacteria* (*Comamonadaceae*, *Marinobacteraceae*, *Nitrosomonadaceae* and *Pseudomonadaceae*), *Actinobacteria* (*Bifidobactericeae* and *Sporichthyaceae*), and *Firmicutes* (*Bacilliaceae* and *Salisediminibacteriaceae*), which have been detected in different saline environments (e.g., Jiang et al., 2012; Crognale et al., 2013; Mirete et al., 2015; Newton et al., 2018; Remonsellez et al., 2018; Zhang et al., 2020). Moreover, members of the families *Chitinophagaceae*, *Ilumatobacteraceae*, *Rubritaleaceae*, *Pedosphaeraceae*, and *Pirellulaceae* have been

detected in various soils and sediments, such as desert surfaces (China), arid biological crusts (United States), and hypersaline lagoons (Chile) (Moquin et al., 2012; An et al., 2013; Fernandez et al., 2016; Asem et al., 2018; Li et al., 2021). Interestingly, the cultivation of clay-rich soil from subsurface samples of Yungay highlighted novel halotolerant bacteria related to *Oceanobacillus*, *Lysinibacillus*, *Virgibacillus*, *Halobacillus* and *Bacillus* (Azua-Bustos et al., 2020).

On the other hand, microbial communities were related to TP and IP (**Figure 6**). In this case, the alkaline pH values, P bonds to Ca as apatite-P (by XANES analyses), and the predominance of the Pi-HCl fraction indicates low P availability in the soil profile. However, in intermediate zone B and deep zone C, slight major P availability was revelated by high values of soluble Pi, as shown in fraction Pi-H_2O (**Supplementary Table 2**). Studies by Oliverio et al. (2020) suggest that the scarce availability of soil P likely constrains microbial growth, favoring slower growing oligotrophic microorganisms that can survive under nutrient limitations, suggesting that bacteria in low P soils may have strategies to permit efficient phosphate uptake, including the utilization of organic P compounds.

As in our study, several authors have found an association between microbial richness and diversity in the Atacama Desert's hyperarid surface soil with water availability and relative humidity (Crits-Christoph et al., 2013; Neilson et al., 2017; Schulze-Makuch et al., 2018; Knief et al., 2020). Moreover, Warren-Rhodes et al. (2019) highlighted the effect of water availability and geochemical parameters down to 80 cm depth. This study shows for the first time that this phenomenon also occurs at soil depths up to 340 cm. To date, the work of Schulze-Makuch et al. (2018) and Warren-Rhodes et al. (2019) have proposed a correlation between microbial community patterns and soil parameters and depths. In this context, our results suggest that soil properties such as moisture content and TC content strongly influence species richness, diversity, community composition, and specific members of microbial communities but that these relationships do not end in the very surface soil but extend several meters deep. Therefore, the search for life in extreme environments should consider soil as a three-dimensional ecosystem. This would increase the prospects of finding moisture hotspots at such extended soil depths, even if hyperarid conditions dominate the land surface.

CONCLUSION

The differential but 'segmented' physico-chemical and mineralogical features observed in our Yungay profile evidenced that it was possible at greater soil depths to find favorable and under-explored hotspots for microbial life in hyperarid Atacama soils. We found that the combined effects of depth, moisture, EC, pH, TC and P availability played a critical role in driving the composition and/or diversity of microbial communities in our hyperarid desert profile. Clearly, extensive and diverse microbial life remains to be discovered at greater soil depths within the hyperarid Atacama Desert, and by inference other extreme environments (including extraterrestrial planets).

DATA AVAILABILITY STATEMENT

The datasets presented in this study can be found in online repositories. The names of the repository/repositories and accession number(s) can be found below: https://www.ncbi.nlm.nih.gov/genbank/, PRJNA638921.

AUTHOR CONTRIBUTIONS

BF, FR, and RB conceived and designed the study. BF, AC, FG, FA, FR, GM, DC, and RB performed the field work. AC, FG, DC, GM, JP, and WK performed the experimental procedures and laboratory work. JA, EC-N, CK, and FR analyzed sequencing data. BF, EC-N, FR, and RB wrote the manuscript. RM, WA, CK, EK, and CS reviewed and edited the manuscript. All authors read and approved the final manuscript.

FUNDING

This work was supported by the Collaborative Project CRC1211 Earth-Evolution at the Dry Limit, funded by German Research Foundation (DFG), Project Number 268236062 – SFB 1211. BF and FR were funded by CONICYT ARIII70001 and CONICYT MEC80180018. EC-N was founded by US Air Force Office for Scientific Research FA9550-20-1-0337. CS was founded by ANID-FONDECYT regular 1200834 and Universidad Andrés Bello Núcleo DI-3–17/N. AC and FA were funded by ANID National Doctoral Fellowship.

ACKNOWLEDGMENTS

We want to thank the technician team at beamline 8 of the SLRI for assistance during the P XANES measurements.

SUPPLEMENTARY MATERIAL

The Supplementary Material for this article can be found online at: https://www.frontiersin.org/articles/10.3389/fmicb.2021.794743/full#supplementary-material

REFERENCES

Al-Busaidi, A., and Cookson, P. (2003). Salinity–pH relationships in calcareous soils. *J. Agric. Mar. Sci.* 8, 41–46. doi: 10.24200/jams.vol8iss1pp41-46

An, S., Couteau, C., Luo, F., Neveu, J., and DuBow, M. S. (2013). Bacterial diversity of surface sand samples from the Gobi and Taklamaken deserts. *Microb. Ecol.* 66, 850–860. doi: 10.1007/s00248-013-0276-2

Andersen, K. S. S., Kirkegaard, R. H., Karst, S. M., and Albertsen, M. (2018). ampvis2: an R package to analyse and visualise 16S rRNA amplicon data. *bioRxiv* [preprint] doi: 10.1101/299537

Asem, M. D., Shi, L., Jiao, J. Y., Wang, D., Han, M. X., Dong, L., et al. (2018). *Desertimonas flava* gen. nov., sp. nov. isolated from a desert soil, and proposal of *Ilumatobacteraceae* fam. nov. *Int. J. Syst. Evol. Microbiol.* 68, 3593–3599. doi: 10.1099/ijsem.0.003038

Azua-Bustos, A., Caro-Lara, L., and Vicuña, R. (2015). Discovery and microbial content of the driest site of the hyperarid Atacama Desert, Chile. *Environ. Microbiol. Rep.* 7, 388–394. doi: 10.1111/1758-2229.12261

Azua-Bustos, A., Fairén, A. G., González-Silva, C., Ascaso, C., Carrizo, D., Fernández-Martínez, M. Á, et al. (2018). Unprecedented rains decimate surface microbial communities in the hyperarid core of the Atacama Desert. *Sci. Rep.* 8:16706. doi: 10.1038/s41598-018-35051-w

Azua-Bustos, A., Fairén, A. G., Silva, C. G., Carrizo, D., Fernández-Martínez, M. A., Arenas-Fajardo, C., et al. (2020). Inhabited subsurface wet smectites in the hyperarid core of the Atacama Desert as an analog for the search for life on Mars. *Sci. Rep.* 10:19183. doi: 10.1038/s41598-020-76302-z

Azua-Bustos, A., Urrejola, C., and Vicuña, R. (2012). Life at the dry edge: microorganisms of the Atacama Desert. *FEBS Lett.* 586, 2939–2945. doi: 10.1016/j.febslet.2012.07.025

Bonilla, R. (1972). *Hidrología del Salar de Aguas Blancas. Departamento de Recursos Hidráulicos*. Moneda: Corporación de Fomento de la Producción (CORFO). Disponible en Biblioteca Universidad Católica del Norte.

Bottos, E. M., Laughlin, D. C., Herbold, C. W., Lee, C. K., McDonald, I. R., and Cary, S. C. (2020). Abiotic factors influence patterns of bacterial diversity and community composition in the Dry Valleys of Antarctica. *FEMS Microbiol. Ecol.* 96:fiaa042. doi: 10.1093/femsec/fiaa042

Bull, A. T., and Asenjo, A. (2013). Microbiology of hyper-arid environments: recent insights from the Atacama Desert, Chile. *Antonie Van Leeuwenhoek* 103, 1173–1179. doi: 10.1007/s10482-013-9911-7

Callahan, B. J., McMurdie, P. J., Rosen, M. J., Han, A. W., Johnson, A. J. A., and Holmes, S. P. (2016). DADA2: high-resolution sample inference from Illumina amplicon data. *Nat. Methods* 13:581. doi: 10.1038/nmeth.3869

Caporaso, J. G., Kuczynski, J., Stombaugh, J., Bittinger, K., Bushman, F. D., Costello, E. K., et al. (2010). QIIME allows analysis of high-throughput community sequencing data. *Nat. Methods* 7, 335–336. doi: 10.1038/nmeth.f.303

Caporaso, J. G., Lauber, C. L., Walters, W. A., Berg-Lyons, D., Huntley, J., Fierer, N., et al. (2012). Ultra-high-throughput microbial community analysis on the Illumina HiSeq and MiSeq platforms. *ISME J.* 6:1621. doi: 10.1038/ismej.2012.8

Churchman, G. J., Singh, M., Schapel, A., Sakar, B., and Bolan, N. (2020). Clay minerals as the key to the sequestration of carbon in soils. *Clays Clay Miner.* 68, 135–143. doi: 10.1007/s42860-020-00071-z

Connon, S. A., Lester, E. D., Shafaat, H. S., Obenhuber, D. C., and Ponce, A. (2007). Bacterial diversity in hyperarid Atacama Desert soils. *J. Geophys. Res.* 112:G04S17. doi: 10.1029/2006JG000311

Crits-Christoph, A., Robinson, C. K., Barnum, T., Fricke, W. F., Davila, A. F., Jedynak, B., et al. (2013). Colonisation patterns of soil microbial communities in the Atacama Desert. *Microbiome* 1:28. doi: 10.1186/2049-2618-1-28

Crognale, S., Máthé, I., Cardone, V., Stazi, S. R., and Ráduly, B. (2013). Halobacterial community analysis of Mierlei saline lake in Transylvania (Romania). *Geomicrobiol. J.* 30, 801–812. doi: 10.1080/01490451.2013.774073

Davis, N. M., Proctor, D. M., Holmes, S. P., Relman, D. A., and Callahan, B. J. (2018). Simple statistical identification and removal of contaminant sequences in marker-gene and metagenomics data. *Microbiome* 6, 1–14. doi: 10.1186/s40168-018-0605-2

Dirección General de Aguas (2017). *Inventario Nacional de Acuíferos. División de Estudios y Planificación SDT N° 403*. Available online at: https://snia.mop.gob.cl/sad/SUB5748.pdf

Dormann, C. F., Gruber, B., and Fründ, J. (2008). Introducing the bipartite package: analysing ecological networks. *R News* 8, 8–11.

Eisenhofer, R., Minich, J. J., Marotz, C., Cooper, A., Knight, R., and Weyrich, L. S. (2019). Contamination in low microbial biomass microbiome studies: issues and recommendations. *Trends Microbiol.* 27, 105–117. doi: 10.1016/j.tim.2018.11.003

Ericksen, G. E. (1981). *Geology and Origin of the Chilean Nitrate Deposits. Geological Survey Professional paper 1188*. Reston, VA: United States Geological survey. doi: 10.3133/pp1188

Ewing, S. A., Sutter, B., Owen, J., Nishiizumi, K., Sharp, W., Cliff, S. S., et al. (2006). A threshold in soil formation at Earth's arid–hyperarid transition. *Geochim. Cosmochim. Acta* 70, 5293–5322. doi: 10.1016/j.gca.2006.08.020

Fernandez, A. B., Rasuk, M. C., Visscher, P. T., Contreras, M., Novoa, F., Poire, D. G., et al. (2016). Microbial diversity in sediment ecosystems (evaporites domes, microbial mats, and crusts) of hypersaline Laguna Tebenquiche, Salar de Atacama, Chile. *Front. Microbiol.* 7:1284. doi: 10.3389/fmicb.2016.01284

Finstad, K. M., Probst, A. J., Thomas, B. C., Andersen, G. L., Demergasso, C., Echeverría, A., et al. (2017). Microbial community structure and the persistence of cyanobacterial populations in salt crusts of the hyperarid Atacama Desert from genome-resolved metagenomics. *Front. Microbiol.* 8:1435. doi: 10.3389/fmicb.2017.01435

Fletcher, L. E., Valdivia-Silva, J. E., Pérez-Montaño, S., Condori-Apaza, R. M., Conley, C. A., and McKay, C. P. (2012). Variability of organic material in surface horizons of the hyper-arid Mars-like soils of the Atacama Desert. *Adv. Space Res.* 49, 271–279. doi: 10.1016/j.asr.2011.10.001

Fox, J. (2003). Effect displays in R for generalised linear models. *J. Stat. Softw.* 8, 1–27.

Fuentes, B., Mora, M. L., Bol, R., San Martin, F., Pérez, E., and Cartes, P. (2014). Sorption of inositol hexaphosphate on desert soils. *Geoderma* 232, 573–580. doi: 10.1016/j.geoderma.2014.06.016

Gómez-Silva, B., Rainey, F. A., Warren-Rhodes, K. A., McKay, C. P., and Navarro-González, R. (2008). "Atacama desert soil microbiology," in *Microbiology of Extreme Soils*, eds P. Dion and C. S. Nautiyal (Berlin: Springer).

Hedley, M. J., Stewart, J. W. B., and Chauhan, B. S. (1982). Changes in inorganic and organic soil phosphorus fractions induced by cultivation practices and by laboratory Incubations. *Soil Sci. Soc. Am. J.* 46, 970–976. doi: 10.2136/sssaj1982.03615995004600050017x

Herrera, C., and Custodio, E. (2014). Origin of waters from small springs located at the northern coast of Chile, in the vicinity of Antofagasta. *Andean Geol.* 41, 314–341. doi: 10.5027/andgeoV41n2-a03

Houston, J. (2006). Variability of precipitation in the Atacama Desert: its causes and hydrological impact. *Int. J. Climatol.* 26, 2181–2198. doi: 10.1002/joc.1359

Houston, J., and Hartley, A. J. (2003). The central Andean west-slope rainshadow and its potential contribution to the origin of hyper-aridity in the Atacama Desert. *Int. J. Climatol.* 23, 1453–1464. doi: 10.1002/joc.938

Hubalek, V., Wu, X., Eiler, A., Buck, M., Heim, C., Dopson, M., et al. (2016). Connectivity to the surface determines diversity patterns in subsurface aquifers of the Fennoscandian shield. *ISME J.* 10, 2447–2458. doi: 10.1038/ismej.2016.36

Jiang, F., Cao, S. J., Li, Z. H., Fan, H., Li, H. F., Liu, W. J., et al. (2012). *Salisediminibacterium halotolerans* gen. nov., sp. nov., a halophilic bacterium from soda lake sediment. *Int. J. Syst. Evol. Micr.* 62, 2127–2132. doi: 10.1099/ijs.0.034488-0

Klysubun, W., Tarawarakarn, P., Thamsanong, N., Amonpattaratkit, P., Cholsuk, C., Lapboonrueng, S., et al. (2019). Upgrade of SLRI BL8 beamline for XAFS spectroscopy in a photon energy range of 1–13keV. *Radiat. Phys. Chem.* 175:108145. doi: 10.1016/j.radphyschem.2019.02.004

Knief, C., Bol, R., Amelung, W., Kush, S., Frindte, K., Eckmeier, E., et al. (2020). Tracing elevational changes in microbial life and organic carbon sources in soils of the Atacama Desert. *Global Planet. Change* 184:103078. doi: 10.1016/j.gloplacha.2019.103078

Kormas, K. A., Smith, D. C., Edgcomb, V., and Teske, A. (2003). Molecular analysis of deep subsurface microbial communities in Nankai Trough sediments (ODP Leg 190, Site 1176). *FEMS Microbiol. Ecol.* 45, 115–125. doi: 10.1016/S0168-6496(03)00128-4

Li, Q., Song, A., Yang, H., and Müller, W. E. (2021). Impact of rocky desertification control on soil bacterial community in Karst Graben Basin, Southwestern China. *Front. Microbiol.* 12:448. doi: 10.3389/fmicb.2021.636405

McMurdie, P. J., and Holmes, S. (2013). phyloseq: an r package for reproducible interactive analysis and graphics of microbiome census data. *PLoS One* 8:e61217. doi: 10.1371/journal.pone.0061217

Melchiorre, E. B., Sickman, J. O., Talyn, B. C., and Noblet, J. (2018). Isotope stratigraphy: insights on paleoclimate and formation of nitrate deposits in the Atacama Desert, Chile. *J. Arid Environ.* 148, 45–53. doi: 10.1016/j.jaridenv.2017.09.013

Mirete, S., Mora-Ruiz, M. R., Lamprecht-Grandío, M., de Figueras, C. G., Sorelló-Móra, R., and Gónzalez-Pastor, J. E. (2015). Salt resistance genes revealed by functional metagenomics from brines and moderate-salinity rhizosphere within a hypersaline environment. *Front. Microbiol.* 2:1121.

Moquin, S. A., Garcia, J. R., Brantley, S. L., Takacs-Vesbach, C. D., and Shepherd, U. L. (2012). Bacterial diversity of bryophyte-dominant biological soil crusts and associated mites. *J. Arid Environ.* 87, 110–117.

Moradi, G., Bol, R., Trbojevic, L., Missong, A., Mörchen, R., Fuentes, B., et al. (2020). Contrasting depth distribution of colloid-associated phosphorus in the active and abandoned sections of an alluvial fan in a hyper-arid region of the Atacama Desert. *Global Planet. Change* 185:103090. doi: 10.1016/j.gloplacha.2019.103090

Mörchen, R., Lehndorff, E., Arenas-Díaz, F., Moradi, G., Bol, R., Fuentes, B., et al. (2019). Carbon accrual in the Atacama Desert. *Global Planet. Change* 181:102993. doi: 10.1016/j.gloplacha.2019.102993

Murphy, J., and Riley, J. P. (1962). A modified single solution method for the determination of phosphate in natural waters. *Anal. Chim. Acta* 27, 31–36. doi: 10.1016/S0003-2670(00)88444-5

Navarro-González, R., Rainey, F. A., Molina, P., Bagaley, D. R., Hollen, B. J., de la Rosa, J., et al. (2003). Mars-like soils in the Atacama Desert, Chile, and the dry limit of microbial life. *Science* 302, 1018–1021. doi: 10.1126/science.1089143

Neilson, J. W., Califf, K., Cardona, C., Copeland, A., van Treuren, W., Josephson, K. L., et al. (2017). Significant impacts of increasing aridity on the arid soil microbiome. *mSystems* 2:e00195-16. doi: 10.1128/mSystems.00195-16

Neilson, J. W., Quade, J., Ortiz, O., Nelson, W. M., Legatzki, A., Tian, F., et al. (2012). Life at the hyperarid margin: novel bacterial diversity in arid soils of the Atacama Desert, Chile. *Extremophiles* 16, 553–566. doi: 10.1007/s00792-012-0454-z

Newton, K., Jeffries, T. C., Smith, R. J., Seymour, J. R., Seuront, L., and Mitchell, J. G. (2018). Taxonomic and metabolic shifts in the Coorong bacterial metagenome driven by salinity and external inputs. *J. Ocean Limnol.* 36, 2033–2049. doi: 10.1007/s00343-018-7387-z

Oades, J. M. (1988). The retention of organic matter in soils. *Biogeochemistry* 5, 35–70. doi: 10.1007/BF02180317

Oliverio, A. M., Bissett, A., McGuire, K., Saltonstall, K., Turner, B. L., and Fierer, N. (2020). The role of phosphorus limitation in shaping soil bacterial communities and their metabolic capabilities. *mBio* 11:e01718-20.

Pfeiffer, M., Latorre, C., Santoro, C. M., Gayo, E. M., Rojas, R., Carrevedo, M. L., et al. (2018). Chronology, stratigraphy and hydrological modelling of extensive wetlands and paleolakes in the hyperarid core of the Atacama Desert during the late quaternary. *Quat. Sci. Rev.* 197, 224–245.

Plaza, C., Zaccone, C., Sawicka, K., Méndez, A. M., Tarquis, A., Gascó, G., et al. (2018). Soil resources and element stocks in drylands to face global issues. *Sci. Rep.* 8:13788. doi: 10.1038/s41598-018-32229-0

Prietzel, J., Harrington, G., Häusler, W., Heister, K., Werner, F., and Klysubun, W. (2016). Reference spectra of important adsorbed organic and inorganic phosphate binding forms for soil P speciation using synchrotron-based K-edge XANES spectroscopy. *J. Synchrotron Radiat.* 23, 532–544. doi: 10.1107/S1600577515023085

Puente-Sánchez, F., Arce-Rodríguez, A., Oggerin, M., García-Villadangos, M., Moreno-Paz, M., Blanco, Y., et al. (2018). Viable cyanobacteria in the deep continental subsurface. *Proc. Natl. Acad. Sci. U. S. A.* 115, 10702–10707. doi: 10.1073/pnas.1808176115

Quast, C., Pruesse, E., Yilmaz, P., Gerken, J., Schweer, T., Yarza, P., et al. (2013). The SILVA ribosomal RNA gene database proj- ect: improved data processing and web-based tools. *Nucleic Acids Res.* 41, D590–D596. doi: 10.1093/nar/gks1219

R Core Team (2018). *R: A Language and Environment for Statistical Computing*. Vienna: R Foundation for Statistical Computing.

Rastogi, G., Osman, S., Kukkadapu, R., Engelhard, M., Vaishampayan, P. A., Andersen, G. L., et al. (2010). Microbial and mineralogical characterizations of soils collected from the deep biosphere of the former Homestake gold mine, South Dakota. *Microb. Ecol.* 60, 539–550. doi: 10.1007/s00248-010-9657-y

Remonsellez, F., Castro-Severyn, J., Pardo-Esté, C., Aguilar, P., Fortt, J., Salinas, C., et al. (2018). Characterization and salt response in recurrent halotolerant *Exiguobacterium* sp. SH31 isolated from sediments of Salar de Huasco, Chilean Altiplano. *Front. Microbiol.* 9:2228. doi: 10.3389/fmicb.2018.02228

Ritter, B., Stuart, F. M., Binnie, S. A., Gerdes, A., Wennrich, V., and Dunai, T. J. (2018). Neogene fluvial landscape evolution in the hyperarid core of the Atacama Desert. *Sci. Rep.* 8:13952. doi: 10.1038/s41598-018-32339-9

RStudio Team (2016). *Integrated Development for R*. Boston, MA: RStudio Inc.

Sáez, A., Godfrey, L. V., Herrera, C., Chong, G., and Pueyo, J. J. (2016). Timing of wet episodes in Atacama Desert over the last 15 ka. The Groundwater Discharge Deposits (GWD) from Domeyko Range at 25°S. *Quat. Sci. Rev.* 145, 82–93.

Saunders, W. M. H., and Williams, E. G. (1955). Observations on the determination of total organic phosphorus in soil. *Eur. J. Soil Sci.* 6, 254–267. doi: 10.1111/j.1365-2389.1955.tb00849.x

Schulze-Makuch, D., Lipus, D., Arens, F. L., Baqué, M., Bornermann, T. L. V., de Vera, J. P., et al. (2021). Microbial hotspots in lithic microhabitats inferred from DNA fractionation and metagenomics in the Atacama Desert. *Migroorganisms* 9:1038. doi: 10.3390/microorganisms9051038

Schulze-Makuch, D., Wagner, D., Kounaves, S. P., Mangelsdorf, K., Devine, K. G., de Vera, J. P., et al. (2018). Transitory microbial habitat in the hyperarid Atacama Desert. *Proc. Natl. Acad. Sci. U.S.A.* 115, 2670–2675. doi: 10.1073/pnas.1714341115

UNEP (1997). *World Atlas of Desertification*, 2nd Edn. Nairobi: United Nations Environmental Programme.

Valdivia-Silva, J., Navarro-González, R., Fletcher, L., Perez-Montaño, S., Condori-Apaza, R., and Mckay, C. P. (2012). Soil carbon distribution and site characteristics in hyper-arid soils of the Atacama Desert: a site with mars-like soils. *Adv. Space Res.* 50, 108–122. doi: 10.1016/j.asr.2012.03.003

Wang, Q., Garrity, G. M., Tiedje, J. M., and Cole, J. R. (2007). Naive Bayesian classifier for rapid assignment of rRNA sequences into the new bacterial taxonomy. *Appl. Environ. Microbiol.* 73, 5261–5267. doi: 10.1128/AEM.00062-07

Wang, Y., Moradi, G., Klumpp, E., von Sperber, C., Tamburini, F., Ritter, B., et al. (2021). Phosphate oxygen isotope fingerprints of past biological activity in the Atacama Desert. *Geochim. Cosmochim. Acta* 311, 1–11. doi: 10.1016/j.gca.2021.07.027

Warren-Rhodes, K. A., Lee, K. C., Archer, S. D. J., Cabrol, N., Ng-Boyle, L., Wetthergreen, D., et al. (2019). Subsurface microbial habitats in an extreme desert mars-analog environment. *Front. Microbiol.* 10:69. doi: 10.3389/fmicb.2019.00069

Warren-Rhodes, K. A., Rhodes, K. L., Pointing, S. B., Ewing, S. A., Lacap, D. C., Gómez-Silva, B., et al. (2006). Hypolithic Cyanobacteria, dry limit of photosynthesis, and microbial ecology in the Hyperarid Atacama desert. *Microb. Ecol.* 52, 389–398. doi: 10.1007/s00248-006-9055-7

Werner, F., and Prietzel, J. (2015). Standard protocol and quality assessment of soil phosphorus speciation by P K-Edge XANES spectroscopy. *Environ. Sci. Tech.* 49, 10521–10528. doi: 10.1021/acs.est.5b03096

Wickham, H. (2016). *ggplot2: Elegant Graphics for Data Analysis*. New York, NY: Springer-Verlag.

Wierzchos, J., Ascaso, C., and Mckay, C. P. (2006). Endolithic cyanobacteria in halite rocks from the Hyperarid core of the Atacama desert. *Astrobiology* 6, 415–422. doi: 10.1089/ast.2006.6.415

Wright, E. S. (2016). Using DECIPHER v2.0 to Analyse big biological sequence data in R. *R J.* 8, 352–359.

Zhang, L., Cai, Y., Jiang, M., Dai, J., Guo, X., Li, W., et al. (2020). The levels of microbial diversity in different water layers of saline Chagan Lake, China. *J. Oceanol. Limnol.* 38, 395–407. doi: 10.1007/s00343-019-9027-7

Zhong, Z., Zhengxing, C., Yadong, X., Chengjie, R., Gaihe, Y., Xinhui, H., et al. (2018). Relationship between soil organic carbon stocks and clay content under different climatic conditions in Central China. *Forests* 9:598. doi: 10.3390/f9100598

Conflict of Interest: The authors declare that the research was conducted in the absence of any commercial or financial relationships that could be construed as a potential conflict of interest.

Publisher's Note: All claims expressed in this article are solely those of the authors and do not necessarily represent those of their affiliated organizations, or those of the publisher, the editors and the reviewers. Any product that may be evaluated in this article, or claim that may be made by its manufacturer, is not guaranteed or endorsed by the publisher.

frontiers in Microbiology

ORIGINAL RESEARCH
published: 15 February 2022
doi: 10.3389/fmicb.2021.822229

Integrative Genomics Sheds Light on Evolutionary Forces Shaping the Acidithiobacillia Class Acidophilic Lifestyle

*Carolina González-Rosales[1,2], Eva Vergara[1], Mark Dopson[3], Jorge H. Valdés[4] and David S. Holmes[1,5]**

[1] Center for Bioinformatics and Genome Biology, Centro Ciencia & Vida, Fundación Ciencia & Vida, Santiago, Chile, [2] Center for Genomics and Bioinformatics, Faculty of Sciences, Universidad Mayor, Santiago, Chile, [3] Centre for Ecology and Evolution in Microbial Model Systems, Linnaeus University, Kalmar, Sweden, [4] Center for Bioinformatics and Integrative Biology, Facultad de Ciencias de la Vida, Universidad Andrés Bello, Santiago, Chile, [5] Facultad de Medicina y Ciencia, Universidad San Sebastián, Santiago, Chile

OPEN ACCESS

Edited by:
Martina Cappelletti, University of Bologna, Italy

Reviewed by:
Aleksandr G. Bulaev, Federal Center Research Fundamentals of Biotechnology, Russian Academy of Sciences (RAS), Russia
Ruiyong Zhang, Institute of Oceanology, Chinese Academy of Sciences (CAS), China

***Correspondence:**
David S. Holmes
dsholmes2000@yahoo.com

Specialty section:
This article was submitted to Extreme Microbiology, a section of the journal Frontiers in Microbiology

Received: *25 November 2021*
Accepted: *30 December 2021*
Published: *15 February 2022*

Citation:
González-Rosales C, Vergara E, Dopson M, Valdés JH and Holmes DS (2022) Integrative Genomics Sheds Light on Evolutionary Forces Shaping the Acidithiobacillia Class Acidophilic Lifestyle. Front. Microbiol. 12:822229. doi: 10.3389/fmicb.2021.822229

Extreme acidophiles thrive in environments rich in protons (pH values <3) and often high levels of dissolved heavy metals. They are distributed across the three domains of the Tree of Life including members of the Proteobacteria. The Acidithiobacillia class is formed by the neutrophilic genus *Thermithiobacillus* along with the extremely acidophilic genera *Fervidacidithiobacillus*, *Igneacidithiobacillus*, *Ambacidithiobacillus*, and *Acidithiobacillus*. Phylogenomic reconstruction revealed a division in the Acidithiobacillia class correlating with the different pH optima that suggested that the acidophilic genera evolved from an ancestral neutrophile within the Acidithiobacillia. Genes and mechanisms denominated as "first line of defense" were key to explaining the Acidithiobacillia acidophilic lifestyle including preventing proton influx that allows the cell to maintain a near-neutral cytoplasmic pH and differ from the neutrophilic Acidithiobacillia ancestors that lacked these systems. Additional differences between the neutrophilic and acidophilic Acidithiobacillia included the higher number of gene copies in the acidophilic genera coding for "second line of defense" systems that neutralize and/or expel protons from cell. Gain of genes such as hopanoid biosynthesis involved in membrane stabilization at low pH and the functional redundancy for generating an internal positive membrane potential revealed the transition from neutrophilic properties to a new acidophilic lifestyle by shaping the *Acidithiobacillaceae* genomic structure. The presence of a pool of accessory genes with functional redundancy provides the opportunity to "hedge bet" in rapidly changing acidic environments. Although a core of mechanisms for acid resistance was inherited vertically from an inferred neutrophilic ancestor, the majority of mechanisms, especially those potentially involved in resistance to extremely low pH, were obtained from other extreme acidophiles by horizontal gene transfer (HGT) events.

Keywords: acidophiles, pH homeostasis, extremophiles, acid mine drainage (AMD), evolution, comparative genomics

INTRODUCTION

Microbial cells present a variety of genetic mechanisms allowing them to manage stressful situations such as changes in temperature, pH values, and oxidative stress (Li et al., 2011). Organisms with an acidic optimal growth pH are termed "acidophiles," and this classification has been further divided into moderate acidophiles with a pH optimum $\leq$5 and extreme acidophiles that grow optimally at pH $\leq$3. To survive and grow in low pH environments, acidophiles must maintain a near-neutral cytoplasm when faced with an external to internal proton gradient across the cytoplasmic membrane up to 10^5-fold (Slonczewski et al., 2009; Zammit and Watkin, 2016; Quatrini and Johnson, 2018). Different pH homeostasis mechanisms have been proposed to explain the acidophilic resistance including some that are shared with neutrophiles. These are (i) proton export pumps and antiporters (Michels and Bakker, 1985); (ii) cytoplasmic buffering *via* an overproduction of alkaline amino acids (Parro et al., 2007); (iii) proton consuming reactions such as glutamate decarboxylase (Mangold et al., 2013); (iv) alterations in the membrane structure to reduce fluidity by the inclusion of hopanoids (Mykytczuk et al., 2010); (v) reduction in the outer membrane permeability *via* porins using polyamines such as spermidine (Samartzidou et al., 2003); and (vi) pH homeostatic systems such as an internal positive membrane potential thought to be generated by potassium ions (Buetti-Dinh et al., 2016). However, as pH homeostatic mechanisms are often shared between neutrophiles and acidophiles, those most important to mediating homeostasis in highly acidic conditions are not always apparent.

Low pH mitigation mechanisms have been investigated in acidophiles (Baker-Austin and Dopson, 2007; Li et al., 2011; Ullrich et al., 2016a; Colman et al., 2018; Vergara et al., 2020; Chen et al., 2021; Mayer et al., 2021; Sriaporn et al., 2021). These studies show that horizontal gene transfer (HGT), gene mutation, and gene loss trajectories in evolution allow adaptation and survival of prokaryotes in extreme conditions (Foster, 2004; Ullrich et al., 2016a; Zhang et al., 2017; Vergara et al., 2020). Extensive HGT events are also documented in acidophiles such as *Sulfolobus islandicus* (Whitaker et al., 2005), *Leptospirillum* (Simmons et al., 2008; Vergara et al., 2020), and the extremophilic red alga *Galdieria sulphuraria* (Schonknecht et al., 2013; Colman et al., 2018) that acquired genes by HGT from bacteria and archaea to be able to thrive in thermophilic, acidic, and metal-rich environments. To cope with the high acidity, *G. sulphuraria* lowers the proton permeability of its plasma membrane by having a single copy of a voltage-gated ion channel gene compared to three copies in the neutrophilic *Cyanidioschyzon merolae* from which it diverged one billion years ago (Schonknecht et al., 2013). However, the events that led to the evolution of acidophiles and their role in the generation of acidic habitats are underexplored.

The Acidithiobacillia is a newly recognized class of Proteobacteria at the root of the Betaproteobacteria/Gammaproteobacteria division (Williams and Kelly, 2013). Two families make up this class, family I comprising the acidophilic *Acidithiobacillaceae* and the neutrophilic family II *Thermithiobacillaceae*. Due to their acidophilic nature, the *Acidithiobacillaceae* are largely recalcitrant to standard genetic manipulation (Inaba et al., 2018; Jung et al., 2021), and consequently, the use of bioinformatics approaches advances our understanding of the biology of these extremophiles. The research of Moya-Beltrán et al. (2021) describes four *Acidithiobacillaceae* genera (Nuñez et al., 2016), namely, (i) sulfur oxidizing *Ambacidithiobacillus* that includes the recently described species *Am. sulfuriphilus* (ex *Acidithiobacillus sulfuriphilus*) (Falagán et al., 2019); (ii) *Igneacidithiobacillus* including species *I. copahuensis* (Moya-Beltrán et al., 2021), *Candidatus I. taiwanensis* (Moya-Beltrán et al., 2021), and *Candidatus I. yellowstonensis* (Moya-Beltrán et al., 2021); (iii) *Fervidacidithiobacillus* with *F. caldus* (ex-*Acidithiobacillus caldus*) (Hallberg and Lindström, 1994; Valdes et al., 2009; You et al., 2011; Zhang et al., 2016b); and (iv) the *Acidithiobacillus* genus formed by *A. thiooxidans* (Waksman and Joffe, 1922; Valdes et al., 2011; Travisany et al., 2014; Yin et al., 2014; Zhang et al., 2016a, 2018; Quatrini et al., 2017; Camacho et al., 2020), *A. albertensis* (Bryant et al., 1983; Castro et al., 2017), *Acidithiobacillus* sp. SH (Kamimura et al., 2018) plus the iron/sulfur oxidizers *A. ferrooxidans* (Temple and Colmer, 1951; Valdés et al., 2008; Chen P. et al., 2015; Yan et al., 2015; Kucera et al., 2016; Ulloa et al., 2019), *A. ferridurans* (Hedrich and Johnson, 2013; Miyauchi et al., 2018), *A. ferrivorans* (Hallberg et al., 2010; Liljeqvist et al., 2011; Talla et al., 2014; Tran et al., 2017), and *A. ferriphilus* (Falagán and Johnson, 2016) represented by *A. ferrooxidans* BY0502 for which phylogenetic and nucleotide identity analysis is suggested to be reclassified as an *A. ferriphilus*-like species (González et al., 2016; Fariq et al., 2019).

Genome sequences are available for many of the acidophilic species (Neira et al., 2020) including *A. ferrooxidans* (Valdés et al., 2008; Chen P. et al., 2015; Yan et al., 2015; Kucera et al., 2016; Ulloa et al., 2019), *A. ferrivorans* (Liljeqvist et al., 2011; Talla et al., 2014; Tran et al., 2017), *A. ferridurans* (Hedrich and Johnson, 2013; Miyauchi et al., 2018), *A. ferrianus* (Norris et al., 2020), *A. thiooxidans* (Valdes et al., 2011; Travisany et al., 2014; Yin et al., 2014; Zhang et al., 2016a, 2018; Quatrini et al., 2017; Camacho et al., 2020), *F. caldus* (Valdes et al., 2009; You et al., 2011; Zhang et al., 2016b), and *Am. sulfuriphilus* (Falagán et al., 2019) along with the neutrophile *Thermithiobacillus tepidarius* (Boden et al., 2016).

Three populations of uncultivated hot spring *Acidithiobacillus* strains and ten publicly available genomes were analyzed for the presence or absence of predicted genes for acid resistance, identifying a similar number of gene copies encoding for K^+ transporters, deiminases/deaminase group and adenosine deaminase shared between genomes, and a difference in the number of amino acid decarboxylases, Na^+/H^+ antiporters, and plasma membrane proton-efflux P-type ATPases (Sriaporn et al., 2021). In addition, the mechanisms of resistance to low temperature and pH from an extreme microbial community where *A. ferrivorans* was the dominant member revealed an adaptation to low temperature by the presence trehalose synthase pathways, oxidative stress pathways, cold shock proteins, and genes encoding for biofilm formation (González et al., 2014; Liljeqvist et al., 2015). This study investigates the genes present

in the Acidithiobacillia class by phylogenomic and comparative genomic analyses deepening our understanding of how the acidophilic genera *Fervidacidithiobacillus*, *Igneacidithiobacillus*, *Ambacidithiobacillus*, and *Acidithiobacillus* obtained genes coding for pH homeostasis that allows them to survive at extremely low pH values of ≤3.

MATERIALS AND METHODS

Genome Selection and Representative Selection

Thirty-seven permanent draft or complete genomes from the Acidithiobacillia class were downloaded from NCBI with those genomes passing CheckM (Parks et al., 2015) quality control for completeness (>90%) and lack of contamination (<10%) retained. The Acidithiobacillia class conserved core genome was identified using the GET_Homologues (Contreras-Moreira and Vinuesa, 2013) software suite, selecting conserved proteins with at least 50% identity and alignment coverage. Core protein families were aligned using MAFFT (Katoh, 2002; Katoh and Standley, 2013; Katoh et al., 2019) with L-INS-i iterative refinement. Alignments were masked to remove unreliable aligned regions with GBLOCK (Castresana, 2000) followed by concatenation of families. A maximum likelihood tree was constructed based on concatenated alignment of core genes using IQ-TREE (Nguyen et al., 2015; Hoang et al., 2018) with 1,000 replicates and the best-fit model predicted by IQ-TREE (Nguyen et al., 2015; Kalyaanamoorthy et al., 2017) according to Bayesian information criterion and the *T. tepidarius* DSM 3134 genome as an outgroup for the *Acidithiobacillaceae* (Boden et al., 2016). The phylogenomic tree was visualized with iTOL6 (Letunic and Bork, 2021).

A representative genome was selected from each clade of core genomes according to the following criteria (**Supplementary Figure 1**): (i) using the type strain genome if available and complete; (ii) if this was unavailable or a draft, a strain with a complete genome was selected; and (iii) a strain genome sequence was selected according to the quality as calculated by CheckM.

Protein Family Prediction

Conserved orthologous proteins were selected based on the classification of all protein-coding genes in protein families. The selected proteins were sorted using the GET_Homologues (Contreras-Moreira and Vinuesa, 2013) software suite, with BLAST (Altschul, 1997) and orthoMCL (Fischer et al., 2011) programs. Protein families were constructed using a 50/50 rule of 50% of identity and 50% of alignment coverage (Altschul et al., 1990; Altschul, 1997; Snipen and Ussery, 2010) and each protein was then assigned to one protein family. The protein families were classified in core (proteins shared by all strains), dispensable (proteins assigned to some strains), and unique (proteins assigned to only a single strain) genomes according to their distribution (**Supplementary Data Sheet 1**). The sum of all three groups form the pangenome, i.e., the union of the genomes under consideration (Tettelin et al., 2005; Snipen and Ussery, 2010).

Selection of Acid Resistance Genes

Genes and protein sequences that were either predicted or experimentally validated to be involved in low pH responses in extreme acidophiles were extracted from the literature (Gassel et al., 1998; Foster, 2004; Zhou et al., 2010; Krulwich et al., 2011; Mangold et al., 2013; De Biase and Lund, 2015; Mühling et al., 2016; Vergara et al., 2020). The list of potential genes was extended by keyword literature searches in Google Scholar and species description journals (e.g., International Journal of Systematic and Evolutionary Microbiology). Additionally, the JGI pH metadata and NCBI's BIOSAMPLE database were used to collect gene and protein information linked to low pH environments. The collected assemblage of potential acid resistance gene/protein sequences was used to formulate Blast searches against Acidithiobacillia genomes using a minimal *E*-value cutoff of $1e^{-5}$ (**Supplementary Figure 1**).

Protein Properties

Prediction of transmembrane regions in protein sequences was carried out using TMHMM (Sonnhammer et al., 1998; Krogh et al., 2001) and TMPRED (Chen et al., 2002). Signal peptide and subcellular localization predictions were made with SignalP 5.0 (Almagro Armenteros et al., 2019), PSORTb (Yu et al., 2010), and CELLO (Yu et al., 2006). Prediction of lipoprotein signals, search of lipobox, plus identification of conserved sequences, motifs, and domains were made with LipoP Server (Juncker et al., 2003) and WebLogo (Schneider and Stephens, 1990; Crooks et al., 2004) using AliView (Larsson, 2014) and MAFFT (Katoh, 2002; Katoh and Standley, 2013; Katoh et al., 2019) as alignment tools.

Mobile Element Analysis and Horizontal Gene Transfer Prediction

Mobile genetic elements as insertion sequences in Acidithiobacillia genomes were predicted with ISsaga (Varani et al., 2011) of ISFINDER (Kichenaradja et al., 2010; Varani et al., 2011) and TnpPred (Riadi et al., 2012). Potential HGT events were predicted by HGTector (Zhu et al., 2014). Genes and pathways related to acid resistance were analyzed to identify mobile genetic elements as transposases, integrases, or phage elements in close genomic context using IslandViewer (Bertelli et al., 2017), Artemis (Carver et al., 2012), MAUVE (Darling et al., 2004, 2010), and STRING (von Mering et al., 2005; Szklarczyk et al., 2019).

Phylogenetic Tree Construction of Acid Resistance Genes

Trees of acid resistance proteins were constructed for proteins identified in the Acidithiobacillia class and orthologs from other microorganisms to propose a common or different evolutionary origin. Orthologous proteins from acid resistance genes were obtained by selection of best hits from BlastP comparison of Acidithiobacillia acid resistance genes versus the NCBI database. Phylogenies were constructed using acid resistance genes from

Acidithiobacillia plus orthologous proteins from NCBI, which were aligned with MAFFT using L-INS-i iterative refinement (Katoh, 2002; Katoh and Standley, 2013; Katoh et al., 2019) and IQ-TREE (Nguyen et al., 2015; Kalyaanamoorthy et al., 2017; Hoang et al., 2018) for prediction of best suited model and phylogenetic construction. Visualization of the trees was with Figtree[1] and iTOL6 (Letunic and Bork, 2021).

RESULTS AND DISCUSSION

General Features of Acidithiobacillia Pangenome

Thirty-seven Acidithiobacillia class genomes met the CheckM quality criteria while the pangenome analysis showed a core genome of 440 protein families (**Supplementary Data Sheet 1**). A maximum likelihood phylogenetic tree of Acidithiobacillia core concatenated proteins showed ten clades, separating the neutrophilic *T. tepidarius* from the acidophilic genera *Ambacidithiobacillus*, *Fervidacidithiobacillus*, and *Acidithiobacillus* (**Figure 1**). The acidophiles were further grouped into nine clades, of which two represented different genera (clades 2 and 3); meanwhile, clades 4–10 grouped species from the *Acidithiobacillus* genus, which is divided into clades according to their capacity to obtain energy such as sulfur oxidizers (clades 4 and 5) and iron/sulfur oxidizers (clades 6–10). While the association between the *Acidithiobacillaceae* and *Thermithiobacillaceae* families was consistent with previous analyses (Williams et al., 2010; Williams and Kelly, 2013; Boden et al., 2016; Moya-Beltrán et al., 2021), the tree also suggested a need for deeper phylogenomic analysis such as for the *Acidithiobacillus* clade, questioning if this clade includes more than a single genus according to their energy properties. Representative genomes from the ten clades of the core tree were selected for this study with their accession numbers and isolation data summarized in **Table 1**.

Acidithiobacillia Acid Resistance Mechanisms

Genes with predicted or experimental evidence for acid resistance mechanisms were searched in the Acidithiobacillia class using a bioinformatic pipeline (**Supplementary Figure 1**) that generated the list in **Supplementary Data Sheet 2**. The acid resistance genes were further labeled into first and second line of defense, according to the classification system proposed by the research of Vergara et al. (2020), which proposes that genes involved in the prevention of the entry of proton into the cell correspond to the "first line of defense," and those related to neutralization or expulsion of protons inside the cell belong to the "second line of defense."

First Line of Defense of Acidophilic Lifestyle in the Acidithiobacillia

Genes related to the first line of defense involved in the prevention of entry of protons into the cell, membrane rigidity, reduced membrane permeability to protons, and maintenance of cellular integrity are summarized in **Figure 2**.

The putrescine biosynthesis pathway was identified in the Acidithiobacillia class including genes *spe*A, *agu*A, and one or more copies of *agu*B (**Figure 3A**). Acidophilic genomes from the *Acidithiobacillaceae* family present several copies of *agu*B clustered in four clades *agu*B1–*agu*B4 (**Figure 3B**). The *agu*B1 and *agu*B3 clades associated *agu*B from acidophiles with the neutrophile *T. tepidarius* although the *agu*B3 genome context in the acidophiles displayed a cupin domain gene with high similarity to copies in the acidophiles *Acidocella* and *Acidiphilium*. In addition, *agu*B3 genes were predicted to result from HGT in the *Acidithiobacillus* genus. The clade of acidophile *agu*B2 genes were downstream from an *feo*ABC operon related to iron management (Osorio et al., 2008).

Putrescine is required for spermidine synthesis (**Figure 3A**), which protects the cell against acid stress by cytoplasmic buffering (Rhee et al., 2007; Kanjee and Houry, 2013; Vergara et al., 2020) such as in *F. caldus* (Mangold et al., 2013). S-adenosylmethionine decarboxylase (*spe*D) and spermidine synthase (*spe*E) are essential for the biosynthesis of spermidine (Xie et al., 1989), which are significantly upregulated in acidic environments (Li et al., 2012). This gene cluster was conserved in the Acidithiobacillia, separating into two clades between the neutrophile *T. tepidarius* and acidophiles of *Acidithiobacillaceae* with different genome contexts. The acidophile spermidine synthesis genes were downstream of *mla*DCEF (**Figure 4**); the latter acts as an ABC transporter driving translocation of phospholipids between the inner and outer membrane of Gram-negative bacteria (Hughes et al., 2019; Chi et al., 2020). The *mla*D outer membrane lipid and *mla*C phospholipid ABC transporter maintain outer membrane integrity in osmotic stress conditions in the halotolerant acidophile *Acidihalobacter prosperus* (Malinverni and Silhavy, 2009; Dopson et al., 2017; Khaleque et al., 2019). Phylogenetic analysis of concatenated *spe*D-*spe*E genes showed similarity to the extreme acidophile *Acidiferrobacter* (**Figure 4**). The close genomic context between *spe*DE and the *mla*DCEF gene complex observed in acidophiles highlights the relevance of these genes for membrane maintenance as a stress response.

An aquaporin AqpF was conserved in the *Ambacidithiobacillus* and *Acidithiobacillus* genera (**Supplementary Figure 2**), including three copies in *A. ferrivorans*. The aquaporin AqpF with an asparagine residue (Asn39) is proposed to be involved in enhancing the capability for proton-blocking in extreme acidophiles (Duarte et al., 2009). This difference was identified in the Acidithiobacillia where the AqpF in the neutrophiles *T. tepidarius* lacked this residue in contrast to AqpF in acidophiles *Am. sulfuriphilus* and *Acidithiobacillus* iron oxidizers. Aquaporin genes identified in *A. ferrianus* and *A. ferriphilus*-like presented signals of HGT events with the extreme acidophile *Acidihalobacter*-like as the potential donor.

Cell envelope *nlp*C, *oml*A, *omp*AT1, and *omp*AT2 genes were conserved in the Acidithiobacillia class with a single copy per genome that is upregulated in response to low pH conditions in *A. ferrooxidans* (Chao et al., 2008). The gene

[1]http://tree.bio.ed.ac.uk/software/figtree/

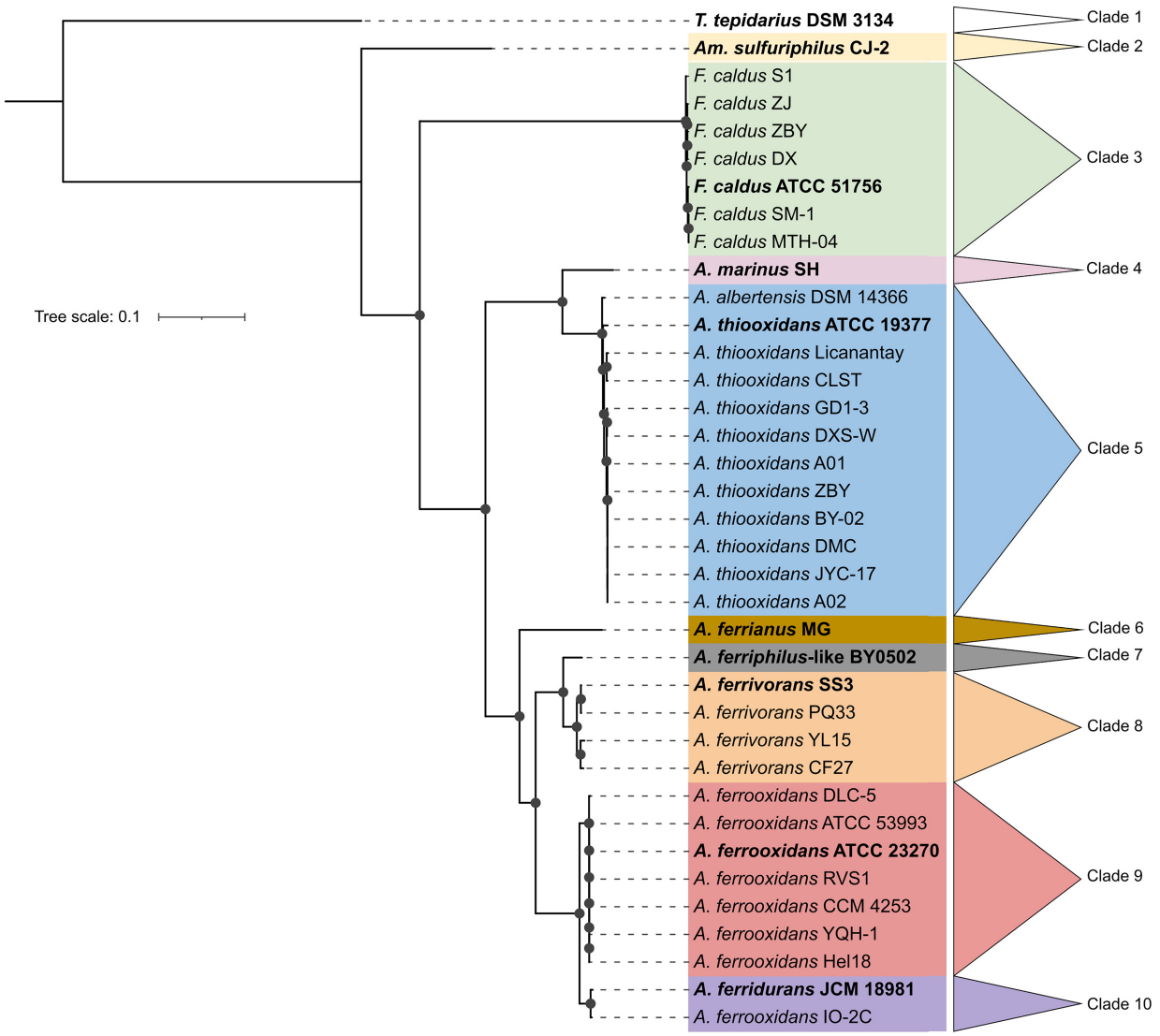

FIGURE 1 | Maximum likelihood phylogenetic tree showing the neutrophilic ancestral origins of the Acidithiobacillia class. The bold genomes were selected to represent the ten clades from Acidithiobacillia class core tree, including *T. tepidarius* DSM 3134 for the neutrophilic *Thermithiobacillus* genus and nine genomes for the acidophilic genera *Ambacidithiobacillus* (*Am.*), *Fervidacidithiobacillus* (*F.*), and *Acidithiobacillus* (*A.*). The tree was constructed using 440 conserved proteins using 1,000 replicates. Bootstraps values ≥60% are represented by black dots on the nodes. The scale bar represents 0.1 amino acid substitution per position.

*omp*40 was exclusively identified in acidophilic members of the Acidithiobacillia including three copies in *Am. sulfuriphilus* CJ-2. The Omp40 is a major outer membrane ion channel protein that increases in expression in response to low pH and phosphate starvation in *F. caldus* and *A. ferrooxidans* (Amaro et al., 1991; Mangold et al., 2013; Hu et al., 2020), suggesting that it controls proton influx across the outer membrane (Guiliani and Jerez, 2000; Baker-Austin and Dopson, 2007). A further cell envelope gene *slp* prevents the flux of organic acids across the outer membrane counteracting their toxic effect in acidophiles (Alexander et al., 1987; Mates et al., 2007; Vergara et al., 2020) and ameliorating low pH stress conditions in *Escherichia coli* (Mates et al., 2007). The *slp* genes contain a characteristic lipobox motif with an Asn amino acid residue in the +2 position, indicative that the protein is located at the inner membrane, and a different residue if Slp protein is exported (Zückert, 2014; Vergara et al., 2020). The *slp* gene was present in all Acidithiobacillia genomes (including several copies in some species; **Supplementary Figure 3A**) and was predicted to be exported. Phylogenetic analysis grouped *slp* into three clades (**Supplementary Figure 3B**) with the neutrophilic *slp* genes separated from those in the acidophile genomes.

Capsule polysaccharides constitute a mechanical defense layer (Feng et al., 2015) that acts as a protective barrier around the cell (Li et al., 2011), preventing influx of protons (Baker-Austin and Dopson, 2007; Mykytczuk et al., 2010) and other harmful external factors (Plante, 2000; Feng et al., 2015; Hu et al., 2020). The *A. thiooxidans* capsule became significantly

TABLE 1 | Strains, genome accession, and features of the selected representatives of the Acidithiobacillia class.

	Genome state and accession number	Source	Size (Mbp)	G+C (%)	#CDS	# contigs/# scaffolds	References
T. tepidarius 3134^T	Draft AUIS00000000	United Kingdom	2.96	66.8	2903	0/43	Boden et al., 2016
Am. sulfuriphilus CJ-2^T	Draft RIZI01000000	United Kingdom	2.82	61.5	2738	0/195	Falagán et al., 2019
F. caldus ATCC 51756^T	Complete CP005986	United Kingdom	2.78	61.7	2681	1/0	Valdes et al., 2009
Megaplasmid mpAca1.1	CP005987	United Kingdom	0.17	57.4	208	1/0	
Plasmid pACA1.1	CP005988	United Kingdom	0.03	59.4	33	1/0	
Plasmid pACA1.2	CP005989	United Kingdom	0.01	50.3	11	1/0	
A. marinus SH^T	Draft MXAV01000000	Japan	2.9	54.3	2828	0/65	Kamimura et al., 2018
A. thiooxidans ATCC 19377^T	Complete CP045571.1	United Kingdom	3.42	53	3388	1/0	[a], Valdes et al., 2011; Camacho et al., 2020
A. ferrianus MG^T	Draft WNJL01000000	Greece	3.17	58.2	3020	0/90	Norris et al., 2020
"*A. ferriphilus*-like BY0502" (formerly *A. ferrooxidans* BY0502)	Draft LVXZ01000000	China	2.98	56.8	2816	0/295	[b]
A. ferrivorans SS3	Complete CP002985	Russia	3.21	56.6	3093	1/0	Liljeqvist et al., 2011
A. ferridurans JCM 18981	Complete AP018795	Japan	2.92	58.4	3026	1/0	Miyauchi et al., 2018
A. ferrooxidans ATCC 23270^T	Complete CP001219	United States	2.98	58.8	3147	1/0	Valdés et al., 2008

[a] *Wang et al. unpublished. Acidithiobacillus thiooxidans genome sequencing and assembly. Submitted (OCT-2019) to EMBL/GenBank/DDBJ databases.*
[b] *Zhou et al. unpublished. Acidithiobacillus ferrooxidans genome sequencing and assembly. Submitted (APR-2016) to the EMBL/GenBank/DDBJ databases.*

thicker at the sub-optimal acid pH 0.8, and at super acid pH 0.4 began to fade, owing to that extreme acid stress became an unbearable threat to the cell survival (Feng et al., 2015, 2019). Three Acidithiobacillia capsule polysaccharide pathways were identified. These were the Lpt (Ma et al., 2008; Renzi et al., 2016), Wzy-dependent (Yuan et al., 2013; Barahona et al., 2014; Wen and Zhang, 2015; Renzi et al., 2016; Oetiker et al., 2018), and Kps (Barton, 2005; Vera et al., 2013; Nzakizwanayo et al., 2015) systems (**Figure 2**). The Lpt system was conserved in the Acidithiobacillia, with additional copies of the ABC transporter *msb*A in the *Acidithiobacillaceae* and absence of *lpt*D in the *A. ferriphilus*-like genome (probably due to its draft state). The *Acidithiobacillaceae* family encode genes for the Wzy system such as *wzx* for flippases that transport capsule polysaccharides across the cytoplasmic membrane along with the accessory genes *wzz*, *wza*, *wzb*, and *wba*P. The accessory genes *wzx, wzz*, and *wza* were predicted to result from HGT events from potential Proteobacteria, *Acidihalobacter*-like, and Bacteroidetes donors. The Kps system includes KfiC and KfiD required for polysaccharide biosynthesis and the export pathway consisting of the Wza integral outer membrane protein that acts in conjunction with KpsE to move polysaccharide between the KpsMT cytoplasmic membrane transporter and the outer membrane (Dong et al., 2006). The genes encoding polysaccharide biosynthesis and transport by the Kps system were identified in *F. caldus*, *A. thiooxidans*, *A. ferrianus* [absence of *kps*C encoding Kdo linker (Willis, 2013)], *A. ferridurans*, and *A. ferrooxidans*. Analysis of HGT events suggested that the Kps system was from donor acidophiles, such as *kps*E, *wza*, and *kps*S genes from *Acidihalobacter*-like (Khaleque et al., 2019, 2020); *kfi*C and *kps*T from *Acidiferrobacter*-like (Issotta et al., 2018); plus *kfi*D, *kps*M, and *kps*C from Proteobacteria. Finally, the capsule formation systems Wzy and Kps were exclusively identified in *Acidithiobacillaceae* acidophiles and presented signals of HGT events from other extreme acidophiles.

An inside positive membrane potential (Baker-Austin and Dopson, 2007; Vergara et al., 2020) suppresses the inflow of protons by creation of a chemical permeation barrier (Hu et al., 2020) and is suggested to be generated by potassium ions accumulated by Trk, Kch, Kup, and Kdo potassium channel proteins (Cholo et al., 2015; Buetti-Dinh et al., 2016; Christel et al., 2018; Wang et al., 2019). While the neutrophile *T. tepidarius* contained *trk*AH genes for TrK activity (**Supplementary Figure 4**), one or more of these genes were disrupted in the acidophiles *A. marinus* SH and *A. thiooxidans*. The disrupted *A. thiooxidans trk*AH genes were preceded by a NhaP antiporter and surrounded by mobile genetic elements, suggesting that they were gained by HGT events. The gene encoding NhaP antiporter, denominated *nha*P-K^+, was classified within the first line of defense as it was in a cluster with a TrK system, suggesting a relation to potassium transport. The TrK system is a rapid-transport system at neutral or alkaline pH (Bossemeyer et al., 1989; Trchounian and Kobayashi, 2000; Epstein, 2003; Su et al., 2009) corresponding with its presence in *T. tepidarius*. Despite the disruption of the TrK system in acidophiles, the *Acidithiobacillaceae* contain three potassium transport systems that were not identified in the closest neutrophile. These were Kup (Trchounian and Kobayashi, 1999, 2000; Zakharyan and Trchounian, 2001; You et al., 2011), Kch (Voges and Jap, 1998; Munsey et al., 2002), and Kdp (Gassel et al., 1998; Yan et al., 2011; Cholo et al., 2015). The presence of three potassium transport systems in extreme acidophiles can be explained by the need to induce K^+ uptake genes at different pH. An example is *E. coli* where the K^+ transport TrK system is the most powerful system for K^+ accumulation upon hyper-osmotic stress at neutral pH (Bossemeyer et al., 1989; Trchounian and Kobayashi, 2000; Epstein, 2003; Su et al., 2009; Yan et al., 2011) that is downregulated at low pH and Kup acts to compensate (Trchounian and Kobayashi, 1999; Yan et al., 2011), highlighting

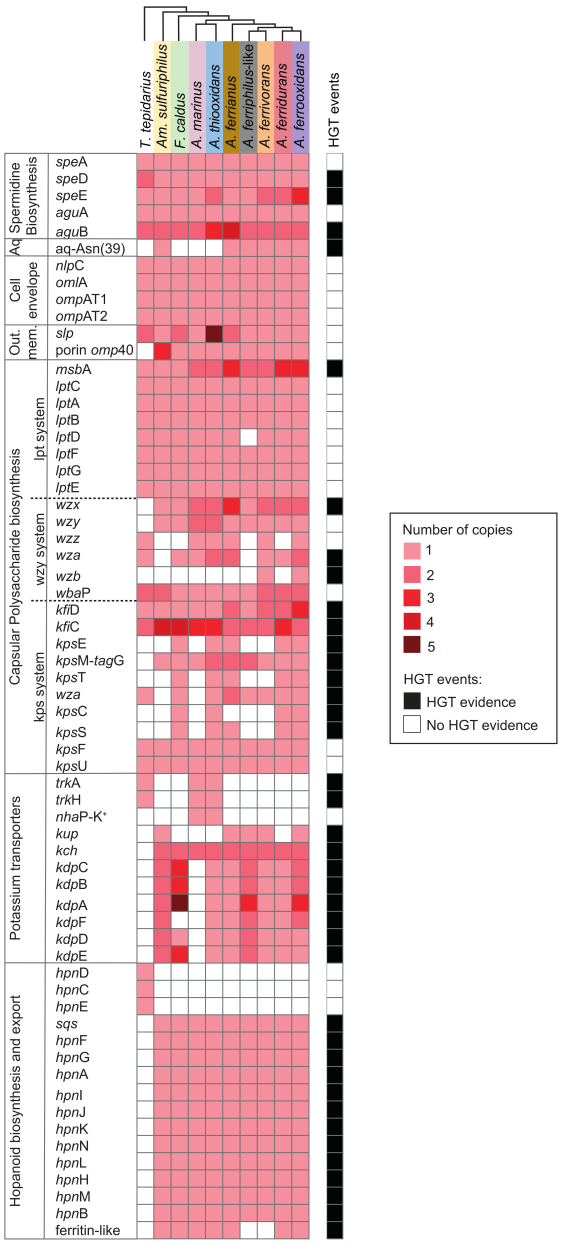

FIGURE 2 | Heatmap of presence (red) and absence (white) of genes involved in the first line of Acidithiobacillia class acid resistance including spermidine biosynthesis; aquaporine (Aq) with an asparagine residue (Asn39); cell envelope; outer membrane proteins (Out. mem.); capsular polysaccharide biosynthesis with pathways Lpt-, Wzy-, and Kps-systems; potassium transporters; and hopanoid biosynthesis plus export. The color intensity represents higher gene copy number per genome. The presence of genes (black; right-hand side) denotes HGT events by genome context with mobile genetic elements, phylogenetic trees, or if it was signaled as part of an HGT event by HGTector (Zhu et al., 2014). *T. tepidarius*, *Thermithiobacillus tepidarius* DSM 3134; *Am. Sulfuriphilus*, *Ambacidithiobacillus sulfuriphilus* CJ-2; *F. caldus*, *Fervidacidithiobacillus caldus* ATCC 51756; *A. marinus*, *Acidithiobacillus marinus* SH; *A. thiooxidans*, *A. thiooxidans* ATCC 19377; *A. ferrianus*, *A. ferrianus* MG; *A. ferriphilus*-like, *A. ferriphilus*-like BY0502; *A. ferrivorans*, *A. ferrivorans* SS3; *A. ferridurans*, *A. ferridurans* JCM 18981; and *A. ferrooxidans*, *A. ferrooxidans* ATCC 23270 (shaded colors correspond to those used in **Figure 1**).

the role of different K^+ uptake according to pH environment (Trchounian and Kobayashi, 1999; Yan et al., 2011). Phylogenetic analysis confirmed the similarity of Kup and Kch (**Figure 5**) to other extreme acidophiles such as *Acidiferrobacter* (Issotta et al., 2018), *Methylacidimicrobium* (van Teeseling et al., 2014), *Verrucomicrobium* (Schmitz et al., 2021), *Leptospirillum* (Vergara et al., 2020), and *Acidiphilium* (Li et al., 2020). This similarity was supported by HGTector prediction that suggested that Kup and Kch were transferred from Gammaproteobacteria and the acidophile *Acidihalobacter*-like. The Kup system was identified in *Am. sulfuriphilus* CJ-2 and the *Acidithiobacillus* iron oxidizers with the exception of *A. ferridurans* (**Figure 5A**). The Kch voltage-gated potassium channel was coded by two gene copies, *kch*1 and *kch*2, which were conserved in the *Acidithiobacillaceae* (**Supplementary Figure 5**). These gene copies had the highest similarity to homologs in the extreme acidophiles *Leptospirillum*, *Acidiphilium*, *Acidihalobacter*, and *Acidiferrobacter* (**Figure 5B**). The Kdp is a complex of four inner membrane subunits KdpF, KdpA, KdpB, and kdpC, with a KdpD sensor kinase and KdpE response regulator (Gassel et al., 1998) that are upregulated at low extracellular pH as a survival strategy for *Mycobacterium tuberculosis* (Cholo et al., 2015). The genes coding for the Kdp complex and regulatory proteins were identified exclusively in acidophiles from the class with three forms according to the gene contexts (**Supplementary Figure 6**). These were (i) the *kdp*CBAFED cluster conserved in *Acidithiobacillaceae* genomes except *A. marinus* SH that lacked a complete system and *Am. sulfuriphilus* with *kdp*DE genes disrupted by transposases; (ii) a second copy of the *kdp*CBAFED cluster in *Am. sulfuriphilus* and *A. ferriphilus*-like, a *kdp*ABC cluster in *F. caldus*, and *kdp*FABC in *A. ferrooxidans*; and (iii) a *kdp*ABCE gene cluster in the *F. caldus* plasmid. Mobile genetic elements were identified in the genome context of three forms of Kdp systems and BLAST analysis of Kdp encoding genes showed similarity to acidophile *Acidiferrobacter*, suggesting that the Kdp complex could be the result of an HGT event from *Acidiferrobacter*-like to *Acidithiobacillaceae* acidophiles as a mechanism to uptake potassium ions and thus improve acid resistance.

Comparative genomic analysis also revealed major differences between the hopanoid biosynthesis pathways of Acidithiobacillia and neutrophiles. Hopanoid biosynthesis regulates membrane fluidity, maintaining membrane integrity and permeability of cells and promoting resistance to antibiotics, detergents, extreme pH, high osmolarity (Welander et al., 2009; Wu et al., 2015), and surviving general environmental stressors such as in the cyanobacterium genus *Nostoc* (Ricci et al., 2017; Mayer et al., 2021). The neutrophile *T. tepidarius* synthesizes squalene *via* the *hpn*CDE gene products compared to the one step through *sqs* gene product in the acidophiles (**Figure 6**). A further hopanoid cluster was conserved in the *Acidithiobacillaceae*, including the *hpn*ABFGHIJKLMN genes conferring the ability to produce several hopanoids such as bacteriohopanetetrol (BHT), cyclitol, and hopan-22-ol. This was consistent with *A. thiooxidans* as a source of bacteriohopanepolyols (BHPs) including BHT, aminotriol, and BHT cyclitol ether (Jones et al., 2012) and the Acidithiobacillales for BHT cyclitol

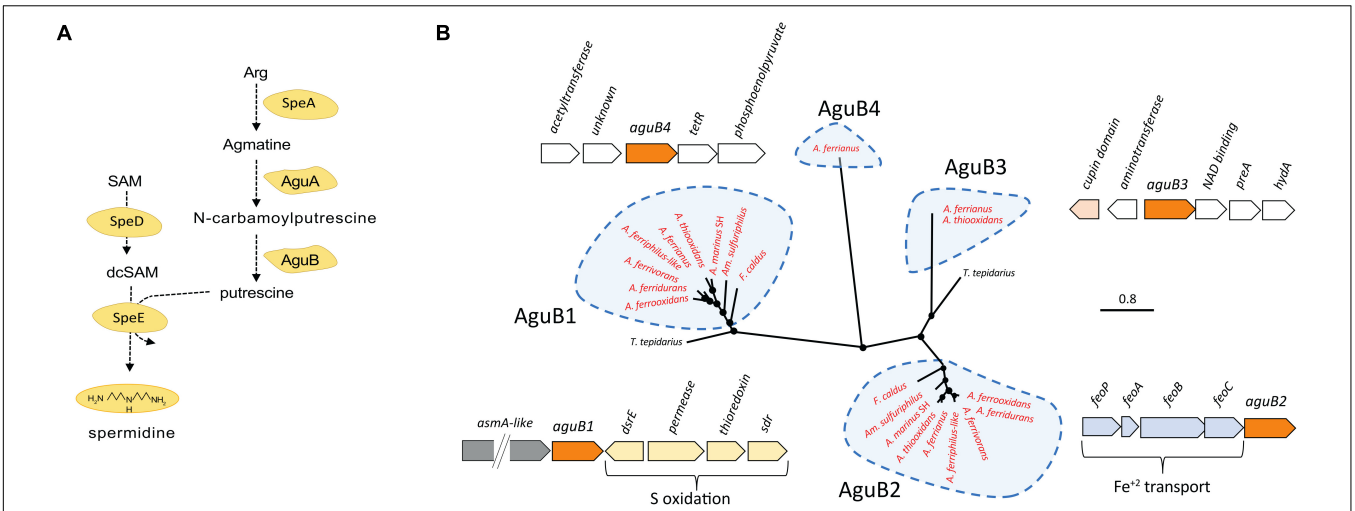

FIGURE 3 | (A) Putrescine and spermidine biosynthesis pathway. **(B)** Unrooted phylogenetic tree of Acidithiobacillia class *agu*B amino acid sequences and their best hits in the NCBI databases plus their genomic context in the *Acidithiobacillaceae* (*agu*B in orange color). Sequences of *agu*B group in four clades denominated *agu*B1–*agu*B4. Acidophilic sequences are highlighted in red. Filled circles at the nodes indicate bootstrap support ≥60%. The scale bar represents 0.8 amino acid substitution per site.

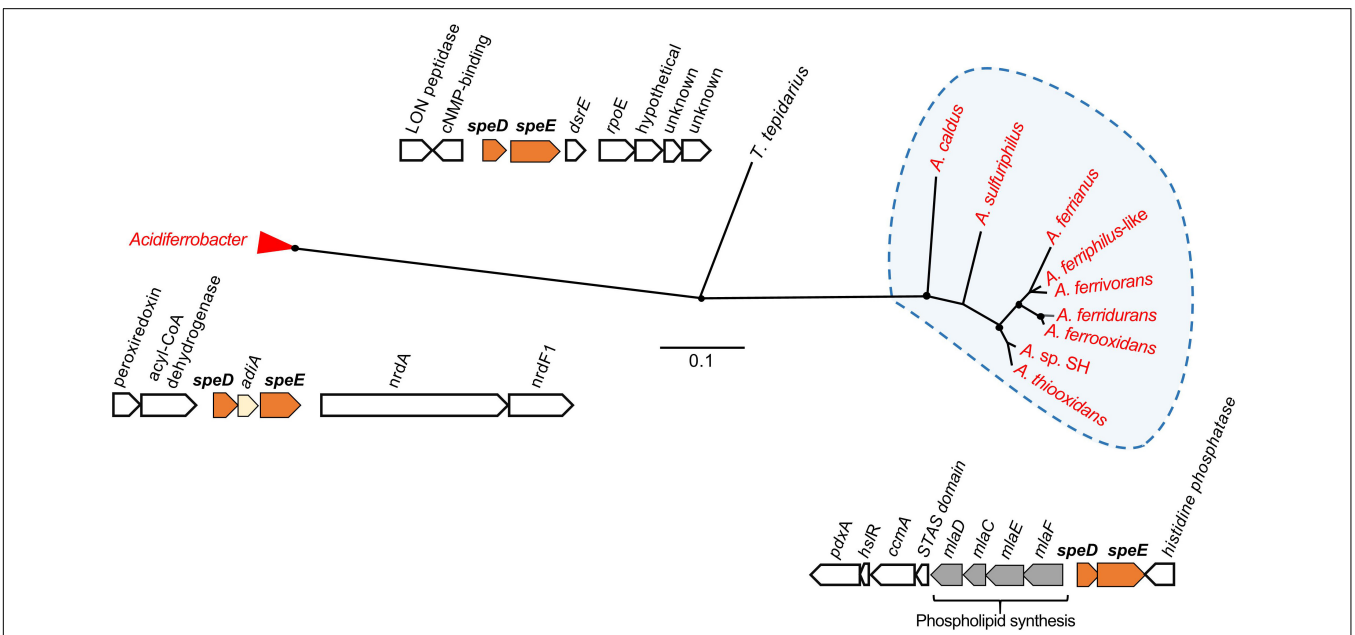

FIGURE 4 | Unrooted phylogenetic tree of concatenated amino acid sequences of *spe*D and *spe*E in the Acidithiobacillia and their best hits in the NCBI databases. *Acidithiobacillaceae* sequences group in a clade from neutrophilic *T. tepidarius*, and had highest similarity to homologs in extreme acidophiles of the *Acidiferrobacter* group. Acidophilic sequences are highlighted in red. Filled circles at the nodes indicate bootstrap support ≥60%. The scale bar represents 0.1 amino acid substitution per site.

ether, aminotriol, BHT, and adenosylhopane at geothermal vents (Gibson et al., 2014). RNA transcripts confirmed the expression and functionality of *sqs* gene in *A. ferrivorans* (Christel et al., 2016). Phylogenomic analysis of the *hpn* cluster showed similarity with *hpn* from the acidophile *Acidiferrobacter* sp. SPIII (**Supplementary Figure 7**), highlighting the role of this pathway for extreme acidophiles.

Second Line of Defense in Acidithiobacillia

The second line of defense includes genes coding for proton export from the cell (**Figure 7**). Phosphorus is of utmost importance for living organisms (Li et al., 2011) and may also ameliorate low pH stress *via* cytoplasmic buffering of protons (Baker-Austin and Dopson, 2007; Chen L. et al.,

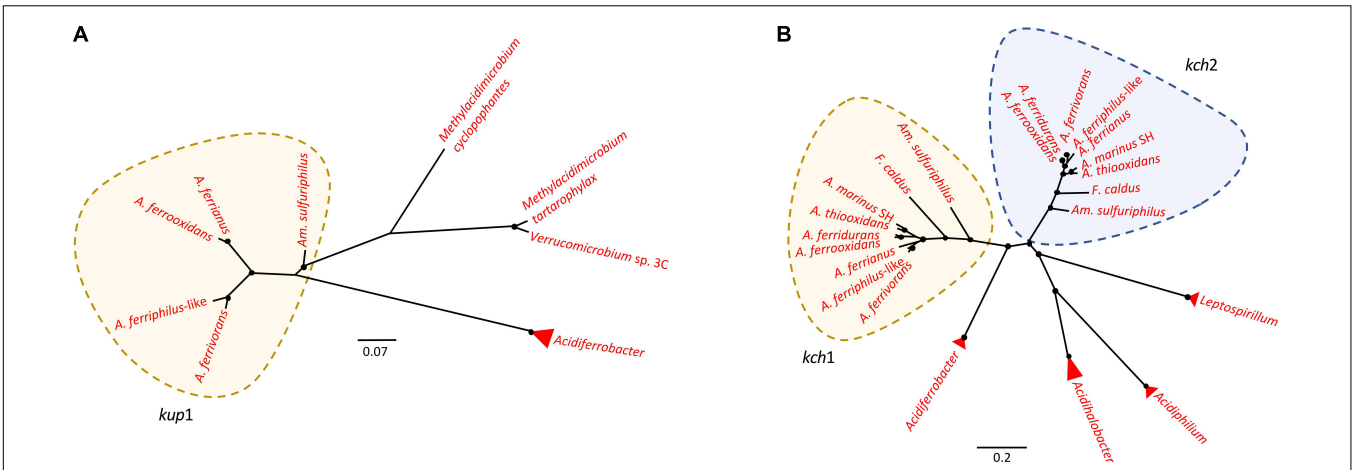

FIGURE 5 | Unrooted phylogenetic tree of potassium transporters in Acidithiobacillia and their best hits in NCBI. **(A)** *kup* gene coding for Kup system had the highest similarity to homologs in extreme acidophiles *Acidiferrobacter*, *Methylacidimicrobium*, and *Verrucomicrobium*. **(B)** *kch* coding for Kch system had the highest similarity to Kch homologs in acidophiles *Leptospirillum*, *Acidiphilium*, *Acidihalobacter*, and *Acidiferrobacter*. Acidophilic sequences are highlighted in red. Filled circles at nodes represent bootstrap support of ≥60%. The scale bar represents amino acid substitution per site.

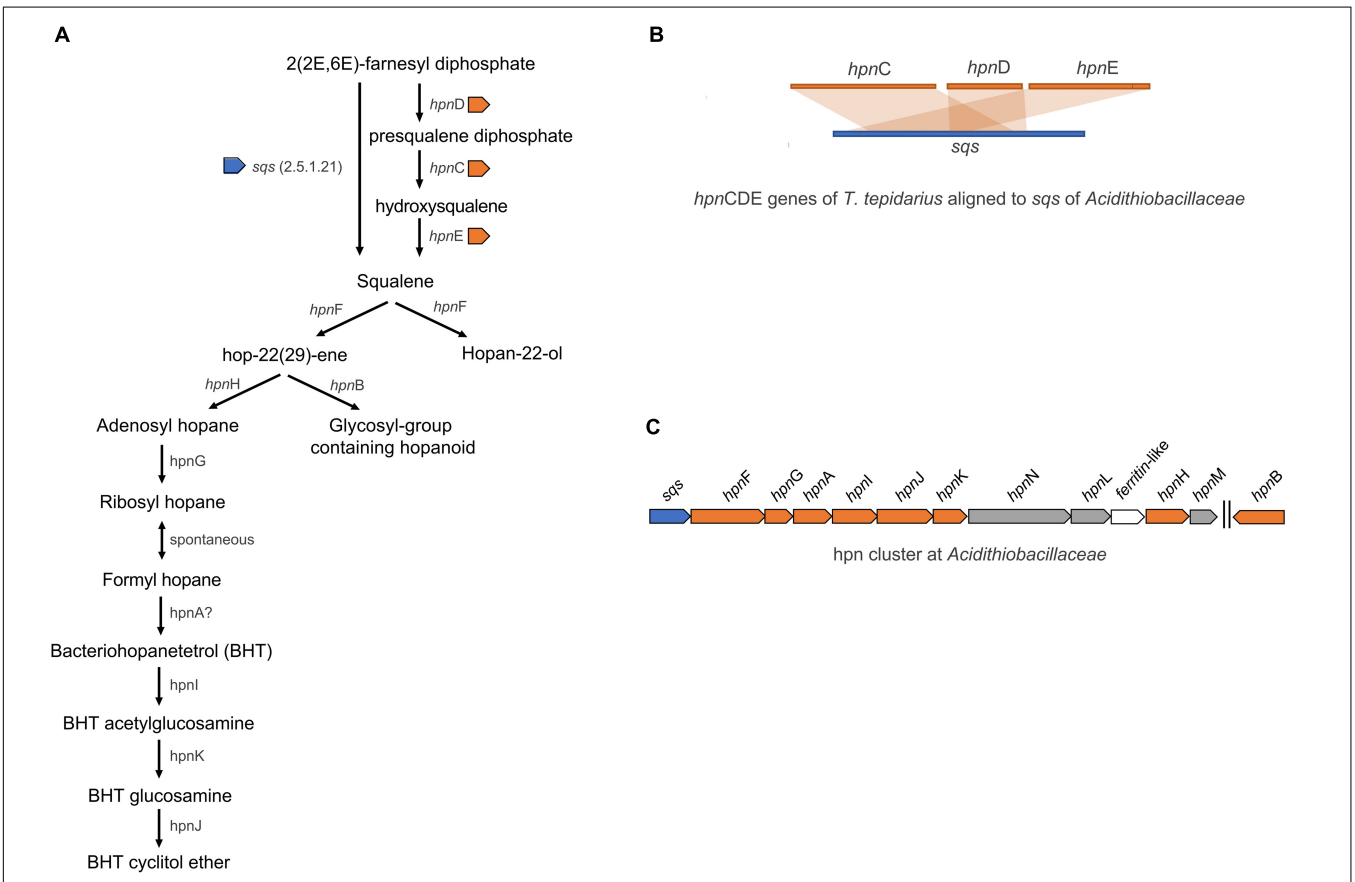

FIGURE 6 | (A) Hopanoid biosynthesis in *Acidithiobacillaceae*. **(B)** Biosynthesis of squalene, that is required for hopanoid, is synthetized by *sqs* in acidophiles in contrast to *hpn*CDE in the neutrophile *T. tepidarius*. **(C)** The *hpn* cluster was identified in *Acidithiobacillaceae* including sqs-*hpn*FGAIJKNL-*ferritin-hpn*HM genes.

2015). The phosphate transport system genes *pst*SCAB are abundant in acidophilic *Acidithiobacillus*, *Leptospirillum*, and *Acidiphilium* taxa in acid mine drainage (Chen L. et al., 2015). A complete repertoire of phosphate uptake genes was identified in the Acidithiobacillia class including the two-component regulatory proteins PhoB/PhoR, Pst-transport system PstSCAB

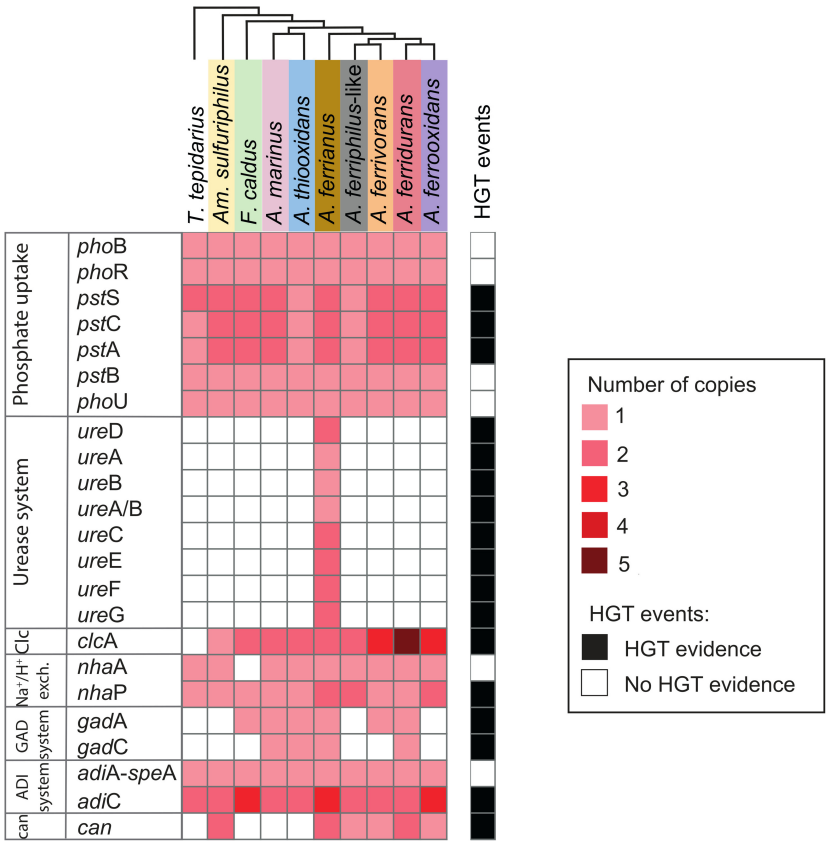

FIGURE 7 | Heatmap of presence (red) and absence (white) of genes involved in second line of defense acid resistance in the Acidithiobacillia class. The red color intensity represents gene copy number per genome. The presence of genes (black; right-hand side) denotes HGT events by genome context with mobile genetic elements, phylogenetic trees, or if it was signaled as part of HGT event by HGTector (Zhu et al., 2014). Species abbreviations are as described in the **Figure 3** legend. Second line of acid resistance genes include phosphate uptake, urease system, ClcA antiporter (Clc), proton antiporter (Na^+/H^+ exch.), amino acid decarboxylation (GAD and ADI systems), and carbonic anhydrase (can) (shaded colors correspond to those used in **Figure 1**).

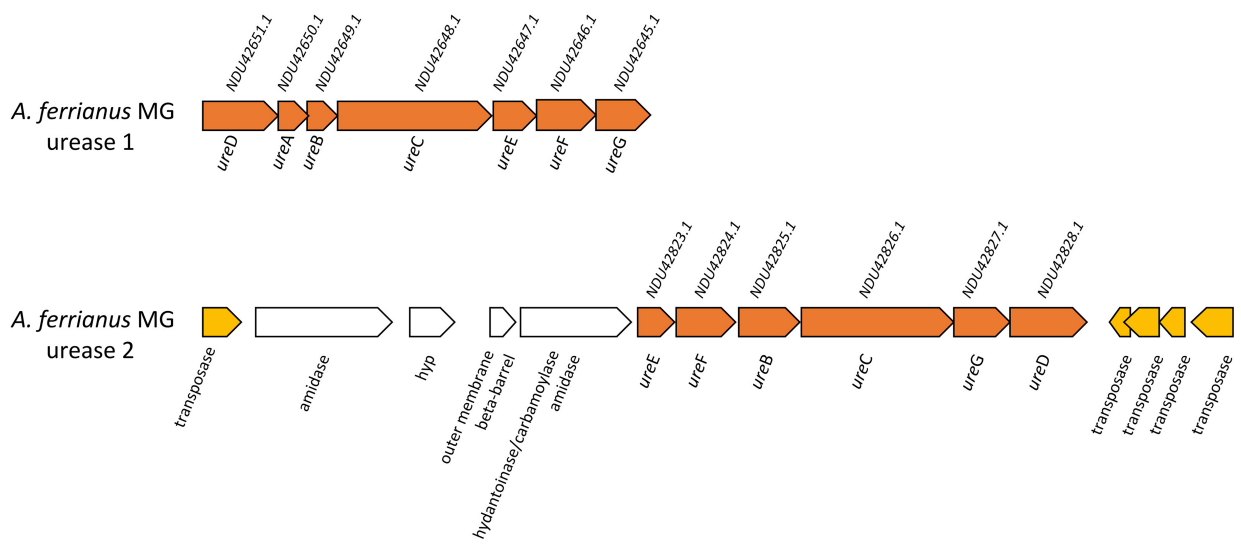

FIGURE 8 | Genetic organization of urease 1 and urease 2 system in *A. ferrianus* MG. Genome context of urease 1 and extended urease 2 in *A. ferrianus* MG formed by *ure*ABCDEFG (orange) with their corresponding accession numbers. Mobile genetic elements are highlighted by yellow arrows.

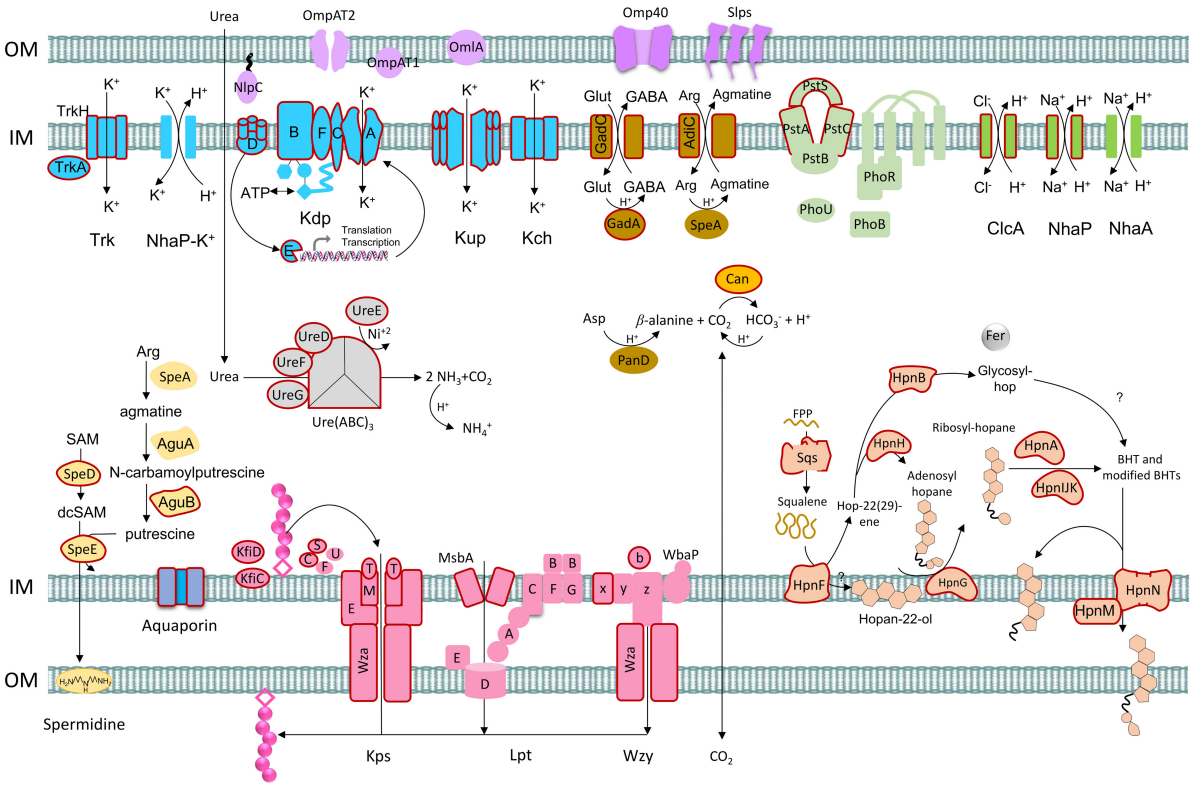

FIGURE 9 | Model of acid resistance genes and mechanisms in acidophiles from the *Acidithiobacillaceae* including first and second lines of defense. Gene gain events proposed by HGT are represented with outline colors in red according to phylogenetic/phylogenomic and prediction (Zhu et al., 2014) analysis.

(Valdés et al., 2008), and auxiliary PhoU (Vuppada et al., 2018). The *Acidithiobacillaceae* genomes maintained two copies of the *pst*SCA gene cluster except *A. thiooxidans* and *A. ferriphilus*-like BY0502. HGT event signals were identified for *pst*SCA genes in *A. ferriphilus*-like BY0502 from a Bacteria donor.

The urease complex can act as buffering capacity of the intracellular pH using ammonia derived from urea hydrolysis such in *Ferrovum* group 2 strains (Ullrich et al., 2016a). The role of urease in pH homeostasis has been shown for *Helicobacter pylori* during gastric colonization (Scott et al., 1998; Stingl et al., 2002; Schoep et al., 2010) and suggested for "*Ferrovum*" strain JA12 (Ullrich et al., 2016b) and *Thiomonas* sp. CB2 (Farasin et al., 2015). The three sub-unit cytoplasmic apoenzyme urease (UreABC) synthesizes CO_2 and NH_3 from urea, interacting with UreDFG and UreE (Carter et al., 2009). Urease complexes were found in *A. ferrianus* MG (**Figure 8**) encoded by *ure*DABCEFG (urease 1) and *ure*EF(A/B)CGD (urease 2) where *ure*A and *ure*B genes were fused in a single gene denominated *ure*(A/B) as identified in *H. pylori* (Voland et al., 2003). A manual curation of genomic context of urease 2 displayed closeness with transposase elements that suggested an origin by HGT event, which was confirmed by HGTector displaying transfer of *ure*F(A/B)CG genes from Proteobacteria donors. HGT signal events were also identified for all urease 1 complex genes that were associated with Bacteria and Cyanobacteria donors. Other urease clusters, with the same gene distribution as urease 1, were identified in other *Acidithiobacillaceae* species including *A. ferrooxidans* IO-2C (new proposed annotation *A. ferridurans*), *F. caldus* BC13, and *A. ferriphilus* DSM 100412 (**Supplementary Figure 8**).

The Cl^-/H^+ antiporter ClcA prevents inner-membrane hyperpolarization at extreme acidic pH in *E. coli* (Richard and Foster, 2004) and *Bacillus coagulans* (McLaggan et al., 1990). This antiporter was gained by the extreme acidophile *Leptospirillum* as demonstrated by remaining mobile elements (Vergara et al., 2020). The acidophilic *Acidithiobacillaceae* contained two contiguous *clc*A genes with the exception of *A. ferrianus* where the genes were present in separate genomic regions (different contigs) and *Am. sulfuriphilus* that only had a single copy. In addition, the iron oxidizing species *A. ferrivorans*, *A. ferrooxidans*, and *A. ferridurans* contained more than two copies in their genomes. Phylogenetic trees indicated an association of *Acidithiobacillaceae* ClcA with other extreme acidophiles (**Supplementary Figure 9**) such as *Acidihalobacter prosperus*, *Ac. ferrooxydans* (Khaleque et al., 2019), *Ac. yilgarnensis* (Khaleque et al., 2020), *Thermodesulfobium acidiphilum* (Frolov et al., 2017), and *Sulfolobus acidocaldarius* (Chen et al., 2005). In addition, HGTector predicted an HGT signal from Bacteria, Proteobacteria, and acidophilic *Ferrovum*-like donors. The neutrophilic *T. tepidarius* lacked the *clc*A antiporter, which agreed with Vergara et al. (2020) who suggested that *clc*A could be gained by HGT events as a mechanism to resist extreme acid environments. A proton

antiporter NhaA was identified in *T. tepidarius* and the *Acidithiobacillaceae* with the exception of *F. caldus*, which was suggested to have lost this gene according to MAUVE synteny analysis. A second proton antiporter, NhaP, was identified in the Acidithiobacillia class with additional copies in the acidophiles *A. ferrianus*, *A. ferriphilus*-like, and *A. ferrooxidans*. Finally, both *nha*P genes from *A. ferriphilus*-like were from HGT events with possible Bacteria and *Ferrovum*-like donors.

Amino acid decarboxylation systems such as glutamic acid-dependent acid resistance (GDAR) catalyze proton consumption. These systems consist of glutamic acid decarboxylases GadA/GadB enzymes and the glutamate/γ-aminobutyric acid (GABA) antiporter GadC while the arginine-dependent acid resistance (ADAR) system involves arginine decarboxylase AdiA and the arginine/agmatine antiporter AdiC (Foster, 2004; Kanjee and Houry, 2013). The GAD system encoded by *gad*A and *gad*C was identified in *A. marinus* SH, *A. thiooxidans*, *A. ferrianus*, and *A. ferridurans*. Phylogenetic analysis of GadA showed a clade of *Acidithiobacillaceae* genes sharing a common ancestor with *Acidihalobacter* acidophiles (**Supplementary Figure 10**), which was supported by the prediction of an HGT event from Gammaproteobacteria to *Acidithiobacillaceae* for *gad*C in *A. marinus* and *A. ferridurans*, and the presence of a mobile genetic elements (MGE) upstream of *gad*C in *A. ferrianus*. These results suggested that the GAD system was gained by acidophiles by obtention of decarboxylase GadA and amino acid permease GadC. Analysis revealed that the *F. caldus* and *A. ferrivorans* genomes only encoded *gad*A and they lacked the *gad*C antiporter (Mangold et al., 2011). However, it is proposed that the decarboxylated GABA product from glutamate decarboxylation might be retained in the cell where it can be incorporated into the TCA cycle (Karatzas et al., 2010; Feehily and Karatzas, 2013; Sriaporn et al., 2021). Even though a complete glutamate decarboxylase exporting system was not identified, previous studies have shown that amino acid decarboxylation is highly expressed in *F. caldus* under acid stress conditions (Mangold et al., 2013; Sriaporn et al., 2021). The *adi*A gene contained the domain *spe*A that also participates in putrescine synthesis and explains why this gene is associated with both pathways (*adi*A-*spe*A; **Figure 7**). The ADAR system was identified in both Acidithiobacillia neutrophiles and acidophiles with a single gene encoding arginine-decarboxylate AdiA and amino acid permease AdiC. However, *F. caldus*, *A. ferrianus*, and *A. ferrooxidans* had three copies of *adi*C. Finally, *adi*C genes were suggested to be acquired by HGT transfer from Proteobacteria and *Acidiferrobacter*-like donors that suggested an evolutionary gain event for acidophiles.

Carbonic anhydrase (*can*) aids pH homeostasis by catalyzing the interconversion of CO_2 to HCO_3^- (Bury-Moné et al., 2008; Valdés et al., 2008; Frost and Mckenna, 2014; Ansari and Yamaoka, 2017; Hu et al., 2020) and was identified in acidophilic microorganisms such as *Leptospirillum*, *Ferrovum* spp., *S. thermosulfidooxidans*, and *Sulfobacillus* sp. (Ullrich et al., 2016a,b; Zhang et al., 2017; Hu et al., 2020). Depending on the direction of reaction, the β-carbonic anhydrase may prevent cytoplasmic acidification by breakdown of HCO_3^- (consuming H^+) or conversion of CO_2 to HCO_3^- for carbon fixation (Lehtovirta-Morley et al., 2016). A cytoplasmic carbonic anhydrase of the β-class clade B (Valdés et al., 2008; Esparza et al., 2019) was identified in *Am. sulfuriphilus* and iron oxidizer genomes with two copies in *Am. sulfuriphilus, A. ferrianus*, and *A. ferridurans.* The additional copy of *can* in the *A. ferridurans* genome was proposed to result from a transfer event from a Bacteria donor according to HGTector. This concept was reinforced by interpretation of phylogenetic trees (clade *can*1–*can*2, **Supplementary Figure 11**) displaying similarity of Can from *A. ferrianus* and *Am. sulfuriphilus* with acidophiles *Acidihalobacter* and *Sulfobacillus*. Finally, a truncated *can* was found in the neutrophile *T. tepidarius*. However, its activity needs to be experimentally investigated.

Model of *Acidithiobacillaceae* Acid Resistance

The model proposes the transition of a neutrophilic Acidithiobacillia ancestor to the extremely acidophilic *Acidithiobacillaceae* family by reinforcing the outer membrane and generating a positive membrane potential to restrict the influx of protons into the cytoplasm (**Figure 9**). Three mechanisms were exclusively identified in extreme *Acidithiobacillaceae* acidophiles, namely, (i) capsular biosynthesis pathways, (ii) influx of potassium ions, and (iii) hopanoid biosynthesis. NhaP, Kup, Kch, and Kdp were identified in acidophiles generating a transmembrane electrical potential and redundancy of genes for potassium influx. The presence of *sqs* gene in *Acidithiobacillaceae* coding for squalene biosynthesis in a single reaction (as compared with the three reactions in *T. tepidarius*) may also represent an important evolutionary energetic advantage for hopanoid biosynthesis, which, along with the *hpn*FGAIJKNLHM gene cluster, allows to synthetize and modify hopanoids. The second line in *Acidithiobacillaceae* presented a pool of accessory genes for buffering of intracellular pH, including decarboxylation of glutamate, urea hydrolysis, and hydration of CO_2, and antiporters export excess protons by coupling the uptake of Na^+ (Chen et al., 2021). This functional redundancy may represent a key strategy for acidophiles to live across different pH ranges and "hedge bet" in rapidly changing acidic environments, where it is hypothesized that the cost of maintaining genetic redundancy is offset by the ability to expeditiously adjust to environmental fluxes.

CONCLUSION

The core genome phylogenomic and acid resistance protein phylogenetic trees confirmed the transition across the Acidithiobacillia class from an ancestral neutrophile to an extreme acidophile (Williams et al., 2010; Williams and Kelly, 2013; González et al., 2016). Acidithiobacillia acid resistance genes were classified into first and second lines of defense, where most were identified in the extremely acidophilic *Acidithiobacillaceae* family. The analysis suggested that whereas a major fraction of genes involved in acid resistance were inherited vertically, genome reprograming including duplication, gain by

HGT from extreme acidophiles, and mutation of genes played a role in the evolution of the acidophilic lifestyle. Especially prominent in our analysis was the prediction of a large number of HGT events from other extreme acidophiles, suggesting that this mode of gene acquisition played a major role in the evolution of an inferred neutrophilic ancestor into a clade of extreme acidophiles.

DATA AVAILABILITY STATEMENT

The original contributions presented in the study are included in the article/**Supplementary Material**, further inquiries can be directed to the corresponding author.

AUTHOR CONTRIBUTIONS

DH and JV conceived and designed the research. CG-R performed the research. CG-R, EV, MD, JV, and DH analyzed the data. All authors participated in the writing and approval of the final manuscript.

FUNDING

This work was supported by the ANID FONDECYT 3190792 (CG-R), FONDECYT 1181717 (DH), Centro Ciencia & Vida, and FB210008 Financiamiento Basal para Centros Científicos y Tecnológicos de Excelencia de ANID.

SUPPLEMENTARY MATERIAL

The Supplementary Material for this article can be found online at: https://www.frontiersin.org/articles/10.3389/fmicb.2021.822229/full#supplementary-material

Supplementary Data Sheet 1 | List of conserved core genes in Acidithiobacillia class.

Supplementary Data Sheet 2 | List of genes involved into first and second line of defense acid resistance in the Acidithiobacillia class.

Supplementary Image 1 | Supplementary figures.

REFERENCES

Alexander, B., Leach, S., and Ingledew, W. J. (1987). The relationship between chemiosmotic parameters and sensitivity to anions and organic acids in the acidophile *Thiobacillus ferrooxidans*. *Microbiology* 133, 1171–1179. doi: 10.1099/00221287-133-5-1171

Almagro Armenteros, J. J., Tsirigos, K. D., Sønderby, C. K., Petersen, T. N., Winther, O., Brunak, S., et al. (2019). SignalP 5.0 improves signal peptide predictions using deep neural networks. *Nat. Biotechnol.* 37, 420–423. doi: 10.1038/s41587-019-0036-z

Altschul, S. (1997). Gapped BLAST and PSI-BLAST: a new generation of protein database search programs. *Nucleic Acids Res.* 25, 3389–3402. doi: 10.1093/nar/25.17.3389

Altschul, S. F., Gish, W., Miller, W., Myers, E. W., and Lipman, D. J. (1990). Basic local alignment search tool. *J. Mol. Biol.* 215, 403–410. doi: 10.1016/S0022-2836(05)80360-2

Amaro, A. M., Chamorro, D., Seeger, M., Arredondo, R., Peirano, I., and Jerez, C. A. (1991). Effect of external pH perturbations on in vivo protein synthesis by the acidophilic bacterium *Thiobacillus ferrooxidans*. *J. Bacteriol.* 173, 910–915. doi: 10.1128/jb.173.2.910-915.1991

Ansari, S., and Yamaoka, Y. (2017). Survival of *Helicobacter* pylori in gastric acidic territory. *Helicobacter* 22:12386. doi: 10.1111/hel.12386

Baker-Austin, C., and Dopson, M. (2007). Life in acid: pH homeostasis in acidophiles. *Trends Microbiol.* 15, 165–171. doi: 10.1016/j.tim.2007.02.005

Barahona, S., Dorador, C., Zhang, R., Aguilar, P., Sand, W., Vera, M., et al. (2014). Isolation and characterization of a novel *Acidithiobacillus ferrivorans* strain from the Chilean Altiplano: attachment and biofilm formation on pyrite at low temperature. *Res. Microbiol.* 165, 782–793. doi: 10.1016/j.resmic.2014.07.015

Barton, L. L. (ed.) (2005). "Capsules, pili, and internal structures," in *Structural and Functional Relationships in Prokaryotes*, (New York, NY: Springer), 190–233. doi: 10.1007/0-387-27125-2_5

Bertelli, C., Laird, M. R., Williams, K. P., Fraser University Research Computing Group, Lau, B. Y., Hoad, G., et al. (2017). Island viewer 4: expanded prediction of genomic islands for larger-scale datasets. *Nucleic Acids Res.* 45, W30–W35. doi: 10.1093/nar/gkx343

Boden, R., Hutt, L. P., Huntemann, M., Clum, A., Pillay, M., Palaniappan, K., et al. (2016). Permanent draft genome of *Thermithiobacillus tepidarius* DSM 3134^{T}, a moderately thermophilic, obligately chemolithoautotrophic member of the acidithiobacillia. *Stand. Genomic Sci.* 11:74. doi: 10.1186/s40793-016-0188-0

Bossemeyer, D., Borchard, A., Dosch, D. C., Helmer, G. C., Epstein, W., Booth, I. R., et al. (1989). K^{+}-transport protein TrkA of *Escherichia coli* is a peripheral membrane protein that requires other trk gene products for attachment to the cytoplasmic membrane. *J. Biol. Chem.* 264, 16403–16410.

Bryant, R. D., McGroarty, K. M., Costerton, J. W., and Laishley, E. J. (1983). Isolation and characterization of a new acidophilic *Thiobacillus* species (*T. albertis*). *Can. J. Microbiol.* 29, 1159–1170. doi: 10.1139/m83-178

Buetti-Dinh, A., Dethlefsen, O., Friedman, R., and Dopson, M. (2016). Transcriptomic analysis reveals how a lack of potassium ions increases *Sulfolobus acidocaldarius* sensitivity to pH changes. *Microbiology* 162, 1422–1434. doi: 10.1099/mic.0.000314

Bury-Moné, S., Mendz, G. L., Ball, G. E., Thibonnier, M., Stingl, K., Ecobichon, C., et al. (2008). Roles of alpha and beta carbonic anhydrases of *Helicobacter* pylori in the urease-dependent response to acidity and in colonization of the murine gastric mucosa. *Infect. Immun.* 76, 497–509. doi: 10.1128/IAI.00993-07

Camacho, D., Frazao, R., Fouillen, A., Nanci, A., Lang, B. F., Apte, S. C., et al. (2020). New insights into *Acidithiobacillus thiooxidans* sulfur metabolism through coupled gene expression, solution chemistry, microscopy, and spectroscopy analyses. *Front. Microbiol.* 11:411. doi: 10.3389/fmicb.2020.00411

Carter, E. L., Flugga, N., Boer, J. L., Mulrooney, S. B., and Hausinger, R. P. (2009). Interplay of metal ions and urease. *Metallomics* 1, 207–221. doi: 10.1039/B903311D

Carver, T., Harris, S. R., Berriman, M., Parkhill, J., and McQuillan, J. A. (2012). Artemis: an integrated platform for visualization and analysis of high-throughput sequence-based experimental data. *Bioinformatics* 28, 464–469. doi: 10.1093/bioinformatics/btr703

Castresana, J. (2000). Selection of conserved blocks from multiple alignments for their use in phylogenetic analysis. *Mol. Biol. Evol.* 17, 540–552. doi: 10.1093/oxfordjournals.molbev.a026334

Castro, M., Moya-Beltrán, A., Covarrubias, P. C., Gonzalez, M., Cardenas, J. P., Issotta, F., et al. (2017). Draft genome sequence of the type strain of the sulfur-oxidizing acidophile, *Acidithiobacillus albertensis* (DSM 14366). *Stand. Genom. Sci.* 12:77. doi: 10.1186/s40793-017-0282-y

Chao, J., Wang, W., Xiao, S., and Liu, X. (2008). Response of *Acidithiobacillus ferrooxidans* ATCC 23270 gene expression to acid stress. *World J. Microbiol. Biotechnol.* 24, 2103–2109. doi: 10.1007/s11274-008-9715-5

Chen, C. P., Kernytsky, A., and Rost, B. (2002). Transmembrane helix predictions revisited. *Protein Sci.* 11, 2774–2791. doi: 10.1110/ps.0214502

Chen, J., Liu, Y., Diep, P., and Mahadevan, R. (2021). Genomic analysis of a newly isolated *Acidithiobacillus ferridurans* JAGS strain reveals its adaptation to acid mine drainage. *Minerals* 11:74. doi: 10.3390/min11010074

Chen, L., Brügger, K., Skovgaard, M., Redder, P., She, Q., Torarinsson, E., et al. (2005). The genome of *Sulfolobus acidocaldarius*, a model organism of the

crenarchaeota. *J. Bacteriol.* 187, 4992–4999. doi: 10.1128/JB.187.14.4992-4999.2005

Chen, L., Hu, M., Huang, L., Hua, Z., Kuang, J., Li, S., et al. (2015). Comparative metagenomic and metatranscriptomic analyses of microbial communities in acid mine drainage. *ISME J.* 9, 1579–1592. doi: 10.1038/ismej.2014.245

Chen, P., Yan, L., Wu, Z., Xu, R., Li, S., Wang, N., et al. (2015). Draft genome sequence of extremely acidophilic bacterium *Acidithiobacillus ferrooxidans* DLC-5 isolated from acid mine drainage in northeast China. *Genom. Data* 6, 267–268. doi: 10.1016/j.gdata.2015.10.018

Chi, X., Fan, Q., Zhang, Y., Liang, K., Wan, L., Zhou, Q., et al. (2020). Structural mechanism of phospholipids translocation by MlaFEDB complex. *Cell Res.* 30, 1127–1135. doi: 10.1038/s41422-020-00404-6

Cholo, M. C., van Rensburg, E. J., Osman, A. G., and Anderson, R. (2015). Expression of the genes encoding the Trk and Kdp potassium transport systems of *Mycobacterium tuberculosis* during growth in vitro. *BioMed Res. Int.* 2015:e608682. doi: 10.1155/2015/608682

Christel, S., Fridlund, J., Watkin, E. L., and Dopson, M. (2016). *Acidithiobacillus ferrivorans* SS3 presents little RNA transcript response related to cold stress during growth at 8 °C suggesting it is a eurypsychrophile. *Extremophiles* 20, 903–913. doi: 10.1007/s00792-016-0882-2

Christel, S., Herold, M., Bellenberg, S., Hajjami, M. E., Buetti-Dinh, A., Pivkin, I. V., et al. (2018). Multi-omics reveals the lifestyle of the acidophilic, mineral-oxidizing model species *Leptospirillum ferriphilum*^{T}. *Appl. Environ. Microbiol.* 84, e02091-17. doi: 10.1128/AEM.02091-17

Colman, D. R., Poudel, S., Hamilton, T. L., Havig, J. R., Selensky, M. J., Shock, E. L., et al. (2018). Geobiological feedbacks and the evolution of thermoacidophiles. *ISME J.* 12, 225–236. doi: 10.1038/ismej.2017.162

Contreras-Moreira, B., and Vinuesa, P. (2013). GET_HOMOLOGUES, a versatile software package for scalable and robust microbial pangenome analysis. *Appl. Environ. Microbiol.* 79, 7696–7701. doi: 10.1128/AEM.02411-13

Crooks, G. E., Hon, G., Chandonia, J.-M., and Brenner, S. E. (2004). WebLogo: a sequence logo generator. *Genome Res.* 14, 1188–1190. doi: 10.1101/gr.849004

Darling, A. C. E., Mau, B., Blattner, F. R., and Perna, N. T. (2004). Mauve: multiple alignment of conserved genomic sequence with rearrangements. *Genome Res.* 14, 1394–1403. doi: 10.1101/gr.2289704

Darling, A. E., Mau, B., and Perna, N. T. (2010). Progressive mauve: multiple genome alignment with gene gain. Loss and Rearrangement. *PLoS One* 5:e11147. doi: 10.1371/journal.pone.0011147

De Biase, D., and Lund, P. A. (2015). "Chapter two - the *Escherichia coli* acid stress response and its significance for pathogenesis," in *Advances in Applied Microbiology*, eds S. Sariaslani and G. M. Gadd (Academic Press), 49–88. doi: 10.1016/bs.aambs.2015.03.002

Dong, C., Beis, K., Nesper, J., Brunkan, A. L., Clarke, B. R., Whitfield, C., et al. (2006). The structure of Wza, the translocon for group 1 capsular polysaccharides in *Escherichia coli*, identifies a new class of outer membrane protein. *Nature* 444, 226–229. doi: 10.1038/nature05267

Dopson, M., Holmes, D. S., Lazcano, M., McCredden, T. J., Bryan, C. G., Mulroney, K. T., et al. (2017). Multiple osmotic stress responses in *Acidihalobacter prosperus* result in tolerance to chloride ions. *Front. Microbiol.* 7:2132. doi: 10.3389/fmicb.2016.02132

Duarte, F., Araya-Secchi, R., González, W., Perez-Acle, T., González-Nilo, D., and Holmes, D. S. (2009). Protein function in extremely acidic conditions: molecular simulations of a predicted aquaporin and a potassium channel in *Acidithiobacillus ferrooxidans*. *Adv. Mat. Res.* 7, 211–214.

Epstein, W. (2003). The roles and regulation of potassium in bacteria. *Prog. Nucleic Acid Res. Mol. Biol.* 75, 293–320. doi: 10.1016/S0079-6603(03)75008-9

Esparza, M., Jedlicki, E., González, C., Dopson, M., and Holmes, D. S. (2019). Effect of CO_2 concentration on uptake and assimilation of inorganic carbon in the extreme acidophile *Acidithiobacillus ferrooxidans*. *Front. Microbiol.* 10:603. doi: 10.3389/fmicb.2019.00603

Falagán, C., and Johnson, D. B. (2016). *Acidithiobacillus ferriphilus* sp. nov., a facultatively anaerobic iron- and sulfur-metabolizing extreme acidophile. *Int. J. Syst. Evol. Microbiol.* 66, 206–211. doi: 10.1099/ijsem.0.000698

Falagán, C., Moya-Beltrán, A., Castro, M., Quatrini, R., and Johnson, D. B. (2019). *Acidithiobacillus sulfuriphilus* sp. nov.: an extremely acidophilic sulfur-oxidizing chemolithotroph isolated from a neutral pH environment. *Int. J. Syst. Evol. Microbiol.* 69, 2907–2913. doi: 10.1099/ijsem.0.003576

Farasin, J., Andres, J., Casiot, C., Barbe, V., Faerber, J., Halter, D., et al. (2015). *Thiomonas* sp. CB2 is able to degrade urea and promote toxic metal precipitation in acid mine drainage waters supplemented with urea. *Front. Microbiol.* 6:993. doi: 10.3389/fmicb.2015.00993

Fariq, A., Blazier, J. C., Yasmin, A., Gentry, T. J., and Deng, Y. (2019). Whole genome sequence analysis reveals high genetic variation of newly isolated *Acidithiobacillus ferrooxidans* IO-2C. *Sci. Rep.* 9:13049. doi: 10.1038/s41598-019-49213-x

Feehily, C., and Karatzas, K. A. G. (2013). Role of glutamate metabolism in bacterial responses towards acid and other stresses. *J. Appl. Microbiol.* 114, 11–24. doi: 10.1111/j.1365-2672.2012.05434.x

Feng, S., Li, K., Huang, Z., Tong, Y., and Yang, H. (2019). Specific mechanism of *Acidithiobacillus caldus* extracellular polymeric substances in the bioleaching of copper-bearing sulfide ore. *PLoS One* 14:e0213945. doi: 10.1371/journal.pone.0213945

Feng, S., Yang, H., and Wang, W. (2015). System-level understanding of the potential acid-tolerance components of *Acidithiobacillus thiooxidans* ZJJN-3 under extreme acid stress. *Extremophiles* 19, 1029–1039. doi: 10.1007/s00792-015-0780-z

Fischer, S., Brunk, B. P., Chen, F., Gao, X., Harb, O. S., Iodice, J. B., et al. (2011). Using OrthoMCL to assign proteins to OrthoMCL-db groups or to cluster proteomes into new ortholog groups. *Curr. Prot. Bioinform.* 35, 6.12.1–6.12.19. doi: 10.1002/0471250953.bi0612s35

Foster, J. W. (2004). *Escherichia coli* acid resistance: tales of an amateur acidophile. *Nat. Rev. Microbiol.* 2, 898–907. doi: 10.1038/nrmicro1021

Frolov, E. N., Kublanov, I. V., Toshchakov, S. V., Samarov, N. I., Novikov, A. A., Lebedinsky, A. V., et al. (2017). *Thermodesulfobium acidiphilum* sp. nov., a thermoacidophilic, sulfate-reducing, chemoautotrophic bacterium from a thermal site. *Int. J. Syst. Evol. Microbiol.* 67, 1482–1485. doi: 10.1099/ijsem.0.001745

Frost, S., and Mckenna, R. (2014). *Carbonic Anhydrase: Mechanism, Regulation, Links to Disease, and Industrial Applications*. Dordrecht: Springer. doi: 10.1007/978-94-007-7359-2

Gassel, M., Siebers, A., Epstein, W., and Altendorf, K. (1998). Assembly of the Kdp complex, the multi-subunit K^{+}-transport ATPase of *Escherichia coli*. *Biochimica et Biophysica Acta* 1415, 77–84. doi: 10.1016/S0005-2736(98)00179-5

Gibson, R. A., Sherry, A., Kaur, G., Pancost, R. D., and Talbot, H. M. (2014). Bacteriohopanepolyols preserved in silica sinters from champagne pool (new zealand) indicate a declining temperature gradient over the lifetime of the vent. *Org. Geochem.* 69, 61–69. doi: 10.1016/j.orggeochem.2014.02.004

González, C., Lazcano, M., Valdés, J., and Holmes, D. S. (2016). Bioinformatic analyses of unique (orphan) core genes of the genus *Acidithiobacillus*: functional inferences and use as molecular probes for genomic and metagenomic/transcriptomic interrogation. *Front. Microbiol.* 7:e02035. doi: 10.3389/fmicb.2016.02035

González, C., Yanquepe, M., Cardenas, J. P., Valdes, J., Quatrini, R., Holmes, D. S., et al. (2014). Genetic variability of psychrotolerant *Acidithiobacillus ferrivorans* revealed by (meta)genomic analysis. *Res. Microbiol.* 165, 726–734. doi: 10.1016/j.resmic.2014.08.005

Guiliani, N., and Jerez, C. A. (2000). Molecular cloning, sequencing, and expression of omp-40, the gene coding for the major outer membrane protein from the acidophilic bacterium *Thiobacillus ferrooxidans*. *Appl. Environ. Microbiol.* 66, 2318–2324. doi: 10.1128/AEM.66.6.2318-2324.2000

Hallberg, K. B., González-Toril, E., and Johnson, D. B. (2010). *Acidithiobacillus ferrivorans*, sp. nov.; facultatively anaerobic, psychrotolerant iron-, and sulfur-oxidizing acidophiles isolated from metal mine-impacted environments. *Extremophiles* 14, 9–19. doi: 10.1007/s00792-009-0282-y

Hallberg, K. B., and Lindström, E. B. (1994). Characterization of *Thiobacillus caldus* sp. nov., a moderately thermophilic acidophile. *Microbiology (Reading)* 140, 3451–3456. doi: 10.1099/13500872-140-12-3451

Hedrich, S., and Johnson, D. B. (2013). *Acidithiobacillus ferridurans* sp. nov., an acidophilic iron-, sulfur- and hydrogen-metabolizing chemolithotrophic gammaproteobacterium. *Int. J. Syst. Evol. Microbiol.* 63, 4018–4025. doi: 10.1099/ijs.0.049759-0

Hoang, D. T., Chernomor, O., von Haeseler, A., Minh, B. Q., and Vinh, L. S. (2018). UFBoot2: improving the ultrafast bootstrap approximation. *Mol. Biol. Evol.* 35, 518–522. doi: 10.1093/molbev/msx281

Hu, W., Feng, S., Tong, Y., Zhang, H., and Yang, H. (2020). Adaptive defensive mechanism of bioleaching microorganisms under extremely environmental acid stress: advances and perspectives. *Biotechnol. Adv.* 42:107580. doi: 10.1016/j.biotechadv.2020.107580

Hughes, G. W., Hall, S. C. L., Laxton, C. S., Sridhar, P., Mahadi, A. H., Hatton, C., et al. (2019). Evidence for phospholipid export from the bacterial inner membrane by the Mla ABC transport system. *Nat. Microbiol.* 4, 1692–1705. doi: 10.1038/s41564-019-0481-y

Inaba, Y., Banerjee, I., Kernan, T., and Banta, S. (2018). Transposase-mediated chromosomal integration of exogenous genes in *Acidithiobacillus ferrooxidans*. *Appl. Environ. Microbiol.* 84, e01381-18. doi: 10.1128/AEM.01381-18

Issotta, F., Moya-Beltrán, A., Mena, C., Covarrubias, P. C., Thyssen, C., Bellenberg, S., et al. (2018). Insights into the biology of acidophilic members of the *Acidiferrobacteraceae* family derived from comparative genomic analyses. *Res. Microbiol.* 169, 608–617. doi: 10.1016/j.resmic.2018.08.001

Jones, D. S., Albrecht, H. L., Dawson, K. S., Schaperdoth, I., Freeman, K. H., Pi, Y., et al. (2012). Community genomic analysis of an extremely acidophilic sulfur-oxidizing biofilm. *ISME J.* 6, 158–170. doi: 10.1038/ismej.2011.75

Juncker, A. S., Willenbrock, H., Von Heijne, G., Brunak, S., Nielsen, H., and Krogh, A. (2003). Prediction of lipoprotein signal peptides in gram-negative bacteria. *Protein Sci.* 12, 1652–1662. doi: 10.1110/ps.0303703

Jung, H., Inaba, Y., and Banta, S. (2021). Genetic engineering of the acidophilic chemolithoautotroph *Acidithiobacillus ferrooxidans*. *Trends Biotechnol.* [Epub ahead of print]. doi: 10.1016/j.tibtech.2021.10.004

Kalyaanamoorthy, S., Minh, B. Q., Wong, T. K. F., von Haeseler, A., and Jermiin, L. S. (2017). Model finder: fast model selection for accurate phylogenetic estimates. *Nat. Methods* 14, 587–589. doi: 10.1038/nmeth.4285

Kamimura, K., Sharmin, S., Yoshino, E., Tokuhisa, M., and Kanao, T. (2018). Draft genome sequence of *Acidithiobacillus* sp. strain SH, a marine acidophilic sulfur-oxidizing bacterium. *Genome Ann.* 6:e01603-17. doi: 10.1128/genomeA.01603-17

Kanjee, U., and Houry, W. A. (2013). Mechanisms of acid resistance in *Escherichia coli*. *Annu Rev. Microbiol.* 67, 65–81. doi: 10.1146/annurev-micro-092412-155708

Karatzas, K.-A. G., Brennan, O., Heavin, S., Morrissey, J., and O'Byrne, C. P. (2010). Intracellular accumulation of high levels of γ-aminobutyrate by *Listeria monocytogenes* 10403S in response to low pH: uncoupling of γ-aminobutyrate synthesis from efflux in a chemically defined medium. *Appl. Environ. Microbiol.* 76, 3529–3537. doi: 10.1128/AEM.03063-09

Katoh, K. (2002). MAFFT: a novel method for rapid multiple sequence alignment based on fast fourier transform. *Nucleic Acids Res.* 30, 3059–3066. doi: 10.1093/nar/gkf436

Katoh, K., Rozewicki, J., and Yamada, K. D. (2019). MAFFT online service: multiple sequence alignment, interactive sequence choice and visualization. *Br. Bioinform.* 20, 1160–1166. doi: 10.1093/bib/bbx108

Katoh, K., and Standley, D. M. (2013). MAFFT multiple sequence alignment software version 7: improvements in performance and usability. *Mol. Biol. Evol.* 30, 772–780. doi: 10.1093/molbev/mst010

Khaleque, H. N., González, C., Johnson, D. B., Kaksonen, A. H., Holmes, D. S., and Watkin, E. L. J. (2020). Genome-based classification of *Acidihalobacter prosperus* F5 (=DSM 105917=JCM 32255) as *Acidihalobacter yilgarnensis* sp. nov. *Int. J. Syst. Evol. Microbiol.* 70, 6226–6234. doi: 10.1099/ijsem.0.004519

Khaleque, H. N., González, C., Kaksonen, A. H., Boxall, N. J., Holmes, D. S., and Watkin, E. L. J. (2019). Genome-based classification of two halotolerant extreme acidophiles, *Acidihalobacter prosperus* V6 (=DSM 14174 =JCM 32253) and "*Acidihalobacter ferrooxidans*" V8 (=DSM 14175 =JCM 32254) as two new species, *Acidihalobacter aeolianus* sp. nov. and *Acidihalobacter ferrooxydans* sp. nov., respectively. *Int. J. Syst. Evol. Microbiol.* 69, 1557–1565. doi: 10.1099/ijsem.0.003313

Kichenaradja, P., Siguier, P., Pérochon, J., and Chandler, M. (2010). ISbrowser: an extension of ISfinder for visualizing insertion sequences in prokaryotic genomes. *Nucleic Acids Res.* 38, D62–D68. doi: 10.1093/nar/gkp947

Krogh, A., Larsson, B., von Heijne, G., and Sonnhammer, E. L. (2001). Predicting transmembrane protein topology with a hidden markov model: application to complete genomes. *J. Mol. Biol.* 305, 567–580. doi: 10.1006/jmbi.2000.4315

Krulwich, T. A., Sachs, G., and Padan, E. (2011). Molecular aspects of bacterial pH sensing and homeostasis. *Nat. Rev. Microbiol.* 9, 330–343. doi: 10.1038/nrmicro2549

Kucera, J., Sedo, O., Potesil, D., Janiczek, O., Zdrahal, Z., and Mandl, M. (2016). Comparative proteomic analysis of sulfur-oxidizing *Acidithiobacillus ferrooxidans* CCM 4253 cultures having lost the ability to couple anaerobic elemental sulfur oxidation with ferric iron reduction. *Res. Microbiol.* 167, 587–594. doi: 10.1016/j.resmic.2016.06.009

Larsson, A. (2014). AliView: a fast and lightweight alignment viewer and editor for large datasets. *Bioinformatics* 30, 3276–3278. doi: 10.1093/bioinformatics/btu531

Lehtovirta-Morley, L. E., Sayavedra-Soto, L. A., Gallois, N., Schouten, S., Stein, L. Y., Prosser, J. I., et al. (2016). Identifying potential mechanisms enabling acidophily in the ammonia-oxidizing archaeon "*Candidatus* Nitrosotalea devanaterra". *Appl. Environ. Microbiol.* 82, 2608–2619. doi: 10.1128/AEM.04031-15

Letunic, I., and Bork, P. (2021). Interactive tree of life (iTOL) v5: an online tool for phylogenetic tree display and annotation. *Nucleic Acids Res.* 49, W293–W296. doi: 10.1093/nar/gkab301

Li, L., Liu, Z., Zhang, M., Meng, D., Liu, X., Wang, P., et al. (2020). Insights into the metabolism and evolution of the genus acidiphilium, a typical acidophile in acid mine drainage. *mSystems* 5, e00867-20. doi: 10.1128/mSystems.00867-20

Li, Q., Li, N., Liu, X., Zhou, Z., Fang, Y., Fan, X., et al. (2012). Characterization of the acid stress response of *Acidithiobacillus ferrooxidans* ATCC 23270 based on the method of microarray. *J. Biol. Res.* 17, 3–15.

Li, Q., Ren, Y., Qiu, G., Li, N., Liu, H., Dai, Z., et al. (2011). Insights into the pH up-shift responsive mechanism of *Acidithiobacillus ferrooxidans* by microarray transcriptome profiling. *Folia Microbiol. (Praha)* 56, 439–451. doi: 10.1007/s12223-011-0067-4

Liljeqvist, M., Ossandon, F. J., González, C., Rajan, S., Stell, A., Valdes, J., et al. (2015). Metagenomic analysis reveals adaptations to a cold-adapted lifestyle in a low-temperature acid mine drainage stream. *FEMS Microbiol. Ecol.* 91:fiv011. doi: 10.1093/femsec/fiv011

Liljeqvist, M., Valdes, J., Holmes, D. S., and Dopson, M. (2011). Draft genome of the psychrotolerant acidophile *Acidithiobacillus ferrivorans* SS3. *J. Bacteriol.* 193, 4304–4305. doi: 10.1128/JB.05373-11

Ma, B., Reynolds, C. M., and Raetz, C. R. H. (2008). Periplasmic orientation of nascent lipid A in the inner membrane of an *Escherichia coli* LptA mutant. *Proc. Natl. Acad. Sci. U.S.A.* 105, 13823–13828. doi: 10.1073/pnas.0807028105

Malinverni, J. C., and Silhavy, T. J. (2009). An ABC transport system that maintains lipid asymmetry in the gram-negative outer membrane. *Proc. Natl. Acad. Sci. U.S.A.* 106, 8009–8014. doi: 10.1073/pnas.0903229106

Mangold, S., Rao Jonna, V., and Dopson, M. (2013). Response of *Acidithiobacillus caldus* toward suboptimal pH conditions. *Extremophiles* 17, 689–696. doi: 10.1007/s00792-013-0553-5

Mangold, S., Valdés, J., Holmes, D. S., and Dopson, M. (2011). Sulfur metabolism in the extreme acidophile *Acidithiobacillus caldus*. *Front. Microbiol.* 2:17. doi: 10.3389/fmicb.2011.00017

Mates, A. K., Sayed, A. K., and Foster, J. W. (2007). Products of the *Escherichia coli* acid fitness island attenuate metabolite stress at extremely low pH and mediate a cell density-dependent acid resistance. *J. Bacteriol.* 189, 2759–2768. doi: 10.1128/JB.01490-06

Mayer, M. H., Parenteau, M. N., Kempher, M. L., Madigan, M. T., Jahnke, L. L., and Welander, P. V. (2021). Anaerobic 3-methylhopanoid production by an acidophilic photosynthetic purple bacterium. *Arch. Microbiol.* 203, 6041–6052. doi: 10.1007/s00203-021-02561-7

McLaggan, D., Keyhan, M., and Matin, A. (1990). Chloride transport pathways and their bioenergetic implications in the obligate acidophile *Bacillus coagulans*. *J. Bacteriol.* 172, 1485–1490. doi: 10.1128/jb.172.3.1485-1490.1990

Michels, M., and Bakker, E. P. (1985). Generation of a large, protonophore-sensitive proton motive force and pH difference in the acidophilic bacteria *Thermoplasma acidophilum* and *Bacillus acidocaldarius*. *J. Bacteriol.* 161, 231–237. doi: 10.1128/jb.161.1.231-237.1985

Miyauchi, T., Kouzuma, A., Abe, T., and Watanabe, K. (2018). Complete genome sequence of *Acidithiobacillus ferridurans* JCM 18981. *Microbiol. Res. Ann.* 7:e01028-18. doi: 10.1128/MRA.01028-18

Moya-Beltrán, A., Beard, S., Rojas-Villalobos, C., Issotta, F., Gallardo, Y., Ulloa, R., et al. (2021). Genomic evolution of the class *Acidithiobacillia*: deep-branching *Proteobacteria* living in extreme acidic conditions. *ISME J.* 15, 3221–3238. doi: 10.1038/s41396-021-00995-x

Mühling, M., Poehlein, A., Stuhr, A., Voitel, M., Daniel, R., and Schlömann, M. (2016). Reconstruction of the metabolic potential of acidophilic *Sideroxydans* strains from the metagenome of an microaerophilic enrichment culture of acidophilic iron-oxidizing bacteria from a pilot plant for the treatment of acid mine drainage reveals metabolic versatility and adaptation to life at low pH. *Front. Microbiol.* 7:e02082. doi: 10.3389/fmicb.2016.02082

Munsey, T. S., Mohindra, A., Yusaf, S. P., Grainge, A., Wang, M.-H., Wray, D., et al. (2002). Functional properties of Kch, a prokaryotic homologue of eukaryotic potassium channels. *Biochem. Biophys. Res. Commun.* 297, 10–16. doi: 10.1016/S0006-291X(02)02095-8

Mykytczuk, N. C. S., Trevors, J. T., Ferroni, G. D., and Leduc, L. G. (2010). Cytoplasmic membrane fluidity and fatty acid composition of *Acidithiobacillus ferrooxidans* in response to pH stress. *Extremophiles* 14, 427–441. doi: 10.1007/s00792-010-0319-2

Neira, G., Cortez, D., Jil, J., and Holmes, D. S. (2020). AciDB 1.0: a database of acidophilic organisms, their genomic information and associated metadata. *Bioinformatics* 36, 4970–4971. doi: 10.1093/bioinformatics/btaa638

Nguyen, L.-T., Schmidt, H. A., von Haeseler, A., and Minh, B. Q. (2015). IQ-TREE: a fast and effective stochastic algorithm for estimating maximum-likelihood phylogenies. *Mol. Biol. Evol.* 32, 268–274. doi: 10.1093/molbev/msu300

Norris, P. R., Falagán, C., Moya-Beltrán, A., Castro, M., Quatrini, R., and Johnson, D. B. (2020). *Acidithiobacillus ferrianus* sp. nov.: an ancestral extremely acidophilic and facultatively anaerobic chemolithoautotroph. *Extremophiles* 24, 329–337. doi: 10.1007/s00792-020-01157-1

Nuñez, H., Covarrubias, P. C., Moya-Beltrán, A., Issotta, F., Atavales, J., Acuña, L. G., et al. (2016). Detection, identification and typing of *Acidithiobacillus* species and strains: a review. *Res. Microbiol.* 167, 555–567. doi: 10.1016/j.resmic.2016.05.006

Nzakizwanayo, J., Kumar, S., Ogilvie, L. A., Patel, B. A., Dedi, C., Macfarlane, W. M., et al. (2015). Disruption of *Escherichia coli* Nissle 1917 K5 capsule biosynthesis, through loss of distinct kfi genes, modulates interaction with intestinal epithelial cells and impact on cell health. *PLoS One* 10:e0120430. doi: 10.1371/journal.pone.0120430

Oetiker, N., Norambuena, R., Martínez-Bussenius, C., Navarro, C. A., Amaya, F., Álvarez, S. A., et al. (2018). Possible role of envelope components in the extreme copper resistance of the biomining *Acidithiobacillus ferrooxidans*. *Genes* 9:347. doi: 10.3390/genes9070347

Osorio, H., Martínez, V., Nieto, P. A., Holmes, D. S., and Quatrini, R. (2008). Microbial iron management mechanisms in extremely acidic environments: comparative genomics evidence for diversity and versatility. *BMC Microbiol.* 8:203. doi: 10.1186/1471-2180-8-203

Parks, D. H., Imelfort, M., Skennerton, C. T., Hugenholtz, P., and Tyson, G. W. (2015). CheckM: assessing the quality of microbial genomes recovered from isolates, single cells, and metagenomes. *Genome Res.* 25, 1043–1055. doi: 10.1101/gr.186072.114

Parro, V., Moreno-Paz, M., and González-Toril, E. (2007). Analysis of environmental transcriptomes by DNA microarrays. *Environ. Microbiol.* 9, 453–464. doi: 10.1111/j.1462-2920.2006.01162.x

Plante, C. (2000). Role of bacterial exopolymeric capsules in protection from deposit-feeder digestion. *Aquat. Microb. Ecol.* 21, 211–219. doi: 10.3354/ame021211

Quatrini, R., Escudero, L. V., Moya-Beltrán, A., Galleguillos, P. A., Issotta, F., Acosta, M., et al. (2017). Draft genome sequence of *Acidithiobacillus thiooxidans* CLST isolated from the acidic hypersaline gorbea salt flat in northern Chile. *Stand. Genom. Sci.* 12:84. doi: 10.1186/s40793-017-0305-8

Quatrini, R., and Johnson, D. B. (2018). Microbiomes in extremely acidic environments: functionalities and interactions that allow survival and growth of prokaryotes at low pH. *Curr. Opin. Microbiol.* 43, 139–147. doi: 10.1016/j.mib.2018.01.011

Renzi, F., Ittig, S. J., Sadovskaya, I., Hess, E., Lauber, F., Dol, M., et al. (2016). Evidence for a LOS and a capsular polysaccharide in *Capnocytophaga canimorsus*. *Sci. Rep.* 6:38914. doi: 10.1038/srep38914

Rhee, H. J., Kim, E.-J., and Lee, J. K. (2007). Physiological polyamines: simple primordial stress molecules. *J. Cell. Mol. Med.* 11, 685–703. doi: 10.1111/j.1582-4934.2007.00077.x

Riadi, G., Medina-Moenne, C., and Holmes, D. S. (2012). TnpPred: a web service for the robust prediction of prokaryotic transposases. *Comparat. Funct. Genom.* 2012:e678761. doi: 10.1155/2012/678761

Ricci, J. N., Morton, R., Kulkarni, G., Summers, M. L., and Newman, D. K. (2017). Hopanoids play a role in stress tolerance and nutrient storage in the cyanobacterium nostoc punctiforme. *Geobiology* 15, 173–183. doi: 10.1111/gbi.12204

Richard, H., and Foster, J. W. (2004). *Escherichia coli* glutamate- and arginine-dependent acid resistance systems increase internal ph and reverse transmembrane potential. *J. Bacteriol.* 186, 6032–6041. doi: 10.1128/JB.186.18.6032-6041.2004

Samartzidou, H., Mehrazin, M., Xu, Z., Benedik, M. J., and Delcour, A. H. (2003). Cadaverine inhibition of porin plays a role in cell survival at acidic pH. *J. Bacteriol.* 185, 13–19. doi: 10.1128/JB.185.1.13-19.2003

Schmitz, R. A., Peeters, S. H., Versantvoort, W., Picone, N., Pol, A., Jetten, M. S. M., et al. (2021). *Verrucomicrobial methanotrophs*: ecophysiology of metabolically versatile acidophiles. *FEMS Microbiol. Rev.* 45:fuab007. doi: 10.1093/femsre/fuab007

Schneider, T. D., and Stephens, R. M. (1990). Sequence logos: a new way to display consensus sequences. *Nucleic Acids Res.* 18, 6097–6100. doi: 10.1093/nar/18.20.6097

Schoep, T. D., Fulurija, A., Good, F., Lu, W., Himbeck, R. P., Schwan, C., et al. (2010). Surface properties of *Helicobacter* pylori urease complex are essential for persistence. *PLoS One* 5:e15042. doi: 10.1371/journal.pone.0015042

Schonknecht, G., Chen, W.-H., Ternes, C. M., Barbier, G. G., Shrestha, R. P., Stanke, M., et al. (2013). Gene transfer from bacteria and archaea facilitated evolution of an extremophilic eukaryote. *Science* 339, 1207–1210. doi: 10.1126/science.1231707

Scott, D. R., Weeks, D., Hong, C., Postius, S., Melchers, K., and Sachs, G. (1998). The role of internal urease in acid resistance of *Helicobacter* pylori. *Gastroenterology* 114, 58–70. doi: 10.1016/s0016-5085(98)70633-x

Simmons, S. L., DiBartolo, G., Denef, V. J., Goltsman, D. S. A., Thelen, M. P., and Banfield, J. F. (2008). Population genomic analysis of strain variation in *Leptospirillum* group II bacteria involved in acid mine drainage formation. *PLoS Biol.* 6:e177. doi: 10.1371/journal.pbio.0060177

Slonczewski, J. L., Fujisawa, M., Dopson, M., and Krulwich, T. A. (2009). "Cytoplasmic pH measurement and homeostasis in bacteria and archaea," in *Advances in Microbial Physiology*, ed. R. K. Poole (Academic Press), 1–317. doi: 10.1016/S0065-2911(09)05501-5

Snipen, L., and Ussery, D. W. (2010). Standard operating procedure for computing pangenome trees. *Stand. Genom. Sci.* 2, 135–141. doi: 10.4056/sigs.38923

Sonnhammer, E. L., von Heijne, G., and Krogh, A. (1998). A hidden markov model for predicting transmembrane helices in protein sequences. *Proc. Int. Conf. Int. Syst. Mol. Biol.* 6, 175–182.

Sriaporn, C., Campbell, K. A., Van Kranendonk, M. J., and Handley, K. M. (2021). Genomic adaptations enabling *Acidithiobacillus* distribution across wide-ranging hot spring temperatures and pHs. *Microbiome* 9:135. doi: 10.1186/s40168-021-01090-1

Stingl, K., Altendorf, K., and Bakker, E. P. (2002). Acid survival of *Helicobacter pylori*: how does urease activity trigger cytoplasmic pH homeostasis? *Trends Microbiol.* 10, 70–74. doi: 10.1016/s0966-842x(01)02287-9

Su, J., Gong, H., Lai, J., Main, A., and Lu, S. (2009). The potassium transporter Trk and external potassium modulate *Salmonella enterica* protein secretion and virulence. *Infect. Immun.* 77, 667–675. doi: 10.1128/IAI.01027-08

Szklarczyk, D., Gable, A. L., Lyon, D., Junge, A., Wyder, S., Huerta-Cepas, J., et al. (2019). STRING v11: protein–protein association networks with increased coverage, supporting functional discovery in genome-wide experimental datasets. *Nucleic Acids Res.* 47, D607–D613. doi: 10.1093/nar/gky1131

Talla, E., Hedrich, S., Mangenot, S., Ji, B., Johnson, D. B., Barbe, V., et al. (2014). Insights into the pathways of iron- and sulfur-oxidation, and biofilm formation from the chemolithotrophic acidophile *Acidithiobacillus ferrivorans* CF27. *Res. Microbiol.* 165, 753–760. doi: 10.1016/j.resmic.2014.08.002

Temple, K. L., and Colmer, A. R. (1951). The autotrophic oxidation of iron by a new bacterium, *Thiobacillus ferrooxidans*. *J. Bacteriol.* 62, 605–611. doi: 10.1128/jb.62.5.605-611.1951

Tettelin, H., Masignani, V., Cieslewicz, M. J., Donati, C., Medini, D., Ward, N. L., et al. (2005). Genome analysis of multiple pathogenic isolates of *Streptococcus agalactiae*: implications for the microbial "pan-genome". *Proc. Natl. Acad. Sci. U.S.A.* 102, 13950–13955. doi: 10.1073/pnas.0506758102

Tran, T. T. T., Mangenot, S., Magdelenat, G., Payen, E., Rouy, Z., Belahbib, H., et al. (2017). Comparative genome analysis provides insights into both the

lifestyle of *Acidithiobacillus ferrivorans* strain CF27 and the chimeric nature of the iron-oxidizing acidithiobacilli genomes. *Front. Microbiol.* 8:e01009. doi: 10.3389/fmicb.2017.01009

Travisany, D., Cortés, M. P., Latorre, M., Di Genova, A., Budinich, M., Bobadilla-Fazzini, R. A., et al. (2014). A new genome of *Acidithiobacillus thiooxidans* provides insights into adaptation to a bioleaching environment. *Res. Microbiol.* 165, 743–752. doi: 10.1016/j.resmic.2014.08.004

Trchounian, A., and Kobayashi, H. (1999). Kup is the major K^+ uptake system in *Escherichia coli* upon hyper-osmotic stress at a low pH. *FEBS Lett.* 447, 144–148. doi: 10.1016/s0014-5793(99)00288-4

Trchounian, A., and Kobayashi, H. (2000). K^+ uptake by fermenting *Escherichia coli* cells: pH dependent mode of the TrkA system operating. *Biosci. Rep.* 20, 277–288. doi: 10.1023/A:1026493024066

Ulloa, R., Moya-Beltrán, A., Rojas-Villalobos, C., Nuñez, H., Chiacchiarini, P., Donati, E., et al. (2019). Domestication of local microbial consortia for efficient recovery of gold through top-down selection in airlift bioreactors. *Front. Microbiol.* 10:60. doi: 10.3389/fmicb.2019.00060

Ullrich, S. R., González, C., Poehlein, A., Tischler, J. S., Daniel, R., Schlömann, M., et al. (2016a). Gene Loss and horizontal gene transfer contributed to the genome evolution of the extreme acidophile "*Ferrovum*". *Front. Microbiol.* 7:797. doi: 10.3389/fmicb.2016.00797

Ullrich, S. R., Poehlein, A., Tischler, J. S., González, C., Ossandon, F. J., Daniel, R., et al. (2016b). Genome analysis of the biotechnologically relevant acidophilic iron oxidising strain JA12 indicates phylogenetic and metabolic diversity within the novel genus "*Ferrovum*.". *PLoS One* 11:e0146832. doi: 10.1371/journal.pone.0146832

Valdes, J., Ossandon, F., Quatrini, R., Dopson, M., and Holmes, D. S. (2011). Draft genome sequence of the extremely acidophilic biomining bacterium *Acidithiobacillus thiooxidans* ATCC 19377 provides insights into the evolution of the *Acidithiobacillus* genus. *J. Bacteriol.* 193, 7003–7004. doi: 10.1128/JB.06281-11

Valdés, J., Pedroso, I., Quatrini, R., Dodson, R. J., Tettelin, H., Blake, R., et al. (2008). *Acidithiobacillus ferrooxidans* metabolism: from genome sequence to industrial applications. *BMC Genom.* 9:597. doi: 10.1186/1471-2164-9-597

Valdes, J., Quatrini, R., Hallberg, K., Dopson, M., Valenzuela, P. D. T., and Holmes, D. S. (2009). Draft genome sequence of the extremely acidophilic bacterium *Acidithiobacillus caldus* ATCC 51756 reveals metabolic versatility in the genus *Acidithiobacillus*. *J. Bacteriol.* 191, 5877–5878. doi: 10.1128/JB.00843-09

van Teeseling, M. C. F., Pol, A., Harhangi, H. R., van der Zwart, S., Jetten, M. S. M., Op, et al. (2014). Expanding the verrucomicrobial methanotrophic world: description of three novel species of *Methylacidimicrobium gen*. nov. *Appl. Environ. Microbiol.* 80, 6782–6791. doi: 10.1128/AEM.01838-14

Varani, A. M., Siguier, P., Gourbeyre, E., Charneau, V., and Chandler, M. (2011). ISsaga is an ensemble of web-based methods for high throughput identification and semi-automatic annotation of insertion sequences in prokaryotic genomes. *Genome Biol.* 12:R30. doi: 10.1186/gb-2011-12-3-r30

Vera, M., Krok, B., Bellenberg, S., Sand, W., and Poetsch, A. (2013). Shotgun proteomics study of early biofilm formation process of *Acidithiobacillus ferrooxidans* ATCC 23270 on pyrite. *Proteomics* 13, 1133–1144. doi: 10.1002/pmic.201200386

Vergara, E., Neira, G., González, C., Cortez, D., Dopson, M., and Holmes, D. S. (2020). Evolution of predicted acid resistance mechanisms in the extremely acidophilic leptospirillum genus. *Genes (Basel)* 11:389. doi: 10.3390/genes11040389

Voges, D., and Jap, B. K. (1998). Recombinant expression, purification and characterization of Kch, a putative *Escherichia coli* potassium channel protein. *FEBS Lett.* 429, 104–108. doi: 10.1016/S0014-5793(98)00509-2

Voland, P., Weeks, D. L., Marcus, E. A., Prinz, C., Sachs, G., and Scott, D. (2003). Interactions among the seven *Helicobacter* pylori proteins encoded by the urease gene cluster. *Am. J. Physiol. Gastr. Liver Physiol.* 284, G96–G106. doi: 10.1152/ajpgi.00160.2002

von Mering, C., Jensen, L. J., Snel, B., Hooper, S. D., Krupp, M., Foglierini, M., et al. (2005). STRING: known and predicted protein-protein associations, integrated and transferred across organisms. *Nucleic Acids Res.* 33, D433–D437. doi: 10.1093/nar/gki005

Vuppada, R. K., Hansen, C. R., Strickland, K. A. P., Kelly, K. M., and McCleary, W. R. (2018). Phosphate signaling through alternate conformations of the PstSCAB phosphate transporter. *BMC Microbiol.* 18:8. doi: 10.1186/s12866-017-1126-z

Waksman, S. A., and Joffe, J. S. (1922). Microörganisms concerned in the oxidation of sulfur in the soil: II. *Thiobacillus thiooxidans*, a new sulfur-oxidizing organism isolated from the soil. *J. Bacteriol.* 7, 239–256. doi: 10.1128/jb.7.2.239-256.1922

Wang, X., Cai, X., Ma, H., Yin, W., Zhu, L., Li, X., et al. (2019). A c-di-AMP riboswitch controlling *kdpFABC* operon transcription regulates the potassium transporter system in *Bacillus thuringiensis*. *Commun. Biol.* 2, 1–10. doi: 10.1038/s42003-019-0414-6

Welander, P. V., Hunter, R. C., Zhang, L., Sessions, A. L., Summons, R. E., and Newman, D. K. (2009). Hopanoids play a role in membrane integrity and pH homeostasis in *Rhodopseudomonas palustris* TIE-1. *J. Bacteriol.* 191, 6145–6156. doi: 10.1128/JB.00460-09

Wen, Z., and Zhang, J.-R. (2015). "Chapter 3 - bacterial capsules," in *Molecular Medical Microbiology (Second Edition)*, eds Y.-W. Tang, M. Sussman, D. Liu, I. Poxton, and J. Schwartzman (Boston: Academic Press), 33–53. doi: 10.1016/B978-0-12-397169-2.00003-2

Whitaker, R. J., Grogan, D. W., and Taylor, J. W. (2005). Recombination shapes the natural population structure of the hyperthermophilic archaeon *Sulfolobus islandicus*. *Mol. Biol. Evol.* 22, 2354–2361. doi: 10.1093/molbev/msi233

Williams, K. P., Gillespie, J. J., Sobral, B. W. S., Nordberg, E. K., Snyder, E. E., Shallom, J. M., et al. (2010). Phylogeny of gamma *Proteobacteria*. *J. Bacteriol.* 192, 2305–2314. doi: 10.1128/JB.01480-09

Williams, K. P., and Kelly, D. P. (2013). Proposal for a new class within the phylum *Proteobacteria, Acidithiobacillia classis* nov., with the type order *Acidithiobacillales*, and emended description of the class *Gammaproteobacteria*. *Int. J. Syst. Evol. Microbiol.* 63, 2901–2906. doi: 10.1099/ijs.0.049270-0

Willis, L. M. (2013). KpsC and KpsS are retaining 3-deoxy-d-manno-oct-2-ulosonic acid (Kdo) transferases involved in synthesis of bacterial capsules. *Proc. Natl. Acad. Sci. U.S.A.* 110, 20753–20758. doi: 10.1073/pnas.1312637110

Wu, C.-H., Bialecka-Fornal, M., and Newman, D. K. (2015). Methylation at the C-2 position of hopanoids increases rigidity in native bacterial membranes. *eLife* 4:e05663. doi: 10.7554/eLife.05663

Xie, Q. W., Tabor, C. W., and Tabor, H. (1989). Spermidine biosynthesis in *Escherichia coli*: promoter and termination regions of the *speED* operon. *J. Bacteriol.* 171, 4457–4465. doi: 10.1128/jb.171.8.4457-4465.1989

Yan, H., Fukamachi, T., Saito, H., and Kobayashi, H. (2011). Expression and activity of Kdp under acidic conditions in *Escherichia coli*. *Biol. Pharmaceut. Bull.* 34, 426–429. doi: 10.1248/bpb.34.426

Yan, L., Zhang, S., Wang, W., Hu, H., Wang, Y., Yu, G., et al. (2015). Draft genome sequence of *Acidithiobacillus ferrooxidans* YQH-1. *Genom. Data* 6, 269–270. doi: 10.1016/j.gdata.2015.10.009

Yin, H., Zhang, X., Li, X., He, Z., Liang, Y., Guo, X., et al. (2014). Whole-genome sequencing reveals novel insights into sulfur oxidation in the extremophile *Acidithiobacillus thiooxidans*. *BMC Microbiol.* 14:179. doi: 10.1186/1471-2180-14-179

You, X.-Y., Guo, X., Zheng, H.-J., Zhang, M.-J., Liu, L.-J., Zhu, Y.-Q., et al. (2011). Unraveling the *Acidithiobacillus caldus* complete genome and its central metabolisms for carbon assimilation. *J. Genet. Genom.* 38, 243–252. doi: 10.1016/j.jgg.2011.04.006

Yu, C.-S., Chen, Y.-C., Lu, C.-H., and Hwang, J.-K. (2006). Prediction of protein subcellular localization. *Proteins* 64, 643–651. doi: 10.1002/prot.21018

Yu, N. Y., Wagner, J. R., Laird, M. R., Melli, G., Rey, S., Lo, R., et al. (2010). PSORTb 3.0: improved protein subcellular localization prediction with refined localization subcategories and predictive capabilities for all prokaryotes. *Bioinformatics* 26, 1608–1615. doi: 10.1093/bioinformatics/btq249

Yuan, B., Cheng, A., and Wang, M. (2013). Polysaccharide export outer membrane proteins in Gram-negative bacteria. *Future Microbiol.* 8, 525–535. doi: 10.2217/fmb.13.13

Zakharyan, E., and Trchounian, A. (2001). K^+ influx by kup in *Escherichia coli* is accompanied by a decrease in H^+ efflux. *FEMS Microbiol. Lett.* 204, 61–64. doi: 10.1111/j.1574-6968.2001.tb10863.x

Zammit, C. M., and Watkin, E. L. J. (2016). "Adaptation to extreme acidity and osmotic stress," in *Acidophiles: Life in Extremely Acidic Environments*, eds R. Quatrini and D. B. Johnson (Caister Academic Press), 49–62. doi: 10.21775/9781910190333.03

Zhang, X., Liu, X., He, Q., Dong, W., Zhang, X., Fan, F., et al. (2016b). Gene turnover contributes to the evolutionary adaptation of *Acidithiobacillus caldus*: insights from comparative genomics. *Front. Microbiol.* 7:e01960. doi: 10.3389/fmicb.2016.01960

Zhang, X., Feng, X., Tao, J., Ma, L., Xiao, Y., Liang, Y., et al. (2016a). Comparative genomics of the extreme acidophile *Acidithiobacillus thiooxidans* reveals intraspecific divergence and niche adaptation. *Int. J. Mol. Sci.* 17:1355. doi: 10.3390/ijms17081355

Zhang, X., Liu, X., Liang, Y., Guo, X., Xiao, Y., Ma, L., et al. (2017). Adaptive evolution of extreme acidophile *Sulfobacillus thermosulfidooxidans* potentially driven by horizontal gene transfer and gene loss. *Appl. Environ. Microbiol.* 83, e03098-16. doi: 10.1128/AEM.03098-16

Zhang, X., Liu, Z., Wei, G., Yang, F., and Liu, X. (2018). In silico genome-wide analysis reveals the potential links between core genome of *Acidithiobacillus thiooxidans* and its autotrophic lifestyle. *Front. Microbiol.* 9:e01255. doi: 10.3389/fmicb.2018.01255

Zhou, X., Chua, T. K., Tkaczuk, K. L., Bujnicki, J. M., and Sivaraman, J. (2010). The crystal structure of *Escherichia coli* spermidine synthase SpeE reveals a unique substrate-binding pocket. *J. Struct. Biol.* 169, 277–285. doi: 10.1016/j.jsb.2009.12.024

Zhu, Q., Kosoy, M., and Dittmar, K. (2014). HGTector: an automated method facilitating genome-wide discovery of putative horizontal gene transfers. *BMC Genom.* 15:717. doi: 10.1186/1471-2164-15-717

Zückert, W. R. (2014). Secretion of bacterial lipoproteins: through the cytoplasmic membrane, the periplasm and beyond. *Biochim. Biophys. Acta* 1843, 1509–1516. doi: 10.1016/j.bbamcr.2014.04.022

Conflict of Interest: The authors declare that the research was conducted in the absence of any commercial or financial relationships that could be construed as a potential conflict of interest.

Publisher's Note: All claims expressed in this article are solely those of the authors and do not necessarily represent those of their affiliated organizations, or those of the publisher, the editors and the reviewers. Any product that may be evaluated in this article, or claim that may be made by its manufacturer, is not guaranteed or endorsed by the publisher.

frontiers in Microbiology

ORIGINAL RESEARCH
published: 23 February 2022
doi: 10.3389/fmicb.2022.840205

Microbial Biofilms Along a Geochemical Gradient at the Shallow-Water Hydrothermal System of Vulcano Island, Mediterranean Sea

Valentina Sciutteri[1,2†], Francesco Smedile[1†], Salvatrice Vizzini[2,3], Antonio Mazzola[2,3] and Costantino Vetriani[1,4]*

[1] Department of Marine and Coastal Sciences, Rutgers, The State University of New Jersey, New Brunswick, NJ, United States, [2] Department of Earth and Marine Sciences, University of Palermo, Palermo, Italy, [3] Consorzio Nazionale Interuniversitario per le Scienze del Mare, Rome, Italy, [4] Department of Biochemistry and Microbiology, Rutgers, The State University of New Jersey, New Brunswick, NJ, United States

OPEN ACCESS

Edited by:
Davide Zannoni, University of Bologna, Italy

Reviewed by:
Anne Godfroy, Centre de Bretagne, Institut Français de Recherche pour l'Exploitation de la Mer, France
Antonella Penna, University of Urbino Carlo Bo, Italy

***Correspondence:**
Costantino Vetriani
vetriani@marine.rutgers.edu

†Present address:
Valentina Sciutteri, Department of Integrated Marine Ecology, Stazione Zoologica Anton Dohrn, Sicily Marine Centre, Messina, Italy
Francesco Smedile, Institute of Polar Sciences, National Research Council, Messina, Italy

Specialty section:
This article was submitted to Extreme Microbiology, a section of the journal Frontiers in Microbiology

Received: *20 December 2021*
Accepted: *24 January 2022*
Published: *23 February 2022*

Citation:
Sciutteri V, Smedile F, Vizzini S, Mazzola A and Vetriani C (2022) Microbial Biofilms Along a Geochemical Gradient at the Shallow-Water Hydrothermal System of Vulcano Island, Mediterranean Sea. Front. Microbiol. 13:840205. doi: 10.3389/fmicb.2022.840205

Shallow water hydrothermal vents represent highly dynamic environments where strong geochemical gradients can shape microbial communities. Recently, these systems are being widely used for investigating the effects of ocean acidification on biota as vent emissions can release high CO_2 concentrations causing local pH reduction. However, other gas species, as well as trace elements and metals, are often released in association with CO_2 and can potentially act as confounding factors. In this study, we evaluated the composition, diversity and inferred functional profiles of microbial biofilms in Levante Bay (Vulcano Island, Italy, Mediterranean Sea), a well-studied shallow-water hydrothermal vent system. We analyzed 16S rRNA transcripts from biofilms exposed to different intensity of hydrothermal activity, following a redox and pH gradient across the bay. We found that elevated CO_2 concentrations causing low pH can affect the response of bacterial groups and taxa by either increasing or decreasing their relative abundance. H_2S proved to be a highly selective factor shaping the composition and affecting the diversity of the community by selecting for sulfide-dependent, chemolithoautotrophic bacteria. The analysis of the 16S rRNA transcripts, along with the inferred functional profile of the communities, revealed a strong influence of H_2S in the southern portion of the study area, and temporal succession affected the inferred abundance of genes for key metabolic pathways. Our results revealed that the composition of the microbial assemblages vary at very small spatial scales, mirroring the highly variable geochemical signature of vent emissions and cautioning for the use of these environments as models to investigate the effects of ocean acidification on microbial diversity.

Keywords: microbial biofilms, active microbial communities, ocean acidification, Vulcano island, sulfide oxidizing bacteria, shallow-water hydrothermal vents, Epsilonproteobacteria/*Campylobacteria*, Gammaproteobacteria

INTRODUCTION

Biofilms are typically defined as assemblages of microbial cells of either single or multiple species, enclosed in a gelatinous matrix adhering to living and inert surfaces (Costerton, 1999). The formation of biofilms is a multi-step process where nude surfaces are initially conditioned with organic and inorganic molecules forming a primary film, which successively attracts the microbial

cells (Flemming and Wingender, 2010). After adhesion to the surface, these microorganisms start producing extracellular polymers (EPS) forming the amorphous matrix surrounding their cells (Flemming et al., 2007). A complex three-dimensional structure including multiple layers of microcolonies (microbial cells and EPS) separated by interstitial channels characterizes mature biofilms, which constitute heterogeneous and dynamic communities attached to the surfaces (Davey and O'toole, 2000). Biofilms represent the predominant form of microbial life in the marine environment, ranging from the surface to the deep ocean as well as in the water column where they constitute the precursor nucleus of marine snow (Dobretsov, 2010). In the photic zone, bacteria and microalgae are the main organisms constituting microbial biofilms which include also microscopic fungi, heterotrophic flagellates and sessile ciliates (Decho, 2000).

The importance of biofilms in the ecology of benthic ecosystems is widely recognized. Indeed, biofilms not only represent the main food source for a variety of grazers, but can actively control the development of benthic communities by influencing the settlement of algal spores and invertebrate larvae, including relevant aquaculture species such as *Mytilus galloprovincialis* (Bao et al., 2007; Hadfield, 2011). Biofilms also provide valuable ecosystem services including primary production, nutrient recycling, organic matter degradation and sediment trapping (Bhaskar and Bhosle, 2005; Ortega-Morales et al., 2010). Several compounds with potential application in biotechnology are isolated from microorganisms within biofilms, particularly from those living in extreme marine environments (Mancuso Nichols et al., 2005). On the other hand, biofilms colonizing artificial surfaces such as oil and gas installations, aquaculture nets and ship hulls alter the physical and chemical properties of these structures causing great economic losses in the maritime industry (Qian et al., 2007; Garrett et al., 2008; Salta et al., 2013). For all the reasons stated above, microbial biofilms are both ecologically and economically relevant.

In recent years, microbial biofilms have been investigated also in the context of climate change and its effects, including ocean acidification. In this regard, Lidbury et al. (2012) reported increased biomass as well as shifts in the assemblage of the community of biofilms along a natural pCO_2/pH gradient in Levante Bay at Vulcano vents. In the same area, chlorophyll-*a* concentration in microphytobenthos communities were higher at low pH sites (pH: 7.9) compared to control sites (pH: 8.1), with changes in the composition of benthic diatom assemblages observed on both artificial (Johnson et al., 2013) as well as natural surfaces (Johnson et al., 2015). Although some changes in the community composition of biofilms could be explained by taxa specific response to acidification (Witt et al., 2011; Taylor et al., 2014), metabolic activity measured as oxygen fluxes (i.e., oxygen production and consumption rates) would not be affected by ocean acidification (Witt et al., 2011). More recently, Hassenrück et al. (2017) demonstrated that the diversity of mature biofilms in coral reef systems was scarcely influenced by pH changes, whereas other biotic and abiotic factors such as light exposure and grazing intensity controlled the biofilm community which, in turn, conditioned the settlement of coral larvae. Furthermore, sediment bacterial community composition showed variations in the abundance of few taxa in relation to long-term acidification at Vulcano vents, but overall the organisms appeared to persist under the acidified conditions (Kerfahi et al., 2014). Based on these observations, and the fact that pH variations naturally occurring in the aquatic environments are well tolerated by microorganisms, some authors argue that, overall, the degree of pH variations due to anthropogenic ocean acidification might not dramatically affect microbial communities (Joint et al., 2011). In order to investigate the response of microbial biofilms to ocean acidification, a colonization experiment was conducted in the shallow-water vent system of Levante Bay (Vulcano Island), a site considered as analog of future acidified oceans (Boatta et al., 2013; Aiuppa et al., 2021). The aim of this study was to evaluate the influence of hydrothermal vent emissions at Vulcano island on the diversity, composition and inferred functional profiles of microbial biofilms, based on the hypothesis that natural acidification induced by the elevated CO_2 concentrations of vents emissions could affect the structure and functionality of these communities. We also aimed at evaluating the combined effect of CO_2 and H_2S emissions on the biofilm communities, as the latter is also present at detectable concentrations in the southern part of Levante Bay (a detailed description of the area is provided in the following section).

MATERIALS AND METHODS

Study Area

Vulcano Island is part of the active volcanic arc of the Aeolian Islands archipelago in the Southern Tyrrhenian Sea (Mediterranean Sea, **Figure 1**). Since its last eruption (1888–1890), the volcano has been in a state of solfataric activity, characterized by the presence of both aerial as well as submerged fumaroles mainly releasing CO_2 for a total of 482 t day^{-1} and, to a lesser extent, H_2S and other gas species (Inguaggiato et al., 2012). In Levante Bay small fumarolic emissions occur offshore at shallow depths (<10 m). Volcanic emissions are visible as bubble trains rising from the sea-bottom and are dominated by CO_2 (98–99% vol of CO_2), for a total estimated value of 3.6 t day^{-1} of CO_2 (Inguaggiato et al., 2012). In the southernmost point of Levante Bay, bubbling gas discharges are also characterized by a variable concentration of H_2S (1.57–2.47 vol%, Carapezza et al., 2011) probably derived by alkaline hydrolysis of metal sulfides promoted by weakly acidic waters (Capaccioni et al., 2001). However, the concentration of H_2S decreases with the distance from the vents and only a small portion of the gas enters into the aqueous phase where it oxidizes to sulfate due to the high O_2 saturation recorded in the bay, particularly in the northern area (Boatta et al., 2013). Due to the intense venting in the southern part of the Levante Bay, a pH gradient (pH: 5.65–8.1) runs parallel to the north-eastern coast of the island, with pCO_2 ranging from 3361.7 ± 2971.3 μatm to 424.6 ± 61.5 μatm (Boatta et al., 2013). After a preliminary survey assessing the physicochemical parameters of Levante Bay, including temperature, salinity, pH and ORP, four sites along a pCO_2/pH gradient were selected as suitable stations to conduct a biofilm colonization experiment (**Figure 1**): Vent 1 (38°24′59.05″N, 14°57′38.76″E), located in

the southern point and representing the main venting area of the bay, is characterized by intense CO_2 and H_2S gas fluxes; Vent 2 (38°25′9.40″N, 14°57′42.14″E), located about 330 m north of Vent 1, is not a vent *sensu stricto* but rather an area characterized by small and sparse CO_2-dominated emissions; REF 1 (38°25′14.33″N, 14°57′52.94″E) and REF 2 (38°25′17.12″N, 14°57′56.77″E), located about 560 m and 760 m north of the main venting area respectively, represent reference sites where neither vent emissions nor their influence have been detected.

Experimental Design and Sampling Procedure

The taxonomic composition of microbial biofilm communities along the Levante Bay pCO_2/pH gradient was assessed via a colonization experiment that took place between October and December 2016. Physicochemical parameters including temperature, pH, Oxidation-Reduction Potential (ORP) and salinity were periodically recorded over the duration of the experiment using a multiparameter probe (model HI98194; HANNA Instruments, Woonsocket, RI, United States).

Sterile microscope glass slides were used as substrate for biofilm colonization. Slides were assembled into a satellite-like structure connected to a float and, at the lower end, to a dead weight to secure the full structure to the sea bottom (**Figure 1**). These substrates were deployed at a depth of 3 m at the four sites along the pCO_2/pH gradient (Vent 1, Vent 2, REF 1, and REF 2). Three structures ($n = 3$ replicates) were collected by scuba divers from each site at two times: t1 (17 days after the deployment) and t2 (57 days after the deployment) corresponding to the end of the experiment. Immediately after collection, the glass slides were disassembled from the structures. Biofilms were removed from each glass slide with a sterile blade, stored in RNA Later (Thermofisher, Waltham, MA, United States), transferred to the laboratory and preserved at –20°C for further analyses.

Analytical Methods

In order to assess the diversity, composition and inferred functional profiles of microbial biofilm communities from Levante Bay experiments, both molecular and bioinformatic analyses were performed.

RNA Extraction, cDNA Synthesis, Amplification of the 16S RNA and Sequencing

RNA was extracted from RNA Later-stored biofilms using a phenol:chloroform extraction protocol. Briefly, 850 μl of extraction buffer (50 mM Tris-HCl, 20 mM EDTA, 100 mM NaCl; pH 8.0) and 100 μl of lysozyme (100 mg/ml) were added to 0.5 g of biofilm sample. After incubation at 37°C for 30 min, the samples were supplemented with 5 μl of proteinase K (20 mg/ml) and incubated as previously. This mix was then supplemented with 50 μl of SDS (20%) and incubated in a water bath at 65°C for 1 h. RNA was extracted in a series of phenol:chloroform:isoamylalcohol (25:24:21, pH 4.3) and chloroform:isoamylalcohol (24:21) extractions. Overnight precipitation of the extracted supernatant was performed using 3M sodium acetate and isopropanol. The precipitated sample was washed twice with 70% ice cold ethanol and resuspended in ultrapure water. A DNAse treatment (TURBO DNAse kit, Invitrogen, Carlsbad, CA, United States) was performed according to the manufacturer's instructions to remove any DNA carryover from the extracted samples. The resulting RNA was used as a template in a reverse transcription reaction generating cDNA (Invitrogen cDNA synthesis kit, Invitrogen, Carlsbad, CA, United States), following the specifications of the manufacturer. To evaluate the integrity of the cDNA, the product of the reverse transcription reaction was used as a template for the polymerase chain reaction amplification (PCR) of 16S rRNA transcripts using primers Bact 8F (5′-AGAGTTTGATCCTGGCTCAG-3′) and Univ 519R (5′-ATTACCGCGGCTGCTGG- 3′). The diversity of biofilm communities from Levante Bay was evaluated by amplifying the variable 4 (V4) region of 16S rRNA transcripts using the prokaryotic universal primers (515f 5′-GTG CCA GCM GCC GCG GTA A-3′ and 806r 5′-GGA CTA CVS GGGTAT CTA AT-3′; Caporaso et al., 2011), and the HotStarTaq Plus Master Mix Kit (Qiagen, Hilden, Germany), under the following conditions: 94°C for 3 min, followed by 30 cycles at 94°C for 30 s, 53°C for 40 s and 72°C for 1 min, and by a final elongation step at 72°C for 5 min. Multiple PCR reactions were combined to reduce potential bias. The total number of reads16S rRNA amplicons were sequenced using a PMG Ion Torrent platform at the Molecular Research LP facility (Shallowater, TX, United States). Sequences are available through the NCBI Short Read Archive database with accession number PRJNA789583. At the research facility, sequences were depleted of barcodes and primers, then sequences < 150 bp were removed along with sequences with ambiguous base calls and with homopolymer runs > 6 bp. The total number of reads for all samples after the chimera check was 2,095,467. The average number of reads per sample was 87,311.

Bioinformatics

The 16S rRNA sequence analysis was conducted using the QIIME 1.9 software package (Caporaso et al., 2010). Chimeric sequences were removed using ChimeraSlayer (Haas et al., 2011). Operational Taxonomic Units (OTUs) were picked at 97% similarity using the "pick_open_reference_otus.py." Clustering of OTUs was performed using the Greengenes database (McDonald et al., 2012). Taxonomic classification of clustered OTUs was done using the Ribosomal Database Project Classifier against the Silva 123 Database (Quast et al., 2013; Glöckner et al., 2014; Yilmaz et al., 2014). Functional profiles of biofilms communities were predicted using the software Tax4Fun, a tool for functional community profiling based on 16S rRNA data (Aßhauer et al., 2015). Briefly, Tax4Fun uses the normalized taxonomic abundances to linearly combine 16S rRNA gene-based biodiversity structure to a precomputed genomic reference profiles for the prediction of the functional profile of the microbial community (see Aßhauer et al., 2015 for further details).

Phylogenetic Analyses

Sequences of the V4 region of 16S rRNA genes of OTUs and 16S rRNA sequences of their closest cultured relatives (obtained by searching the NCBI non-redundant database by nucleotide

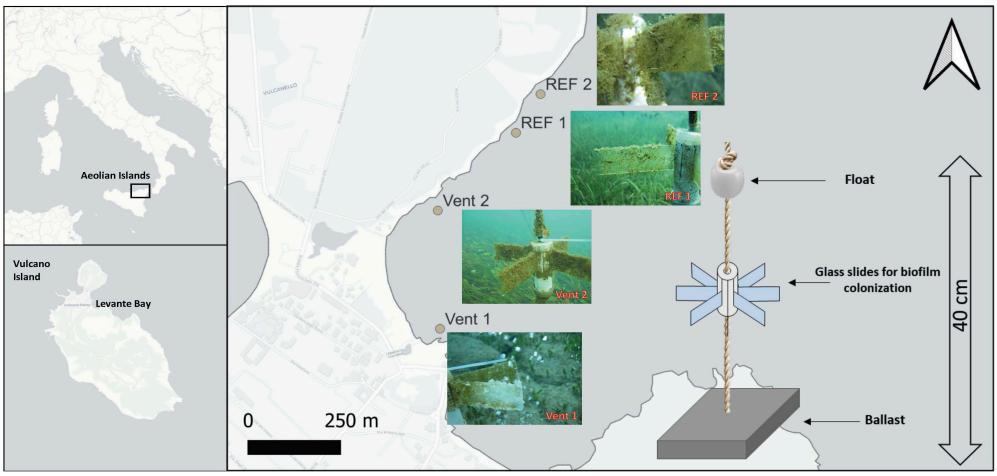

FIGURE 1 | Map showing the location of the study site (Vulcano Island-Levante Bay) and the four sites chosen for the experiments. **(Right)** scheme of the satellite-like structure used for the experiment. **(Left)** pictures of the biofilms collected from the different sites at the end of the experiment.

BLAST search) were aligned using Clustal Omega (Sievers et al., 2011) within SEAVIEW (Galtier et al., 1996; Gouy et al., 2010). The resulting alignment was used to reconstruct phylogenetic trees using the Maximum Likelihood algorithm with PhyML (Guindon and Gascuel, 2003) using the general time reversible (GTR) model, aLRT scores calculated.

Statistical Elaboration

Differences between sites and among times in the physicochemical variables, taxonomic composition (at the Phylum, Class, and Genus levels) and predicted functional profiles of biofilms were tested through Permutational Analysis of Variance (PERMANOVA). In all cases, a 4 × 2 orthogonal design with "Site" and "Time" set as fixed factors was used to conduct the analysis on square root transformed data. The effect of the interaction of the two factors "Site" and "Time" was tested as well. Pair-wise tests were performed on significant results. Square-root transformed data were used in order to construct resemblance matrices based on Euclidean distance for physicochemical variables and Bray–Curtis distance for the taxonomic composition. Gower distance was applied for elaboration of the predicted functional profiles (Gower, 1971; Anderson et al., 2008). All statistical elaborations were performed at both multivariate and univariate level. Similarities among 16S RNA transcripts was visualized using non-metric multidimensional scale (nMDS) coupled with Cluster analysis. A SIMPER test was conducted in order to understand the relative contribution of single OTUs to the observed difference between samples using PAST Paleontological Statistics V3.25[1]; after that, a BLASTn (megablast) search was performed against the NCBI-National Center for Biotechnology Information nucleotide database[2] in order to identify the most similar prokaryotic-derived sequence entry on the first twelve taxa identified by the SIMPER test.

Diversity indexes (Taxa_S, Individuals, Dominance, Simpson, Shannon, Evenness, Margalef, Chao-1) were also calculated on the PAST Paleontological Statistics V3.25 software using a Bray Curtis similarity matrix obtained from the OTUs abundance table. The PRIMER + PERMANOVA v6 software package (PRIMER-E Ltd., Plymouth, United Kingdom, Anderson et al., 2008) was used to perform the statistical elaborations on the physicochemical variables, the community structure and diversity of microbial biofilms as well as their predicted functional profiles.

RESULTS

Environmental Settings

Physicochemical parameters were measured at least once every 2 weeks throughout the experiment (**Table 1**). Temperature ranged from 18.3 to 22.7°C, showing similar values among sites and decreasing significantly over time (**Supplementary Table S1**). pH values, ranging from 6.7 to 8.3, showed significant differences between the vent and reference sites, as well as between Vent 1 and Vent 2 (**Table 1** and **Figure 2**). ORP values ranged from –67.8 mV to 180.8 mV and showed a trend similar to the pH, with values increasing from Vent 1 toward the other sites, and significant differences over time. On the contrary, salinity remained relatively constant over time and across all sites (**Table 1** and **Figure 2**).

Community Structure and Diversity

In the biofilms collected from Levante Bay, up to >98% of the OTUs were affiliated to the domain Bacteria, while the remaining OTUs were associated to Archaea and unclassified sequences. Among the Archaea that could be classified, sequences related to *Nitrosopumilus* and *Methanobacterium* spp. were

[1]https://palaeoelectronica.org/2001_1/past/issue1_01.htm
[2]https://www.ncbi.nlm.nih.gov/nucleotide/

TABLE 1 | Physicochemical parameters of the study sites for the duration of the experiment.

	Vent 1	Vent 2	REF 1	REF 2
October				
T [°C]	22.74 ± 0.35	22.58 ± 0.08	22.75 ± 0.37	22.65 ± 0.23
pH [unit]	7.39 ± 0.49	8.03 ± 0.13	8.18 ± 0.04	8.28 ± 0.14
ORP [mV]	–49.68 ± 14.05	119.71 ± 25.94	145.66 ± 5.87	115.58 ± 7.08
Sal.[psu]	38.40 ± 0.00	38.38 ± 0.04	38.35 ± 0.14	38.41 ± 0.03
November				
T [°C]	21.02 ± 1.20	20.91 ± 1.14	20.88 ± 1.12	20.86 ± 1.09
pH [unit]	7.14 ± 0.46	7.88 ± 0.25	8.10 ± 0.09	8.14 ± 0.08
ORP [mV]	–32.99 ± 43.02	90.67 ± 76.05	73.38 ± 85.99	66.47 ± 78.79
Sal.[psu]	38.39 ± 0.06	38.39 ± 0.04	37.64 ± 1.36	38.22 ± 0.32
December				
T [°C]	18.51 ± 0.36	18.35 ± 0.61	18.28 ± 0.63	18.26 ± 0.63
pH [unit]	6.70 ± 0.77	7.89 ± 0.03	8.07 ± 0.04	8.15 ± 0.04
ORP [mV]	–11.51 ± 21.37	122.58 ± 48.50	164.71 ± 13.42	173.78 ± 10.01
Sal.[psu]	38.27 ± 0.01	38.27 ± 0.02	38.25 ± 0.06	38.28 ± 0.06

Values are reported as mean ± standard deviation for each site in each month.

detected at very low abundances (<0.0025%). At the phylum level (**Supplementary Figure S1A**), the most abundant sequences across all samples were Proteobacteria (47.9%), Cyanobacteria (27.3%), and Bacteroidetes (11.8%). Multivariate analysis at this taxonomic level revealed, overall, significant differences among biofilms at Vent 1 *vs.* Vent 2, as well as Vent 1 *vs.* REF 1 (**Supplementary Table S2**).

On average at the class level (**Supplementary Figure S1B**), Gammaproteobacteria were numerically dominant at Vent 1 at the beginning of the experiment (45.8%) and were followed by chloroplast-related sequences (19.9%) and Alphaproteobacteria (8.1%). Other abundant groups in this site at t1 were Epsilonproteobacteria (aka *Campylobacteria*) and Deltaproteobacteria (4.8% and 3.7%, respectively). At the end of the experiment (t2), the abundance of Gammaproteobacteria in Vent 1 decreased considerably (22%), while Alphaproteobacteria doubled their abundance (16.5%); chloroplast-related sequences, Deltaproteobacteria and Epsilonproteobacteria slightly increased toward the end of the experiment (23.1, 5.7, 6.2% respectively at t2).

On average, the biofilm community of Vent 2 at t1 was dominated by chloroplast-related sequences and Gammaproteobacteria (25.5 and 23.5%, respectively), followed by Alpha- and Deltaproteobacteria (15.4 and 5.6%, respectively). After 57 days (t2), the community composition remained substantially similar, with a slight decrease in the relative abundance of chloroplast-related sequences and Gammaproteobacteria (22.5 and 22.9%, respectively), and

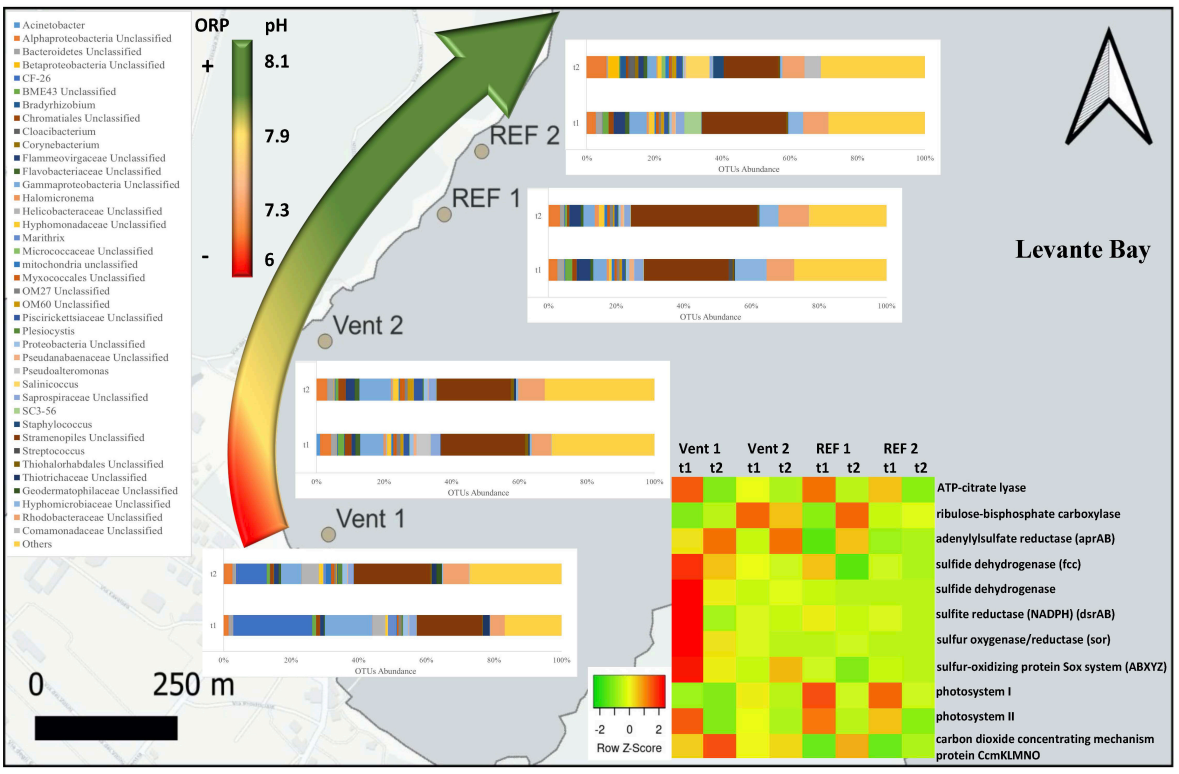

FIGURE 2 | Genus-level taxonomic affiliation of 16S rRNA transcripts recovered from the biofilms located at the four study sites of Levante Bay, Vulcano island. Taxa representing genera that account for at least 1% (on average) of the overall abundance in all samples are shown. The curved arrow on the left indicates the redox (ORP) and pH observed along the pCO_2/pH gradient. The heatmap on the right shows the abundance of genes for inferred central metabolic pathways of the biofilms.

a minor increase in the relative abundance of Alpha- and Deltaproteobacteria (17 and 6.2%, respectively). In REF 1, chloroplast-related 16S rRNA transcripts were always numerically dominant in the community, with their abundance increasing over time (from 26.1 to 38.1% for t1 and t2, respectively). Alphaproteobacteria were the second most abundant bacterial group at this site and remained relatively constant during the experiment (24.5 and 24.1% for t1 and t2, respectively).

The abundance of Gammaproteobacteria at REF 1 was lower than that of the other groups at this site, and lower than Gammaproteobacteria at both Vent sites. On average, Gammaproteobacteria decreased over the duration of the experiment (from 12.5% at t1, to 9.6% at t2). A similar trend was observed for Deltaproteobacteria (4.3 and 3.7% at t1 and t2, respectively). Cytophagia were numerically higher at this site compared to Vent 1 and Vent 2, although their abundance slightly decreased over time (from 5.2% at t1, to 3.9% at t2).

The composition of the biofilm community at REF 2 was similar to REF 1 at t1, with chloroplast-related sequences constituting 25.9% of the community, followed by Alphaproteobacteria (20.3% on average), Gammaproteobacteria (14.8%), Cytophagia (9.2%), and Deltaproteobacteria (4.1%). At the end of the experiment (t2), the relative average abundance of chloroplast-related sequences, Gammaproteobacteria, Cytophagia, and Deltaproteobacteria decreased (16.9, 11, 2.1, and 2.5%, respectively), whereas Alphaproteobacteria remained relatively constant (20.6%). Bacilli and Betaproteobacteria, which were scarcely present at t1, increased numerically in mature biofilms (t2), reaching an average of 10.3 and 10% of the overall community, respectively.

At the class level, the biofilm community of Vent 1 was significantly different compared to all the other sites, whereas biofilms of Vent 2 were significantly different compared to those of REF 1 (**Supplementary Table S2**).

At the genus level (**Figure 2**), sequences related to the *Thiothrix*-related group CF-26 were, on average, the most abundant (23.3%) in young biofilms (t1) at Vent 1; the other abundant groups were unclassified sequences of Stramenopiles and Gammaproteobacteria, representing respectively 19.3 and 14% of the total sequences, followed by unclassified taxa affiliated with the families Rhodobacteraceae and Helicobacteraceae (4.2 and 3.7%, respectively), and with the genus *Candidatus* Marithrix (2.4%). At the end of the experiment (t2), the relative abundance of these groups changed: the abundance of the *Thiothrix*-related group CF-26 decreased to 9.1%, while *Candidatus* Marithrix and unclassified sequences of Gammaproteobacteria decreased to 0.7 and 6%, respectively, and the relative abundance of unclassified Stramenopiles as well as of taxa affiliated with Rhodobacteraceae and Helicobacteraceae families increased (22.5, 7.6, and 5%, respectively).

At Vent 2, unclassified Stramenopiles constituted the 24.7% of the overall average abundance of young biofilms (t1). The most abundant genus belonging to the Gammaproteobacteria was *Pseudoalteromonas* (4% on average), while unclassified Gammaproteobacteria accounted for 6.9%. Within the Alphaproteobacteria, members of the Rhodobacteraceae accounted for 5.7%, while 3.2% remained unclassified. At the same site, the mature biofilm community (t2) showed a similar taxa assemblage, with the exception of *Pseudoalteromonas*-related sequences, whose abundance decreased drastically (<0.01%).

Chloroplast-related 16S rRNA transcripts from unclassified Stramenopiles constituted the major group at REF 1, with their abundance increasing from 25.1 to 37.4% over time. Sequences of unclassified Hyphomicrobiaceae and unclassified Rhodobacteraceae were also relatively abundant and showed different patterns, with the former decreasing (from 9.5 to 5.6%) and the latter remaining relatively constant during the experiment (from 8.1 to 8.3%).

The most abundant groups at the beginning of the experiment (t1) at REF 2 were unclassified Stramenopiles (24.8%) and unclassified Rhodobacteraceae (7.3%), followed by unclassified Gammaproteobacteria (5.1%), group SC3-56 of the phylum Bacteroidetes (5%) and unclassified Hyphomicrobiaceae (4.4%). At the end of the experiment, all these groups decreased in their abundance, while other taxa such as *Salinicoccus, Staphylococcus*, unclassified Alphaproteobacteria and unclassified Comamonadaceae increased greatly (6.9, 3.1, 5.9, and 4.8%, respectively).

Permanova analysis of the community composition at the genus level revealed significant differences for the factor "Site." "Time" was also significant for the community structure, although to a lesser extent (**Supplementary Table S2**). Pair-wise tests revealed significant differences between Vent 1 vs. all the other sites for the factor "Site," as well between Vent 2 and REF 1 (**Supplementary Table S2**).

SIMPER analysis conducted on Bray-Curtis matrix highlighted the taxa that mostly contributed to the dissimilarity among the samples (**Supplementary Table S3**). The highest contribution (3.4%) was attributed to OTU ID 1836083, which was related OTU ID 95 and to uncultured Gammaproteobacteria belonging to the *Thiothrix*-related group CF-26 sequences, previously recovered from a shallow-water gas vent in the Mediterranean Sea (Tor Caldara OTU 27, **Figure 3**; Patwardhan et al., 2018) and other marine hydrothermal environments. The second taxa which contributed to 2.4% of the total dissimilarity was OTU ID 264, whose closest relative was an uncultured cyanobacterium retrieved from microbial biofilms from the Great Barrier Reef. Several sequences related to phototrophs, including Bacillariophyta as well as Foraminifera, contributed between 1.6 and 0.1% of the total dissimilarity. Interestingly, 1.2% of the sequences were related to halophilic bacteria such as *Salinicoccus* spp., hydrocarbon-degrading, sulfate-reducing Deltaproteobacteria (0.7%) as well as sulfide-oxidizing bacteria related to *Thiothrix* spp. (0.6%).

Similarity among communities from different sites at the genus level is shown by the nMDS plot (**Figure 4**), based on Bray-Curtis similarity calculated on the occurrence of sequences from the OTU table (n-MDS 2-D stress was 0.1). The nMDS ordination plot, coupled with Cluster analysis at 70% similarity level, showed the separation of two main groups: samples from Vent 1 formed a unique cluster, distinct from the majority of samples from the other sites which, in general, clustered in another group. Four samples (one from each site) clustered independently. The

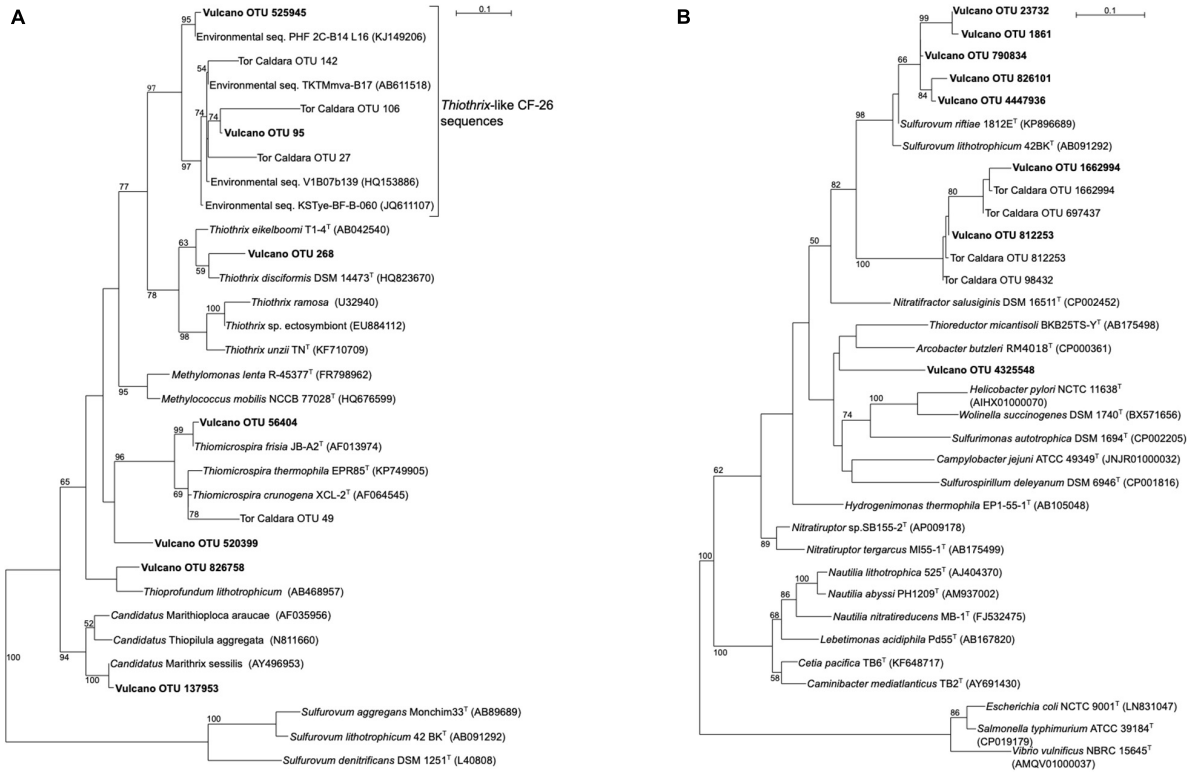

FIGURE 3 | Maximum-likelihood phylogenetic trees derived from 16S rRNA transcript sequences from Vulcano. aLRT branch support values higher than 50% were based on 1000 replicates and are shown at each node. Bar, 0.1% substitutions per position. Tor Caldara sequences were reported in Patwardhan et al. (2018). **(A)** Phylogenetic tree showing sequences related to sulfide-oxidizing Gammaproteobacteria (in boldface). Sequences belonging to the class Epsilonproteobacteria were used as outgroup. **(B)** Phylogenetic tree showing sequences related to sulfide-oxidizing Epsilonproteobacteria (in boldface). Sequences belonging to the class Gammaproteobacteria were used as outgroup.

over-imposition of vectors representing environmental parameters showed that pH and ORP were responsible for the separation of Vent 1 from the other sites.

Diversity indexes showed similar values across sites and times with the exception of dominance and evenness, which differed significantly for the factor "Site." Dominance was significantly different between Vent 1 and Vent 2 as well as between both Vent sites and REF 1. Evenness was significantly lower in Vent 1 compared to Vent 2 (see **Supplementary Tables S4–S6** for detailed results).

Predicted Functional Profiles of Vulcano Biofilm Communities

The inferred *in situ* expression of the central metabolic pathways in the marine biofilm communities collected in Levante Bay is reported in **Figure 5** (numerical values in **Supplementary Table S7**). We reported the normalized abundances of inferred key genes involved in carbon fixation, nitrogen and sulfur metabolism, photosynthesis, oxygen reduction, heavy metals detoxification and carbon dioxide concentrating mechanisms (CCMs). Overall, genes for oxygen reduction, photosynthesis and sulfur metabolism were prevalent in the biofilm communities of Levante Bay. Multivariate analyses of each pathway revealed significant differences for carbon fixation cycles, sulfur metabolism, photosynthesis and CCMs only. **Carbon fixation:** the ATP-citrate lyase gene (encoding a diagnostic enzyme for the reductive tricarboxylic acid cycle) and the ribulose-bisphosphate carboxylase gene (RuBisCO, Calvin-Benson-Bassham cycle) were inferred to be significantly more prevalent in Vent 1 with respect to the other sites. However, RuBisCO decreased significantly over time (**Supplementary Table S8**). **Sulfur metabolism:** the genes for sulfur metabolism were inferred to be significantly more prevalent in the biofilms of Vent 1 compared to both REF sites at the beginning of the experiment (t1), while in mature biofilms (t2) significant changes occurred between Vent 1 and Vent 2 and REF 1, as well as between Vent 2 and REF 1. Time significantly affected the prevalence of genes involved in the sulfur metabolism in Vent 1 and REF 1. SIMPER analysis showed that the adenylylsulfate reductase *(aprAB)* gene contributed the most to the dissimilarity between Vent and REF sites, while the sulfate adenylyltransferase *(sat)* gene was the most determinant in the differences across time (**Supplementary Tables S9**, **S10**). **Photosynthesis:** the inferred prevalence of genes involved in photosynthesis was relatively high compared to the other metabolic pathways and showed significant changes in time (**Supplementary Table S11**). Indeed, the abundance of the two genes for photosystem II

and photosystem I, which respectively contributed to the 49.7 and 34.7% of dissimilarity between t1 and t2, decreased significantly across time at all sites, while the genes for the photosystem P840 reaction center was inferred to be present only at Vent 1, t1. **Carbon concentrating mechanisms:** the genes for carbon dioxide concentrating mechanisms were inferred to be significantly lower in Vent 1 compared to both REF sites, as well as at t1 vs. t2 for the factor "Time" (**Supplementary Table S11**). The gene encoding for the carbon dioxide concentrating mechanism protein (*CcmKLMNO*) was responsible for the differences detected overall (**Supplementary Table S11**). **Nitrogen metabolism:** The gene encoding for the NADH-nitrite reductase [EC:1.7.1.15] was inferred to be the most abundant of the nitrogen metabolism genes in the biofilms communities of Levante Bay, followed by the gene encoding the nitrogenase complex (*Nif*; EC:1.18.6.1). The inferred abundance pattern for the nitrogen metabolism-related genes was similar across sites and times (**Supplementary Table S7**). **Oxygen reduction:** the gene encoding for the cytochrome cbb3 [EC:1.9.3.1] was inferred to be the most abundant of all the genes included in this analysis, followed by cytochrome bd encoding gene [EC:1.10.3.14] (**Supplementary Table S7**). **Heavy metal detoxification:** the arsenate reductase encoding gene [EC:1.20.4.1] was predicted to occur frequently, albeit with no significant changes overall.

DISCUSSION

Although microbial biofilms are key components of benthic communities and provide relevant ecosystem services in the marine environment, their response to ocean acidification is not clear. This study aimed at filling this gap by investigating the community composition of biofilms exposed to natural acidification in Levante Bay (Vulcano Island, Mediterranean Sea), a site considered analog for future acidified oceans. Based on previous studies of the Vulcano hydrothermal system, we hypothesized that acidification induced by elevated CO_2 concentration might affect the abundance and/or the metabolic activity of photosynthetic microorganisms within the biofilms. Alternatively, we posited that the elevated concentration of H_2S, serving as the main electron donor for the biofilm communities, might become the main driver of microbial metabolism and overcome the effect of CO_2. In that case, we expected that sulfide-oxidizing bacteria would achieve a competitive advantage in the biofilm community.

Our findings showed that the distribution and abundance of few bacterial groups varied along the pCO_2/pH gradient and identified significant changes in the diversity of the microbial communities and of their predicted functional profiles. These changes, however, were not always attributable exclusively to elevated concentration of CO_2. Indeed, we found that factors related to hydrothermal vent activity in Levante Bay, such as the concentration of H_2S (Boatta et al., 2013) and the consequent negative ORP values detected in the southern portion of the Bay (site Vent 1 in our study), significantly affected the composition and functionality of microbial biofilms by selecting microorganisms able to use sulfide an energy source. The lowest pH and ORP value were measured at Vent 1, the main venting area of the bay, in line with the elevated H_2S and pCO_2 values previously measured at this site (Capaccioni et al., 2001; Boatta et al., 2013).

The Characteristics of the Vent 1 Biofilm Community Set It Apart From the Other Sites

Gammaproteobacteria were abundant in biofilms from Vent 1 and Epsilonproteobacteria were also detected, albeit to a lesser extent (**Figure 2**). Both these taxa include sulfide-oxidizing bacteria and are usually dominant in microbial communities of shallow and deep-sea hydrothermal vents. Gammaproteobacteria are usually more prevalent in lower sulfide habitats, while Epsilonproteobacteria dominate in higher sulfide habitats (Engel et al., 2004; Macalady et al., 2008; Reigstad et al., 2011; Giovannelli et al., 2013; O'Brien et al., 2015; Miranda et al., 2016; Meier et al., 2017; Patwardhan et al., 2018, 2021). Phylogenetic analyses of representative gammaproteobacterial sequences revealed that *Thiothrix*-, *Thiomicrospira*-, *Thioprofundum*-, and *Candidatus* Marithrix -related bacteria were active at Vent 1 (**Figure 3A**), while active members of the Epsilonproteobacteria were mainly related to *Sulfurovum* spp. (**Figure 3B**). These bacteria are chemolithoautotrophs that conserve energy by sulfide-oxidation (Jannasch et al., 1985; Lentini et al., 2014; Giovannelli et al., 2016; Patwardhan et al., 2021) suggesting that the oxidation of reduced sulfur species is one of the main energy-yielding process within the biofilm community at Vent 1. These observations are in line with the geochemical characteristics of Vent 1 (CO_2 and H_2S availability) and with the predicted metabolic pathways at this site, which revealed sulfide oxidation (mainly via the Sox, Fcc, and SQR pathways) and carbon fixation (via the CBB cycle) to be the main metabolisms (**Supplementary Tables S7–S9**). Within the Gammaproteobacteria, the relatively higher abundance of *Thiothrix*- and *Candidatus* Marithrix -related sequences compared to Epsilonproteobacteria (**Figure 2**) is likely due to the lower concentration of sulfide at Vent 1 compared to other geothermal habitats colonized by these organisms, such as deep-sea and shallow-water hydrothermal systems (Macalady et al., 2008; Giovannelli et al., 2013; O'Brien et al., 2015; Meier et al., 2017; Patwardhan et al., 2018, 2021). Interestingly, the gamma- and epsilonproteobacterial sequences from the Vulcano biofilms at Vent 1 were closely related to those retrieved from Tor Caldara, a coastal CO_2 and H_2S gas vent in the Mediterranean Sea (**Figures 3A,B**; Patwardhan et al., 2018). A metaproteogenomic study of the Tor Caldara biofilms demonstrated that *Thiothrix*- and *Thiomicrospira*-related Gammaproteobacteria, as well as *Sulfurovum*-related Epsilonproteobacteria, expressed pathways for sulfide oxidation and carbon fixation (Patwardhan et al., 2021), in line with the inferred metabolism of the Vulcano biofilms at the Vent 1 site (**Figure 5**). At Vent 1, biofilms were visually different compared to those from the other sites, and white and brown biofilms colonized the same glass slides and were very close to each other (**Figure 1**). Indeed, the biofilm community of Vent 1 formed a unique cluster, whose separation from the other biofilms was driven by pH and ORP (**Figure 4**).

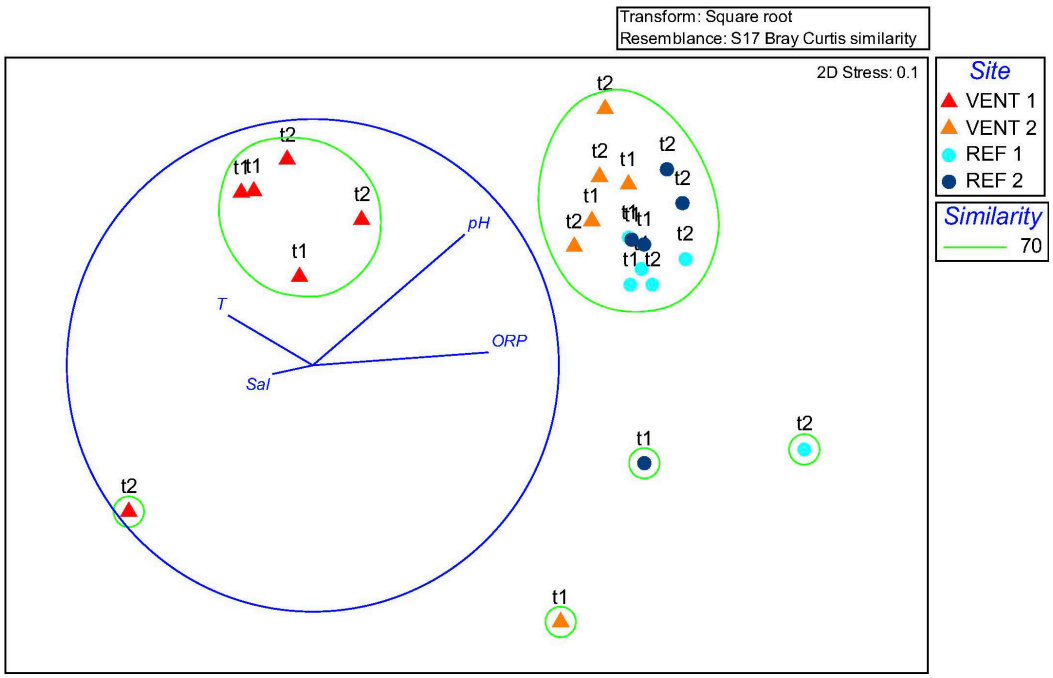

FIGURE 4 | Non-metric multidimensional scaling (nMDS) plot of biofilms 16S rRNA transcript.

PATHWAY	GENE	Vent 1		Vent 2		REF 1		REF 2	
		t1	t2	t1	t2	t1	t2	t1	t2
CARBON (rTCA)	ATP-citrate lyase [EC:2.3.3.8]								
CARBON (CBB)	ribulose-bisphosphate carboxylase [EC:4.1.1.39]								
NITROGEN	nitrate reductase / nitrite oxidoreductase [EC:1.7.5.1 1.7.99.-]								
	nitric oxide reductase [EC:1.7.2.5]								
	nitrite reductase (cytochrome c-552) [EC:1.7.2.2]								
	nitrite reductase (NADH) [EC:1.7.1.15]								
	nitrite reductase (NO-forming) / hydroxylamine reductase [EC:1.7.2.1 1.7.99.1]								
	nitrite reductase (NO-forming) [EC:1.7.2.1]								
	nitrogen fixation protein NifBQTUXZ								
	nitrogenase protein Nif [EC:1.18.6.1]								
	nitroreductase								
	nitrous-oxide reductase [EC:1.7.2.4]								
SULFUR	adenylylsulfate reductase (aprAB) [EC:1.8.99.2]								
	polysulfide reductase (psrBC)								
	sulfate adenylyltransferase (sat) [EC:2.7.7.4]								
	sulfide dehydrogenase (fcc) [EC:1.8.2.3]								
	sulfide dehydrogenase [EC:1.8.1.19]								
	sulfide:quinone oxidoreductase (sqr) [EC:1.8.5.4]								
	sulfite reductase (NADPH) (dsrAB) [EC:1.8.1.2]								
	sulfur oxygenase/reductase (sor) [EC:1.13.11.55]								
	sulfur-oxidizing protein Sox system (ABXYZ)								
PHOTOSYNTHESIS	photosynthetic reaction center								
	photosystem I								
	photosystem II								
	photosystem P840 reaction center								
OXYGEN REDUCTION	cytochrome aa3 [EC:1.10.3.12]								
	cytochrome bd [EC:1.10.3.14]								
	cytochrome cbb3 [EC:1.9.3.1]								
HEAVY METAL DETOXIFICATION	arsenate reductase [EC:1.20.4.1]								
	mercuric reductase [EC:1.16.1.1]								
CCMs	carbon dioxide concentrating mechanism protein CcmKLMNO								
	carbonic anhydrase [EC:4.2.1.1]								

FIGURE 5 | Predicted gene abundance (bars, normalized data) of key metabolic pathways in the biofilms collected from Levante Bay.

The simultaneous inputs of H_2S and CO_2 from hydrothermal vents causing low pH and negative ORP values at Vent 1 allowed the assemblage of a metabolically diverse community, where the distribution of organisms with different trophic strategies followed a geochemical gradient at a very small spatial scale. Indeed, the exposure to different environmental conditions was responsible for the co-existence of two communities on the same glass slide: the portion of slide directly exposed to

the sulfide-rich hydrothermal emissions was covered with white biofilms of chemosynthetic sulfide-oxidizing Epsilon- and Gammaproteobacteria; the portion of the slide less directly exposed to the vent emissions was instead covered with brown biofilms likely composed of photo- and heterotrophic bacteria (**Figure 1**). These observations suggest that at the southern area of Levante Bay (Vent 1), where hydrothermal vents activity is particularly intense, high H_2S emissions have a stronger effect on the composition of the microbial communities than CO_2, which might cause bias in the interpretation of data relative to ocean acidification. At sites where H_2S was undetectable and conditions more realistically simulate the ocean acidification scenario (e.g., Vent 2), the composition of the biofilm community shifted from chemosynthetic, sulfide-oxidizing Gammaproteobacteria to phototrophic and heterotrophic microorganisms (e.g., *Pseudoalteromonas* spp.; **Figure 2**).

The Vulcano Hydrothermal System as Proxy to Study Ocean Acidification

The response of bacteria to natural acidification was highly variable in our study and for some groups partially in contrast with previous observations on intertidal biofilm communities from the same area (Taylor et al., 2014). These differences could be attributed to seasonal (autumn = this study; spring = Taylor et al., 2014), as well as habitat (subtidal = this study; intertidal = Taylor et al., 2014) effects, as microbial biofilms are dynamic complex entities and rapidly respond to environmental variations. In this study, sequences identified as Chloroplast (class-level, **Supplementary Figure S1B**) or unclassified Stramenopiles (genus-level, **Figure 2**) refer to Cyanobacteria and other oxygenic phototrophs, as the genomes of eukaryotic plastid contain Cyanobacteria-related 16S rRNA genes due to their prokaryotic origin (*sensu de* Lynn Margulis' theory on Endosymbiotic Origin). Considering the high degree of conservation of the sequences, a more detailed taxonomic classification was not obtained as further analysis would be beyond the scope of this study. Diatoms, along with Cyanobacteria, have been indicated as potential "winners" in the future high-CO_2 world, especially for the advantage they can gain by regulating the activity of their carbon concentrating mechanisms (Raven et al., 2012; Sandrini et al., 2014). Contrary to this expectation, the abundance of oxygenic phototrophs (unclassified Stramenopiles in **Figure 2**) did not increase in low pH conditions compared to the reference sites. Biofilms in reference sites showed an assemblage typical for marine biofilm communities, where Alphaproteobacteria (Rhodobacteraceae), Bacteroidetes (Cytophagia and Flavobacteria), Cyanobacteria and other phototrophs are usually abundant. These communities were relatively stable in their composition over time, except in one reference site (REF 2) where biofilms at the end of the experiment were characterized by elevated abundance of Bacilli, in particular *Salinicoccus* and *Staphylococcus* taxa, as well as members of Comamonadaceae family (Betaproteobacteria). Since these organisms typically inhabit sediments, wastewaters and activated sludge (Rosenberg, 2013), their presence may indicate that runoff from terrestrial sources might have occurred at this site before the end of the experiment, causing the shifts observed in the community over time.

Predicted Functional Profiles

The analysis of the inferred functional profiles revealed differences in the abundance of functional genes in relation to both sites and times for carbon fixation, sulfur metabolism, photosynthesis, and CCMs. The predicted occurrence of RuBisCO, the key gene of the CBB cycle for carbon fixation, common both the sulfur-oxidizing Gammaproteobacteria and oxygenic phototrophs, along with genes for carbon fixation via the rTCA cycle and for sulfur metabolism (**Figures 2**, **5**), characterized the functional profile of Vent 1 and reflected the abundance patterns of sulfur-oxidizing bacteria detected at this site such as *Thiothrix*, *Candidatus* Marithrix and *Thiothrix*-related group CF-26 and (Gammaproteobacteria) as well as *Sulfurovum spp*. (Epsilonproteobacteria; **Figures 2**, **3A,B**). Genes for photosynthesis and the CBB cycle (RuBisCO) showed a decreasing pattern in their abundance over time (compare t1 and t2 at the various sites, **Figures 2**, **5**). This trend suggests a time-dependent relative increase of heterotrophic bacteria over autotrophs in the biofilm communities of Levante Bay.

CONCLUSION

In conclusion, this study showed shifts in the assemblage of biofilm community across the geochemical gradient of Levante Bay, Vulcano island. The effect of the emissions was particularly evident in the southern part of the bay (Vent 1) where the biofilm community included chemosynthetic, photo- and heterotrophic microorganisms. Here, the main environmental drivers were the low pH and the negative ORP resulting from the elevated concentrations of CO_2 and H_2S released from the vents, respectively (**Figure 2** and **Table 1**). Their combined effect was evident on the diversity of the community which was characterized by higher dominance and lower evenness compared to the other sites. Following the pH gradient northwards in the bay, H_2S concentrations decreased significantly while CO_2 was still elevated resulting in positive ORP and low pH detected at Vent 2, respectively (**Figure 2** and **Table 1**). The differences detected in the taxonomic composition were reflected in the inferred functionality of the biofilm communities, with increased abundance in genes for sulfur respiration in Vent 1 and Vent 2 compared to the reference sites (**Figure 2**). Although shallow-water vents are recognized as natural laboratories for testing the effects of ocean acidification on marine biota, the influence of other environmental variables cannot be excluded (Hassenrück et al., 2016; Dahms et al., 2018). Compared to previous studies conducted in the same area (Lidbury et al., 2012; Kerfahi et al., 2014; Taylor et al., 2014), our study highlights the importance of H_2S in shaping marine biofilm communities in Levante Bay along with the effect of CO_2. Further, acidification is likely to occur along with other environmental changes related to climate changes such as deoxygenation of the oceans (Keeling et al., 2010). In this regard, experimental investigations conducted at hydrothermal vents can provide insights on the response of microbial

communities to multiple environmental stressors (i.e., elevated pCO_2, low pH and low ORP) in the wide context of the global climate change scenario.

DEDICATION

We dedicate this manuscript to the memory of Prof. Mario Giordano, dear mentor and colleague.

DATA AVAILABILITY STATEMENT

The datasets presented in this study can be found in online repositories. The names of the repository/repositories and accession number(s) can be found in the article/**Supplementary Material**.

AUTHOR CONTRIBUTIONS

VS, SV, AM, and CV designed the experimental procedure. VS collected the samples, performed the experiments, analyzed the data, and wrote the manuscript. SV and AM participated in the writing, review and editing of the manuscript. CV and FS participated to the data analysis and wrote the manuscript. All authors contributed to the article and approved the submitted version.

FUNDING

This work was partially supported by NSF grant MCB 15-17567, NSF grant OCE 19-48623, and NASA grant 20-EXO20-0084 to CV.

ACKNOWLEDGMENTS

We thank A. Savona for his support in setting up the experiments, V. Costa, C. Andolina, and A. Mirasole for assistance during the fieldwork activities and S. Patwardhan for her valuable comments and suggestions.

SUPPLEMENTARY MATERIAL

The Supplementary Material for this article can be found online at: https://www.frontiersin.org/articles/10.3389/fmicb.2022.840205/full#supplementary-material

REFERENCES

Aiuppa, A., Hall-Spencer, J. M., Milazzo, M., Turco, G., Caliro, S., and Di Napoli, R., (2021). Volcanic CO2 seep geochemistry and use in understanding ocean acidification. *Biogeochemistry* 152, 93–115. doi: 10.1007/s10533-020-00737-9

Anderson, M. J., Gorley, R. N., and Clarke, K. R. (2008). *PERMANOVA+for PRIMER: Guide to Software and Statistical Methods*. Plymouth: PRIMER-E.

Aßhauer, K. P., Wemheuer, B., Daniel, R., and Meinicke, P. (2015). Tax4Fun: predicting functional profiles from metagenomic 16S rRNA data. *Bioinformatics* 31, 2882–2884. doi: 10.1093/bioinformatics/btv287

Bao, W. Y., Satuito, C. G., Yang, J. L., and Kitamura, H. (2007). Larval settlement and metamorphosis of the mussel *Mytilus galloprovincialis* in response to biofilms. *Mar. Biol.* 150, 565–574. doi: 10.1007/s00227-006-0383-4

Bhaskar, P. V., and Bhosle, N. B. (2005). Microbial extracellular polymeric substances in\rmarine biogeochemical processes. *Curr. Sci.* 88:922.

Boatta, F., D'Alessandro, W., Gagliano, A. L., Liotta, M., Milazzo, M., Rodolfo-Metalpa, R., et al. (2013). Geochemical survey of Levante Bay, Vulcano Island (Italy), a Natural Laboratory for the Study of Ocean acidification. *Mar. Pollut. Bull.* 73, 485–494. doi: 10.1016/j.marpolbul.2013.01.029

Capaccioni, B., Tassi, F., and Vaselli, O. (2001). Organic and inorganic geochemistry of low temperature gas discharges at the Baia Di Levante Beach, Vulcano Island, Italy. *J. Volcanol. Geotherm. Res.* 108, 173–185. doi: 10.1016/S0377-0273(00)00284-5

Caporaso, J. G., Kuczynski, J., Stombaugh, J., Bittinger, K., Bushman, F. D., Costello, E. K., et al. (2010). QIIME allows analysis of high-throughput community sequencing data. *Nat. Methods* 7, 335–336. doi: 10.1038/nmeth.f.303.QIIME

Caporaso, J. G., Lauber, C. L., Walters, W. A., Berg-Lyons, D., Lozupone, C. A., Turnbaugh, P. J., et al. (2011). Global patterns of 16S rRNA diversity at a depth of millions of sequences per sample. *Proc. Natl. Acad. Sci. U.S.A.* 108, 4516–4522. doi: 10.1073/pnas.1000080107

Carapezza, M. L., Barberi, F., Ranaldi, M., Ricci, T., Tarchini, L., Barrancos, J., et al. (2011). Diffuse CO2soil degassing and CO2and H2S concentrations in air and related hazards at Vulcano Island (Aeolian Arc, Italy). *J. Volcanol. Geotherm. Res.* 207, 130–144. doi: 10.1016/j.jvolgeores.2011.06.010

Costerton, J. W. (1999). Introduction to biofilm. *Int. J. Antimicrob. Agents* 11, 217–221. doi: 10.1016/S0924-8579(99)00018-7

Dahms, H. U., Schizas, N. V., James, R. A., Wang, L., and Hwang, J. S. (2018). Marine hydrothermal vents as templates for global change scenarios. *Hydrobiologia* 818, 1–10. doi: 10.1007/s10750-018-3598-8

Davey, M. E., and O'toole, G. A. (2000). Microbial biofilms : from ecology to molecular genetics. *Microbiol. Mol. Biol. Rev.* 64, 847–867. doi: 10.1128/MMBR.64.4.847-867.2000.Updated

Decho, A. W. (2000). Microbial biofilms in intertidal systems: an overview. *Continent. Shelf Res.* 20, 1257–1273. doi: 10.1016/S0278-4343(00)00022-4

Dobretsov, S. (2010). "Marine biofilms," in *Biofouling*, eds S. Dürr and J. C. Thomason (Hoboken, NJ: Wiley), 123–136.

Engel, A. S., Porter, M. L., Stern, L. A., Quinlan, S., and Bennett, P. C. (2004). Bacterial diversity and ecosystem function of filamentous microbial mats from aphotic (cave) sulfidic springs dominated by chemolithoautotrophic "Epsilonproteobacteria". *FEMS Microbiol. Ecol.* 51, 31–53. doi: 10.1016/j.femsec.2004.07.004

Flemming, H., and Wingender, J. (2010). The biofilm matrix. *Nat. Rev. Microbiol.* 8, 623–633. doi: 10.1038/nrmicro2415

Flemming, H. C., Neu, T. R., and Wozniak, D. J. (2007). The EPS matrix: the 'house of biofilm cells'. *J. Bacteriol.* 189, 7945–7947. doi: 10.1128/JB.00858-07

Galtier, N., Gouy, M., and Gautier, C. (1996). SEAVIEW and PHYLO_WIN: two graphic tools for sequence alignment and molecular phylogeny. *Comput. Appl. Biosci. CABIOS* 12, 543–548. doi: 10.1093/bioinformatics/12.6.543

Garrett, T. R., Bhakoo, M., and Zhang, Z. (2008). Bacterial adhesion and biofilms on surfaces. *Prog. Nat. Sci.* 18, 1049–1056. doi: 10.1016/j.pnsc.2008.04.001

Giovannelli, D., Chung, M., Staley, J., Starovoytov, V., Le Bris, N., and Vetriani, C. (2016). *Sulfurovum riftiae* sp. nov., a mesophilic, thiosulfate-oxidizing, nitrate-reducing chemolithoautotrophic *Epsilonproteobacterium* isolated from the tube of the deep-sea hydrothermal vent polychaete, *Riftia*

pachyptila. *Intl. J. Syst. Evol. Microbiol.* 66, 2697–2701. doi: 10.1099/ijsem.0.001106

Giovannelli, D., d'Errico, G., Manini, E., Yakimov, M., and Vetriani, C. (2013). Diversity and phylogenetic analyses of bacteria from a shallow-water hydrothermal vent in Milos Island (Greece). *Front. Microbiol.* 4:184. doi: 10.3389/fmicb.2013.00184

Glöckner, F. O., Yilmaz, P., Quast, C., Gerken, J., Beccati, A., Ciuprina, A., et al. (2014). The SILVA ribosomal RNA gene database project: improved data processing and web-based tools. *Nucleic Acids Res.* 41, 643–648. doi: 10.1093/nar/gks1219

Gouy, M., Guindon, S., and Gascuel, O., (2010). SeaView version 4: a multiplatform graphical user interface for sequence alignment and phylogenetic tree building. *Mol. Biol. Evol.* 27, 221–224. doi: 10.1093/molbev/msp259

Gower, J. C. (1971). A general coefficient of similarity and some of its properties. *Biometrics* 27, 857–871. doi: 10.2307/2528823

Guindon, S., and Gascuel, O. (2003). A simple, fast, and accurate algorithm to estimate large phylogenies by maximum likelihood. *Syst. Biol.* 52, 696–704. doi: 10.1080/10635150390235520

Haas, B. J., Gevers, D., Earl, A. M., Feldgarden, M., Ward, D. V., Giannoukos, G., et al. (2011). Chimeric 16S RRNA sequence formation and detection in sanger and 454-Pyrosequenced PCR amplicons. *Genome Res.* 21, 494–504. doi: 10.1101/gr.112730.110.Freely

Hadfield, M. G. (2011). Biofilms and marine invertebrate larvae: what bacteria produce that larvae use to choose settlement sites. *Annu. Rev. Mar. Sci.* 3, 453–470. doi: 10.1146/annurev-marine-120709-142753

Hassenrück, C., Fink, A., Lichtschlag, A., Tegetmeyer, H. E., De Beer, D., and Ramette, A. (2016). Quantification of the effects of ocean acidification on sediment microbial communities in the environment: the importance of ecosystem approaches. *FEMS Microbiol. Ecol.* 92, 1–12. doi: 10.1093/femsec/fiw027

Hassenrück, C., Tegetmeyer, H. E., Ramette, A., and Fabricius, K. E. (2017). Minor impacts of reduced PH on bacterial biofilms on settlement tiles along natural PH gradients at two CO 2 seeps in Papua New Guinea. *ICES J. Mar. Sci. J. Conseil* 74:fsw204. doi: 10.1093/icesjms/fsw204

Inguaggiato, S., Mazot, A. I, Diliberto, S., Inguaggiato, C., Madonia, P., Rouwet, D., et al. (2012). Total CO<inf>2</Inf> Output from Vulcano Island (Aeolian Islands, Italy). *Geochem. Geophys. Geosyst.* 13, 1–19. doi: 10.1029/2011GC003920

Jannasch, H. W., Wirsen, C. O., Douglas, C. N., and Robertson, L. A. (1985). *Thiomicrospira crunogena* sp. nov., a colorless, sulfur-oxidizing bacterium from a deep-sea hydrothermal vent". *Intl. J. Syst. Evol. Microbiol.* 35, 422–424. doi: 10.1099/00207713-35-4-422

Johnson, V. R., Brownlee, C., Milazzo, M., and Hall-Spencer, J. M. (2015). Marine microphytobenthic assemblage shift along a natural shallow-water CO2 gradient subjected to multiple environmental stressors. *J. Mar. Sci. Eng.* 3, 1425–1447. doi: 10.3390/jmse3041425

Johnson, V. R., Brownlee, C., Rickaby, R. E. M., Graziano, M., Milazzo, M., and Hall-Spencer, J. M. (2013). Responses of marine benthic microalgae to elevated CO2. *Mar. Biol.* 160, 1813–1824. doi: 10.1007/s00227-011-1840-2

Joint, I., Doney, S. C., and Karl, D. M. (2011). Will ocean acidification affect marine microbes? *ISME J.* 5, 1–7. doi: 10.1038/ismej.2010.79

Keeling, R. F., Körtzinger, A., and Gruber, N. (2010). Ocean deoxygenation in a warming world. *Annu. Rev. Mar. Sci.* 2, 199–229.

Kerfahi, D., Hall-Spencer, J. M., Tripathi, B. M., Milazzo, M., Lee, J., and Adams, J. M. (2014). Shallow water marine sediment bacterial community shifts along a natural CO2 gradient in the Mediterranean Sea Off Vulcano. *Italy Microb. Ecol.* 67, 819–828. doi: 10.1007/s00248-014-0368-7

Lentini, V., Gugliandolo, C., Bunk, B., Overmann, J., and Maugeri, T. L. (2014). Diversity of prokaryotic community at a shallow marine hydrothermal site elucidated by illumina sequencing technology. *Curr. Microbiol.* 69, 457–466. doi: 10.1007/s00284-014-0609-5

Lidbury, I., Johnson, V., Hall-Spencer, J. M., Munn, C. B., and Cunliffe, M. (2012). Community-level response of coastal microbial biofilms to ocean acidification in a natural carbon dioxide vent ecosystem. *Mar. Pollut. Bull.* 64, 1063–1066. doi: 10.1016/j.marpolbul.2012.02.011

Macalady, J. L., Dattagupta, S., Schaperdoth, I., Jones, D. S., Druschel, G. K., and Eastman, D. (2008). Niche differentiation among sulfur-oxidizing bacterial populations in cave waters. *ISME J.* 2, 590–601.

Mancuso Nichols, C. A., Guezennec, J., and Bowman, J. P. (2005). Bacterial exopolysaccharides from extreme marine environments with special consideration of the southern ocean, sea ice, and deep-sea hydrothermal vents: a review. *Mar. Biotechnol.* 7, 253–271. doi: 10.1007/s10126-004-5118-2

McDonald, D., Price, M. N., Goodrich, J., Nawrocki, E. P., Desantis, T. Z., Probst, A., et al. (2012). An improved greengenes taxonomy with explicit ranks for ecological and evolutionary analyses of bacteria and archaea. *ISME J.* 6, 610–618. doi: 10.1038/ismej.2011.139

Meier, D. V., Pjevac, P., Bach, W., Hourdez, S., Girguis, P. R., Vidoudez, C., et al. (2017). Niche partitioning of diverse sulfur-oxidizing bacteria at hydrothermal vents. *ISME J.* 11, 1545–1558.

Miranda, P. J., McLain, N. K., Hatzenpichler, R., Orphan, V. J., and Dillon, J. G. (2016). Characterization of chemosynthetic microbial mats associated with intertidal hydrothermal sulfur vents in white point, San Pedro, CA, USA. *Front. Microbiol.* 7:1163. doi: 10.3389/fmicb.2016.01163

O'Brien, C. E., Giovannelli, D., Govenar, B., Luther, G. W., Lutz, R. A., Shank, T. M., et al. (2015). Microbial biofilms associated with fluid chemistry and megafaunal colonization at post-eruptive deep-sea hydrothermal vents. *Deep Sea Res. Part II Top. Stud. Oceanogr.* 121, 31–40. doi: 10.1016/j.dsr2.2015.07.020

Ortega-Morales, B. O., Chan-Bacab, M. J., De la Rosa-García Sdel, C., and Camacho-Chab, J. C. (2010). Valuable processes and products from marine intertidal microbial communities. *Curr. Opin. Biotechnol.* 21, 346–352. doi: 10.1016/j.copbio.2010.02.007

Patwardhan, S., Foustoukos, D. I., Giovannelli, D., Yucel, M., and Vetriani, C. (2018). Ecological succession of sulfur-oxidizing Epsilon- and Gammaproteobacteria during colonization of a shallow-water gas vent. *Front. Microbiol.* 9:2970. doi: 10.3389/fmicb.2018.02970

Patwardhan, S., Smedile, F., Giovannelli, D., and Vetriani, C. (2021). Metaproteogenomic profiling of chemosynthetic microbial biofilms reveals metabolic flexibility during colonization of a shallow-water gas vent. *Front. Microbiol.* 12:638300. doi: 10.3389/fmicb.2021.638300

Qian, P. Y., Lau, S. C. K., Dahms, H. U., Dobretsov, S., and Harder, T. (2007). Marine biofilms as mediators of colonization by marine macroorganisms: implications for antifouling and aquaculture. *Mar. Biotechnol.* 9, 399–410. doi: 10.1007/s10126-007-9001-9

Quast, C., Pruesse, E., Yilmaz, P., Gerken, J., Schweer, T., Yarza, P., et al. (2013). The SILVA ribosomal RNA gene database project: improved data processing and web-based tools. *Nucleic Acids Res.* 41, 590–596. doi: 10.1093/nar/gks1219

Raven, J. A., Giordano, M., Beardall, J., and Maberly, S. C. (2012). Algal evolution in relation to atmospheric CO2: carboxylases, carbon-concentrating mechanisms and carbon oxidation cycles. *Philos. Trans. R. Soc. B Biol. Sci.* 367, 493–507. doi: 10.1098/rstb.2011.0212

Reigstad, L. J., Jorgensen, S. L., Lauritzen, S.-E., Schleper, C., and Urich, T. (2011). Sulfur-oxidizing chemolithotrophic *Proteobacteria* dominate the microbiota in high arctic thermal springs on svalbard. *Astrobiology* 11, 665–678. doi: 10.1089/ast.2010.0551

Rosenberg, E. (2013). "The Prokaryotes: alphaproteobacteria and Betaproteobacteria," in *The Prokaryotes: Alphaproteobacteria and Betaproteobacteria*, eds E. Rosenberg, E. F. DeLong, S. Lory, E. Stackebrandt, and F. Thompson (Cham: Springer).

Salta, M., Wharton, J. A., Blache, Y., Stokes, K. R., and Briand, J. F. (2013). Marine biofilms on artificial surfaces: structure and dynamics. *Environ. Microbiol.* 15, 2879–2893. doi: 10.1111/1462-2920.12186

Sandrini, G., Matthijs, H. C. P., Verspagen, J. M. H., Muyzer, G., and Huisman, J. (2014). Genetic diversity of inorganic carbon uptake systems causes variation in CO2response of the *Cyanobacterium microcystis*. *ISME J.* 8, 589–600. doi: 10.1038/ismej.2013.179

Sievers, F., Wilm, A., Dineen, D., Gibson, T. J., Karplus, K., Li, W., et al. (2011). Fast, scalable generation of high-quality protein multiple sequence alignments using Clustal Omega. *Mol. Syst. Biol.* 7:539. doi: 10.1038/msb.2011.75

Taylor, J. D., Ellis, R., Milazzo, M., Hall-Spencer, J. M., and Cunliffe, M. (2014). Intertidal epilithic bacteria diversity changes along a naturally occurring carbon

dioxide and PH gradient. *FEMS Microbiol. Ecol.* 89, 670–678. doi: 10.1111/1574-6941.12368

Witt, V., Wild, C., and Uthicke, S. (2011). Effect of substrate type on bacterial community composition in biofilms from the great barrier reef. *FEMS Microbiol. Lett.* 323, 188–195. doi: 10.1111/j.1574-6968.2011.02374.x

Yilmaz, P., Parfrey, L. W., Yarza, P., Gerken, J., Pruesse, E., Quast, C., et al. (2014). The SILVA and 'all-species Living Tree Project (LTP)' taxonomic frameworks. *Nucleic Acids Res.* 42, 643–648. doi: 10.1093/nar/gkt1209

Conflict of Interest: The authors declare that the research was conducted in the absence of any commercial or financial relationships that could be construed as a potential conflict of interest.

Publisher's Note: All claims expressed in this article are solely those of the authors and do not necessarily represent those of their affiliated organizations, or those of the publisher, the editors and the reviewers. Any product that may be evaluated in this article, or claim that may be made by its manufacturer, is not guaranteed or endorsed by the publisher.

frontiers in Microbiology

ORIGINAL RESEARCH
published: 25 February 2022
doi: 10.3389/fmicb.2022.820714

Membrane and Extracellular Matrix Glycopolymers of *Colwellia psychrerythraea* 34H: Structural Changes at Different Growth Temperatures

Angela Casillo, Caterina D'Angelo, Ermenegilda Parrilli, Maria Luisa Tutino and Maria Michela Corsaro*

Department of Chemical Sciences, University of Naples "Federico II," Complesso Universitario Monte S. Angelo, Naples, Italy

OPEN ACCESS

Edited by:
Davide Zannoni, University of Bologna, Italy

Reviewed by:
Thomas R. Neu, Helmholtz Centre for Environmental Research, Helmholtz Association of German Research Centres (HZ), Germany
Amir Bouallegue, National Engineering School of Sfax, Tunisia

***Correspondence:**
Angela Casillo
angela.casillo@unina.it

Specialty section:
This article was submitted to Extreme Microbiology, a section of the journal Frontiers in Microbiology

Received: *23 November 2021*
Accepted: *11 January 2022*
Published: *25 February 2022*

Citation:
Casillo A, D'Angelo C, Parrilli E, Tutino ML and Corsaro MM (2022) Membrane and Extracellular Matrix Glycopolymers of Colwellia psychrerythraea 34H: Structural Changes at Different Growth Temperatures. Front. Microbiol. 13:820714. doi: 10.3389/fmicb.2022.820714

Colwellia psychrerythraea 34H is a marine Gram-negative psychrophile; it was isolated from Arctic marine sediments, but it is considered cosmopolitan in cold environments. This microorganism is considered a model to study adaptive strategies to sub-zero temperatures, and its lifestyle has been the object of numerous studies. In the last few years, we focused our studies on the glycoconjugates produced by *C. psychrerythraea* 34H at 4°C, resulting in the isolation and characterization of very interesting molecules. It produces an unusual lipooligosaccharide molecule and both capsular and medium released polysaccharides. In this study, we described the response of these glycoconjugates in terms of production and chemical structure produced by *C. psychrerythraea* 34H grown in planktonic conditions at −2, 4, and 8°C. The glycopolymers have been detected by chemical methods and spectroscopic analyses. Moreover, the glycopolymer content of the biofilm matrix of *C. psychrerythraea* 34H has been evaluated, through confocal microscopy and glycosyl analysis. The results highlighted that *C. psychrerythraea* 34H adjusts both the production and the typology of its glyconjugates in response to temperature fluctuations.

Keywords: biofilm, cold-adapted bacterium, extracellular polysaccharides, temperature changes, structural characterization, CLSM

INTRODUCTION

Arctic and Antarctic sea-ice, glaciers, and deep ocean waters are some of the examples of environments where the temperature is below 0°C. These habitats create the perfect niches for the colonization of psychrophiles, microorganism able to grow well at temperatures around the freezing point of water. These bacteria evolved several strategies to counteract the lowering temperatures (Siddiqui et al., 2013; Collins and Margesin, 2019). The main studies concerning the adaptation strategies are focused on the overexpression or the production of cold shock proteins, and ice-binding proteins (IBPs). Furthermore, the modulation of enzymes involved in synthesis of the membrane components, such as acyl chains of lipids, LPS, peptidoglycan, and outer membrane

protein biosynthesis, is reported. Recently, the role of the surface glycoconjugates molecules in the cold adaptation mechanism has been investigated (Nichols et al., 2005; Carillo et al., 2015; Casillo et al., 2019a).

The outer membrane (OM) of Gram-negative bacteria is an asymmetric bilayer with the inner monolayer composed of phospholipids and the outer leaflet mainly composed of lipopolysaccharides (LPS). The main role of the OM is to protect the cell by forming a protective barrier (Nikaido and Vaara, 1985; Nikaido, 1994), which makes the bacteria resistant to a variety of host defense factors, antibiotics, and stress conditions (Daugelavičius et al., 2000; Guyard-Nicodème et al., 2008).

The LPSs are embedded in the OM through the lipid A domain, a glycolipid portion consisting of two phosphorylated glucosamines (GlcN) that carry long-chain fatty acids. In addition to this, the LPS contains two saccharide portions: the core oligosaccharide linked to the lipid A, and the O-polysaccharide region (O-chain) exposed to the outside. The last portion is responsible for the different phenotypes of Gram-negative bacteria. The smooth phenotype occurs when the O-chain is linked to the core, while the rough phenotype occurs when bacteria are unable to add the O-chain repeating unit to their outer core region. The alteration of cell membrane composition to preserve the membrane fluidity at low temperatures has been observed in terms of phospholipid composition (Russell, 1990; Ernst et al., 2016). Since the lipid A moiety represents a major part of the outer leaflet, its chemical structure is also crucial in the maintenance of the membrane integrity.

Finally, many of the LPSs characterized from cold-adapted bacteria lack the O-chain when grown at a temperature above 20°C (Casillo et al., 2019a). The investigation on the response of the cell membrane to lower temperature is well studied in mesophilic bacteria (Cronan and Gelmann, 1975; Janoff et al., 1979; Kropinski et al., 1987), while too few investigations are conducted on psychrophiles (Ray et al., 1994; Kumar et al., 2002; Corsaro et al., 2004). Additionally, some bacteria are reported to produce extracellular polysaccharides, strictly associated with the cell surface as a capsule (capsular polysaccharide) or totally released in the surrounding medium (medium released polysaccharide, MRP) (Casillo et al., 2018). Extracellular polysaccharides facilitate the adhesion on the biotic and abiotic surfaces, cellular aggregation, and nutrient trapping (Quintero and Weiner, 1995; Rinker and Kelly, 1996; Langille and Weiner, 1998)WeinerKelly, and confer cryoprotection to the bacterial cell (Kim and Yim, 2007; Marx et al., 2009; Carillo et al., 2015; Casillo et al., 2017a). Extracellular polysaccharides are also essential structural components of the biofilm matrix. Biofilm has been defined as an aggregate of microorganisms in which the cells are surrounded by a self-produced matrix of extracellular polymeric substances (EPS) (Flemming and Wingender, 2010). Although the precise chemical and physical composition of the EPS varies according to the species and the growth conditions, the main biofilm matrix building blocks are bacterial proteins, extracellular DNA (eDNA) (Whitchurch et al., 2002), lipids, and polysaccharides (Flemming and Wingender, 2010).

In the natural environment, the biofilm formation has several advantages, i.e., the matrix captures resources such as the nutrients that are present in the environment (Flemming and Wingender, 2010) and affords protection from a wide range of environmental challenges (Flemming et al., 2016), such as UV exposure, metal toxicity, dehydration, and salinity and phagocytosis. Therefore, the ability to form biofilm is a selective advantage for bacteria. Correspondingly, bacteria living in extreme environments, like the Polar region, can be found as biofilms, and this ability is believed to aid their adaptation and survival in the environment (Liao et al., 2016; Ricciardelli et al., 2018).

To deeply investigate the implication of carbohydrate-based molecules in cold adaptation mechanism, we have been interested in the structural elucidation of glycoconjugates isolated from the psychrophile *Colwellia psychrerythraea* 34H.

C. psychrerythraea 34H (henceforth *Colwellia* 34H) is a psychrophilic bacterium, originally isolated from subzero Arctic sediments (Methé et al., 2005), considered a cosmopolitan species to both poles and sea-ice (Boetius et al., 2015). *Colwellia* 34H is used as model species for investigating the metabolism of cold-adapted microbes. This bacterium can grow in a heterotrophic medium over a temperature range of −4 to 10°C, with an optimum of 8°C (Marx et al., 2009). Recently, the genome of *Colwellia* 34H was used as type strain to construct the whole genome phylogeny. The obtained phylogenomic trees showed that the genus *Colwellia* was paraphyletic, and that four members of the genus *Colwellia*, including *Colwellia* 34H, formed a clade (Liu et al., 2020).

In the last years, we focused our research on the elucidation of the surface carbohydrate molecules produced by the model psychrophile *Colwellia* 34H. The large-scale cultivation of *Colwellia* 34H at 4°C allowed to isolate and characterize very intriguing and original glycoconjugates moiety. The inner portion of the LPS, the lipid A, displays the presence of phosphoglycerol moiety that can be additionally acylated, resulting in a lipid A carrying up to seven fatty acids (Casillo et al., 2017b). The core oligosaccharide structure confers a high negative charge density to the entire molecule since it contains many acidic residues. In addition, it showed a phosphoglycerol, and the core structure ends with the rare sugar colitose (Carillo et al., 2013). *Colwellia* 34H produces both CPS and MRP (Carillo et al., 2015: Casillo et al., 2017a) decorated with amino acids, the structures of which resemble those of the antifreeze glycoproteins (AFGP). These polysaccharides, through their peculiar primary structures and three-dimensional conformation, inhibit the ice crystal growth, exhibiting their anti-freezing effect. Since *Colwellia* 34H genome lacks genes encoding for AFGP, this alternative mechanism to contrast the freezing of the cells makes these polymers even more fascinating. Finally, the large-scale cultivation of *Colwellia* 34H at 8°C allowed to isolate a CPS (Casillo et al., 2017c) containing all amino sugars.

The complex mechanism adopted by *Colwellia* 34H to face the low temperatures makes this bacterium the perfect candidate to get to the bottom of the understanding of cold adaptation.

In this paper, we analyzed the effect of the temperature changes on the production and the structures of the surface

carbohydrate molecules, and on the biofilm produced by *Colwellia* 34H.

EXPERIMENTAL SECTION

Bacteria Growth in Planktonic and Sessile Conditions

Colwellia 34H was grown aerobically at −2, 4, and 8°C in Marine Broth medium (DIFCO 2216). Cells were harvested at different times of growth (48, 72, and 96 h) by centrifugation for 20 min at 5,000 rpm and 4°C. The biofilm formation was assessed in the static condition in the Marine Broth medium at 8 and 4°C for 48 h while −2°C for 96 h. The kinetic of the biofilm formation was performed at 4°C at different times (24, 48, 72, 96, and 120 h).

Transmission Electron Microscopy Images

The samples were prepared for TEM observations as detailed in Escalera et al. (2014). Briefly, specimens were fixed with 2.5% glutaraldehyde, post-fixed with 1% osmium tetroxide, dehydrated in a graded ethanol series further substituted by propylene oxide, and embedded in Epon 812 (TAAB, TAAB Laboratories Equipment Ltd., Berkshire, United Kingdom). Ultrathin sections (60 nm thick) were collected on nickel grids and stained with uranyl acetate and lead citrate, and transmission electron microscopy (TEM) images were acquired with a Zeiss LEO 912AB TEM (Zeiss, Oberkochen, Germany) operating at an accelerating voltage of 80 kV.

Lipopolysaccharides Isolation Purification

Dried cells were extracted three times with a mixture of aqueous phenol 90%/chloroform/light petroleum ether (2:5:8) (PCP) as described by Galanos et al. (1969). After removal of the organic solvents under vacuum, LPS was precipitated from phenol with drops of water, then washed with cold acetone, and then lyophilized (LPS yields: 1.1, 3, and 0.6% at −2, 4, and 8°C, respectively).

Lipid A Isolation

The PCP extracts were hydrolyzed with 1% CH_3COOH (10 mg/ml, 100°C for 3 h). The obtained suspensions were then centrifuged (7,000 rpm, 4°C, 30 min) (Casillo et al., 2017b). The precipitates containing the lipid A were washed several times with chloroform/methanol (1:2) mixture to obtain purified samples and then analyzed by GC-MS.

Core Oligosaccharide Isolation

An aliquot of the PCP extracts was incubated with hydrazine at 37°C (20–30 mg/ml, 1.5 h). The precipitation of the *O*-deacylated LOSs was achieved by adding cold acetone and recovered after centrifugation (4°C, 7,000 rpm, 30 min). The LOS-OH samples were lyophilized, and then dissolved in 4 M KOH (120°C for 16 h). The mixtures were neutralized and extracted three times with $CHCl_3$, and finally desalted on a Sephadex G-10 column (Amersham Biosciences, 2.5 × 43 cm, 35 ml/h, fraction volume 2.5 ml, eluent NH_4HCO_3 10 mM). The eluted oligosaccharide mixtures were then lyophilized.

Capsular Polysaccharides Isolation and Purification

The cell residues after PCP extraction were extracted by phenol/water method according to Westphal and Jann (1965) procedure. The cells were suspended in aqueous phenol/water 90%/(1:1 v/v) at 68°C as already reported. The collected water phases were dialyzed against water (cutoff 3,500 Da) and freeze-dried. The extracts were subjected to enzymatic digestion with DNase, RNase, and protease K (Sigma-Aldrich) to remove nucleic acids. The water extracts were hydrolyzed with 1% aqueous CH_3COOH (10 mg/ml, 100°C, 3 h), and centrifuged (7,000 rpm, 4°C, 30 min). The supernatant portion was fractionated on a Sephacryl S-400HR (Sigma, 0.5 × 110 cm, fraction volume 2.5 ml) eluted with 0.05 M ammonium hydrogen carbonate, to isolate the polysaccharidic material (CPS yields:1.4, 1.6, and 1.2% at −2, 4, and 8°C, respectively).

Medium Released Polysaccharide Isolation and Purification

The cell-free supernatants were dialyzed against water (cutoff 3,500 Da) and lyophilized, and subsequently hydrolyzed with 5% aqueous CH_3COOH (100°C, 3 h). The resulting suspensions were centrifuged (7,000 rpm, 4°C, 30 min), and the supernatant portions were then fractionated on a Sephacryl S-400 HR column (Sigma, 1.5 × 95 cm, flow 16.8 ml/h, fraction volume 2.5 ml), eluted with 0.05 M ammonium hydrogen carbonate. The obtained polysaccharides were further analyzed by chemical analyses.

Chemical Analyses

Monosaccharides were analyzed as acetylated methyl glycoside (AMG) derivatives as reported (Adinolfi et al., 1996). Briefly, 0.5–1 mg of sample was subjected to a methanolysis reaction (1.25 M HCl/MeOH, 1 ml, 80°C, 16 h). The obtained *O*-methyl-glycosides were extracted three times with hexane and the methanol layers were acetylated with Ac_2O (50 μl) and Py (50 μl) at 100°C for 30 min and analyzed by using an Agilent Technologies gas chromatograph 7,820A equipped with a mass selective detector 5977B and an HP-5 capillary column (Agilent, 30 m × 0.25 mm i.d.; flow rate, 1 ml/min, He as carrier gas). The following temperature program was used for the analysis of the AMG: 140°C for 3 min, 150°C → 240°C at 3°C/min. The hexane layer containing fatty acid methyl esters (FAME) were analyzed by GC-MS to obtain fatty acid composition, by using the following temperature program: 140°C for 3 min, 140°C → 280°C at 10°C/min, and 280°C for 20 min.

Deoxycholate-PAGE

PAGE was performed using the system of Laemmli (Laemmli and Favre, 1970) with sodium deoxycholate (DOC) as the detergent, as already described (Casillo et al., 2019b). The gels were fixed in an aqueous solution of 40% ethanol and 5% acetic

acid and visualized after Alcian Blue and silver nitrate staining (Tsai and Frasch, 1982).

MALDI TOF/TOF

MALDI-TOF mass spectra were acquired on an ABSCIEX TOF/TOF^{TM}5800 (AB SCIEX, Darmstadt, Germany). The core oligosaccharide samples were desalted on a Dowex 50WX8 (H + form) and dissolved in 2-propanol/water (v/v 1:1). The 2, 5-dihydroxybenzoic acid (DHB) dissolved in 20% CH_3CN in water (25 mg/ml) was used as matrix. The spectra were calibrated with a hyaluronan oligosaccharide mixture and processed under computer control by using Data Explorer software v.0.2.0 (Microsoft, Albuquerque, NM, United States).

Biofilm

Biofilm Formation and Assays

The quantification of the *in vitro* biofilm production was based on the method described by Christensen with slight modifications (Christensen et al., 1999). Briefly, the wells of a sterile 24-well flat-bottomed polystyrene plate were filled with 1 ml of a medium with a suitable dilution of the Artic bacterial culture in the exponential growth phase (about 0.2 OD 600 nm). For the analysis of the temperature effect on *Colwellia* 34H biofilm formation, the plates were incubated at −2°C for 96 h, and at 4 and 8°C for 48 h, while for the kinetics of the biofilm formation, the plates were incubated at 4°C for different times (24, 48, 72, 96, and 120 h). After rinsing with PBS, the adherent cells were stained with 0.1% (w/v) crystal violet, rinsed twice with double-distilled water, and thoroughly dried. Subsequently, the dye bound to the adherent cells was solubilized with 20% (v/v) acetone and 80% (v/v) ethanol. After 10 min of incubation at room temperature, the OD 590 nm was measured to quantify the total biomass of biofilm formed in each well. Each data point was composed of six independent samples.

Biofilm Recovery

The biofilm formation at the air–liquid interface was assessed in the Marine Broth medium at 4°C. Briefly, the wells of a sterile 24-well flat-bottomed polystyrene plate were filled with 1 ml of a medium with a suitable dilution of a culture of *Colwellia* 34H in the exponential growth phase (about 0.2 OD 600 nm). The plates were incubated at 4°C for 120 h to allow the formation of compact and resistant pellicles at the air–liquid interface. After incubation, the pellicles were recovered using a pipette and stored at −20°C. The samples were freeze-dried for further analysis.

DNase I and Proteinase K Effects on Biofilm Formation

To understand if DNase I and proteinase K can affect the *Colwellia* 34H biofilm formation process, a static biofilm assay was performed in the presence of DNase I or proteinase K. The biofilm formation was assessed in Marine Broth medium at 4°C for 96 h. In detail, 200 μl of the medium with a suitable dilution of *Colwellia* 34H culture in the exponential growth phase (about 0.2 OD 600 nm) were added into each well of a sterile 96-well flat-bottomed polystyrene plate in the absence and presence of DNase I or proteinase K (100 μg/ml). After incubation, biofilm quantification was performed by means of the crystal violet method, as previously described (Christensen et al., 1999).

Confocal Laser Scanning Microscopy

For the confocal microscopy analysis, the biofilm formation was performed on Nunc^{TM} Lab-Tek® 8-well Chamber Slides (n° 177445; Thermo Scientific, Ottawa, ON, Canada) in Marine Broth medium at 8 and 4°C for 72 h while at −2°C for 96 h. All the microscopic observations and image acquisitions were performed with a confocal laser scanning microscope (CLSM) (LSM700-Zeiss, Germany) equipped with an Ar laser (488 nm), and a He-Ne laser (555 nm). The biofilm observed by CLSM was formed at the bottom of the well.

Bacterial Viability and Biofilm Thickness Determination

The biofilm cell viability was determined with the FilmTracer^{TM} LIVE/DEAD® Biofilm Viability Kit (Molecular Probes, Invitrogen) following the manufacturer's instructions. Briefly, 300 μl of the medium with a suitable dilution of a *Colwellia* 34H culture in the exponential growth phase (about 0.2 OD 600 nm) were added into each well of a sterile Chamber Slide. After the incubation, the plates were rinsed with filter-sterilized PBS. Then, each well of the chamber slide was filled with 300 μl of a working solution of fluorescent stains, containing the SYTO 9 green-fluorescent nucleic acid stain (10 μM) and propidium iodide, the red-fluorescent nucleic acid stain (60 μM), and incubated for 20–30 min at room temperature, protected from light. All the excess staining was removed by rinsing gently with filter-sterilized PBS. The Z-stacks images were obtained using a 20X NA 0.8 objective and acquired using these parameters: scaling (per pixel) of 63 (X) × 0.63 (Y) × 1 μm (Z); image size (pixels) of 512 × 512; bit depth of 8 bit; pixel dwell of 1.58 μm. The excitation/emission maxima for these dyes are approximately 480/500 nm for the SYTO® 9 stain and 490/635 nm for propidium iodide. Z-stacks (XYZ isosurface) were obtained by driving the microscope to a point just out of focus on both the top and the bottom of the biofilms with a step size of 1 μm. The images were analyzed with ZEN black Imaging Software 3.0 and recorded as a series of. tif files with a file depth of 16 bits. The COMSTAT software package (Heydorn et al., 2000) was used to determine the biomasses ($\mu m^3/\mu m^2$), mean thicknesses (μm), and roughness coefficients (Ra*). For each condition, two independent biofilm samples were used.

Qualitative Imaging of the Matrix Components

To identify the polysaccharide and protein contents of the biofilm matrix, the biofilms were labeled with wheat germ agglutinin (WGA), from Triticum vulgaris, FITC conjugated (L4895; Sigma-Aldrich), which binds di-*N*-acetylglucosamine and *N*−acetylneuraminic acid (415/518 nm), and with FilmTracer^{TM} SYPRO® Ruby Biofilm Matrix stain (Molecular Probes, Invitrogen), which labels most classes of proteins including glycoproteins, phosphoproteins, lipoproteins, calcium-binding proteins, fibrillar proteins, and other proteins that are difficult to stain (450/610 nm). Briefly, 300 μl of the medium with a suitable dilution of the Arctic culture in the exponential growth

phase (about 0.2 OD 600 nm) were added into each well of a sterile Chamber Slide. After the incubation, the plates were rinsed with filter-sterilized PBS. Next, each well of the chamber slide was filled with 300 μl of a working solution of fluorescent stains (WGA or SYPRO Ruby), following the manufacturer's instructions, and incubated for 20–30 min at room temperature, protected from light. All the excess staining was removed by rinsing gently with filter-sterilized PBS. The 2D images ("snap") were obtained using a 20 × NA 0.8 objective and acquired using these parameters: scaling (per pixel) of 63 μm (X) × 0.63 μm (Y); image size (pixels) of 512 × 512; bit depth of 8 bit; pixel dwell of 1.58 μm. Then, the images were analyzed with ZEN black Imaging Software 3.0 and recorded as a series of. tif files with a file depth of 16 bits. For each condition, two independent biofilm samples were used.

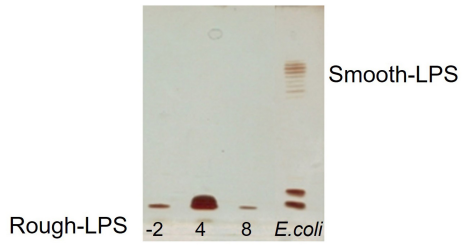

FIGURE 1 | DOC-PAGE analysis of the PCP extracts from *Colwellia* 34H cells grown at −2, 4, and 8°C.

TABLE 1 | Temperature dependence in fatty acid composition reported for *Colwellia* 34H.

Growth temperature (°C)	***−2***	***4***	***8***
Fatty acid	**Fatty acid composition (%)**		
C10:0	8.33	8.84	9.72
C12:0	13.40	9.01	13.09
C14:0	2.87	4.10	3.24
C15:0	0.61	0.75	0.05
C16:0	32.85	41.98	30.36
Sum saturated	**58.08**	**64.68**	**56.46**
C14.1	4.61	5.26	5.20
C15:1	0.53	0.70	1.07
C16:1	15.37	10.05	10.02
Sum monounsaturated	**20.51**	**16.01**	**16.29**
C12:3OH	19.38	16.12	22.73
C14:3OH	0.12	0.67	0.69
C14:1 3OH	1.92	2.52	3.83
Sum hydroxylated	**21.41**	**19.31**	**27.25**

RESULTS

Bacteria Growth Conditions

C. psychrerythraea strain 34H was grown aerobically at −2, 4, and 8°C in the Marine Broth medium, and the cells were separated from spent medium by a gentle centrifugation and freeze-dried. The supernatants were dialyzed against water and lyophilized. The obtained biomasses for all the conditions are reported in **Supplementary Table 1**.

As previously performed in case of *Colwellia* 34H grown at 4°C, a preliminary analysis on the Arctic bacterium grown at −2 and 8°C was performed by transmission electron microscopy, and the presence of a capsular structure around the cells was visible either at −2 or at 8°C (**Supplementary Figure 1**).

Lipopolysaccharides Isolation, Purification, and Characterization

The dried cells from *Colwellia* 34H grown at the temperatures of −2, 4, and 8°C were extracted by the PCP method to recover the crude LPSs. The DOC-PAGE analysis, visualized after silver nitrate (**Figure 1**), confirmed that *Colwellia* 34H produces a rough-LPS (LOS) in all the conditions, as shown by the absence of the typical ladder-like pattern in the upper part of the gel attributable to the O-chain moiety. Moreover, differences in the yield of the produced LPSs at the three different temperatures were observed (yields: −2°C 1.1%; 4°C 3%; 8°C 0.6%).

Chemical analyses performed on the pure LOS for each growth revealed the presence of colitose, glucuronic acid, mannose, and glucosamine. The presence of Kdo in the three samples was confirmed after the HF treatment.

Lipid A

The intact LOS extracts were subjected to mild acid hydrolysis with acetic acid to separate the lipid A portion from the saccharidic one. The mixtures were centrifuged, and the precipitates were freeze-dried, and then washed several times with a chloroform/methanol mixture to obtain the purified samples. The analysis of fatty acid composition was performed for each sample and the results are reported in **Table 1**. The data suggested that *Colwellia* 34H exhibited slight changes in fatty acid composition in response to the growth temperature. The growth at −2°C resulted in an increased percentage of mono-unsaturated fatty acids (C16:1), confirming the role of the lipid A in the modulation of membrane fluidity. In contrast with the results obtained for *P. syringae*, in *Colwellia* 34H, the hydroxylated acyl chains do not seem to participate in the adaptation mechanism since the highest amount of the last was found for *Colwellia* 34H grown at 8°C (27.25%). Finally, we observed that saturated fatty acids did not change significantly. Although the obtained results in this study are counterintuitive when compared with those reported for mesophilic bacteria, they agree with the findings reported for other cold-adapted bacteria. It is also evident that if we limit our analysis by considering only the temperature of −2 and 4°C, the variations in unsaturation, hydroxylation, and acyl chain length are all in agreement with the available data. A similar response was also observed for *P. haloplanktis* TAC 125. This uncommon trend could find a right explanation in the capacity of *Colwellia* 34H to grow at 8°C, which probably represents a limit in growth temperature in the lab, whereas −2 and 4°C are close to those of the natural environments.

Core Oligosaccharide Structure

An aliquot of each LOS sample was deacylated with anhydrous hydrazine. The LOS-OH product obtained from both samples

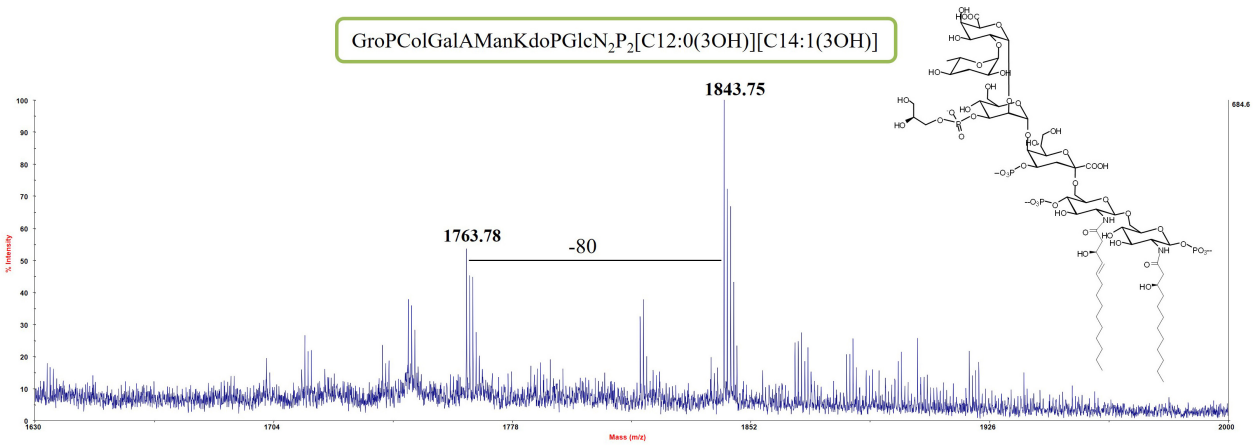

FIGURE 2 | MS spectrum and chemical structure of the partially deacylated LOS (LOS-OH) from *Colwellia* 34H grown at 8°C.

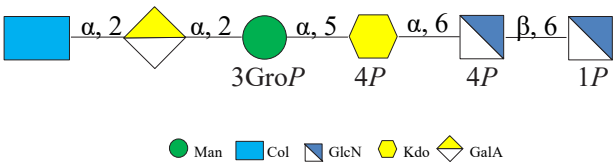

SCHEME 1 | Core oligosaccharide structure from *Colwellia* 34H.

was analyzed by MALDI MS. The partially deacylated LOS (LOS-OH) obtained for both LOS from cells grown at −2°C and 8°C revealed the identical composition with the LOS from *Colwellia* 34H at 4°C (**Figure 2** and **Supplementary Figure 2**).

The LOS-OH were completely deacylated by strong alkaline hydrolysis and purified by gel filtration chromatography. The resulting core oligosaccharides (OSs) were analyzed by NMR experiments.

Both MS results of the LOS-OH and ^{1}H NMR spectra of the OS (**Supplementary Figure 3**) revealed that *Colwellia* 34H produces the same core oligosaccharide structure at all temperatures (**Scheme 1**).

Capsular Polysaccharides

The phenol/water extracts were analyzed by GC-MS. The samples derivatized as AMG suggested the presence of glucuronic (GlcA) and galacturonic (GalA) acids, galactosamine (GalN), and glucosamine (GlcN), together with traces of mannose (Man) in all the tested conditions. Finally, at 8°C, traces of glucosaminuronic acid (GlcNA) were found. The analysis of the monosaccharide composition confirmed the production of the CPS_A isolated from the large-scale cultivation at 4°C. Furthermore, the analysis also revealed the production of the CPS_B only at 8°C. Similarly to the fatty acids, the effect of the growth temperature on the percentage composition of monosaccharides was evaluated (**Table 2**).

Since the monosaccharides constituting the CPS_A, the CPS_B, and the LOS are almost the same, it is difficult to correlate the production of the capsular polysaccharides (CPSs) in response to the temperature changes. Therefore, the extracts were analyzed by 14% DOC-PAGE and visualized after Alcian Blue and silver staining (**Figure 3**). Moving from −2 to 8°C, together with fast-migrating bands typical of the LOS, the electrophoretic profile showed bands at high molecular masses due to the presence of the CPS_A and CPS_B. The DOC-PAGE analysis revealed to be more suitable to describe the production and the relative abundance of the polymers, demonstrating that the polysaccharide production exhibited changes in response to the growth temperature. The cultivation at the very low temperature suggested that the CPS_A endowed with IRI activity is the only produced, confirming the key role of this capsular in the survival of the bacterium. The cultivation of *Colwellia* 34H to 8°C resulted in the production of both CPS_A and CPS_B.

TABLE 2 | Temperature dependence in monosaccharide composition reported for *Colwellia* 34H.

Growth temperature (°C)	−2	4	8
	Monosaccharide composition (%)		
GlcA	14,18	15,23	17,68
GalA	33,24	27,06	24,25
GalN	16,13	15,59	16,25
GlcN	36,45	42,12	41,82
GlcNA	–	–	Traces

GlcA, CPS_A; GalA, CPS_A and LPS; GalN, CPS_A and CPS_B; GlcN, CPS_A and LPS.

To confirm the primary structures of all the CPSs, all the extracts were purified from nucleic acid and LOS molecules through an enzymatic hydrolysis and a mild acid hydrolysis, respectively. The pure CPSs obtained after gel filtration chromatography were analyzed by ^{1}H NMR (**Supplementary Figure 4**), confirming that the changing temperature did not affect either the production or the primary structure (**Scheme 2**).

Medium Released Polysaccharides

The cell culture supernatants were dialyzed against water and freeze-dried. The monosaccharide composition revealed the

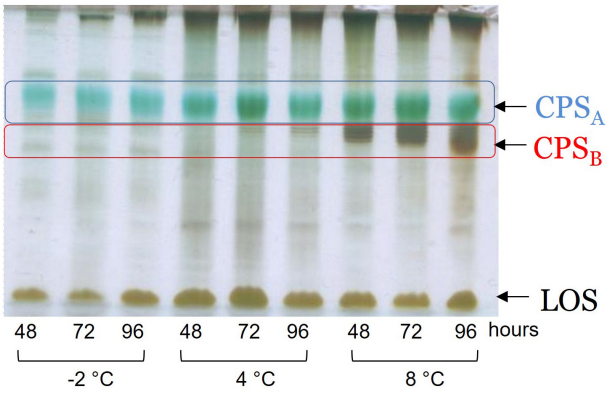

FIGURE 3 | DOC-PAGE of the water extract from *Colwellia* 34H cell cultivation at −2, 4, and 8°C.

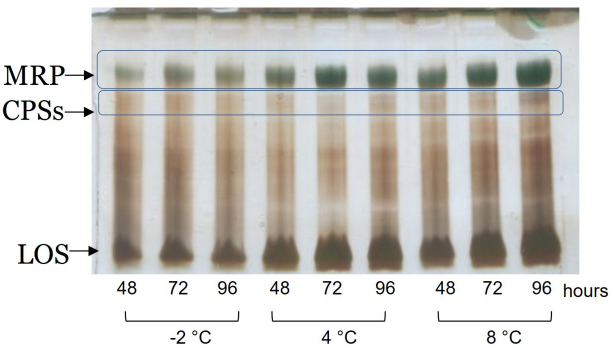

FIGURE 4 | DOC-PAGE analysis of the dialyzed supernatant from *Colwellia* 34H.

presence of quinovosamine (QuiN) and galacturonic (GalA) residues, attributable to the MRP, as main components. Furthermore, the AMG analysis showed traces of GlcA, GalN, and GlcN, attributable to CPS$_A$ and CPS$_B$. The samples were analyzed by 14% DOC-PAGE, visualized after Alcian Blue and silver nitrate. The results of the DOC-PAGE experiment (**Figure 4**) suggested that moving from −2 to 8°C *Colwellia* 34H, the production of the EPS increased at higher temperatures.

The samples were subjected to mild acid hydrolysis and purified by S400 gel filtration chromatography column. The obtained polysaccharide fractions were analyzed by chemical analyses and NMR spectroscopy. The comparison of the ^{1}H NMR spectra (**Supplementary Figure 5**) allowed confirming the structure of the MRP characterized from cultivation at 4°C in all the tested conditions (**Scheme 3**).

Biofilm Production and Characterization

To investigate the capability of *Colwellia* 34H to form biofilm at different growth temperatures, the bacterium was grown in static conditions at −2, 4, and 8°C in Marine Broth medium, and biofilms were evaluated at different incubation times. The bacterium was able to form biofilm in all the tested conditions, and its formation occurs at the air—liquid interface forming pellicles or floating biofilms (Wimpenny et al., 2000). The amount of the biofilm formed in the diverse conditions was different; at −2°C, the amount of the biofilm produced by the bacterium was lower than that produced at 4 and 8°C. Biofilms produced by *Colwellia* 34H at different temperatures were further investigated by confocal laser scanning microscopy (CLSM) to analyze the structure and the biomass distribution.

The biofilm structures were obtained using the live/dead staining, indicating viable cells by green fluorescence and red for dead (cell membrane damaged) bacteria (**Figure 5A**). The CLSM image stack data were further analyzed using the COMSTAT image analysis software package to evaluate the different parameters describing the biofilm structure (**Figure 5B**). The analysis revealed that the biofilm at −2°C proved to be less compact and structured worse than that produced at 4 and 8°C.

Moreover, the polysaccharide and the protein content of the biofilm matrix was explored by CLSM. A fluorescence lectin-binding analysis was carried out to obtain preliminary information on polysaccharide presence in *Colwellia* 34H biofilms. In particular, the biofilms obtained in the three studied conditions were stained with WGA, from Triticum vulgaris, FITC conjugated (**Figure 6**). WGA generally binds β-GlcNAc-(1→4)-β-GlcNAc-(1→4)-GlcNAc and Neu5Ac (sialic acid). SYPRO Ruby Biofilm Matrix FilmTracer was used to reveal the proteins present in the biofilm matrix, and the analysis revealed the presence of polysaccharides and proteins in all the tested conditions (**Figure 6**).

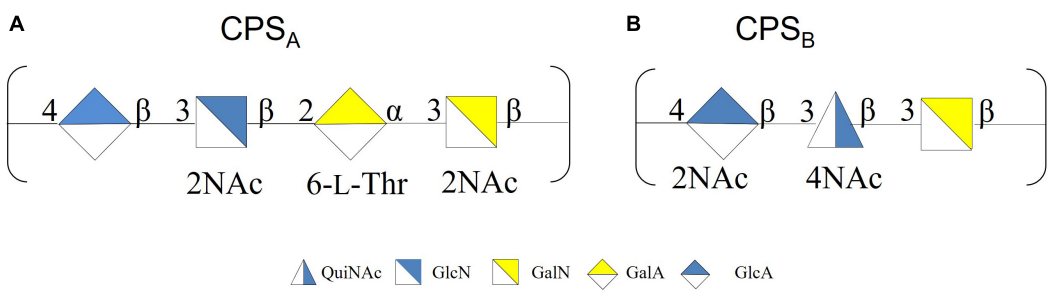

SCHEME 2 | (A) CPS$_A$ produced at −2, 4, and 8°C. **(B)** CPS$_B$ produced at 8°C.

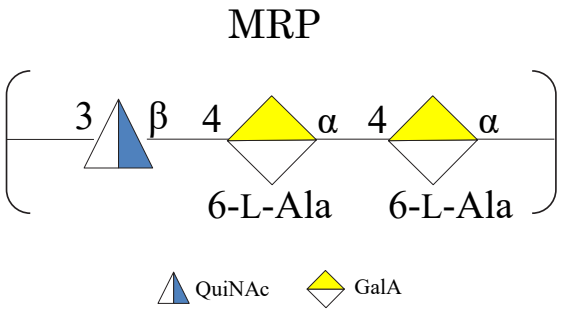

SCHEME 3 | MRP isolated from *Colwellia* 34H at −2, 4, and 8°C.

To better characterize the biofilm at 4°C, we analyzed the kinetics of the biofilm formation at 4°C (**Supplementary Figure 6**), and the highest biomass value was reached after 96 h. Therefore, the studies to assess the role of eDNA and proteins in the biofilm formation were performed, growing the cells in static conditions in the presence of either in the absence of DNase I or proteinase K for 96 h. The quantification of the biofilms obtained in these conditions (**Figure 7**) revealed that the treatment with DNaseI reduced the biofilm formation with respect to the biofilm obtained in the absence of the DNaseI. The proteinase K presence also affected the Arctic bacterium biofilm formation, suggesting the key role of proteins and eDNA during the biofilm formation of *Colwellia* 34H.

To investigate the biofilm in terms of polysaccharide composition, the air–liquid pellicles of *Colwellia* 34H grown in static condition at 4°C were recovered and analyzed by 14% DOC-PAGE experiment (**Figure 8**).

The gel visualized after Alcian Blue and silver nitrate staining showed the presence of one band at low molecular masses, corresponding to the LOS, and several bands at high molecular weight corresponding to the polysaccharide components. In agreement with the fact that in the biofilm the main biomass is attributable to the cells, glycosyl analysis performed on the *Colwellia* 34H biofilm confirmed the presence of the LOS and CPSs components. Moreover, the finding of ribose confirmed the occurrence of nucleic acids in the samples (data not shown).

DISCUSSION

Colwellia 34H is considered an excellent model for studying the lifestyle in cold environments (Methé et al., 2005) and is suitable for biotechnological applications since it produces cold-active enzymes with high catalytic efficiency at low temperatures (Park et al., 2017; Lee et al., 2019). Bacteria populating cold habitats evolved several strategies to avoid the freezing of their cells due to the low temperatures. The dropping of the temperature mainly affects the fluidity of the cellular membrane, thus compromising its functionality. The outer membrane of Gram-negative bacteria actively participates with all its constituents to reach this purpose. It is well known that the phospholipid composition changes vs. a higher amount of unsaturated fatty acids, an increased branching of acyl chains, and a decreased length. Consistent with these observations, the lipid A isolated from cold-adapted bacteria showed shortened acyl chains with respect to the mesophiles (Casillo et al., 2019a). This observation is mainly derived from

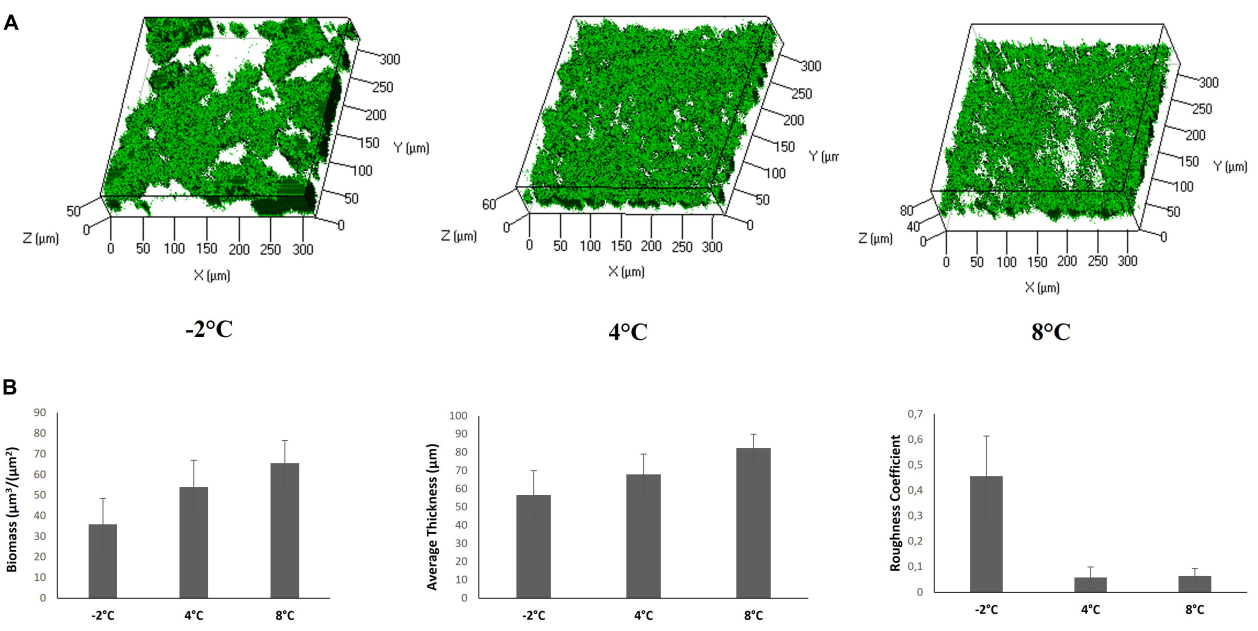

FIGURE 5 | CLSM of *Colwellia* 34H biofilms in Marine Broth medium. **(A)** Z-stack (XYZ isosurface) analysis of *Colwellia* 34H biofilms at −2, 4, and 8°C. The bacteria were grown in chamber slides and then stained with LIVE/DEAD reagents. The green fluorescence (SYTO9) indicates viable cells. **(B)** COMSTAT quantitative analysis of the biomass, average thickness, and roughness coefficient of *Colwellia* 34H biofilms at −2, 4, and 8°C.

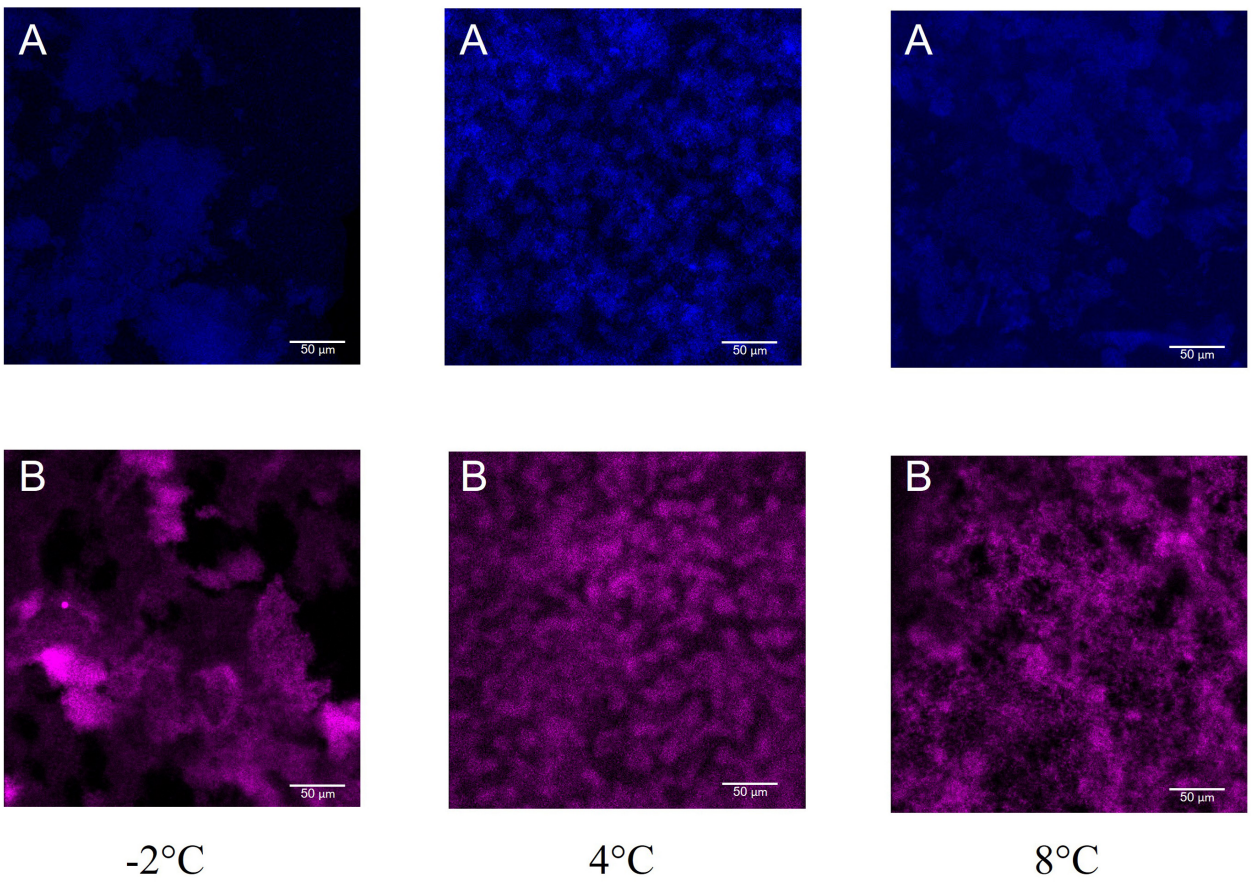

FIGURE 6 | CLSM of *Colwellia* 34H biofilms at −2, 4, and 8°C. 2D images of *Colwellia* 34H biofilms. Biofilms were stained with wheat germ agglutinin (WGA), from Triticum vulgaris, FITC conjugated **(A)** that binds β-GlcNAc-(1→4)-β-GlcNAc-(1→4)-GlcNAc and Neu5Ac (sialic acid), and SYPRO® Ruby Biofilm Matrix FilmTracer **(B)** used to reveal the proteins present in the biofilm matrix.

the investigation of the temperature effect on mesophilic bacteria (Janoff et al., 1979; Kropinski et al., 1987), since a limited number of such studies are carried out on psychrophiles.

In the past, the effect of growth temperature on the LPS has been evaluated for the psychrotolerant *P. haloplanktis* TAC125. In that case, the change of the growth temperature among 4, 15, and 25°C resulted in two LOS structural variations: the presence of free lipid A at 4°C suggesting an incomplete biosynthesis in this condition, and a higher phosphate content from 4 to 25°C (Corsaro et al., 2004).

In the last few years, we focused our studies on the glycoconjugates produced by *Colwellia* 34H at 4°C, resulting in the isolation and characterization of very interesting molecules. In this paper, we analyzed the response of these glycoconjugates in terms of production and chemical structure by changing the growth temperature. The DOC-PAGE and chemical analyses of the extracted cells at −2, 4, and 8°C confirmed the rough nature of the LPS, with a slight difference in the yields. To compare the primary structure, the core oligosaccharides have been isolated and characterized. Our results demonstrated that no differences were found in the carbohydrate moiety of the lipooligosaccharides obtained from all the tested conditions.

The different amounts of some of the acyl chains obtained from the analyses of the fatty acid composition highlighted that the homeoviscous adaptation of the outer membrane is also attributable to the lipid A structures, as already reported for *Colwellia hornerae* and *Colwellia piezophila* (Sweet et al., 2015). At −2°C, increased production of monounsaturated fatty acids (C16:1) is observed, in agreement with the data available for other cold-adapted bacteria (Corsaro et al., 2004; Sweet et al., 2015).

The effect of temperature variation was also evaluated on the production of extracellular polysaccharides. The phenol/water extracts have been analyzed to compare the CPSs production. Moving from −2 to 8°C, the production and the structures of the CPS_A and MRP are confirmed, whereas the production of the CPS_B is verified to occur only at 8°C. Interestingly, this result indicated that *Colwellia* 34H was able to switch to a different polysaccharide biosynthesis instead of a mere downregulation of the polymers synthesized at low temperature.

The ability of bacteria to form biofilms in many environments is undoubtedly related to the selective advantage that the association offers; therefore, in this paper we also evaluated the ability of *Colwellia* 34H to form biofilm at different temperatures. The data demonstrated that this model organism responds to

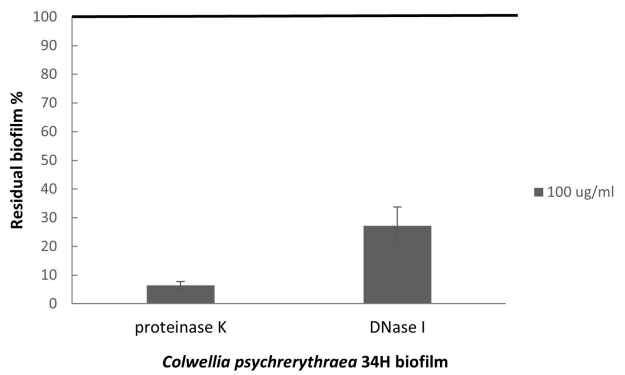

FIGURE 7 | Analysis of the effect of proteinase K and DNase I on *Colwellia* 34H biofilm formation. *Colwellia* 34H biofilm formation obtained at 4°C for 96 h in the absence (100% biofilm obtained in absence of proteinase K or DNase I) and in the presence of proteinase K or DNase I at a concentration of 100 μg/ml. The data are reported as a percentage of the residual biofilm after the treatment. Each data point represents the mean ± the SD of six independent samples.

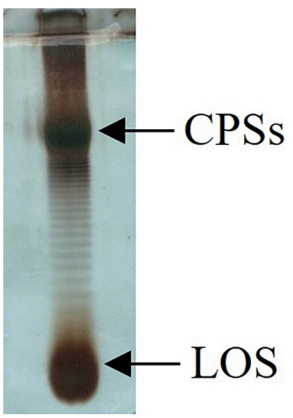

FIGURE 8 | DOC-PAGE analysis of *Colwellia* 34H biofilm.

different temperatures producing a different amount of air–liquid biofilm. In all the tested conditions, the biofilm matrix obtained is quite similar, even if the analysis revealed that, at −2°C, the biofilm is less compact.

A more detailed investigation on the sugar content of biofilm at 4°C uncovered the absence of MRP molecules in the biofilm matrix, whereas further experiments revealed that the MRP molecules were present in the extracellular medium of the biofilm growth (data not shown). In many bacteria, the biofilm matrix contains MRPs (Karygianni et al., 2020), and in several strains, the MRPs have not only a structural role but also a functional one, for example, in *V. vulnificus* where MRPs are required for maturation of biofilm structures (Kim et al., 2009). The absence of MRP in the *Colwellia* 34H biofilm matrix could be related to the MRP role in cell cryoprotection; indeed, this function could be better accomplished if the MRP molecules are present in the culture medium where they can interact with the water molecules avoiding the formation of the tetrahydric geometry distinctive of ice crystals.

Since the analyses on *Colwellia* 34H biofilms revealed that the matrix contains not only sugar but also proteins and nucleic acids, we investigated the role of protein and eDNA on biofilm formation. Indeed, for some bacteria eDNA, besides its structural role, it is required for the initial step of biofilm formation, whereas in other bacteria, it plays a role during the transition from the attachment phase to the biofilm maturation phase (Okshevsky and Meyer, 2015). The reported data suggested that either eDNA or proteins seemed to be crucial for the biofilm formation of *Colwellia* 34H.

CONCLUSION

In conclusion, we analyzed the cell culture of the model bacterium *C. psychrerythraea* 34H at three different temperatures to describe the variations in surface glycoconjugates and extracellular matrix glycopolymers. It is interesting to note that *C. psychrerythraea* 34H modulates in different ways all the analyzed glycoconjugates in response to different temperatures, by working on the fatty acid structural motifs or on the amount of the polymers. Finally, while the production of the CPS_A at all the temperatures is confirmed and its role in survival at low temperatures is clear, the physiological role of the CPS_B at 8°C is still under investigation.

DATA AVAILABILITY STATEMENT

The original contributions presented in the study are included in the article/**Supplementary Material**, further inquiries can be directed to the corresponding author/s.

AUTHOR CONTRIBUTIONS

AC performed the experiments, suggested critical parameters in design of experiments, and co-wrote the manuscript. CD'A performed the experiments and co-wrote the manuscript. EP and MT suggested critical parameters in the design of experiments and co-wrote the manuscript. MC designed the experiments, provided advice in the performance of experiments, and wrote the manuscript. All authors contributed to the article and approved the submitted version.

ACKNOWLEDGMENTS

We thank the Italian National Programme for Antarctic Research (PNRA) (Project PNRA18_00007).

SUPPLEMENTARY MATERIAL

The Supplementary Material for this article can be found online at: https://www.frontiersin.org/articles/10.3389/fmicb.2022.820714/full#supplementary-material

REFERENCES

Adinolfi, M., Corsaro, M. M., De Castro, C., Evidente, A., Lanzetta, R., Lavermicocca, P., et al. (1996). Analysis of the polysaccharide components of the lipopolysaccharide fraction of *Pseudomonas caryophylli*. *Carbohydr. Res.* 284, 119–133.

Boetius, A., Anesio, A. M., Deming, J. W., Mikucki, J. A., and Rapp, J. Z. (2015). Microbial ecology of the cryosphere: sea ice and glacial habitats. *Nat. Rev. Microbiol.* 13, 677–690. doi: 10.1038/nrmicro3522

Carillo, S., Casillo, A., Pieretti, G., Parrilli, E., Sannino, F., Bayer-Giraldi, M., et al. (2015). A unique capsular polysaccharide structure from the psychrophilic marine bacterium *Colwellia psychrerythraea* 34H that mimics antifreeze (Glyco)proteins. *J. Am. Chem. Soc.* 137, 179–189. doi: 10.1021/ja5075954

Carillo, S., Pieretti, G., Lindner, B., Parrilli, E., Filomena, S., Tutino, M. L., et al. (2013). Structural Characterization of the Core Oligosaccharide Isolated from the Lipopolysaccharide of the Psychrophilic Bacterium *Colwellia psychrerythraea* Strain 34H. *Eur. J. Org. Chem.* 3771–3779.

Casillo, A., Lanzetta, R., Parrilli, M., and Corsaro, M. M. (2018). Exopolysaccharides from marine and marine extremophilic bacteria: structures, properties, ecological roles and applications. *Mar. Drugs* 16:69. doi: 10.3390/md16020069

Casillo, A., Ziaco, M., Lindner, B., Parrilli, E., Schwudke, D., Holgado, A., et al. (2017b). Unusual lipid a from a cold-adapted bacterium: detailed structural characterization. *Chem. Bio Chem.* 18, 1845–1854. doi: 10.1002/cbic.201700287

Casillo, A., Parrilli, E., Sannino, F., Mitchell, D. E., Gibson, M. I., Marino, G., et al. (2017a). Structure-activity relationship of the exopolysaccharide from a psychrophilic bacterium: a strategy for cryoprotection. *Carbohydr. Polym.* 156, 364–371. doi: 10.1016/j.carbpol.2016.09.037

Casillo, A., Ståhle, J., Parrilli, E., Sannino, F., Mitchell, D. E., Pieretti, G., et al. (2017c). Structural characterization of an all-aminosugar-containing capsular polysaccharide from *Colwellia psychrerythraea* 34H. *Antonie Van Leeuwenhoek* 110, 1377–1387. doi: 10.1007/s10482-017-0834-6

Casillo, A., Parrilli, E., Tutino, M. L., and Corsaro, M. L. (2019a). The outer membrane glycolipids of bacteria from cold environments: isolation, characterization, and biological activity. *FEMS Microbiol. Ecol.* 95:fiz094. doi: 10.1093/femsec/fiz094

Casillo, A., Di Guida, R., Carillo, S., Chen, C., Kamasaka, K., Kawamoto, J., et al. (2019b). Structural elucidation of a novel lipooligosaccharide from the Antarctic bacterium OMVs producer Shewanella sp. HM13. *Mar. Drugs* 17:34. doi: 10.3390/md17010034

Christensen, A. J., Moran, P. J., and Wiebe, J. S. (1999). "Assessment of irrational health beliefs: relation to health practices and medical regimen adherence": correction to Christensen et al. (1999). *Health Psychol.* 18:220. doi: 10.1037//0278-6133.18.2.169

Collins, T., and Margesin, R. (2019). Psychrophilic lifestyles: mechanisms of adaptation and biotechnological tools. *Appl. Microbiol. Biotechnol.* 103, 2857–2871. doi: 10.1007/s00253-019-09659-5

Corsaro, M. M., Lanzetta, R., Parrilli, E., Parrilli, M., Tutino, M. L., and Ummarino, S. (2004). Influence of growth temperature on lipid and phosphate contents of surface polysaccharides from the antarctic bacterium *Pseudoalteromonas haloplanktis* TAC 125. *J. Bacteriol.* 186, 29–34. doi: 10.1128/JB.186.1.29-34.2004

Cronan, J. E., and Gelmann, E. P. (1975). Physical properties of membrane lipids: biological relevance and regulation. *Bacteriol. Rev.* 39, 232–256. doi: 10.1128/br.39.3.232-256.1975

Daugelavičius, R., Bakiene, E., and Bamford, D. H. (2000). Stages of polymyxin B interaction with the *Escherichia coli* cell envelope. *Antimicrob. Agents Chemother.* 44, 2969–2978. doi: 10.1128/AAC.44.11.2969-2978.2000

Ernst, R., Ejsing, C. S., and Antonny, B. (2016). Homeoviscous adaptation and the regulation of membrane lipids. *J. Mol. Biol.* 428, 4776–4791. doi: 10.1016/j.jmb.2016.08.013

Escalera, L., Benvenuto, G., and Scalco, E. (2014). Ultrastructural features of the benthic dinoflagellate *Ostreopsis* cf. *ovata* (Dinophyceae). *Protist* 165, 260–274.

Flemming, H. C., and Wingender, J. (2010). The biofilm matrix. *Nat. Rev. Microbiol.* 8, 623–633. doi: 10.3390/nano10081527

Flemming, H. C., Wingender, J., Szewzyk, U., Steinberg, P., Rice, S. A., and Kjelleberg, S. (2016). Biofilms: an emergent form of bacterial life. *Nat. Rev. Microbiol.* 14, 563–575.

Galanos, C., Lüderitz, O., and Westphal, O. (1969). A new method for the extraction of R Lipopolysaccharides. *Eur. J. Biochem.* 9, 245–249. doi: 10.1111/j.1432-1033.1969.tb00601.x

Guyard-Nicodème, M., Bazire, A., Hémery, G., Meylheuc, T., Mollé, D., Orange, N., et al. (2008). Outer membrane Modifications of *Pseudomonas fluorescens* MF37 in response to hyperosmolarity. *J. Proteome Res.* 7, 1218–1225. doi: 10.1021/pr070539x

Heydorn, A., Nielsen, A. T., Hentzer, M., Sternberg, C., Givskov, M., Ersbøll, B. K., et al. (2000). Quantification of biofilm structures by the novel computer program COMSTAT. *Microbiology* 146, 2395–2407. doi: 10.1099/00221287-146-10-2395

Janoff, A. S., Haug, A., and McGroarty, E. J. (1979). Relationship of growth temperature and thermotropic lipid phase changes in cytoplasmic and outer membranes from *Escherichia coli* K12. *Biochim. Biophys. Acta* 555, 56–66. doi: 10.1016/0005-2736(79)90071-3

Karygianni, L., Ren, Z., Koo, H., and Thurnheer, T. (2020). Biofilm matrixome: extracellular components in structured microbial communities. *Trends Microbiol.* 28, 668–681. doi: 10.1016/j.tim.2020.03.016

Kim, H.-S., Park, S.-J., and Lee, K.-H. (2009). Role of NtrC-regulated exopolysaccharides in the biofilm formation and pathogenic interaction of *Vibrio vulnificus*. *Mol. Microbiol.* 74, 436–453.

Kim, S. J., and Yim, H. J. (2007). Cryoprotective properties of exopolysaccharide (P-21653). produced by the Antarctic bacterium, *Pseudoalteromonas arctica* KOPRI 21653. *J. Microbiol.* 45, 510–514.

Kropinski, A. M., Lewis, V., and Berry, D. (1987). Effect of growth temperature on the lipids, outer membrane proteins, and lipopolysaccharides of *Pseudomonas aeruginosa* PAO. *J. Bacteriol.* 169, 1960–1966. doi: 10.1128/jb.169.5.1960-1966.1987

Kumar, G. S., Jagannadham, M. V., and Ray, M. K. (2002). Low-temperature-induced changes in composition and fluidity of lipopolysaccharides in the Antarctic psychrotrophic bacterium *Pseudomonas syringae*. *J. Bacteriol.* 184, 6746–6749. doi: 10.1128/JB.184.23.6746-6749.2002

Laemmli, U., and Favre, M. (1970). SDS Polyacrylamide gel electrophoresis. *Nature* 227, 680–682.

Langille, S. E., and Weiner, R. M. (1998). Spatial and temporal deposition of *Hyphomonas* strain vp-6 capsules involved in biofilm formation. *Appl. Environ. Microbiol.* 64, 2906–2913. doi: 10.1128/AEM.64.8.2906-2913.1998

Lee, C. W., Park, S. H., Jeong, C. S., Cha, S., Park, H., and Lee, J. H. (2019). Structural basis of small RNA hydrolysis by oligoribonuclease (CpsORN). from *Colwellia psychrerythraea* strain 34H. *Sci. Rep.* 9:2649. doi: 10.1038/s41598-019-39641-0

Liao, Y., Williams, T., Ye, J., Charlesworth, J., Burns, B. P., Poljak, A., et al. (2016). Morphological and proteomic analysis of biofilms from the Antarctic archaeon. *Halorubrum lacusprofundi*. *Sci. Rep.* 6:37454. doi: 10.1038/srep37454

Liu, A., Zhang, Y. J., Cheng, P., Peng, Y. J., Blom, J., and Xue, Q. J. (2020). Whole genome analysis calls for a taxonomic rearrangement of the genus *Colwellia*. *Antonie Van Leeuwenhoek* 113, 919–931. doi: 10.1007/s10482-020-01405-6

Marx, J. G., Carpenter, S. D., and Deming, J. W. (2009). Production of cryoprotectant extracellular polysaccharide substances (EPS). by the marine psychrophilic bacterium *Colwellia psychrerythraea* strain 34H under extreme conditions. *Can. J. Microbiol.* 55, 63–72. doi: 10.1139/W08-130

Methé, B. A., Nelson, K. E., Deming, J. W., Momen, B., Melamud, E., Zhang, X., et al. (2005). The psychrophilic lifestyle as revealed by the genome sequence of *Colwellia psychrerythraea* 34H through genomic and proteomic analyses. *Proc. Natl. Acad. Sci. U. S. A.* 102, 10913–10918. doi: 10.1073/pnas.0504766102

Nichols, C. M., Lardiere, S. G., Bowman, J. P., Nichols, P. D., Gibson, J. A. E., and Guezennec, J. (2005). Chemical characterization of exopolysaccharides from Antarctic marine bacteria. *Microb. Ecol.* 49, 578–589. doi: 10.1007/s00248-004-0093-8

Nikaido, H. (1994). Prevention of drug access to bacterial targets: permeability barriers and active efflux. *Science* 264, 382–388. doi: 10.1126/science.8153625

Nikaido, H., and Vaara, M. (1985). Molecular basis of bacterial outer membrane permeability. *Microbiol. Rev.* 49, 1–32.

Okshevsky, M., and Meyer, R. L. (2015). The role of extracellular DNA in the establishment, maintenance and perpetuation of bacterial biofilms. *Crit. Rev. Microbiol.* 41, 341–352.

Park, S.-H., Lee, C. W., Lee, S. G., Shin, S. C., Kim, H. J., Park, H., et al. (2017). Crystal structure and functional characterization of an isoaspartyl dipeptidase (CpsIadA). from *Colwellia psychrerythraea* strain 34H. *PLoS One* 12:e0181705. doi: 10.1371/journal.pone.0181705

Quintero, E. J., and Weiner, R. M. (1995). Evidence for the adhesive function of the exopolysaccharide of *Hyphomonas* strain MHS-3 in its attachment to surfaces. *Appl. Environ. Microbiol.* 61, 1897–1903. doi: 10.1128/aem.61.5.1897-1903.1995

Ray, M. K., Kumar, G. S., and Shivaji, S. (1994). Phosphorylation of lipopolysaccharides in the Antarctic psychrotroph *Pseudomonas syringae*: a possible role in temperature adaptation. *J. Bacteriol.* 176, 4243–4249. doi: 10.1128/jb.176.14.4243-4249.1994

Ricciardelli, A., Casillo, A., Papa, R., Monti, D. M., Imbimbo, P., Vrenna, G., et al. (2018). Pentadecanal inspired molecules as new anti-biofilm agents against *Staphylococcus epidermidis*. *Biofouling* 34, 1110–1120. doi: 10.1080/08927014.2018.1544246

Rinker, K. D., and Kelly, R. M. (1996). Growth physiology of the hyperthermophilic Archaeon *Thermococcus litoralis*: development of a sulfur-free defined medium, characterization of an exopolysaccharide and evidence of biofilm formation. *Appl. Environ. Microbiol.* 62, 4478–4485. doi: 10.1128/aem.62.12.4478-4485.1996

Russell, N. J. (1990). Cold adaptation of microorganisms. *Philos. Trans. R Soc. Lond. B* 326, 595–611. doi: 10.1098/rstb.1990.0034

Siddiqui, K. S., Williams, T. J., Wilkins, D., Yau, S., Allen, M. A., Mark, V., et al. (2013). Psychrophiles. *Annu. Rev. Earth Planet. Sci.* 41, 87–115.

Sweet, C. R., Watson, R. E., Landis, C. A., and Smith, J. P. (2015). Temperature-dependence of lipid A acyl structure in *Psychrobacter cryohalolentis* and arctic isolates of *Colwellia hornerae* and *Colwellia piezophile*. *Mar. Drugs* 13, 4701–4720. doi: 10.3390/md13084701

Tsai, C. M., and Frasch, C. E. (1982). A sensitive silver stain for detecting lipopolysaccharides in polyacrylamide gels. *Anal. Biochem.* 119, 115–119. doi: 10.1016/0003-2697(82)90673-x

Westphal, O., and Jann, K. (1965). Bacterial lipopolysaccharides extraction with phenol-water and further applications of the procedure. *Methods Carbohydr. Chem.* 5, 83–91.

Whitchurch, C. B., Tolker-Nielsen, T., Ragas, P. C., and Mattick, J. S. (2002). Extracellular DNA required for bacterial biofilm formation. *Science* 295:1487. doi: 10.1126/science.295.5559.1487

Wimpenny, J., Manz, W., and Szewzyk, U. (2000). Heterogeneity in biofilms. *FEMS Microbiol. Rev.* 24, 661–671. doi: 10.1111/j.1574-6976.2000.tb00565.x

Conflict of Interest: The authors declare that the research was conducted in the absence of any commercial or financial relationships that could be construed as a potential conflict of interest.

Publisher's Note: All claims expressed in this article are solely those of the authors and do not necessarily represent those of their affiliated organizations, or those of the publisher, the editors and the reviewers. Any product that may be evaluated in this article, or claim that may be made by its manufacturer, is not guaranteed or endorsed by the publisher.

frontiers in Microbiology

ORIGINAL RESEARCH
published: 04 March 2022
doi: 10.3389/fmicb.2022.816605

Acetate Degradation at Low pH by the Moderately Acidophilic Sulfate Reducer *Acididesulfobacillus acetoxydans* gen. nov. sp. nov.

Irene Sánchez-Andrea[1†], Charlotte M. van der Graaf[1†], Bastian Hornung[2], Nicole J. Bale[3], Monika Jarzembowska[1], Diana Z. Sousa[1], W. Irene C. Rijpstra[3], Jaap S. Sinninghe Damsté[3,4] and Alfons J. M. Stams[1,5]*

[1]Laboratory of Microbiology, Wageningen University & Research, Wageningen, Netherlands, [2]Laboratory of Systems and Synthetic Biology, Wageningen University & Research, Wageningen, Netherlands, [3]Department of Marine Microbiology and Biogeochemistry, NIOZ Royal Netherlands Institute for Sea Research, Den Burg, Netherlands, [4]Department of Earth Sciences, Faculty of Geosciences, Utrecht University, Utrecht, Netherlands, [5]Centre of Biological Engineering, University of Minho, Braga, Portugal

OPEN ACCESS

Edited by:
Claudia P. Saavedra, Andres Bello University, Chile

Reviewed by:
Axel Schippers, Federal Institute For Geosciences and Natural Resources, Germany
Shawn E. McGlynn, Tokyo Institute of Technology, Japan

***Correspondence:**
Irene Sánchez-Andrea
irene.sanchezandrea@wur.nl

[†]These authors have contributed equally to this work

Specialty section:
This article was submitted to Extreme Microbiology, a section of the journal Frontiers in Microbiology

Received: *16 November 2021*
Accepted: *31 January 2022*
Published: *04 March 2022*

Citation:
Sánchez-Andrea I, van der Graaf CM, Hornung B, Bale NJ, Jarzembowska M, Sousa DZ, Rijpstra WIC, Sinninghe Damsté JS and Stams AJM (2022) Acetate Degradation at Low pH by the Moderately Acidophilic Sulfate Reducer Acididesulfobacillus acetoxydans gen. nov. sp. nov. Front. Microbiol. 13:816605. doi: 10.3389/fmicb.2022.816605

In acid drainage environments, biosulfidogenesis by sulfate-reducing bacteria (SRB) attenuates the extreme conditions by enabling the precipitation of metals as their sulfides, and the neutralization of acidity through proton consumption. So far, only a handful of moderately acidophilic SRB species have been described, most of which are merely acidotolerant. Here, a novel species within a novel genus of moderately acidophilic SRB is described, *Acididesulfobacillus acetoxydans* gen. nov. sp. nov. strain INE, able to grow at pH 3.8. Bioreactor studies with strain INE at optimum (5.0) and low (3.9) pH for growth showed that strain INE alkalinized its environment, and that this was more pronounced at lower pH. These studies also showed the capacity of strain INE to completely oxidize organic acids to CO_2, which is uncommon among acidophilic SRB. Since organic acids are mainly in their protonated form at low pH, which increases their toxicity, their complete oxidation may be an acid stress resistance mechanism. Comparative proteogenomic and membrane lipid analysis further indicated that the presence of saturated ether-bound lipids in the membrane, and their relative increase at lower pH, was a protection mechanism against acid stress. Interestingly, other canonical acid stress resistance mechanisms, such as a Donnan potential and increased active charge transport, did not appear to be active.

Keywords: acid rock/mine drainage, acidophiles, sulfate-reducing bacteria, *Acididesulfobacillus*, *Desulfosporosinus*, *Desulfitobacterium*, acetate oxidation, bioremediation

INTRODUCTION

Acid rock and acid mine drainage (ARD and AMD) environments are among the most extreme habitats on Earth due to their high acidity and high metal concentrations. Acid drainage is generated by the oxidative dissolution of metal sulfides to sulfuric acid and dissolved metals upon exposure to water and oxidants such as oxygen (O_2) or ferric iron

(Fe^{3+}; Sand et al., 2001; Johnson and Hallberg, 2005). This can be triggered naturally (ARD) or by mining operations (AMD; Lottermoser, 2010). The Tinto River, which flows through the massive sulfide deposits of the Iberian Pyrite Belt (IPB; Huelva, Southwestern Spain), is one of the best-known examples of ARD. Although mining activity reportedly occurred in the IPB already >5,000 years ago, the acid drainage does not exclusively originate on the surface by mining activities but also in the subsurface, as a result of chemolithotrophic microbial activity (Amils et al., 2011).

Microorganisms thriving in acid drainage environments are polyextremophiles, as they need to withstand high acidity (the mean pH of the water column of the Tinto River is 2.3), extremely high metal concentrations (e.g., Fe 2.26 g/L, Cu 0.11 g/L, and Zn 0.24 g/L; López-Archilla et al., 2001) and high salinity due to high sulfate concentrations. Although much emphasis has been placed on the extreme acidophiles involved in the iron cycle and the oxidative part of the sulfur cycle, studies of anoxic Tinto River sediments showed the importance of more moderately acidophilic microorganisms, most notably acidophilic sulfate-reducing bacteria (SRB; Sánchez-Andrea et al., 2011, 2012b). SRB have been shown to have an attenuating effect on the extreme characteristics of the Tinto River through the formation of sulfide (biosulfidogenesis), enabling the precipitation of metals as metal sulfides, and the consumption of protons required for sulfate reduction at low pH, resulting in alkalinization (Sánchez-Andrea et al., 2012a). In specific layers of Tinto River sediments, a higher pH (up to 6.2), a lower redox potential, and lower sulfate and metal concentrations were accompanied by a higher abundance of SRB from the family *Peptococcaceae* (Sánchez-Andrea et al., 2012a), representing up to 40% of the total cell counts in the sediment layers. Geomicrobiological studies of abandoned open pit mines filled with AMD revealed that, similar to observations in AMD sediments, biosulfidogenesis by SRB also had an attenuating effect on acidity and metal concentrations in the water column (Wendt-Potthoff et al., 2012; Santofimia et al., 2013; Falagán et al., 2014; Sánchez-España et al., 2020; van der Graaf et al., 2020).

The in-depth study of the physiology and dominant stress resistance mechanisms of acidophilic SRB requires pure culture isolates. So far, only a few moderately acidophilic or acidotolerant SRB species have been described, *Thermodesulfobium narugense* (pH 4.0–6.5; Mori et al., 2003) and *T. acidiphilum* (pH 3.7–6.5; Frolov et al., 2017), both from the genus *Thermodesulfobium* within the family *Thermodesulfobiaceae*; *Desulfothermobacter acidiphilus* (pH 2.9–6.5; Frolov et al., 2018) from the family *Thermoanaerobacteraceae*; and *Desulfosporosinus acididurans* (pH 3.8-7.0; Sánchez-Andrea et al., 2015), *D. acidiphilus* (pH 3.6–5.5; Alazard et al., 2010), and *D. metallidurans* (pH 4.0–7.0; Panova et al., 2021) from the genus *Desulfosporosinus* in the family *Peptococcaceae* of the *Clostridia* class in the *Firmicutes* phylum. Here, we report the characterization of a novel moderately acidophilic SRB from a novel genus, *Acididesulfobacillus acetoxydans* strain INE, enriched from Tinto River sediments (Sánchez-Andrea et al., 2013). We use comparative proteomics and cell membrane lipid analysis performed on cells grown at optimum (5.0) and low (3.9) pH of growth to determine the main strategies enabling *A. acetoxydans* to grow at acidic pH.

MATERIALS AND METHODS

Microorganisms

Strain INE was isolated from an enrichment culture containing acidic sediments from *JL* dam (37.691207 N, 6.560587 W) in the Tinto River basin (southwestern Spain) by incubation with 5 mM of lactate and 10 mM sulfate at pH 4.5 (Sánchez-Andrea et al., 2013). Detailed physicochemical information on the site has been published previously (Sánchez-Andrea et al., 2012a). For comparison purposes, *D. orientis* DSM 765^T, *Desulfitobacterium dehalogenans* DSM 9161^T and *D. acidiphilus* DSM 22704^T were obtained from the DSMZ (Braunschweig, Germany). *Desulfosporosinus acididurans* DSM 27692^T was taken from the laboratory collection.

Phenotypic Characterization: Morphology and Physiology

Cell morphology, motility and spore formation were examined by phase contrast microscopy using a Leica DM2000 microscope (Leica, Hesse, Germany). Cell size was determined by SEM microscopy. To this end, samples were fixed by immersion in glutaraldehyde (2.5%) for 2 h, and subsequently washed twice in sodium cacodylate buffer (0.2 M, pH 7.1). Samples were dehydrated in a graded series (10%, 30%, 50%, 70%, 90%, and 100%) of ethanol/water mixtures, leaving them 20 min in each mixture. After dehydration, samples were critical point dried and mounted on stubs. After gold shadowing, samples were examined in a Phillips XL30 EDAX DX4i SEM (Philips, Netherlands). The lengths and widths of several cells were measured, and mean dimensions recorded. Gram staining was performed according to standard procedures (Doetsch, 1981), and Gram-structure was checked by mixing cells with a drop of 3% (w/v) solution of KOH.

Gram-structure was further checked by TEM microscopy. For this, cells were pelleted, incubated in fixative solution (2.5% glutaraldehyde, 2% paraformaldehyde in a 0.1 M phosphate citrate buffer pH 5.0) for 1 h at room temperature, washed twice in 0.1 M phosphate citrate buffer (wash buffer), resuspended in 100 ml 2% gelatin in 0.1 M phosphate citrate buffer and incubated at 4°C until gelatin solidified. The gelatin pellet was incubated for 15 min at room temperature in fixative solution, cut into small pieces (maximum 0.5 cm^3), and incubated for 30 min at room temperature. Gelatin sections were washed six times with wash buffer, stained and fixed in a 1% osmium tetroxide solution for 1 h at room temperature. The samples were then washed three times in distilled water, dehydrated in successive ethanol incubations (30%, 50%, 70%, 80%, 90%, and 96%), with a final dehydration step in 100% ethanol. Samples were embedded in Spurr epoxy resin as described previously (Spurr, 1969), cut into ultrathin sections with a Leica EM UC7 ultramicrotome (Leica, Wetzlar, Hesse, Germany),

and poststained with uranyl-acetate and lead citrate. Samples were imaged using a JEOL JEM-1400 series 120 kV TEM (JEOL, Tokyo, Japan).

Catalase activity was determined by reaction with 15% (w/v) solution of H_2O_2. An oxidase test was performed with a filter impregnated in 1% (w/v) solution of tetramethyl-*p*-phenylenediamine in dimethyl sulfoxide (Sigma-Aldrich, St. Louis, MO). Indole and urease formation as well as gelatin and esculin hydrolysis were determined with API® 20A (bioMérieux, France) according to manufacturer's instructions. Analysis of respiratory quinones of biomass grown on glycerol was carried out by the DSMZ Deutsche Sammlung von Mikroorganismen und Zellkulturen GmbH (Braunschweig, Germany; Tindall, 1990a,b).

Growth experiments were performed in triplicate, using 120 ml-serum bottles as described elsewhere (Sánchez-Andrea et al., 2013). Growth conditions were pH 5.0 and $T_a = 30°C$, unless indicated otherwise. Growth was monitored by measuring optical density at 600 nm (OD_{600}) with a spectrophotometer (U-1500 Hitachi, Tokyo, Japan). Soluble substrates and intermediates (sugars and volatile fatty acids) were measured using a thermo electron spectrasystem high performance liquid chromatography (HPLC) equipped with an Agilent Metacarb 67H column. Gaseous compounds (H_2) were analyzed using a Shimadzu GC-2014 Gas Chromatograph equipped with a Mol sieve 13X column. Sulfide was measured photometrically with the methylene blue method (Cline, 1969). Different electron donors and acceptors were tested at final concentrations of 5 or 10 mM, respectively, except sulfite, which was tested at 5 mM. Electron donors and acceptors were added to the media from sterile 1 M stock solutions. When electron donors were tested, sulfate (10 mM) was used as acceptor and when acceptors were tested, glycerol (5 mM) was used as donor. Growth was also studied at different incubation temperatures (from 10°C to 45°C), pH (from 3.0 to 7.5), salinity (up to 0.5 M NaCl), oxygen concentrations, and with different reducing agents: L-cysteine, sodium sulfide, titanium citrate, and $FeCl_2$ (2 mM). Sulfate reduction rates were determined during the exponential phase of the cultures grown between pH 4 and 7 at 30°C.

Bioreactor Cultivation

Bioreactor cultivation was performed in duplicate in two pH-controlled batch reactors at pH 3.9 and pH 5.0. Basal medium was supplemented with 0.1 g yeast extract L^{-1}, 5 mM glycerol, 10 mM sulfate, and 2 mM L-cysteine as reducing agent. Glass reactors (Applikon, Netherlands) of 5 L volume capacity filled with 4 L of medium were operated with an ADI 1010 Bio-controller and the ADI 1025 Bio-console (Applikon). Autoclavation of the whole system enabled reactor operation under sterile conditions. Stirring speed was 50 rpm, temperature was maintained at 30°C, and pH was maintained at pH 5.0 or pH 3.9 by addition of 0.5 M HCl. The growth rates at pH 3.9 and pH 5.0 were calculated from semi-logarithmic plots of changes in OD_{600} values against time at 30°C. Values were obtained by implementing the modified Gompertz model (Zwietering et al., 1990). Biomass for lipid and proteome analysis was obtained from the reactors at 80% of maximum OD_{600}.

Membrane Lipid Analysis

For comparison of the cellular fatty acid composition all strains were grown at their optimum pH in the medium described elsewhere (Sánchez-Andrea et al., 2013). Bicarbonate buffer was added to the medium for the cultivation of neutrophilic strains. For *A. acetoxydans* strain INE, biomass grown at both pH 3.9 and 5.0 was analyzed. Fatty acid analyses were carried out by acid hydrolysis of total cell material with 5% HCl in methanol by refluxing for 3 h, and analysis by gas chromatography, gas chromatography–mass spectrometry, following procedures described previously (Sinninghe Damsté et al., 2011), and were performed in duplicate. Intact polar lipids (IPLs) were extracted from freeze-dried biomass using a modified Bligh–Dyer procedure and analyzed by ultra-high-pressure liquid chromatography–high resolution mass spectrometry (UHPLC-HRMS) under conditions described previously (Bale et al., 2019).

Phylogenetic Analysis

Cloning of the 16S rRNA gene was performed to determine the phylogenetic affiliation of strain INE. Total genomic DNA was extracted using the FastDNA® SPIN Kit for Soil and the FastPrep® Instrument (MP Biomedicals, Santa Ana, CA). The 16S rRNA genes were amplified with the primers set 27F-1492R ($T_a = 57°C$) for *Bacteria* and cloned in *Escherichia coli* DH5α competent cells by using the pGEM-T vector (Promega, Madison, WI). Sequences were assembled with the DNABaser software 3.5.3 and prior to phylogenetic analysis, vector sequences flanking the 16S rRNA gene inserts were identified using the VecScreen tool (NCBI) and removed.[1] Clone sequences were checked for chimeras (Wright et al., 2012), aligned with SINA (v1.2.11; Pruesse et al., 2012), and added to a database of over 230,000 homologous prokaryotic 16S rRNA gene primary structures by using the merging tool of the ARB program package (Ludwig et al., 2004). Sequences were then manually corrected with the alignment tool of the same software and added by parsimony to the tree generated in the *Living Tree Project* (LTP; Yarza et al., 2008). Phylogenetic reconstruction was performed using the three algorithms as implemented in the ARB package. The maximum-likelihood method was used for the generation of the consensus tree and bootstrap analysis performance. The bar indicates 10% estimated sequence divergence. The 16S rRNA gene sequence is available in the EMBL database under accession number LN551924.

Genomic Analysis and Annotation Workflow

Genomic DNA was extracted with the MasterPure™ Gram Positive DNA Purification Kit (Epicentre, Madison, Wisconsin). Pacific Biosciences sequencing was performed on a PacBio RSII at GATC Biotech (Konstanz, Germany), and Illumina sequencing on a MiSeq sequencer (250 bp paired-end with 500 bp insert). The genome was assembled with the smrt analysis pipeline version 2.3.0 and the protocol HGAP version 3. After

[1]http://www.ncbi.nlm.nih.gov/VecScreen/VecScreen.html

assembly, the taxonomy of all contigs was determined with megablast (Altschul et al., 1990) and a custom version of the LCA algorithm (Huson et al., 2007). In detail, a blast search was performed against various database of the NCBI (NCBI NT database, the draft bacteria genome database, the human genome, the protozoa database; NCBI Resource Coordinators, 2013), the Hungate 1,000 database (Seshadri et al., 2018) and the human microbiome database (Human Microbiome Project, 2012), using an e value of 0.0001. A custom script with the implementation of the LCA algorithm was used (Huson et al., 2007), with the exception that only the hits exceeding a bitscore of 50 and not deviating >10% in length from the longest hit were used to determine the taxonomy. After the taxonomy was obtained, all contigs not belonging to the family *Peptococcaceae* were discarded as contamination. A correction of the PacBio assembly was performed with Pilon 1.19 (Walker et al., 2014), and the Illumina MiSeq data, which was mapped to the assembly with bowtie2 (Langmead and Salzberg, 2012). The Illumina MiSeq data were additionally used as verification that the discarded contigs of the PacBio assembly were contaminating contigs. Average amino acid identity (AAI) was calculated with compareM v0.1.1.[2]

The annotation of the genome was performed with an early version of SAPP (Koehorst et al., 2018). Gene calling was performed with prodigal 2.6.3 (Hyatt et al., 2010). RNA genes were predicted with RNAmmer 1.2 (Lagesen et al., 2007), Aragorn 1.2.36 (Laslett and Canback, 2004), and the CRISPR Recognition tool version 1.2 (Bland et al., 2007). Protein coding genes were further annotated with InterproScan 5.19–58.0, PRIAM version March 2015 (Claudel-Renard et al., 2003), EnzDP version 1.0 (Nguyen et al., 2015), tmHMM version 2.0c (Krogh et al., 2001), and SignalP 4.1 (Petersen et al., 2011). Additional EC numbers were derived *via* Gene Ontology terms (Ashburner et al., 2000) predicted by InterproScan. Furthermore, blastp searches against the COG database (Galperin et al., 2015) and the Swissprot database (Release 06 Jul 2016; UniProt, 2014) were performed. The annotations were partially manually curated. To avoid repetition, locus ID is displayed without the locus tag "DEACI_."

Proteomics

Duplicate samples at each pH value of the biomass grown in reactors (pH 3.5 A + B and pH 5.0 A + B) were taken at 80% of maximum OD_{600}, centrifuged, washed, and transferred to 2-ml low-binding microcentrifuge tubes (Eppendorf, Netherlands) prior to protein extraction. Around 0.1 g of wet weight pellet was resuspended in 500 ml of 4% sodium dodecyl sulfate in 100 mM Tris-HCl pH 7.6. Cells were lysed by sonication with a 3-mm tip using a Branson sonifier in six pulses of 30 s. Around 40 µg of protein was separated by gel electrophoresis (SDS-PAGE) and cut into five slices per sample to fractionate proteins. The gel slices were subjected to in-gel tryptic digestion and peptides were loaded on STAGE-tips (STop And Go Elution, C18-reversed phase SPE) for desalting and concentration.

The resulting purified and concentrated peptide mixtures were analyzed by nanoflow C18 reversed phase HPLC coupled with a maXis 4G ETD ultra-high resolution Qq-TOF mass spectrometer (Bruker Daltonics) with collision-induced dissociation (CID) as fragmentation technique. Chromatographic separation was achieved *via* a linear gradient of 7–32% acetonitrile in 90 min using 0.1% formic acid as ion pair reagent. For data analysis, a custom *Acididesulfobacillus* database with added sequences for typical contaminant proteins (e.g., skin and hair proteins) was used. For database searches, validation, and relative quantification the MaxQuant software package was used (version 1.5.0.0).[3] A false discovery rate of 1% was tolerated at both peptide and protein level.

In total, 1,258 *Acididesulfobacillus* proteins were identified. These proteins were quantified in both replicate samples of at least one of the conditions (pH 3.9 or 5.0). Known contaminants like human keratins were excluded from these lists. Please note that no correction for multiple testing has been applied due to the number of replicates ($n = 2$) for each condition.

Data Accessibility

All data has been uploaded to the European Nucleotide Archive under bioproject number PRJEB7665 composed by PacBio raw data (ERR3835955), Illumina MiSeq raw data (ERR665276), and genome assembly (ERZ1286184). The mass spectrometry proteomics data have been deposited to the ProteomeXchange Consortium (Deutsch et al., 2020) *via* the PRIDE (Perez-Riverol et al., 2019) partner repository with the dataset identifier PXD022508.

RESULTS AND DISCUSSION

Characterization of *Acididesulfobacillus acetoxydans* gen. nov. sp. nov. strain INE

Morphology and Physiology

Acididesulfobacillus acetoxydans gen. nov. sp. nov. strain INE was isolated previously from enrichment cultures inoculated with Tinto River sediments, supplemented with lactate (5 mM) and sulfate (10 mM) at pH 4.5 (Sánchez-Andrea et al., 2013). Strain INE grew between pH 3.8 and 6.5, with a maximum specific growth rate at pH 5.0 (0.051 h^{-1}). The temperature range of growth was between 25°C and 42°C, with an optimum at 30°C. Growth occurred in the presence of up to 15.3 g L^{-1} of NaCl. Cells of strain INE were single, straight rods, 4–7 µm long and *ca.* 0.6 µm wide (**Figure 1A**), with motility associated with observed lateral flagella (**Figure 1B**). Although strain INE stains Gram-negative, the double membrane characteristic of Gram-negative bacteria is absent (**Figure 1C**). Its Gram-positive cell wall structure was further supported by the negative KOH test and its susceptibility to vancomycin, as well as the membrane structure observed by TEM (**Figure 1C**).

[2]https://github.com/dparks1134/CompareM

[3]http://www.maxquant.org/

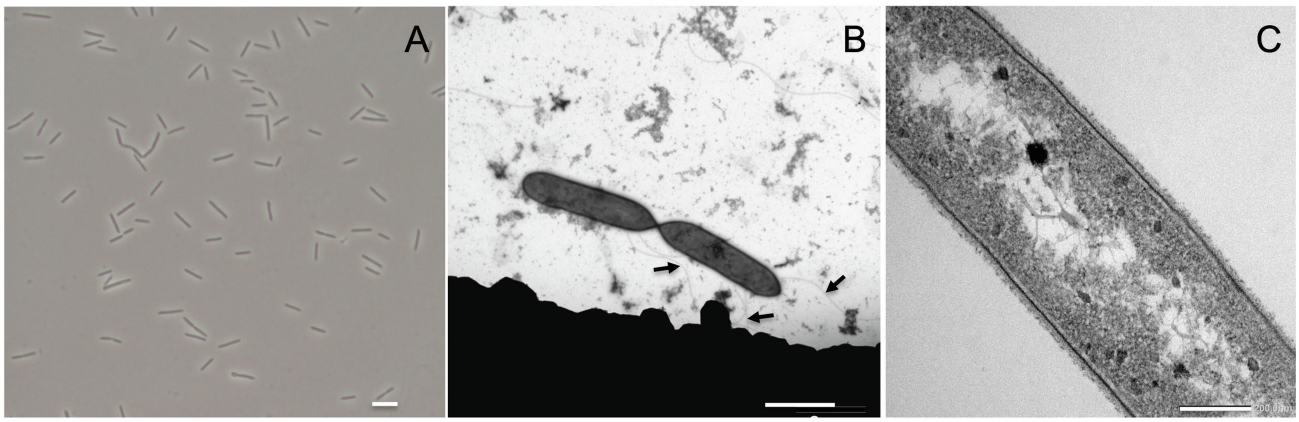

FIGURE 1 | *Acididesulfobacillus acetoxydans* gen. nov. sp. nov. strain INE microscopy images: **(A)** phase contrast microscopy and **(B,C)** transmission electron microscopy. Scale bars represent 5 mm, 2 mm, and 200 nm, respectively. Arrows in **(B)** indicate flagella.

Strain INE is a strict anaerobe as it grew only in the presence of L-cysteine, ferrous iron, titanium citrate, or sulfide as reducing agents. With sulfate as electron acceptor, strain INE utilized a wide range of compounds as electron donors (**Table 1**): hydrogen, complex substrates such as yeast extract, carbohydrates such as xylose, glucose, fructose, maltose, sucrose, and raffinose, a variety of C1–C4 organic acids (formate, acetate, glycolate, pyruvate, lactate, malate, fumarate, butyrate, and succinate), the amino acid L-cysteine, and alcohols, such methanol, ethanol, glycerol, and 1- and 2-propanol. Strain INE was capable of the complete oxidation of substrates to CO_2. No growth was observed with propionate, citrate, or benzoate as electron donor. With glycerol as electron donor, strain INE used a range of compounds as electron acceptor in addition to sulfate including elemental sulfur, thiosulfate, arsenate, selenate, nitrate, and DMSO. It could not reduce ferric iron as Fe(III)NTA, sulfite, dithionate, polysulfide, perchlorate, perchloroethylene, fumarate, humic acids, chromate, molybdate, manganese, or AQDS. Strain INE was also capable of disproportionation of elemental sulfur and thiosulfate, and of fermentation of cysteine, glucose, pyruvate, and yeast extract. The only detected menaquinone of strain INE was MK-7 (100%), as also detected for the closely related *Desulfosporosinus* spp., except for *Ds. lacus* which contained up to 36% MK-5 (Ramamoorthy et al., 2006).

Phylogenetic and Genomic Analysis

Genome assembly indicated the presence of one chromosome with a size of 4.52 Mbp, with a GC content of 53.65%, and 4,104 predicted protein coding sequences, of which 3,443 contained at least one protein domain, and 639 were identified as hypothetical proteins. In total 53 tRNAs and 3 full rRNA operons were identified. The phylogenetic position of the complete 16S rRNA gene sequence of strain INE (LN551924) showed that the strain is related to the *Desulfosporosinus* and *Desulfitobacterium* genera (**Figure 2**): the 16S rRNA gene sequence identity with its closest relatives, *Ds. meridiei* DSM 13257^T, *Ds. auripigmenti* DSM 13351^T and *D. metallireducens* DSM 15288^T was 93.8%, 93.5%, and 93.5%, respectively. This is below the minimum similarity threshold of 94.5% for genus-delineation (Yarza et al., 2014), indicating that strain INE belongs to a new genus. This is further supported by the average amino acid identity (AAI) derived from the genome comparison of strain INE with *Desulfosporosinus* and *Desulfitobacterium* spp. (**Supplementary Table S1**). The highest similarity was observed with *Peptococcaceae* bacterium CEB3 (89.3%; Ňancucheo and Johnson, 2012), followed by *Ds. acidiphilus* DSM 22704 (64.4%). Based on the observed AAI values of more than 96% in most strains within one species and 62–64% within the same genus, respectively (Konstantinidis and Tiedje, 2005), AAI values also suggest that *A. acetoxydans* strain INE forms a new genus. Although the AAI with *Ds. acidiphilus* is close to the threshold of 64%, the 16S rRNA gene similarity is 92.7%, supporting the separation in a new genus. The 16S rRNA sequence identity further indicates that the novel genus *Acididesulfobacillus* encompasses the isolates CL4 and CEB3 (Jameson et al., 2010; Ňancucheo and Johnson, 2012). Although strain CL4 was formerly proposed as "*Desulfobacillus acidavidus*" (Jameson et al., 2010), it was never formally described, and current nomenclature regulations prevented us from using the proposed name. We therefore hereby propose the alternative name *Acididesulfobacillus*.

The *Desulfosporosinus* and *Desulfitobacterium* genera and the novel genus *Acididesulfobacillus* form a separate cluster from the other recognized genera and species of the family *Peptococcaceae*, order *Clostridiales* of the phylum *Firmicutes*. Members of the *Desulfosporosinus* and *Desulfitobacterium* genera are rod-shaped, Gram-positive, free-living, strictly anaerobic, and spore-forming bacteria. They display a diversity of metabolic traits relevant to bioremediation of polluted sites, e.g., reductive dehalogenation and reduction of metals such as arsenic or ferric iron, sulfur compounds, or nitrate (Spring and Rosenzweig, 2006; Alazard et al., 2010; Pester et al., 2012; Petzsch et al., 2015; Sánchez-Andrea et al., 2015; Mardanov et al., 2016). Members of *Desulfosporosinus* are known sulfate reducers in AMD environments (Nevin et al., 2003; Petrie et al., 2003; Suzuki et al., 2004; Kimura et al., 2006; Rowe et al., 2007;

TABLE 1 | Main characteristics differentiating strain INE from its closest phylogenetic relatives.

Name	*Acididesulfobacillus*	*Desulfosporosinus*				*Desulfitobacterium*	
	***A. acetoxydans* DSM 29876^T**	***Ds. acididurans* DSM 27692^T**	***Ds. acidiphilus* DSM 22704^T**	***Ds. metallidurans DSM 104464T***	***Ds. orientis* DSM 765^T**	***D. dehalogenans* DSM 9161^T**	***D. metallireducens* DSM 15228^T**
Type strain	INE	M1^T	SJ4^T	OL^T	Singapore^T	JW/IU-DC1^T	853-15A^T
Isolation source	ARD sediments	AMD/ARD sediments	AMD sediments	AMD microbial mat	Soil	Freshwater pond sediment	Aquifer sediment (uranium-contaminated)
Cell size (μm)	0.7 × 5.5	0.7 × 3–5	0.8–1 × 4–7	0.5 × 2–3	1.5 × 5	0.5–0.7 × 2.5–4	
DNA G + C mol %	53.7	41.8	42.3		41.7; 42.8[1]; 45.9[2]	45	42
Quinones	MK-7 (100%)	MK-7 (98%)			MK-7		
Genome size (Mb)	4.52	4.64	4.99	5.29	5.86	4.32	3.17
Endospore position	Subterminal	Subterminal	Subterminal	Subterminal	Subterminal, paracentral or central	–	–
Motility	+	Variable	–	–	+	+	–
Gram staining	–	–	–	–	–	+	+
T range (°C)	25–42	15–40	25–40	4–37	</42		20–37
T opt (°C)	25–35	30	30	28	30–37	38	30
pH range (opt.)	3.8–6.5 (5.0)	3.8–7 (5.5)	3.6–5.6 (5.2)	4.0–7.0 (5.5)	5.6–7.4 (6.4–7)	(7.5)	(7.0)
NaCl range (%; opt)	0.5–1.5 (<0.5)	0–1.5 (0.6)	0–0.6 (1.5)	0–6 (0–0.1)	<4.5		<0.5
Catalase	–	+					
Oxidase	–	–/+	–,+		–,+		
Electron donors							
H_2	+ (with 0.1 YE)	+	+	+	+	+	+
Formate	+	(+)	–	+	+	+	+
Acetate	+	–	–		–		
Pyruvate	+	+		+	+	+	+
Propionate	–	–	–	+	–		
Lactate	+	+	(+)	+	+	+	+
Malate	+	+	–	+	–		
Fumarate	+	+	–		+		
Butyrate	+	+	–		-[4],+[1]		
Succinate	+	–	–		–		
Methanol	+	(+)	–		+		
Ethanol	+	+	–	+	+		
Glycerol	+	+	+	+	–[1], +[3]		
Xylose	+	+	–		–		
Fructose	+	(+)	+	+	–		
Glucose	+	(+)	(+)	+	–		
Electron acceptors							
Sulfate	+	+	+	+	+	–	–
Sulfur	+	+	–, +[3]	–	+	+	+
Sulfite	–	–	–	+	+	+	–
Thiosulfate	+	+	+	+	+[3], –[4]	+	+
DMSO	+						
Arsenate	+	+	–		–[1,2,3], +[5]	–	
Fumarate	–	–	–	+	+	+	–
Fe(III) sol./insol.	–	Variable[3]	–		+	+	+
Nitrate	+	+	(+)[1]	+	–	+	–
PCE	–						
Se(VI)	+					+	–
Mn(IV)	–					+	+

Desulfosporosinus acididurans (Sánchez-Andrea et al., 2015), Desulfosporosinus acidiphilus (Alazard et al., 2010), Desulfosporosinus metallidurans (Panova et al., 2021), Desulfosporosinus orientis (Adams and Postgate, 1959; Campbell and Postgate, 1965; Klemps et al., 1985; Robertson et al., 2001; Ramamoorthy et al., 2006), Desulfitobacterium dehalogenans (Utkin et al., 1994), Desulfitobacterium metallireducens (Finneran et al., 2002). +, supported growth; –, did not support growth; (+), weak growth.

[1]*Ramamoorthy et al. (2006).*

[2]*Robertson et al. (2001).*

[3]*Sánchez-Andrea et al. (2015).*

[4]*Adams and Postgate (1959).*

[5]*Campbell and Postgate (1965).*

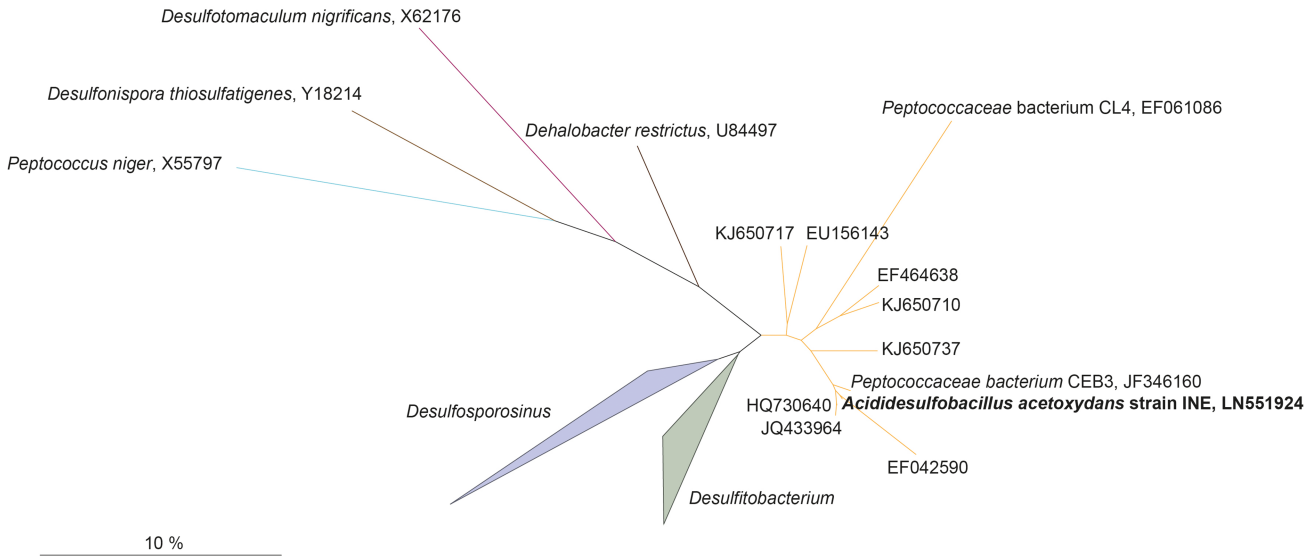

FIGURE 2 | Maximum-likelihood tree showing phylogenetic affiliation of 16S rRNA gene sequences of *Acididesulfobacillus acetoxydans* (in bold) with related environmental sequences found in acidic environments, and closely related species in the *Peptococcaceae* family of the *Firmicutes* phylum. The accession numbers represent sequences retrieved from different acid drainage environments. KJ650710, KJ650737, or KJ650717: sulfidic mine tailings dumps in Botswana; EF042590: an abandoned copper mine in Odiel (Huelva, Spain); HQ730640, JQ433964: Tinto River sediments; EU156143: a thermal spring in Yellowstone National Park (WY, United States); EF464638: acidic enrichment cultures. JF346160 and EF061086: *Peptococcaceae* bacteria CEB3 and CL4. Scalebar indicates 10% sequence difference.

Cardenas et al., 2008; Lee et al., 2009; Madden et al., 2009; Senko et al., 2009; Ňancucheo and Johnson, 2014), and other low pH ecosystems such as peatlands (Hausmann et al., 2016, 2019). Three moderately acidophilic or acidotolerant *Desulfosporosinus* species were isolated so far: *Ds. acidiphilus* (pH 3.6–5.5, optimum pH 5.2; Alazard et al., 2010), *Ds. acididurans* (pH 3.8–7.0, optimum 5.5; Sánchez-Andrea et al., 2015), and *Ds. metallidurans* (pH 4.0–7.0, optimum 5.5; Panova et al., 2021).

All 16S rRNA gene amplicon sequences found in the public databases (SILVA and NCBI) that cluster together with *A. acetoxydans* strain INE were identified in AMD or ARD environments (**Figure 2**): in sulfidic mine tailings dumps in Botswana (pH 3.2–3.5; Korehi et al., 2014), in a stream of an abandoned copper mine in Odiel (Huelva, Spain; pH 2.5–2.75; Rowe et al., 2007), in Tinto River sediments (pH 5; Sánchez-Andrea et al., 2011) and in a thermal spring in Yellowstone National Park (pH 5.75–6.91; Hall et al., 2008). In addition, they were detected in enrichment cultures inoculated with samples from acid mine tailings (Winch et al., 2009). The two isolates included in the cluster, *Peptococcaceae* bacteria CL4 and CEB3 (Jameson et al., 2010; Ňancucheo and Johnson, 2012), were both obtained from reactors treating acid mine waters at a pH of about 2.5. The genome sequence from CEB3 is publicly available, but the two isolates were not characterized further. Interestingly, sequences of CEB3, which according to 16S rRNA gene sequence similarity corresponds to the same species as strain INE, became dominant in a reactor inoculated with an acidophilic consortium when the operating pH of the reactor was lowered, showing their predominance at more acidic conditions over other acidophilic SRB such as *Ds. acididurans* (Ňancucheo and Johnson, 2012). Its inability to grow at pH 7, combined with the lower pH optimum of strain INE (5.0), compared to *Ds. acididurans* (5.5) and *Ds. acidiphilus* (5.2; **Table 1**), this indicates that the SRB in this novel cluster are more acidophilic than the SRB described so far.

Chemotaxonomy

The lipid composition, including fatty acids (FAs), of strain INE grown at optimal pH (5.0) was compared with the type strains of the phylogenetically closest genera, *Ds. orientis* (Adams and Postgate, 1959; Stackebrandt et al., 1997) and *D. dehalogenans* (Utkin et al., 1994; **Table 1**). As these type strains are neutrophilic, lipid profiles were also compared with two acidophilic/acidotolerant strains from the *Desulfosporosinus* genus: *Ds. acididurans* (Sánchez-Andrea et al., 2015) and *Ds. acidiphilus* (Alazard et al., 2010).

The lipid profile of strain INE was dominated by the *iso*-$C_{15:0}$ FA (representing almost 60%; **Table 2**), followed by *iso*-$C_{15:0}$ dimethylacetal (DMA) as the second most abundant lipid. DMAs are formed upon acid hydrolysis from ether lipids containing an alk-1-enyl ether substituent at the sn-1 carbon of glycerol, so called plasmalogens (Jackson et al., 2021). Interestingly, the *iso*-$C_{15:0}$ FA was also abundant in the acidophilic/acidotolerant strains *Ds. acididurans* (25.8%) and *Ds. acidiphilus* (16.6%), but absent in both the neutrophilic strains, *Ds. orientis* and *D. halogenans*. *Iso*-$C_{17:0}$ and 10-methyl *n*-$C_{17:0}$ FA and corresponding DMAs were also present in strain INE. Small amounts (i.e., 5% of total lipids) of 1-alkyl glycerol ethers with *iso*-C_{15} and 10-methyl *n*-C_{17} groups were also detected

TABLE 2 | Relative abundance (% of total) of fatty acids and ether lipids of *Acididesulfobacillus acetoxydans* strain INE and its phylogenetically closest relatives grown on glycerol and sulfate.

Lipid	*A. acetoxydans* strain INE		Acidophilic/acidotolerant type strains		Neutrophilic type strains	
			Ds. acidiphilus	*Ds. acididurans*	*Ds. orientis*	*D. dehalogenans*
	pH 3.9	pH_{opt} 5.0	pH_{opt} 5.2	pH_{opt} 5.5	pH_{opt} 6.8	pH_{opt} 7.5
Fatty acids						
iC_{14}	2.5	1.1				
$C_{14:1}$						1.4
$C_{14:0}$	0.9		**20.4**	7.5	2.0	**15.8**
i$C_{15:1}$	1.5	2.4		1.3		
iC_{15}	**48.0**	**59.5**	**16.6**	**25.8**		
aiC_{15}	6.5	2.4	1.4	1.5		
$C_{15:0}$				2.4		
iC_{16}	1.9		1.1	2.8		
$C_{16:1}$			1.3	1.3	2.2	6.3
$C_{16:1}$			2.6	3.9	6.3	**15.9**
$C_{16:0}$	1.1		**32.3**	**25.9**	**35.7**	**23.6**
diMeC_{15}	1.5					
10MeC_{16}	2.6	1.3				
$C_{17:1}$				3.3		
iC_{17}	1.1	1.3	1.1	2.9		
$C_{17:0}$				1.2		
10MeC_{17}	2.1	2.5				
$C_{18:1}$					2.4	3.8
$C_{18:1}$					8.3	**10.3**
$C_{18:0}$			1.4	1.5	1.1	3.8
Sum	**69.7**	**70.5**	**78.2**	**81.3**	**58**	**80.9**
Sum saturated	**68.2**	**68.1**	**74.3**	**71.5**	**38.8**	**43.2**
Sum unsaturated	**1.5**	**2.4**	**3.9**	**9.8**	**19.2**	**37.7**
β-Hydroxy-fatty acids						
$C_{14:0}$					1.6	
$C_{16:1}$					1.0	
$C_{16:0}$			1.1		2.0	
$C_{18:1}$					1.2	
$C_{18:1}$					1.4	
Sum	**0**	**0**	**1.1**	**0**	**7.2**	**0**
Dimetyl-acetals						
iC_{15}	4.9	**14.7**	1.4			
iC_{16}	3.2	1.9				
$C_{16:1}$			1.3	1.2	3.3	1.3
$C_{16:0}$	5.4	2.1	**15.7**	7.5	9.4	6.9
$C_{17:1}$				3.8		
iC_{17}	4.1	5.1	1.5	4.3		
$C_{17:0}$				1.9		
10MeC_{17}		1.1				
$C_{18:1}$					4.3	2.8
$C_{18:1}$					**16.4**	6.7
$C_{18:0}$			0.9		1.4	1.6
Sum	**17.6**	**24.9**	**20.8**	**18.7**	**34.8**	**19.3**
1-Monoglycerol ethers						
iC_{15}	2.6	3.5				
iC_{16}	1.1					
$C_{16:0}$	2.5					
10MeC_{16}	3.7					
10MeC_{17}	2.3	1.5				
$C_{18:1}$	1.0					
Sum	**13.2**	**5.0**	**0**	**0**	**0**	**0**

Strains: Acididesulfobacillus acetoxydans strain INE at pH 3.9 and at pH 5.0; Desulfosporosinus acidiphilus; Desulfosporosinus acididurans; Desulfosporosinus orientis, and Desulfitobacterium dehalogenans. Major lipids (>10% of total) are indicated in bold.

in strain INE, but saturated glycerol monoethers were absent in any of the other strains. The two most abundant FAs in *Ds. orientis* were *n*-$C_{16:0}$ FA (35.7%) and the *n*-$C_{18:1}$ DMA (16.4%). Both lipids are absent in strain INE and the latter is missing in all three acidophilic strains. Similarly, the abundant FAs *n*-$C_{16:0}$ (23.6%), *n*-$C_{16:1}$ (15.9%), and *n*-$C_{14:0}$ (15.8%) in *D. dehalogenans*, the (neutrophilic) type strain of the second closest phylogenetic genus *Desulfitobacterium*, also showed a negligible presence in strain INE. The saturated branched-chain acid iso-$C_{15:0}$ and the 1-alkyl glycerol ether lipids may therefore be characteristic for acidophilic SRB.

Analysis of the IPL of strain INE showed a high diversity of polar head groups (**Supplementary Table S2**), including sulfoquinovosyls (SQs), phosphoglycerols (PGs), phosphoethanolamines (PE), and diphosphatidylglycerols (DPG; commonly known as cardiolipins). Additionally, a series of glycolipids with hexosamine moieties were present. The dominant group was tentatively assigned a structure with a hexose group bound to the glycerol backbone and a hexosamine bound to this. The assignment was made based on their MS^2 fragmentation and their accurate masses (**Supplementary Figure S1**; **Supplementary Table S2**). The second group also contained a hexosamine head group but the complete structure could not be elucidated (**Supplementary Figure S1**; **Supplementary Table S2**). Amino sugars are not routinely reported as components of polar headgroups in bacterial lipids but have been reported in a range of Archaea (Koga et al., 1993, 1998; Oger and Cario, 2013; Meador et al., 2014). Lipid-A, found in the outer-membrane of most Gram-negative bacteria, consists of two glucosamine moieties. However, the mass spectra of the hexosamine components detected in this study did not agree with published spectra of lipid A (Larrouy-Maumus et al., 2016; Crittenden et al., 2017). The IPL-bound core lipids (**Supplementary Table S2**) were in agreement with the hydrolysis-derived core lipid analysis (**Table 2**) and included diacylglycerols (DAGs) and mixed acyl/ether glycerols (AEGs; including plasmalogen lipids).

Dominant Acid Stress Resistance Mechanisms in *Acididesulfobacillus acetoxydans*

Proton Consumption and Complete Organic Acid Oxidation at Optimum and Minimum pH

The pH dependence of growth of *A. acetoxydans* strain INE^T (pH 3.8–6.5 with pH optimum at 5.0) indicated that it is moderately acidophilic rather than acid-tolerant, since it is unable to grow at pH 7.0. As aforementioned, members of *Acididesulfobacillus* spp. were found to be more tolerant to low pH than other acidophilic/acidotolerant SRB such as *Desulfosporosinus* spp. The capacity for complete oxidation of organic acids to CO_2 is not common in other acidophilic/acidotolerant SRB described so far (Alazard et al., 2010; Sánchez-Andrea et al., 2013, 2015) and was only recently reported to promote limited growth in *Ds. metallidurans* (Panova et al., 2021). Because of the increasing toxicity of organic acids at pH values below their pK_a, lowering their concentration by complete oxidation likely constituted an important detoxification mechanism for *A. acetoxydans* strain INE. In order to elucidate the main strategies conferring increased robustness at low pH, we investigated this in more detail by monitoring its metabolism through quantifying proton consumption rates, and glycerol, sulfate, and acetic acid concentrations at optimum (5.0) and low (3.9) pH in pH-controlled batch bioreactors fed with glycerol.

By monitoring the acid addition required for pH control, the proton consumption rates could be calculated. A higher net consumption of protons was observed at pH 3.9 than at 5.0 (**Table 3**): 128 mM H^+ g^{-1} biomass (dry weight) vs. to 58 mM H^+ g^{-1} biomass (dry weight), respectively. Doubling times at pH 3.9 and 5.0 were 17.6 and 13.8 h, respectively. The maximum OD_{600} reached in the late exponential phase after complete oxidation of glycerol was 0.41 at pH 3.9 and 0.44 at pH 5.0, corresponding to a maximum biomass dry weight of 102 and 115 mg L^{-1}, respectively (**Table 3**). This difference likely indicated increased energetic costs for cell maintenance at pH values below the optimum. The increased maintenance energy requirements could have been partly compensated for by the slightly larger theoretical Gibbs free energy change (Δ_rG') for sulfate reduction with glycerol at pH 3.9 (−1186.7 kJ/mol) compared to pH 5.0 (−1142.8 kJ/mol), as calculated with Equilibrator (Flamholz et al., 2012; **Table 4**).

Consumption of glycerol and sulfate was accompanied by an initial increase of total acetate concentrations to 2.4 mM at pH 3.9 and 2 mM at pH 5.0, followed by its complete

TABLE 3 | Summary parameters of bioreactor cultivation of *Acididesulfobacillus acetoxydans* gen. nov. sp. nov. strain INE at pH 3.9 and pH 5.0 when grown on 5 mM glycerol and 10 mM sulfate.

	pH 3.9	pH 5.0
Doubling time t_d (h)	17.6	13.8
Maximum OD_{600}	0.41	0.44
$C_{DW,final}$* (mg·L^{-1})	102	115
H^+ consumption (mM H^+·g_{DW}^{-1})	128	58

$C_{DW,final}$ was calculated from OD_{600} and ratio c_{DW} (mg·L^{-1})/OD_{600} = 254.84.

TABLE 4 | Gibbs free energy of complete and incomplete oxidation of glycerol to CO_2 and acetic acid, respectively.

Reaction equation	Δ_rG' (kJ/reaction)	
	pH 3.9	pH 5.0
Eq. 1—Complete oxidation of glycerol to CO_2		
$4\ C_3H_8O_3 + 7\ SO_4^{2-} + 14\ H^+ \rightarrow 12\ CO_2 + 7\ H_2S + 16\ H_2O$	−1142.8	−1099.0
Eq. 2—Oxidation of glycerol to acetic acid		
$4\ C_3H_8O_3 + 3\ SO_4^{2-} + 6\ H^+ \rightarrow 4\ C_2H_4O_2 + 3\ H_2S + 8\ H_2O + 4\ CO_2$	−781.3	−776.6
Eq. 3—Oxidation of acetic acid to CO_2		
$C_2H_4O_2 + SO_4^{2-} + 2\ H^+ \rightarrow 2\ CO_2 + H_2S + 2\ H_2O$	−90.4	−80.6

Δ_rG' was calculated with Equilibrator (Flamholz et al., 2012) using concentrations of 1 mM for all reactants.

removal (**Figure 3**). Total acetic acid concentrations started to decrease before all glycerol was consumed, indicating a co-consumption phase. Biomass concentrations remained approximately constant once glycerol was completely consumed, while total acetic acid concentrations kept decreasing, indicating that under these conditions, energy derived from acetate degradation was invested in cell maintenance rather than in net growth. This was also reflected in the continued addition of acid (HCl) required to maintain constant pH after the maximum optical density (OD_{600}) was reached. Overall, approximately 30% of the carbon added as glycerol was not coupled to dissimilatory sulfate reduction but used for anabolism.

The ability to use acetic acid as electron donor is advantageous in extreme environments such as AMD for several reasons. Firstly, acetic acid is a typical end product of other microorganisms such as fermenters present in AMD sediments (Sánchez-Andrea et al., 2018). The ability to metabolize a variety of organic acids, but especially a metabolic end product such as acetic acid (**Table 1**) increases the carbon and energy available to strain INE in nutrient-limited AMD/ARD environments. Furthermore, at pH values below their pK_a, organic acids occur in their undissociated (protonated) form and can freely diffuse across the cell membrane, resulting in the acidification of the cytoplasm. Removal of intracellular protons is energetically costly and can be detrimental for growth. Complete oxidation of organic acids to CO_2 prevents their accumulation in the environment, thereby lowering organic acid toxicity. For example, at the pH conditions compared in this study, maximum total extracellular acetic acid (dissociated and undissociated) concentrations reached 2.4 mM at pH 3.9 and 2.0 mM at pH 5.0 removal (**Figure 3**). Considering the pK_a of acetic acid (4.8), its extracellular concentration (undissociated) at pH 3.9 is 2.1 mM, vs. 0.7 mM at pH 5.0. The higher extracellular acetic acid concentration measured at pH 3.9 could correspond to a higher consumption of acetic acid at the optimum pH 5.

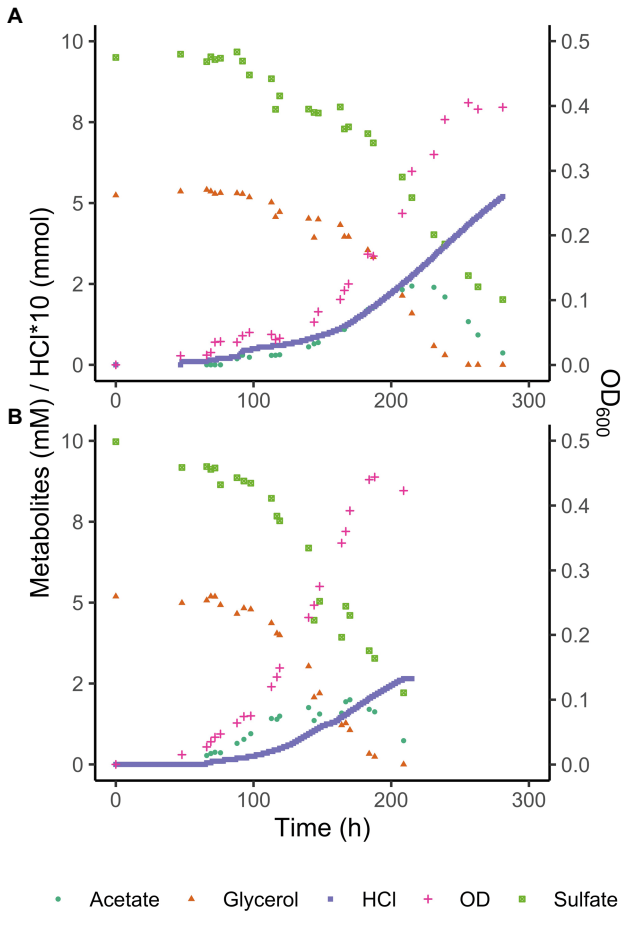

FIGURE 3 | Glycerol, total acetate (undissociated + dissociated) and sulfate concentrations, and OD_{600} of *Acididesulfobacillus acetoxydans* strain INE grown in bioreactors at pH 3.9 **(A)** and pH 5 **(B)**. Concentration profiles of glycerol, sulfate, acetic acid, as well as OD_{600} and HCl addition are shown for one reactor at each pH value for clarity.

Metabolic Pathways for Complete Acetic Acid Oxidation Coupled to Sulfate Reduction

To enable the more informed prediction of acetotrophic potential in acidophilic SRB from (meta)genomic data, the metabolic pathway for complete oxidation of acetic acid by *A. acetoxydans* was determined through proteome analysis. The Acetyl-CoA pathway seemed to be responsible for the complete oxidation of acetic acid to CO_2, since all of its enzymes were present in the proteome (**Figure 4**). Additionally, the absence of citrate synthase indicated that acetyl-CoA could not be degraded through the tricarboxylic acid (TCA) cycle, the other potential pathway for acetate oxidation. Two genes encoding bifurcating enzymes related to the reverse Acetyl-CoA pathway were detected, the NADH-dependent reduced ferredoxin:$NADP^+$ oxidoreductase (*nfnAB*, 2795-96), and the cytoplasmic NADH-dependent formate dehydrogenase (*fdh*, 1374–1377). NfnAB catalyses the NAD^+-dependent reduction of ferredoxin by NADPH, acting possibly on the $NADP^+$ generated in the conversion of methylene-THF to methenyl-THF in the Acetyl-CoA pathway. The *nfnAB* genes, both encoding iron–sulfur flavoproteins, are present in a diversity of microorganisms (Wang et al., 2010), but often incorrectly annotated as sulfide dehydrogenase. The *nfnAB* genes were detected in the proteome of strain INE and were found in the same operon as two genes encoding methylene-H_4F-DH/methenyl-H_4F cyclohydrolase and the methenyl-H_4F cyclohydrolase (2793-94), both part of the Acetyl-CoA pathway. The second bifurcating enzyme detected in the proteome of strain INE, the cytoplasmic NADH-dependent formate dehydrogenase (Sebban et al., 1995; Costa et al., 1997), is a selenocysteine-containing Fdh that oxidizes formate while reducing ferredoxin and NAD^+. The Fdh detected in the genome of strain INE resembled the Fdh protein encoded in the genome of *Desulfotomaculum kuznetsovii* (Deasku_2987-2991), and consisted of a catalytic subunit (*fdhA*, 1377), two subunits for oxidoreduction of NADH/NAD^+ (*fdhGH*, 1374), the proton-translocating quinone (*fdhE*, 1375), and the 5-formyltetrahydrofolate cyclo-ligase (*fdhH*, 1373). This Fdh is predicted to act in the Acetyl-CoA pathway (Ragsdale and Pierce, 2008), and it was found next to a gene encoding a histidine kinase (1378), suggesting that it has a regulatory

function (Pereira et al., 2011). Although the complete Acetyl-CoA pathway is also present in the genome of sulfate reducers from the genus *Desulfosporosinus* (Alazard et al., 2010; Pester et al., 2012; Sánchez-Andrea et al., 2015), complete oxidation of acetic acid in moderately acidophilic SRB was so far only observed in the recently described *Ds. metallidurans*, where weak growth on acetic acid was reported. However, acetate oxidation was proposed to occur through the TCA cycle instead of the Acetyl-CoA pathway based on genome analysis (Panova et al., 2021).

Enzymes of the metabolic pathways used for oxidation of glycerol coupled to sulfate reduction were also identified in the proteome (**Figure 4**). Glycerol is taken up by a glycerol transporter (DEACI_1309-DEACI_1310, hereafter "DEACI_" will be omitted for simplicity) and oxidized to dihydroxyacetone-P (DHAP) by glycerol kinase (0310) and glycerol-3-phosphate dehydrogenase (1301-1303). DHAP is converted to pyruvate involving enzymes of the Embden-Meyerhoff pathway (0305-0308, 2591-2592, 3679) and subsequently to acetyl-coA by pyruvate:ferredoxin oxidoreductase (0330, 0621, 1130, 1144, 2105, 2107, 2770). Acetyl-CoA is converted to acetate through P_i acetyltransferase (3443) and acetate kinase (3414), or completely oxidized to CO_2 through the reverse Acetyl-CoA pathway, discussed above. Reducing equivalents are transferred to NAD^+ and oxidized ferredoxin. Electrons flow to sulfate through the respiratory chain, for which the key enzymes were identified. Sulfate is activated with ATP to adenosine-phosphosulfate (APS) and pyrophosphate by ATP sulfurylase (Sat, 0463). Heterodisulfide reductase (HdrF1, 0461) is predicted to receive electrons from the quinone pool and direct them

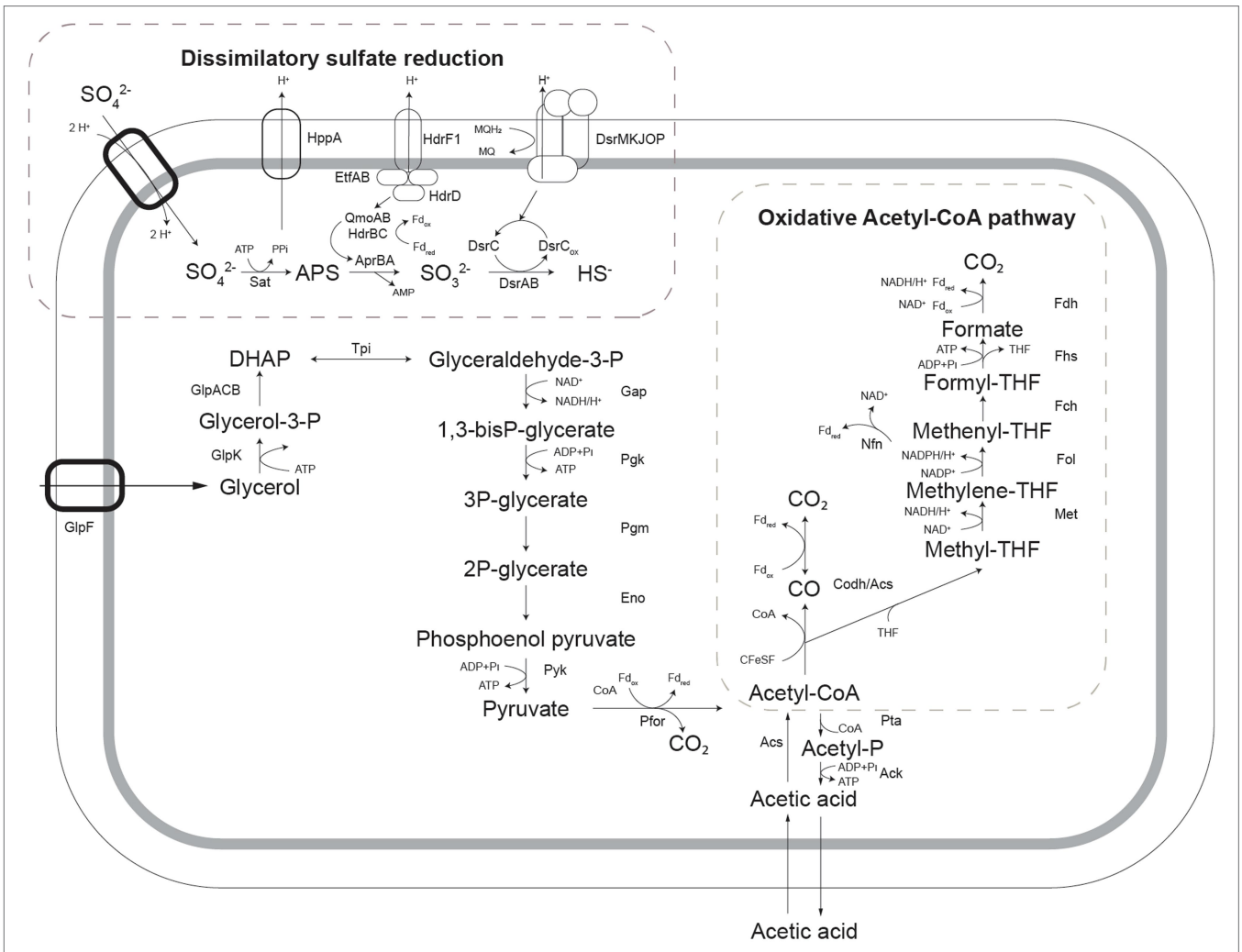

FIGURE 4 | Schematic representation of pathways for glycerol oxidation and sulfate reduction as detected in the genome of *Acididesulfobacillus acetoxydans*. Sat: ATP sulfurylase, Apr: APS reductase, Dsr: dissimilatory sulfite reductase, Qmo: quinone-interacting membrane oxidoreductase complex, Hdr: heterodisulfide reductase, GlpF: glycerol transporter, GlpK: glycerol kinase, Tpi: triose phosphate isomerase, Gap: glyceraldehyde-3-phosphate dehydrogenase, Pgk: phosphoglycerate kinase, Pgm: phosphoglycerate mutase, Eno: phosphoenolpyruvate hydratase, Pyk: pyruvate kinase, Pfor: pyruvate:ferredoxin oxidoreductase, Pta: Phosphate acetyltransferase, Ack: acetate kinase, Acs: acetyl-coA synthase, Codh: carbon monoxide dehydrogenase, Met: methylene-tetrahydrofolate reductase, Fol: methylene-tetrahydrofolate dehydrogenase/methenyl-tetrahydrofolate cyclohydrolase, Fch: 5-formyltetrahydrofolate_cyclo-ligase, Fhs: Formate-tetrahydrofolate ligase/ formyl-H4F synthethase, Fdh: formate dehydrogenase, Nfn: NADH-dependent reduced ferredoxin:$NADP^+$ oxidoreductase.

to the cytoplasmic QmoAB/HdrBC complex (0456, 0457, 0470, 0471; Rabus et al., 2015), reducing APS to sulfite through the AprAB (0464, 0465) complex, as described for other SRB (Ramos et al., 2012). The sulfur in sulfite is then reduced and transferred to DsrC (0677) forming DsrC trisulfide by DsrAB (0668, 0669; Santos et al., 2015), which is finally reduced to sulfide by electrons received from the DsrMKJOP complex (0672-0676; Pires et al., 2006).

The increased specific proton consumption rate at pH 3.9 compared to pH 5.0, and the ability to oxidize organic acids to CO_2 has important effects on the biogeochemistry of ARD/AMD environments, as it contributes to the natural attenuation of the extreme conditions. In the Tinto River, for example, the pH values can be as low as 2 in the water column (Sánchez-Andrea et al., 2012; Amils et al., 2014). Consequently, the microbial diversity in the water column of the Tinto River is generally low, and dominated by only a few species belonging to the *Acidithiobacillus*, *Leptospirillum*, and *Acidiphilium* genera (López-Archilla et al., 2001). Microbial diversity is higher in the sediments (Sánchez-Andrea et al., 2011), partly due to the wider range of physicochemical characteristics found in the different layers. As strain INE was isolated from Tinto River sediments, its detoxifying characteristics indicate that it could assist in the creation of milder conditions, where less acidophilic microorganisms can thrive. This could facilitate the higher microbial diversity found in the sediments compared to the water column, where the environment is more dynamic due to the water flow.

Additional Stress Resistance Mechanisms at Low pH

Other possible pH homeostasis mechanisms enabling *A. acetoxydans* to grow at low pH besides acetate oxidation were also investigated. Protein abundance at optimum and minimum pH were compared to detect increased translation of proteins involved in acid stress response mechanisms at minimum pH. Protein abundances in cultures grown at optimum (5.0) and low (3.9) pH showed 1258 proteins present in at least one of the growth conditions, of which 949 were present in both. Using a value of p cut-off of 0.05 (student t-test), 30 proteins were present in at least two-fold higher abundance at pH 3.9 compared to pH 5.0, with 15 proteins unique for pH 3.9. At pH 5.0, 56 proteins were present in at least 2-fold higher abundance, of which 32 were uniquely present at pH 5.0 (**Supplementary Table S3**).

Donnan Potential and Transporters

A Donnan potential serves as a chemiosmotic barrier to the influx of protons at low extracellular pH as described for extreme acidophiles (Baker-Austin and Dopson, 2007). A key element in creating a positive membrane potential is the K^+-transporting ATPase, encoded by the *kdpABC* operon, which was indeed detected in the genome of *A. acetoxydans* (3037-39). However, this K^+ ATPase was not detected in the proteome of cells grown at either pH 3.9 or 5.0. Therefore, despite its apparent importance in other acidophiles (Baker-Austin and Dopson, 2007), it did not appear to play an important role in acid stress resistance of *A. acetoxydans*. Although the detection of membrane proteins such as ATPases with standard proteomics methods is difficult, and their presence cannot be completely dismissed based on these results alone, comparative transcriptomics analysis also verified the absence of the K^+-transporting ATPase from the transcriptome (Sánchez-Andrea, unpublished data).

In addition to K^+-ATPase, genes encoding secondary cation transporters such as Na^+/P_i co-transporters (3752, 0312, 1305) and solute symporters (1779, 2169, 2179, 2830, 3466, 3909) were identified in the genome, and the corresponding proteins (1305, 2179, 3466, and 2830) were present in the proteome. Interestingly, a bile acid:Na^+ symporter (2179) and a transporter from the major facilitator superfamily (0284) were only present at pH 3.9, indicating a potentially important role in ion transport at low pH. Build-up of excess protons in the cytoplasm can be further countered by active H^+ export by ATPase. The proton ATPase found in strain INE (0352-0361) was present in the proteome at both pH values, but not in significantly different abundance at lower pH, suggesting that this system is not upregulated in response to increased acid stress. Antiporters such as the Na^+/H^+ antiporter (2829) or the H^+/Cl^- exchange transporter (*clcA*, 0494) also contribute to H^+ removal. ClcA was detected in the proteome, albeit not in significantly different abundance at lower pH.

Cytoplasmic Buffering Capacity

The modification of the cytoplasmic buffering capacity through a change in the metabolism of certain amino acids could mitigate acid stress (Baker-Austin and Dopson, 2007; Slonczewski et al., 2009). The decarboxylation of arginine, glutamate and aspartate, for example, releases CO_2 and amines, and consumes protons (Slonczewski et al., 2009). This would be net H^+-consuming when the amino acids can be taken up from the environment, and it could be speculated that the yeast extract present in the medium served as an external source of amino acids. L-Aspartate decarboxylase (2148) was found in the proteome at pH 5.0, but not at pH 3.9, indicating that this reaction does not contribute to pH homeostasis at increased proton stress. Glutamate decarboxylase (2571), catalyzing the H^+ consuming conversion of glutamate to g-aminobutyrate (GABA; Castanie-Cornet et al., 1999), and L-arginine decarboxylase (0577), catalyzing the H^+-consuming conversion of L-arginine to agmatine, were detected in the proteome at both conditions, albeit not at a significantly different abundance. Furthermore, glutamate decarboxylase forms the GABA shunt together with GABA aminotransferase and succinate semialdehyde dehydrogenase, which is also proposed to be involved in acid stress resistance in bacteria (Feehily and Karatzas, 2013). Through the GABA shunt, glutamate is converted to GABA by glutamate decarboxylase (2571), consuming a proton, and GABA is converted to succinate semialdehyde (SSA) by GABA aminotransferase (4212, 3258), regenerating the glutamate. Succinate semialdehyde dehydrogenase then converts SSA to succinate (3872, 3892). Glutamate decarboxylase (2571) and GABA aminotransferase (3258, 4212) were detected in the proteome of strain INE, albeit not at a significantly different abundance at pH 5.0 or 3.9. Succinate

semialdehyde dehydrogenase was not detected in the proteome; however, and the role of the GABA shunt in resistance to acid stress in strain INE could, therefore, not be clearly established.

Interestingly, agmatinase (0579), converting agmatine to urea and putrescine, was detected in the proteome at both pH values. Urea may play a role in pH homeostasis through its degradation into two molecules of ammonium and one CO_2, catalyzed by urease. This requires incorporation of 2 H^+ and is known to play a role in acid stress resistance (Young et al., 1996). However, the gene encoding urease was not detected in the genome of strain INE. An alternative route for urea degradation could be through urea amidolyase; genes (0170, 0171) were detected in the genome, but the corresponding proteins were absent in the proteome. Urea does seem to play a role in pH homeostasis of strain INE at low pH—four out of the five enzymes of the urea cycle are present in increased abundance at pH 3.9. A carbamoyl phosphate synthase (0932) was found only at pH 3.9, and ornithine carbamoyltransferase (0934), and argininosuccinate synthase (0935) were present in twofold higher abundance. Argininosuccinate lyase (0936) was present in the proteome at both conditions in similar abundance. Arginase (0853), converting arginine to urea and ornithine and completing the urea cycle, was, however, not detected in the proteome, and the role of the urea cycle in acid stress resistance of strain INE, therefore, remains enigmatic.

DNA, Protein, and Lipid Repair Mechanisms

The extreme acidity and high metal concentrations in acid drainage environments increase the risk of damage to DNA, RNA, and proteins. A number of DNA, protein, and lipid repair systems were present in the proteome of strain INE. Ferroxidase (0081), linked to protection of DNA upon exposure to acid stress in *Helicobacter pylori* (Huang et al., 2010), was present in the proteome at both conditions. Several chaperones involved in protein refolding (0004, 2293, 3249, 0692, 2491, 2469, 1389, 1390) were present in the proteome, and a ferredoxin signature (3253) upstream of a chaperone (3249) was *ca.* 6-fold more abundant at pH 3.9 than at pH 5.0. An upregulation of chaperones was found to accompany growth at lower pH in many acidophiles (Jerez et al., 1988). Furthermore, six peroxiredoxins, potentially involved in lipid repair (Cárdenas et al., 2012), were detected in the proteomes at both conditions (2671, 0858, 0888, 0966, 1064, 2671, 3052). One of these (2671) was *ca.* twofold more abundant at low pH.

Altered Membrane Permeability

Comparison of the lipid composition in *A. acetoxydans* strain INE at pH 5.0 and at pH 3.9 showed a transition, with decreasing pH, from acyl/ether glycerol (AEG) lipids with an unsaturated ether moiety (plasmalogens) to AEG lipids with a saturated ether moiety (**Table 2**). This was evident in the core lipids through an increase in saturated monoalkyl glycerol ether lipids from 5.0% at pH 5.0 to 13.0% at pH 3.9 and a concomitant decrease in DMAs (from 24.9% to 17.6%). The increase in saturated ether moieties may represent an adaptation to maintain membrane homeostasis at lower pH. Increasing saturation of FAs in response to lower pH has been described some in bacterial species, but the opposite effect has been observed in others (Siliakus et al., 2017; Sohlenkamp, 2017). It should be noted that there was no change in the saturation of the diacyl glycerols (DAGs), as seen from the FAs (**Table 2**). With decreasing growth pH there was also a clear diversification in acyl and ether moieties (**Table 2**). Bacterial glycerol ether lipids likely play a role in cell resistance or adaptation to adverse environmental conditions (Grossi et al., 2015) since ether linkages are less sensitive to acid hydrolysis than ester bonds. Indeed, AEG lipids are thought to improve cell resistance to extreme external conditions, relative to DAGs (Grossi et al., 2015).

At both pH values, the *A. acetoxydans* fatty acids were dominated by branched-chain FAs (97% of FAs at pH 3.9, 100% at pH 5.0), including iso, anti-iso and mid-chain methylated FAs. Similarly, the percentage of FAs that were branch-chained was moderate to high in the other acidophilic strains, *Ds. acididurans* (26%) and *Ds. acidiphilus* (42%), while they were absent in both neutrophilic strains *Ds. orientis* and *Ds. halogenans*. In particular, the branched-chain acid iso-$C_{15:0}$ was abundant in strain INE (48.1% at pH 3.9, 60.7% at pH 5.0) and in the acidophilic strains *Ds. acididurans* (25.8%) and *Ds. acidiphilus* (16.6). An increasing proportion of branched-chain FAs is a known adaption to maintain membrane homeostasis under external stress, and a number of extreme acidophilic bacteria have been reported to have high levels of branched-chain fatty acids (Siliakus et al., 2017).

In addition to an altered membrane FAs composition, a putative poly-gamma-glutamate (PGA) bacterial capsule synthesis protein CapA (2151) was found in 2-fold higher abundance at low pH in the proteome, providing another means to create physical separation between the cell and the acidic environment as a defense mechanism. PGA is a natural polymer that may be involved in avoiding dehydration in high salt concentrations and neutralizing pH in alkaliphiles (Ashiuchi and Misono, 2002) by forming a protective PGA capsule. Furthermore, spermidine is hypothesized to play a role in the protection against acid stress through lowering the permeability of the membrane to protons (Christel et al., 2017). Spermidine synthase (0578) was detected in both proteome sets at similar abundances, indicating spermidine could play a role in acid stress resistance of *A. acetoxydans* at both pH values tested.

CONCLUSION

Acididesulfobacillus acetoxydans strain INE, isolated from Tinto River sediments, represents a novel species of a novel genus of moderately acidophilic SRB. The increased specific proton consumption rates at low pH (3.9) compared to optimum pH (5.0) when grown with glycerol and sulfate demonstrated the alkalinizing effect of its metabolism in acidic environments. The capacity for complete oxidation of organic acids to CO_2 can reduce organic acid toxicity and provide increased access to organic carbon compounds in nutrient-limited acid drainage environments. Interestingly, canonical acid stress resistance mechanisms such as an inverted membrane (Donnan) potential,

increased abundance of charge transporters, and cytoplasmic buffering capacity were not detected in the proteome during growth at low pH. Instead, an increased fraction of ether-bound fatty acids in the overall membrane lipid composition appeared to be an important acid stress resistance mechanism for *A. acetoxydans* during growth at pH below optimum. In addition, the increased abundance of CapA could suggest that the response to proton stress in *A. acetoxydans* resembles the response to high salinity.

Description of *Acididesulfobacillus* gen. nov.

A.ci.di.de.sul.fo.ba.cil'lus. L. masc. adj. *acidus*, sour; N.L. masc. n. *'Desulfobacillus'*, a (not validly published) bacterial genus name; N.L. masc. n. *Acididesulfobacillus*, an acid-loving relative of the genus '*Desulfobacillus*'.

Cells present sub-terminal spores and are rod-shaped, strictly anaerobic, motile, and stain Gram-negative, but lack the characteristic double membrane. The genus is closely related to *Desulfosporosinus* and *Desulfitobacterium*. The type species is *A. acetoxydans*.

Description of *Acididesulfobacillus acetoxydans* sp. nov.

Acididesulfobacillus acetoxydans: a.cet.o'xy.dans. L. neut. n. *acetum*, vinegar; N.L. v. *oxydo* (from Gr. masc. adj. *oxys*, acid, sour), to oxidize; N.L. part. adj. *acetoxydans*, oxidizing acetate

Straight single rods are 4–7 µm long and about 0.6 µm wide. Motile in the exponential phase by lateral flagellation. Subterminal, oval endospores are formed in the stationary growth phase. Cells are Gram-positive that stain Gram-negative. The pH range for growth is pH 3.8–6.5, with an optimum at pH 5.0. The temperature range for growth is 25–42°C, with an optimum at 30°C. The upper limit for salt tolerance is 15.3 g L^{-1} NaCl. Strain INE uses a wide range of electron donors in the presence of sulfate such as H_2; organic acids (formate, acetate, pyruvate, lactate, malate, fumarate, butyrate, and succinate); alcohols (methanol, ethanol, propanol, and glycerol); the amino acid L-cysteine; sugars (xylose, fructose, glucose, maltose, sucrose, and raffinose) and yeast extract or starch; but not propionate, citrate, or benzoate. Organic substrates are oxidized completely to CO_2. Strain INE uses selenate, arsenate, nitrate, sulfate, elemental sulfur, thiosulfate, and DMSO as electron acceptors; but not iron, fumarate, PCE, perchlorate, sulfite, or dithionate. It also ferments some substrates such as cysteine, pyruvate, glucose, and yeast extract. It couples the disproportionation of sulfur and thiosulfate to growth, but not sulfite. Strain INE is susceptible to vancomycin. The predominant whole cell membrane lipids of the type strain INE at pH 5 are iso-C15:0 fatty acid (60.7%), and iso-C15:0 DMA (14.3%). Its genomic G + C content is 53.65 mol %. Phylogenetically, it is a member of the family *Peptococcaceae*, order *Clostridiales* within the Firmicutes phylum. The type strain *A. acetoxydans*, strain INE (=DSM 29876^T = JCM 30553^T), was isolated from the Tinto River, Spain.

DATA AVAILABILITY STATEMENT

The datasets presented in this study can be found in online repositories. The names of the repository/repositories and accession number(s) can be found at: https://www.ebi.ac.uk/ena, PRJEB7665; https://www.ebi.ac.uk/pride/archive/, PXD022508.

AUTHOR CONTRIBUTIONS

IS-A and AS initiated the study and designed the experiments. IS-A and MJ performed experiments. IS-A and CG processed and analyzed the reactor, genome, and proteome data and wrote the draft manuscript. BH assembled and compared genome data. NB, JS, and WR performed membrane lipid analysis. All authors contributed to the article and approved the submitted version.

FUNDING

This work was financed by ERC grants to AS (project 323009) and JS (project 694569), the research program TTW under project number 14797, which is financed by the Dutch Research Council (NWO) to IS-A, and a Gravitation grant (SIAM 024.002.002) of the Netherlands Ministry of Education, Culture and Science to AS and JS.

ACKNOWLEDGMENTS

We thank Hans Wessels from Radboud University Nijmegen for the proteomics services, Marcel Giesbers and Jelmer Vroom from the Wageningen Electron Microscopy Center for TEM imaging, and Ellen Hopmans for advice on lipid identification. We thank Aharon Oren for fruitful discussion over nomenclature regulations and Barrie Johnson for his pioneering work on acidophilic SRB.

SUPPLEMENTARY MATERIAL

The Supplementary Material for this article can be found online at: https://www.frontiersin.org/articles/10.3389/fmicb.2022.816605/full#supplementary-material

Supplementary Table S1 | AAI matrix.

Supplementary Table S2 | The intact polar lipid (IPL) composition of *Acididesulfobacillus acetoxydans* gen. nov. sp. nov. grown at pH 5.0 (growth optimum) as determined by UHPLC-HRMS analysis.

Supplementary Table S3 | Proteins detected at 2-fold or higher increased abundance at pH 3.9 or pH 5.0 (p-value < 0.05, student t-test). Locus tag DEACI_**** is followed by the annotation. U: unique at this condition.

Supplementary Table S4 | (A) Example MS2 spectra of a hexosamine-hexose lipid. [M+H]+ of parent ion in MS1 = 864.604. Placement of amine group in structure is tentative. Table insert of ion assignments, mmu = milli mass unit, Δ mmu = (measured mass – calculated mass) x 1000. **(B)** Example MS2 spectra of one of the unknown hexosamine-containing lipids. [M+H]+ of parent ion in MS1 = 880.599.

REFERENCES

Adams, M. E., and Postgate, J. R. (1959). A new sulphate-reducing vibrio. *J. Gen. Microbiol.* 20, 252–257. doi: 10.1099/00221287-20-2-252

Alazard, D., Joseph, M., Battaglia-Brunet, F., Cayol, J. L., and Ollivier, B. (2010). *Desulfosporosinus acidiphilus* sp. nov.: a moderately acidophilic sulfate-reducing bacterium isolated from acid mining drainage sediments. *Extremophiles* 14, 305–312. doi: 10.1007/s00792-010-0309-4

Altschul, S. F., Gish, W., Miller, W., Myers, E. W., and Lipman, D. J. (1990). Basic local alignment search tool. *J. Mol. Biol.* 215, 403–410. doi: 10.1016/S0022-2836(05)80360-2

Amils, R., Fernández-Remolar, D., and IPBSL Team (2014). Río Tinto: a geochemical and mineralogical terrestrial analogue of Mars. *Life. 4*, 511–534. doi: 10.3390/life4030511

Amils, R., González-Toril, E., Aguilera, A., Rodríguez, N., Fernández-Remolar, D., Gómez, F., et al. (2011). From Río Tinto to Mars: the terrestrial and extraterrestrial ecology of acidophiles. *Adv. Appl. Microbiol.* 77, 41–70. doi: 10.1016/B978-0-12-387044-5.00002-9

Ashburner, M., Ball, C. A., Blake, J. A., Botstein, D., Butler, H., Cherry, J. M., et al. (2000). Gene ontology: tool for the unification of biology. *Nat. Genet.* 25, 25–29. doi: 10.1038/75556

Ashiuchi, M., and Misono, H. (2002). Biochemistry and molecular genetics of poly-γ-glutamate synthesis. *Appl. Microbiol. Biotechnol.* 59, 9–14. doi: 10.1007/s00253-002-0984-x

Baker-Austin, C., and Dopson, M. (2007). Life in acid: pH homeostasis in acidophiles. *Trends Microbiol.* 15, 165–171. doi: 10.1016/j.tim.2007.02.005

Bale, N. J., Sorokin, D. Y., Hopmans, E. C., Koenen, M., Irene Rijpstra, W. C., Villanueva, L., et al. (2019). New insights into the polar lipid composition of extremely halo(alkali)philic euryarchaea from hypersaline lakes. *Front. Microbiol.* 10:377. doi: 10.3389/fmicb.2019.00377

Bland, C., Ramsey, T. L., Sabree, F., Lowe, M., Brown, K., Kyrpides, N. C., et al. (2007). CRISPR recognition tool (CRT): a tool for automatic detection of clustered regularly interspaced palindromic repeats. *BMC Bioinformatics* 8:209. doi: 10.1186/1471-2105-8-209

Campbell, L. L., and Postgate, J. R. (1965). Classification of the spore-forming sulfate-reducing bacteria. *Microbiol. Mol. Biol. Rev.* 29, 359–363. doi: 10.1128/br.29.3.359-363.1965

Cardenas, E., Wu, W. M., Leigh, M. B., Carley, J., Carroll, S., Gentry, T., et al. (2008). Microbial communities in contaminated sediments, associated with bioremediation of uranium to submicromolar levels. *Appl. Environ. Microbiol.* 74, 3718–3729. doi: 10.1128/AEM.02308-07

Cárdenas, J. P., Moya, F., Covarrubias, P., Shmaryahu, A., Levicán, G., Holmes, D. S., et al. (2012). Comparative genomics of the oxidative stress response in bioleaching microorganisms. *Hydrometallurgy* 127-128, 162–167. doi: 10.1016/j.hydromet.2012.07.014

Castanie-Cornet, M.-P., Penfound, T. A., Smith, D., Elliott, J. F., and Foster, J. W. (1999). Control of acid resistance in *Escherichia coli*. *J. Bacteriol.* 181, 3525–3535. doi: 10.1128/JB.181.11.3525-3535.1999

Christel, S., Herold, M., Bellenberg, S., El Hajjami, M., Buetti-Dinh, A., Pivkin, I. V., et al. (2017). Multi-omics reveals the lifestyle of the acidophilic, mineral-oxidizing model species *Leptospirillum ferriphilum*. *Appl. Environ. Microbiol.* 84, e02091–e02017. doi: 10.1128/AEM.02091-17

Claudel-Renard, C., Chevalet, C., Faraut, T., and Khan, D. (2003). Enzyme-specific profiles for genome annotation – PRIAM. *Nucleic Acids Res.* 31, 6633–6639. doi: 10.1093/nar/gkg847

Cline, J. (1969). Spectrophotometric determination of hydrogen sulfide in natural waters. *Limnol. Oceanogr.* 14, 454–458. doi: 10.4319/lo.1969.14.3.0454

Costa, C., Teixeira, M., LeGall, J., Moura, J. J. G., and Moura, I. (1997). Formate dehydrogenase from *Desulfovibrio desulfuricans* ATCC 27774: isolation and spectroscopic characterization of the active sites (heme, iron- sulfur centers and molybdenum). *J. Biol. Inorg. Chem.* 2, 198–208. doi: 10.1007/s007750050125

Crittenden, C. M., Akin, L. D., Morrison, L. J., Trent, M. S., and Brodbelt, J. S. (2017). Characterization of lipid A variants by energy-resolved mass spectrometry: impact of acyl chains. *J. Am. Soc. Mass Spectrom.* 28, 1118–1126. doi: 10.1007/s13361-016-1542-6

Deutsch, E. W., Bandeira, N., Sharma, V., Perez-Riverol, Y., Carver, J. J., Kundu, D. J., et al. (2020). The ProteomeXchange consortium in 2020: enabling "big data" approaches in proteomics. *Nucleic Acids Res.* 48, D1145–D1152. doi: 10.1093/nar/gkz984

Doetsch, R. N. (1981). "Determinative methods of light microscopy," in *Manual of Methods for General Bacteriology* (Washington, D.C.: American Society for Microbiology), 21–33.

Falagán, C., Sánchez-España, J., and Johnson, D. B. (2014). New insights into the biogeochemistry of extremely acidic environments revealed by a combined cultivation-based and culture-independent study of two stratified pit lakes. *FEMS Microbiol. Ecol.* 87, 231–243. doi: 10.1111/1574-6941.12218

Feehily, C., and Karatzas, K. A. G. (2013). Role of glutamate metabolism in bacterial responses towards acid and other stresses. *J. Appl. Microbiol.* 114, 11–24. doi: 10.1111/j.1365-2672.2012.05434.x

Finneran, K. T., Forbush, H. M., VanPraagh, C. V., and Lovley, D. R. (2002). *Desulfitobacterium metallireducens* sp. nov., an anaerobic bacterium that couples growth to the reduction of metals and humic acids as well as chlorinated compounds. *Int. J. Syst. Evol. Microbiol.* 52, 1929–1935. doi: 10.1099/ijs.0.02121-0

Flamholz, A., Noor, E., Bar-Even, A., and Milo, R. (2012). eQuilibrator—The biochemical thermodynamics calculator. *Nucleic Acids Res.* 40, D770–D775. doi: 10.1093/nar/gkr874

Frolov, E. N., Kublanov, I. V., Toshchakov, S. V., Samarov, N. I., Novikov, A. A., Lebedinsky, A. V., et al. (2017). *Thermodesulfobium acidiphilum* sp. nov., a thermoacidophilic, sulfate-reducing, chemoautotrophic bacterium from a thermal site. *Int. J. Syst. Evol. Microbiol.* 67, 1482–1485. doi: 10.1099/ijsem.0.001745

Frolov, E. N., Zayulina, K. S., Kopitsyn, D. S., Kublanov, I. V., Bonch-Osmolovskaya, E. A., and Chernyh, N. A. (2018). *Desulfothermobacter acidiphilus* gen. Nov., sp. nov., a thermoacidophilic sulfate-reducing bacterium isolated from a terrestrial hot spring. *Int. J. Syst. Evol. Microbiol.* 68, 871–875. doi: 10.1099/ijsem.0.002599

Galperin, M. Y., Makarova, K. S., Wolf, Y. I., and Koonin, E. V. (2015). Expanded microbial genome coverage and improved protein family annotation in the COG database. *Nucleic Acids Res.* 43, D261–D269. doi: 10.1093/nar/gku1223

Grossi, V., Mollex, D., Vinçon-Laugier, A., Hakil, F., Pacton, M., and Cravo-Laureau, C. (2015). Mono- and dialkyl glycerol ether lipids in anaerobic bacteria: biosynthetic insights from the mesophilic sulfate reducer *Desulfatibacillum alkenivorans* PF2803 T. *Appl. Environ. Microbiol.* 81, 3157–3168. doi: 10.1128/AEM.03794-14

Hall, J. R., Mitchell, K. R., Jackson-Weaver, O., Kooser, A. S., Cron, B. R., Crossey, L. J., et al. (2008). Molecular characterization of the diversity and distribution of a thermal spring microbial community by using rRNA and metabolic genes. *Appl. Environ. Microbiol.* 74, 4910–4922. doi: 10.1128/AEM.00233-08 [doi]

Hausmann, B., Knorr, K. H., Schreck, K., Tringe, S. G., Glavina Del Rio, T., Loy, A., et al. (2016). Consortia of low-abundance bacteria drive sulfate reduction-dependent degradation of fermentation products in peat soil microcosms. *ISME J.* 10, 2365–2375. doi: 10.1038/ismej.2016.42

Hausmann, B., Pelikan, C., Rattei, T., Loy, A., and Pester, M. (2019). Long-term transcriptional activity at zero growth of a cosmopolitan rare biosphere member. *MBio* 10, 1–16. doi: 10.1128/mBio.02189-18

Huang, C. H., Lee, I. L., Yeh, I. J., Liao, J. H., Ni, C. L., Wu, S. H., et al. (2010). Upregulation of a non-heme iron-containing ferritin with dual ferroxidase and DNA-binding activities in *helicobacter pylori* under acid stress. *J. Biochem.* 147, 535–543. doi: 10.1093/jb/mvp200

Human Microbiome Project Consortium (2012). Structure, function and diversity of the healthy human microbiome. *Nature* 486, 207–214. doi: 10.1038/nature11234

Huson, D. H., Auch, A. F., Qi, J., and Schuster, S. C. (2007). MEGAN analysis of metagenomic data. *Genome Res.* 17, 377–386. doi: 10.1101/gr.5969107

Hyatt, D., Chen, G. L., Locascio, P. F., Land, M. L., Larimer, F. W., and Hauser, L. J. (2010). Prodigal: prokaryotic gene recognition and translation initiation site identification. *BMC Bioinformatics* 11, 119. doi: 10.1186/1471-2105-11-119

Jackson, D. R., Cassilly, C. D., Plichta, D. R., Vlamakis, H., Liu, H., Melville, S. B., et al. (2021). Plasmalogen biosynthesis by anaerobic bacteria: identification of a two-gene operon responsible for Plasmalogen production in Clostridium perfringens. *ACS Chem. Biol.* 16, 6–13. doi: 10.1021/acschembio.0c00673

Jameson, E., Rowe, O. F., Hallberg, K. B., and Johnson, D. B. (2010). Sulfidogenesis and selective precipitation of metals at low pH mediated by Acidithiobacillus

spp. and acidophilic sulfate-reducing bacteria. *Hydrometallurgy* 104, 488–493. doi: 10.1016/j.hydromet.2010.03.029

Jerez, C., Chamorro, D., Peirano, I., and Toledo, H. (1988). Studies of the stress response in chemolithotrophic acidophilic bacteria. *Biochem. Int.* 17, 989–999.

Johnson, D. B., and Hallberg, K. B. (2005). Acid mine drainage remediation options: A review. *Sci. Total Environ.* 338, 3–14. doi: 10.1016/j.scitotenv.2004.09.002

Kimura, S., Hallberg, K. B., and Johnson, D. B. (2006). Sulfidogenesis in low pH (3.8-4.2) media by a mixed population of acidophilic bacteria. *Biodegradation* 17, 159–167. doi: 10.1007/s10532-005-3050-4

Klemps, R., Cypionka, H., Widdel, F., and Pfennig, N. (1985). Growth with hydrogen, and further physiological characteristics of *Desulfotomaculum* species. *Arch. Microbiol.* 143, 203–208. doi: 10.1007/BF00411048

Koehorst, J. J., van Dam, J. C. J., Saccenti, E., Martins Dos Santos, V. A. P., Suarez-Diez, M., and Schaap, P. J. (2018). SAPP: functional genome annotation and analysis through a semantic framework using FAIR principles. *Bioinformatics* 34, 1401–1403. doi: 10.1093/bioinformatics/btx767

Koga, Y., Morn, H., Akagawa-Matsushita, M., and Ohga, M. (1998). Correlation of polar lipid composition with 16S rRNA phylogeny in methanogens. Further analysis of lipid component parts. *Biosci. Biotechnol. Biochem.* 62, 230–236. doi: 10.1271/bbb.62.230

Koga, Y., Nishihara, M., Morii, H., and Akagawa-Matsushita, M. (1993). Ether polar lipids of methanogenic bacteria: structures, comparative aspects, and biosyntheses. *Microbiol. Rev.* 57, 164–182. doi: 10.1128/mmbr.57.1.164-182.1993

Konstantinidis, K. T., and Tiedje, J. M. (2005). Towards a genome-based taxonomy for prokaryotes. *J. Bacteriol.* 187, 6258–6264. doi: 10.1128/JB.187.18.6258-6264.2005

Korehi, H., Blöthe, M., and Schippers, A. (2014). Microbial diversity at the moderate acidic stage in three different sulfidic mine tailings dumps generating acid mine drainage. *Res. Microbiol.* 165, 713–718. doi: 10.1016/j.resmic.2014.08.007

Krogh, A., Larsson, B., Von Heijne, G., and Sonnhammer, E. L. L. (2001). Predicting transmembrane protein topology with a hidden Markov model: application to complete genomes. *J. Mol. Biol.* 305, 567–580. doi: 10.1006/jmbi.2000.4315

Lagesen, K., Hallin, P., Rodland, E. A., Staerfeldt, H. H., Rognes, T., and Ussery, D. W. (2007). RNAmmer: consistent and rapid annotation of ribosomal RNA genes. *Nucleic Acids Res.* 35, 3100–3108. doi: 10.1093/nar/gkm160

Langmead, B., and Salzberg, S. L. (2012). Fast gapped-read alignment with bowtie 2. *Nat. Methods* 9, 357–359. doi: 10.1038/nmeth.1923

Larrouy-Maumus, G., Clements, A., Filloux, A., McCarthy, R. R., and Mostowy, S. (2016). Direct detection of lipid A on intact gram-negative bacteria by MALDI-TOF mass spectrometry. *J. Microbiol. Methods* 120, 68–71. doi: 10.1016/j.mimet.2015.12.004

Laslett, D., and Canback, B. (2004). ARAGORN, a program to detect tRNA genes and tmRNA genes in nucleotide sequences. *Nucleic Acids Res.* 32, 11–16. doi: 10.1093/nar/gkh152

Lee, Y. J., Romanek, C. S., and Wiegel, J. (2009). *Desulfosporosinus youngiae* sp. nov., a spore-forming, sulfate-reducing bacterium isolated from a constructed wetland treating acid mine drainage. *Int. J. Syst. Evol. Microbiol.* 59, 2743–2746. doi: 10.1099/ijs.0.007336-0

López-Archilla, A. I., Marin, I., and Amils, R. (2001). Microbial community composition and ecology of an acidic aquatic environment: the Tinto River, Spain. *Microb. Ecol.* 41, 20–35. doi: 10.1007/s002480000044

Lottermoser, B. G. (2010). "Tailings" in *Mine Wastes*. (Verlag Berlin Heidelberg: Springer), 205–241.

Ludwig, W., Strunk, O., Westram, R., Richter, L., and Meier, H. (2004). ARB: a software environment for sequence data. *Nucleic Acids Res.* 32, 1363–1371. doi: 10.1093/nar/gkh293

Madden, A. S., Palumbo, A. V., Ravel, B., Vishnivetskaya, T. A., Phelps, T. J., Schadt, C. W., et al. (2009). Donor-dependent extent of uranium reduction for bioremediation of contaminated sediment microcosms. *J. Environ. Qual.* 38, 53–60. doi: 10.2134/jeq2008.0071

Mardanov, A. V., Panova, I. A., Beletsky, A. V., Avakyan, M. R., Kadnikov, V. V., Antsiferov, D. V., et al. (2016). Genomic insights into a new acidophilic, copper-resistant *Desulfosporosinus* isolate from the oxidized tailings area of an abandoned gold mine. *FEMS Microbiol. Ecol.* 92, 1–14. doi: 10.1093/femsec/fiw111

Meador, T. B., Gagen, E. J., Loscar, M. E., Goldhammer, T., Yoshinaga, M. Y., Wendt, J., et al. (2014). *Thermococcus kodakarensis* modulates its polar membrane lipids and elemental composition according to growth stage and phosphate availability. *Front. Microbiol.* 5:10. doi: 10.3389/fmicb.2014.00010

Mori, K., Kim, H., Kakegawa, T., and Hanada, S. (2003). A novel lineage of sulfate-reducing microorganisms: *Thermodesulfobiaceae* fam. Nov., *Thermodesulfobium narugense*, gen. nov., sp. nov., a new thermophilic isolate from a hot spring. *Extremophiles* 7, 283–290. doi: 10.1007/s00792-003-0320-0

Ñancucheo, I., and Johnson, D. B. (2012). Selective removal of transition metals from acidic mine waters by novel consortia of acidophilic sulfidogenic bacteria. *Microb. Biotechnol.* 5, 34–44. doi: 10.1111/j.1751-7915.2011.00285.x

Ñancucheo, I., and Johnson, D. B. (2014). Removal of sulfate from extremely acidic mine waters using low pH sulfidogenic bioreactors. *Hydrometallurgy* 150, 222–226. doi: 10.1016/j.hydromet.2014.04.025

NCBI Resource Coordinators (2013). Database resources of the National Center for biotechnology information. *Nucleic Acids Res.* 41, D8–D20. doi: 10.1093/nar/gks1189

Nevin, K. P., Finneran, K. T., and Lovley, D. R. (2003). Microorganisms associated with uranium bioremediation in a high-salinity subsurface sediment. *Appl. Environ. Microbiol.* 69, 3672–3675. doi: 10.1128/AEM.69.6.3672-3675.2003

Nguyen, N.-N., Srihari, S., Leong, H. W., and Chong, K.-F. (2015). EnzDP: improved enzyme annotation for metabolic network reconstruction based on domain composition profiles. *J. Bioinforma. Comput. Biol.* 13:1543003. doi: 10.1142/S0219720015430039

Oger, P. M., and Cario, A. (2013). Adaptation of the membrane in Archaea. *Biophys. Chem.* 183, 42–56. doi: 10.1016/j.bpc.2013.06.020

Panova, I. A., Ikkert, O., Avakyan, M. R., Kopitsyn, D. S., Mardanov, A. V., Pimenov, N. V., et al. (2021). *Desulfosporosinus metallidurans* sp. Nov., an acidophilic, metal-resistant sulfate-reducing bacterium from acid mine drainage. *Int. J. Syst. Evol. Microbiol.* 71. doi: 10.1099/ijsem.0.004876

Pereira, I. A. C., Ramos, A. R., Grein, F., Marques, M. C., da Silva, S. M., Venceslau, S. S., et al. (2011). A Comparative genomic analysis of energy metabolism in sulfate reducing bacteria and archaea. *Front. Microbiol.* 2:69 doi: 10.3389/fmicb.2011.00069

Perez-Riverol, Y., Csordas, A., Bai, J., Bernal-Llinares, M., Hewapathirana, S., Kundu, D. J., et al. (2019). The PRIDE database and related tools and resources in 2019: improving support for quantification data. *Nucleic Acids Res.* 47, D442–D450. doi: 10.1093/nar/gky1106

Pester, M., Brambilla, E., Alazard, D., Rattei, T., Weinmaier, T., Han, J., et al. (2012). Complete genome sequences of *Desulfosporosinus orientis* DSM765T, *Desulfosporosinus youngiae* DSM17734T, *Desulfosporosinus meridiei* DSM13257T, and *Desulfosporosinus acidiphilus* DSM22704T. *J. Bacteriol.* 194, 6300–6301. doi: 10.1128/JB.01392-12

Petersen, T. N., Brunak, S., von Heijne, G., and Nielsen, H. (2011). SignalP 4.0: discriminating signal peptides from transmembrane regions. *Nat. Methods* 8, 785–786. doi: 10.1038/nmeth.1701

Petrie, L., North, N. N., Dollhopf, S. L., Balkwill, D. L., and Kostka, J. E. (2003). Enumeration and characterization of iron(III)-reducing microbial communities from acidic subsurface sediments contaminated with uranium(VI). *Appl. Environ. Microbiol.* 69, 7467–7479. doi: 10.1128/AEM.69.12.7467-7479.2003

Petzsch, P., Johnson, D. B., Daniel, R., and Schlömann, M. (2015). Genome sequence of the moderately acidophilic sulfate-reducing firmicute *Desulfosporosinus acididurans* (strain M1T). *Genome Announc.* 3, 5–6. doi: 10.1128/genomeA.00881-15.Copyright

Pires, R. H., Venceslau, S. S., Morais, F., Teixeira, M., Xavier, A. V., and Pereira, I. A. C. (2006). Characterization of the *Desulfovibrio desulfuricans* ATCC 27774 DsrMKJOP complex - A membrane-bound redox complex involved in the sulfate respiratory pathway. *Biochemistry* 45, 249–262. doi: 10.1021/bi0515265

Pruesse, E., Peplies, J., and Glöckner, F. O. (2012). SINA: accurate high-throughput multiple sequence alignment of ribosomal RNA genes. *Bioinformatics* 28, 1823–1829. doi: 10.1093/bioinformatics/bts252

Rabus, R., Venceslau, S. S., Wöhlbrand, L., Voordouw, G., Wall, J. D., and Pereira, I. A. C. (2015). A post-genomic view of the ecophysiology, catabolism and biotechnological relevance of sulphate-reducing prokaryotes. *Adv. Microb. Physiol.* 66, 55–321. doi: 10.1016/bs.ampbs.2015.05.002

Ragsdale, S. W., and Pierce, E. (2008). Acetogenesis and the wood-Ljungdahl pathway of CO_2 fixation. *Biochim. Biophys. Acta* 1784, 1873–1898. doi: 10.1016/j.bbapap.2008.08.012

Ramamoorthy, S., Sass, H., Langner, H., Schumann, P., Kroppenstedt, R. M., Spring, S., et al. (2006). *Desulfosporosinus lacus* sp. nov., a sulfate-reducing bacterium isolated from pristine freshwater lake sediments. *Int. J. Syst. Evol. Microbiol.* 56, 2729–2736. doi: 10.1099/ijs.0.63610-0

Ramos, A. R., Keller, K. L., Wall, J. D., and Pereira, I. A. (2012). The membrane QmoABC complex interacts directly with the dissimilatory adenosine 5′-phosphosulfate reductase in sulfate reducing bacteria. *Front. Microbiol.* 3:137. doi: 10.3389/fmicb.2012.00137

Robertson, W. J., Bowman, J. P., Franzmann, P. D., and Mee, B. J. (2001). *Desulfosporosinus meridiei* sp. nov., a spore-forming sulfate-reducing bacterium isolated from gasolene-contaminated groundwater. *Int. J. Syst. Evol. Microbiol.* 51, 133–140. doi: 10.1099/00207713-51-1-133

Rowe, O. F., Sánchez-España, J., Hallberg, K. B., and Johnson, D. B. (2007). Microbial communities and geochemical dynamics in an extremely acidic, metal-rich stream at an abandoned sulfide mine (Huelva, Spain) underpinned by two functional primary production systems. *Environ. Microbiol.* 9, 1761–1771. doi: 10.1111/j.1462-2920.2007.01294.x

Sánchez-Andrea, I., Florentino, A. P., Semerel, J., Strepis, N., Sousa, D. Z., and Stams, A. J. M. (2018). Co-culture of a novel fermentative bacterium, *Lucifera butyrica* gen. Nov. sp. nov., with the sulfur reducer *Desulfurella amilsii* for enhanced sulfidogenesis. *Front. Microbiol.* 9:3108. doi: 10.3389/fmicb.2018.03108

Sánchez-Andrea, I., Knittel, K., Amann, R., Amils, R., and Sanz, J. L. (2012a). Quantification of Tinto River sediment microbial communities: importance of sulfate-reducing bacteria and their role in attenuating acid mine drainage. *Appl. Environ. Microbiol.* 78, 4638–4645. doi: 10.1128/AEM.00848-12

Sánchez-Andrea, I., Rodriguez, N., Amils, R., and Sanz, J. L. (2011). Microbial diversity in anaerobic sediments at Rio Tinto, a naturally acidic environment with a high heavy metal content. *Appl. Environ. Microbiol.* 77, 6085–6093. doi: 10.1128/AEM.00654-11

Sánchez-Andrea, I., Rojas-Ojeda, P., Amils, R., and Sanz, J. L. (2012b). Screening of anaerobic activities in sediments of an acidic environment: Tinto River. *Extremophiles* 16, 829–839. doi: 10.1007/s00792-012-0478-4

Sánchez-Andrea, I., Stams, A. J. M., Amils, R., and Sanz, J. L. (2013). Enrichment and isolation of acidophilic sulfate-reducing bacteria from Tinto River sediments. *Environ. Microbiol. Rep.* 5, 672–678. doi: 10.1111/1758-2229.12066

Sánchez-Andrea, I., Stams, A. J. M., Hedrich, S., Ňancucheo, I., and Johnson, D. B. (2015). *Desulfosporosinus acididurans* sp. nov.: an acidophilic sulfate-reducing bacterium isolated from acidic sediments. *Extremophiles* 19, 39–47. doi: 10.1007/s00792-014-0701-6

Sánchez-España, J., Yusta, I., Ilin, A., van der Graaf, C. M., and Sánchez-Andrea, I. (2020). Microbial geochemistry of the acidic saline pit lake of Brunita mine (La Unión, SE Spain). *Mine Water Environ.* 39, 535–555. doi: 10.1007/s10230-020-00655-0

Sand, W., Gehrke, T., Jozsa, P.-G., and Schippers, A. (2001). (bio)chemistry of bacterial leaching—direct vs. indirect bioleaching. *Hydrometallurgy* 59, 159–175. doi: 10.1016/S0304-386X(00)00180-8

Santofimia, E., González-Toril, E., López-Pamo, E., Gomariz, M., Amils, R., and Aguilera, Á. (2013). Microbial diversity and its relationship to physicochemical characteristics of the water in two extreme acidic pit lakes from the Iberian Pyrite Belt (SW Spain). *PLoS One* 8, 1–12. doi: 10.1371/journal.pone.0066746

Santos, A. A., Venceslau, S. S., Grein, F., Leavitt, W. D., Dahl, C., Johnston, D. T., et al. (2015). A protein trisulfide couples dissimilatory sulfate reduction to energy conservation. *Science* 350, 1541–1545. doi: 10.1126/science.aad3558

Sebban, C., Blanchard, L., Bruschi, M., and Guerlesquin, F. (1995). Purification and characterization of the formate dehydrogenase from *Desulfovibrio vulgaris* Hildenborough. *FEMS Microbiol. Lett.* 133, 143–149. doi: 10.1016/0378-1097(95)00339-7

Senko, J. M., Zhang, G., McDonough, J. T., Bruns, M. A., and Burgos, W. D. (2009). Metal reduction at low pH by a *Desulfosporosinus* species: implications for the biological treatment of acidic mine drainage. *Geomicrobiol J.* 26, 71–82. doi: 10.1080/01490450802660193

Seshadri, R., Leahy, S. C., Attwood, G. T., Teh, K. H., Lambie, S. C., Cookson, A. L., et al. (2018). Cultivation and sequencing of rumen microbiome members from the Hungate1000 collection. *Nat. Biotechnol.* 36, 359–367. doi: 10.1038/nbt.4110

Siliakus, M. F., van der Oost, J., and Kengen, S. W. M. (2017). Adaptations of archaeal and bacterial membranes to variations in temperature, pH and pressure. *Extremophiles* 21, 651–670. doi: 10.1007/s00792-017-0939-x

Sinninghe Damsté, J., Rijpstra, W. I., Hopmans, E. C., Weijers, J. W., Foesel, B. U., Overmann, J., et al. (2011). 13,16-dimethyl octacosanedioic acid (iso-diabolic acid), a common membrane-spanning lipid of Acidobacteria subdivisions 1 and 3. *Appl. Environ. Microbiol.* 77, 4147–4154. doi: 10.1128/AEM.00466-11

Slonczewski, J. L., Fujisawa, M., Dopson, M., and Krulwich, T. A. (2009). "Cytoplasmic pH measurement and homeostasis in bacteria and Archaea," in *Advances in Microbial Physiology* (Elsevier), 1–317.

Sohlenkamp, C. (2017). Biogenesis of fatty acids, lipids and membranes. *Biog. Fat. Acids, Lipids Membr.* 1–13. doi: 10.1007/978-3-319-43676-0

Spring, S., and Rosenzweig, F. (2006). "The genera *Desulfitobacterium* and *Desulfosporosinus*: taxonomy," in *The Prokaryotes. 3rd Edn.* eds. M. Dworkin (Editor-in-Chief), S. Falkow, E. Rosenberg, K.-H. Schleifer and E. Stackebrandt (NY: Springer).

Spurr, A. R. (1969). A low-viscosity epoxy resin embedding medium for electron microscopy. *J. Ultrastruct. Res.* 26, 31–43. doi: 10.1016/S0022-5320(69)90033-1

Stackebrandt, E., Sproer, C., Rainey, F. A., Burghardt, J., Pauker, O., and Hippe, H. (1997). Phylogenetic analysis of the genus *Desulfotomaculum*: evidence for the misclassification of *Desulfotomaculum guttoideum* and description of *Desulfotomaculum orientis* as *Desulfosporosinus orientis* gen. nov., comb. nov. *Int. J. Syst. Evol. Microbiol.* 47, 1134–1139. doi: 10.1099/00207713-47-4-1134

Suzuki, Y., Kelly, S. D., Kemner, K. M., and Banfield, J. F. (2004). Enzymatic U(VI) reduction by *Desulfosporosinus* species. *Radiochim. Acta* 92, 11–16. doi: 10.1524/ract.92.1.11.25404

Tindall, B. J. (1990a). A comparative study of the lipid composition of *Halobacterium saccharovorum* from various sources. *Syst. Appl. Microbiol.* 13, 128–130. doi: 10.1016/S0723-2020(11)80158-X

Tindall, B. J. (1990b). Lipid composition of *Halobacterium lacusprofundi*. *FEMS Microbiol. Lett.* 66, 199–202. doi: 10.1111/j.1574-6968.1990.tb03996.x

UniProt, C. (2014). Activities at the universal protein resource (UniProt). *Nucleic Acids Res.* 42, D191–D198. doi: 10.1093/nar/gkt1140

Utkin, I., Woese, C. R., and Wiegel, J. (1994). Isolation and characterization of *Desulfitobacterium dehalogenans* gen. Nov., sp. nov., an anaerobic bacterium which reductively dechlorinates chlorophenolic compounds. *Int. J. Syst. Bacteriol.* 44, 612–619. doi: 10.1099/00207713-44-4-612

van der Graaf, C. M., Sánchez-España, J., Yusta, I., Ilin, A., Shetty, S. A., Bale, N. J., et al. (2020). Biosulfidogenesis mediates natural attenuation in acidic mine pit lakes. *Microorganisms* 8, 1–26. doi: 10.3390/microorganisms8091275

Walker, B. J., Abeel, T., Shea, T., Priest, M., Abouelliel, A., Sakthikumar, S., et al. (2014). Pilon: an integrated tool for comprehensive microbial variant detection and genome assembly improvement. *PLoS One* 9:e112963. doi: 10.1371/journal.pone.0112963

Wang, S., Huang, H., Moll, J., and Thauer, R. K. (2010). $NADP^+$ reduction with reduced ferredoxin and $NADP^+$ reduction with NADH are coupled via an electron-bifurcating enzyme complex in *clostridium kluyveri*. *J. Bacteriol.* 192, 5115–5123. doi: 10.1128/JB.00612-10

Wendt-Potthoff, K., Koschorreck, M., Diez Ercilla, M., and Sánchez España, J. (2012). Microbial activity and biogeochemical cycling in a nutrient-rich meromictic acid pit lake. *Limnologica* 42, 175–188. doi: 10.1016/j.limno.2011.10.004

Winch, S., Mills, H. J., Kostka, J. E., Fortin, D., and Lean, D. R. S. (2009). Identification of sulfate-reducing bacteria in methylmercury-contaminated mine tailings by analysis of SSU rRNA genes. *FEMS Microbiol. Ecol.* 68, 94–107. doi: 10.1111/j.1574-6941.2009.00658.x

Wright, E. S., Yilmaz, L. S., and Noguera, D. R. (2012). DECIPHER, a search-based approach to chimera identification for 16S rRNA sequences. *Appl. Environ. Microbiol.* 78, 717–725. doi: 10.1128/AEM.06516-11

Yarza, P., Richter, M., Peplies, J., Euzeby, J., Amann, R., Schleifer, K.-H., et al. (2008). The all-species living tree project: A 16S rRNA-based phylogenetic tree of all sequenced type strains. *Syst. Appl. Microbiol.* 31, 241–250. doi: 10.1016/j.syapm.2008.07.001

Yarza, P., Yilmaz, P., Pruesse, E., Glöckner, F. O., Ludwig, W., Schleifer, K. H., et al. (2014). Uniting the classification of cultured and uncultured bacteria and archaea using 16S rRNA gene sequences. *Nat. Rev. Microbiol.* 12, 635–645. doi: 10.1038/nrmicro3330

Young, G. M., Amid, D., and Miller, V. L. (1996). A bifunctional urease enhances survival of pathogenic Yersinia enterocolitica and Morganella morganii at low pH. *J. Bacteriol.* 178, 6487–6495. doi: 10.1128/jb.178.22.6487-6495.1996

Zwietering, M. H., Jongenburger, I., Rombouts, F. M., and van 't Riet, K., (1990). Modeling of the bacterial growth curve. *Appl. Environ. Microbiol.* 56, 1875–1881. doi: 10.1128/aem.56.6.1875-1881.1990

Conflict of Interest: The authors declare that the research was conducted in the absence of any commercial or financial relationships that could be construed as a potential conflict of interest.

Publisher's Note: All claims expressed in this article are solely those of the authors and do not necessarily represent those of their affiliated organizations, or those of the publisher, the editors and the reviewers. Any product that may be evaluated in this article, or claim that may be made by its manufacturer, is not guaranteed or endorsed by the publisher.

frontiers | Frontiers in Microbiology

ORIGINAL RESEARCH
published: 18 April 2022
doi: 10.3389/fmicb.2022.848410

Prediction and Inferred Evolution of Acid Tolerance Genes in the Biotechnologically Important *Acidihalobacter* Genus

Katelyn Boase[1†], Carolina González[2†], Eva Vergara[2], Gonzalo Neira[2], David Holmes[2,3] and Elizabeth Watkin[1]**

[1] Curtin Medical School, Curtin University, Perth, WA, Australia, [2] Center for Bioinformatics and Genome Biology, Centro Ciencia & Vida, Santiago, Chile, [3] Facultad de Medicina y Ciencias, Universidad San Sebastián, Santiago, Chile

OPEN ACCESS

Edited by:
Claudia P. Saavedra, Andres Bello University, Chile

Reviewed by:
Mario Tello, University of Santiago, Chile
Daniel Aguayo, Universidad Andres Bello, Santiago, Chile

***Correspondence:**
David S. Holmes
dsholmes2000@yahoo.com
Elizabeth Watkin
E.Watkin@curtin.edu.au

[†]These authors share first authorship

Specialty section:
This article was submitted to Extreme Microbiology, a section of the journal Frontiers in Microbiology

Received: *04 January 2022*
Accepted: *28 February 2022*
Published: *18 April 2022*

Citation:
Boase K, González C, Vergara E, Neira G, Holmes D and Watkin E (2022) Prediction and Inferred Evolution of Acid Tolerance Genes in the Biotechnologically Important Acidihalobacter Genus. Front. Microbiol. 13:848410. doi: 10.3389/fmicb.2022.848410

Acidihalobacter is a genus of acidophilic, gram-negative bacteria known for its ability to oxidize pyrite minerals in the presence of elevated chloride ions, a capability rare in other iron-sulfur oxidizing acidophiles. Previous research involving *Acidihalobacter* spp. has focused on their applicability in saline biomining operations and their genetic arsenal that allows them to cope with chloride, metal and oxidative stress. However, an understanding of the molecular adaptations that enable *Acidihalobacter* spp. to thrive under both acid and chloride stress is needed to provide a more comprehensive understanding of how this genus can thrive in such extreme biomining conditions. Currently, four genomes of the *Acidihalobacter* genus have been sequenced: *Acidihalobacter prosperus* DSM 5130^T, *Acidihalobacter yilgarnensis* DSM 105917^T, *Acidihalobacter aeolianus* DSM 14174^T, and *Acidihalobacter ferrooxydans* DSM 14175^T. Phylogenetic analysis shows that the *Acidihalobacter* genus roots to the Chromatiales class consisting of mostly halophilic microorganisms. In this study, we aim to advance our knowledge of the genetic repertoire of the *Acidihalobacter* genus that has enabled it to cope with acidic stress. We provide evidence of gene gain events that are hypothesized to help the *Acidihalobacter* genus cope with acid stress. Potential acid tolerance mechanisms that were found in the *Acidihalobacter* genomes include multiple potassium transporters, chloride/proton antiporters, glutamate decarboxylase system, arginine decarboxylase system, urease system, *slp* genes, squalene synthesis, and hopanoid synthesis. Some of these genes are hypothesized to have entered the *Acidihalobacter* via vertical decent from an inferred non-acidophilic ancestor, however, horizontal gene transfer (HGT) from other acidophilic lineages is probably responsible for the introduction of many acid resistance genes.

Keywords: polyextremophile, extreme acidophile, acid resistance, genome evolution, phylogenomics, potassium transporters, urease, chloride/proton antiporters

INTRODUCTION

Environments that exhibit both acidic and saline conditions are relatively rare. There are few studies aimed at understanding acid stress responses in halophiles and these typically show that halophiles are unable to grow in low pH environments (Bowers and Wiegel, 2011; Moran-Reyna and Coker, 2014; He et al., 2016; Zammit and Watkin, 2016). For example, it has been hypothesized that chloride ions, present in saline conditions, can disrupt the reversed membrane potential of acidophiles making them potentially sensitive to acidification of their cytoplasm followed by subsequent cellular death (Suzuki et al., 1999).

Acidihalobacter is one of a limited number of genera of bacteria that has been shown to be an extreme acidophile (pH $\leq$ 3.0) and halophile (Minegishi, 2013; Zammit and Watkin, 2016) and is thus a polyextremophile. Currently four organisms belonging to the *Acidihalobacter* genus have been isolated and cultivated in laboratory conditions: *Acidihalobacter prosperus* DSM 5130^{T} from the geothermally heated seafloor at Porto di Levante, Vulcano, Italy; *Acidihalobacter aeolianus* DSM 14174^{T}, and *Acidihalobacter ferrooxydans* DSM 14175^{T} from the hydrothermal pools at the Aeolian Islands, Vulcano Italy and *Acidihalobacter yilgarnensis* DSM 105917^{T} from an acidic saline lake drain in Western Australia (Huber and Stetter, 1989; Simmons and Norris, 2002; Zammit et al., 2009). Several studies have been conducted on the *Acidihalobacter* genus, understanding its response to chloride ions, osmotic stress, metal stress and oxidative stress (Dopson et al., 2016; Khaleque et al., 2018, 2019, 2020) but there has been limited focus on their mechanisms of survival at extremely low pH. The *Acidihalobacter* are interesting not only because they are deeply intriguing polyextremophiles but also because they are among the few organisms that can be used for copper recovery (bioleaching) from chalcopyrite (Khaleque et al., 2017a). Extreme acidophiles capable of oxidizing iron and sulfur have been of interest to the scientific and industrial communities regarding their biotechnological and biomining applications (Johnson and Schippers, 2017; Gumulya et al., 2018) and their potential in protein engineering (Parashar and Satyanarayana, 2018).

Acidophilic microorganisms are found in all three domains of life. When describing acid stress responses in microorganisms, it is useful to make a distinction between "extreme" acidophiles (pH opt $<$ 3.0) and "moderate" acidophiles (pH opt between 3 and 5). Both share multiple acid tolerance mechanisms, however, extreme acidophiles have additional adaptations absent in moderate acidophiles (reviewed in Baker-Austin and Dopson, 2007). Both categories of acidophiles thrive in acidic conditions by maintaining a circumneutral cytoplasmic pH despite a large proton gradient compared to their environment. In contrast, another class of acidophiles, the so-called "amateur" acidophiles, e.g., *Helicobacter pylori*, survive by neutralizing their acidic environment (Foster, 2004; Baker-Austin and Dopson, 2007; Slonczewski et al., 2009; Quatrini and Barrie Johnson, 2016). The maintenance of a circumneutral cytoplasmic pH is achieved through multiple mechanisms including the generation of a reversed membrane potential, creating a positive charge, referred to as the Donnan potential. This chemi-osmotic barrier effectively repels positive ions from entering the cell, preventing the acidification of their cytoplasm and has been defined as the first line of defense (Vergara et al., 2020). The use of potassium transporters, importing K^{+} ions, are thought to be the most likely mechanism acidophiles use to generate this membrane potential (Cholo et al., 2015; Buetti-Dinh et al., 2016; Christel et al., 2018). The potassium channel transporters Kdp, Trk, and Kch have been identified in extreme acidophiles (Cholo et al., 2015; Buetti-Dinh et al., 2016; Christel et al., 2018; Vergara et al., 2020). Extreme acidophiles are also hypothesized to have membranes that are less permeable to protons through membrane adaptations (Yamauchi et al., 1993; Macalady et al., 2004; Chao et al., 2008; Mykytczuk et al., 2010). Hopanoids, spermidine, and starvation-inducible membrane-altering lipoproteins are all associated with conferring a higher resistance to proton permeability (Alexander and St John, 1994; Hommais et al., 2004; Jones et al., 2012). Second line of defense mechanisms (Vergara et al., 2020) describe processes that consume or expel protons that have entered the cell including buffering reactions, for example the glutamate decarboxylase system, the arginine decarboxylase system, spermidine synthesis, the urease system and Na^{+}/H^{+} antiporters (Hommais et al., 2004; Richard and Foster, 2004; Zhao and Houry, 2010; Feehily and Karatzas, 2013; Mangold et al., 2013; Marcus and Scott, 2016). These mechanisms are commonly found in both extreme and moderate acidophiles. To deepen our understanding of acid stress response in the *Acidihalobacter* genus, a genome-wide comparison study was undertaken to generate an inventory of predicted acid resistance genes. Using phylogenomic approaches, we suggest possible events, including gene gain/loss and gene duplication, that led to the evolution of the acidophilic *Acidihalobacter* from an inferred non-acidophilic ancestor.

MATERIALS AND METHODS

Genomes and Phylogenetic Analysis

The four currently published *Acidihalobacter* assembly sequences (GCF_000754095.2, GCF_001753245.1, GCF_001753165.1 and GCF_001975725.1) as well as the outgroup *Halothiobacillus neapolitanus* c2 (GCF_000024765.1) were downloaded from the National Center for Biotechnology Information (NCBI) GenBank genomic database in October 2019 (Pruitt et al., 2012). Phylogenetic analysis of four *Acidihalobacter* genomes in the context of the Chromatiales order was conducted using 52 NCBI reference proteomes of the Chromatiales order available from the GenBank database (**Supplementary Table 1**) in October 2019. PhyloPhlAn3 was used to construct a phylogenetic tree of the Chromatiales proteomes, using the Phylophlan database and diversity set to low (set of 400 conserved proteins) (Asnicar et al., 2020). Diamond (Buchfink et al., 2015) was used for mapping the database to the proteomes in study, MAFFT (Katoh and Standley, 2013) for the multiple sequence alignment and the maximum likelihood tree was constructed with IQTREE (Nguyen et al., 2015), using 1000 replicates, with the best suited evolutionary

model proposed by IQTREE. The final tree was visualized using iTOL.[1]

Prediction of Mobile Genetic Elements and Genome Islands

Mobile genetic elements (MGEs) were predicted and classified using TnpPred and ISsaga (Siguier et al., 2006; Varani et al., 2011; Riadi et al., 2012). Horizontal gene transfer events were predicted by HGTector (Waack et al., 2006; Zhu et al., 2014). Genome context of mobile elements and genome islands were analyzed using STRING, MAUVE, and ARTEMIS (Darling et al., 2010; Carver et al., 2012; Szklarczyk et al., 2019). These bioinformatic tools were used to predict genes involved in mechanisms of HGT (see **Supplementary Information 1**).

Identification of Genes Related to Low pH Resistance

Genes and mechanisms involved in acidic resistance were identified through previous research (Vergara et al., 2020; González-Rosales et al., 2022). Identification of these genes in the *Acidihalobacter* genus genomes and the outgroup was done using BlastP comparison with a minimum E-value cutoff of $1e^{-5}$. Synteny blocks were predicted and visualized using MAUVE Progressive alignment (Darling et al., 2010). Genome contexts were visualized using Artemis (Carver et al., 2012). Acid tolerance proteins found in the *Acidihalobacter* genomes and *H. neapolitanus* were back-blast to assess orthologous proteins in other organisms. To assess the relatedness of these proteins, phylogenetic trees were made as previously described in section 2.1 using MAFFT, IQTREE, and iTOL.

Mapping Evolutionary Events

To infer branch-site-specific evolutionary events across genomes of the *Acidihalobacter* genus, a conserved markers tree of 400 proteins was constructed between the *Acidihalobacter* genomes and using *H. neapolitanus* c2 as outgroup using Phylophlan3 (Asnicar et al., 2020). The presence of genes predicted to be involved in acid resistance were mapped onto each branch of the phylogenomic tree to model gene gain and loss events. Inference of evolutionary events were based on parsimony criteria.

RESULTS AND DISCUSSION

Genomic Features of the Acidihalobacter Genus

Acidihalobacter spp. are aerobic, chemolithotrophic, mesophilic, halotolerant acidophiles with pH optimums between 1.9 and 2.75. The four publicly available *Acidihalobacter* genomes were analyzed together with the *H. neapolitanus* outgroup genome (**Table 1**). *A. yilgarnensis* is the only complete genome of the *Acidihalobacter*, with the other three being high quality permanent draft genomes. GC% content between the *Acidihalobacter* genomes varies between 59.9 and 64.4%. *Acidihalobacter* genomes are larger than the *H. neapolitanus* c2 outgroup genome with a range of 0.78–0.99 Mb.

[1]https://itol.embl.de/

Phylogeny of *Acidihalobacter* Within the Chromatiales Order

To understand the recent evolutionary history of the *Acidihalobacter* genus, we compared the relative chloride and acid tolerance of microbes in the Chromatiales order to that of the *Acidihalobacter* spp. Using the complete reference genomes in the Chromatiales order, a phylogenetic tree was constructed, and literature was reviewed to identify the chloride and acid tolerances of the genomes used (**Figure 1**). Most microbes in the Chromatiales order were halotolerant and either neutrophilic or alkaliphilic. The *Acidihalobacter* microbes were the only microbes in the Chromatiales order that tolerate pH environments below four. This is an indication that *Acidihalobacter* has likely evolved from a halophilic past and has gained the ability to cope with acidic stress.

Acid Resistance: First Line of Defense

"First line of defense" (Vergara et al., 2020) mechanisms are involved in reducing the influx of protons into the cytoplasm of acidophiles. Potassium pumps are primarily responsible for this by creating the reversed membrane potential, limiting proton influx (reviewed in Quatrini and Barrie Johnson, 2016). Membrane alterations that limit proton permeability across the cellular membrane also fall under the "first line of defense" mechanisms and include hopanoid synthesis, Slp proteins and porin alterations, as described in the following sections.

Membrane Potential and Potassium Transporters

Potassium transport systems are found in many bacteria as potassium is the major intracellular cation responsible for osmotic regulation, activating intracellular enzymes, regulating internal pH and as a secondary messenger (Epstein, 2003; Korolev, 2021; Raven, 2021). It is widely accepted that potassium transporters are regulated by ion concentrations and turgor pressure (Epstein, 2003). In terms of acid tolerance in extreme acidophiles, potassium transporters are hypothesized to be responsible for the reversed membrane potential, which is the primary mechanism reducing proton influx (Baker-Austin and Dopson, 2007). In halophiles, it has been shown that potassium transport systems aid in osmotic stress and typically halophiles have multiple copies of potassium transport genes (Epstein, 2003; Kraegeloh et al., 2005; Mongodin et al., 2005).

The Trk potassium system symports K^+ and H^+ into the cell and has been identified in plants, Bacteria and Archaea (reviewed in Epstein, 2003; Pandey and Mahiwal, 2020). In prokaryotes the most studied Trk system is in *Escherichia coli* and consists of TrkH and TrkG, the multimeric functional transporters; TrkA, the cytoplasmic regulating subunit; and TrkE (also known as *sapD*), the ATP-binding component of the Trk system (Epstein, 2003; reviewed in Stautz et al., 2021). In *E. coli,* the genes involved in the Trk system are distributed throughout the genome, however in halophilic organisms *trk*A and *trk*H have been found clustered together (Nakamura et al., 1998; Kraegeloh et al., 2005). Many acidophile genomes lack *trk*HG,

TABLE 1 | Genomic information of the *Acidihalobacter* spp. genomes and *Halothiobacillus neapolitanus* genome used in the study.

Genome	Size (Mb)	No. predicted genes	G+C (%)	Stat-us	RefSeq Assembly Accession	Origin	pH optima [range]	NaCl (M) optima [range]	Ref
A. prosperus^T DSM 5130	3.36	3264	64.4	D	GCF_000754095.2	Italy	2 [1–4.5]	0.34 [0.07–1]	Nicolle et al., 2009; Ossandon et al., 2014
A. yilgarnensis^T DSM 105917	3.57	3459	59.9	C	GCF_001753245.1	WA	2.5 [2–4]	0.4 [0.005–1.28]	Khaleque et al., 2017a
A. aeolianus^T DSM 14174	3.36 (0.16)	3234 (165)	62.1 (57.3)	D (C)	GCF_001753165.1	Italy	1.8 [1.5–3]	0.4 [0.06–1.28]	Khaleque et al., 2017c
A. ferrooxydans^T DSM 14175	3.45	3220	61.6	D	GCF_001975725.1	Italy	1.8 [1–3]	0.4 [0.06–0.85]	Khaleque et al., 2017b
H. neapolitanus c2 DSM 15147	2.58	2407	54.7	C	GCF_000024765.1	VA	6.5–6.9 [3-8.5]	0-0.86 [ND]	Boden, 2017; Kelly and Wood, 2000

A. aeolianus is the only species to have a plasmid (termed pABPV6, displayed in parentheses). D, draft genome; C, closed (finished) genome. Square brackets show the range of pH and NaCl for growth. WA, Western Australia; VA, Victoria Australia.

and only contain the *trk*A homolog (exception *Alicyclobacillus ferrooxidans*) (Rivera-Araya et al., 2020). In *Acidihalobacter* spp. and *H. neapolitanus c2* the TrkAH potassium transporter system was present. The system is in a highly conserved syntenic region in all genomes and the genes are arranged contiguously (**Supplementary Figure 1**). A second copy of *trk*H was also found in the *Acidihalobacter* genomes directly downstream of the first *trk*H copy. The genomic arrangement of the Trk system in *Acidihalobacter* and *H. neapolitanus* c2 is very similar to that found in *Vibrio alinolyticus* (a halophile) with *fmt* (methionyl-tRNA formyltransferase) and *rsmB* (a ribosomal RNA small subunit methyltransferase B, also identified as *fmu* in other bacteria) being present upstream of *trk*A (**Supplementary Figure 1**) (Nakamura et al., 1998). Three extra genes were found between *rsm*B and *trk*A in *Acidihalobacter* and *H. neapolitanus,* a predicted gene that produces a protein with an unknown function, a histidine kinase, and a sigma-54 RNA polymerase holoenzyme. Both the histidine kinase and σ-54 proteins are predicted to be nitrogen regulated and involved in nitrogen assimilation (*ntr*Y and *ato*C also known as *ntr*X). Trk proteins have been identified in the genomes of other acidophiles such as *Leptospirillum* (Vergara et al., 2020), however, information about how the Trk system is arranged in their genome is lacking. No other case of a Trk system with two adjacent TrkH proteins has been published. Multiple copies of *trk*A and *trk*H have been found in the same region in *Salinibacter ruber*, however, they are not juxtaposed (López-Pérez et al., 2013). Whether this alteration results in a more efficient adaptation to acidity or salinity remains to be explored. Evidence of HGT in the genome surrounding the Trk system in *Acidihalobacter* was not found, and phylogenetic analysis of the protein sequences and their best BlastP hits show the *Acidihalobacter* TrkH proteins clustering with other TrkH proteins found in other organisms in the same Chromatiales order (**Supplementary Figure 2**). In light of the Trk system being in a highly conserved region of the genome in both *Acidihalobacter* and *H. neapolitanus* c2 and the Trk proteins all clustering with Trk proteins in the Chromatiales order, vertical descent of the Trk system in *Acidihalobacter* is likely. Whether the alteration of the gene structure in *Acidihalobacter* and *H. neapolitanus* when compared to Trk systems in other halophiles results in differential control or efficiency of Trk in these bacteria remains to be investigated.

Kdp is a high-affinity potassium transport system known to be involved in potassium homeostasis and the osmotic stress response in many bacteria, encompassing halophiles and non-halophiles, and is responsible for the active influx of potassium ions in environments with low potassium concentrations (Epstein, 2003; Strahl and Greie, 2008; Kixmüller et al., 2011; Price-Whelan et al., 2013). The Kdp system is also present in many acidophiles and has been found to be actively transcribed in acidic environments (Bakker et al., 1987; Acuña et al., 2013; Cholo et al., 2015; Rivera-Araya et al., 2019, 2020; Vergara et al., 2020). In *E. coli* the Kdp system consists of two operons, one encompassing the structural genes *kdp*FABC, and the other encompassing the regulatory genes *kdp*DE (Walderhaug et al., 1992). These two operons overlap in *E. coli,* however, different genetic arrangements of the system are found in other bacteria (Walderhaug et al., 1992; Epstein, 2003). KdpF is involved in stabilizing the Kdp complex but is not essential. KdpA is responsible for binding and translocating the K^+ and KdpB and KdpC are responsible for the ATP hydrolysis (Hesse et al., 1984; Gaßel et al., 1998, 1999; Dorus et al., 2001; Reviewed in Epstein, 2003). The *kdp*DE operon is a two-component response regulator responsible for regulating the Kdp complex as KdpD is a histidine kinase and KdpE is a response regulator (Walderhaug et al., 1992; Reviewed in Epstein, 2003). The Kdp system was only identified in the genome of *A. aeolianus.* The gene arrangement of the system was similar to that of *E. coli* (**Supplementary Figure 3A**) (Walderhaug et al., 1992). Both carbonic anhydrase (*can*) and the sigma-54 regulator (σ-54) have been identified in the same genomic context and previously have been indicated to be involved in acid tolerance of other microorganisms (Sachs et al., 2006; Bury-Moneì et al., 2008; Mitra et al., 2012, 2014). HGTector analysis predicts KdpA, KdpB, KdpC, KdpD, KdpE, and the

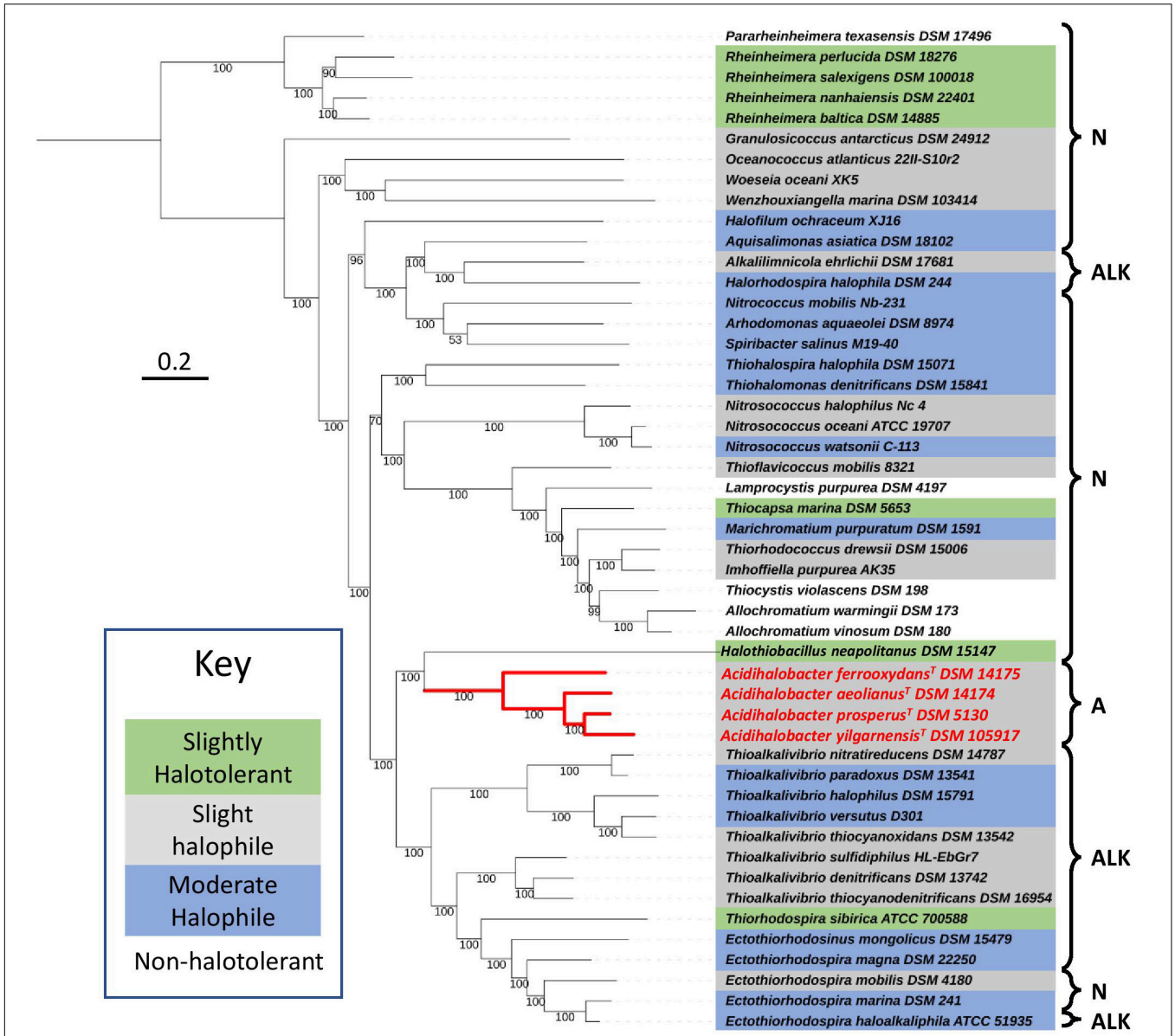

FIGURE 1 | Phylogenomic tree constructed, using 400 protein markers of 52 representative complete genomes of the Chromatiales order, using the Phylophlan3 program. Gray highlights slightly halophilic genomes (optimum growth 2–5% w/v NaCl), blue highlights moderately halophilic genomes (optimum growth 5–20% w/v NaCl), green highlights slightly halotolerant genomes (no NaCl required to grow however optimum growth in 2–8% w/v NaCl) and no highlight represents non-halophiles. A, acidophiles (optimum growth < pH 5); N, neutrophiles (optimum growth between pH 5 and 9); and ALK, alkaliphiles (optimum growth > pH 9). Red lines indicate the phylogenetic relationships between the acidophiles. The sequences were aligned with MAFFT and the concatenated alignment was used to construct the phylogenetic tree with IQTREE and LG+R3 as the best-suited evolutionary model. Scale bar indicates 0.2 substitutions per amino acid. See **Supplementary Table 1** for the full information on the microorganisms used in the tree.

sigma-54 transcription regulator to have been gained through HGT from a Bacteria, and the *can* from a Proteobacteria. The sigma-54 regulator, a hypothetical zinc-containing protein and the *can* upstream of the Kdp system all have significant similarity to their corresponding proteins in multiple *Acidithiobacillus* spp. (*Acidithiobacillus ferriphilus* and *Acidithiobacillus ferrivorans*) as well as the closely related *Ambacidithiobacillus sulfuriphilus* and *Fervidacidithiobacillus caldus* acidophiles. The lack of *kdp* genes in all other *Acidihalobacter* genomes and the outgroup suggests it has been acquired via HGT, as well as the genes and gene contexts having significant similarity to species in the Burkholderiales order. We propose that the Kdp system in *A. aeolianus* was a result of HGT and has the potential to aid acid tolerance in low potassium environments.

Kch is a voltage-gated membrane potassium transporter commonly found in plants but has also been identified in *E. coli*, although its biological role is currently not understood (Reviewed in Epstein, 2003; Lundbäck et al., 2009). In eukaryotes, it is

recognized as a voltage-gated ion channel that is associated with membrane potential regulation (Capera et al., 2019). The Kch protein was identified in all *Acidihalobacter* genomes and was not identified in *H. neapolitanus*. Best-hit analysis of the Kch proteins to the NCBI BlastP non-redundant database revealed that the Kch proteins in *Acidihalobacter* have significant similarity (46–53%) to Kch proteins from the acidophiles, *F. caldus* and *Am. sulfuriphilus*. *put*A (a bifunctional proline dehydrogenase/L-glutamate gamma-semialdehyde dehydrogenase) was found closely associated with *kch* in *A. yilgarnensis* and *A. prosperus* and is known to be involved in osmotolerance. Phylogenetic analysis, however, shows the Kch proteins from *Acidihalobacter* clustering closely to Kch proteins from other Chromatiales, and not the acidophiles Kch proteins (see **Supplementary Figure 4**). As Kch proteins are present, and cluster closely to the Chromatiales proteins, it is likely the Kch protein is a result of vertical decent in the *Acidihalobacter* genomes. The proximity of the *kch* to other osmotic tolerance genes may point to this area of the genome being important to both acid and osmotolerance in *Acidihalobacter*.

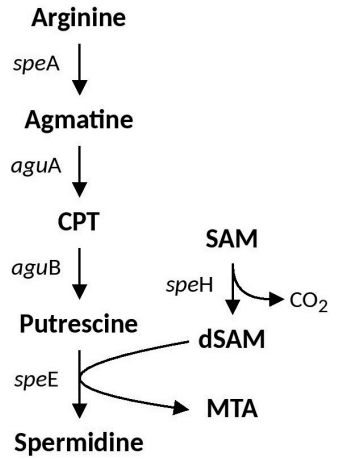

FIGURE 2 | Spermidine biosynthesis pathway identified in *Acidihalobacter*. CPT, N-carbamoylputrescine; SAM, S-Adenosyl methionine; dSAM, decarboxylated-Adenosyl methionine; MTA, methylthioadenosine.

Spermidine Biosynthesis and Associated Genes

Spermidine is a positively charged membrane associated aliphatic, polycation polyamine that is possibly involved in acid and osmotic stress responses in *E. coli* and has been shown to reduce the outer membrane permeability caused by porins (Samartzidou et al., 2003). Spermidine biosynthesis pathways vary between bacterial species. Arginine is the precursor which can either be converted to citrulline or ornithine (via ArcB and RocF, respectively) which is then converted to putrescine (via SpeC) and subsequently converted to Spermidine via SpeE. An alternative pathway also includes arginine conversion to agmatine (AguA), which can be either converted directly to putrescine via SpeB, or to an intermediate CPT by AguA. The full spermidine biosynthesis pathway identified in *Acidihalobacter* is summarized in **Figure 2**. Both *spe*E and *spe*H (involved in the production of dSAM important in the conversion of putrescine to spermidine) were identified in all *Acidihalobacter* genomes and had significant similarity (66–68%) to SpeE and (73–79%) SpeH proteins in the closely related sister clade *Thioalkalivibrio* genus and other bacteria in the Chromatiales order. *spe*E is found in the same genomic context as the urease accessory genes. *spe*H is in a separate part of the genome that is also conserved between the *Acidihalobacter* genomes. Genes involved in osmotic tolerance are found upstream of *spe*H including *yhf* A (a protein belonging to the osmotically inducible OsmC superfamily). As spermidine has been shown to be involved in both acid and osmotic stress responses, it is likely that spermidine synthesis in *Acidihalobacter* has been acquired via vertical descent from a common ancestor considering the presence of spermidine genes in other organisms from Chromatiales order and has possibly been lost in the *H. neapolitanus* outgroup genome.

Hopanoid Biosynthesis

Hopanoid biosynthesis is hypothesized to be involved in regulating the fluidity and permeability of bacterial membranes, aiding in stress responses involved in acidity, temperature and salinity (Belin et al., 2018). Squalene is the precursor to hopanoid biosynthesis and the genes involved in it (*hpn*DE and *hpn*C) were predicted in all *Acidihalobacter* genomes, and were not identified in the *H. neapolitanus* genome. *hpn*DEC all had high similarity to orthologous proteins in the *Thioalkalivibrio* genus (>90%). *A. ferrooxydans* was the only genome that had the complete set of genes required to produce bacteriohopanetetrol (BHT) (*hpn*FHG) (the full hopanoid biosynthesis pathway can be seen in **Figure 3**). HpnF and HpnH both had high similarity to proteins from the *Nitrosomonas* genus (61.5 and 74–68%, respectively) and HpnH also had high similarity to proteins from microbes in the Methylococcaceae family (70–67%). *hpn*H, *isp*H, *hpn*F, *hp*G, and *hpn*A are all in a region of the genome with no synteny with the other *Acidihalobacter* genomes. An assembly gap was detected in the genome adjacent to *hpn*A, thus the full genomic context and evidence of HGT could not be determined.

Starvation Lipoprotein Slp

The outer membrane "starvation lipoprotein" gene *slp* is associated with the protection of *E. coli* during carbon starvation and metabolites that are toxic in low pH environments (namely organic acids) (Alexander and St John, 1994; Hommais et al., 2004; Mates et al., 2007). *slp* is located in the "acid fitness island" of *E. coli* and is co-expressed with other acid resistance genes. Two copies of *slp* were identified in all species of *Acidihalobacter,* excluding *A. ferrooxydans,* which only had one copy, and was absent in the outgroup. Slp copies contained a characteristic lipobox motif (Zückert, 2014; Vergara et al., 2020) with an Alanine amino acid residue in the position +2, suggesting an exportation of Slp (**Supplementary Figure 5**). Both copies, named *slp-1 and slp-2,* are adjacent to each other in *A. yilgarnensis, A. prosperus and A. aeolianus,* and the area of the genome is conserved between the three species (see **Supplementary Figure 6**). A cardiolipin synthase (*cls*) gene was found upstream of *slp* in all *Acidihalobacter* genomes and is involved in the structural organization of membranes and is

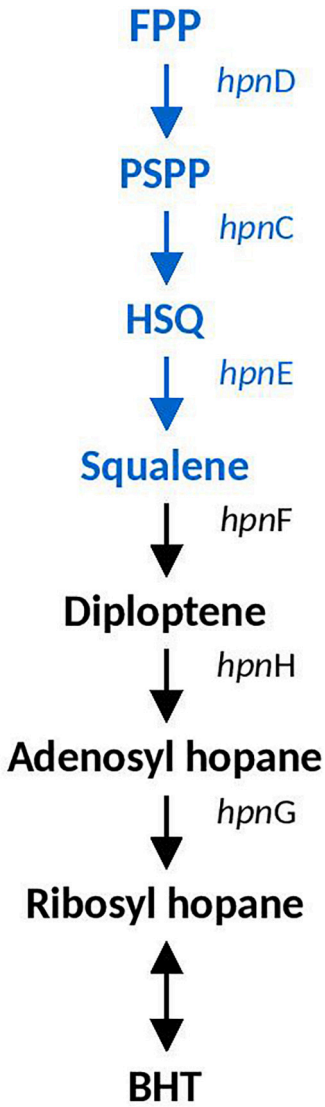

FIGURE 3 | Hopanoid biosynthesis pathway identified in *Acidihalobacter.* Blue text indicates pathway identified in all *Acidihalobacter* genomes, black text indicates hopanoid biosynthesis pathway found in *A. ferrooxydans*. HSQ, hydroxysqualene; BHT, bacteriohopanetetrol.

associated with osmoregulation and acidic resistance (Romantsov et al., 2009; MacGilvray et al., 2012). The cardiolipin synthase presented higher similarity with Planctomycetes microorganisms according BlastP results. *engB*, a gene associated with the *slp* and glutamate decarboxylase genes in *E. coli,* was also identified in the same genomic context as *Acidihalobacters slp* (Mates et al., 2007). *NhaP,* a $K^+(Na^+)/H^+$ antiporter, and *lysR,* a transcriptional regulator, were identified downstream of *slp* in *A. ferrooxydans* and both are associated with acid stress response of *Vibrio cholerae* (Kovacikova et al., 2010; Ante et al., 2015; Mourin et al., 2019). Phylogenetic analysis of the proteins shows the Slp-1 protein clustering with Slp proteins of *Acidithiobacillus*, and Slp-2 clustered with Chromatiales Slp proteins (see **Figure 4**). HGT events signals were identified for two genes upstream of slp-1 (AOU99095.1–AOU99096.1) by HGTector, suggesting Proteobacteria donor. This information, in addition to the genomic arrangement and phylogenetic analysis, allow us to hypothesize that genomic segment of *Acidihalobacter* including *slp*-1, cardiolipin synthase and genes upstream were gained by HGT events from a Proteobacteria donor, such as the extreme acidophile *Acidithiobacillaceae*; meanwhile *slp*-2 copies correspond to an ancestral gene from Chromatiales.

Acid Resistance Mechanisms: Second Line of Defense

"Second line of defense" (Vergara et al., 2020) mechanisms are involved in removing excess protons that have passed the cellular membrane and have entered the cytoplasm. Such mechanisms consist of cytoplasmic buffering systems and proton antiporters, pumping protons out of the cell. The glutamate decarboxylase system, the arginine decarboxylase system, the urease system, carbonic anhydrase and the ClcA antiporters found in *Acidihalobacter* are described below.

Glutamate Decarboxylase System

The glutamate decarboxylase system has been identified as a major mechanism in the acid stress response of *E. coli* (reviewed in Foster, 2004). Glutamate is transported into the cell by GadC (an amino acid permease), and GadA or GadB (the glutamate decarboxylase isozymes) replaces the *a*-carboxyl group of glutamate with H^+, creating *y*-amino butyric acid (GABA) and CO_2 removing a proton from the cytoplasm in the process. GABA is subsequently removed from the cell by GadC. The Gad decarboxylase system has also been identified in extreme acidophiles such as *Leptospirillum* spp. and *F. caldus* (Mangold et al., 2013; Vergara et al., 2020). GadA and GadC were both identified in all *Acidihalobacter* genomes but was missing in the *H. neapolitanus* genome. *gad*A and *gad*C in *A. aeolianus* and *A. ferrooxydans* were separated by a protein with no predicted putative domains. This hypothetical protein was predicted to be 248 amino acids and 7 transmembrane domains by HMMER, and has matches to ArcD, an arginine/ornithine antiporter in the HMMER database. In all genomes, best-hit analysis of GadA and GadC proteins showed 100% coverage and high amino acid percentage identity (ranging from 75 to 85.12%) to orthologs in *Salinisphaera* sp. LB1 (a haloacidophile), *Mangrovitalea sediminis* (a halophile), and *Acidithiobacillus* spp. (including *At. thiooxidans, At. Ferridurans*, and *At. ferrivorans*). This is an indication of a possible gene gain event in *Acidihalobacter* (see **Supplementary Figures 7A,B**).

Arginine Decarboxylase System

The Arginine decarboxylase system is another acid stress tolerance system identified in *E. coli* that works in the same way as the glutamate decarboxylase system (reviewed in Richard and Foster, 2004). Arginine decarboxylase, encoded by the *adiA*, replaces the *a*-carboxyl group of arginine with a proton, producing CO_2 and agmatine, which is removed from the cell via antiporter AdiC. All *Acidihalobacter* genomes had hits to *adiA*, however, no hit to *adiC* was identified (no arginine decarboxylase

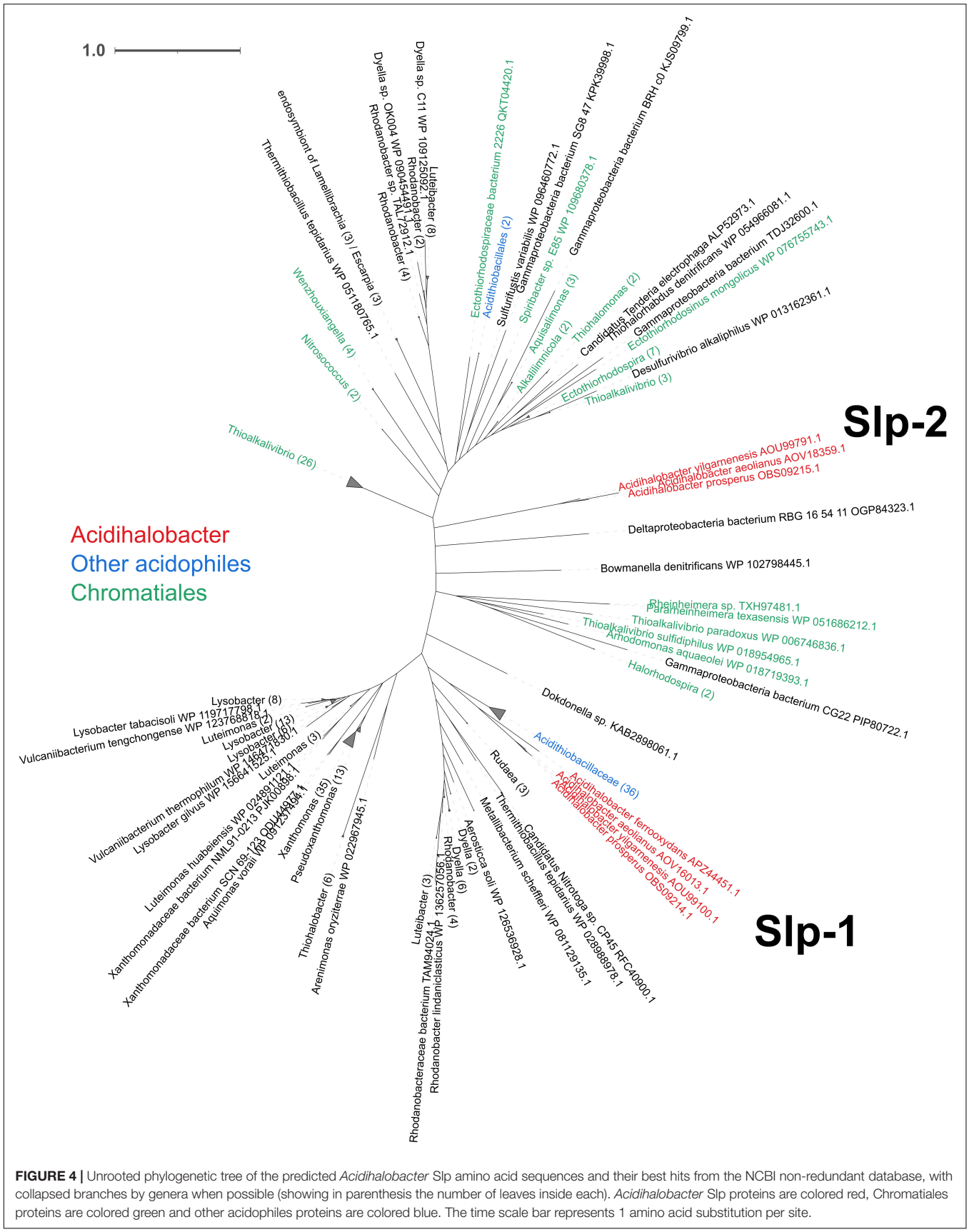

FIGURE 4 | Unrooted phylogenetic tree of the predicted *Acidihalobacter* Slp amino acid sequences and their best hits from the NCBI non-redundant database, with collapsed branches by genera when possible (showing in parenthesis the number of leaves inside each). *Acidihalobacter* Slp proteins are colored red, Chromatiales proteins are colored green and other acidophiles proteins are colored blue. The time scale bar represents 1 amino acid substitution per site.

genes were found in the *H. neapolitanus* genome). The complete arginine synthesis pathway was identified (*arg*ABCDEFGHO), thus *Acidihalobacter* may be capable of producing its own arginine, to be used in the arginine decarboxylase system. Best hits of the *Acidihalobacter* AdiA proteins to the BlastP non-redundant database indicated significant similarity to AdiA proteins of other Chromatiales organisms, suggesting vertical descent.

Urease System

One of the key mechanisms used by the enteric pathogen *H. pylori* to combat acid stress is the production of a highly expressed urease enzyme (Marcus and Scott, 2016). Urease converts urea to ammonia which is protonated to NH_4^+, neutralizing its environment. Urea import in *H. pylori* is controlled by UreI, a proton gated inner membrane urea channel, found to be activated by low pH (Bury-Moné et al., 2001; McNulty et al., 2013). Further buffering capacity is achieved by carbonic anhydrase which converts the carbon dioxide produced as a by-product of the urease activity into carbonic acid, which has a higher buffering capacity compared to ammonium (Marcus et al., 2005). The urease enzyme is coded for by *ure*A, *ure*B, and *ure*C (urease subunit gamma, beta, and alpha, respectively) and *ure*D (an ortholog of *ure*H), *ure*E, *ure*F, and *ure*G all of which are accessory proteins necessary for the expression of a functional urease enzyme (Akada et al., 2000). In *H. pylori* the regulation in the expression of the urease complex is dependent on the cellular pH and environmental pH, conditions sensed by the ArsRS and FlgRS two-component system. Urease is also found widely in soil bacteria, cyanobacteria and the extreme acidophile *Ferrovum* (Ullrich et al., 2016a) and studied in halophilic alkaliphiles in the production of biocement (Burbank et al., 2012; Dhami et al., 2013; Stabnikov et al., 2013; Veaudor et al., 2019). In the previously mentioned cases the urease activity is largely related to nitrogen assimilation and microbially induced calcite precipitation (Burbank et al., 2012). In cyanobacteria urea transport is controlled by the urea transport genes *urt*ABCDE (Veaudor et al., 2019).

In all the *Acidihalobacter* genomes, *ure*A, *ure*B, *ure*C, *ure*D, *ure*E, *ure*F, and *ure*G were detected (*ure*C in *A. yilganensis* has multiple frameshift mutations resulting in a truncated version of UreC). These genes were not detected in the outgroup *H. neapolitanus* c2. The gene cluster structure of the urease system was unique in the *Acidihalobacter* genomes with a cyanase (*cyn*S) gene between *ure*A and *ure*B. Cyanase is an enzyme that converts cyanate to carbamate, which spontaneously converts to ammonia and carbon dioxide ($OCN^- + HCO_3^- + 2H^+ \leftrightarrow NH_3 + 2CO_2$), directly consuming two protons as well as more protons consumed via the spontaneous conversion of ammonia to ammonium ($NH_3 + H^+ \leftrightarrow NH_4^+$) (Anderson and Little, 1986). Reporting of *cyn*S incorporated into the urease operon in other genomes has not been found and could possibly be a novel alteration in *Acidihalobacter* allowing for further buffering capacity. As previously stated, *H. pylori* contains *ars*R, a pH activated transcriptional regulator, responsible for the transcription of the urease operon in low pH environments (Pflock et al., 2005). The *ars*R transcriptional regulator was found in *A. yilgarnensis, A. prosperus*, and *A. aeolianus.* This regulator was found upstream of the urease operon and also encompasses the genes *adi*A and *spe*E (**Figure 5**). SpeE is a polyamine aminopropyltransferase in *E. coli* that is involved in the production of spermidine and is found to be involved in the acid tolerance of *E. coli,* possibly through the regulation of a wide range of acid tolerance genes including the glutamate decarboxylase system and the arginine decarboxylase system (Rhee et al., 2007). Whether or not the urease operon, *adi*A and *spe*E are controlled by the *ars*R transcriptional regulator remains to be seen and must be tested further. The only urease transport system detected was *urt*ABCDE in *A. ferrooxydans* and two copies in *H. nepolitanus* c2. In the case of *H. pylori,* gastrointestinal urea concentrations are very low (∼3 mM), and thus requires the active transport of urea into its cell for the urease system to be effective at combating acid stress (Scott et al., 2000). Environmental urea typically ranges from 0 to 13uM in concentration, over 2 orders of magnitude lower than the case of *H. pylori*; thus, it is unclear if the urease system found in *A. yilgarnensis, A. prosperus* and *A. aeolianus* would be effective enough in combating acid stress if no active urea transport system is found. *A. ferrooxydans* may be able to use the urease system as an acid resistance mechanism more effectively than the other member of *Acidihalobacter* due to the presence of the active urease transporter system in its genome. Further proteomic studies would be needed to validate this hypothesis. Due to the lack of the urease gene cluster in the outgroup and the similarity of the *Acidihalobacter* and Betaproteobacteria urease gene clusters, we speculate that the urease system was acquired via HGT in an ancestral *Acidihalobacter*.

Carbonic Anhydrase

Carbonic anhydrase (CA) is a proton-consuming enzyme that has been found to be upregulated in response to acid stress in *H. pylori* and the lack of the enzyme delays growth of *H. pylori* in acidic conditions (Sachs et al., 2006; Bury-Moneì et al., 2008). CAs are found in the cytoplasm and thus would directly contribute to minimizing the effect of protons leaking into the cytoplasm. CA is also known to catalyze the dissolution of carbonate minerals and in *Aspergillus fumigatus* is upregulated in potassium limited environments to increase the dissolution of potassium minerals to obtain potassium (Xiao et al., 2012; Sun et al., 2013). CA have also been found in acidophiles, but conclusions about their involvement in acid tolerance is not clear (Levicán et al., 2008; Li et al., 2012; Acuña et al., 2013). HGTector predicted the CA gene to have been acquired in the *A. aeolianus* and the *A. yilgarnensis* genomes from a Proteobacteria. The proximity of the CA to the Kdp system in *A. aeolianus*, as well as its clustering with CA proteins from the extreme acidophile class *Acidithiobacillia* may indicate an involvement in acid tolerance. Although, best BlastP hit analysis had many top hits to CAs of the extreme acidophile class *Acidithiobacillia,* phylogenetic analysis reveals clustering of the *Acidihalobacter* CAs to both *Acidithiobacillia and Chromatiales* CAs (see **Supplementary Figure 8**). This makes it unclear as to whether the horizontal gene transfer occurred from the acidophiles to the *Acidihalobacter* genomes, and subsequent loss in *A. prosperus* and *A. ferrooxydans,* or if the

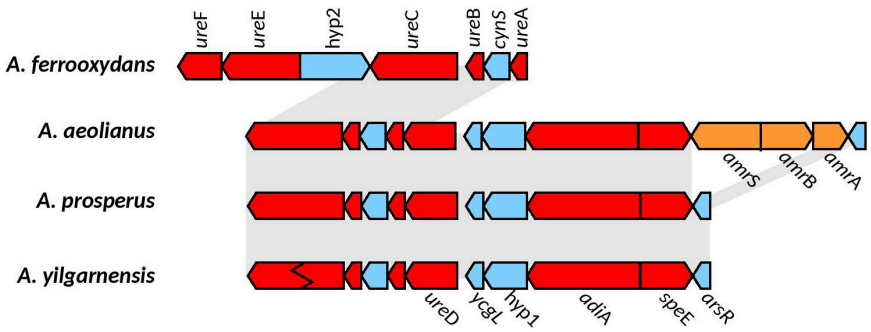

FIGURE 5 | Genomic context of the urease gene cluster in the *Acidihalobacter* spp. genomes. Gray background shows synteny between genomes; blue genes are found in all genomes; red shows genes hypothesized to be involved in acid and osmotic tolerance; genes in orange correspond to unique genes (only found in their respective genomes). Ziz-zag pattern indicates a frameshift mutation in the gene. Hyp1, hypothetical 1; Hyp2, hypothetical 2; *cyn*S, cynanate hydratase; *ycg*L, protein YcgL; *ars*R, arsenic resistance transcriptional regulator; *amr*S, AmmeMemoRadiSam system radical SAM enzyme; *amr*B, AmmeMedoRadiSam system protein B; *amr*A, AmmeMedoRadiSam system protein A.

HGT occurred from an early *Acidihalobacter* common ancestor to the acidophiles.

ClcA Antiporters

Voltage gated ClC-type Cl^-/H^+ transporters found in *E. coli* are thought to be important in acid resistance systems. These proteins are hypothesized to function as a "electrical shunt for an outwardly directed virtual proton pump, linked to amino acid decarboxylation" (Iyer et al., 2002). Although chloride regulation is important in halophiles, no studies have indicated ClcA proteins to be involved in osmotic tolerance. Multiple predicted ClcA proteins were identified in the *Acidihalobacter* genomes, two in *A. yilgarnensis,* three in *A. prosperus* and *A. aeolianus,* four in *A. ferrooxydans* and one in the outgroup. Phylogenetic analysis of the ClcA proteins reveal five distinct clades of ClcA proteins which were named ClcA-1, ClcA-2, ClcA-3, ClcA-4, and ClcA-5 (see **Supplementary Figure 9**). *clc*A-1 and *clc*A-3 are located in the same area of the genome in *A. yilgarnensis, A. prosperus*, and *A. aeolianus.* Evidence of the loss of *clcA-3* in *A. yilgarnensis* is evident as genomic synteny is conserved between these genomes (see **Figure 6A**). Both *clc*A-1 and *clc*A-3 are hypothesized to have been inherited via HGT, as phylogenetic analysis reveals *clc*A-1 clustering closely to ClcA proteins from *Acidithiobacillaceae* and *clc*A-3 clustering with *Sneathiella* spp., *Symmachiella* spp., *Desulfobacteraceae* spp., and *Thiomicrospira* spp. The genes surrounding *clc*A-1 *and clc*A-3 may also be involved in both acid and osmotic tolerance; *pst*ACS (proton buffering), *ygg*TUS (osmotic stress signaling), *pro*H (associated with the production of proline as a compatible solute), and *pil*U and *pil*T (involved in cell adhesion, colonization, biofilm maturation and twitching) (Ito et al., 2009; Chen et al., 2015). *pil*G was identified to be upregulated in *Acidihalobacter* during increasing osmotic stress, thus these proteins may also play a role in osmotic tolerance, although no direct evidence is available of this mechanism in other bacteria (Dopson et al., 2016). This area of the genome may be important to acidic and osmotic tolerance in the *Acidihalobacter*, given that many of the genes in the same context are possibly involved in both osmotic and acidic tolerance. *A. ferrooxydans* is the only *Acidihalobacter* that had a second copy of the *clc*A-1 and is hypothesized to have been acquired via gene duplication of the original *clc*A-1 gene and has undergone further diversification. The second copy of *clc*A-1 in *A. ferrooxydans* is directly upstream of the hypothesized original *clc*A-1 gene and clusters closely with the original *clc*A-1 proteins (**Figure 6B**). *clc*A-2 was only identified in *A. ferrooxydans* and was in an area of the genome with no synteny between any other *Acidihalobacter* genomes (**Figure 6A**). Phylogenetic analysis indicates the *clc*A-2 protein also clustered closely with ClcA proteins in *Acidithiobacillaceae,* and is hypothesized to have been acquired via HGT from said Acidithiobacillaceae ClcA-4 clusters closely to ClcA proteins from other Chromatiales ClcA proteins, and is in a conserved region of the genome across all the *Acidihalobacter* genomes (see **Supplementary Figure 10**), thus we suspect that *clc*A-4 was acquired via vertical descent, and subsequently lost in *H. neapolitanus*. ClcA-5 was the only ClcA protein found in the outgroup *H. neapolitanus c2* genome, however, is hypothesized to not be orthologous to any of the ClcA proteins found in the *Acidihalobacter* genomes as it was not phylogenetically related to any of the *Acidihalobacter* ClcA proteins. We hypothesize that the multiple copies of *clc*A in *Acidihalobacter* may point to its usefulness in the acidic response of *Acidihalobacter*. The abundance of chloride ions in *Acidihalobacter* environments could possibly allow for the ClcA mechanism of exporting H^+ in exchange for Cl^- is an effective and energetically favored mechanism, due to the abundance of chloride in *Acidihalobacter* environment. Although this mechanism is found in other acidophiles, it may be more useful for a haloacidophile like *Acidihalobacter* as it is adapted to a high chloride environment.

Acid Tolerance Genes Absent in the *Acidihalobacter* Genus

Multiple genes that are hypothesized to be involved in acid tolerance were not identified in the *Acidihalobacter* genomes (the complete list of genes queried against *Acidihalobacter* can be found in the **Supplementary Table 2**). *Acidihalobacter*

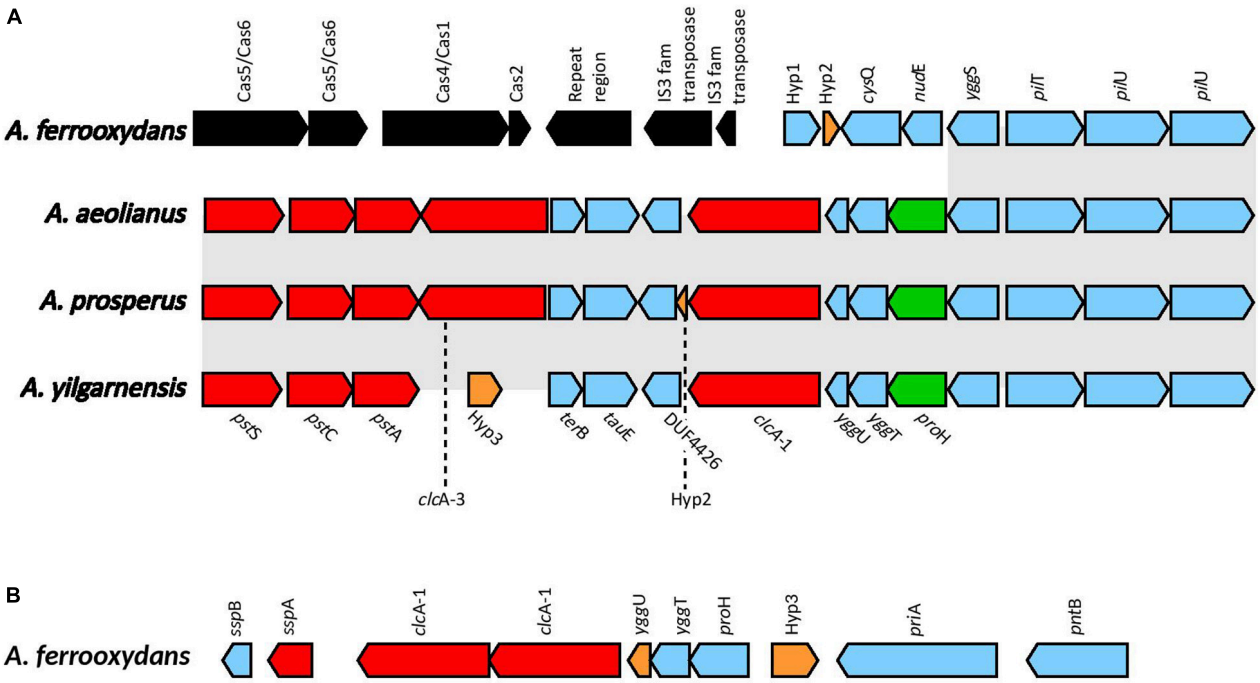

FIGURE 6 | (A) The genomic context of *clc*A-1 in *A. yilgarnensis, A. prosperus* and *A. aeolianus*. **(B)** The genomic context of the *clcA-1* genes in *A. ferrooxydans.* Genes in red; involved in acid tolerance, in green; involved in osmotolerance, in blue; others, in black; genes associated with HGT. Hyp, hypothetical proteins with no predicted putative domains; *cys*Q, 3′(2′),5′-bisphosphate nucleotidase; *nud*E, ADP compounds hydrolase; *ygg*S, Pyridoxal phosphate homeostasis protein; *pil*T, type IV pilus twitching motility protein; *pil*U, type IV pilus ATPase; *ter*B, tellurite resistance protein; *tau*E, sulfite exporter; DUF4426, domain of unknown function 4426; *ygg*U, UPF0235 protein YggU; *ygg*T, uncharacterized protein; *pro*H, pyrroline-5-carboxylate reductase 1; *ssp*B, stringent starvation protein B; *ssp*A, stringent starvation protein A; *pri*A, primosomal protein N′; *pnt*B, NAD(P) transhydrogenase subunit beta.

lacked the lysine, ornithine and agmatine decarboxylase systems. Regulatory genes involved in the glutamate decarboxylase system were absent, including *yba*S, *gad*X, *gad*W, and *gad*E. Alternative regulatory genes could be responsible for the glutamate decarboxylase system in *Acidihalobacter,* and further experimental data may shed light on such genes. Multiple hopanoid biosynthesis genes that produce alternative hopanoid proteins were either absent in the *Acidihalobacter* genomes, or lacked essential intermediate genes. Genes involved in producing general stress proteins were not covered in this study as they are not specialized acid tolerance cellular mechanisms.

Model of *Acidihalobacter* Acid Resistance

A model explaining the acid resistance mechanisms identified in *Acidihalobacter* is proposed in **Figure 7**. We propose the major mechanisms aiding in the acid resistance of the *Acidihalobacter* spp. to be a combination of potassium transporters, multiple cytoplasmic buffering systems and cellular membrane alterations. The potassium transporters including TrkAH and Kch are likely involved in generating a reversed membrane potential, repelling protons from entering the cell in *Acidihalobacter* spp. *A. aeolianus* has the additional Kdp potassium transport system, possibly aiding it in maintaining a reversed membrane potential when exposed environments low in potassium ions. *Acidihalobacter* has multiple cytoplasmic buffering systems including the glutamate decarboxylase system, the urease system, and carbonic anhydrase. These buffering systems likely contribute to removing any protons that have leaked through the membrane and thus aid in maintaining a circumneutral intracellular pH. The urease system is reported as a strong buffering system, allowing *H. pylori* to survive in the acidity of the stomach. The effectiveness of this system in *Acidihalobacter* is unknown, however, as only *A. ferrooxydans* has a urea transport system. The glutamate decarboxylase system is another well-known buffering system used by enteric bacteria that have transient exposure to the acidic conditions of the stomach. It is evident in the study that the glutamate decarboxylase system is present in *Acidihalobacter* spp. and was likely acquired from acidophilic bacteria. Interestingly, glutamate is also commonly accumulated as an osmoprotectant in halophilic bacteria (Dinnbier et al., 1988; Csonka et al., 1994; Kang and Hwang, 2018), therefore the import of glutamate by the glutamate decarboxylase system may also aid during osmotic stress. Membrane alterations also likely play a role in the acid resistance of *Acidihalobacter* spp. including Slp lipoprotein, spermidine and BHT production in *A. ferrooxydans.* Multiple Slp lipoproteins identified in *Acidihalobacter* likely provide resistance to organic acids, that are detrimental to many chemolithotrophic acidophiles, including *Acidihalobacter.* This area of the genome has also uncovered many genes involved

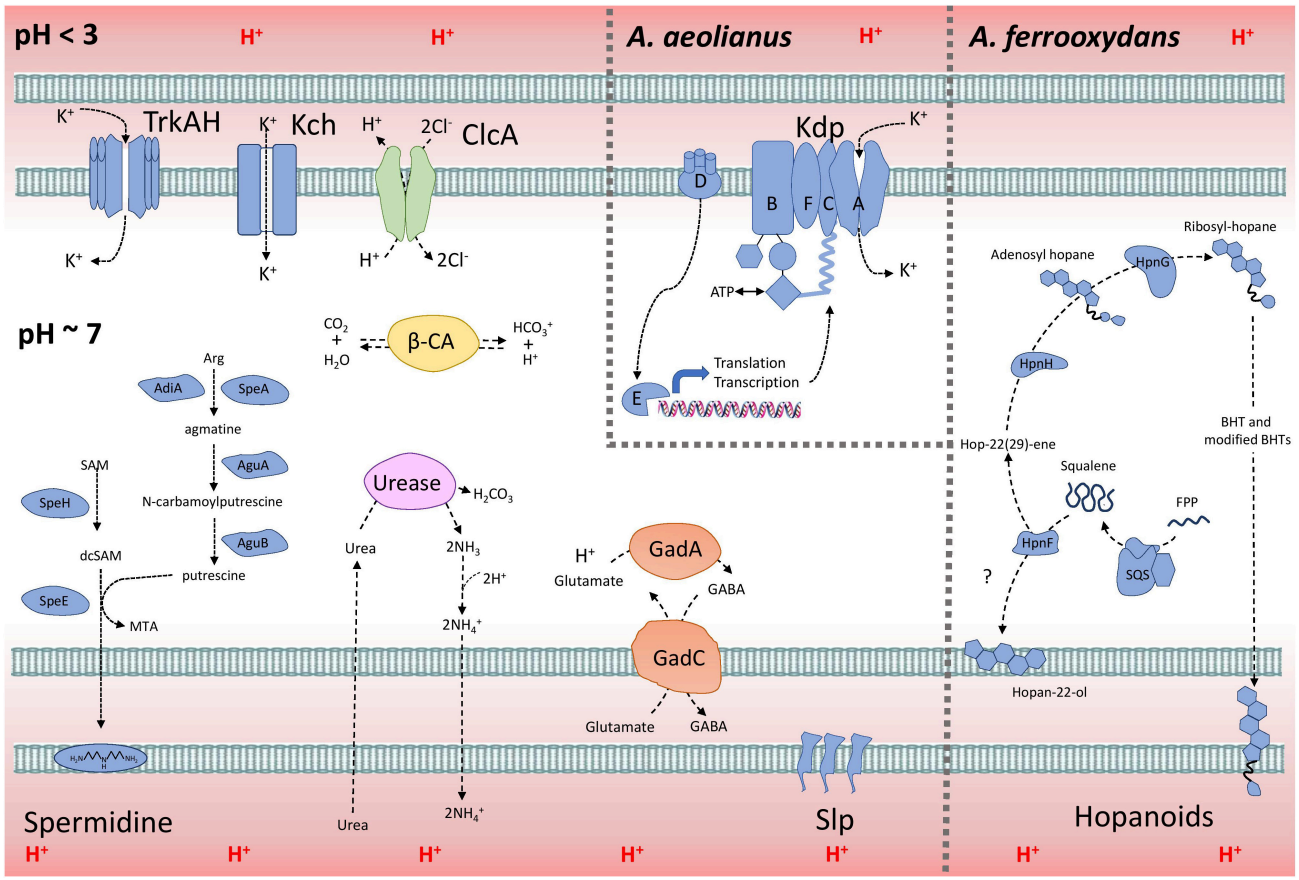

FIGURE 7 | The model of acid resistance in the *Acidihalobacter* spp. First line of defense mechanisms are displayed in blue and second line of defense mechanisms are displayed in other colors (green = *Clc*A; yellow = β-CA; purple = urease system; and orange = Gad system).

in outer membrane proteins, that may be important to assess for their function in *Acidihalobacter* response to acidic and osmotic stress. BHTs produced in *A. ferrooxydans* likely aid in its resistance to acidic conditions as hopanoids have been identified in acid mine drainage and other acidic environments (Jones et al., 2012). Although the mechanism of spermidine in acid tolerance is not fully understood, *Acidihalobacter* spp. have the genetic potential to produce spermidine, and may aid in its acid tolerance. Multiple ClcA proteins identified in *Acidihalobacter* likely exchange chloride for the removal of protons, which may be especially effective in *Acidihalobacter* as opposed to other acidophiles sensitive to chloride ions.

Phylogenetic Distribution of Acid Resistance Genes and Their Inferred Evolutionary Trajectories

The hypothesized evolutionary trajectory leading to the *Acidihalobacter* genus becoming acidophilic from an inferred neutrophilic ancestor is summarized in **Figure 8**, displaying gene gain and gene loss events and gene inheritance through vertical descent. Many genes involved in acid resistance, were hypothesized to be in the last inferred common ancestor including the potassium transporters (*trk*AH, *kch*) and membrane alterations (*hpn*JCDE, *isp*H and *spe*EH). It is evident that the accumulation of potassium via potassium pumps is vital when responding to both osmotic and acidic stress. In this study we hypothesize the TrkAH low affinity potassium transporter to have been acquired via vertical descent from a common halophilic ancestor. Although the Kch proteins have Best-BlastP hits to many Kch proteins from the Acidithiobacillaceae family, phylogenetic analysis reveals the *Acidihalobacter* spp. Kch proteins cluster closely with Kch proteins from organisms of the Chromatiales class. Thus, we inferred the Kch protein to have also been inherited via vertical descent, and subsequently lost in the outgroup. The Kdp high affinity potassium transport system was hypothesized to have been acquired in the *A. aeolianus* genome via HGT likely from Betaproteobacteria, according to the phylogenetic tree (**Supplementary Figure 3B**). *A. ferrooxydans* BHT synthesis genes were likely obtained in the genome via both vertical descent and HGT. HpnCDE are involved in squalene synthesis, an early intermediate product of BHT production. These protein sequences were phylogenetically related to the same proteins in other Chromatiales species, indicating they were likely vertically inherited. Squalene is known to be associated with halophilic

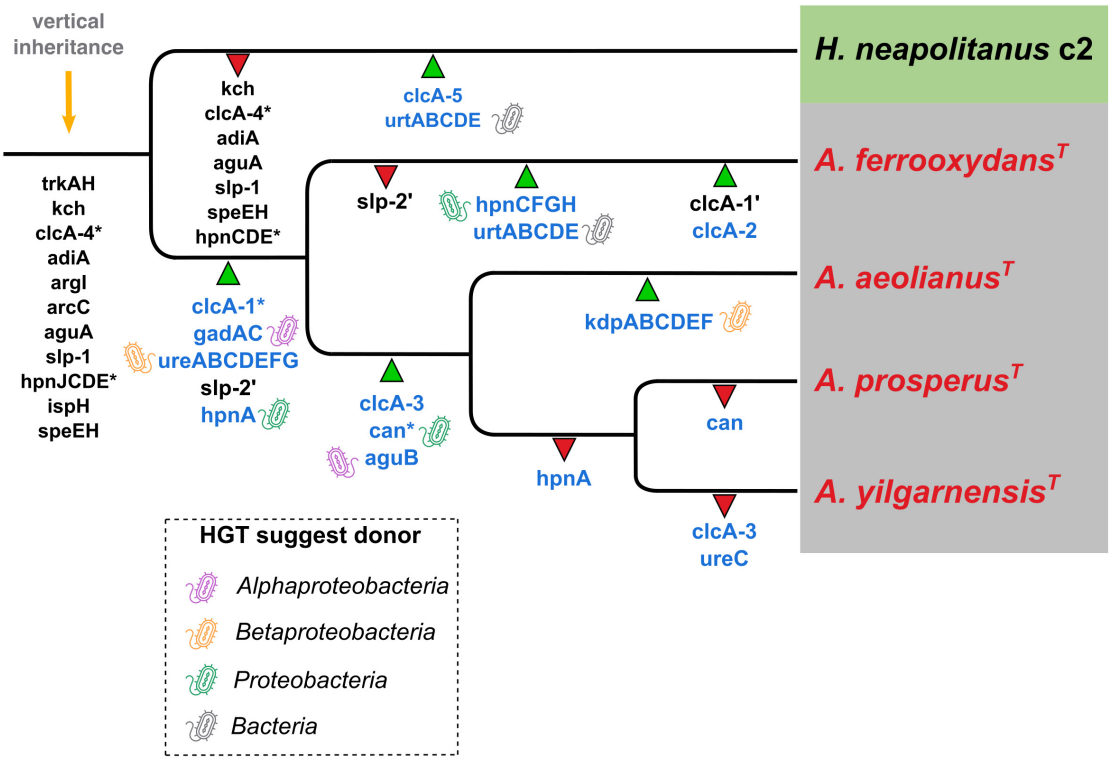

FIGURE 8 | Inferred phylogenetic distribution of acid resistance genes. Green triangles represent gene gain events (the ' in *slp* and *clc*A genes represent a duplication event) and red triangles represent gene loss events. Gene names in blue indicate hypothesized HGT events (* marks the uncertain origin for that gene) and the bacteria-icon represents the putative origin of those events. Orange arrow = predicted genes inherited by vertical descent.

archaea's membranes, integrating with cellular lipids, helping them to pack closer together, thus is supports HpnCDE likely being inherited from a halophilic common ancestor (Gilmore et al., 2013). Hopanoids are also associated with saline stress, however, the remainder of the BHT synthesis genes (*hpn*FGH) had best-BlastP hits to non-Chromatiales proteins and due to the lack of these genes in the other *Acidihalobacter* genomes, as well as the outgroup, we hypothesize these genes were gained via HGT in the *A. ferrooxydans* genome. All the typical "first line of defense" mechanisms described in extreme acidophiles, in the case of *Acidihalobacter*, seem to originate from a neutrophilic-halophilic ancestry. When it comes to second line of defense mechanisms, it is clear in this study that *Acidihalobacter* has likely gained two cytoplasmic buffering systems through HGT. The glutamate decarboxylase system (*gad*AC) was acquired via HGT into the *Acidihalobacter* genome from a possible acidophilic microbe. Urease (*ure*ABCDEFG) genes were also acquired into the *Acidihalobacter* genome via HGT, but we hypothesize from a non-acidophilic counterpart. Although not acquired from an acidophile, the urease system is known to be a strong buffering system for non-acidophilic enteric bacteria such as *H. pylori,* thus may be able to contribute to acid tolerance in *Acidihalobacter*. Urease was identified in the extreme acidophile *Ferrovum* sp. JA12, and it was also noted in the study that urease has not been identified in any other iron oxidizing acidophiles (Ullrich et al., 2016b). As mentioned previously, it is unclear how effective the urease system is in *A. yilgarnensis, A. prosperus*, and *A. aeolianus*, as no urea transporter was identified in these genomes. ClcA proteins in the *Acidihalobacter* genomes were hypothesized to have independent evolutionary histories. *clc*A-1 was likely acquired via HGT in the *Acidihalobacter* genomes from an acidophilic counterpart and underwent a duplication event in *A. ferrooxydans.* clcA-2 we hypothesize was also acquired via HGT in *A. ferrooxydans* independently. *clc*A-3 was likely acquired via HGT, however, from a non-acidophilic counterpart. *clc*A-4 was the only ClcA protein to have been vertically inherited and subsequently lost in the outgroup as it is phylogenetically related to other ClcA proteins from Chromatiales species. Although ClcA proteins are recognized in the acid stress responses of acidophiles, they have also been identified in some halophilic bacteria, although the function of ClcA proteins in halophiles has not been discussed (John et al., 2019). The evolutionary origin of carbonic anhydrase remains unclear. *Acidihalobacter* has been identified in shared environments with acidophilic microorganisms that we hypothesize had HGT events between species namely members of the Acidithiobacillaceae family (Norris et al., 2020; Abramov et al., 2021). Both *Acidihalobacter* and Acidithiobacillaceae species have been isolated from the acidified sulfide-rich seawater sites from the islands of Vulcano and Milos (Simmons and Norris, 2002; Norris et al., 2020). Other environments that have identified *Acidihalobacter* and other acidophiles inhabiting the same ecological niche include arid

soils in the Atacama desert Chile (Neilson et al., 2012) and acidic hypersaline river sediments of Western Australia (Lu et al., 2016). The evidence of professional acidophiles and *Acidihalobacter* supports environmental scenarios for HGT events to have occurred between these bacteria. These environmental niches hypothetically provide the ideal conditions for acidophiles and halophiles to live in close proximity and also apply the selection pressure for existing halophiles and acidophiles alike to share genetic capabilities. We hypothesize *Acidihalobacter* is an example of a halophile gaining acid tolerance mechanisms, however, the opposite case may still be discovered in other bacteria.The cellular mechanisms for microorganisms to thrive in saline and acidophilic conditions independently is well established. Understanding what combination of these cellular mechanisms *Acidihalobacter* has, that allows it to cope in both extreme acidity and saline conditions will give insight into the unique capabilities of haloacidophiles. The current understanding of *Acidihalobacter* as a halophile, is that it utilizes potassium pumps, periplasmic glucans and multiple compatible solutes to regulate its internal osmotic pressure to its saline environment. It is proposed by Khaleque et al. (2019) that initially potassium accumulation and the production of periplasmic glucans are the primary mechanisms used to respond to initial saline stress, and as salinity increases, the accumulation and production of compatible solutes would take priority. Identifying the genetic capabilities *Acidihalobacter* spp. possess that allows the genus to thrive in acidic conditions is vital to understand its evolution as a polyextremophile.

It is evident that *Acidihalobacter* is a genus rooted in a class of bacteria that are mostly halophilic/halotolerant neutrophiles and alkaliphiles. *Acidihalobacter* is also the only genus in the Chromatiales order that has been found to be acidophilic. We hypothesize that the ancestor of *Acidihalobacter* was a halophile that subsequently gained the genetic capability to thrive in acidic conditions. This research has identified some of these hypothesized genes involved in acid tolerance and uncovered evidence of HGT events that may have been involved in *Acidihalobacter* becoming acidophilic. The main mechanisms identified that likely are involved in acid tolerance in *Acidihalobacter* spp. include the potassium transporters TrkAH, Kch, and Kdp, membrane-associated alterations Slp, spermidine and BHTs, cytoplasmic buffering mechanisms, glutamate decarboxylase, urease and carbonic anhydrase, and the antiporters ClcA's. This study can inform further experimentation studying the acid tolerance of *Acidihalobacter*.

DATA AVAILABILITY STATEMENT

Publicly available datasets were analyzed in this study. This data can be found here: NCBI GCF_000754095.2, GCF_001753245.1, GCF_001753165.1 GCF_001975725.1, and GCF_000024765.1.

AUTHOR CONTRIBUTIONS

DH and EW conceived the study. KB carried out the research. All authors contributed to data collection, analysis, and manuscript preparation and read and approved the final manuscript.

FUNDING

This work was supported by Fondecyt 1181717 (DH), ANID FONDECYT 3190792 (CG), and Centro Ciencia & Vida, FB210008, Financiamiento Basal para Centros Científicos y Tecnológicos de Excelencia de ANID.

ACKNOWLEDGMENTS

We thank Diego Cortez for his insightful input. KB acknowledges support through an Australian Government Research Training Program Scholarship.

SUPPLEMENTARY MATERIAL

The Supplementary Material for this article can be found online at: https://www.frontiersin.org/articles/10.3389/fmicb.2022.848410/full#supplementary-material

REFERENCES

Abramov, S. M., Straub, D., Tejada, J., Grimm, L., Schädler, F., Bulaev, A., et al. (2021). Biogeochemical niches of fe-cycling communities influencing heavy metal transport along the rio tinto, Spain. *Appl. Environ. Microbiol.* 88:e0229021. doi: 10.1128/AEM.02290-21

Acuña, L. G., Cárdenas, J. P., Covarrubias, P. C., Haristoy, J. J., Flores, R., Nuñez, H., et al. (2013). Architecture and repertoire of the flexible genome of the extreme acidophile *Acidithiobacillus caldus*. *PLoS One* 8:e78237. doi: 10.1371/journal.pone.0078237

Akada, J. K., Shirai, M., Takeuchi, H., Tsuda, M., and Nakazawa, T. (2000). Identification of the urease operon in *Helicobacter pylori* and its control by mRNA decay in response to pH. *Mol. Microbiol.* 36, 1071–1084. doi: 10.1046/j.1365-2958.2000.01918.x

Alexander, D. M., and St John, A. C. (1994). Characterization of the carbon starvation-inducible and stationary phase-inducible gene slp encoding an outer membrane lipoprotein in *Escherichia coli*. *Mol. Microbiol.* 11, 1059–1071. doi: 10.1111/j.1365-2958.1994.tb00383.x

Anderson, P. M., and Little, R. M. (1986). Kinetic properties of cyanase. *Biochemistry* 25, 1621–1626. doi: 10.1021/bi00355a026

Ante, V. M., Bina, X. R., and Bina, J. E. (2015). The LysR-type regulator LeuO regulates the acid tolerance response in *Vibrio cholerae*. *Microbiology* 161, 2434–2443. doi: 10.1099/mic.0.000194

Asnicar, F., Thomas, A. M., Beghini, F., Mengoni, C., Manara, S., Manghi, P., et al. (2020). Precise phylogenetic analysis of microbial isolates and genomes from metagenomes using PhyloPhlAn 3.0. *Nat. Commun.* 11:2500. doi: 10.1038/s41467-020-16366-7

Baker-Austin, C., and Dopson, M. (2007). Life in acid: pH homeostasis in acidophiles. *Trends Microbiol.* 15, 165–171. doi: 10.1016/j.tim.2007.02.005

Bakker, E. P., Borchard, A., Michels, M., Altendorf, K., and Siebers, A. (1987). High-affinity potassium uptake system in Bacillus acidocaldarius showing

immunological cross-reactivity with the Kdp system from *Escherichia coli*. *J. Bacteriol.* 169, 4342–4348. doi: 10.1128/jb.169.9.4342-4348.1987

Belin, B. J., Busset, N., Giraud, E., Molinaro, A., Silipo, A., and Newman, D. K. (2018). Hopanoid lipids: from membranes to plant–bacteria interactions. *Nat. Rev. Microbiol.* 16, 304–315. doi: 10.1038/nrmicro.2017.173

Boden, R. (2017). Reclassification of *Halothiobacillus hydrothermalis* and *Halothiobacillus halophilus* to *Guyparkeria* gen. nov. in the *Thioalkalibacteraceae* fam. nov., with emended descriptions of the genus *Halothiobacillus* and family *Halothiobacillaceae*. *Int. J. Syst. Evol. Microbiol.* 67, 3919–3928. doi: 10.1099/ijsem.0.002222

Bowers, K. J., and Wiegel, J. (2011). Temperature and pH optima of extremely halophilic archaea: a mini-review. *Extremophiles* 15, 119–128. doi: 10.1007/s00792-010-0347-y

Buchfink, B., Xie, C., and Huson, D. H. (2015). Fast and sensitive protein alignment using DIAMOND. *Nat. Methods* 12, 59–60. doi: 10.1038/nmeth.3176

Buetti-Dinh, A., Dethlefsen, O., Friedman, R., and Dopson, M. (2016). Transcriptomic analysis reveals how a lack of potassium ions increases *Sulfolobus acidocaldarius* sensitivity to pH changes. *Microbiology* 162, 1422–1434. doi: 10.1099/mic.0.000314

Burbank, M. B., Weaver, T. J., Williams, B. C., and Crawford, R. L. (2012). Urease activity of ureolytic bacteria isolated from six soils in which calcite was precipitated by indigenous bacteria. *Geomicrobiol. J.* 29, 389–395. doi: 10.1080/01490451.2011.575913

Bury-Moneì, S., Mendz, G. L., Ball, G. E., Thibonnier, M., Stingl, K., Ecobichon, C., et al. (2008). Roles of α and β carbonic anhydrases of *Helicobacter pylori* in the urease-dependent response to acidity and in colonization of the murine gastric mucosa. *Infect. Immunity* 76, 497–509. doi: 10.1128/iai.00993-07

Bury-Moné, S., Skouloubris, S., Labigne, A., and De Reuse, H. (2001). The *Helicobacter* pylori UreI protein: role in adaptation to acidity and identification of residues essential for its activity and for acid activation. *Mol. Microbiol.* 42, 1021–1034. doi: 10.1046/j.1365-2958.2001.02689.x

Capera, J., Serrano-Novillo, C., Navarro-Pérez, M., Cassinelli, S., and Felipe, A. (2019). The potassium channel odyssey: mechanisms of traffic and membrane arrangement. *Int. J. Mol. Sci.* 20:734. doi: 10.3390/ijms20030734

Carver, T., Harris, S. R., Berriman, M., Parkhill, J., and McQuillan, J. A. (2012). Artemis: an integrated platform for visualization and analysis of high-throughput sequence-based experimental data. *Bioinformatics* 28, 464–469. doi: 10.1093/bioinformatics/btr703

Chao, J., Wang, W., Xiao, S., and Liu, X. (2008). Response of *Acidithiobacillus ferrooxidans* ATCC 23270 gene expression to acid stress. *World J. Microbiol. Biotechnol.* 24, 2103–2109. doi: 10.1007/s11274-008-9715-5

Chen, L.-X., Hu, M., Huang, L.-N., Hua, Z.-S., Kuang, J.-L., Li, S.-J., et al. (2015). Comparative metagenomic and metatranscriptomic analyses of microbial communities in acid mine drainage. *ISME J.* 9, 1579–1592. doi: 10.1038/ismej.2014.245

Cholo, M. C., van Rensburg, E. J., Osman, A. G., and Anderson, R. (2015). Expression of the Genes encoding the Trk and Kdp potassium transport systems of *Mycobacterium tuberculosis* during growth in vitro. *Biomed Res. Int.* 2015:608682. doi: 10.1155/2015/608682

Christel, S., Herold, M., Bellenberg, S., El Hajjami, M., Buetti-Dinh, A., Pivkin, I. V., et al. (2018). Multi-omics reveals the lifestyle of the acidophilic, mineral-oxidizing model species *Leptospirillum ferriphilum*. *Appl. Environ. Microbiol.* 84:e02091–17. doi: 10.1128/AEM.02091-17

Csonka, L. N., Ikeda, T. P., Fletcher, S. A., and Kustu, S. (1994). The accumulation of glutamate is necessary for optimal growth of *Salmonella typhimurium* in media of high osmolality but not induction of the proU operon. *J. Bacteriol.* 176, 6324–6333. doi: 10.1128/jb.176.20.6324-6333.1994

Darling, A. E., Mau, B., and Perna, N. T. (2010). progressiveMauve: multiple genome alignment with gene gain, loss and rearrangement. *PLoS One* 5:e11147. doi: 10.1371/journal.pone.0011147

Dhami, N. K., Reddy, M. S., and Mukherjee, A. (2013). Biomineralization of calcium carbonates and their engineered applications: a review. *Front. Microbiol.* 4:314. doi: 10.3389/fmicb.2013.00314

Dinnbier, U., Limpinsel, E., Schmid, R., and Bakker, E. P. (1988). Transient accumulation of potassium glutamate and its replacement by trehalose during adaptation of growing cells of *Escherichia coli* K-12 to elevated sodium chloride concentrations. *Arch. Microbiol.* 150, 348–357. doi: 10.1007/BF00408306

Dopson, M., Holmes, D. S., Lazcano, M., McCredden, T. J., Bryan, C. G., Mulroney, K. T., et al. (2016). Multiple osmotic stress responses in result in tolerance to chloride ions. *Front. Microbiol.* 7:2132. doi: 10.3389/fmicb.2016.02132

Dorus, S., Mimura, H., and Epstein, W. (2001). Substrate-binding clusters of the k -transporting Kdp ATPase of *Escherichia coli* investigated by amber suppression scanning mutagenesis. *J. Biol. Chem.* 276, 9590–9598. doi: 10.1074/jbc.m009365200

Epstein, W. (2003). The roles and regulation of potassium in bacteria. *Prog. Nucleic Acid Res. Mol. Biol.* 75, 293–320. doi: 10.1016/s0079-6603(03)75008-9

Feehily, C., and Karatzas, K. A. G. (2013). Role of glutamate metabolism in bacterial responses towards acid and other stresses. *J. Appl. Microbiol.* 114, 11–24. doi: 10.1111/j.1365-2672.2012.05434.x

Foster, J. W. (2004). *Escherichia coli* acid resistance: tales of an amateur acidophile. *Nat. Rev. Microbiol.* 2, 898–907. doi: 10.1038/nrmicro1021

Gaßel, M., Möllenkamp, T., Puppe, W., and Altendorf, K. (1999). The KdpF subunit is part of the K -translocating Kdp complex of *Escherichia coli* and is responsible for stabilization of the complex in vitro. *J. Biol. Chem.* 274, 37901–37907. doi: 10.1074/jbc.274.53.37901

Gaßel, M., Siebers, A., Epstein, W., and Altendorf, K. (1998). Assembly of the Kdp complex, the multi-subunit K -transport ATPase of *Escherichia coli*. *Biochim. Biophys. Acta BBA Biomembranes* 1415, 77–84. doi: 10.1016/s0005-2736(98)00179-5

Gilmore, S. F., Yao, A. I., Tietel, Z., Kind, T., Facciotti, M. T., and Parikh, A. N. (2013). Role of squalene in the organization of monolayers derived from lipid extracts of *Halobacterium salinarum*. *Langmuir* 29, 7922–7930. doi: 10.1021/la401412t

González-Rosales, C., Vergara, E., Dopson, M., Valdés, J. H., and Holmes, D. S. (2022). Integrative genomics shed light on evolutionary forces shaping the acidithiobacillia class acidophilic lifestyle. *Front. Microbiol.* 12:822229. doi: 10.3389/fmicb.2021.822229

Gumulya, Y., Boxall, N. J., Khaleque, H. N., Santala, V., Carlson, R. P., and Kaksonen, A. H. (2018). In a quest for engineering acidophiles for biomining applications: challenges and opportunities. *Genes* 9:116. doi: 10.3390/genes9020116

He, G., Wu, C., Huang, J., and Zhou, R. (2016). Acid tolerance response of *Tetragenococcus halophilus*: a combined physiological and proteomic analysis. *Process Biochem.* 51, 213–219. doi: 10.1016/j.procbio.2015.11.035

Hesse, J. E., Wieczorek, L., Altendorf, K., Reicin, A. S., Dorus, E., and Epstein, W. (1984). Sequence homology between two membrane transport ATPases, the Kdp-ATPase of *Escherichia coli* and the Ca2 -ATPase of sarcoplasmic reticulum. *Proc. Natl. Acad. Sci. U.S.A.* 81, 4746–4750. doi: 10.1073/pnas.81.15.4746

Hommais, F., Krin, E., Coppée, J.-Y., Lacroix, C., Yeramian, E., Danchin, A., et al. (2004). GadE (YhiE): a novel activator involved in the response to acid environment in *Escherichia coli*. *Microbiology* 150, 61–72. doi: 10.1099/mic.0.26659-0

Huber, H., and Stetter, K. O. (1989). *Thiobacillus prosperus* sp. nov., represents a new group of halotolerant metal-mobilizing bacteria isolated from a marine geothermal field. *Arch. Microbiol.* 151, 479–485. doi: 10.1007/bf00454862

Ito, T., Uozumi, N., Nakamura, T., Takayama, S., Matsuda, N., Aiba, H., et al. (2009). The implication of YggT of *Escherichia coli* in osmotic regulation. *Biosci. Biotechnol. Biochem.* 73, 2698–2704. doi: 10.1271/bbb.90558

Iyer, R., Iverson, T. M., Accardi, A., and Miller, C. (2002). A biological role for prokaryotic ClC chloride channels. *Nature* 419, 715–718. doi: 10.1038/nature01000

John, J., Siva, V., Richa, K., Arya, A., and Kumar, A. (2019). Life in high salt concentrations with changing environmental conditions: insights from genomic and phenotypic analysis of *Salinivibrio* sp. *Microorganisms* 7:577. doi: 10.3390/microorganisms7110577

Johnson, D. B., and Schippers, A. (2017). Editorial: recent advances in acidophile microbiology: fundamentals and applications. *Front. Microbiol.* 8:428. doi: 10.3389/fmicb.2017.00428

Jones, D. S., Albrecht, H. L., Dawson, K. S., Schaperdoth, I., Freeman, K. H., Pi, Y., et al. (2012). Community genomic analysis of an extremely acidophilic sulfur-oxidizing biofilm. *ISME J.* 6, 158–170. doi: 10.1038/ismej.2011.75

Kang, Y., and Hwang, I. (2018). Glutamate uptake is important for osmoregulation and survival in the rice pathogen *Burkholderia glumae*. *PLoS One* 13:e0190431. doi: 10.1371/journal.pone.0190431

Katoh, K., and Standley, D. M. (2013). MAFFT multiple sequence alignment software version 7: improvements in performance and usability. *Mol. Biol. Evol.* 30, 772–780. doi: 10.1093/molbev/mst010

Kelly, D. P., and Wood, A. P. (2000). Reclassification of some species of *Thiobacillus* to the newly designated genera *Acidithiobacillus* gen. nov., *Halothiobacillus* gen. nov. and *Thermithiobacillus* gen. nov. *Int. J. Syst. Evol. Microbiol.* 50 Pt 2, 511–516. doi: 10.1099/00207713-50-2-511

Khaleque, H. N., Corbett, M. K., Ramsay, J. P., Kaksonen, A. H., Boxall, N. J., and Watkin, E. L. J. (2017a). Complete genome sequence of *Acidihalobacter prosperus* strain F5, an extremely acidophilic, iron- and sulfur-oxidizing halophile with potential industrial applicability in saline water bioleaching of chalcopyrite. *J. Biotechnol.* 262, 56–59. doi: 10.1016/j.jbiotec.2017.10.001

Khaleque, H. N., Fathollazadeh, H., González, C., Shafique, R., Kaksonen, A. H., Holmes, D. S., et al. (2020). Unlocking survival mechanisms for metal and oxidative stress in the extremely acidophilic, halotolerant acidihalobacter Genus. *Genes* 11:1392. doi: 10.3390/genes11121392

Khaleque, H. N., González, C., Shafique, R., Kaksonen, A. H., Holmes, D. S., and Watkin, E. L. J. (2019). Uncovering the mechanisms of halotolerance in the extremely acidophilic members of the acidihalobacter genus through comparative genome analysis. *Front. Microbiol.* 10:155. doi: 10.3389/fmicb.2019.00155

Khaleque, H. N., Ramsay, J. P., Murphy, R. J. T., Kaksonen, A. H., Boxall, N. J., and Watkin, E. L. J. (2017c). Draft genome sequence of the acidophilic, halotolerant, and iron/sulfur-oxidizing *Acidihalobacter prosperus* DSM 14174 (Strain V6). *Genome Announc.* 5:e01469–16. doi: 10.1128/genomeA.01469-16

Khaleque, H. N., Ramsay, J. P., Murphy, R. J. T., Kaksonen, A. H., Boxall, N. J., and Watkin, E. L. J. (2017b). Draft genome sequence of acidihalobacter ferrooxidans DSM 14175 (Strain V8), a new iron- and sulfur-oxidizing, halotolerant, acidophilic species. *Genome Announcements* 5:e00413–17. doi: 10.1128/genomea.00413-17

Khaleque, H. N., Shafique, R., Kaksonen, A. H., Boxall, N. J., and Watkin, E. L. J. (2018). Quantitative proteomics using SWATH-MS identifies mechanisms of chloride tolerance in the halophilic acidophile *Acidihalobacter prosperus* DSM 14174. *Res. Microbiol.* 169, 638–648. doi: 10.1016/j.resmic.2018.07.002

Kixmüller, D., Strahl, H., Wende, A., and Greie, J.-C. (2011). Archaeal transcriptional regulation of the prokaryotic KdpFABC complex mediating K uptake in *H. salinarum*. *Extremophiles* 15, 643–652. doi: 10.1007/s00792-011-0395-y

Korolev, N. (2021). How potassium came to be the dominant biological cation: of metabolism, chemiosmosis, and cation selectivity since the beginnings of life. *BioEssays* 43:2000108. doi: 10.1002/bies.202000108

Kovacikova, G., Lin, W., and Skorupski, K. (2010). The LysR-type virulence activator AphB regulates the expression of Genes in *Vibrio cholerae* in response to low pH and *Anaerobiosis*. *Journal of Bacteriology* 192, 4181–4191. doi: 10.1128/jb.00193-10

Kraegeloh, A., Amendt, B., and Kunte, H. J. (2005). Potassium transport in a halophilic member of the bacteria domain: identification and characterization of the K uptake systems TrkH and TrkI from *Halomonas elongata* DSM 2581 T. *J. Bacteriol.* 187, 1036–1043. doi: 10.1128/jb.187.3.1036-1043.2005

Levicán, G., Ugalde, J. A., Ehrenfeld, N., Maass, A., and Parada, P. (2008). Comparative genomic analysis of carbon and nitrogen assimilation mechanisms in three indigenous bioleaching bacteria: predictions and validations. *BMC Genomics* 9:581. doi: 10.1186/1471-2164-9-581

Li, L., Fu, M.-L., Zhao, Y.-H., and Zhu, Y.-T. (2012). Characterization of carbonic anhydrase II from *Chlorella vulgaris* in bio-CO2 capture. *Environ. Sci. Pollut. Res.* 19, 4227–4232. doi: 10.1007/s11356-012-1077-8

López-Pérez, M., Ghai, R., Leon, M. J., Rodríguez-Olmos, Á, Copa-Patiño, J. L., Soliveri, J., et al. (2013). Genomes of "Spiribacter", a streamlined, successful halophilic bacterium. *BMC Genomics* 14:787. doi: 10.1186/1471-2164-14-787

Lu, S., Peiffer, S., Lazar, C. S., Oldham, C., Neu, T. R., Ciobota, V., et al. (2016). Extremophile microbiomes in acidic and hypersaline river sediments of Western Australia. *Environ. Microbiol. Rep.* 8, 58–67. doi: 10.1111/1758-2229.12351

Lundbäck, A.-K., Müller, S. A., Engel, A., and Hebert, H. (2009). Assembly of Kch, a putative potassium channel from *Escherichia coli*. *J. Struct. Biol.* 168, 288–293. doi: 10.1016/j.jsb.2009.07.018

Macalady, J. L., Vestling, M. M., Baumler, D., Boekelheide, N., Kaspar, C. W., and Banfield, J. F. (2004). Tetraether-linked membrane monolayers in Ferroplasma spp: a key to survival in acid. *Extremophiles* 8, 411–419. doi: 10.1007/s00792-004-0404-5

MacGilvray, M. E., Lapek, J. D., Friedman, A. E., and Quivey, R. G. (2012). Cardiolipin biosynthesis in Streptococcus mutans is regulated in response to external pH. *Microbiology* 158, 2133–2143. doi: 10.1099/mic.0.057273-0

Mangold, S., Rao Jonna, V., and Dopson, M. (2013). Response of *Acidithiobacillus caldus* toward suboptimal pH conditions. *Extremophiles* 17, 689–696. doi: 10.1007/s00792-013-0553-5

Marcus, E. A., and Scott, D. R. (2016). "Gastric colonization by *H. pylori*," in *Helicobacter pylori*, 1st Edn, ed. N. Kim (Singapore: Springer), 23–34. doi: 10.1007/978-981-287-706-2_2

Marcus, E. A., Moshfegh, A. P., Sachs, G., and Scott, D. R. (2005). The periplasmic α-carbonic anhydrase activity of *Helicobacter pylori* is essential for acid acclimation. *J. Bacteriol.* 187, 729–738. doi: 10.1128/jb.187.2.729-738.2005

Mates, A. K., Sayed, A. K., and Foster, J. W. (2007). Products of the *Escherichia coli* acid fitness island attenuate metabolite stress at extremely low ph and mediate a cell density-dependent acid resistance. *J. Bacteriol.* 189, 2759–2768. doi: 10.1128/jb.01490-06

McNulty, R., Ulmschneider, J. P., Luecke, H., and Ulmschneider, M. B. (2013). Mechanisms of molecular transport through the urea channel of *Helicobacter* pylori. *Nat. Commun.* 4:2900. doi: 10.1038/ncomms3900

Minegishi, H. (2013). "Halophilic, acidophilic, and haloacidophilic prokaryotes," in *Polyextremophiles. Cellular Origin, Life in Extreme Habitats and Astrobiology*, Vol. 27, eds J. Seckbach, A. Oren, and H. Stan-Lotter (Dordrecht: Springer), 201–213. doi: 10.1007/978-94-007-6488-0_7

Mitra, A., Fay, P. A., Morgan, J. K., Vendura, K. W., Versaggi, S. L., and Riordan, J. T. (2012). Sigma factor n, liaison to an ntrc and rpos dependent regulatory pathway controlling acid resistance and the lee in enterohemorrhagic *Escherichia coli*. *PLoS One* 7:e46288. doi: 10.1371/journal.pone.0046288

Mitra, A., Fay, P. A., Vendura, K. W., Alla, Z., Carroll, R. K., Shaw, L. N., et al. (2014). σ N −dependent control of acid resistance and the locus of enterocyte effacement in enterohemorrhagic E scherichia coli is activated by acetyl phosphate in a manner requiring flagellar regulator FlhDC and the σ S antagonist FliZ. *Microbiol. Open* 3, 497–512. doi: 10.1002/mbo3.183

Mongodin, E. F., Nelson, K. E., Daugherty, S., Deboy, R. T., Wister, J., Khouri, H., et al. (2005). The genome of Salinibacter ruber: convergence and gene exchange among hyperhalophilic bacteria and archaea. *Proc. Natl. Acad. Sci. U.S.A.* 102, 18147–18152. doi: 10.1073/pnas.0509073102

Moran-Reyna, A., and Coker, J. A. (2014). The effects of extremes of pH on the growth and transcriptomic profiles of three haloarchaea. *F1000Research* 3:168. doi: 10.12688/f1000research.4789.2

Mourin, M., Wai, A., O'Neil, J., Hausner, G., and Dibrov, P. (2019). Physiological, structural, and functional analysis of the paralogous cation–proton antiporters of nhap type from *Vibrio cholerae*. *Int. J. Mol. Sci.* 20:2572. doi: 10.3390/ijms20102572

Mykytczuk, N. C. S., Trevors, J. T., Ferroni, G. D., and Leduc, L. G. (2010). Cytoplasmic membrane fluidity and fatty acid composition of *Acidithiobacillus ferrooxidans* in response to pH stress. *Extremophiles* 14, 427–441. doi: 10.1007/s00792-010-0319-2

Nakamura, T., Yamamuro, N., Stumpe, S., Unemoto, T., and Bakker, E. P. (1998). Cloning of the trkAH gene cluster and characterization of the Trk K(+)-uptake system of Vibrio alginolyticus. *Microbiology* 144 (Pt 8), 2281–2289. doi: 10.1099/00221287-144-8-2281

Neilson, J. W., Quade, J., Ortiz, M., Nelson, W. M., Legatzki, A., Tian, F., et al. (2012). Life at the hyperarid margin: novel bacterial diversity in arid soils of the Atacama Desert, Chile. *Extremophiles* 16, 553–566. doi: 10.1007/s00792-012-0454-z

Nguyen, L.-T., Schmidt, H. A., von Haeseler, A., and Minh, B. Q. (2015). IQ-TREE: a fast and effective stochastic algorithm for estimating maximum-likelihood phylogenies. *Mol. Biol. Evol.* 32, 268–274. doi: 10.1093/molbev/msu300

Nicolle, J. L. C., Le, C., Nicolle, J., Simmons, S., Bathe, S., and Norris, P. R. (2009). Ferrous iron oxidation and rusticyanin in halotolerant, acidophilic "*Thiobacillus prosperus*.". *Microbiology* 155, 1302–1309. doi: 10.1099/mic.0.023192-0

Norris, P. R., Davis-Belmar, C. S., Calvo-Bado, L. A., and Ogden, T. J. (2020). Salt-tolerant *Acidihalobacter* and *Acidithiobacillus* species from Vulcano (Italy) and Milos (Greece). *Extremophiles* 24, 593–602. doi: 10.1007/s00792-020-01178-w

Ossandon, F. J., Cárdenas, J. P., Corbett, M., Quatrini, R., Holmes, D. S., and Watkin, E. (2014). Draft genome sequence of the iron-oxidizing, acidophilic, and halotolerant "*Thiobacillus prosperus*" type strain DSM 5130. *Genome Announc.* 2:e01042–14. doi: 10.1128/genomeA.01042-14

Pandey, G. K., and Mahiwal, S. (2020). "Potassium homeostasis," in *Role of Potassium in Plants*, eds G. K. Pandey and S. Mahiwal New York, NY: Springer International Publishing, 11–18. doi: 10.1007/978-3-030-45953-6_2

Parashar, D., and Satyanarayana, T. (2018). An insight into ameliorating production, catalytic efficiency, thermostability and starch saccharification of acid-stable α-amylases from acidophiles. *Front. Bioeng. Biotechnol.* 6:125. doi: 10.3389/fbioe.2018.00125

Pflock, M., Kennard, S., Delany, I., Scarlato, V., and Beier, D. (2005). Acid-induced activation of the urease promoters is mediated directly by the ArsRS two-component system of *Helicobacter* pylori. *Infect. Immun.* 73, 6437–6445. doi: 10.1128/IAI.73.10.6437-6445.2005

Price-Whelan, A., Poon, C. K., Benson, M. A., Eidem, T. T., Roux, C. M., Boyd, J. M., et al. (2013). Transcriptional profiling of Staphylococcus aureus during growth in 2 M NaCl leads to clarification of physiological roles for Kdp and Ktr K+ uptake systems. *MBio* 4:e00407–13. doi: 10.1128/mBio.00407-13

Pruitt, K. D., Tatusova, T., Brown, G. R., and Maglott, D. R. (2012). NCBI Reference Sequences (RefSeq): current status, new features and genome annotation policy. *Nucleic Acids Res.* 40, D130–D135. doi: 10.1093/nar/gkr1079

Quatrini, R., and Barrie Johnson, D. (2016). *Acidophiles: Life in Extremely Acidic Environments*. Norfolk: Caister Academic Press.

Raven, J. A. (2021). Origin of the roles of potassium in biology. *Bioessays* 43:e2000302. doi: 10.1002/bies.202000302

Rhee, H. J., Kim, E.-J., and Lee, J. K. (2007). Physiological polyamines: simple primordial stress molecules. *J. Cell. Mol. Med.* 11, 685–703. doi: 10.1111/j.1582-4934.2007.00077.x

Riadi, G., Medina-Moenne, C., and Holmes, D. S. (2012). TnpPred: a web service for the robust prediction of prokaryotic transposases. *Comp. Funct. Genomics* 2012:678761. doi: 10.1155/2012/678761

Richard, H., and Foster, J. W. (2004). *Escherichia coli* glutamate- and arginine-dependent acid resistance systems increase internal pH and reverse transmembrane potential. *J. Bacteriol.* 186, 6032–6041. doi: 10.1128/JB.186.18.6032-6041.2004

Rivera-Araya, J., Huynh, N. D., Kaszuba, M., Chávez, R., Schlömann, M., and Levicán, G. (2020). Mechanisms of NaCl-tolerance in acidophilic iron-oxidizing bacteria and archaea: comparative genomic predictions and insights. *Hydrometallurgy* 194:105334. doi: 10.1016/j.hydromet.2020.105334

Rivera-Araya, J., Pollender, A., Huynh, D., Schlömann, M., Chávez, R., and Levicán, G. (2019). Osmotic imbalance, cytoplasm acidification and oxidative stress induction support the high toxicity of chloride in acidophilic bacteria. *Front. Microbiol.* 10:2455. doi: 10.3389/fmicb.2019.02455

Romantsov, T., Guan, Z., and Wood, J. M. (2009). Cardiolipin and the osmotic stress responses of bacteria. *Biochim. Biophys. Acta* 1788, 2092–2100. doi: 10.1016/j.bbamem.2009.06.010

Sachs, G., Kraut, J. A., Wen, Y., Feng, J., and Scott, D. R. (2006). Urea transport in bacteria: acid acclimation by gastric *Helicobacter* spp. *J. Membr. Biol.* 212, 71–82. doi: 10.1007/s00232-006-0867-7

Samartzidou, H., Mehrazin, M., Xu, Z., Benedik, M. J., and Delcour, A. H. (2003). Cadaverine inhibition of porin plays a role in cell survival at Acidic pH. *J. Bacteriol.* 185, 13–19. doi: 10.1128/jb.185.1.13-19.2003

Scott, D. R., Marcus, E. A., Weeks, D. L., Lee, A., Melchers, K., and Sachs, G. (2000). Expression of the *Helicobacter* pylori ureI gene is required for acidic pH activation of cytoplasmic urease. *Infect. Immun.* 68, 470–477. doi: 10.1128/IAI.68.2.470-477.2000

Siguier, P., Perochon, J., Lestrade, L., Mahillon, J., and Chandler, M. (2006). ISfinder: the reference centre for bacterial insertion sequences. *Nucleic Acids Res.* 34, D32–D36. doi: 10.1093/nar/gkj014

Simmons, S., and Norris, R. (2002). Acidophiles of saline water at thermal vents of Vulcano, Italy. *Extremophiles* 6, 201–207. doi: 10.1007/s007920100242

Slonczewski, J. L., Fujisawa, M., Dopson, M., and Krulwich, T. A. (2009). Cytoplasmic pH measurement and homeostasis in bacteria and archaea. *Adv. Microb. Physiol.* 55, 1–79, 317. doi: 10.1016/S0065-2911(09)05501-5

Stabnikov, V., Chu, J., Ivanov, V., and Li, Y. (2013). Halotolerant, alkaliphilic urease-producing bacteria from different climate zones and their application for biocementation of sand. *World J. Microbiol. Biotechnol.* 29, 1453–1460. doi: 10.1007/s11274-013-1309-1

Stautz, J., Hellmich, Y., Fuss, M. F., Silberberg, J. M., Devlin, J. R., Stockbridge, R. B., et al. (2021). Molecular mechanisms for bacterial potassium homeostasis. *J. Mol. Biol.* 433:166968. doi: 10.1016/j.jmb.2021.166968

Strahl, H., and Greie, J.-C. (2008). The extremely halophilic archaeon *Halobacterium salinarum* R1 responds to potassium limitation by expression of the K+-transporting KdpFABC P-type ATPase and by a decrease in intracellular K+. *Extremophiles* 12, 741–752. doi: 10.1007/s00792-008-0177-3

Sun, L., Xiao, L., Xiao, B., Wang, W., Pan, C., Wang, S., et al. (2013). Differences in the gene expressive quantities of carbonic anhydrase and cysteine synthase in the weathering of potassium-bearing minerals by *Aspergillus niger*. *Sci. China Earth Sci.* 56, 2135–2140. doi: 10.1007/s11430-013-4704-4

Suzuki, I., Lee, D., Mackay, B., Harahuc, L., and Oh, J. K. (1999). Effect of various ions, pH, and osmotic pressure on oxidation of elemental sulfur by *Thiobacillus thiooxidans*. *Appl. Environ. Microbiol.* 65, 5163–5168. doi: 10.1128/AEM.65.11.5163-5168.1999

Szklarczyk, D., Gable, A. L., Lyon, D., Junge, A., Wyder, S., Huerta-Cepas, J., et al. (2019). STRING v11: protein-protein association networks with increased coverage, supporting functional discovery in genome-wide experimental datasets. *Nucleic Acids Res.* 47, D607–D613. doi: 10.1093/nar/gky1131

Ullrich, S. R., González, C., Poehlein, A., Tischler, J. S., Daniel, R., Schlömann, M., et al. (2016a). Gene Loss and horizontal gene transfer contributed to the genome evolution of the extreme acidophile "ferrovum.". *Front. Microbiol.* 7:797. doi: 10.3389/fmicb.2016.00797

Ullrich, S. R., Poehlein, A., Tischler, J. S., González, C., Ossandon, F. J., Daniel, R., et al. (2016b). Genome analysis of the biotechnologically relevant acidophilic iron oxidising strain ja12 indicates phylogenetic and metabolic diversity within the novel genus "ferrovum.". *PLoS One* 11:e0146832. doi: 10.1371/journal.pone.0146832

Varani, A. M., Siguier, P., Gourbeyre, E., Charneau, V., and Chandler, M. (2011). ISsaga is an ensemble of web-based methods for high throughput identification and semi-automatic annotation of insertion sequences in prokaryotic genomes. *Genome Biol.* 12:R30. doi: 10.1186/gb-2011-12-3-r30

Veaudor, T., Cassier-Chauvat, C., and Chauvat, F. (2019). Genomics of urea transport and catabolism in cyanobacteria: biotechnological implications. *Front. Microbiol.* 10:2052. doi: 10.3389/fmicb.2019.02052

Vergara, E., Neira, G., González, C., Cortez, D., Dopson, M., and Holmes, D. S. (2020). Evolution of predicted acid resistance mechanisms in the extremely acidophilic *Leptospirillum* Genus. *Genes* 11:389. doi: 10.3390/genes11040389

Waack, S., Keller, O., Asper, R., Brodag, T., Damm, C., Fricke, W. F., et al. (2006). Score-based prediction of genomic islands in prokaryotic genomes using hidden Markov models. *BMC Bioinformatics* 7:142. doi: 10.1186/1471-2105-7-142

Walderhaug, M. O., Polarek, J. W., Voelkner, P., Daniel, J. M., Hesse, J. E., Altendorf, K., et al. (1992). KdpD and KdpE, proteins that control expression of the kdpABC operon, are members of the two-component sensor-effector class of regulators. *J. Bacteriol.* 174, 2152–2159. doi: 10.1128/jb.174.7.2152-2159.1992

Xiao, B., Lian, B., Sun, L., and Shao, W. (2012). Gene transcription response to weathering of K-bearing minerals by *Aspergillus fumigatus*. *Chem. Geol.* 306–307, 1–9. doi: 10.1016/j.chemgeo.2012.02.014

Yamauchi, K., Doi, K., Yoshida, Y., and Kinoshita, M. (1993). Archaebacterial lipids: highly proton-impermeable membranes from 1,2-diphytanyl-sn-glycero-3-phosphocholine. *Biochim. Biophys. Acta* 1146, 178–182. doi: 10.1016/0005-2736(93)90353-2

Zammit, C. M., and Watkin, E. L. J. (2016). "Adaptation to extreme acidity and osmotic stress," in *Acidophiles: Life in Extremely Acidic Environments*, eds R. Quatrini and D. B. Johnson (Poole: Caister Academic Press), 49–62. doi: 10.21775/9781910190333.03

Zammit, C. M., Mutch, L. A., Watling, H. R., and Watkin, E. L. J. (2009). The characterization of salt tolerance in biomining microorganisms and the search for novel salt tolerant strains. *Adv. Materials Res.* 71-73, 283–286. doi: 10.4028/www.scientific.net/amr.71-73.283

Zhao, B., and Houry, W. A. (2010). Acid stress response in enteropathogenic gammaproteobacteria: an aptitude for survival. *Biochem. Cell Biol.* 88, 301–314. doi: 10.1139/o09-182

Zhu, Q., Kosoy, M., and Dittmar, K. (2014). HGTector: an automated method facilitating genome-wide discovery of putative horizontal gene transfers. *BMC Genomics* 15:717. doi: 10.1186/1471-2164-15-717

Zückert, W. R. (2014). Secretion of bacterial lipoproteins: through the cytoplasmic membrane, the periplasm and beyond. *Biochim. Biophys. Acta* 1843, 1509–1516. doi: 10.1016/j.bbamcr.2014.04.022

Conflict of Interest: The authors declare that the research was conducted in the absence of any commercial or financial relationships that could be construed as a potential conflict of interest.

Publisher's Note: All claims expressed in this article are solely those of the authors and do not necessarily represent those of their affiliated organizations, or those of the publisher, the editors and the reviewers. Any product that may be evaluated in this article, or claim that may be made by its manufacturer, is not guaranteed or endorsed by the publisher.

frontiers | Frontiers in Microbiology

ORIGINAL RESEARCH
published: 03 May 2022
doi: 10.3389/fmicb.2022.841359

Comparative Proteomic Analysis of Psychrophilic vs. Mesophilic Bacterial Species Reveals Different Strategies to Achieve Temperature Adaptation

Laura García-Descalzo[1], Eva García-López[2] and Cristina Cid[2]*

[1] Centro de Astrobiología, Department of Planetology and Habitability, CSIC-INTA, Madrid, Spain, [2] Centro de Astrobiología, Department of Molecular Ecology, CSIC-INTA, Madrid, Spain

The old debate of nature (genes) vs. nurture (environmental variables) is once again topical concerning the effect of climate change on environmental microorganisms. Specifically, the Polar Regions are experiencing a drastic increase in temperature caused by the rise in greenhouse gas emissions. This study, in an attempt to mimic the molecular adaptation of polar microorganisms, combines proteomic approaches with a classical microbiological analysis in three bacterial species *Shewanella oneidensis*, *Shewanella frigidimarina,* and *Psychrobacter frigidicola*. Both shewanellas are members of the same genus but they live in different environments. On the other hand, *Shewanella frigidimarina* and *Psychrobacter frigidicola* share the same natural environment but belong to a different genus. The comparison of the strategies employed by each bacterial species estimates the contribution of genome vs. environmental variables in the adaptation to temperature. The results show a greater versatility of acclimatization for the genus *Shewanella* with respect to *Psychrobacter*. Besides, *S. frigidimarina* was the best-adapted species to thermal variations in the temperature range 4–30°C and displayed several adaptation mechanisms common with the other two species. Regarding the molecular machinery used by these bacteria to face the consequences of temperature changes, chaperones have a pivoting role. They form complexes with other proteins in the response to the environment, establishing cooperation with transmembrane proteins, elongation factors, and proteins for protection against oxidative damage.

Keywords: psychrophiles, proteomics, adaptation, chaperone protein, protein complex

OPEN ACCESS

Edited by:
Gloria Paz Levicán, University of Santiago, Chile

Reviewed by:
Andrés Esteban Marcoleta, University of Chile, Chile
Catherine Duport, University of Avignon, France

****Correspondence:***
Laura García-Descalzo
garciadl@cab.inta-csic.es

Specialty section:
This article was submitted to Extreme Microbiology, a section of the journal Frontiers in Microbiology

Received: *22 December 2021*
Accepted: *08 March 2022*
Published: *03 May 2022*

Citation:
García-Descalzo L, García-López E and Cid C (2022) Comparative Proteomic Analysis of Psychrophilic vs. Mesophilic Bacterial Species Reveals Different Strategies to Achieve Temperature Adaptation. Front. Microbiol. 13:841359. doi: 10.3389/fmicb.2022.841359

Abbreviations: SBd, substrate-binding domain-containing protein; TAXI-TRAP, TAXI family TRAP transporter solute-binding subunit; Omp, outer membrane porine; Phe-tRNA, phenylalanile-tRNA ligase subunit beta; RpiA, ribose-5-phosphate isomerase; cAMP-CRP, cAMP-activated global transcriptional regulator CRP protein; Flav-Sye4-NAD(P)H, flavin oxidoreductase Sye4; RpS1, ribosomal protein S1 30S; Pro-Iso, peptidyl-prolyl isomerase; TolC, outer membrane channel protein TolC; TonB, TonB-dependent siderophore receptor; GDHr, glutathione-disulfide reductase protein; PflB, formate C-acetyltransferase; PrpC, protein 2-methylcitrate synthase; Fur, ferric iron uptake transcriptional regulator; TolB, Tol-Pal system protein TolB; DH-E1, 2-oxoglutarate dehydrogenase E1 component; acyl-CoA DH, acyl-CoA dehydrogenase family protein; NpRibT, nicotinate phosphoribosyltransferase; CTP synthase, cytosine triphosphate synthase; PspA, phage shock protein A; ClpS, protease-dependent ATP adaptor protein Clp; Do-DegQ, periplasmic Do family serine endopeptidase DegQ; DNA-Dps, DNA starvation/stationary phase protection protein; Cyto-c-type, Chain A Tetraheme cytochrome c-type; Tpx-C, Thiol peroxidase protein subunit C; Q-nitroreductase-K, K subunit of the NADH quinone nitroreductase family protein.

INTRODUCTION

Cold is the most frequently spread natural condition that causes stress to live organisms (Rodrigues and Tiedje, 2008). Cold ecosystems are widespread on Earth, given that 80% of the biosphere is permanently frozen (Russell, 1990). About 90% of oceans hold a temperature of ≤5°C (Rodrigues and Tiedje, 2008), and, along with the seas, constitute 70% of the surface of the planet with a medium temperature of 2°C.

The low temperature causes changes in the properties of water even if it does not freeze (Rodrigues and Tiedje, 2008). This restricts its availability for biochemical reactions, limiting the survival of microorganisms that are unable to develop adaptive mechanisms to cope with it. When the temperature decreases, the diffusion of water drops, and its viscosity increases, reducing substrate diffusion rates and disrupting the transport of nutrients in the cells (Rodrigues and Tiedje, 2008). However, the low temperature does also alter other important parameters in cells, such as enzyme activity, membrane fluidity, transcription, translation, cellular division rates, protein folding, and denaturation (Russell, 1990; D'Amico et al., 2006; Rodrigues and Tiedje, 2008; Schumann, 2009; Alcazar et al., 2010).

The study of extremophiles has increased the discovery of new microorganisms and has contributed to understanding how they respond to evolving challenges over time at the molecular level (Irwin and Baird, 2004). Regarding the temperature of growth, microorganisms have been conventionally classified into psychrophiles (cold loving), psychrotrophs (cold tolerant), mesophiles (moderate temperature loving), and thermophiles (heat loving) (Tortora et al., 2010). Psychrophiles are broadly distributed and have developed successful strategies to colonize cold environments and even regions under temperature fluctuations (De Maayer et al., 2014). These strategies include the upward regulation of some genes, enhanced membrane transport, increased biosynthesis of carotenoid pigments, and compatible osmotic solutes (De Maayer et al., 2014; Cray et al., 2015).

Nevertheless, the main actors in these adaptive responses are the proteins, which have a key role in the molecular mechanisms of the cell. They control the balance between nutrients and products, the assembly of macromolecules, the dynamic of nucleic acids, and the correct folding of other proteins (D'Amico et al., 2006). Thus, changes in the composition of the proteome in response to cellular stress conditions are linked with specific adaptive strategies (Maier et al., 2011). Chaperones are a group of essential proteins involved in the quality control of cell machinery (Hartl and Hayer-Hartl, 2002) and in dealing with the consequences of stress (Cooper and Hausman, 2000; Hochachka and Somero, 2002; Beckerman, 2005; Cloutier and Coulombe, 2013). They are constituent proteins responsible for the correct folding and building of other proteins and for eliminating those incorrectly formed during synthesis or as a result of a cell stress situation (Hartl and Hayer-Hartl, 2002; Camberg et al., 2013).

Among the chaperone family, heat-shock proteins (Hsp) play a well-known role in the prevention of aberrant protein aggregates as well as in the facilitation of protein synthesis, translocation, *de novo* folding, and the assembly of multi-protein complexes (Bromfield and Nixon, 2013). Their amount increases in the cell during stress situations like changes in the temperature of the environment. Not only does heat induce these proteins but the exposure of cells to low temperature can also lead to the synthesis of some Hsps (Hochachka and Somero, 2002; García-Descalzo et al., 2011). The main families of Hsps are highly conserved and classified based on their sequence and their molecular weight (Makhnevych and Houry, 2013). Two large and important families are Hsp70 and Hsp60 (Cooper and Hausman, 2000; Beckerman, 2005). Sometimes, members of these families act together sequentially during protein transport and folding of newly synthesized proteins (Langer et al., 1992; Cooper and Hausman, 2000). Protein DnaK is the main representative of the Hsp70 family in the prokaryotes (Thompson et al., 2012), and it is part of a chaperone system together with other co-chaperones, such as DnaJ, from the Hsp 40 family, and the nucleotide exchange factor GrpE (Ahmad et al., 2011; Perrody et al., 2012; Thompson et al., 2012). In the Hsp60 family, a great number of chaperone complexes are activated by cellular stress, including the GroEL-GroES complex (Ventura et al., 2004), which are responsible for facilitating the folding of other proteins from an incorrect or unfolded conformation to their native form in stressful situations (Cooper and Hausman, 2000).

Extremophiles employ different adaptive approaches to cope with environmental changes (Lin, 2008; Metpally and Reddy, 2009; Paredes et al., 2011). Their comparison is a very valuable tool to identify crucial features of adaptation to cold and fluctuating environments. With this purpose, we designed a comparative proteomic study of three bacteria: a mesophile, a psychrophile, and a psychrotroph. They were subjected to different growth temperature conditions to study the underlying molecular actors that are activated under diverse environmental scenarios. Two of these bacteria belong to the same genus but live in environments with different temperatures, while the other two share the same environment but belong to a different genus. In this way, our findings will clarify to what extent the strategies used by these microorganisms are derived from a similar genome or a similar environment. Detailed information about each strain is summarized in **Table 1**.

Moreover, the knowledge of these molecular mechanisms will have application in different research fields, including biotechnology, medicine, astrobiology, ecology, and climate change investigations (Cavicchioli et al., 2002). The molecules involved in these mechanisms range from enzymes that remain active with high efficiency at very low temperature to be used in the food industry (or in cosmetic or textile detergent production) (Cavicchioli et al., 2002) to biosensors that can report about the state of an ecosystem (Irwin and Baird, 2004), providing valuable information related to climate change or even to biomarkers of habitability in planetary exploration and planetary analog research.

MATERIALS AND METHODS

Strains and Culture Conditions

Bacteria included in this study were purchased from culture collections: *Shewanella oneidensis* (MR-1, 700550TM) and *Shewanella frigidimarina* (ACAM 591, 700753TM) from the

TABLE 1 | Main features of the species used.

Specie	Taxonomy	Thermal classification	Optimal growth T[a]	Environment isolation	Available sequenced genome	Total proteome size
S. oneidensis	γ-Proteobacteria	mesophile	30°C	Oneida Lake (New York)	Yes (4,97 Mbp)	4196
S. frigidimarina	γ-Proteobacteria	psychrotroph	20–22°C	Antarctic sea ice	Yes (4,85 Mbp)	4030
P. frigidicola	γ-Proteobacteria	psychrotolerant	15°C	Antarctic ornithogenic soil	No (2,85Mbp)	2298

Germany Microorganisms and Culture Cell collection (DMSZ) and *Psychrobacter frigidicola* (ACAM 304, 700361TM) from the American collection (ATCC®). The two first strains belong to the same genus but are distinct regarding their optimal temperature condition and natural environment. *S. oneidensis* is a mesophile, while *S. frigidimarina* is a psychrotolerant and *P. frigidicola* belongs to a different genus and is a psychrophile.

Individual pre-inocula of the three strains were prepared from vials stored in glycerol at −80°C. Aliquots of 100 μl from these vials were incubated at their corresponding optimal growth temperature in tubes with 5 ml of each specific broth (BactoMarine Broth Difco2216 – MB – for *S. frigidimarina* and *P. frigidicola* and Luria-Bertani Broth – LB – for *S. oneidensis*). Once they reached the half exponential phase (corresponding to an optical density (O.D.) at 600 nm about 0.5), 500 μl of each one was inoculated in 250 ml Erlenmeyer flasks with broth at a final volume of 100 ml. Flasks of each species were incubated in triplicate at each experimental temperature of 4, 12, and 30°C for 5 days in aerobic conditions (150 rpm stirring). The O.D. at 600 nm was checked two times per day until it reached the stationary growth phase. Then, pellets of each flask were obtained by centrifugation for 20 min (10,000 × *g*; 4°C) and washed with phosphate buffer saline (PBS). Pellets were used to extract proteins for subsequent experiments. For the growth curves, statistical analyses were performed using GraphPad Prism version 7.0 (GraphPad Software, La Jolla, CA, United States[1]). The data were the mean ± SD from three replicates.

Sodium Dodecyl Sulfate-Polyacrylamide Gel Electrophoresis and Western-Blot

Proteins from the pellets were extracted to study the potential differences in protein profiles of the three bacteria against different temperature conditions. The preparation of cell extracts and protein determination were performed as described in García-Descalzo et al. (2014).

Protein extracts were separated and analyzed by sodium dodecyl sulfate-polyacrylamide gel electrophoresis (SDS-PAGE) for 1 h at 200 V and 400 mA (PowerPac 200, BioRad) in 12% acrylamide-bisacrylamide gels (2.6% crosslinking) using low molecular weight (LMW) (GE Healthcare) marker. Gels were stained with Coomassie Blue or transferred to polyvinyl-difluoride membranes (PVDF) to perform chaperones immunodetection by western blot (WB).

Membranes were firstly incubated overnight in a cold chamber with antibodies anti-DnaK, anti-GroEL, anti-DnaJ, and anti-GroES (**Table 2**). A second incubation was performed with HRP-linked anti-rabbit or anti-mouse (1:1,000) for 1 h.

[1]www.graphpad.com

TABLE 2 | Antibodies for WB and the dilution used.

Chaperone antibody	Protein MW	Host	Type	Dilution
DnaK	70 kDa	mouse	monoclonal	1:1000
GroEL	60 kDa	mouse	monoclonal	1:1000
DnaJ	41 kDa	rabbit	policlonal	1:5000
GroES	10 kDa	rabbit	policlonal	1:10000

After several washes with PBS, membranes were revealed by chemiluminescence using ECL Western blotting detection reagents (GE Healthcare).

Two-Dimensional Fluorescence Difference Gel Electrophoresis

The proteins produced in each bacterium at the analyzed temperatures were separated by 2-DE (two-dimensional electrophoresis). Samples (150 μg from each extract) were prepared as previously described (García-Descalzo et al., 2014) with slight modifications. After the first dimension by IEF (isoelectric focusing), which separates proteins based on their isoelectric points, IPG-strips (Immobiline Dry Strips, GE; pH 3-11 NL – non-linear – of 24 cm) were equilibrated in two successive steps with SDS equilibration buffer solutions containing a Tris buffer, 100 mM; urea, 6 M; glycerol, 30% (w/v); and DTT, 0.5% (w/v). Then, they were incubated with iodoacetamide, 4.5% (w/v). The second dimension in SDS-PAGE, to separate proteins by their molecular weight, was carried out on 12% acrylamide (2.6% crosslinking) gels (1.-mm thick). Gels were stained with Coomassie Blue or with MALDI-MS-compatible silver reagent for protein identification (Miller et al., 2006).

To compare the proteins over and under synthesized in each temperature condition, proteins from bacterial cells grown at 4 and 30°C were analyzed by 2-D DIGE. Proteins were extracted from the cultures as indicated before, obtaining four biological replicates of each one. Samples (40 μg) from each experimental condition were made using 7 M urea/2 M thiourea and labeled with DIGE Fluor minimal dyes (GE Healthcare) for their electrophoresis separation and analysis. Two replicates of each experimental condition were labeled with Cy3 and the other two with Cy5. A pool of both temperature conditions was also labeled with Cy2 to be used as an internal standard.

Protein gel images were processed and analyzed using the DeCyder Differential In-gel Analysis (DIA). The spots were co-detected, quantified, normalized, and matched between the four replicate experiments. Protein abundance changes between samples from each strain grouped by the temperatures 4 and 30°C (4/30 ratio) were examined by ANOVA test. Spots present in at least three of four gels per group, with significant

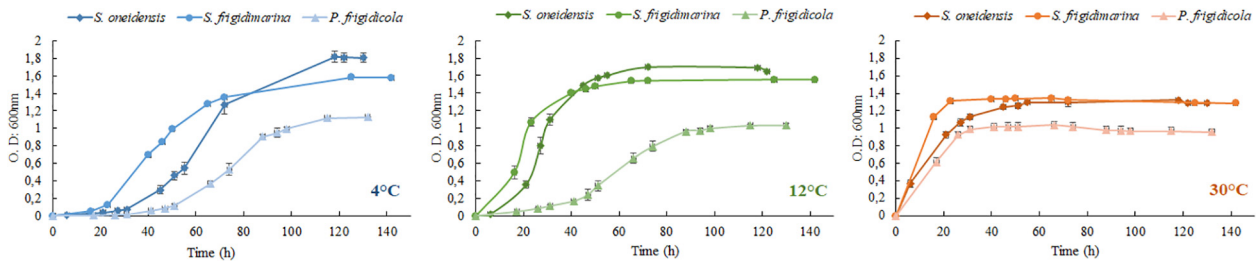

FIGURE 1 | Growth curves of *S. oneidensis*, *S. frigidimarina*, and *P. frigidicola* at 4 (blue), 12 (green), and 30°C (red/orange).

ANOVA test ($p \leq 0.05$ or $p \leq 0.01$), and an averaged 4/30 ratio $\geq \pm 2$ were considered and selected for further MS analysis in preparative gels. Those spots selected in new gels were excised, digested with trypsin, and identified by matrix-assisted laser desorption/ionization time-of-flight mass spectrometry (MALDI-TOF MS).

The identification protocol and data search used were based on the method previously described in Cid et al. (2010) and García-Descalzo et al. (2014) with minor variations. Combined peptide mass fingerprint and MS/MS ion search modes were applied against the NCBInr databases (NCBInr 081217 with 7463447 sequences and 2570742364 residues for *S. oneidensis*; NCBInr 160909 with 9694989 sequences and 3312496757 residues for *S. frigidimarina*; NCBInr 20131020 with 33055681 sequences and 11532217697 residues and NCBInr 14042010 with 10866589 sequences and 3703552722 residues for *P. frigidicola*). The MASCOT^{MT} (Matrix Science, London, United Kingdom) database search algorithm was used for protein identification (search parameters: Enzyme-trypsin; fixed modifications carbamidomethyl (C); variable modifications-oxidation (M); mass values-monoisotopic; protein mass unrestricted; peptide mass tolerance-±50 ppm; peptide charge State- 1+; max-missed cleavages-1).

Immunoprecipitation

Cell extracts were immunoprecipitated with monoclonal anti-DnaK and anti-GroEL antibodies (Enzo Life Sciences, United States) to study the DnaK- and the GroEL-associated proteins in the three bacteria studied.

The immunoprecipitation was carried out using Protein G-Sepharose previously washed with PBS. In the first-step, 600 μg of protein extract from each sample was mixed with 3 μl (1 mg/ml) of an antibody (anti-DnaK or anti-GroEL) for 4 h at 4°C with rotation in an immunoprecipitation buffer (IPB) (Tris HCl, 500 mM; pH: 7.5; NaCl, 200 mM; 0.2% Triton X-100; 0.2% NP-40; EDTA, 5 mM; pH: 8, protease inhibitors – Roche – and phenylmethylsulphonyl fluoride, PMSF, 1 mM). The immunoprecipitation was developed in stringent conditions to minimize unspecific complexes. Second, 30 μl of washed Protein-G-Sepharose (50% of slurry) was added, followed by 1 h of incubation in the same previous conditions. Finally, the immunoprecipitates were washed two times in a cold isotonic protease inhibition buffer (IPIB) (Tris HCl, 1 M; pH: 7.5; EDTA, 0.2 M; NaCl, 150 mM; 0.2% SDS) with protease inhibitors (Roche) to remove the unspecific binding. Then, samples were centrifuged for 5 min at 5,000 rpm, discarding the supernatant. The solid phase was subjected to two-dimensional electrophoresis (2 DE), and the subsequent protein identification was carried out by MALDI-TOF MS or kept at −20°C until use.

RESULTS

Cell Growth at 4 and 30°C (and 12°C)

Despite having different optimal temperatures for growth, the three bacteria studied were able to adapt to changing laboratory conditions, mimicking some of the extreme temperatures they could experience in their natural ecosystems. Their growth achieved high O.D. values in the established temperature range, although their lag phase was very different (**Figure 1** and **Table 3**). In the three bacteria, the growth at 4°C demanded a large lag phase; while warmer temperatures depicted a quicker onset, regardless of whether they were mesophile, psychrotolerant, or strict psychrophile. The differences between lag phase duration were statistically significant for the three strains at 4°C as well as for the case of *P. frigidicola* compared to the other two strains. The exponential phase duration when bacteria grew at 4°C was considerably larger when they grew at 30°C for the three species. Growth rates of each strain at each temperature treatment showed significant differences between

TABLE 3 | Duration of the lag phase in each bacterium at each temperature studied.

		4°C	12°C	30°C
S. oneidensis		32.00 (0.10)	7.00 (0.10)	0
S. frigidimarina		23.00 (0.10)	4.00 (0.11)	0
P. frigidicola		47.33 (0.33)	44.67 (3.22)	0
r^2		0.9993***	0.9993***	NS
Multiplecomparison	*S. oneidensis* vs. *S. frigidimarina*	***	NS	NS
	S. oneidensis vs. *P. frigidicola*	***	***	NS
	S. frigidimarina vs. *P. frigidicola*	***	***	NS

*Data are expressed as mean ± (SD). Statistical differences were studied by ANOVA test (***$p \leq 0.0001$). Statistical significance was achieved by Bonferroni's post-test (NS, not significant;***$p \leq 0.001$).*

TABLE 4 | Growth rates (h^{-1}) of *S. oneidensis*, *S. frigidimarina*, and *P. frigidicola* at 4, 12, and 30°C.

		4°C	12°C	30°C
S. oneidensis		13.91 (0.71)	8.777 (1.91)	11.37 (1.07)
S. frigidimarina		19.86 (1.22)	6.29 (2.15)	32.19 (2.28)
P. frigidicola		16.73 (1.47)	12.12 (2.15)	16.03 (4.42)
r^2		0.8646**	0.7370*	0.9328***
Multiplecomparison	*S. oneidensis* vs. *S. frigidimarina*	**	NS	***
	S. oneidensis vs. *P. frigidicola*	NS	NS	NS
	S. frigidimarina vs. *P. frigidicola*	NS	*	**

Data are expressed as mean ± (SD). Statistical differences were studied by ANOVA test ($p \leq 0.01$; **$p \leq 0.001$; ***$p \leq 0.0001$). Statistical significance was achieved by Bonferroni's post-test (NS, not significant; *$p \leq 0.05$; **$p \leq 0.01$; ***$p \leq 0.001$).*

S. frigidimarina and *S. oneidensis*, growing at 4 and 30°C and between *S. frigidimarina* and *P. frigidicola*, growing at 12 and 30°C (**Table 4**). For the two Shewanellas, the highest rate appeared at 30°C, while the rate of *P. frigidicola* is quite similar in the three temperatures tested.

Synthesis Levels of Chaperones With Temperature Changes Immunodetected by Western Blot

The relative synthesis levels of chaperones GroEL, GroES, DnaK, and DnaJ at 4 and 30°C for each bacterium were studied by WB. Cultures of the mesophile, *S. oneidensis*, at 30°C showed strong signals of chaperones GroEL/GroES and DnaK (**Figure 2A**). Cultures at 4°C revealed a weak band corresponding to DnaK, while a strong immunodetection of chaperonine GoES was observed (**Figure 2A**). These results may suggest that the machinery activated and controlled by these chaperones could be an advantage for the mesophile bacterium, allowing it to thrive in cold conditions and to grow even at temperatures far from its optimum.

The chaperones GroEL, DnaK, and DnaJ were immunodetected in samples from *S. frigidimarina* cultured at 30°C (10°C above their optimal growth temperature). Nevertheless, the immunodetection of chaperones in cultures at 4°C was not possible (**Figure 2B**).

In this case, the chaperone system at 30°C was formed by the chaperone DnaK from the Hsp70 family and its co-chaperonin DnaJ from the Hsp40 family. No levels of the co-chaperonin GroES were detected, despite the strong detection of its partner GroEL.

The immunodetection in samples from cultures of the psychrophile *P. frigidicola* showed detectable levels of GroEL and DnaK chaperones when cells were grown at 30°C but not at 4°C (**Figure 2C**). The optimal growth temperature for this microorganism is 15°C. It seems that it needs these chaperones to cope with warm temperatures, while, at cold temperatures, the levels of these proteins remained undetectable by WB.

Identification of Over- and Under-Synthesized Proteins at Warm and Cold Temperatures

Two-dimensional fluorescence difference gel electrophoresis experiments were performed to compare the whole proteomes of each bacterial species cultured at 4 and 30°C. In that way, the molecular machinery used in the adaptation to changes in temperature could be studied.

Two-Dimensional Differential Electrophoresis Analysis of *Shewanella oneidensis* at 4 and 30°C

2DE-labeled images (**Supplementary Figure 2**) were matched to analyze the results of 2D-DIGE as explained above. The fluorescence intensity of 395 protein spots was significantly altered by an averaged fold change of ±2 (*t*-test, $p < 0.01$). The 51 spots, which showed the greatest change, were selected and excised from the gel (**Supplementary Figure 3**), digested with trypsin, and identified by MALDI-TOF or MALDI-TOF-TOF MS. Finally, from the 51 spots selected, 44 were identified corresponding to 47 proteins, while 7 spots could not be identified (**Table 5**).

The identified proteins were classified into functional groups: carbohydrate metabolism, amino acid metabolism, nucleotide metabolism, protein metabolism, energy, redox homeostasis, transport and transmembrane proteins, chaperones and stress response, replication and translation, hypothetical, and an additional group one of the non-identified spots.

The main increased proteins observed at 30°C were especially from the categories related to stress response (GroEL, ClpB protein, DnaK), transport, and membrane proteins [flagellin, iron (III) ABC transporter, substrate-binding domain-containing protein], TAXI family TRAP transporter solute-binding subunit, and outer membrane porine. In cultures, at 4°C, *S. oneidensis* increased the synthesis of groups involved in replication and translation processes and in the biosynthesis of proteins and aminoacids precursors (Phe-tRNA, elongation factor G (EF-G), RpiA, and the cAMP-CRP). These bacteria also showed an increase in redox enzymes involved in the response to oxidative stress like Flav-Sye4.

Two-Dimensional Differential Electrophoresis Analysis of *Shewanella frigidimarina* at 4 and 30°C

After matching the fluorescence images (**Supplementary Figure 4**) and normalizing data from conditions of 4 and 30°C, 128 protein spots showed significant differences based on changes in the abundance ratio of ±1.5-fold with a *t*-test of $p < 0.005$. The 43 with the greatest differences were selected and cut off for their identification. About 42 spots were identified (**Supplementary Figure 5**) corresponding to 31 proteins – some of them with several isoforms – and 5 without satisfactory identification (**Table 6**).

Samples at 30°C showed a greater number of proteins identified as over-synthesized. The functional groups more represented were chaperones and stress proteins (GroES, Trigger factor, PspA, Clps adaptor, GrpE, GroEL, and DnaK) as well as the replication and translation proteins (elongation factors

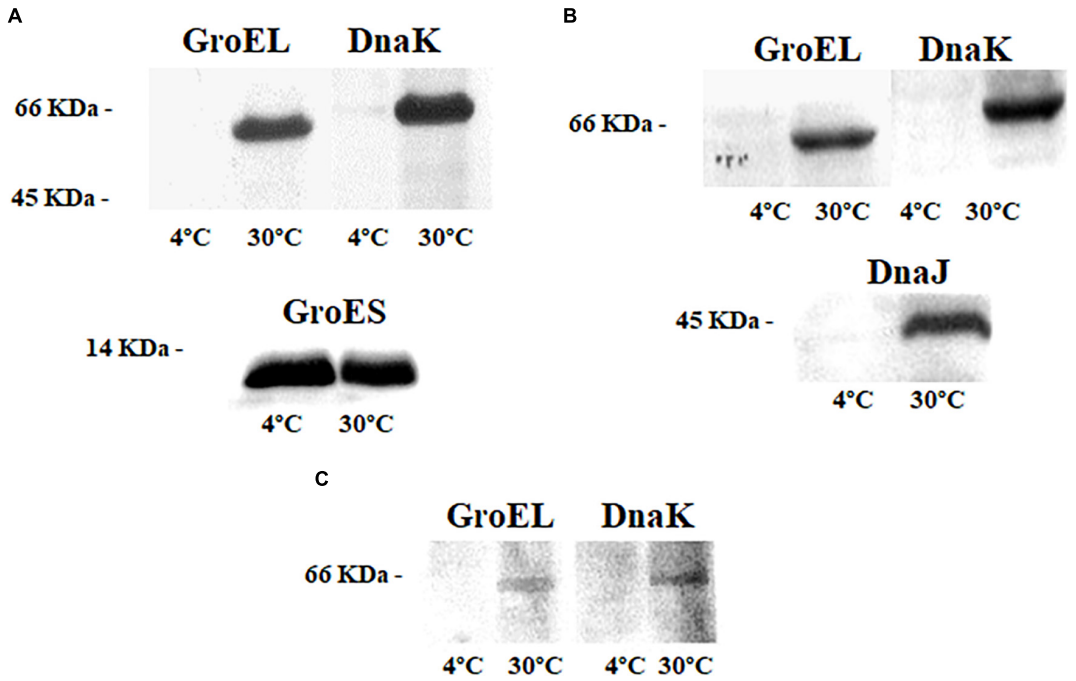

FIGURE 2 | Immunodetection of chaperones in the cell extracts of the three bacteria at 4 and 30°C; **(A)** GroEL, DnaK, and GroES in *Shewanella oneidensis*; **(B)** GroEL, DnaK, and DnaJ in *Shewanella frigidimarina*; and **(C)** GroEL and DnaK *Psychrobacter frigidicola*.

and ribosomal proteins). However, these two groups were not over-synthesized in samples at 4°C. At this temperature, the main groups identified were those of transport and membrane proteins. It is noteworthy that, in the 30°C samples, the redox metabolism was represented mainly by the appearance of three isoforms of the peroxiredoxin C protein. Two other isoforms of the same protein also appeared in cultures at 4°C.

Unlike the other two tested bacteria, cultures of *S. frigidimarina* at both 4°C and 30°C show a high number of isoforms of different proteins [TonB-dependent receptor, peroxiredoxin C, GroEL, DnaK, ferritin, elongation factor Tu (EF-Tu) and RpS1].

Two-Dimensional Differential Electrophoresis Analysis of *Psychrobacter frigidicola* at 4 and 30°C

The merged fluorescence images were analyzed (**Supplementary Figure 6**) and normalized. The data from the extracts at 4 and 30°C determined the protein spots of greatest interest. Thus, based on changes in the abundance ratio of ±2.5 times fold between both temperature conditions and with a $p < 0.05$ as statistically significant, 86 spots were selected. From them, the 39 spots with the greatest differences were cut out (**Supplementary Figure 7**), resulting in 36 (**Table 7**) proteins identified and 5 with no satisfactory identification. Due to the recent sequence project of this species, the identification of spots was carried out using databases of the closest phylogenetic species, such as *Psychrobacter cryohalolentis*, *Psychrobacter arcticus*, or the genus *Psychrobacter* in other cases.

In this species, we identified more than double the number of proteins over-synthesized at 30°C with regard to 4°C. Similarly to *S. frigidimarina*, the main group represented at 30°C, that was not found at 4°C, corresponded to *chaperones and stress proteins* [trigger factor, GrpE, GroES, superoxide dismutase (SOD), thioredoxin, ferritin, peptidyl-prolyl isomerase, and ATPase AAA-2]. Besides, we found, at 30°C, several proteins were involved in redox metabolism that did not appear in the 4°C condition. The main groups over-synthesized in cultures at 4°C were those of transport and transmembrane proteins, like TolC (spot 783), three isoforms of TonB (188, 189, and 195), and porin (1052).

Proteins in Common Revealed by Two-Dimensional Fluorescence Difference Gel Electrophoresis

Those proteins identified in at least two of the three species were grouped by a functional category, comparing their synthesis through changes in the 4/30 ratio and represented in a heatmap (**Figure 3**).

The protein groups most shared between the three bacterial species were those related to thermal stress, oxidative stress, and transmembrane transport. Mainly, the heatmap showed more coincidences in the production of proteins regarding temperature between *S. frigidimarina* and the other two species than between the other two species.

Comparison of Molecular Machinery

To compare the proteins *in vivo* linked to GroEL and DnaK chaperones, immunoprecipitations were carried out with specific

TABLE 5 | Identified proteins in *S. oneidensis* overexpressed at 4 (green) and 30°C (red).

Spot	Ratio 4/30	Identified protein	Specie	Functional group	Score	Pept. N	Accession number	% SC	pI	M.M. (Da)	R*
875	8.23	NAD(P)H:flavin oxidoreductase Sye4//alkene reductasa	*S. oneidensis*	Redox Homeost.	189	26	WP_011073258.1	58%	5.23	36629	
656	4.86	SidA/IucD/PvdA family monooxygenase	*S. oneidensis*	Redox Homeost.	191	11	WP_011072933.1	21%	6.27	48427	
1671	2.44	Ferric iron uptake transcriptional regulator	*S. oneidensis*	Stress/chaperones	176	8	WP_011072035.1	33%	5.77	16504	
1499	5.59	Non-heme ferritin	*S. oneidensis*	Stress/chaperones	128	11	WP_011070543.1	23%	4.77	20362	
706	3.21	Tol-Pal system protein TolB	*S. oneidensis*	Membrane/Transport	146	21	WP_011072687.1	44%	8.89	43897	
115	12.7	TonB-dependent receptor	*S. oneidensis*	Membrane/Transport	200	17	WP_011072815.1	25%	4.54	95930	
271	2.52	Ferric alcaligin siderophore receptor TonB-dependent//ferric putrebactin siderophore receptor PutA	*S. oneidensis MR-1*	Membrane/Transport	273	31	WP_011072936.1	52%	4.74	80853	
543	2.31	TolC family outer membrane protein	*S. oneidensis*	Membrane/Transport	225	26	WP_011073979.1	51%	5.17	52368	
162	3.24	Phenylalanine–tRNA ligase subunit beta	*S. oneidensis*	Replic/Translat.	223	31	WP_011072150.1	39%	5.14	87147	
223	23.02	Elongation factor G	*S. oneidensis*	Replic/Translat.	169	15	WP_011071132.1	22%	4.91	77127	
1307	4.93	Ribose-5-phosphate isomerase RpiA	*S. oneidensis*	Replic/Translat.	108	12	WP_011071382.1	51%	5.03	23354	
1366	2.07	cAMP-activated global transcriptional regulator CRP	*Shewanella*	Replic/Translat.	86	4	WP_011070954.1	19%	7.12	23862	
117	20.94	aminomethyl-transferring glycine dehydrogenase	*S. oneidensis*	AminoacidMetab.	216	15	WP_011071084.1	17%	5.70	105348	
363	23.85	S9 family peptidase	*S. oneidensis*	AminoacidMetab.	111	14	WP_011073927.1	20%	5.49	73874	
248	2.96	Peptidase, putative subfamily S9C unassigned peptidase	*S. oneidensis MR-1*	AminoacidMetab.	182	15	WP_011072247.1	19%	5.28	77948	
868	5.82	Gamma-glutamyltransferase GgtB	*S. oneidensis*	AminoacidMetab.	131	11	WP_011071048.1	14%	6.11	39090	
408	3	Acylase	*S. oneidensis*	Protein Metab.	95	28	WP_011071198.1	30%	5.01	92593	
284	16.35	S46 family peptidase	*S. oneidensis*	Protein Metab.	376	52	WP_011071328.1	66%	5.85	68876	
504	2.45	Phosphoenolpyruvate carboxykinase PckA	*S. oneidensis*	Carbohydrate Metab.	350	33	WP_011070559.1	75%	5.56	56190	
128	2.61	Bifunctional aconitate hydratase 2/2-methylisocitrate dehydratase	*S. oneidensis*	Carbohydrate Metab.	284	34	WP_011070790.1	40%	5.27	94879	
298	7.6	Formate C-acetyltransferase PflB	*S. oneidensis*	Carbohydrate Metab.	143	24	WP_011072817.1	24%	5.55	85205	
867	9.4	2-methylcitrate synthase PrpC	*S. oneidensis*	Carbohydrate Metab.	281	15	WP_011070709.1	38%	6.17	58982	
743	3.36	Acetate kinase	*S. oneidensis*	Energy	224	26	WP_011072820.1	71%	6.60	39407	
388	4.55	DUF885 domain-containing protein	*S. oneidensis*	Hypothetical	175	31	WP_011073230.1	46%	6.62	69137	
1249	3.17	WbqC family protein	*S. oneidensis*	Hypothetical	120	10	WP_011073072.1	28%	5.35	27787	
1102	18.69	–		unidentified							
1219	6.45	–									
826	3.27	–									
859	6.73	–									
1401	2.65	–									
1479	−4.27	Thiol peroxidase	*S. oneidensis*	Redox Homeost.	115	12	WP_011073211.1	58%	5.76	22153	
1379	−3.04	Peroxiredoxin C	*Shewanella*	Stress/chaperones	250	10	WP_011623136.1	37%	5.01	22085	
152	−16.79	ATP-dependent chaperone ClpB	*S. oneidensis*	Stress/chaperones	185	19	WP_011073398.1	23%	5.36	95759	
244	−6.8	Molecular chaperone DnaK	*S. oneidensis*	Stress/chaperones	291	40	WP_011071367.1	60%	4.77	77298	
420	−2.74	Chaperonin GroEL	*S. oneidensis*	Stress/chaperones	354	35	WP_011071022.1	69%	4.84	57101	
1620	−39.67	Universal stress protein	*S. oneidensis*	Stress/chaperones	276	11	WP_011073476.1	54%	5.26	15642	
856	−2.64	Porin	*S. oneidensis*	Membrane/Transport	353	30	WP_011073642.1	69%	4.70	39874	
993	−4.65	Flagellin FliC	*S. oneidensis*	Membrane/Transport	210	23	WP_011073122.1	62%	7.93	33512	
930	−2.62	Fe (3+) ABC transporter substrate-binding protein	*S. oneidensis*	Membrane/Transport	270	28	WP_011071051.1	67%	6.02	37394	
1236	−4.95	Substrate-binding domain-containing protein	*S. oneidensis*	Membrane/Transport	329	32	WP_011074305.1	79%	6.46	29348	
1018	−4.83	TAXI family TRAP transporter solute-binding subunit	*S. oneidensis MR-1*	Membrane/Transport	215	14	WP_011070810.1	31%	7.79	43542	
1159	−3.51	Class I SAM-dependent methyltransferase	*S. oneidensis MR-1*	Replic/Translat.	134	17	WP_011072532.1	61%	7.75	29576	

(Continued)

TABLE 5 | (Continued)

Spot	Ratio 4/30	Identified protein	Specie	Functional group	Score	Pept. N	Accession number	% SC	pI	M.M. (Da)	R*
643	−19.8	Elongation factor Tu	*S. oneidensis MR-1*	Replic/Translat.	306	31	WP_011070604.1	79%	5.13	56562	
818	−2.57	4-hydroxyphenylpyruvate dioxygenase	*S. oneidensis*	AminoacidMetab.	205	22	WP_011072057.1	52%	5.12	39874	
492	−10.82	Amidohydrolase	*S. oneidensis*	AminoacidMetab.	116	18	WP_011071259.1	31%	5.03	62282	
447	−2.28	Amidohydrolase	*S. oneidensis*	AminoacidMetab.	345	34	WP_011074413.1	62%	6.84	65670	
1657	−2.16	Nucleoside-diphosphate kinase	*Shewanella*	Nucleotide Metab.	451	13	WP_011072285.1	66%	5.50	15530	
557	−35.13	IMP dehydrogenase	*Shewanella*	Nucleotide Metab.	200	15	WP_011788710.1	30%	6.36	51929	
641	−2.42	Do family serine endopeptidase Deg Q	*S. oneidensis*	Protein Metab.	151	19	WP_011073684.1	46%	5.95	46522	
80	−4.91	Fe/S-dependent 2-methylisocitrate dehydratase AcnD	*S. oneidensis*	Carbohydrate Metab.	349	41	WP_011070708.1	46%	5.15	93904	
890	−2.38	Type I glyceraldehyde-3-phosphate dehydrogenase	*S. oneidensis*	Carbohydrate Metab.	148	14	WP_011072334.1	27%	5.83	28657	
1222	−3.19	–		unidentified							
192	−4.45	–									

R represents a heatmap of the ratio 4/30 as in* ***Figure 3****. A specie column refers to the organisms (specie or genus) in which protein has been identified according to the NCBI database.*

anti-GroEL and anti-DnaK antibodies. The immunoprecipitates were analyzed by 2DE, and proteins were identified by mass spectrometry (MS). The extended list of proteins identified that co-immunoprecipitate with DnaK or GroEL in each species and at each temperature are summarized in **Supplementary Material** (**Supplementary Tables 1–4**). **Figure 4** represents a comparison of the molecular machinery expressed by each bacterial species at each temperature tested that interacts with chaperones GroEL or DnaK.

Regarding the proteomic machinery, *P. frigidicola* and *S. oneidensis* used different proteins in these interactions. At warm temperatures, they only had one common interaction (GroEL with SOD). On the other hand, the machinery with more proteins in common was found between the two shewanellas at both temperatures and was related to both DnaK and GroEL. These proteins were elongation factors and transmembrane proteins, and the peroxiredoxin C in the case of immunoprecipitation with GroEL in cultures at 4°C. Specifically, *S. oneidensis* displayed a higher number of proteins interacting with chaperone GroEL, at 4 and 30°C, and DnaK, at 4°C, than *S. frigidimarina* and *P. frigidicola*. In contrast, the immunoprecipitation with DnaK in samples at 30°C showed a slight increase in the number of proteins identified in the species *S. frigidimarina* and *P. frigidicola*, compared to *S. oneidensis*. In fact, *P. frigidicola* immuno precipitated more proteins at 30°C with antibodies from both chaperones used than at 4°C, while *S. frigidimarina* showed a similar number of proteins interacting with both chaperone antibodies at 4 and 30°C, with the exception of a slight increase in the case of DnaK at 30°C.

DISCUSSION

The aim of this study was to understand the molecular strategies of three bacteria to cope with temperature changes in their environment. Given that the proteins are the main actors in these strategies and are responsible for the active machinery of the cells (D'Amico et al., 2006), the investigation has mainly focused on them. As mentioned above, this was achieved by comparing the behavior of psychrotolerant bacteria (i) *Shewanella frigidimarina*, which share a great part of the genome with the mesophile (ii) *Shewanella oneidensis* and came from the same environment (Antarctica) as the third bacteria (iii) *Psychrobacter frigidicola* from a different genus.

Growth Dynamics Under Different Temperatures

On the whole, the behavior of the three bacteria studied regarding their growth and biomass multiplication under cold, mild, and warm temperatures appeared relatively similar, with only mild differences in their growth phases (**Table 3**) and growth rates (**Table 4**). These differences could inform whether the bacteria are in a normal or stressful situation, taking into account the length of the lag phase. However, this would be just a potential finding taken as sole data (Hamill et al., 2020) that would need to be supported with further analysis by proteomic experiments.

Shewanella oneidensis is considered a mesophile according to its optimal growth temperature (Venkateswaran et al., 1999), but it was originally isolated from Oneida Lake in New York, which is frozen or at temperatures near 0°C for almost half of the year. This could be the reason why it can multiply at 4°C after a long lag phase with a relatively similar growth rate than at 30°C. Besides, this bacterium can behave as a psychrotolerant after a preadaptation period (Hébraud and Potier, 1999) as it has also been described for *E. coli* (Jones et al., 1987) and other mesophiles isolated from the Arctic and Antarctic permafrost (Steven et al., 2006).

S. frigidimarina and *P. frigidicola*, whose preinocula were set at 20°C, and *S. oneidensis* (preinocula at 30°C) showed marked lag phases in their growth at 4 and 12°C. In general, cold-adapted bacteria possess regulating factors that keep the translating machinery active at low temperatures. When their growth pauses due to a shift in temperature, they can activate

TABLE 6 | Identified proteins in *S. frigidimarina* overexpressed at 4 (green) and 30°C (red).

Spot	Ratio 4/30	Identified protein	Specie	Functional group	Score	Pept. N	Accession number	% SC	pI	M.M (Da)	R*
634	3.73	Glutathione-disulfide reductase	*S. frigidimarina*	Redox Homeost.	171	10	WP_011639286.1	21%	5.55	48293	
2023	12.75	Peroxiredoxin C	*Shewanella*	Estrés/chap.	137	7	WP_011636928.1	34%	5.22	22198	
1602	38.07	Peroxiredoxin C	*Shewanella*	Estrés/chap.	103	12	WP_011636928.1	68%	5.22	22198	
1052	114.95	Porin	*Shewanella*	Membrane/Transport	124	18	WP_011635991.1	47%	4.53	34011	
783	8.48	Outer membrane channel protein TolC	*Shewanella*	Membrane/Transport	153	20	WP_011638771.1	43%	4.97	47015	
195	10.63	TonB-dependent siderophore receptor	*S. frigidimarina*	Membrane/Transport	187	23	WP_011639260.1	32%	4.55	78903	
189	7.15	TonB-dependent siderophore receptor	*S. frigidimarina*	Membrane/Transport	120	10	WP_011639260.1	15%	4.55	78903	
188	5.61	TonB-dependent siderophore receptor	*S. frigidimarina*	Membrane/Transport	153	20	WP_011639260.1	26%	4.55	78903	
951	10.2	Agmatine deiminase	*S. frigidimarina*	AminoacidMetab.	89	11	WP_011637082.1	39%	4.61	41039	
1689	24.66	(Hypothetical protein Sfri_2875) YceI family protein	*S. frigidimarina*	Protein Metab.	139	13	WP_011638323.1	52%	5.92	20372	
358	9.57	M61 family metallopeptidase	*S. frigidimarina*	Protein Metab.	144	12	WP_011638221.1	14%	5.33	68235	
278	16.91	S46 family peptidase	*Shewanella*	Protein Metab.	158	21	WP_011636061.1	31%	5.57	80465	
993	18.01	Class 1 fructose-bisphosphatase	*S. frigidimarina*	Carbohydrate Metab.	74	10	WP_011636019.1	32%	4.46	35885	
293	7.71	DUF1302 domain-containing protein	*Shewanella*	Unknown	141	22	WP_011637681.1	36%	4.40	75029	
1033	2.8	–		unidentified							
1020	2.78	–		unidentified							
288	5.7	–		unidentified							
1985	−6.78	Chain A, Tetraheme cytochrome c-type	*S. frigidimarina*	Redox Homeost.	89	4	2K3V_A	53%	4.61	9310	
2022	−11.34	Peroxiredoxin C	*Shewanella*	Estrés/chap.	319	13	WP_011636928.1	41%	5.22	22198	
1522	−5.94	Peroxiredoxin C	*Shewanella*	Estrés/chap.	222	9	WP_011636928.1	34%	5.22	22198	
1519	−7.17	Peroxiredoxin C	*Shewanella*	Estrés/chap.	223	11	WP_011636928.1	41%	5.22	22198	
1888	−26	co-chaperone GroES	*Shewanella*	Stress/chaperones	120	10	WP_011639076.1	100%	5.81	10153	
1418	−2.92	Phage shock protein PspA	*Shewanella*	Stress/chaperones	137	13	WP_011638028.1	49%	5.42	25743	
1398	−8.24	Nucleotide exchange factor GrpE	*S. frigidimarina*	Stress/chaperones	138	7	WP_011638240.1	19%	4.43	22235	
420	−4.8	Trigger factor	*Shewanella*	Stress/chaperones	72	7	WP_011638047.1	24%	4.73	47835	
387	−9.15	Chaperonin GroEL	*Shewanella*	Stress/chaperones	177	26	WP_011639075.1	51%	4.83	57115	
374	−9.3	Chaperonin GroEL	*Shewanella*	Stress/chaperones	139	4	WP_011639075.1	6%	4.83	57115	
224	−6.16	Molecular chaperone DnaK	*Shewanella*	Stress/chaperones	143	18	WP_011636443.1	43%	4.70	68893	
215	−6.17	Molecular chaperone DnaK	*Shewanella*	Stress/chaperones	123	17	WP_011636443.1	42%	4.70	68893	
205	−6.95	Molecular chaperone DnaK	*Shewanella*	Stress/chaperones	207	14	WP_011636443.1	21%	4.70	68893	
1773	−24.2	DNA starvation/stationary phase protection protein	*Shewanella*	Stress/chaperones	196	5	WP_011637305.1	23%	5.78	17684	
1767	−27.15	DNA starvation/stationary phase protection protein	*Shewanella*	Stress/chaperones	172	18	WP_011637305.1	73%	5.78	17684	
805	−3.49	Flagellar hook-associated protein FlgL	*S. frigidimarina*	Membrane/Transport	141	18	WP_011636645.1	32%	4.35	42352	
1220	−5.41	DUF4097 family beta strand repeat protein	*Shewanella*	Membrane/Transport	182	10	WP_011636320.1	35%	4.88	33161	
1198	−6.16	Elongation factor Ts	*Shewanella*	Replic/Translat.	92	11	WP_011636745.1	40%	5.12	30304	
711	−3.18	Elongation factor Tu	*Shewanella*	Replic/Translat.	248	28	WP_011635638.1	72%	5.07	43547	
708	−4.13	Elongation factor Tu	*Shewanella*	Replic/Translat.	183	20	WP_011635638.1	63%	5.07	43547	
701	−5.81	Elongation factor Tu	*Shewanella*	Replic/Translat.	94	14	WP_011635638.1	39%	5.07	43547	
459	−7.54	tRNA uridine-5-carboxymethylaminomethyl (34) synthesis GTPase MnmE	*S. frigidimarina*	Replic/Translat.	77	9	WP_011639467.1	30%	4.84	49300	
266	−6.49	30S ribosomal protein S1	*Shewanella*	Replic/Translat.	82	10	WP_011637579.1	24%	4.88	61260	
258	−9.09	30S ribosomal protein S1	*Shewanella*	Replic/Translat.	95	10	WP_011637579.1	30%	4.88	61260	
152	−4.24	elongation factor G	*Shewanella*	Replic/Translat.	148	5	WP_011636038.1	6%	4.95	77026	
1409	−5.37	5′/3′-nucleotidase SurE	*Shewanella*	Nucleotide Metab.	98	9	WP_011636531.1	34%	5.00	26351	
1832	−3.34	Nucleoside diphosphate kinase (NDP kinase)	*Shewanella*	Nucleotide Metab.	101	8	WP_041413046.1	38%	5.38	15477	
791	−4.06	Do family serine endopeptidase DegQ	*S. frigidimarina*	Protein Metab.	92	14	WP_011638799.1	41%	5.87	47095	
1884	−5.89	ATP-dependent Clp protease adapter ClpS	*Shewanella*	Protein Metab.	87	11	WP_011637710.1	64%	5.08	11852	
169	−5.03	–		unidentified							
170	−4.45	–		unidentified							

R represents a heatmap of the ratio 4/30 as in* ***Figure 3****. A specie column refers to the organisms (specie or genus) in which protein has been identified according to the NCBI database.*

TABLE 7 | Identified proteins in *P. frigidicola* overexpressed at 4 (green) and 30°C (red).

Spot	Ratio 4/30	Identified protein	Specie	Functional group	Score	Pept. N	Accession number	% SC	pI	M.M. (Da)	R*
417	14.94	Nicotinate phosphoribosyltransferase	*P. cryohalolentis*	Replic/Translat.	111	16	WP_011514515.1	35%	5.90	51410	
540	4.61	Phenylalanine–tRNA ligase subunit alpha	*P. cryohalolentis*	Replic/Translat.	222	17	WP_011514607.1	30%	5.39	39695	
431	3.73	Elongation factor Tu	*Psychrobacter*	Replic/Translat.	235	23	WP_011512793.1	74%	5.04	43277	
172	3.98	Translational GTPase TypA	*Psychrobacter*	Replic/Translat.	83	5	WP_011512742.1	12%	5.08	67942	
373	2.79	Argininosuccinate synthase	*P. arcticus*	AminoacidMetab.	93	11	WP_011280895.1	34%	5.03	46225	
421	3.36	Glutamate 5-kinase	*Psychrobacter*	AminoacidMetab.	101	11	WP_011514007.1	39%	5.32	42831	
311	3.05	Type I glutamate–ammonia ligase	*Psychrobacter*	AminoacidMetab.	86	10	WP_011513771.1	21%	5.12	52236	
296	4.29	5-guanidino-2-oxopentanoate decarboxylase	*P. cryohalolentis*	AminoacidMetab.	142	10	WP_011513878.1	16%	5.23	62796	
247	4.46	CTP synthase	*Psychrobacter*	Nucleotide Metab.	82	10	WP_011514195.1	20%	5.21	60615	
481	8.62	Acyl-CoA dehydrogenase family protein	*P. cryohalolentis*	Nucleotide Metab.	138	8	WP_011513519.1	24%	5.88	46876	
44	2.88	2-oxoglutarate dehydrogenase E1 component	*P. cryohalolentis*	Carbohydrate Metab.	160	24	WP_011512486.1	24%	5.37	108303	
241	3.04	–		unidentified							
1289	−3.79	NADH-quinone oxidoreductase subunit K (NDH-1 subunit K)	*Psychrobacter sp.* (PRwf-1)	Redox Homeost.	114	5	A5WG39.1	59%	5.59	13504	
645	−4.66	Uroporphyrinogen decarboxylase	*Psychrobacter*	Stress/chaperones	151	12	WP_011514006.1	30%	6.01	42217	
1036	−5.53	Nitroreductase family protein	*P. cryohalolentis*	Stress/chaperones	100	12	WP_011513876.1	49%	5.48	22806	
980	−4.16	VOC family protein	*P. cryohalolentis*	Stress/chaperones	163	10	WP_011513888.1	15%	5.44	22154	
359	−2.53	Trigger factor	*P. frigidicola*	Stress/chaperones	103	9	ABX56853	19%	4,54	50600	
1081	−4.61	Protein GrpE (Hsp-70 cofactor)	*Psychrobacter*	Stress/chaperones	151	8	WP_011514755.1	35%	4,64	22674	
1326	−3.37	GroES protein/Chaperonin 10 kDa	*P. arcticus*	Stress/chaperones	21	1	Q4FU95.1	20%	4,95	10351	
993	−2.88	Superoxide dismutase	*Psychrobacter*	Stress/chaperones	139	13	WP_011514541.1	63%	5.05	23649	
996	−3.19	Superoxide dismutase	*Psychrobacter*	Stress/chaperones	202	9	WP_011514541.2	24%	5.05	23649	
1301	−3.7	Thioredoxin	*P. arcticus*	Stress/chaperones	210	7	WP_011281244.1	32%	4.78	11993	
1126	−6.77	DNA starvation/stationary phase protection protein	*Psychrobacter sp.*	Stress/chaperones	132	7	WP_011960763.1	75%	5,06	17870	
1438	−3.85	Peptidyl-prolyl cis-trans isomerase	*P. cryohalolentis*	Stress/chaperones	296	18	WP_011513014.1	68%	5.02	18696	
76	−4.48	ATP-dependent chaperone ClpB	*P. cryohalolentis*	Stress/chaperones	140	20	WP_011513187.1	31%	5.07	96035	
852	−3.29	Inositol monophosphatase	*Psychrobacter*	Membrane/Transport	190	8	WP_011512618.1	18%	6.07	30665	
584	−7.05	Porin	*P. cryohalolentis*	Membrane/Transport	104	15	WP_011514197.1	45%	4.61	38871	
1437	−2.96	Ribosome recycling factor	*Psychrobacter*	Replic/Translat.	156	11	WP_011514038.1	35%	5.27	20846	
1353	−4.9	4a-hydroxytetrahydrobiopterin dehydratase	*P. cryohalolentis*	Replic/Translat.	109	6	WP_011513882.1	30%	5.48	12736	
816	−3.42	Elongation factor Ts	*P. arcticus*	Replic/Translat.	160	9	WP_011279658.1	35%	4,95	31766	
233	−2.76	Leucyl aminopeptidase	*P. cryohalolentis*	AminoacidMetab.	137	18	WP_011512426.1	38%	5.20	60490	
705	−2.55	Branched-chain amino acid transaminase	*Psychrobacter*	AminoacidMetab.	115	14	WP_011513510.1	44%	5.71	34743	
1253	−14.56	RidA family protein	*P. cryohalolentis*	AminoacidMetab.	137	12	WP_011512622.1	61%	8.89	18648	
618	−3.29	Alanine–glyoxylate aminotransferase family protein	*P. cryohalolentis*	AminoacidMetab.	197	21	WP_011512563.1	66%	5.13	41591	
523	−10.75	Amidohydrolase	*P. cryohalolentis*	AminoacidMetab.	95	13	WP_011513591.1	33%	6.74	46763	
337	−4.9	IMP dehydrogenase	*Psychrobacter*	Nucleotide Metab.	180	25	WP_011280629.1	52%	5.99	52630	
848	−8.83	DUF3298 domain-containing protein	*P. cryohalolentis*	Unknown	182	8	WP_011512791.1	25%	8.59	31941	
285	−3.22	–		unidentified							
851	−4.36	–		unidentified							
968	−3.46	–		unidentified							
1026	−3.74	–		unidentified							

R represents a heatmap of the ratio 4/30 so the level of overexpression in each case being more brilliant at higher values and darker at lower. A specie column refers to the organisms (specie or genus) in which protein has been identified according to the NCBI database.*

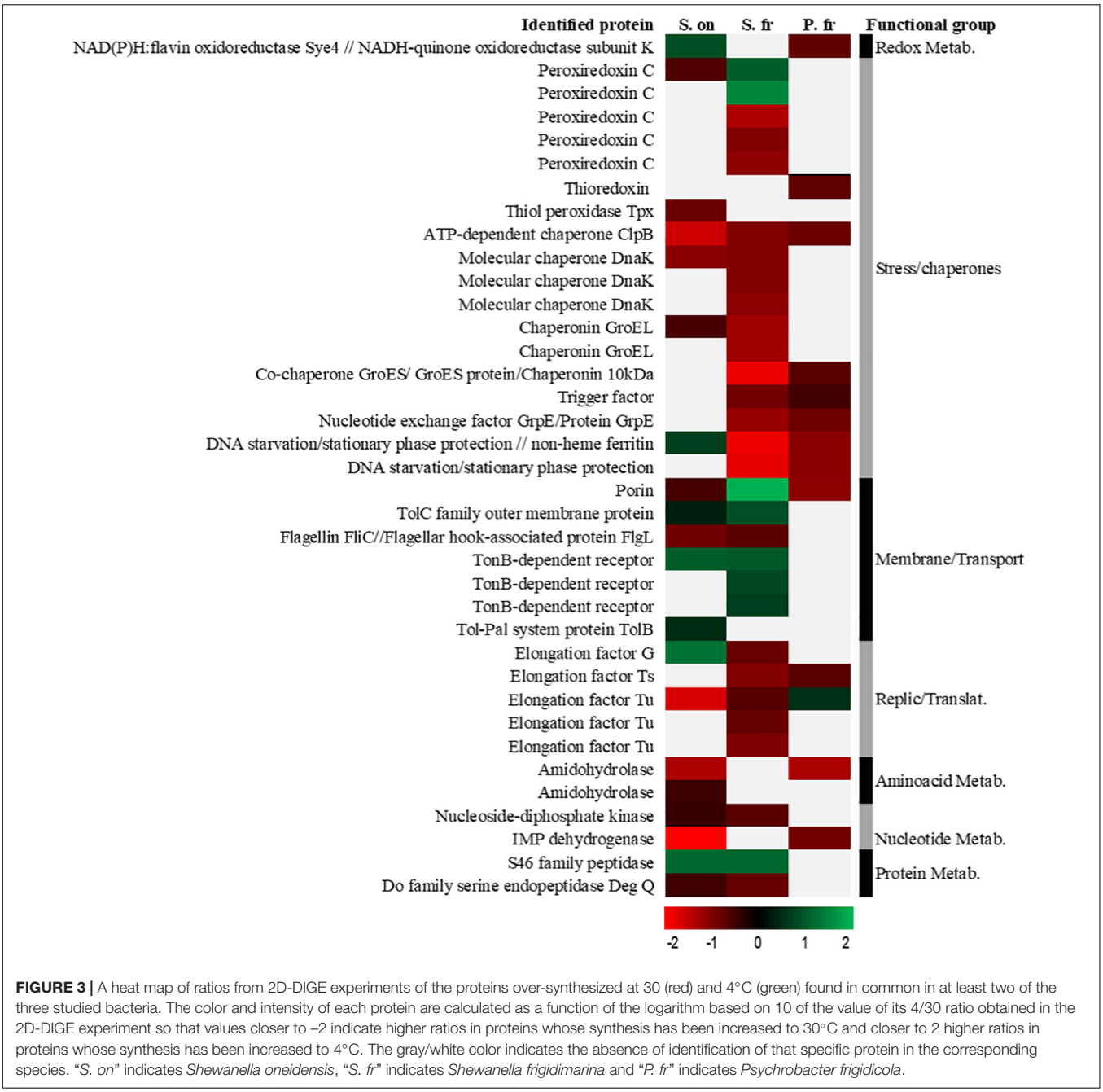

FIGURE 3 | A heat map of ratios from 2D-DIGE experiments of the proteins over-synthesized at 30 (red) and 4°C (green) found in common in at least two of the three studied bacteria. The color and intensity of each protein are calculated as a function of the logarithm based on 10 of the value of its 4/30 ratio obtained in the 2D-DIGE experiment so that values closer to –2 indicate higher ratios in proteins whose synthesis has been increased to 30°C and closer to 2 higher ratios in proteins whose synthesis has been increased to 4°C. The gray/white color indicates the absence of identification of that specific protein in the corresponding species. "*S. on*" indicates *Shewanella oneidensis*, "*S. fr*" indicates *Shewanella frigidimarina* and "*P. fr*" indicates *Psychrobacter frigidicola*.

these regulating mechanisms after an adaptation period and grow again at these new low temperatures (Hébraud and Potier, 1999). For *S. frigidimarina*, this accommodation period is shorter at 12°C than at 4°C, probably due to the small temperature difference from its optimal growth temperature, although the growth rates are different, being higher at 4°C. This may indicate that the strategies activated during the lag period provide efficient molecular machinery for successful bacterial development. The ACAM 304 strain of the psychrophile *P. frigidicola,* which has an optimal growth temperature of 15°C, was isolated from ornithogenic soil in Antarctica (Bowman et al., 1996). Its behavior at 4 and 12°C, with relatively long lag phases, could indicate that it has a generalized decrease in affinity at low temperatures (Nedwell and Rutter, 1994). This bacterium is described as a strict psychrophile from an environment where it is competing with psychrotolerants, which are predominant in polar areas (Nedwell and Rutter, 1994) and are better adapted to temperature changes and fluctuations (Baross and Morita, 1978).

In this study, we have observed that the growth of the three species at warm temperatures (30°C), with almost no lag period, implies a fast entry in the stationary phase, especially for the psychro-species. Nevertheless, and contrary to what one might

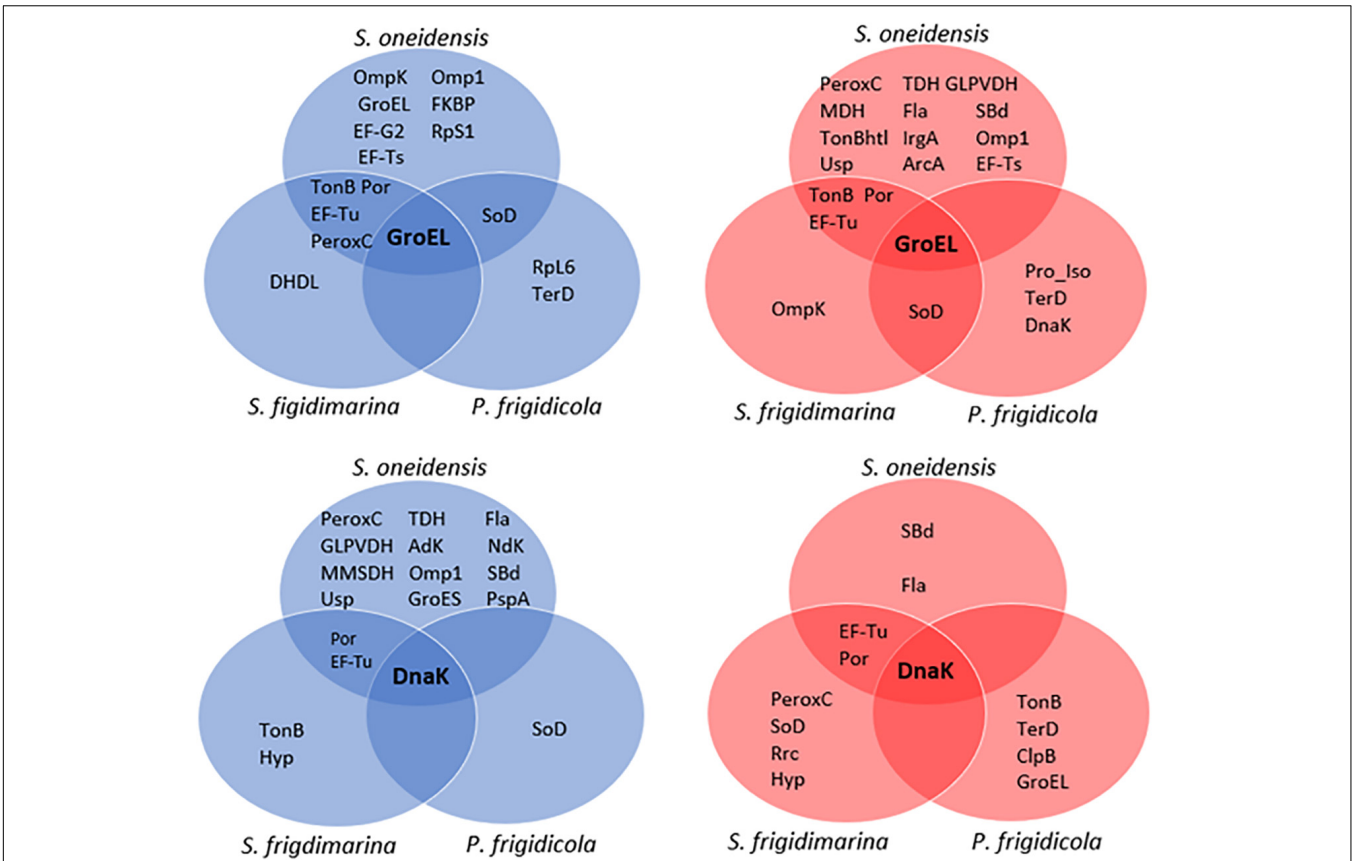

FIGURE 4 | Venn diagrams of identified proteins that coimmunoprecipitate with GroEL (top) and DnaK (down) in the three bacteria at 4 (blue) and 30°C (red).

expect, the psychrotolerant and psychrophilic bacteria showed an effective growth at temperatures slightly higher than those of their described limits. The reason could be the well-known effect of the adaptation of laboratory strains. This can expand cellular limits of medium/environmental conditions (Knöppel et al., 2018), susceptibility against chemicals (Herruzo-Cabrera et al., 2004), or even temperature, such as *Saccharomyces cerevisiae*, which can increase their maximum growth temperature by 3°C (Caspeta and Nielsen, 2015). Furthermore, the growth of the three bacteria at low temperatures reached higher values of O.D., probably due to the improved efficiency in the use of substrates during the first period of incubation, which allows psychrophiles to reach maximum amounts of biomass (Morita, 1975). Microbial growth is the result of a sequence of interrelated chemical reactions (Hébraud and Potier, 1999), and is not only influenced by temperature but also by the availability and quantity of nutrients (Russell, 1990), especially important in the late exponential phase and the entry into the stationary phase.

Changes in Synthesis Levels of Chaperone Systems GroEL/GroES and DnaK/DnaJ With the Temperature

Chaperones GroEL and DnaK have a crucial role in the adaptation to thermal stress through refolding of denatured or misfolded proteins, avoiding the formation of damaging aggregates, or eliminating them by proteolysis (Gragerov et al., 1992; Phadtare, 2004; Robin et al., 2009). On many occasions, they act together in successive steps being the pair DnaK/DnaJ, which first recognizes the substrate protein and stabilizes an intermediate conformation. Subsequently, the pair GroEL/GroES acts by ATP hydrolysis to conform to the native state of the protein (Langer et al., 1992).

The immunodetection in samples at 30°C showed high levels of different chaperones in each strain (GroEL/GroES and DnaK in *S. oneidensis*, GroEL, DnaK/DnaJ in *S. frigidimarina* and GroEL and DnaK in *P. frigidicola*), suggesting that this warm temperature condition represents a stressful situation that promotes the increase of Hsps levels (Lüders et al., 2009; Che et al., 2013). As indicated before, the natural environment of *S. oneidensis* is a lake that remains frozen or at temperatures near 0°C for 6 months of the year. This bacterium, although described as a mesophile, is able to behave as a psychrotolerant, showing similarities with *S. frigidimarina* in responses to temperature conditions. It is also known that mesophiles and psychrotolerants sometimes overlap with their thermal properties (Russell, 1990). The signal of GroES immunodetected in *S. oneidensis* growing at 4°C was relatively strong, which correlates with the fact that this chaperone is greatly produced at low temperatures in some species of the *Shewanella* genus (Miyake et al., 2007), although, in

S. frigidimarina, this chaperone was not detected. *S. frigidimarina* and *P. frigidicola*, which are both originally from Antarctica, had undetectable levels of the chaperones tested in cultures at 4°C, suggesting that, even far from their respective optimal growth temperatures (20°C for *S. frigidimarina* and 15°C for *P. frigidicola*), they do not require the activity of these Hsps to cope with a cold environment such as at 4°C.

Over-Synthesis of Proteins at 4 and 30°C in the Three Bacteria

Over-Synthesized Proteins at Low Temperature

Cultures of the psycrotrophic *S. frigidimarina* at 4°C produce mainly a group of proteins related to the low iron availability or its metabolism, membrane transport, and oxidative stress. At low temperatures, the solubility of gases, especially oxygen, increases, and free radicals are more stable. Psychrophiles possess several mechanisms to cope with the oxidative stress of these reactive oxygen species (ROS). These mechanisms include the synthesis of specific reductases to repair oxidized residues, reduction in the number of oxidizable amino acids in the proteins, and the deletion of metabolic pathways that produce ROS (Piette et al., 2010). The increase of proteins like peroxiredoxin C and GDHr, which are involved in the redox homeostasis of the cell by acting as a reducing disulfide (Aslund and Beckwith, 1999), is presumably triggered to restore reduced cell conditions occurring at low temperatures. Membrane proteins identified in these cultures, system TolC-TonB, conform a membranal system to bond, transport, and chelate iron into the cell (Krewulak and Vogel, 2011), thus regulating iron homeostasis. Since cold affects the membrane fluidity (Bajerski et al., 2017; Siliakus et al., 2017), it could also be prompting these proteins for a better regulation of iron homeostasis to be used as a cofactor for the function of other proteins and respiration and to avoid more ROS emergence (Yang et al., 2008).

Similar to *S. frigidimarina*, when *S. oneidensis* grew at low temperature, there was an increase in the synthesis of redox enzymes and iron metabolism-related, as well, to an increase in proteins of the transport system, consisting of Ton-B-dependent receptor protein (Spot 115), the Tol-Pal system protein TolB (Spot 706), and TolC (Spot 543). This may be an indicator of an oxidative stress situation at the cold that *S. oneidensis* and *S. frigidimarina* face due to the increase of proteins that regulate iron levels and its transport for cell respiration, and accurate homeostasis to avoid oxidative poisoning (Mirus et al., 2009).

Different groups of proteins involved in replication and translation processes and in the biosynthesis of other proteins and aminoacid precursors were also over-accumulated in *S. oneidensis* at 4°C. Among them, the one with a notably higher ratio (23.02) was EF-G, which plays a key role in the elongation of polypeptides during the synthesis of protein (Savelsbergh et al., 2009; Li et al., 2011). In *E. coli*, EF-G has been described as susceptible to oxidative stress (Nagano et al., 2012) and plays a chaperone role in protein folding (Caldas et al., 2000). Furthermore, its marked synthesis increase at 4°C in *S. oneidensis* could be because it behaves like a cold-adapted enzyme, with high molecular flexibility (Ruggiero et al., 2007) and a low activation energy requirement in GTP hydrolysis (Thomas and Cavicchioli, 2000), which is able to keep active at low temperatures.

At 4°C, this bacterium also increased the synthesis of proteins related to intracellular levels of acetyl-CoA. Bacteria often cope with changes in their environment by activating metabolic pathways to produce available nutrients. The phosphorylation of some regulating proteins in response to stress involves mechanisms that include acetyl phosphate, whose gene is induced by a shortage of phosphate in some bacteria (Summers et al., 1999). Temperature and the growth phase are factors that influence intracellular concentrations of acetyl phosphate (Prüss and Wolfe, 1994). Thus, the over-synthesis of enzymes that control intracellular levels of acetyl-CoA, like the acetate kinase, detected in *S. oneidensis* at 4°C, could respond to the need of the bacterium to generate energy and phosphorylate other proteins to be active in response to a stressful situation.

In this line, there was a remarkable increase in the production of the enzyme acyl-CoA dehydrogenase (ACDH) (Spot 481), also in *P. fridigicola* at 4°C that could support the activation of the metabolism of this bacterium at cold temperatures. An active metabolism contributes to the generation of energy and electron transfer in respiration with the participation of acetyl-CoA, a product of the reaction catalyzed by ACDH in metabolic pathways such as the tricarboxylic acid cycle. This enzyme belongs to the family of proteins involved in lipid oxidation and in the metabolism of amino acids and acts as an oxidoreductase for the transfer of electrons in the respiratory chain (Kim and Miura, 2004). Possibly, this active metabolism in *P. frigidicola* cultures at low temperature also requires a high synthesis and presence of NAD co-factors of the main metabolic processes (Gerdes et al., 2006). Interestingly, we did find strong induction of the enzyme nicotine-phosphoribosyl transferase (spot. 417) too, which catalyzes the first reaction in the synthesis of NAD (Dulyaninova et al., 2000).

The active metabolism of this bacterium at 4°C was also depicted by the over-synthesis of proteins involved in the biosynthesis processes of numerous amino acids and nucleotides, as well as in the metabolism of carbohydrates, while there was no induction of chaperons or stress proteins detected by 2D-DIGE. One of the most strongly induced proteins in these samples was the CTP synthase. This enzyme is responsible for the production of CTP from UTP and glutamine, and for the regulation of intracellular levels of CTP (Endrizzi et al., 2004), which is an essential precursor of membrane phospholipids (Chang and Carman, 2008). It also plays a key role in the metabolism of pyrimidines and is very important for the growth rate and the concentration of ribonucleotides and deoxyribonucleotides (Jørgensen et al., 2004).

Over-Synthesized Proteins at High Temperature

When *S. frigidimarina* grew at warm temperatures (30°C), an increase in the synthesis of several chaperones and stress response proteins was observed. They were mainly proteins that face oxidative, osmotic, and thermal stress situations. Some of them appeared in different isoforms like DnaK (posts 224, 215, 205) and GroEL (Spots 387 and 374) and others as single forms like GrpE (Spot 1398), TF (Spot 420), PspA (Spot 1418), and GroES

(Spot 1888). The latter, although undetectable by WB in this study, forms the GroEL-GroES complex that keeps bound in the presence of ATP (Ventura et al., 2004) in the thermal stress response. These chaperones play an important role in the quality control system of post-translational processing. They control the folding and the proper conformation of other proteins to cope with environmental changes such as temperature, cooperating with each other (Liberek et al., 2008; Muga and Moro, 2008; Robin et al., 2009). In response to oxidative stress at warm temperatures, we found in *S. frigidimarina* two isoforms of the DNA-binding ferritin-like proteins region, DNA-Dps (spots 1773 and 1767), which belongs to Dps family proteins. This family is involved in protecting DNA from damage by chelating iron and by ferroxidase activity (Calhoun and Kwon, 2011). DNA-Dps is also required for starvation response and long-term stationary viability (Jeong et al., 2006) that is why we cannot discard some contribution to its high levels detected to the fact that the samples were collected once cultures reached the stationary phase. Nevertheless, another three isoforms of other protein-related to oxidative stress were also overexpressed in these samples, the peroxiredoxin C (Spots 2022, 1522, 1519). It is part of the large and highly conserved family of the peroxiredoxines, which detoxify peroxides by reducing them (Rhee, 2016). This protein is also known as alkyl hydroperoxide reductase (AhpC) described as a protective enzyme against peroxides in *E. coli* (Storz and Imlay, 1999) against osmotic stress in *Staphylococcus aureus* and induced by a temperature increase in *Bacillus subtilis*, while, in *Shewanella putrefaciens*, its activity is related to cold acclimation (Leblanc et al., 2003).

This molecular strategy involving proteins against redox, osmotic, and stationary phase stress during warm conditions seems to be common in the two shewanellas studied, being the peroxiredoxin C also identified as over-accumulated in warm cultures of *S. oneidensis* (Spot 1379). In this bacterium, at 30°C, there were too many other over-synthesized proteins related to oxidative and osmotic stress belonging to the anti-oxidant AhpC-TSA or peroxiredoxin family. That is the case of the Tpx-C (Spot 1479) that protects against oxidative (Storz and Imlay, 1999; Horst et al., 2010; Somprasong et al., 2012), osmotic and cold stress (Leblanc et al., 2003), and that increase in the late stationary phase (Miyake et al., 2007). Thus, the bacteria *S. oneidensis*, as well as *S. frigidimarina,* could share a similar mechanism to that of *Bacillus subtilis* in which this type of enzyme is induced as a response to temperature increase and osmotic stress after the beginning of the stationary phase (Hecker and Völker, 1990; Antelmann et al., 1996).

Regarding other groups of proteins over-synthesized in *S. oneidensis* at 30°C, we found GroEL (Spot 420), which increases the solubilization of aggregates (Niwa et al., 2012), the ClpB protein (Spot 152), and the DnaK (Spot 244), correlating the immunodetection results observed by WB. Protein GroEL belongs to the Hsp100/Clp AAA + ATPase family and cooperates with the chaperone system DnaK/DnaJ/GrpE in efficient solubilization and reactivation of aberrant protein aggregates formed as a consequence of cellular heat stress (Kedzierska et al., 2003; Mogk et al., 2003; Lee et al., 2004; Doyle et al., 2007). This chaperone restores the activity of other membrane proteins that also appeared over-synthesized in *S. oneidensis* at 30°C, the porin (spot 856), which forms hydrophilic channels in the membrane and is refolded by GroEL (Goulhen et al., 2004). Similar to *S. frigidimarina*, several other stress proteins over-accumulated could be indicative of a stress situation for *S. oneidensis* when grown at 30°C and/or due to be in the stationary phase. This is the case of universal stress protein (Usp) (Spot 1620). It is a small cytoplasmic protein that is greatly induced in many bacteria, such as *E. coli*, as a response to a wide range of environmental conditions and stressful situations like heat shock, starvation, or in the presence of stressors that prevent cell growth, and agents that damage DNA (Tkaczuk et al., 2013). This protein increases the survival rate of cells during prolonged exposure to these stressful conditions and is phosphorylated when cells enter the stationary growth phase (Sousa and McKay, 2001).

Again, the majority of proteins over-synthesized at 30°C in the case of the psychrophile *P. frigidicola* belong to the chaperone and stress protein groups. There were several of them involved in redox metabolism, resistance to oxidative stress or in heat stress, and the starvation response as it was observed for the other two bacteria studied. They were oxide and nitro-reductase enzymes that contribute to the defense against oxidative stress by reducing the redox cycle and the toxic nitro-aromatic compounds and quinones (Liochev et al., 1999), as well as degrading ROS and free radicals.

In this regard, two isoforms of the enzyme SOD (Spots 993 and 996), the protein thiorredoxin (Spot 1301) and DNA-Dps (Spot 1126), were induced in *P. frigidicola* at warm temperatures. The first protein plays a pivotal role in maintaining the redox state of the cell and protects it from oxidative stress (Wang et al., 2013; Lu and Holmgren, 2014). DNA-Dps, identified also in *S. frigidimarina*, is highly conserved and operates, as indicated before, against several kinds of stressors (Jeong et al., 2006; Karas et al., 2015) in *E. coli*, including oxidative damage to protect DNA. and it is also required in the normal starvation response and in long-term stationary viability (Almirón et al., 1992; Nair and Finkel, 2004).

Concerning the specific chaperones group, the main proteins found were involved in the heat stress response forming, as was the case for samples of *S. frigidimarina*, a cooperative role in the folding and maintenance of the proper conformation of other proteins to cope with environmental changes such as temperature.

Comparative Molecular Machinery in Each Bacterium Against Temperature Conditions

Both temperature and oxidative stress are closely related, since temperature influences the solubility of oxygen and the formation of ROS (Piette et al., 2010; Chattopadhyay et al., 2011). Stress proteins were required at warm temperatures, whereas cold temperature seems to promote a similar membrane system in the two shewanellas studied.

The analysis of 2D-DIGE revealed common strategies in several groups of proteins between the three species,

depending on growth temperature. The species *S. frigidimarina* shared over/under-synthesized proteins with *S. oneidensis* and *P. frigidicola*, while these two showed fewer proteins in common with one another. The strategy followed by *S. frigidimarina*, especially at warm temperatures, used shame chaperones and stress proteins with both *P. frigidicola* (GroES, TF, GrpE, ferritin, stationary phase protection protein) and *S. oneidensis* (ClpB, GroEL, and DnaK). On the other hand, the mesophile, *S. oneidensis,* and the psychrophile, *P. frigidicola*, employed different strategies at 30°C, except for the ClpB, which works together with DnaK to solubilize and reactivate aggregated proteins (Doyle et al., 2007; Doyle et al., 2015). This interaction is specie specific (Miot et al., 2011) and plays an essential role in cell survival under thermal stress conditions (Nagy et al., 2010; Krajewska et al., 2017).

Regarding oxidative stress, members of the superfamily of peroxiredoxins (peroxiredoxin C, thiorredoxin, and thiol peroxidase) were over-synthesized at 30°C in the two species of *Shewanella* and *Psychrobacter*. This kind of protein removes peroxides that are toxic to the cell (Storz and Imlay, 1999) and does also protects against osmotic stress and temperature changes in several bacteria (Leblanc et al., 2003). Even though oxidative stress is more typical at low temperatures (Chattopadhyay et al., 2011), it could also occur at 30°C as a response to the by-products of the increased metabolism of these bacteria at moderate to warm temperatures (Piette et al., 2010). Interestingly, the psychrotolerant *S. frigidimarina* may need to cope with oxidative stress at low temperatures through over-synthetization of other peroxiredoxin C isoforms. *S. oneidensis* showed a differential behavior in the synthesis of proteins related to the iron homeostasis. While it over-synthesized the non-heme ferritin at 4°C; the other two bacteria increased the levels of the Dps, which, as mentioned before, joins ferritin and protects against oxidative damage (Nair and Finkel, 2004; De Martino et al., 2016).

The metabolism of *S. oneidensis* and *S. frigidimarina* at low temperature, below their optimum, uses channels and siderophores that regulate the entrance of ions in the cell. These species at 4°C there induced synthesis of proteins of the outer membrane channels like TolPal System (TonB, TolC, and TolB) and the porin protein (that appears also in *P. frigidicola*), which interacts with this system for assembling to the membrane (Rigal et al., 1997). The system has an important role in the elimination of toxic compounds from oxidative damage through the membrane (Benz et al., 1993; Fralick, 1996) and its reparation (Zgurskaya et al., 2011) and binds to iron-chelating or siderophore complexes (Mirus et al., 2009). The porin protein, which was present in the three bacteria, could be acting differently in the psychrotolerant than in the other two species. It was over-synthesized at 4°C in *S. frigidimarina*, probably forming aqueous channels and interacting with the TolPal System (Cascales et al., 2002). However, it could be related to the basal apparatus of the flagellum (Chu et al., 2020; Liao et al., 2021) in *S. oneidensis*, in which it is over-synthesized at 30°C along with the flagellin protein.

Concerning replication and translation processes, there was an induction of different elongation factors like EF-G, EF-Tu, and EF-Ts, mainly at warm temperatures, except for factor EF-G in the mesophile and EF-Tu in the psychrophile. The EF-Ts is a guanine nucleotide exchanger for EF-Tu by GTPase activity for the separation of the EF-Tu-GDP complex from the ribosome (Palmer et al., 2013). It has a high similarity in different mesophiles such as *E. coli*, thermophiles such as *Thermus thermophilus*, and psychrophiles such as *Pseudoalteromonas haloplanktis*, but it was observed in higher concentration in the latter (Raimo et al., 2004). EF-G has different associations with ribosomes in response to stressful situations (deLivron et al., 2009). This factor is required for growth at low temperatures, as well as in acidic environments in *Sinorhizobium meliloti* (Kiss et al., 2004) and *E. coli* (Pfennig and Flower, 2001). It has also been described in other extremophiles such as *Psychrobacter cryohalolentis* and *Thiomicrospiracrunogena*, increasing the translation efficiency during the growth at low temperatures (Krishnan and Flower, 2008). Interestingly, EF-Tu that catalyzes the binding of aminoacyl-RNA to the ribosome can also act as a chaperone in the renaturation of other proteins (Masullo et al., 2000). This chaperone role has also been proposed for EF-Ts (Takeshita and Tomita, 2010) in the assembly and maintenance of the Qβ viral RNA polymerase in infected cells.

Regarding the groups of amino acids, nucleic acids, and proteins metabolism, there were no proteins identified that were shared by the three bacteria. Contrary to what has been indicated before for groups of stress and membrane proteins, no coincidences were found for these groups between *S. frigidimarina* and *P. frigidicola*, but both bacteria presented similarities with *S. oneidensis*. This could indicate that the main processes affected by stress and essential for cell survival and adaptation are those involving chaperone activity, detoxifying proteins, and transport through the membrane.

Several protein isoforms of different functional groups (peroxiredoxin C, DnaK, GroEL, EF-Tu, TonB-dependent receptor) present in *S. frigidimarina* were not observed in *S. oneidensis* or *P. frigidicola*. Other psychrotolerant species from Antarctica belonging to the genera *Sphingobacterium* and *Pseudomonas*, which can grow in the temperature range of 0–30°C, display differences in the phosphorylation-dephosphorylation state of membrane and cytosolic proteins in response to temperature changes, acting as cell heat sensors (Ray et al., 1994). The presence of isoforms in *S. frigidimarina* suggested that this psychrotolerant bacterium could have a similar mechanism to recognize environmental conditions and adapt to them, probably by different phosphorylation states or other post-translational modifications (dos Santos et al., 2010; García-Descalzo et al., 2014).

As a further step in understanding the molecular machinery that these three types of bacteria use to adapt to temperature changes, proteins that co-immunoprecipitate alongside the main chaperones DnaK and GroEL were investigated. Analysis of the results revealed protein interactions that could be happening *in vivo* in the cell as part of an adaptive response to different growth temperatures or as part of their normal metabolism at these temperatures (**Figure 4**).

Chaperones are essential components of the quality control machinery in cells. They optimize the physiological responses of

bacteria by interacting directly with other proteins, taking part in cell signaling, and acting as stress response proteins (Hartl and Hayer-Hartl, 2002). Chaperones GroEL and DnaK are the main representatives of their families (Cooper and Hausman, 2000; Beckerman, 2005; Liberek et al., 2008), and their action has been described in a wide range of bacteria, frequently working together (Fourie and Wilson, 2020; Fatima et al., 2021; Mayer, 2021) and taking part in the regulation of transcription and translation (Parsot et al., 2003).

The molecular machinery involving these chaperones according to temperature was more complex in *S. oneidensis*, of intermediate complexity in *S. frigidimarina*, and notably simpler in *P. frigidicola*. While, in *S. oneidensis*, the proteins that co-immunoprecipitate with GroEL and DnaK tended to cluster at both warm and cold temperatures; those of *P. frigidicola* gathered mainly toward warmer temperatures, and *S. frigidimarina* showed a more equal distribution in the established and combined chaperone-temperature conditions. The groups of proteins that co-immunoprecipitated with the chaperones tested in *S. oneidensis* and *S. frigidimarina* shared more elements with each other than they do with proteins co-immunoprecipitated in *P. frigidicola*. These were proteins particularly involved in membrane transport, elongation processes, and oxidative stress. Characteristically, psychrotrophs are a more diverse group than psychrophiles, and their thermal properties overlap with those of some mesophiles (Russell, 1990). For *S. oneidensis*, a noticeably higher number of proteins seem to act together with GroEL at both temperatures and with DnaK at 30°C.

In general, the protein interaction network observed was mainly composed of chaperones and co-chaperones (GroES, Usp), membrane proteins involved in the transport of molecules and ions (porins and Ton-B-dependent receptors), and the formation of flagellar structures (flagellin, Omp family); but also proteins related with the defense against oxidative stress (peroxiredoxine, superoxide dismutase) and the elongation factors EF-Tu, EF-Ts, and EF-G. Co-immunoprecipitation revealed that the main processes to cope with temperature changes in these bacteria were those involved in the stress (temperature and oxidative) response. And that they need, especially *S. oneidensis*, the support of a membrane system that helps to eliminate toxic products resulting in these processes.

It is noteworthy that *P. frigidicola*, with a simpler proteome and a smaller number of proteins that co-immunoprecipitate with GroEL and Dnak than the two shewanellas, showed the co-appearance of the tellurium ion resistance (TerD) and SOD proteins with GroEL at both temperatures and with DnaK at 30°C for the former and DnaK at 4°C for the latter.

The TerD protein is part of a poorly characterized family involved especially in the response to oxidative stress in several organisms (Chasteen et al., 2009; Anantharaman et al., 2012; Daigle et al., 2015) and is also present in different pathogenic bacteria (Taylor, 1999; Turkovicova et al., 2016; Chen et al., 2019). The presence of this enzyme and SOD suggests that this psychrophilic bacterium is adapted to the frequent situation of oxidative stress at low temperatures due to the stability of ROS, and the metabolic processes that can lead to the generation of ROS at high temperatures (Piette et al., 2011).

CONCLUSION

In the adaptation of microorganisms to changes in temperature, proteins are the molecular machine that regulates metabolism and cell functions. This study combines proteomic approaches with classical microbiology analysis, like growth dynamics.

We have observed a similar growing behavior between the three species against cold and warm temperatures, being able to achieve akin biomass under the temperatures tested, regardless of whether it is a stress situation or not. Some differences observed in the first stages of growth could give clues about whether the bacteria are in a normal or stressful situation, considering the duration of the lag phase. This observation had to be corroborated by a more detailed analysis, for which proteomic tools are essential.

The analysis of proteomic data showed that, in general, the two bacteria from the genus *Shewanella* displayed a more versatile adaptive response than the *Psychrobacter* species tested. These findings could suggest a tendency of an adaptation and evolution from mesophilic to psychrophilic microorganisms, maintaining a similar genome, but this would need to be supported with more genomic studies. Within the two *Shewanella* species studied, the psychrotolerant *S. frigidimarina* exhibits temperature-adaptative mechanisms in common with the other two species. This could be due to the genome (common with the mesophile) and the post-translational modifications, which give rise to isoforms (common with the psychrophile). As a result, it is better adapted to thermal variations in the temperature range 4–30°C.

In the molecular machinery to withstand temperature stressful situations, the role of chaperones is essential. In the three species studied, these proteins interact with other proteins forming complexes to provide diverse physiological responses of the cell to different growth temperatures. Equally important for adapting to temperature changes is the establishment of a cooperative system of chaperones with other proteins for the protection against oxidative damage, transmembrane transport, and elongation factors. They, together, are in charge of ensuring the viability and survival of bacteria.

This study is potentially related to pieces of climate change research since microorganisms and their adaptive strategies could be biosensors of the state of environments. An in-depth understanding of how they cope with changes in the temperature conditions could give us information about the molecules overproduced and provide a tool for evaluating the state of the environment. Additionally, it could also contribute to the Astrobiology field. The knowledge about the limits of life and how it adapts to environmental changes is crucial in the study of the habitability of environments with extreme conditions on Earth and in other planetary bodies like Mars or icy moons. The molecules employed to adapt to these extreme conditions could be considered biomarkers of life on Earth and beyond.

DATA AVAILABILITY STATEMENT

The mass spectrometry proteomics data have been deposited to the ProteomeXchange Consortium via the PRIDE repository with the dataset identifier PXD030438.

AUTHOR CONTRIBUTIONS

CC contributed to conceptualization, funding acquisition, editing, and manuscript review. LG-D contributed to experiments performance, analysis, and manuscript writing. EG-L contributed to experiments performance and data acquisition. All authors contributed to the article and approved the submitted version.

FUNDING

This research has been funded by Grant Nos. PID2019-104205GB-C22 and MDM-2017-0737 Unidad de Excelencia "Maria de Maeztu"-Centro de Astrobiología (INTA-CSIC) by the Spanish Ministry of Science and Innovation/State Agency of Research MCIN/AEI/10.13039/501100011033. EG-L is supported by PTA2016-12325-I grant provided by MCIN/AEI/10.13039/501100011033. LG-D was supported by the Instituto Nacional de Técnica Aeroespacial through the grant FPI "Rafael Calvo Rodés." This research is part of POLARCSIC activities.

ACKNOWLEDGMENTS

We thank Paula Alcázar for her assistance in reviewing, and Proteomic Unit of the Parque Científico de Madrid and Proteomic Service at Centro Nacional de Investigaciones Cardiovasculares for 2D-DIGE experiments and identification of proteins.

SUPPLEMENTARY MATERIAL

The Supplementary Material for this article can be found online at: https://www.frontiersin.org/articles/10.3389/fmicb.2022.841359/full#supplementary-material

REFERENCES

Ahmad, A., Bhattacharya, A., McDonald, R. A., Cordes, M., Ellington, B., Bertelsen, E. B., et al. (2011). Heat shock protein 70 kDa chaperone/DnaJ cochaperone complex employs an unusual dynamic interface. *Proc. Natl. Acad. Sci.* 108, 18966–18971. doi: 10.1073/pnas.1111220108

Alcazar, A., Garcia-Descalzo, L., and Cid, C. (2010). "Microbial evolution and adaptation in icy worlds," in *Astrobiology: Physical Origin, Biological Evolution and Spatial Distribution*, eds S. Hegedus and J. Csonka (New York, NY: Nova Science Publishers), 81–95. doi: 10.3389/fmicb.2017.01407

Almirón, M., Link, A. J., Furlong, D., and Kolter, R. (1992). A novel DNA-binding protein with regulatory and protective roles in starved *Escherichia coli*. *Genes Dev.* 6, 2646–2654. doi: 10.1101/gad.6.12b.2646

Anantharaman, V., Iyer, L. M., and Aravind, L. (2012). Ter-dependent stress response systems: novel pathways related to metal sensing, production of a nucleoside-like metabolite, and DNA-processing. *Mol. Biosyst.* 8, 3142–3165. doi: 10.1039/c2mb25239b

Antelmann, H., Engelmann, S., Schmid, R., and Hecker, M. (1996). General and oxidative stress responses in *Bacillus subtilis*: cloning, expression, and mutation of the alkyl hydroperoxide reductase operon. *J. Bacteriol.* 178, 6571–6578. doi: 10.1128/jb.178.22.6571-6578.1996

Aslund, F., and Beckwith, J. (1999). Bridge over troubled waters: sensing stress by disulfide bond formation. *Cell* 96, 751–753. doi: 10.1016/s0092-8674(00)80584-x

Bajerski, F., Wagner, D., and Mangelsdorf, K. (2017). Cell membrane fatty acid composition of *Chryseobacterium frigidisoli* PB4T, isolated from antarctic glacier forefield soils, in response to changing temperature and pH Conditions. *Front. Microbiol.* 8:677. doi: 10.3389/fmicb.2017.00677

Baross, J., and Morita, R. (1978). "Microbial life at low temperatures: ecological aspects," in *Microbial life in Extreme Environments*, ed. D. J. Kushner (London: Academic Press), 9–71.

Beckerman, M. (2005). "Protein folding and binding," in *Molecular and Cellular Signaling*, ed. T. Abl (New York, NY: Springer), 89–110.

Benz, R., Maier, E., and Gentschev, I. (1993). TolC of *Escherichia coli* functions as an outer membrane channel. *Zentralbl Bakteriol.* 278, 187–196. doi: 10.1016/s0934-8840(11)80836-4

Bowman, J. P., Cavanagh, J., Austin, J. J., and Sanderson, K. (1996). Novel Psychrobacter species from Antarctic ornithogenic soils. *Int. J. Syst. Bacteriol.* 46, 841–848. doi: 10.1099/00207713-46-4-841

Bromfield, E. G., and Nixon, B. (2013). The function of chaperone proteins in the assemblage of protein complexes involved in gamete adhesion and fusion processes. *Reproduction* 145, R31–R42. doi: 10.1530/rep-12-0316

Caldas, T., Laalami, S., and Richarme, G. (2000). Chaperone properties of bacterial elongation factor EF-G and initiation factor IF2. *J. Biol. Chem.* 275, 855–860. doi: 10.1074/jbc.275.2.855

Calhoun, L. N., and Kwon, Y. M. (2011). Structure, function and regulation of the DNA-binding protein Dps and its role in acid and oxidative stress resistance in *Escherichia coli*: a review. *J. Appl. Microbiol.* 110, 375–386. doi: 10.1111/j.1365-2672.2010.04890.x

Camberg, J. L., Doyle, S. M., Johnston, D. M., and Wickner, S. (2013). "Molecular Chaperones," in *Brenner's Encyclopedia of Genetics*, 2nd Edn, eds S. Maloy and K. Hughes (San Diego, CA: Academic Press), 456–460.

Cascales, E., Bernadac, A., Gavioli, M., Lazzaroni, J. C., and Lloubes, R. (2002). Pal lipoprotein of *Escherichia coli* plays a major role in outer membrane integrity. *J. Bacteriol.* 184, 754–759. doi: 10.1128/jb.184.3.754-759.2002

Caspeta, L., and Nielsen, J. (2015). Thermotolerant yeast strains adapted by laboratory evolution show trade-off at ancestral temperatures and preadaptation to other stresses. *mBio* 6:e00431. doi: 10.1128/mBio.00431-15

Cavicchioli, R., Siddiqui, K. S., Andrews, D., and Sowers, K. R. (2002). Low-temperature extremophiles and their applications. *Curr. Opin. Biotechnol.* 13, 253–261. doi: 10.1016/s0958-1669(02)00317-8

Chang, Y. F., and Carman, G. M. (2008). CTP synthetase and its role in phospholipid synthesis in the yeast *Saccharomyces cerevisiae*. *Prog. Lipid Res.* 47, 333–339. doi: 10.1016/j.plipres.2008.03.004

Chasteen, T. G., Fuentes, D. E., Tantaleán, J. C., and Vásquez, C. C. (2009). Tellurite: history, oxidative stress, and molecular mechanisms of resistance. *FEMS Microbiol. Rev.* 33, 820–832. doi: 10.1111/j.1574-6976.2009.00177.x

Chattopadhyay, M. K., Raghu, G., Sharma, Y. V., Biju, A. R., Rajasekharan, M. V., and Shivaji, S. (2011). Increase in oxidative stress at low temperature in an antarctic bacterium. *Curr. Microbiol.* 62, 544–546. doi: 10.1007/s00284-010-9742-y

Che, S., Song, W., and Lin, X. (2013). Response of heat-shock protein (HSP) genes to temperature and salinity stress in the antarctic psychrotrophic bacterium Psychrobacter sp. G. *Curr. Microbiol.* 67, 601–608. doi: 10.1007/s00284-013-0409-3

Chen, J., Tan, W., Wang, W., Hou, S., Chen, G., Xia, L., et al. (2019). Identification of common antigens of three pathogenic Nocardia species and development of DNA vaccine against fish nocardiosis. *Fish Shellfish Immunol.* 95, 357–367. doi: 10.1016/j.fsi.2019.09.038

Chu, J., Liu, J., and Hoover, T. R. (2020). Phylogenetic distribution, ultrastructure, and function of bacterial flagellar sheaths. *Biomolecules* 10:363. doi: 10.3390/biom10030363

Cid, C., Garcia-Descalzo, L., Casado-Lafuente, V., Amils, R., and Aguilera, A. (2010). Proteomic analysis of the response of an acidophilic strain of

Chlamydomonas sp. (Chlorophyta) to natural metal-rich water. *Proteomics* 10, 2026–2036. doi: 10.1002/pmic.200900592

Cloutier, P., and Coulombe, B. (2013). Regulation of molecular chaperones through post-translational modifications: decrypting the chaperone code. *Biochim. Biophys. Acta* 1829, 443–454. doi: 10.1016/j.bbagrm.2013.02.010

Cooper, G. M., and Hausman, R. E. (2000). "Protein folding and processing," in *The Cell: A Molecular Approach*, 2nd Edn (Sunderland, MA: Sinauer Associates; Oxford University Press).

Cray, J. A., Stevenson, A., Ball, P., Bankar, S. B., Eleutherio, E. C. A., Ezeji, T. C., et al. (2015). Chaotropicity: a key factor in product tolerance of biofuel-producing microorganisms. *Curr. Opin. Biotechnol.* 33, 228–259. doi: 10.1016/j.copbio.2015.02.010

Daigle, F., Lerat, S., Bucca, G., Sanssouci, É, Smith, C. P., Malouin, F., et al. (2015). A terD domain-encoding gene (SCO2368) is involved in calcium homeostasis and participates in calcium regulation of a DosR-like regulon in *Streptomyces coelicolor*. *J. Bacteriol.* 197, 913–923. doi: 10.1128/jb.02278-14

D'Amico, S., Collins, T., Marx, J.-C., Feller, G., Gerday, C., and Gerday, C. (2006). Psychrophilic microorganisms: challenges for life. *EMBO Rep*. 7, 385–389. doi: 10.1038/sj.embor.7400662

De Maayer, P., Anderson, D., Cary, C., and Cowan, D. A. (2014). Some like it cold: understanding the survival strategies of psychrophiles. *EMBO Rep.* 15, 508–517. doi: 10.1002/embr.201338170

De Martino, M., Ershov, D., van den Berg, P. J., Tans, S. J., and Meyer, A. S. (2016). Single-cell analysis of the dps response to oxidative stress. *J. Bacteriol.* 198, 1662–1674. doi: 10.1128/jb.00239-16

deLivron, M. A., Makanji, H. S., Lane, M. C., and Robinson, V. L. (2009). A novel domain in translational GTPase BipA mediates interaction with the 70S ribosome and influences GTP hydrolysis. *Biochemistry* 48, 10533–10541. doi: 10.1021/bi901026z

dos Santos, M. F., Muniz de Pádua, V. L., de Matos Nogueira, E., Hemerly, A. S., and Domont, G. B. (2010). Proteome of *Gluconacetobacter diazotrophicus* co-cultivated with sugarcane plantlets. *J. Proteomics* 73, 917–931. doi: 10.1016/j.jprot.2009.12.005

Doyle, S. M., Hoskins, J. R., and Wickner, S. (2007). Collaboration between the ClpB AAA+ remodeling protein and the DnaK chaperone system. *Proc. Natl. Acad. Sci. U. S. A.* 104, 11138–11144. doi: 10.1073/pnas.0703980104

Doyle, S. M., Shastry, S., Kravats, A. N., Shih, Y. H., Miot, M., Hoskins, J. R., et al. (2015). Interplay between *E. coli* DnaK, ClpB and GrpE during protein disaggregation. *J. Mol. Biol.* 427, 312–327. doi: 10.1016/j.jmb.2014.10.013

Dulyaninova, N. G., Podlepa, E. M., Toulokhonova, L. V., and Bykhovsky, V. Y. (2000). Salvage pathway for NAD biosynthesis in *Brevibacterium ammoniagenes*: regulatory properties of triphosphate-dependent nicotinate phosphoribosyltransferase. *Biochim. Biophys. Acta* 1478, 211–220. doi: 10.1016/s0167-4838(00)00045-5

Endrizzi, J. A., Kim, H., Anderson, P. M., and Baldwin, E. P. (2004). Crystal structure of *Escherichia coli* cytidine triphosphate synthetase, a nucleotide-regulated glutamine amidotransferase/ATP-dependent amidoligase fusion protein and homologue of anticancer and antiparasitic drug targets. *Biochemistry* 43, 6447–6463. doi: 10.1021/bi0496945

Fatima, K., Naqvi, F., and Younas, H. (2021). A review: molecular chaperone-mediated folding, unfolding and disaggregation of expressed recombinant proteins. *Cell Biochem. Biophys.* 79, 153–174. doi: 10.1007/s12013-021-00970-5

Fourie, K. R., and Wilson, H. L. (2020). Understanding GroEL and DnaK stress response proteins as antigens for bacterial diseases. *Vaccines* 8:773. doi: 10.3390/vaccines8040773

Fralick, J. A. (1996). Evidence that TolC is required for functioning of the Mar/AcrAB efflux pump of *Escherichia coli*. *J. Bacteriol.* 178, 5803–5805. doi: 10.1128/jb.178.19.5803-5805.1996

García-Descalzo, L., Alcazar, A., Baquero, F., and Cid, C. (2011). Identification of *in vivo* HSP90-interacting proteins reveals modularity of HSP90 complexes is dependent on the environment in psychrophilic bacteria. *Cell Stress Chaperones* 16, 203–218. doi: 10.1007/s12192-010-0233-7

García-Descalzo, L., García-López, E., Alcázar, A., Baquero, F., and Cid, C. (2014). Proteomic analysis of the adaptation to warming in the Antarctic bacteria *Shewanella frigidimarina*. *Biochim. Biophys. Acta* 1844, 2229–2240. doi: 10.1016/j.bbapap.2014.08.006

Gerdes, S. Y., Kurnasov, O. V., Shatalin, K., Polanuyer, B., Sloutsky, R., Vonstein, V., et al. (2006). Comparative genomics of NAD biosynthesis in cyanobacteria. *J. Bacteriol.* 188, 3012–3023. doi: 10.1128/jb.188.8.3012-3023.2006

Goulhen, F., Dé, E., Pagès, J. M., and Bolla, J. M. (2004). Functional refolding of the *Campylobacter jejuni* MOMP (major outer membrane protein) porin by GroEL from the same species. *Biochem. J.* 378(Pt 3), 851–856. doi: 10.1042/bj20031239

Gragerov, A., Nudler, E., Komissarova, N., Gaitanaris, G. A., Gottesman, M. E., and Nikiforov, V. (1992). Cooperation of GroEL/GroES and DnaK/DnaJ heat shock proteins in preventing protein misfolding in *Escherichia coli*. *Proc. Natl. Acad. Sci. U. S. A.* 89, 10341–10344. doi: 10.1073/pnas.89.21.10341

Hamill, P. G., Stevenson, A., McMullan, P. E., Williams, J. P., Lewis, A. D. R., Sudharsan, S., et al. (2020). Microbial lag phase can be indicative of, or independent from, cellular stress. *Sci. Rep.* 10:5948. doi: 10.1038/s41598-020-62552-4

Hartl, F. U., and Hayer-Hartl, M. (2002). Molecular chaperones in the cytosol: from nascent chain to folded protein. *Science* 295, 1852–1858. doi: 10.1126/science.1068408

Hébraud, M., and Potier, P. (1999). Cold shock response and low temperature adaptation in psychrotrophic bacteria. *J. Mol. Microbiol. Biotechnol.* 1, 211–219.

Hecker, M., and Völker, U. (1990). General stress proteins in *Bacillus subtilis*. *FEMS Microbiol. Lett.* 74, 197–213. doi: 10.1111/j.1574-6968.1990.tb04065.x

Herruzo-Cabrera, R., Vizcaino-Alcaide, M. J., and Fernández-Aceñero, M. J. (2004). The influence of laboratory adaptation on test strains, such as *Pseudomonas aeruginosa*, in the evaluation of the antimicrobial efficacy of ortho-phthalaldehyde. *J. Hosp. Infect.* 57, 217–222. doi: 10.1016/j.jhin.2004.01.031

Hochachka, P. W., and Somero, G. N. (2002). *Biochemical Adaptation: Mechanism and Process in Physiological Evolution*. Oxford: Oxford University Press.

Horst, S. A., Jaeger, T., Denkel, L. A., Rouf, S. F., Rhen, M., and Bange, F. C. (2010). Thiol peroxidase protects *Salmonella enterica* from hydrogen peroxide stress *in vitro* and facilitates intracellular growth. *J. Bacteriol.* 192, 2929–2932. doi: 10.1128/jb.01652-09

Irwin, J. A., and Baird, A. W. (2004). Extremophiles and their application to veterinary medicine. *Ir. Vet. J.* 57, 348–354. doi: 10.1186/2046-0481-57-6-348

Jeong, K. C., Baumler, D. J., and Kaspar, C. W. (2006). dps expression in *Escherichia coli* O157:H7 requires an extended −10 region and is affected by the cAMP receptor protein. *Biochim. Biophys. Acta* 1759, 51–59. doi: 10.1016/j.bbaexp.2006.02.001

Jones, P. G., VanBogelen, R. A., and Neidhardt, F. C. (1987). Induction of proteins in response to low temperature in *Escherichia coli*. *J. Bacteriol.* 169, 2092–2095. doi: 10.1128/jb.169.5.2092-2095.1987

Jørgensen, C. M., Hammer, K., Jensen, P. R., and Martinussen, J. (2004). Expression of the pyrG gene determines the pool sizes of CTP and dCTP in *Lactococcus lactis*. *Eur. J. Biochem.* 271, 2438–2445. doi: 10.1111/j.1432-1033.2004.04168.x

Karas, V. O., Westerlaken, I., and Meyer, A. S. (2015). The DNA-binding protein from starved cells (Dps) utilizes dual functions to defend cells against multiple stresses. *J. Bacteriol.* 197, 3206–3215. doi: 10.1128/jb.00475-15

Kedzierska, S., Akoev, V., Barnett, M. E., and Zolkiewski, M. (2003). Structure and function of the middle domain of ClpB from *Escherichia coli*. *Biochemistry* 42, 14242–14248. doi: 10.1021/bi035573d

Kim, J. J., and Miura, R. (2004). Acyl-CoA dehydrogenases and acyl-CoA oxidases. Structural basis for mechanistic similarities and differences. *Eur. J. Biochem.* 271, 483–493. doi: 10.1046/j.1432-1033.2003.03948.x

Kiss, E., Huguet, T., Poinsot, V., and Batut, J. (2004). The typA gene is required for stress adaptation as well as for symbiosis of *Sinorhizobium meliloti* 1021 with certain *Medicago truncatula* lines. *Mol. Plant Microbe Interact.* 17, 235–244. doi: 10.1094/mpmi.2004.17.3.235

Knöppel, A., Knopp, M., Albrecht, L. M., Lundin, E., Lustig, U., Näsvall, J., et al. (2018). Genetic adaptation to growth under laboratory conditions in *Escherichia coli* and *Salmonella enterica*. *Front. Microbiol.* 9:756. doi: 10.3389/fmicb.2018.00756

Krajewska, J., Modrak-Wójcik, A., Arent, Z. J., Więckowski, D., Zolkiewski, M., Bzowska, A., et al. (2017). Characterization of the molecular chaperone ClpB from the pathogenic spirochaete *Leptospira interrogans*. *PLoS One* 12:e0181118. doi: 10.1371/journal.pone.0181118

Krewulak, K. D., and Vogel, H. J. (2011). TonB or not TonB: is that the question? *Biochem. Cell Biol.* 89, 87–97. doi: 10.1139/o10-141

Krishnan, K., and Flower, A. M. (2008). Suppression of DeltabipA phenotypes in *Escherichia coli* by abolishment of pseudouridylation at specific sites on the 23S rRNA. *J. Bacteriol.* 190, 7675–7683. doi: 10.1128/jb.00835-08

Langer, T., Lu, C., Echols, H., Flanagan, J., Hayer, M. K., and Hartl, F. U. (1992). Successive action of DnaK, DnaJ and GroEL along the pathway of chaperone-mediated protein folding. *Nature* 356, 683–689. doi: 10.1038/356683a0

Leblanc, L., Leboeuf, C., Leroi, F., Hartke, A., and Auffray, Y. (2003). Comparison between NaCl tolerance response and acclimation to cold temperature in *Shewanella putrefaciens*. *Curr. Microbiol.* 46, 157–162. doi: 10.1007/s00284-002-3837-z

Lee, S., Sowa, M. E., Choi, J. M., and Tsai, F. T. (2004). The ClpB/Hsp104 molecular chaperone-a protein disaggregating machine. *J. Struct. Biol.* 146, 99–105. doi: 10.1016/j.jsb.2003.11.016

Li, W., Trabuco, L. G., Schulten, K., and Frank, J. (2011). Molecular dynamics of EF-G during translocation. *Proteins* 79, 1478–1486. doi: 10.1002/prot.22976

Liao, C. H., Chang, C. L., Huang, H. H., Lin, Y. T., Li, L. H., and Yang, T. C. (2021). Interplay between OmpA and RpoN regulates flagellar synthesis in *Stenotrophomonas maltophilia*. *Microorganisms* 9:1216. doi: 10.3390/microorganisms9061216

Liberek, K., Lewandowska, A., and Zietkiewicz, S. (2008). Chaperones in control of protein disaggregation. *EMBO J.* 27, 328–335. doi: 10.1038/sj.emboj.7601970

Lin, Y. S. (2008). Using a strategy based on the concept of convergent evolution to identify residue substitutions responsible for thermal adaptation. *Proteins* 73, 53–62. doi: 10.1002/prot.22049

Liochev, S. I., Hausladen, A., and Fridovich, I. (1999). Nitroreductase A is regulated as a member of the soxRS regulon of *Escherichia coli*. *Proc. Natl. Acad. Sci. U. S. A.* 96, 3537–3539. doi: 10.1073/pnas.96.7.3537

Lu, J., and Holmgren, A. (2014). The thioredoxin antioxidant system. *Free Radic. Biol. Med.* 66, 75–87. doi: 10.1016/j.freeradbiomed.2013.07.036

Lüders, S., Fallet, C., and Franco-Lara, E. (2009). Proteome analysis of the *Escherichia coli* heat shock response under steady-state conditions. *Proteome Sci.* 7:36. doi: 10.1186/1477-5956-7-36

Maier, T., Schmidt, A., Güell, M., Kühner, S., Gavin, A. C., Aebersold, R., et al. (2011). Quantification of mRNA and protein and integration with protein turnover in a bacterium. *Mol. Syst. Biol.* 7:511. doi: 10.1038/msb.2011.38

Makhnevych, T., and Houry, W. A. (2013). The control of spindle length by Hsp70 and Hsp110 molecular chaperones. *FEBS Lett.* 587, 1067–1072. doi: 10.1016/j.febslet.2013.02.018

Masullo, M., Arcari, P., de Paola, B., Parmeggiani, A., and Bocchini, V. (2000). Psychrophilic elongation factor Tu from the antarctic *Moraxella* sp. Tac II 25: biochemical characterization and cloning of the encoding gene. *Biochemistry* 39, 15531–15539. doi: 10.1021/bi0018133

Mayer, M. P. (2021). The Hsp70-chaperone machines in bacteria. *Front. Mol. Biosci.* 8:694012. doi: 10.3389/fmolb.2021.694012

Metpally, R. P., and Reddy, B. V. (2009). Comparative proteome analysis of psychrophilic versus mesophilic bacterial species: insights into the molecular basis of cold adaptation of proteins. *BMC Genomics* 10:11. doi: 10.1186/1471-2164-10-11

Miller, I., Crawford, J., and Gianazza, E. (2006). Protein stains for proteomic applications: which, when, why? *Proteomics* 6, 5385–5408. doi: 10.1002/pmic.200600323

Miot, M., Reidy, M., Doyle, S. M., Hoskins, J. R., Johnston, D. M., Genest, O., et al. (2011). Species-specific collaboration of heat shock proteins (Hsp) 70 and 100 in thermotolerance and protein disaggregation. *Proc. Natl. Acad. Sci. U. S. A.* 108, 6915–6920. doi: 10.1073/pnas.1102828108

Mirus, O., Strauss, S., Nicolaisen, K., von Haeseler, A., and Schleiff, E. (2009). TonB-dependent transporters and their occurrence in cyanobacteria. *BMC Biol.* 7:68. doi: 10.1186/1741-7007-7-68

Miyake, R., Kawamoto, J., Wei, Y. L., Kitagawa, M., Kato, I., Kurihara, T., et al. (2007). Construction of a low-temperature protein expression system using a cold-adapted bacterium. *Shewanella* sp. strain Ac10, as the host. *Appl. Environ. Microbiol.* 73, 4849–4856. doi: 10.1128/aem.00824-07

Mogk, A., Schlieker, C., Strub, C., Rist, W., Weibezahn, J., and Bukau, B. (2003). Roles of individual domains and conserved motifs of the AAA+ chaperone ClpB in oligomerization. ATP hydrolysis, and chaperone activity. *J. Biol. Chem.* 278, 17615–17624. doi: 10.1074/jbc.M209686200

Morita, R. Y. (1975). Psychrophilic bacteria. *Bacteriol. Rev.* 39, 144–167. doi: 10.1128/br.39.2.144-167.1975

Muga, A., and Moro, F. (2008). Thermal adaptation of heat shock proteins. *Curr. Protein Pept. Sci.* 9, 552–566. doi: 10.2174/138920308786733903

Nagano, T., Kojima, K., Hisabori, T., Hayashi, H., Morita, E. H., Kanamori, T., et al. (2012). Elongation factor G is a critical target during oxidative damage to the translation system of *Escherichia coli*. *J. Biol. Chem.* 287, 28697–28704. doi: 10.1074/jbc.M112.378067

Nagy, M., Guenther, I., Akoyev, V., Barnett, M. E., Zavodszky, M. I., Kedzierska-Mieszkowska, S., et al. (2010). Synergistic cooperation between two ClpB isoforms in aggregate reactivation. *J. Mol. Biol.* 396, 697–707. doi: 10.1016/j.jmb.2009.11.059

Nair, S., and Finkel, S. E. (2004). Dps protects cells against multiple stresses during stationary phase. *J. Bacteriol.* 186, 4192–4198. doi: 10.1128/JB.186.13.4192-4198.2004

Nedwell, D. B., and Rutter, M. (1994). Influence of temperature on growth rate and competition between two psychrotolerant Antarctic bacteria: low temperature diminishes affinity for substrate uptake. *Appl. Environ. Microbiol.* 60, 1984–1992. doi: 10.1128/aem.60.6.1984-1992.1994

Niwa, T., Kanamori, T., Ueda, T., and Taguchi, H. (2012). Global analysis of chaperone effects using a reconstituted cell-free translation system. *Proc. Natl. Acad. Sci. U. S. A.* 109, 8937–8942. doi: 10.1073/pnas.1201380109

Palmer, S. O., Rangel, E. Y., Montalvo, A. E., Tran, A. T., Ferguson, K. C., and Bullard, J. M. (2013). Cloning and characterization of EF-Tu and EF-Ts from *Pseudomonas aeruginosa*. *Biomed. Res. Int.* 2013:585748. doi: 10.1155/2013/585748

Paredes, D. I., Watters, K., Pitman, D. J., Bystroff, C., and Dordick, J. S. (2011). Comparative void-volume analysis of psychrophilic and mesophilic enzymes: structural bioinformatics of psychrophilic enzymes reveals sources of core flexibility. *BMC Struct. Biol.* 11:42. doi: 10.1186/1472-6807-11-42

Parsot, C., Hamiaux, C., and Page, A. L. (2003). The various and varying roles of specific chaperones in type III secretion systems. *Curr. Opin. Microbiol.* 6, 7–14. doi: 10.1016/s1369-5274(02)00002-4

Perrody, E., Cirinesi, A.-M., Desplats, C., Keppel, F., Schwager, F., Tranier, S., et al. (2012). A bacteriophage-encoded J-domain protein interacts with the DnaK/Hsp70 chaperone and stabilizes the heat-shock factor σ32 of *Escherichia coli*. *PLoS Genet.* 8:e1003037. doi: 10.1371/journal.pgen.1003037

Pfennig, P. L., and Flower, A. M. (2001). BipA is required for growth of *Escherichia* coi K12 at low temperature. *Mol. Genet. Genomics* 266, 313–317. doi: 10.1007/s004380100559

Phadtare, S. (2004). Recent developments in bacterial cold-shock response. *Curr. Issues Mol. Biol.* 6, 125–136.

Piette, F., D'Amico, S., Mazzucchelli, G., Danchin, A., Leprince, P., and Feller, G. (2011). Life in the cold: a proteomic study of cold-repressed proteins in the antarctic bacterium pseudoalteromonas haloplanktis TAC125. *Appl. Environ. Microbiol.* 77, 3881–3883. doi: 10.1128/aem.02757-10

Piette, F., D'Amico, S., Struvay, C., Mazzucchelli, G., Renaut, J., Tutino, M. L., et al. (2010). Proteomics of life at low temperatures: trigger factor is the primary chaperone in the Antarctic bacterium *Pseudoalteromonas haloplanktis* TAC125. *Mol. Microbiol.* 76, 120–132. doi: 10.1111/j.1365-2958.2010.07084.x

Prüss, B. M., and Wolfe, A. J. (1994). Regulation of acetyl phosphate synthesis and degradation, and the control of flagellar expression in *Escherichia coli*. *Mol. Microbiol.* 12, 973–984. doi: 10.1111/j.1365-2958.1994.tb01085.x

Raimo, G., Lombardo, B., Masullo, M., Lamberti, A., Longo, O., and Arcari, P. (2004). Elongation factor Ts from the Antarctic eubacterium *Pseudoalteromonas haloplanktis* TAC 125: biochemical characterization and cloning of the encoding gene. *Biochemistry* 43, 14759–14766. doi: 10.1021/bi048949b

Ray, M. K., Kumar, G. S., and Shivaji, S. (1994). Phosphorylation of membrane proteins in response to temperature in an Antarctic *Pseudomonas syringae*. *Microbiology* 140(Pt 12), 3217–3223. doi: 10.1099/13500872-140-12-3217

Rhee, S. G. (2016). Overview on peroxiredoxin. *Mol. Cells* 39, 1–5. doi: 10.14348/molcells.2016.2368

Rigal, A., Bouveret, E., Lloubes, R., Lazdunski, C., and Benedetti, H. (1997). The TolB protein interacts with the porins of *Escherichia coli*. *J. Bacteriol.* 179, 7274–7279. doi: 10.1128/jb.179.23.7274-7279.1997

Robin, S., Togashi, D. M., Ryder, A. G., and Wall, J. G. (2009). Trigger factor from the psychrophilic bacterium *Psychrobacter frigidicola* is a monomeric chaperone. *J. Bacteriol.* 191, 1162–1168. doi: 10.1128/jb.01137-08

Rodrigues, D. F., and Tiedje, J. M. (2008). Coping with our cold planet. *Appl. Environ. Microbiol.* 74, 1677–1686. doi: 10.1128/AEM.02000-07

Ruggiero, I., Raimo, G., Palma, M., Arcari, P., and Masullo, M. (2007). Molecular and functional properties of the psychrophilic elongation factor G from the Antarctic Eubacterium *Pseudoalteromonas haloplanktis* TAC 125. *Extremophiles* 11, 699–709. doi: 10.1007/s00792-007-0088-8

Russell, N. J. (1990). Cold adaptation of microorganisms. *Philos. Trans. R. Soc. Lond. B Biol. Sci.* 326, 595–608, discussion 608-611. doi: 10.1098/rstb.1990.0034

Savelsbergh, A., Rodnina, M. V., and Wintermeyer, W. (2009). Distinct functions of elongation factor G in ribosome recycling and translocation. *RNA* 15, 772–780. doi: 10.1261/rna.1592509

Schumann, W. (2009). Temperature sensors of eubacteria. *Adv. Appl. Microbiol.* 67, 213–256. doi: 10.1016/s0065-2164(08)01007-1

Siliakus, M. F., van der Oost, J., and Kengen, S. W. M. (2017). Adaptations of archaeal and bacterial membranes to variations in temperature, pH and pressure. *Extremophiles* 21, 651–670. doi: 10.1007/s00792-017-0939-x

Somprasong, N., Jittawuttipoka, T., Duang-Nkern, J., Romsang, A., Chaiyen, P., Schweizer, H. P., et al. (2012). *Pseudomonas aeruginosa* thiol peroxidase protects against hydrogen peroxide toxicity and displays atypical patterns of gene regulation. *J. Bacteriol.* 194, 3904–3912. doi: 10.1128/jb.00347-12

Sousa, M. C., and McKay, D. B. (2001). Structure of the universal stress protein of *Haemophilus influenzae*. *Structure* 9, 1135–1141. doi: 10.1016/s0969-2126(01)00680-3

Steven, B., Léveillé, R., Pollard, W. H., and Whyte, L. G. (2006). Microbial ecology and biodiversity in permafrost. *Extremophiles* 10, 259–267. doi: 10.1007/s00792-006-0506-3

Storz, G., and Imlay, J. A. (1999). Oxidative stress. *Curr. Opin. Microbiol.* 2, 188–194. doi: 10.1016/s1369-5274(99)80033-2

Summers, M. L., Denton, M. C., and McDermott, T. R. (1999). Genes coding for phosphotransacetylase and acetate kinase in *Sinorhizobium meliloti* are in an operon that is inducible by phosphate stress and controlled by phoB. *J. Bacteriol.* 181, 2217–2224. doi: 10.1128/jb.181.7.2217-2224.1999

Takeshita, D., and Tomita, K. (2010). Assembly of Q{beta} viral RNA polymerase with host translational elongation factors EF-Tu and -Ts. *Proc. Natl. Acad. Sci. U. S. A.* 107, 15733–15738. doi: 10.1073/pnas.1006559107

Taylor, D. E. (1999). *Bacterial tellurite* resistance. *Trends Microbiol.* 7, 111–115. doi: 10.1016/s0966-842x(99)01454-7

Thomas, T., and Cavicchioli, R. (2000). Effect of temperature on stability and activity of elongation factor 2 proteins from Antarctic and thermophilic methanogens. *J. Bacteriol.* 182, 1328–1332. doi: 10.1128/jb.182.5.1328-1332.2000

Thompson, A. D., Bernard, S. M., Skiniotis, G., and Gestwicki, J. E. (2012). Visualization and functional analysis of the oligomeric states of *Escherichia coli* heat shock protein 70 (Hsp70/DnaK). *Cell Stress Chaperones* 17, 313–327. doi: 10.1007/s12192-011-0307-1

Tkaczuk, K. L., Shumilin, I. A., Chruszcz, M., Evdokimova, E., Savchenko, A., and Minor, W. (2013). Structural and functional insight into the universal stress protein family. *Evol. Appl.* 6, 434–449. doi: 10.1111/eva.12057

Tortora, G., Funke, B., and Case, C. (2010). *Microbiology An Introduction*, 10th Edn. San Francisco, CA: Benjamin Cummings.

Turkovicova, L., Smidak, R., Jung, G., Turna, J., Lubec, G., and Aradska, J. (2016). Proteomic analysis of the TerC interactome: novel links to tellurite resistance and pathogenicity. *J. Proteomics* 136, 167–173. doi: 10.1016/j.jprot.2016.01.003

Venkateswaran, K., Moser, D. P., Dollhopf, M. E., Lies, D. P., Saffarini, D. A., MacGregor, B. J., et al. (1999). Polyphasic taxonomy of the genus Shewanella and description of *Shewanella oneidensis* sp. nov. *Int. J. Syst. Bacteriol.* 49(Pt 2), 705–724. doi: 10.1099/00207713-49-2-705

Ventura, M., Canchaya, C., Zink, R., Fitzgerald, G. F., and van Sinderen, D. (2004). Characterization of the groEL and groES loci in *Bifidobacterium breve* UCC 2003: genetic, transcriptional, and phylogenetic analyses. *Appl. Environ. Microbiol.* 70, 6197–6209. doi: 10.1128/aem.70.10.6197-6209.2004

Wang, Q., Hou, Y., Qu, J., Hong, Y., Lin, Y., and Han, X. (2013). Molecular cloning, expression, purification and characterization of thioredoxin from Antarctic sea-ice bacteria Pseudoalteromonas sp. AN178. *Mol. Biol. Rep.* 40, 6587–6591. doi: 10.1007/s11033-013-2771-4

Yang, Y., Harris, D. P., Luo, F., Wu, L., Parsons, A. B., Palumbo, A. V., et al. (2008). Characterization of the *Shewanella oneidensis* Fur gene: roles in iron and acid tolerance response. *BMC Genomics* 9 (Suppl. 1):S11. doi: 10.1186/1471-2164-9-s1-s11

Zgurskaya, H. I., Krishnamoorthy, G., Ntreh, A., and Lu, S. (2011). Mechanism and function of the outer membrane channel TolC in multidrug resistance and physiology of enterobacteria. *Front. Microbiol.* 2:189. doi: 10.3389/fmicb.2011.00189

Conflict of Interest: The authors declare that the research was conducted in the absence of any commercial or financial relationships that could be construed as a potential conflict of interest.

Publisher's Note: All claims expressed in this article are solely those of the authors and do not necessarily represent those of their affiliated organizations, or those of the publisher, the editors and the reviewers. Any product that may be evaluated in this article, or claim that may be made by its manufacturer, is not guaranteed or endorsed by the publisher.

Advantages of publishing in Frontiers

OPEN ACCESS
Articles are free to read for greatest visibility and readership

FAST PUBLICATION
Around 90 days from submission to decision

HIGH QUALITY PEER-REVIEW
Rigorous, collaborative, and constructive peer-review

TRANSPARENT PEER-REVIEW
Editors and reviewers acknowledged by name on published articles

Frontiers
Avenue du Tribunal-Fédéral 34
1005 Lausanne | Switzerland

Visit us: www.frontiersin.org
Contact us: frontiersin.org/about/contact

REPRODUCIBILITY OF RESEARCH
Support open data and methods to enhance research reproducibility

DIGITAL PUBLISHING
Articles designed for optimal readership across devices

FOLLOW US
@frontiersin

IMPACT METRICS
Advanced article metrics track visibility across digital media

EXTENSIVE PROMOTION
Marketing and promotion of impactful research

LOOP RESEARCH NETWORK
Our network increases your article's readership